mathematics

Special Issue Reprint

Nonlinear Systems

Dynamics, Control, Optimization and Applications in Science and Engineering, 3rd Edition

Edited by
Quanxin Zhu

mdpi.com/journal/mathematics

MDPI

Nonlinear Systems: Dynamics, Control, Optimization and Applications in Science and Engineering, 3rd Edition

Nonlinear Systems: Dynamics, Control, Optimization and Applications in Science and Engineering, 3rd Edition

Guest Editor

Quanxin Zhu

MDPI

Basel • Beijing • Wuhan • Barcelona • Belgrade • Novi Sad • Cluj • Manchester

Guest Editor
Quanxin Zhu
School of Mathematics and
Statistics
Hunan Normal University
Changsha
China

Editorial Office
MDPI AG
Grosspeteranlage 5
4052 Basel, Switzerland

This is a reprint of the Special Issue, published open access by the journal *Mathematics* (ISSN 2227-7390), freely accessible at: https://www.mdpi.com/si/mathematics/41CQ4098PR.

For citation purposes, cite each article independently as indicated on the article page online and as indicated below:

Lastname, A.A.; Lastname, B.B. Article Title. *Journal Name* **Year**, *Volume Number*, Page Range.

ISBN 978-3-7258-4311-4 (Hbk)
ISBN 978-3-7258-4312-1 (PDF)
https://doi.org/10.3390/books978-3-7258-4312-1

Contents

About the Editor

Quanxin Zhu

Professor Quanxin Zhu received his Ph.D. degree from Sun Yatsen (Zhongshan) University, Guangzhou, China, in 2005. He is currently a professor at Hunan Normal University, and he has obtained the Alexander von Humboldt Foundation of Germany. Professor Zhu is a distinguished professor of Furong scholars in Hunan Province, a leading talent in scientific and technological innovation in Hunan Province, and the Deputy Director of the Key Laboratory of Computing and Stochastic Mathematics for the Ministry of Education. Professor Zhu is a globally highly cited scientist. In addition, he is a senior member of the IEEE and has served as the Lead Guest Editor for several international journals. He serves as an Associate Editor for six international SCI journals, including *IEEE Transactions on Automation Science and Engineering*. He obtained the first prize of the Hunan Natural Science Award in 2021, and was listed as part of the top two percent of scientists in 2020–2024. Professor Zhu won the 2011 Annual Chinese "One Hundred Most Influential International Academic Paper" Award and was one of most cited Chinese researchers in 2014–2024, according to Elsevier. Professor Zhu serves as a reviewer for more than 50 journals and he is the author or coauthor of more than 300 journal papers. His research interests include stochastic control, stochastic differential equations, stochastic stability, stochastic nonlinear systems, Markovian jump systems, stochastic neural networks, and stochastic complex networks.

mathematics

MDPI

Article

Discounted Risk-Sensitive Optimal Control of Switching Diffusions: Viscosity Solution and Numerical Approximation

Xianggang Lu and Lin Sun *

School of Mathematics and Statistics, Guangdong University of Technology, Guangzhou 510006, China; luxg@gdut.edu.cn

* Correspondence: yssl12@gdut.edu.cn

Abstract: This work considers the infinite horizon discounted risk-sensitive optimal control problem for the switching diffusions with a compact control space and controlled through the drift; thus, the the generator of the switching diffusions also depends on the controls. Note that the running cost of interest can be unbounded, so a decent estimation on the value function is obtained, under suitable conditions. To solve such a risk-sensitive optimal control problem, we adopt the viscosity solution methods and propose a numerical approximation scheme. We can verify that the value function of the optimal control problem solves the optimality equation as the unique viscosity solution. The optimality equation is also called the Hamilton–Jacobi–Bellman (HJB) equation, which is a second-order partial differential equation (PDE). Since, the explicit solutions to such PDEs are usually difficult to obtain, the finite difference approximation scheme is derived to approximate the value function. As a byproduct, the ϵ-optimal control of finite difference type is also obtained.

Keywords: risk-sensitive control; controlled switching diffusions; HJB equation

MSC: 93E20; 49L20; 49M25

1. Introduction

The past few decades have witnessed the emergence and development of optimal control problems with risk-sensitive criteria. The reason why risk-sensitive criteria are often desirable is that they can capture the effects of higher-order moments of the running costs in addition to their expectations. To the best of our knowledge, refs. [1,2] are the earliest works concerned with risk-sensitive optimal control problems. Since then, there has been a lot of research on risk-sensitive optimal control problems. For the discrete time controlled Markov chains, the risk-sensitive criteria have been studied in [3,4]; for the continuous time Markov chains with risk-sensitive criteria see [5–8] and the reference therein; for piecewise deterministic Markov decision processes see [9] and the reference therein; for the controlled diffusions with risk-sensitive criteria, we refer the readers to [10–13]. Besides the theoretical improvement, it has also has found applications in Q-learning [14], finance [15], insurance [16], missile guidance [17], and many other applications.

As to controlled switching diffusion, it has been paid much attention in theory and application in recent years. The state of such process consists of a continuous part and a discrete part at the same time. Usually, the discrete part of the state is modelled by a continuous time Markov chain with finite states. So much effort has been spent to learn more about the properties of the processes, for instance [18,19] and the reference therein. Much of the study originated from applications arising in manufacturing systems [20,21], filtering [22], and financial engineering [23]. For more general theory on such hybrid systems, we refer the readers to [24,25]. While [24] concerns the case when the generator of the continuous time Markov chain is independent of the continuous part of the state, and [25] studies the case when the generator of the continuous time Markov chain depends on the continuous part of the state. Such models can be widely used in many practical

applications. For example, [26] applies the switching diffusions to the ecosystems and let the discrete part of the state represent the random environment. Within the framework of financial applications, the discrete part of the state is usually used to capture the market environment, say bull or bear, see [27].

However, to the best of our knowledge, there is little literature on controlled switching diffusions with risk-sensitive criteria. The risk-sensitive optimal control problem to the controlled switching diffusions is of interest and such an issue has not received so much attention, which motivates us to consider such topics. In this work, we are going to study the infinite horizon discounted risk-sensitive optimal control problem based on the controlled switching diffusions. To be specific, we work on the process $(X(t), \alpha(t))$ with $X(t)$ being the continuous part of the state and $\alpha(t)$ being the discrete part, which is governed by (1) and (2). Based on the controlled switching diffusion $(X(t), \alpha(t))$ defined above, we are going to minimize

$$J(\theta, x, \alpha, u(\cdot)) = \frac{1}{\theta} \log\left\{ E\left[\exp\left(\theta \int_0^\infty e^{-\rho t} c(X(t), \alpha(t), u(t)) dt \right) \right] \right\},$$

with $\theta \in (0, 1]$ being the risk factor and $\rho > 0$ being the discount factor. Define the value function as follows,

$$V(\theta, x, \alpha) = \inf_{u(\cdot)} J(\theta, x, \alpha, u(\cdot)).$$

Our aim is to find the optimal control $u^*(\cdot)$ such that $V(\theta, x, \alpha) = J(\theta, x, \alpha, u^*(\cdot))$. Since the logarithm function is increasing, to simplify the calculation, we only need to minimize the following functional

$$I(\theta, x, \alpha, u(\cdot)) = E\left[\exp\left(\theta \int_0^\infty e^{-\rho t} c(X(t), \alpha(t), u(t)) dt \right) \right],$$

The corresponding value function is

$$W(\theta, x, \alpha) = \inf_{u(\cdot)} I(\theta, x, \alpha, u(\cdot)).$$

Similarly, if there exists a control $u^*(\cdot)$ such that $W(\theta, x, \alpha) = I(\theta, x, \alpha, u^*(\cdot))$, we call it optimal. It is easy to know that if $u^*(\cdot)$ such that $W(\theta, x, \alpha) = I(\theta, x, \alpha, u^*(\cdot))$, then we can also obtain $V(\theta, x, \alpha) = J(\theta, x, \alpha, u^*(\cdot))$, and vice versa. Therefore, it is sufficient to work on the optimization problem with exponential utility.

To solve such problem, similar to the risk neutral case, see [20,27], we should find suitable characterizations to the value function $W(\theta, x, \alpha)$ and the optimal control $u^*(\cdot)$. Due to the dynamic program principle, such characterizations are usually given via the associated optimality equation, or the HJB equation. Thus we formally derive the associated HJB equation and rigorously prove that the value function $W(\theta, x, \alpha)$ of the optimization problem solves the associated HJB equation as the unique viscosity solution. We will see that such equation is a second-order partial differential equation. The viscosity solution is one of the commonly used weak solutions for this kind of equation; we recommend [27–29] and the reference therein for readers who are not familiar with the concept of viscosity solutions. In particular, the development of viscosity solutions is briefly introduced in reference [28].

As is well known, explicit solutions to such HJB equations are usually difficult to obtain, so we turn to study the numerical solutions. Finite difference approximation scheme is a tool of commonly used. Moreover, associated with the viscosity solution method, we can also give the convergence analysis to the finite difference approximation scheme. As a byproduct, through the convergence analysis of the approximation scheme we can obtain the ϵ-optimal control of finite difference type.

This work has the following contributions: (a) We propose a suitable condition to give a decent estimation on the value function of concerned with unbounded running cost.

Unlike in [10], we do not need the near-monotonicity condition as the structural assumption on the running cost function. Further, compared with the assumptions adopted in [10], under our assumption we can also drop the requirement that the coefficients of the systems should be bounded. (b) We construct an appropriate truncation function to reduce the proof of the global comparison theorem to the local case. To be specific, the difficulty of verifying the uniqueness of viscosity solution is to prove the corresponding comparison theorem, and the large obstacle of proving the corresponding comparison theorem is to construct the corresponding truncation function. (c) We construct a finite difference approximation scheme to approach the value function, and as a byproduct, we can obtain the existence of ϵ-optimal control of finite difference type. This kind of idea can be extended to treat the optimal control of controlled (switching) diffusions with other criteria.

The rest of the work is organized as follows: In Section 2, we introduce the mathematical background and arise the optimization problem. In Section 3, we derive the associated HJB equation and show that the value function to the optimization problem solves the associated HJB equation as the unique viscosity solution. In Section 4, we construct the finite difference approximation scheme and give its convergence analysis, as a byproduct, we also show the existence of ϵ-optimal control of finite difference type.

2. The Model

In this work, the underlying process $(X(t), \alpha(t))$ is defined on the complete filtered probability space $(\Omega, \mathcal{F}, \{\mathcal{F}_t\}_{t\geq 0}, P)$ and governed by the following system,

$$dX(t) = b(X(t), \alpha(t), u(t))dt + \sigma(X(t), \alpha(t))dB(t), \quad (X(0), \alpha(0)) = (x, \alpha), \tag{1}$$

$$P(\alpha(t+\delta) = j | \alpha(t) = i, X(s), \alpha(s), s \leq t) = q_{ij}(X(t), u(t))\delta + o(\delta), \quad i \neq j, \tag{2}$$

with $\delta > 0$ arbitrarily small. $(X(t), \alpha(t)) \in \mathbb{R}^r \times \mathcal{M}$, with $\mathcal{M} = \{1, 2, \cdots, m\}$ be a finite set. $b(\cdot, \cdot, \cdot) : \mathbb{R}^r \times \mathcal{M} \times \mathbb{U} \to \mathbb{R}^r$ and $\sigma(\cdot, \cdot) : \mathbb{R}^r \times \mathcal{M} \to \mathbb{R}^{r\times r}$ are drift term and diffusion term, respectively. $Q(x, u) = (q_{ij}(x, u)) \in \mathbb{R}^{m\times m}$ is the generator of the process of Markov regime switching. The control process $\{u(t)\}_{t\geq 0}$ is taking value in $\mathbb{U}$, which is a given compact metric space. $B(t)$ is a standard Brownian motion.

Remark 1. *The probability space $(\Omega, \mathcal{F}, \{\mathcal{F}_t\}_{t\geq 0}, P)$ mentioned above is constructed in the following way. Firstly, for fixed $x \in \mathbb{R}^r$, define*

$$p(t, x, y) = (2\pi t)^{-r/2} \exp\left\{-\frac{|x-y|^2}{2t}\right\},$$

for $y \in \mathbb{R}^r, t > 0$. If $0 \leq t_1 \leq t_2 \leq \cdots \leq t_k$, define a measure $\nu_{t_1,\ldots,t_k}$ on $\mathbb{R}^{rk}$ by

$$\begin{aligned} & \nu_{t_1,\ldots,t_k}(F_1 \times \cdots \times F_k) \\ = & \int_{F_1\times\cdots\times F_k} p(t_1, x, x_1)p(t_2 - t_1, x_1, x_2) \cdots p(t_k - t_{k-1}, x_{k-1}, x_k)dx_1 \cdots dx_k, \end{aligned}$$

where $F_i, i = 1, 2, \cdots, k$, are members of $\mathcal{B}(\mathbb{R}^r)$, the Borel σ-field of $\mathbb{R}^r$. Additionally, we use the convention that $p(0, x, y)dy = \delta_x(y)$. Then by verifying that $\nu_{t_1,\ldots,t_k}$ satisfies the consistent properties and the Kolmogorov's extension theorem (see [30] (p. 11, Theorem 2.1.5) and the reference therein), there exists a probability space $(\Omega^B, \mathcal{F}^B, P^B)$ and a stochastic process $\{B(t)\}_{t\geq 0}$ on Ω^B such that

$$P^B(B(t_1) \in F_1, \cdots, B(t_k) \in F_k) = \nu_{t_1,\cdots,t_k}(F_1 \times \cdots \times F_k).$$

In fact, $\{B(t)\}_{t\geq 0}$ is a standard Brownian motion.

Moreover, Let λ be the Lebesgue measure on $(\mathbb{R}_+ \times \mathbb{R}, \mathcal{B}(\mathbb{R}_+ \times \mathbb{R}))$ such that $\lambda(dt \times dz) = dt \times m(dz)$, where m is the Lebesgue measure on $\mathbb{R}$. For arbitrary $A \in \mathcal{B}(\mathbb{R}_+ \times \mathbb{R})$ and $\lambda(A) < \infty$, let

$$p_A(n) = e^{-\lambda(A)} \frac{[\lambda(A)]^n}{n!}, \quad n = 0, 1, 2, \cdots.$$

If $\lambda(A) = \infty$, *then let*

$$p_A(\infty) = 1.$$

It is easy to know that p_A *is a probability measure on* $\bar{Z}_+ = Z_+ \cup \{\infty\}$. *Moreover, for each* $k \in Z_+/\{0\}$, $A_i \in \mathcal{B}(\mathbb{R}_+ \times \mathbb{R})$, *and* $\lambda(A_i) < \infty$, $(i = 1, 2, \cdots, k)$ *and* $i_j \in \bar{Z}_+$, $(j = 1, 2, \cdots, k)$, *define the following finite dimensional distribution on* $(\bar{Z}_+)^k$

$$p_{A_1,\cdots,A_k}(i_1, \cdots, i_k) = \Pi_{n=1}^{k} p_{A_n}(i_n).$$

Then by verifying the above finite dimensional distribution admits several consistent properties, the existence theorem of Poisson random measure (see in [31] [Chapter 11]) ensures that there exists a probability space $(\Omega^{\mathfrak{p}}, \mathcal{F}^{\mathfrak{p}}, P^{\mathfrak{p}})$ *and a process of Poisson random measure* $\mathfrak{p}(dt, dz)$ *defined on* $\Omega^{\mathfrak{p}}$ *with intensity* $dt \times m(dz)$, *where* $m(dz)$ *denotes the Lebesgue measure on* $\mathbb{R}$, *such that, for each* $k \in Z_+/\{0\}$, $A_i \in \mathcal{B}(\mathbb{R}_+ \times \mathbb{R})$ *and* $\lambda(A_i) < \infty$, *for* $i = 1, 2, \cdots, k$,

$$P^{\mathfrak{p}}(\mathfrak{p}(A_j) = i_j, j = 1, 2, \cdots, k) = p_{A_1,\cdots,A_k}(i_1, \cdots, i_k).$$

Then by letting $(\Omega, \mathcal{F}, P) := (\Omega^B \times \Omega^{\mathfrak{p}}, \mathcal{F}^B \times \mathcal{F}^{\mathfrak{p}}, P^B \times P^{\mathfrak{p}})$ *and* $\mathcal{F}_t = \sigma\{B(s), \mathfrak{p}(E, F), (E, F) \in \mathcal{B}([0, s)) \times \mathcal{B}(\mathbb{R}), 0 \le s \le t\}$, *we have actually constructed the complete filtered probability space* $(\Omega, \mathcal{F}, \{\mathcal{F}_t\}_{t\ge 0}, P)$. *Throughout the work, we assume that the Poisson random measure* $\mathfrak{p}(dt, dz)$ *is independent of the Brownian motion* $B(\cdot)$.

In order to get convenient compactness property, we introduce the notion of relaxed control. Let $\Pi = \{\pi(t) \in \mathcal{P}(\mathbb{U}), t \ge 0\}$, with $\mathcal{P}(\mathbb{U})$ being the space of all probability measures defined on the control space $\mathbb{U}$. In particular, $u(t)$ is equivalent to $\delta_{u(t)}$, with δ be the Dirac measure, for each $t \ge 0$. To proceed, we also need the following definition of admissible control.

Definition 1. *We say that a relaxed control* $\pi \in \Pi$ *is admissible if* $\pi(t)$ *is* $\mathcal{F}_t$*-adapted measurable and the* σ*-fields* $\mathcal{F}_t^{\pi}$ *and* $\mathcal{F}_{[t,\infty)}^{B,\mathfrak{p}}$ *are independent, with* $\mathcal{F}_t^{\pi} = \sigma\{\pi(s), s \le t\}$ *and* $\mathcal{F}_{[t,\infty)}^{B,\mathfrak{p}} = \sigma\{B(s) - B(t), \mathfrak{p}(E, F), E \in \mathcal{B}([s, \infty)), F \in \mathcal{B}(\mathbb{R}), s \ge t\}$.

Denote by Π_A the collecton of all admissible controls. Furthermore, if $\pi(t) = \varphi(X(t), \alpha(t))$ for a measurable function $\varphi : \mathbb{R}^r \times \mathcal{M} \to \mathcal{P}(\mathbb{U})$, the admissible control $\pi = \{\pi(t), t \ge 0\}$ is called a stationary Markov control. We use Π_{RM} to represent the family of all stationary Markov controls. Moreover, we call $u(\cdot)$ or $\pi(\cdot) = \delta_{u(\cdot)}$ the non-randomized stationary Markov control, if $u(t) = \phi(X(t), \alpha(t))$and $\phi : \mathbb{R}^r \times \mathcal{M} \to \mathbb{U}$ is measurable for all $t \ge 0$. Denote all such controls by Π_{DM}. Obviously, $\Pi_{DM} \subset \Pi_{RM} \subset \Pi_A \subset \Pi$.

In order to guarantee that the system (1) and (2) admits a unique solution, we need the following assumption.

Assumption 1.

(i) $Q(x, u) = (q_{ij}(x, u)) \in \mathbb{R}^{m\times m}$ *with* $q_{ij}(x, u) \ge 0 (i \ne j)$, *for all* $(x, u) \in \mathbb{R}^r \times \mathbb{U}$, *and* $\sum_{j=1}^{m} q_{ij}(x, u) = 0$ *for all* $i \in \mathcal{M}$. *Additionally,* $q_{ij}(x, u)$ *is bounded continuous function for all* $i, j \in \mathcal{M}$

(ii) The drift term $b(\cdot, \cdot, \cdot)$ *and the diffusion term* $\sigma(\cdot, \cdot)$ *are continuous functions. Moreover, both of them are Lipschitz continuous in their first component, uniformly for all* $\alpha \in \mathcal{M}$ *and* $u \in \mathbb{U}$, *with Lipschitz constant* $k_0 > 0$.

(iii) The system is non-degenerate, i.e., $\sigma\sigma^T \ge k_1 I$ *for suitable constant* $k_1 > 0$, *where* $I \in \mathbb{R}^{r\times r}$ *represents the identity matrix.*

Associated with the assumptions above, we can get the following conclusion.

Theorem 1. *Suppose that the Assumption 1 holds, then the system* (1) *and* (2) *admits an unique strong solution* $(X(\cdot), \alpha(\cdot))$ *for a given control* $\pi \in \Pi_{RM}$*, which is a Feller process and the associated operator is given by*

$$\mathcal{L}^{\pi} f(x,\alpha) = \int_{\mathbb{U}} \mathcal{L}^{u} f(x,\alpha)\pi(du|x,\alpha), \quad \pi \in \Pi_{RM}$$

where

$$\mathcal{L}^{u} f(x,\alpha) = \sum_{l=1}^{r} b_l(x,\alpha,u)\frac{\partial f(x,\alpha)}{\partial x_l} + \frac{1}{2}\sum_{l,k=1}^{r} a_{lk}(x,\alpha)\frac{\partial^2 f(x,\alpha)}{\partial x_l \partial x_k} + \sum_{j=1}^{m} q_{\alpha j}(x,u) f(x,j), \quad (3)$$

with $a(x,\alpha) = \sigma(x,\alpha)\sigma^T(x,\alpha) \in \mathbb{R}^{r\times r}$ *and* $f \in C^{2,0}(\mathbb{R}^r \times \mathcal{M})$*, which is the space consisting of all real-valued functions, which are twice continuously differentiable with respect to* x *and continuous with respect to* α*.*

Proof 1. As well known, the Markov regime switching process $\alpha(\cdot)$ can be represented by the stochastic integral with respect to the forementioned Poisson random measure $\mathfrak{p}(dt,dz)$ as given is Remark 1. Then for $\pi = \{\pi(t), t \geq 0\} \in \Pi_{RM}$, (1) and (2) have the following equivalent form

$$\begin{aligned} dX(t) &= b(X(t),\alpha(t),\pi(t))dt + \sigma(X(t),\alpha(t))dB(t), \\ d\alpha(t) &= \int_{\mathbb{R}} h(X(t),\alpha(t-),\pi(t),z)\mathfrak{p}(dt,dz), \end{aligned} \quad (4)$$

with initial state $(X(0),\alpha(0)) = (x,\alpha)$. For more details, we refer the readers to [25,32], [Chapter 2] and the reference therein. Thus the result follows by ([20] Theorem 2.1). □

The Risk-Sensitive Criterion

Now, we are going to introduce the risk-sensitive criterion. For $\theta \in (0,1]$ and $\rho > 0$, define

$$J(\theta,x,\alpha,\pi) = \frac{1}{\theta}\log\left\{E\left[\exp\left(\theta\int_0^{\infty} e^{-\rho t}c(X(t),\alpha(t),\pi(\cdot))dt\right)\right]\right\},$$

where $c(x,\alpha,\pi(\cdot)) := \int_{\mathbb{U}} c(x,\alpha,u)\pi(du|x,\alpha)$ for all control $\pi \in \Pi_{RM}$, θ is the risk-sensitive parameter and ρ is the given discount factor. We are going to minimize $J(\theta,x,\alpha,\pi)$ over Π_{RM}. Let the value function be defined as follows,

$$V(\theta,x,\alpha) := \inf_{\pi\in\Pi_{RM}} J(\theta,x,\alpha,\pi).$$

The aim is to find a suitable control $\pi^* \in \Pi_{RM}$ such that $V(\theta,x,\alpha) = J(\theta,x,\alpha,\pi^*)$, we call such π^* the optimal control. As mentioned in the introduction, to simplify the calculation, we need to work with the following auxiliary functional

$$I(\theta,x,\alpha,\pi) = E\left[\exp\left(\theta\int_0^{\infty} e^{-\rho t}c(X(t),\alpha(t),\pi(\cdot))dt\right)\right],$$

The corresponding value function is

$$W(\theta,x,\alpha) = \inf_{\pi\in\Pi_{RM}} I(\theta,x,\alpha,\pi).$$

Since the logarithm function is an increasing function, thus the optimal control to the auxiliary problem is also optimal to the original risk-sensitive problem. Henceforth, we only need to work with $W(\theta,x,\alpha)$.

To proceed we need the following assumption to ensure that the value function W is well defined, which means that it admits a certain property of boundness.

Assumption 2. *Suppose that the following conditions hold.*

(i) *The running cost function $c(x,\alpha,u)$ is continuous in (x,α,u), and $\sup_\pi |c(x,\alpha,\pi(\cdot))| \le M_0\omega(x,\alpha)$, for suitable $M_0 > 0$, where $\omega : \mathbb{R}^r \times \mathcal{M} \to \mathbb{R}^+$ is a given positive function and twice continuously differentiable in $x \in \mathbb{R}^r$ for each $\alpha \in \mathcal{M}$, and $\omega(x,\alpha) \ge 1$, for all $(x,\alpha) \in \mathbb{R}^r \times \mathcal{M}$.*

(ii) *There have two constants $A, \tilde{A} > 0$ such that $\rho > A > 0$ and*

$$\mathcal{L}^u\omega(x,\alpha) + \frac{1}{2}\sum_{l,k=1}^{r} a_{l,k}(x,\alpha)\frac{\partial\omega(x,\alpha)}{\partial x_l}\frac{\partial\omega(x,\alpha)}{\partial x_k} \le A\omega(x,\alpha) + \tilde{A}.$$

(iii) *And assume that*

$$E\left\{\exp\left[\frac{1}{2}\int_0^\infty \left(e^{-As}\partial\omega(X(s),\alpha(s))\sigma(X(s),\alpha(s))\right)^2 ds\right]\right\} < \infty, \tag{5}$$

with $(\partial\omega(x,\alpha)\sigma(x,\alpha))_k = \sum_{l=1}^r \frac{\partial\omega(x,\alpha)}{\partial x_l}\sigma_{lk}(x,\alpha)$.

Henceforth, we denote $\partial\omega(x,\alpha)\sigma(x,\alpha)$ or its suitable variants $\partial\omega(X(s),\alpha(s))\sigma(X(s),\alpha(s))$ by $\partial\omega\sigma$, for simplicity.

Remark 2. *Since the function ω can be unbounded, thus $c(x,\alpha,u)$ can also be unbounded. Unlike in [10], we do not need the structural assumption on the running cost function, which is known as near-monotonicity, and we also do not assume the cofficients of the diffusion to be bounded.*

Under the assumption above, we can show that the value functions are well defined. In fact, we can obtain the following conclusion.

Proposition 1. *Under the Assumption 2, we have*

$$W(\theta,x,\alpha) \le M_1 \exp\{M_2\omega(x,\alpha)\},$$

with $M_1 = \exp\left\{\frac{M_0}{\rho - A}\right\}$ *and* $M_2 = 2\max\left\{\frac{M_0}{\rho - A}, \frac{M_0\tilde{A}}{\rho(\rho - A)}\right\}$.

Proof 2. Let $f(t,x,\alpha) = e^{-At}\omega(x,\alpha)$, then by using the Itô's formula we have

$$\begin{aligned}
& e^{-At}\omega(X(t),\alpha(t)) \\
= \;& \omega(x,\alpha) + \int_0^t e^{-As}[\mathcal{L}^u\omega(X(s),\alpha(s)) - A\omega(X(s),\alpha(s))]ds + \int_0^t e^{-As}\partial\omega\cdot\sigma dB(s) \\
= \;& \omega(x,\alpha) + \int_0^t e^{-As}[\mathcal{L}^u\omega(X(s),\alpha(s)) - A\omega(X(s),\alpha(s))]ds + \frac{1}{2}\int_0^t \left(e^{-As}\partial\omega\cdot\sigma\right)^2 ds \\
& + \int_0^t e^{-As}\partial\omega\cdot\sigma dB(s) - \frac{1}{2}\int_0^t \left(e^{-As}\partial\omega\cdot\sigma\right)^2 ds \\
\le \;& \omega(x,\alpha) + \int_0^t e^{-As}\tilde{A}ds + \int_0^t e^{-As}\partial\omega\cdot\sigma dB(s) - \frac{1}{2}\int_0^t \left(e^{-As}\partial\omega\cdot\sigma\right)^2 ds
\end{aligned} \tag{6}$$

Thus

$$\omega(X(t),\alpha(t)) \le e^{At}\omega(x,\alpha) + \frac{\tilde{A}}{A}(e^{At} - 1) + e^{At}Z_t \tag{7}$$

with

$$Z_t = \int_0^t e^{-As}\partial\omega\cdot\sigma dB(s) - \frac{1}{2}\int_0^t \left(e^{-As}\partial\omega\cdot\sigma\right)^2 ds \tag{8}$$

In addition, we have

$$\begin{aligned}
& E\left\{\exp\left[\theta\int_0^\infty e^{-\rho t}c(X(t),\alpha(t),\pi(\cdot))dt\right]\right\} \\
\leq\ & E\left\{\exp\left[\theta\int_0^\infty e^{-\rho t}|c(X(t),\alpha(t),\pi(\cdot))|dt\right]\right\} \\
\leq\ & E\left\{\exp\left[\int_0^\infty e^{-\rho t}M_0\omega(X(t),\alpha(t))dt\right]\right\} \quad \text{(by Assumption 2(i) and } \theta\leq 1) \qquad (9)\\
\leq\ & E\left\{\exp\left[\int_0^\infty e^{-\rho t}M_0\left(e^{At}\omega(x,\alpha)+\frac{\tilde{A}}{A}(e^{At}-1)\right)dt\right]\right\} \\
& \times E\left\{\exp\left[\int_0^\infty e^{-\rho t}M_0\left(e^{At}Z_t\right)dt\right]\right\}.
\end{aligned}$$

Furthermore, note that $\rho > A$, by direct calculation, we can derive that

$$\begin{aligned}
& E\left\{\exp\left[\int_0^\infty e^{-\rho t}M_0\left(e^{At}\omega(x,\alpha)+\frac{\tilde{A}}{A}(e^{At}-1)\right)dt\right]\right\} \\
=\ & \frac{M_0}{\rho-A}\omega(x,\alpha)+\frac{M_0\tilde{A}}{\rho(\rho-A)} \\
\leq\ & M_2\omega(x,\alpha) \quad (\text{by } \omega(x,\alpha)\geq 1),
\end{aligned}$$

with $M_2 := 2\max\left\{\frac{M_0}{\rho-A}, \frac{M_0\tilde{A}}{\rho(\rho-A)}\right\}$.

Moreover, by letting $\nu(dt) := (\rho-A)e^{-(\rho-A)t}dt$, and noting that it is a probability measure on $[0,\infty)$, we can derive that

$$\begin{aligned}
& E\left\{\exp\left[\int_0^\infty e^{-\rho t}M_0\left(e^{At}Z_t\right)dt\right]\right\} \\
=\ & E\left\{\exp\left[\int_0^\infty \frac{M_0}{\rho-A}Z_t\nu(dt)\right]\right\} \\
\leq\ & E\left\{\int_0^\infty \exp\left[\frac{M_0}{\rho-A}Z_t\right]\nu(dt)\right\} \\
=\ & \int_0^\infty \exp\left[\frac{M_0}{\rho-A}\right]E[e^{Z_t}]\nu(dt).
\end{aligned}$$

By the condition (5), we can derive that Z_t is an exponential martingale and

$$E[e^{Z_t}] = E[e^{Z_0}] = 1.$$

Thus we have

$$E\left\{\exp\left[\int_0^\infty e^{-\rho t}M_0\left(e^{At}Z_t\right)dt\right]\right\} = \exp\left[\frac{M_0}{\rho-A}\right] =: M_1.$$

Therefore, we can conclude that

$$W(\theta,x,\alpha)\leq M_1\exp\{M_2\omega(x,\alpha)\},$$

for all $\theta\in(0,1]$, with $M_1 = \exp\left[\frac{M_0}{\rho-A}\right]$ and $M_2 = 2\max\left\{\frac{M_0}{\rho-A}, \frac{M_0\tilde{A}}{\rho(\rho-A)}\right\}$. We are done. □

Let $\tilde{\omega}(x,\alpha) = \exp\{M_2\omega(x,\alpha)\}$. Now, we can introduce the $\tilde{\omega}$-norm and the definition of $\tilde{\omega}$ bounded. A function $\psi : (0,1]\times\mathbb{R}^r\times\mathcal{M}\to\mathbb{R}$, is called $\tilde{\omega}$-bounded if

$$\|\psi\|_{\tilde{\omega}} := \sup_{(\theta,x,\alpha)\in\mathbb{R}^r\times\mathcal{M}}\frac{|\psi(\theta,x,\alpha)|}{\tilde{\omega}(x,\alpha)} < \infty.$$

Then, we can see that W is a member of $B_{\tilde{\omega}}((0,1]\times\mathbb{R}^r\times\mathcal{M})$, the collection of all $\tilde{\omega}$-bounded real valued functions defined on $(0,1]\times\mathbb{R}^r\times\mathcal{M}$, which is a Banach space. Thus, the value function W is well defined. For simplicity, henceforth, let $\mathcal{Q}_0 := (0,1]\times\mathbb{R}^r\times\mathcal{M}$, then $B_{\tilde{\omega}}((0,1]\times\mathbb{R}^r\times\mathcal{M})$ can be simply denoted by $B_{\tilde{\omega}}(\mathcal{Q}_0)$.

To proceed, we need to illustrate that the set of models which satisfy Assumptions 1 and 2 is nonempty. We show this fact by giving a representative example.

Example 1. *For simplicity, we consider the one-dimensional Ornstein–Uhlenbeck type process with regime switching. Let* $(X(t),\alpha(t))\in\mathbb{R}\times\mathcal{M}$, *with* $\mathcal{M}=\{1,2\}$, *and*

$$dX(t)=(\mu(\alpha(t))+u(t))X(t)dt+\sigma(\alpha(t))dB(t) \tag{10}$$

$$Q(x,u)=\begin{pmatrix} q_{11}(x,u) & -q_{11}(x,u)\\ -q_{22}(x,u) & q_{22}(x,u)\end{pmatrix} \tag{11}$$

with $q_{ii}<0, |q_{ii}|<\infty, i=1,2$ *and* $\mathbb{U}=[0,U_0]$, *and consider the functional*

$$I(\theta,x,\alpha,\pi(\cdot))=E\left[\exp\left(\theta\int_0^\infty e^{-\rho t}c(X(t),\alpha(t),\pi(\cdot))dt\right)\right],$$

with $c(x,\alpha,u)=x+\alpha+u$, *and* $\rho>\mu_M+U_0$, *with* $\sigma_M=\max\{\sigma(1),\sigma(2)\}$, $\mu_M=\max\{\mu(1),\mu(2)\}$.

It is obvious to know that Assumption 1 holds and by taking $\omega(x,\alpha)=x+\alpha+1$, it is easy to verify that Assumption 2 (i) and (ii) also hold with $A=\mu_M+U_0<\rho$, $\tilde{A}=\max\{|q_{11}|,|q_{22}|\}$ and $M_0=\max\{U_0,1\}$. Now it remains to verify that Assumption 2 (iii) also holds. In fact,

$$\begin{aligned} & E\left\{\exp\left[\frac{1}{2}\int_0^\infty\left(e^{-As}\partial\omega(X(s),\alpha(s))\sigma(X(s),\alpha(s))\right)^2ds\right]\right\}\\ =\ & E\left\{\exp\left[\frac{1}{2}\int_0^\infty(e^{-2As}\sigma(\alpha(s))^2ds\right]\right\}\\ \le\ & \exp\left[\frac{1}{2}\int_0^\infty e^{-2As}\sigma_M^2ds\right]\\ =\ & \exp\left[\frac{\sigma_M^2}{4A}\right]<\infty. \end{aligned}$$

Therefore, Assumption 2 (iii) has been verified.

To conclude this section, now we formally derive the HJB equation for W. For any $T>0$ and given Markov control $\pi\in\Pi_{RM}$, it is easy to know that

$$\begin{aligned} & W(\theta,x,\alpha)\\ =\ & \inf_{\pi\in\Pi_{RM}} I(\theta,x,\alpha,\pi)\\ =\ & \inf_{\pi\in\Pi_{RM}} E\left[\exp\left(\theta\int_0^T e^{-\rho t}c(X(t),\alpha(t),\pi(\cdot))dt+\theta\int_T^\infty e^{-\rho t}c(X(t),\alpha(t),\pi(\cdot))dt\right)\right]\\ =\ & \inf_{\pi\in\Pi_{RM}} E\left\{\exp\left(\theta\int_0^T e^{-\rho t}c(X(t),\alpha(t),\pi(\cdot))dt\right)\right.\\ & \left.\times E_{(X(T),\alpha(T))}\left[\exp\left(\theta e^{-\rho T}\int_0^\infty e^{-\rho t}c(X(t),\alpha(t),\pi(\cdot))dt\right)\right]\right\}. \end{aligned}$$

Thus, formally we have

$$W(\theta,x,\alpha)=\inf_{\pi\in\Pi_{RM}} E\left\{\exp\left(\theta\int_0^T e^{-\rho t}c(X(t),\alpha(t),\pi(\cdot))dt\right)W(\theta e^{-\rho T},X(T),\alpha(T))\right\}, \tag{12}$$

then by using Itô's formula for $\exp\Big(\theta \int_0^T e^{-\rho t} c(X(t), \alpha(t), \pi(\cdot))dt\Big) W(\theta e^{-\rho T}, X(T), \alpha(T))$, and letting T approach 0, we obtain

$$-\theta\rho \frac{\partial W(\theta, x, \alpha)}{\partial \theta} + \inf_{u \in \mathbb{U}} \{\theta c(x, \alpha, u) W(\theta, x, \alpha) + \mathcal{L}^u W(\theta, x, \alpha)\} = 0. \tag{13}$$

Remark 3. *In fact,* (12) *is the direct consequence of the multiplicative dynamic programming principle, whose proof can be find in [12] and the reference therein.*

Later in this work, we will show that the value function W is the unique viscosity solution to the associated HJB equation and construct a decent approximation scheme to such equation. As a byproduct, we can also obtain the existence of the ϵ-optimal control of finite difference type.

3. The Main Results

3.1. The Optimality Equation And Viscosity Property

One of the main result of this work is to verify that W is the unique viscosity solution of the following optimality equation, also called the HJB equation:

$$-\theta\rho \frac{\partial \phi(\theta, x, \alpha)}{\partial \theta} + \inf_{u \in \mathbb{U}} \{\theta c(x, \alpha, u) \phi(\theta, x, \alpha) + \mathcal{L}^u \phi(\theta, x, \alpha)\} = 0. \tag{14}$$

Before giving the definition of viscosity solution, we introduce two notations, $C(\mathcal{Q}_0)$ the set of all continuous real-valued functions on $\mathcal{Q}_0$, and $C^{1,2,0}(\mathcal{Q}_0)$ the collection of all real-valued functions on $\mathcal{Q}_0$, which are continuously differentiable, twice continuously differentiable and continuous with respect to its corresponding components.

Definition 2.

(i) *If $w(\theta, x, \alpha) \in C(\mathcal{Q}_0) \bigcap B_{\tilde{\omega}}(\mathcal{Q}_0)$ such that*

$$-\theta\rho \frac{\partial \psi(\theta_0, x_0, \alpha_0)}{\partial \theta} + \inf_{u \in \mathbb{U}} \{\theta c(\theta_0, x_0, \alpha_0) \psi(\theta_0, x_0, \alpha_0) + \mathcal{L}^u \psi(\theta_0, x_0, \alpha_0)\} \geq 0,$$

at every $(\theta_0, x_0, \alpha_0) \in \mathcal{Q}_0$ which is a maximum of $w - \psi$, with $w(\theta_0, x_0, \alpha_0) = \psi(\theta_0, x_0, \alpha_0)$, whenever $\psi(\theta, x, \alpha) \in C^{1,2,0}(\mathcal{Q}_0)$ and $\lim_{t \to \infty} \psi(\theta e^{-\rho t}, x, \alpha) = 1$, then we say that w is a viscosity subsolution of (14) *on $\mathcal{Q}_0$.*

(ii) *If $w(\theta, x, \alpha) \in C(\mathcal{Q}_0) \bigcap B_{\tilde{\omega}}(\mathcal{Q}_0)$ such that*

$$-\theta\rho \frac{\partial \psi(\theta_0, x_0, \alpha_0)}{\partial \theta} + \inf_{u \in \mathbb{U}} \{\theta c(\theta_0, x_0, \alpha_0) \psi(\theta_0, x_0, \alpha_0) + \mathcal{L}^u \psi(\theta_0, x_0, \alpha_0)\} \leq 0,$$

at every $(\theta_0, x_0, \alpha_0) \in \mathcal{Q}_0$ which is a minimum of $w - \psi$, with $w(\theta_0, x_0, \alpha_0) = \psi(\theta_0, x_0, \alpha_0)$, whenever $\psi(\theta, x, \alpha) \in C^{1,2,0}(\mathcal{Q}_0)$ and $\lim_{t \to \infty} \psi(\theta e^{-\rho t}, x, \alpha) = 1$, then we say that w is a viscosity supsolution of (14) *on $\mathcal{Q}_0$.*

(iii) *We say that w is a viscosity solution of* (14) *on $\mathcal{Q}_0$ if it is both a viscosity subsolution and a viscosity supsolution of* (14).

In order to show that $W(\theta, x, \alpha)$ is the unique viscosity solution to the corresponding HJB equation, we define the following operator on $C(\mathcal{Q}_0) \bigcap B_{\tilde{\omega}}(\mathcal{Q}_0)$,

$$\mathcal{T}_t \phi(\theta, x, \alpha) = \min_{\pi \in \Pi_{RM}} E^{\pi}_{(x,\alpha)} \left\{ \exp\left(\theta \int_0^t e^{-\rho s} c(X(s), \alpha(s), \pi(s)) ds \right) \phi(\theta e^{-\rho t}, X(t), \alpha(t)) \right\},$$

where $E^{\pi}_{(x,\alpha)}[f(X(t), \alpha(t))] = E[f(X(t), \alpha(t))]$ for every bounded function f on $\mathcal{Q}_0$, with $E^{\pi}_{(x,\alpha)}$ be the expectation operator with respect to $P^{\pi}_{(x,\alpha)}$, the probability law deduced by

$(X(t), \alpha(t))$, the process corresponding to control π and initial state (x, α). E is the expectation operator with respect to the given probability measure P.

To proceed, we first need to verify that the operator has the following properties. Set

$$\mathcal{H}(\theta, x, \alpha, \psi, D_\theta\psi, D_x\psi, D_x^2\psi) = -\theta\rho\frac{\partial\psi(\theta, x, \alpha)}{\partial\theta} + \inf_{u\in\mathbb{U}}\{\theta c(x, \alpha, u)\psi(\theta, x, \alpha) + \mathcal{L}^u\psi(\theta, x, \alpha)\}.$$

Lemma 1. *If Assumptions 1 and 2 hold, then we have the following conclusions:*

(i) $\mathcal{T}_0\phi(\theta, x, \alpha) = \phi(\theta, x, \alpha)$, *for all* $\phi \in C(\mathcal{Q}_0)\bigcap B_{\tilde{\omega}}(\mathcal{Q}_0)$;

(ii) $\mathcal{T}_t\phi(\theta, x, \alpha) \le \mathcal{T}_t\psi(\theta, x, \alpha)$, *if* $\phi \le \psi$, *with* $\phi, \psi \in C(\mathcal{Q}_0)\bigcap B_{\tilde{\omega}}(\mathcal{Q}_0)$;

(iii) and for each $\psi(\theta, x, \alpha) \in C^{1,2,0}(\mathcal{Q}_0)\bigcap B_{\tilde{\omega}}(\mathcal{Q}_0)$, *we have*

$$\lim_{r\downarrow 0}\frac{1}{r}(\mathcal{T}_r\psi(\theta, x, \alpha) - \psi(\theta, x, \alpha)) = \mathcal{H}(\theta, x, \alpha, \psi, D_\theta\psi, D_x\psi, D_x^2\psi).$$

Proof 3. The conclusions (i) and (ii) are obvious by the definition. Now, the verification of conclusion (iii) remains. For fixed $u \in \mathbb{U}$, let $\pi(\cdot) = \delta_u(\cdot)$, thus by definition, it is easy to obtain that

$$\begin{aligned}
&\frac{1}{r}(\mathcal{T}_r\psi(\theta, x, \alpha) - \psi(\theta, x, \alpha))\\
\le\ &\frac{1}{r}\left\{E^u_{(x,\alpha)}\left[\exp\left(\theta\int_0^r e^{-\rho s}c(X(s), \alpha(s), u)ds\right)\psi(\theta e^{-\rho r}, X(r), \alpha(r))\right] - \psi(\theta, x, \alpha)\right\}.
\end{aligned}$$

Let $f(r, X(r), \alpha(r)) := \exp\big(\theta\int_0^r e^{-\rho s}c(X(s), \alpha(s), u)ds\big)\psi(\theta e^{-\rho r}, X(r), \alpha(r))$, by Itô's formula, we have

$$\begin{aligned}
&E[f(r, X(r), \alpha(r))] - f(0, x, \alpha)\\
=\ &E\left\{\int_0^r\left[\frac{\partial}{\partial s}f(s, X(s), \alpha(s)) + \mathcal{L}^u f(s, X(s), u)\right]ds\right\}\\
=\ &E\left\{\int_0^r \exp\left(\theta\int_0^s e^{-\rho t}c(X(t), \alpha(t), u)dt\right)\left[\theta(-\rho)e^{-\rho s}\frac{\partial}{\partial\theta}\psi(\theta e^{-\rho s}, X(s), \alpha(s))\right.\right.\\
&+\psi(\theta e^{-\rho s}, X(s), \alpha(s))\theta e^{-\rho s}c(X(s), \alpha(s), u)\\
&\left.\left.+\mathcal{L}^u\psi(\theta e^{-\rho s}, X(s), \alpha(s))\right]ds\right\}.
\end{aligned}$$

Thus, we have

$$\begin{aligned}
&\lim_{r\downarrow 0}\frac{1}{r}(\mathcal{T}_r\psi(\theta, x, \alpha) - \psi(\theta, x, \alpha))\\
\le\ &\theta(-\rho)\frac{\partial}{\partial\theta}\psi(\theta, x, \alpha) + \psi(\theta, x, \alpha)\theta c(x, \alpha, u) + \mathcal{L}^u\psi(\theta, x, \alpha).
\end{aligned}$$

Moreover, we have

$$\begin{aligned}
&\lim_{r\downarrow 0}\frac{1}{r}(\mathcal{T}_r\psi(\theta, x, \alpha) - \psi(\theta, x, \alpha))\\
\le\ &\theta(-\rho)\frac{\partial}{\partial\theta}\psi(\theta, x, \alpha) + \min_{u\in\mathbb{U}}\{\psi(\theta, x, \alpha)\theta c(x, \alpha, u) + \mathcal{L}^u\psi(\theta, x, \alpha)\}.
\end{aligned}$$

On the other hand, let $\{r_n\}$ be a sequence of positive numbers, such that $r_n < r_m$ for $n > m$ and $\lim_{n\to\infty} r_n = 0$. Obviously, for given r_n, we have a control $\pi_n(\cdot) := \pi_{r_n}(\cdot) \in \Pi_{RM}$ such that

$$\begin{aligned}
&\mathcal{T}_{r_n}\psi(\theta, x, \alpha) + (r_n)^2\\
\ge\ &E\left\{\exp\left(\theta\int_0^{r_n} e^{-\rho s}c(X_n(s), \alpha_n(s), \pi_n(s))ds\right)\psi(\theta e^{-\rho r_n}, X_n(r_n), \alpha_n(r_n))\right\},
\end{aligned}$$

with $(X_n(\cdot), \alpha_n(\cdot)), n \geq 1$ be the process corresponding to the control $\pi_n(\cdot)$ and initial state (x, α).

Let $\pi_n(0) \equiv \delta_u$ for all $n \geq 1$, with u arbitrarily taken from $\mathbb{U}$ and assume that $\{\pi_n(\cdot)\}$ convergents to $\pi := \pi_\infty \in \Pi_{RM}$, with $\pi_\infty(0) = \delta_u$. Then we can derive that

$$\begin{aligned} & \frac{1}{r_n}(\mathcal{T}_{r_n}\psi(\theta,x,\alpha) - \psi(\theta,x,\alpha)) \\ \geq\ & \frac{1}{r_n}\left\{E\left\{\exp\left(\theta\int_0^{r_n} e^{-\rho s}c(X_n(s),\alpha_n(s),\pi_n(s))ds\right)\psi(\theta e^{-\rho r_n}, X_n(r_n),\alpha_n(r_n))\right\}\right. \\ & \left. -\psi(\theta,x,\alpha)\right\} - r_n. \end{aligned}$$

By Itô's formula, we have

$$\begin{aligned} & E\left\{\exp\left(\theta\int_0^{r_n} e^{-\rho s}c(X_n(s),\alpha_n(s),\pi_n(s))ds\right)\psi(\theta e^{-\rho r_n}, X_n(r_n),\alpha_n(r_n))\right\} - \psi(\theta,x,\alpha) \\ =\ & E\left\{\int_0^{r_n}\exp\left(\theta\int_0^s e^{-\rho t}c(X_n(t),\alpha_n(t),\pi_n(t))dt\right)\left[\theta(-\rho)e^{-\rho s}\frac{\partial}{\partial\theta}\psi(\theta e^{-\rho s}, X_n(s),\alpha_n(s))\right.\right. \\ & +\psi(\theta e^{-\rho s}, X_n(s),\alpha_n(s))\theta e^{-\rho s}c(X_n(s),\alpha_n(s),\pi_n(s)) \\ & \left.\left.+\mathcal{L}^{\pi_n}\psi(\theta e^{-\rho s}, X_n(s),\alpha_n(s))\right]ds\right\}. \end{aligned}$$

Since $\psi \in C^{1,2,0}(\mathcal{Q}_0)\bigcap B_{\tilde{\omega}}(\mathcal{Q}_0)$, and the fact that $r_n > 0$ small enough, there exists a $\xi_n \in [0, r_n]$ such that

$$\begin{aligned} & \lim_{n\to\infty}\frac{1}{r_n}E\left\{\int_0^{r_n}\exp\left(\theta\int_0^s e^{-\rho t}c(X_n(t),\alpha_n(t),\pi_n(t))dt\right)\right. \\ & \left[\theta(-\rho)e^{-\rho s}\frac{\partial}{\partial\theta}\psi(\theta e^{-\rho s}, X_n(s),\alpha_n(s)) + \psi(\theta e^{-\rho s}, X_n(s),\alpha_n(s))\theta e^{-\rho s}c(X_n(s),\alpha_n(s),\pi_n(s))\right. \\ & \left.\left.+\mathcal{L}^{\pi_n}\psi(\theta e^{-\rho s}, X_n(s),\alpha_n(s))\right]ds\right\} \\ =\ & \lim_{n\to\infty}E\left\{\exp\left(\theta\int_0^{\xi_n} e^{-\rho t}c(X_n(\xi_n),\alpha_n(\xi_n),\pi_n(\xi_n))dt\right)\right. \\ & \left[\theta(-\rho)e^{-\rho\xi_n}\frac{\partial}{\partial\theta}\psi(\theta e^{-\rho\xi_n}, X_n(\xi_n),\alpha_n(\xi_n))\right. \\ & +\psi(\theta e^{-\rho\xi_n}, X_n(\xi_n),\alpha_n(\xi_n))\theta e^{-\rho\xi_n}c(X_n(\xi_n),\alpha_n(\xi_n),\pi_n(\xi_n)) \\ & \left.\left.+\mathcal{L}^{\pi_n}\psi(\theta e^{-\rho\xi_n}, X_n(\xi_n),\alpha_n(\xi_n))\right]\right\} \\ =\ & \theta(-\rho)\frac{\partial}{\partial\theta}\psi(\theta,x,\alpha) + \psi(\theta,x,\alpha)\theta c(x,\alpha,u) + \mathcal{L}^u\psi(\theta,x,\alpha). \end{aligned}$$

So we have

$$\begin{aligned} & \lim_{r_n\downarrow 0}\frac{1}{r_n}(\mathcal{T}_r\psi(\theta,x,\alpha) - \psi(\theta,x,\alpha)) \\ \geq\ & \theta(-\rho)\frac{\partial}{\partial\theta}\psi(\theta,x,\alpha) + \psi(\theta,x,\alpha)\theta c(x,\alpha,u) + \mathcal{L}^u\psi(\theta,x,\alpha) \\ \geq\ & \theta(-\rho)\frac{\partial}{\partial\theta}\psi(\theta,x,\alpha) + \min_{u\in\mathbb{U}}\{\psi(\theta,x,\alpha)\theta c(x,\alpha,u) + \mathcal{L}^u\psi(\theta,x,\alpha)\}. \end{aligned}$$

Thus, the result follows. □

Now we can give one of the main results of this work.

Theorem 2. *Under Assumptions 1 and 2, the value function $W(\theta, x, \alpha)$ is the unique positive viscosity solution of the HJB Equation* (14).

Proof 4. Firstly, we should show that the value function W is continuous in (θ, x, α). It should be pointed out that the continuity of W with respect to α is in the topological sense. Let

$$I^M(\theta, x, \alpha, \pi) = E\left[\exp\left(\theta \int_0^\infty e^{-\rho t}(c(X(t), \alpha(t), \pi(\cdot)) \wedge M)dt\right)\right],$$

for given $\pi(\cdot)$ with $c(x, \alpha, u) \wedge M := \min\{c(x, \alpha, u), M\}$. By the estimation in Proposition 1, there is no doubt that $\lim_{M\to\infty} I^M(\theta, x, \alpha, \pi) = I(\theta, x, \alpha, \pi)$. By the Feller property of the process $(X(t), \alpha(t))$, it is obvious that $I^M(\theta, x, \alpha, \pi)$ is continuous in (θ, x, α) for given π. Then, associated with the following inequality

$$\begin{aligned} &|I(\theta, x, \alpha, \pi) - I(\theta, y, \alpha, \pi)| \\ \leq\ &|I(\theta, x, \alpha, \pi) - I^M(\theta, x, \alpha, \pi)| + |I^M(\theta, x, \alpha, \pi) - I^M(\theta, y, \alpha, \pi)| + |I^M(\theta, y, \alpha, \pi) - I(\theta, y, \alpha, \pi)|, \end{aligned}$$

we conclude that $I(\theta, x, \alpha, \pi)$ is continuous in (θ, x, α), for given π. Then, it follows that $W(\theta, x, \alpha)$ is continuous in (θ, x, α).

Now, we can verify that W solves the HJB Equation (14) as a viscosity solution. Let $\psi \in C^{1,2,0}(\mathcal{Q}_0)$ and $\lim_{t\to\infty} \psi(\theta e^{-\rho t}, x, \alpha) = 1$. Denote by $(\theta_0, x_0, \alpha_0)$ the maximizer of $W - \psi$, with $W(\theta_0, x_0, \alpha_0) = \psi(\theta_0, x_0, \alpha_0)$. Then, $\psi(\theta, x, \alpha) \geq W(\theta, x, \alpha)$, and associated with Lemma 1 and (12), we can derive that

$$\mathcal{T}_r\psi(\theta, x, \alpha) \geq \mathcal{T}_r W(\theta, x, \alpha) = W(\theta, x, \alpha).$$

Furthermore, we can obtain that

$$\mathcal{H}(\theta_0, x_0, \alpha_0, \psi, D_\theta\psi, D_x\psi, D_x^2\psi) = \lim_{r\downarrow 0} \frac{1}{r}(\mathcal{T}_r\psi(\theta_0, x_0, \alpha_0) - \psi(\theta_0, x_0, \alpha_0)) \geq 0,$$

thus, W is the subsolution of the HJB Equation (14). Similarly, we can also verify that W is also a supsolution of the HJB equation. Then we conclude that W is a viscosity solution of the HJB equation.

As to the uniqueness, it is the direct consequence of the following comparison result. □

3.2. Comparison Result

In order to prove the uniqueness, we need some more preparations as follows. Let $\mathcal{Q}_R^\nu = [\nu, 1] \times B_R \times \mathcal{M}$, where B_R is the open ball in $\mathbb{R}^r$ with radius R and $\nu > 0$ is arbitrarily small. Suppose that $w(\theta, x, \alpha) \in C^{1,2,0}(\overline{\mathcal{Q}_0})$ is a classical solution of the HJB equation, i.e.,

$$-\theta\rho\frac{\partial w(\theta, x, \alpha)}{\partial\theta} + \inf_{u\in\mathbb{U}}\{\theta c(x, \alpha, u)w(\theta, x, \alpha) + \mathcal{L}^u w(\theta, x, \alpha)\} = 0, \tag{15}$$

Let $\xi^R(\theta, x) \in C^{1,2}([\nu, 1] \times \bar{B}_R)$ the space of all real-valued functions defined on $[\nu, 1] \times \bar{B}_R$, which are continuously differentiable with respect to θ and twice continuously differentiable with respect to x. Further, we assume that $\xi^R > 0$, for all $(\theta, x) \in [\nu, 1] \times \bar{B}_R$, with ν arbitrarily small. Moreover, $\lim_{R\to\infty} \xi^R(\theta, x) = 1$ for all $(\theta, x) \in [\nu, 1] \times B_R$ and $\lim_{R\to\infty} \xi^R(\theta, x) = 0$ for all $(\theta, x) \in [\nu, 1] \times \partial B_R$. Set

$$\hat{w}(\theta, x, \alpha) = \xi^R w(\theta, x, \alpha), \quad (\theta, x, \alpha) \in (0, 1] \times \bar{B}_R \times \mathcal{M}.$$

Let $(D_\theta\phi, D_x\phi) = (\phi_\theta, \phi_{x_1}, \cdots, \phi_{x_r})$ and $D_x^2\phi = (\phi_{x_ix_j}), \quad i, j = 1, 2, \cdots, r$, with $\phi = \xi^R, w$ or $\hat{w}$. Then, we can directly calculate that

$$\hat{w}_\theta = \xi_\theta^R w + \xi^R w_\theta, \quad \hat{w}_{x_i} = \xi^R w_{x_i} + \xi_{x_i}^R w,$$

and

$$\hat{w}_{x_ix_j} = \xi^R w_{x_ix_j} + \xi_{x_i}^R w_{x_j} + \xi_{x_j}^R w_{x_i} + \xi_{x_ix_j}^R w.$$

Multiplying the HJB Equation (15) by $\xi^R(\theta,x)$ we have

$$-\theta\rho\xi^R(\theta,x)\frac{\partial w(\theta,x,\alpha)}{\partial\theta}+\inf_{u\in\mathbb{U}}\{\xi^R(\theta,x)[\theta c(x,\alpha,u)w(\theta,x,\alpha)+\mathcal{L}^u w(\theta,x,\alpha)]\}=0. \quad (16)$$

Note that

$$\xi^R w_\theta=\hat{w}_\theta-w\xi^R_\theta,\quad \xi^R w_{x_i}=\hat{w}_{x_i}-w\xi^R_{x_i},$$

and

$$\begin{aligned}\xi^R w_{x_ix_j} &= \hat{w}_{x_ix_j}-w\xi^R_{x_ix_j}-\xi^R_{x_i}w_{x_j}-\xi^R_{x_j}w_{x_i}\\ &= \hat{w}_{x_ix_j}-w\xi^R_{x_ix_j}-\frac{\xi^R_{x_i}}{\xi^R}\hat{w}_{x_j}-\frac{\xi^R_{x_j}}{\xi^R}\hat{w}_{x_i}+2w\frac{\xi^R_{x_i}\xi^R_{x_j}}{\xi^R},\end{aligned}$$

we can derive that

$$-\theta\rho\frac{\partial\hat{w}(\theta,x,\alpha)}{\partial\theta}+\inf_{u\in\mathbb{U}}\{\theta\hat{c}(x,\alpha,u)\hat{w}(\theta,x,\alpha)+\hat{\mathcal{L}}^u\hat{w}(\theta,x,\alpha)\}=-\theta\rho\xi^R_\theta w, \quad (17)$$

with

$$\hat{c}:=c(x,\alpha,u)-\frac{1}{\xi^R}\left(\sum_{l=1}^r b_l(x,\alpha,u)\xi^R_{x_l}+\frac{1}{2}\sum_{l,k=1}^r a_{lk}(x,\alpha)\xi^R_{x_lx_k}\right),$$

and

$$\hat{\mathcal{L}}^u:=\sum_{l=1}^r\hat{b}_l(x,\alpha,u)\frac{\partial}{\partial x_l}+\frac{1}{2}\sum_{l,k=1}^r a_{l,k}(x,\alpha)\frac{\partial^2}{\partial x_l\partial x_k}+\sum_{j=1}^m q_{\alpha j}(x,u),$$

where

$$\hat{b}_l(x,\alpha,u):=b_l(x,\alpha,u)-\frac{1}{\xi^R}\sum_{k=1}^r a_{lk}(x,\alpha)\xi^R_{x_k}.$$

In order to show that the value function W is the unique viscosity solution of the HJB Equation (14) in $\mathcal{Q}_0$, we only need to show the following comparison result. To proceed, let $\phi(x,\alpha):=W(1,x,\alpha),(x,\alpha)\in\mathbb{R}^r\times\mathcal{M}$.

Theorem 3. *Assume that Assumptions 1 and 2 hold. Let $w,v\in C(\mathcal{Q}_0)\bigcap B_{\tilde{\omega}}(\mathcal{Q}_0)$ be the viscosity subsolution and viscosity supsolution of the HJB Equation* (14) *in $\mathcal{Q}_0$, respectively. And suppose that $w>0$ and $v>0$ for all $(\theta,x,\alpha)\in\mathcal{Q}_0$ with $w(1,x,\alpha)=v(1,x,\alpha)=\phi(x,\alpha)$. Then, we have*

$$\sup_{\mathcal{Q}_0}(w-v)=\sup_{\mathbb{R}^r\times\mathcal{M}}(w(1,x,\alpha)-v(1,x,\alpha)).$$

Proof 5. Set

$$\zeta^R(x)=\exp\left\{\frac{1}{R}\right\}-\exp\left\{|x|^2-R^2\right\},\quad x\in\bar{B}_R.$$

Then it is easy to note that $\zeta^R\in C^2(\bar{B}_R)$ and $\zeta^R>0$, for all $x\in\bar{B}_R$ with ν arbitrarily small. We can also verify that $\lim_{R\to\infty}\zeta^R(x)=1$, for all $x\in B_R$ and $\lim_{R\to\infty}\zeta^R(x)=0$, for all $x\in\partial B_R$. Denote

$$w^R(\theta,x,\alpha)=\zeta^R(x)\exp\left\{-\frac{K_2\theta}{R}\right\}w(\theta,x,\alpha),\quad K_2>0.$$

Suppose that $\psi^R(\theta,x,\alpha)\in C^{1,2,0}(\overline{\mathcal{Q}^\nu_R})\bigcap B_{\tilde{\omega}}(\overline{\mathcal{Q}^\nu_R})$ and $\lim_{t\to\infty}\lim_{R\to\infty}\psi^R(\theta e^{-\rho t},x,\alpha)=1$ for all $(\theta,x,\alpha)\in\mathcal{Q}_R$, and $w^R-\psi^R$ has a maximum at $(\theta_0,x_0,\alpha_0)\in\mathcal{Q}_R$ with $w^R(\theta_0,x_0,\alpha_0)=\psi^R(\theta_0,x_0,\alpha_0)$. Let $\psi(\theta,x,\alpha)=\psi^R(\theta,x,\alpha)\exp\left\{\frac{K_2\theta}{R}\right\}/\zeta^R$. Thus it is easy to verify that $\psi(\theta,x,\alpha)\in C^{1,2,0}(\overline{\mathcal{Q}^\nu_R})\bigcap B_{\tilde{\omega}}(\overline{\mathcal{Q}^\nu_R})$ and $\lim_{t\to\infty}\psi(\theta e^{-\rho t},x,\alpha)=1$ for all $(\theta,x,\alpha)\in\mathcal{Q}_R$, and

$w-\psi$ has a maximum at $(\theta_0, x_0, \alpha_0) \in \mathcal{Q}_R$ with $w(\theta_0, x_0, \alpha_0) = \psi(\theta_0, x_0, \alpha_0)$. Since $w(\theta, x, \alpha)$ is a viscosity subsolution of the HJB Equation (14), by definition we have

$$-\theta\rho\frac{\partial\psi(\theta_0, x_0, \alpha_0)}{\partial\theta} + \inf_{u\in\mathbb{U}}\{\theta c(\theta_0, x_0, \alpha_0)\psi(\theta_0, x_0, \alpha_0) + \mathcal{L}^u\psi(\theta_0, x_0, \alpha_0)\} \geq 0,$$

Note that $\psi^R(\theta, x, \alpha) = \zeta^R \exp\left\{-\frac{K_2\theta}{R}\right\}\psi(\theta, x, \alpha)$, and the calculations preceding the theorem, we can verify that

$$\begin{aligned}&-\theta\rho\frac{\partial\psi^R(\theta_0, x_0, \alpha_0)}{\partial\theta} + \inf_{u\in\mathbb{U}}\{\theta\hat{c}(\theta_0, x_0, \alpha_0)\psi^R(\theta_0, x_0, \alpha_0) + \hat{\mathcal{L}}^u\psi^R(\theta_0, x_0, \alpha_0)\}\\ &\geq \theta\rho\exp\left\{-\frac{K_2\theta}{R}\right\}w(\theta_0, x_0, \alpha_0)\frac{K_2}{R}\zeta^R \geq 0.\end{aligned}$$

Since the constant $K_2 > 0$, we conclude that w^R is the viscosity subsolution of the the following modified HJB equation

$$-\theta\rho\frac{\partial\psi(\theta, x, \alpha)}{\partial\theta} + \inf_{u\in\mathbb{U}}\{\theta\hat{c}(\theta, x, \alpha)\psi(\theta, x, \alpha) + \hat{\mathcal{L}}^u\psi(\theta, x, \alpha)\} = 0, \tag{18}$$

on $\mathcal{Q}_R$. Similarly, we can also verify that

$$v^R = \zeta^R\exp\left(\theta\frac{K_3}{R}\right)v(\theta, x, \alpha),$$

with given constant $K_3 > 0$, is the viscosity supsolution of the modified HJB Equation (18) on $\mathcal{Q}_R$. Then, by Lemma A1, we obtain that

$$\sup_{\overline{\mathcal{Q}_R^\nu}}(w^R - v^R) = \sup_{\partial^*Q_R^\nu}(w^R - v^R), \tag{19}$$

with $\partial^*\mathcal{Q}_R^\nu := ([\nu, 1]\times\partial B_R)\cup(\{1\}\times B_R)$. Note that w^R, v^R approach w, v uniformly on bounded subsets of $\overline{\mathcal{Q}_0}$ as $R\to\infty$, respectively. Moreover, since $\lim_{R\to\infty}\zeta^R(x) = 0$, for all $x\in\partial B_R$, we have

$$\lim_{R\to\infty}\sup_{[\nu,1]\times\partial B_R} w^R - v^R \leq \lim_{R\to\infty}\tilde{M}(\|w\|_{\tilde{\omega}} + \|v\|_{\tilde{\omega}})\zeta^R(x) = 0,$$

for a suitable constant $\tilde{M}$. Since $\nu > 0$ can be arbitrarily small, the result follows by letting R approaches to infinity in (19). □

4. The Approximation Scheme

In order to solve the HJB equation numerically, we are going to introduce the finite difference approximation scheme. For numerical purpose, we only need to work on the case with the cutoff as follows,

$$I^M(\theta, x, \alpha, \pi) = E\left[\exp\left(\theta\int_0^\infty e^{-\rho t}(c(X(t), \alpha(t), \pi(\cdot))\wedge M)dt\right)\right],$$

for given $\pi(\cdot)$, and we can also define

$$W^M(\theta, x, \alpha) = \inf_{\pi\in\Pi_{RM}} I^M(\theta, x, \alpha, \pi).$$

By the estimation in Proposition 1, we can conclude that $W^M \to W$, as $M \to \infty$. This means that it is enough to work with W^M when constructing the approximation scheme. To proceed, we set

$$\Delta_\theta^- W^M = \frac{W^M(\theta, x, \alpha) - W^M(\theta - h, x, \alpha)}{h},$$

$$\Delta_{x_i}^+ W^M = \frac{W^M(\theta, x + \delta e_i, \alpha) - W^M(\theta, x, \alpha)}{\delta},$$

$$\Delta_{x_i}^- W^M = \frac{W^M(\theta, x, \alpha) - W^M(\theta, x - \delta e_i, \alpha)}{\delta},$$

$$\Delta_{x_i}^2 W^M = \frac{W^M(\theta, x + \delta e_i, \alpha) + W^M(\theta, x - \delta e_i, \alpha) - 2W^M(\theta, x, \alpha)}{\delta^2},$$

$$\begin{aligned} &\Delta_{x_i x_j}^+ W^M \\ = \; & \frac{2W^M(\theta, x, \alpha) + W^M(\theta, x + \delta e_i + \delta e_j, \alpha) + W^M(\theta, x - \delta e_i - \delta e_j, \alpha)}{2\delta^2} \\ & - \frac{W^M(\theta, x + \delta e_i, \alpha) + W^M(\theta, x - \delta e_i, \alpha) + W^M(\theta, x + \delta e_j, \alpha) + W^M(\theta, x - \delta e_j, \alpha)}{2\delta^2}, \end{aligned}$$

$$\begin{aligned} &\Delta_{x_i x_j}^- W^M \\ = \; & -\frac{2W^M(\theta, x, \alpha) + W^M(\theta, x + \delta e_i + \delta e_j, \alpha) + W^M(\theta, x - \delta e_i - \delta e_j, \alpha)}{2\delta^2} \\ & + \frac{W^M(\theta, x + \delta e_i, \alpha) + W^M(\theta, x - \delta e_i, \alpha) + W^M(\theta, x + \delta e_j, \alpha) + W^M(\theta, x - \delta e_j, \alpha)}{2\delta^2}, \end{aligned}$$

Replacing the derivatives by their corresponding finite difference quotients, and rearranging the terms we have the following approximation scheme

$$\begin{aligned} &W_{h,\delta}^M(\theta, x, \alpha) \\ = \; & \inf_{u \in \mathbb{U}} \Bigg\{ C(h, \delta, x, \alpha, u)^{-1} \Bigg[\frac{\theta}{h} W_{h,\delta}^M(\theta - h, x, \alpha) + \sum_{l=1}^{r} \Bigg(C_l^+(h, \delta, x, \alpha, u) W_{h,\delta}^M(\theta, x + \delta e_l, \alpha) \\ & + C_l^-(h, \delta, x, \alpha, u) W_{h,\delta}^M(\theta, x - \delta e_l, \alpha) + \frac{1}{2} \sum_{k \neq l} \frac{|a_{lk}|}{2\delta^2} W_{h,\delta}^M(\theta, x + \delta e_l + \delta e_k, \alpha) \\ & + \frac{1}{2} \sum_{k \neq l} \frac{|a_{lk}|}{2\delta^2} W_{h,\delta}^M(\theta, x - \delta e_l - \delta e_k, \alpha) \Bigg) + \sum_{j \neq \alpha} q_{\alpha j}(x, u) W_{h,\delta}^M(\theta, x, j) \Bigg] \Bigg\}, \end{aligned}$$

with

$$\begin{aligned} C(h, \delta, x, \alpha, u) \; := \; & \frac{\theta \rho}{h} - \theta(c(x, \alpha, u) \wedge M) - q_{\alpha\alpha} \\ & + \sum_{l=1}^{r} \Bigg(\frac{|b_l(x, \alpha, u)|}{\delta} + \frac{|a_{ll}(x, \alpha)|}{\delta^2} - \frac{\sum_{k \neq l} |a_{lk}(x, \alpha)|}{2\delta^2} \Bigg), \end{aligned}$$

and

$$C_l^+(h, \delta, x, \alpha, u) := \frac{b_l^+(x, \alpha, u)}{\delta} + \frac{a_{ll}(x, \alpha)}{2\delta^2} - \frac{\sum_{k \neq l} |a_{lk}(x, \alpha)|}{2\delta^2},$$

$$C_l^-(h, \delta, x, \alpha, u) := \frac{b_l^-(x, \alpha, u)}{\delta} + \frac{a_{ll}(x, \alpha)}{2\delta^2} - \frac{\sum_{k \neq l} |a_{lk}(x, \alpha)|}{2\delta^2}.$$

To proceed, we should first show that the above approximation scheme makes sense. To show this, for given $h, \delta > 0$, we need to verify that $C(h, \delta, x, \alpha, u) \neq 0$ for all (x, α, u). We also need the following assumption.

Assumption 3. *Supposing that*

$$a_{ll}(x,\alpha) - \sum_{k\neq l} |a_{lk}(x,\alpha)| \geq 0.$$

Then under Assumptions 1 and 3, we can derive that $C(h,\delta,x,\alpha,u) \neq 0$. In fact, by Assumption 1 (i) and the fact that $q_{\alpha\alpha} < 0$, we have $\tilde{M} > -q_{\alpha\alpha}(x,u) > 0$ for suitable constant $\tilde{M}$ and all x and u. Additionally, by Assumption 3 we conclude that

$$\sum_{l=1}^{r}\left(\frac{|b_l(x,\alpha,u)|}{\delta} + \frac{|a_{ll}(x,\alpha)|}{\delta^2} - \frac{\sum_{k\neq l}|a_{lk}(x,\alpha)|}{2\delta^2}\right) > 0.$$

Moreover, if we choose that $h = \frac{\rho}{M+1}$, then it is easy to have $c(x,\alpha,u)\wedge M < \frac{\rho}{h} = M+1$, thus $\frac{\theta\rho}{h} - \theta(c(x,\alpha,u)\wedge M) > 0$, for all x,α,u. Based on the statement above we conclude that

$$C(h,\delta,x,\alpha,u) > 0.$$

Thus, the approximation scheme constructed above is well defined. Furthermore, we also know that the value of h can be chosen such that $h \to 0$, as $M \to \infty$. Moreover, we can also choose the value of δ such that $\delta \to 0$ as $M \to \infty$. Then $h,\delta \to 0$ is equivalent to $M \to \infty$.

Let

$$\begin{aligned}
&\mathcal{S}(h,\delta,\theta,x,\alpha,t,v)\\
=\ &\inf_{u\in\mathbb{U}}\Bigg\{-C(h,\delta,x,\alpha,u)t + \Bigg[\frac{\theta}{h}v(\theta-h,x,\alpha) + \sum_{l=1}^{r}\Bigg(C_l^+(h,\delta,x,\alpha,u)v(\theta,x+\delta e_l,\alpha)\\
&+C_l^-(h,\delta,x,\alpha,u)v(\theta,x-\delta e_l,\alpha) + \frac{1}{2}\sum_{k\neq l}\frac{|a_{lk}(x,\alpha)|}{2\delta^2}v(\theta,x+\delta e_l+\delta e_k,\alpha)\\
&+\frac{1}{2}\sum_{k\neq l}\frac{|a_{lk}(x,\alpha)|}{2\delta^2}v(\theta,x-\delta e_l-\delta e_k,\alpha)\Bigg) + \sum_{j\neq\alpha}q_{\alpha j}(x,u)v(\theta,x,j)\Bigg]\Bigg\}.
\end{aligned}$$

Then the approximation scheme can be rewritten as

$$\mathcal{S}(h,\delta,\theta,x,\alpha,W_{h,\delta}^M(\theta,x,\alpha),W_{h,\delta}^M) = 0.$$

Because of Assumption 3, it is easy to derive that the coefficients of v is positive. Thus, we can easily verify that $\mathcal{S}(h,\delta,\theta,x,\alpha,t,v)$ is monotone in v, i.e., for arbitrary $t\in\mathbb{R}$, $h,\delta\in(0,1)$, $(\theta,x,\alpha)\in\mathcal{Q}_0$,

$$\mathcal{S}(h,\delta,\theta,x,\alpha,t,v) \leq \mathcal{S}(h,\delta,\theta,x,\alpha,t,w),$$

with $v\leq w$ and $v,w\in C(\mathcal{Q}_0)\bigcap B_{\tilde{\omega}}(\mathcal{Q}_0)$. In addition, we can also verify that $\mathcal{S}(h,\delta,\theta,x,\alpha,t,v)$ is consistent which means that

$$\begin{aligned}
&\lim_{\epsilon\to 0,h\downarrow 0,\delta\downarrow 0,\zeta\to\theta,\xi\to x}\mathcal{S}(h,\delta,\theta,x,\alpha,v(\zeta,\xi,\alpha)+\epsilon,v+\epsilon)\\
=\ &\mathcal{H}(\theta,x,\alpha,v(\theta,x,\alpha),D_\theta v(\theta,x,\alpha),D_x v(\theta,x,\alpha),D_x^2 v(\theta,x,\alpha))
\end{aligned}$$

Now we are going to verify the stability. Let $\mathcal{O}_{h,\delta}:(C(\mathcal{Q}_0)\bigcap B_{\tilde{\omega}}(\mathcal{Q}_0))^m \to (C(\mathcal{Q}_0)\bigcap B_{\tilde{\omega}}(\mathcal{Q}_0))^m$, such that

$$\mathcal{O}_{h,\delta}(v(\theta,x,1),\cdots,v(\theta,x,m)) = (\mathcal{G}_{h,\delta}^1 v(\theta,x,1),\cdots,\mathcal{G}_{h,\delta}^m v(\theta,x,m)),$$

with

$$\begin{aligned}
&\mathcal{G}^{\alpha}_{h,\delta}v(\theta,x,\alpha)\\
=\ &\inf_{u\in\mathbb{U}}\Bigg\{C(h,\delta,x,\alpha,u)^{-1}\Bigg[\frac{\theta}{h}v(\theta-h,x,\alpha)+\sum_{l=1}^{r}\Bigg(C_l^{+}(h,\delta,x,\alpha,u)v(\theta,x+\delta e_l,\alpha)\\
&+C_l^{-}(h,\delta,x,\alpha,u)v(\theta,x-\delta e_l,\alpha)+\frac{1}{2}\sum_{k\neq l}\frac{|a_{lk}(x,\alpha)|}{2\delta^2}v(\theta,x+\delta e_l+\delta e_k,\alpha)\\
&+\frac{1}{2}\sum_{k\neq l}\frac{|a_{lk}(x,\alpha)|}{2\delta^2}v(\theta,x-\delta e_l-\delta e_k,\alpha)\Bigg)+\sum_{j\neq\alpha}q_{\alpha j}(x,u)v(\theta,x,j)\Bigg]\Bigg\}.
\end{aligned}$$

If we claim that $\mathcal{O}_{h,\delta}$ is a strict contraction mapping, the stability can be verified. Thus we need to show that there exists a constant $\kappa\in(0,1)$ such that

$$\|\mathcal{O}_{h,\delta}v-\mathcal{O}_{h,\delta}w\|\leq\kappa\|v-w\|,$$

for all $v,w\in C(\mathcal{Q}_0)\bigcap B_{\tilde{\omega}}(\mathcal{Q}_0)$. Note that

$$|\mathcal{O}_{h,\delta}v-\mathcal{O}_{h,\delta}w|^2\leq|\mathcal{G}^1_{h,\delta}v(\theta,x,1)-\mathcal{G}^1_{h,\delta}w(\theta,x,1)|^2+\cdots+|\mathcal{G}^m_{h,\delta}v(\theta,x,m)-\mathcal{G}^m_{h,\delta}w(\theta,x,m)|^2,$$

and

$$\begin{aligned}
&\mathcal{G}^{\alpha}_{h,\delta}v(\theta,x,\alpha)-\mathcal{G}^{\alpha}_{h,\delta}w(\theta,x,\alpha)\\
=\ &\inf_{u\in\mathbb{U}}\Bigg\{C(h,\delta,x,\alpha,u)^{-1}\Bigg[\frac{\theta}{h}v(\theta-h,x,\alpha)+\sum_{l=1}^{r}\Bigg(C_l^{+}(h,\delta,x,\alpha,u)v(\theta,x+\delta e_l,\alpha)\\
&+C_l^{-}(h,\delta,x,\alpha,u)v(\theta,x-\delta e_l,\alpha)+\frac{1}{2}\sum_{k\neq l}\frac{|a_{lk}(x,\alpha)|}{2\delta^2}v(\theta,x+\delta e_l+\delta e_k,\alpha)\\
&+\frac{1}{2}\sum_{k\neq l}\frac{|a_{lk}(x,\alpha)|}{2\delta^2}v(\theta,x-\delta e_l-\delta e_k,\alpha)\Bigg)+\sum_{j\neq\alpha}q_{\alpha j}(x,u)v(\theta,x,j)\Bigg]\Bigg\}\\
&-\inf_{u\in\mathbb{U}}\Bigg\{C(h,\delta,x,\alpha,u)^{-1}\Bigg[\frac{\theta}{h}w(\theta-h,x,\alpha)+\sum_{l=1}^{r}\Bigg(C_l^{+}(h,\delta,x,\alpha,u)w(\theta,x+\delta e_l,\alpha)\\
&+C_l^{-}(h,\delta,x,\alpha,u)w(\theta,x-\delta e_l,\alpha)+\frac{1}{2}\sum_{k\neq l}\frac{|a_{lk}(x,\alpha)|}{2\delta^2}w(\theta,x+\delta e_l+\delta e_k,\alpha)\\
&+\frac{1}{2}\sum_{k\neq l}\frac{|a_{lk}(x,\alpha)|}{2\delta^2}w(\theta,x-\delta e_l-\delta e_k,\alpha)\Bigg)+\sum_{j\neq\alpha}q_{\alpha j}(x,u)w(\theta,x,j)\Bigg]\Bigg\},
\end{aligned}$$

thus

$$|\mathcal{G}^{\alpha}_{h,\delta}v(\theta,x,\alpha)-\mathcal{G}^{\alpha}_{h,\delta}w(\theta,x,\alpha)|\leq\max_{u\in\mathbb{U}}\{F_{h,\delta}(x,\alpha,u)\}\|v-w\|_{\tilde{\omega}}\tilde{\omega}(x,\alpha),$$

with

$$F_{h,\delta}(x,\alpha,u)=\frac{\frac{\theta}{h}+\sum_{l=1}^{r}\Big(C_l^{+}(h,\delta,x,\alpha,u)+C_l^{-}(h,\delta,x,\alpha,u)+\sum_{k\neq l}^{r}\frac{|a_{lk}(x,\alpha)|}{2\delta^2}\Big)}{C(h,\delta,x,\alpha,u)}.$$

Since we can choose that $h=\frac{\rho}{M+1}$, thus it is easy to know that

$$\frac{\theta}{h}<\frac{\theta\rho}{h}-\theta(c(x,\alpha,u)\wedge M),$$

for all (x,α,u). Furthermore, we can derive that

$$\max_{u\in\mathbb{U}}\{F_{h,\delta}(x,\alpha,u)\}<1.$$

Thus, let $\kappa=\max_{u\in\mathbb{U}}\{F_{h,\delta}(u)\}$ we have

$$\|\mathcal{O}_{h,\delta}v-\mathcal{O}_{h,\delta}w\|_{\tilde{\omega}}\leq\kappa\|v-w\|_{\tilde{\omega}},$$

for all $v, w \in C(\mathcal{Q}_0) \cap B_{\tilde{\omega}}(\mathcal{Q}_0)$. This means that $\mathcal{O}_{h,\delta}$ is a strict contraction mapping. Then, there is a unique fixed point to $\mathcal{O}_{h,\delta}$, by the Banach fixed point theorem. We denote it by $v_{h,\delta}$. Moreover, we define

$$v^*(\theta, x, \alpha) = \lim_{(\zeta,\xi)\to(\theta,x)} \sup_{h,\delta\downarrow 0} v_{h,\delta}(\zeta, \xi, \alpha),$$

and

$$v_*(\theta, x, \alpha) = \lim_{(\zeta,\xi)\to(\theta,x)} \inf_{h,\delta\downarrow 0} v_{h,\delta}(\zeta, \xi, \alpha).$$

Note that $h, \delta \to 0$ is equivalent to $M \to \infty$. If we can verify that v^* and v_* are sub- and supersolutions of the HJB Equation (14), respectively, then the result that follows is associated with the comparison result. In fact, as in [27], we can show that

$$\mathcal{H}(\theta_0, x_0, \alpha_0, \varphi(\theta_0, x_0, \alpha_0), D_\theta\varphi(\theta_0, x_0, \alpha_0), D_x\varphi(\theta_0, x_0, \alpha_0), D_x^2\varphi(\theta_0, x_0, \alpha_0)) \geq 0,$$

for any test function $\varphi \in C^{1,2,0}(\mathcal{Q}_0) \cap B_{\tilde{\omega}}(\mathcal{Q}_0)$ such that $(\theta_0, x_0, \alpha_0)$ is a strictly local maximum of $v^* - \varphi$ with $v^*(\theta_0, x_0, \alpha_0) = \varphi(\theta_0, x_0, \alpha_0)$. Since the proofs are alike, we omit the details. Based on the statement above, we can obtain the following conclusion.

Theorem 4. *The solution $v_{h,\delta}$ of the approximation scheme $\mathcal{S}$ converges to the unique viscosity solution of the HJB Equation* (14)*.*

4.1. Existence of ϵ-Optimal Controls of Finite-Difference-Type

In this section, we will first introduce the definition of the so-said ϵ-optimal control and talk about its existence. Let

$$\begin{aligned}
&\overline{H}_{W_M^{h,\delta}}(\theta, x, \alpha, u) \\
:= \;& C(h, \delta, \theta, x, \alpha, u)^{-1}\Bigg[\frac{\theta}{h}W_M^{h,\delta}(\theta - h, x, \alpha) + \sum_{l=1}^{r}\Bigg(C_l^+(h, \delta, \theta, x, \alpha, u)W_M^{h,\delta}(\theta, x + \delta e_l, \alpha) \\
&+C_l^-(h, \delta, \theta, x, \alpha, u)W_M^{h,\delta}(\theta, x - \delta e_l, \alpha) + \frac{1}{2}\sum_{k\neq l}\frac{|a_{lk}(x, \alpha)|}{2\delta^2}W_M^{h,\delta}(\theta, x + \delta e_l + \delta e_k, \alpha) \\
&+\frac{1}{2}\sum_{k\neq l}\frac{|a_{lk}(x, \alpha)|}{2\delta^2}W_M^{h,\delta}(\theta, x - \delta e_l - \delta e_k, \alpha)\Bigg) + \sum_{j\neq\alpha} q_{\alpha j}(x, u)W_M^{h,\delta}(\theta, x, j)\Bigg],
\end{aligned}$$

with $W_M^{h,\delta}$ such that $\mathcal{S}(h, \delta, \theta, x, \alpha, W_M^{h,\delta}(\theta, x, \alpha), W_M^{h,\delta}) = 0$.

Definition 3. *We call $u_{h,\delta}^*(\theta, x, \alpha)$ the ϵ-optimal control, if there exists a pair of constants $(h_\epsilon, \delta_\epsilon)$ such that $h \leq h_\epsilon, \delta \leq \delta_\epsilon$ and*

$$\overline{H}_{W_M^{h,\delta}}(\theta, x, \alpha, u_{h,\delta}^*) = \inf_{u\in\mathbb{U}}\Big\{\overline{H}_{W_M^{h,\delta}}(\theta, x, \alpha, u)\Big\}.$$

Now, we first illustrate why such controls are called ϵ-optimal controls. Note that $h, \delta \to 0$ is equivalent to $M \to \infty$ and $u_{h,\delta}^*(\theta, x, \alpha)$ is corresponding to $W_M^{h,\delta}(\theta, x, \alpha)$. By Theorem 4, we know that for arbitrary $\epsilon > 0$, there exists a constant $M_0 > 0$ such that for all $M > M_0$,

$$|W_M^{h,\delta} - W| < \epsilon.$$

Thus, it is understandable to say that $u_{h,\delta}^*(\theta, x, \alpha)$ is the ϵ-optimal control.

Lemma 2. *Under Assumptions 1–3, there always exist ϵ-optimal controls.*

Proof 6. If Assumptions 1–3 are all satisfied. Then it is easy to find that $\overline{H}_{W_M^{h,\delta}}(\theta, x, \alpha, u)$ is continuous in u, for given $(h, \delta, \theta, x, \alpha)$. Note that we assume that $\mathbb{U}$ is compact. Thus it is obvious that there exist a control $u^*_{h,\delta}(\theta, x, \alpha)$, such that

$$\overline{H}_{W_M^{h,\delta}}(\theta, x, \alpha, u^*_{h,\delta}) = \inf_{u\in\mathbb{U}}\Big\{\overline{H}_{W_M^{h,\delta}}(\theta, x, \alpha, u)\Big\}.$$

Thus the result follows. □

4.2. Numerical Simulation

In order to demonstrate our theoretical results, we will give a numerical simulation example in this section. We consider the one-dimensional stochastic process with regime switching given in Example 1. Let $(X(t), \alpha(t)) \in \mathbb{R} \times \mathcal{M}$, with $\mathcal{M} = 1, 2$, and

$$dX(t) = (\mu(\alpha(t)) + u(t))X(t)dt + \sigma(\alpha(t))dB(t), \tag{20}$$

$$Q(x, u) = \begin{pmatrix} q_{11}(x, u) & -q_{11}(x, u) \\ -q_{22}(x, u) & q_{22}(x, u) \end{pmatrix}, \tag{21}$$

with $q_{ii} < 0$, $|q_{ii}| < \infty$, $i = 1, 2$ and $\mathbb{U} = [0, U_0]$, consider the functional

$$I(\theta, x, \alpha, \pi(\cdot))) = E[\exp(\theta \int_0^\infty e^{-\rho t} c(X(t), \alpha(t), \pi(\cdot))dt)], \tag{22}$$

with $c(x, \alpha, u) = x + \alpha + u$, and $\rho > \mu_M + U_0$, with $\sigma_M = max\{\sigma(1), \sigma(2)\}$, $\mu_M = max\{\mu(1), \mu(2)\}$.

Previously, we have verified that the model in Example 1 satisfies the assumptions proposed in this paper, so based on the approximation scheme in the previous section, for the one-dimensional example mentioned above, we can obtain the following iterative format of the value function with $\alpha, j = 1, 2$ and $\alpha \neq j$,

$$\begin{aligned} W^M_{h,\delta}(\theta, x, \alpha) = \inf_{u\in U}\{C(h, \delta, x, \alpha, u)^{-1}[\frac{\theta}{h} W^M_{h,\delta}(\theta - h, x, \alpha) + C^+_l(h, \delta, x, \alpha, u) W^M_{h,\delta}(\theta, x + \delta, \alpha) \\ + C^-_l(h, \delta, x, \alpha, u) W^M_{h,\delta}(\theta, x - \delta, \alpha) + q_{\alpha j} W^M_{h,\delta}(\theta, x, j)]\}, \end{aligned} \tag{23}$$

with

$$C(h, \delta, x, \alpha, u) = \frac{\theta\rho}{h} - \theta(c(x, \alpha, u) \wedge M) - q_{\alpha\alpha} + \frac{|b_l(x, \alpha, u)|}{\delta} + \frac{|a_{ll}(x, \alpha)|}{\delta^2}, \tag{24}$$

$$C^+_l(h, \delta, x, \alpha, u) = \frac{b^+_l(x, \alpha, u)}{\delta} + \frac{a_{ll}(x, \alpha)}{2\delta^2}, \tag{25}$$

$$C^-_l(h, \delta, x, \alpha, u) = \frac{b^-_l(x, \alpha, u)}{\delta} + \frac{a_{ll}(x, \alpha)}{2\delta^2}, \tag{26}$$

and

$$b_l(x, \alpha, u) = (\mu(\alpha(t) + u(t))X(t),\ a_{ll}(x, \alpha) = \sigma(\alpha(t)) \tag{27}$$

$$b^+_l(x, \alpha, u) = max\{b_l(x, \alpha, u), 0\},\ b^-_l(x, \alpha, u) = max\{-b_l(x, \alpha, u), 0\} \tag{28}$$

Furthermore, we choose the appropriate parameters for this example as follows, $\delta = 0.1$, h=0.1, $M = 5$, $\mu(1) = -0.2$, $\mu(2) = 0.2$, $\sigma(1) = -0.1$, $\sigma(2) = 0.1$, $\rho = 0.8$, $u \in \mathbb{U} = [0, U_0] = [0, 0.5]$, thus the following condition $\rho > \mu_M + U_0$ holds. The interval of θ is selected as $[0, 1]$, and we set $q_{11} = -u$, $q_{12} = u$, $q_{21} = 2u$, $q_{22} = -2u$.

According to the iterative format and parameter settings mentioned above, we conduct the numerical experiments by using the Matlab software (latest version R2023b) to obtain the following results:

In Figure 1, we can observe that the value function decreases with respect to X, and increases with respect to θ, and it can also be observed that the value function at state 2 is significantly larger than the value function at state 1.

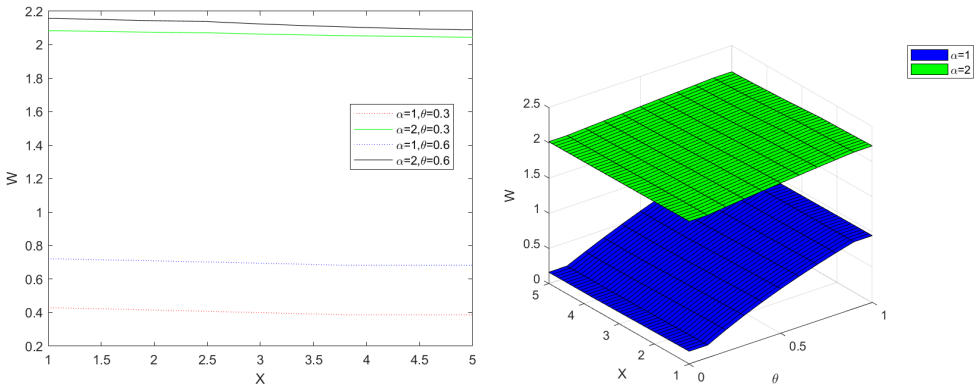

Figure 1. Optimal value function W.

Figure 2 shows that the ϵ-optimal control μ remains almost constant with the change of X, and the control in state 2 is larger than that in state 1.

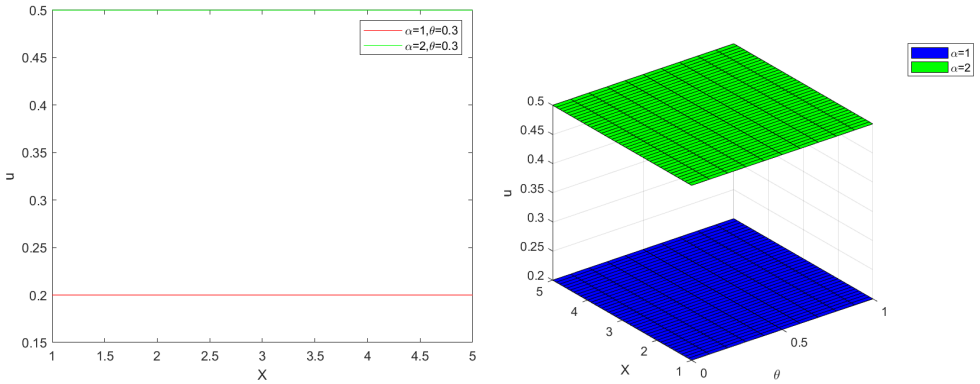

Figure 2. ϵ-optimal control μ.

5. Discussion

This work considers the controlled switching diffusions with infinite horizon discounted risk-sensitive criterion. The associated HJB equation has been derived. Since the explicit solution to such an equation is not easy to obtain, we figure out a numerical approximation scheme through the finite difference method. However, there is still an open problem. As to the existence of optimal control, in the risk-neutral case [20,27], the occupation measure method is usually used. By introducing the occupation measure method, one can pose the risk-neutral optimal control problem as a convex optimization problem. Moreover, as in [29] (Chapter 2, Section 5), except for the conditions similar to Assumption 1, by supposing that the pair of functions, consisting of the coefficients of the dynamic system and the running cost, maps the control space $\mathbb{U}$ into a convex set, one can show the existence of the optimal control for the controlled diffusion model. Such a technique can also be extended to deal with the risk-neutral optimal control problem within the controlled switching diffusion model. However, it seems that such methods can not be directly used to handle the risk-sensitive case. Thus, we need to find other ways to show the existence of optimal control to the risk-sensitive optimal control problem to the controlled switching model. **Open problem:** We guess that $u^*_{h,\delta}(\theta, x, \alpha)$ is the approximation of the optimal control when h, δ approach 0, under suitable conditions.

Author Contributions: Conceptualization, X.L.; methodology, X.L. and L.S.; validation, X.L. and L.S.; formal analysis, L.S.; investigation, X.L. and L.S.; writing—original draft preparation, X.L.; writing—review and editing, X.L. and L.S. All authors have read and agreed to the published version of the manuscript.

Funding: This research is partly supported by the National Natural Science Foundation of China (No. 12126313, 11801590 and 61673019), Basic Research Project of Guangzhou Science and Technology Plan (No. 2023A04J1320), Research Foundation for Young Teachers of Guangdong University of Technology, Humanities and Social Sciences Research and Planning Fund of the Ministry of Education of China (No. 20YJA630053).

Data Availability Statement: No new data were created or analyzed in this study. Data sharing is not applicable to this article.

Acknowledgments: Thanks to the editors and anonymous reviewers for their valuable comments and suggestions

Conflicts of Interest: The authors declare no conflicts of interest.

Appendix A

To complete the proof of the comparison result in Theorem 3, we also need the following result. Before going further we need to introduce the following notions. Such notions are original from [28]. We modified them for our own purpose. Let S^r be the set of all $r \times r$ symmetric matrices.

Definition A1. *Let $w \in C(\overline{\mathcal{Q}_R^\nu})$, with $\mathcal{Q}_R^\nu$ as given in Theorem 3.*

(i) The set of second-order superdifferentials of w at $(\theta, x) \in [\nu, 1] \times B_R$ for each α is

$$\begin{aligned} & D^{+(1,2)}w(\theta, x, \alpha) \\ = & \Big\{(q, p, A) \in \mathbb{R} \times \mathbb{R}^r \times S^r : \\ & \lim_{(h,y)\to 0} \sup_{(\theta+h, x+y)\in \mathcal{Q}_R^\nu} \frac{w(\theta+h, x+y) - w(t, x) - qh - py - \frac{1}{2}Ay \cdot y}{|h| + |y|^2} \le 0\Big\}. \end{aligned}$$

(ii) The set of second-order subdifferentials of w at $(\theta, x) \in [\nu, 1] \times B_R$ for each α is

$$\begin{aligned} & D^{-(1,2)}w(\theta, x, \alpha) \\ = & \Big\{(q, p, A) \in \mathbb{R} \times \mathbb{R}^r \times S^r : \\ & \lim_{(h,y)\to 0} \inf_{(\theta+h, x+y)\in \mathcal{Q}_R^\nu} \frac{w(\theta+h, x+y) - w(t, x) - qh - py - \frac{1}{2}Ay \cdot y}{|h| + |y|^2} \ge 0\Big\}. \end{aligned}$$

We also need the closure of the set of second-order subdifferentials and supdifferentials for the continuous functions. That is, for $w \in C(\overline{\mathcal{Q}_R^\nu})$ and $(\theta, x) \in [\nu, 1] \times B_R$, $(q, p, A) \in cD^{\pm}(1,2)w(\theta, x, \alpha)$ if and only if there exist sequences $(\theta_n, x_n) \in [\nu, 1] \times B_R$ and $(q_n, p_n, A_n) \in D^{\pm(1,2)}w(\theta_n, x_n, \alpha) \to (q, p, A)$, with α fixed.

If we assume that $w \in C^{1,2,0}(\overline{\mathcal{Q}_R^\nu})$, $(\theta, x) \in [\nu, 1] \times B_R$ and fixed α,

$$\begin{aligned} cD^{+(1,2)}w(\theta, x, \alpha) &= \left\{\left(\frac{\partial}{\partial\theta}w(\theta, x, \alpha), D_x w(\theta, x, \alpha), D_x^2 w(\theta, x, \alpha) + B\right) \middle| B \ge 0\right\}, \\ cD^{-(1,2)}w(\theta, x, \alpha) &= \left\{\left(\frac{\partial}{\partial\theta}w(\theta, x, \alpha), D_x w(\theta, x, \alpha), D_x^2 w(\theta, x, \alpha) - B\right) \middle| B \ge 0\right\} \end{aligned}$$

Now, also assume that $w \in C^{1,2,0}(\overline{\mathcal{Q}_R^\nu})$ is a classical solution of the HJB Equation (14) in $\mathcal{Q}_R$. Since for every semidefinite matrix $B \ge 0$

$$tr[\sigma\sigma^T(x, \alpha)B] \ge 0.$$

Then the above characterization of the second order sub- and supdifferentials yields

$$-\theta\rho q + H(\theta, x, \alpha, p, A, w(\theta, x, \alpha)) \geq 0, \quad \forall (q, p, A) \in cD^{+(1,2)}w(\theta, x, \alpha),$$
$$-\theta\rho q + H(\theta, x, \alpha, p, A, w(\theta, x, \alpha)) \leq 0, \quad \forall (q, p, A) \in cD^{-(1,2)}w(\theta, x, \alpha),$$

with

$$H(\theta, x, \alpha, p, A, \psi(\theta, x, \alpha)) = \inf_{u \in \mathbb{U}} \{\theta c(x, \alpha, u)\psi + bp + \frac{1}{2} tr(\sigma\sigma')A + \sum_{j=1}^{m} q_{\alpha j}(x, u)\psi(\theta, x, j)\}.$$

Now we can give the comparison result in the local case.

Lemma A1. *Let $w \in C(\overline{\mathcal{Q}_R^\nu})$ be a viscosity subsolution of the HJB Equation* (14) *in $\mathcal{Q}_R$, and $v \in C(\overline{\mathcal{Q}_R^\nu})$ be a viscosity supsolution of the HJB Equation* (14) *in $\mathcal{Q}_R$, with $\mathcal{Q}_R^\nu$ as given in Theorem 3. Then*

$$\sup_{\overline{\mathcal{Q}_R^\nu}}(w - v) = \sup_{\partial^* \mathcal{Q}_R^\nu}(w - v),$$

with $\partial^* \mathcal{Q}_R^\nu := ([\nu, 1] \times \partial B_R) \cup (\{1\} \times B_R)$.

Proof A1. Suppose the contrary of the conclusion holds, i.e.,

$$\sup_{\overline{\mathcal{Q}_R^\nu}}(w - v) - \sup_{\partial^* \overline{\mathcal{Q}_R^\nu}}(w - v) > 0.$$

And for $\beta_1, \beta_2 > 0$, consider the auxiliary function

$$\Phi(\theta, x, y, \alpha) = w(\theta, x, \alpha) - v(\theta, y, \alpha) - \beta_1|x - y|^2 - \beta_2(\theta - 1),$$

for $\theta \in [\nu, 1], x, y \in \bar{B}_R$. Note that w, v are continuous on $\overline{\mathcal{Q}_R^\nu}$, We can verify that for fixed α and any $(\theta, x) \in [\nu, 1] \times B_R$, if $(q, p, A) \in cD^{+(1,2)}w(\theta, x, \alpha)$ and $\|(\theta, x, p, A, w(\theta, x, \alpha))\| \leq M$, for every $M > 0$, there exists a constant $C = C(M)$ such that $q \leq C(M)$. Also, if $(q, p, A) \in cD^{-(1,2)}w(\theta, x, \alpha)$ and $\|(\theta, x, p, A, w(\theta, x, \alpha))\| \leq M$ for every $M > 0$, there exists a constant $C = C(M)$ such that $q \geq -C(M)$. Moreover, since we suppose that $\sup_{\overline{\mathcal{Q}_R^\nu}}(w - v) - \sup_{\partial^* \overline{\mathcal{Q}_R^\nu}}(w - v) > 0$, we can derive that for each given α,

$$\sup_{[\nu,1] \times \bar{B}_R \times \bar{B}_R} \Phi(\theta, x, y, \alpha) > \sup_{\partial([\nu,1] \times \bar{B}_R \times \bar{B}_R)} \Phi(\theta, x, y, \alpha),$$

when choosing suitable constants β_1 and β_2. For fixed α, let $(\bar{\theta}, \bar{x}, \bar{y})$ be a local maximum of Φ. Then, by the Crandall–Ishii maximum principle (see [28] (p. 216, Theorem 6.1) and [33] (Theorem 8.3)), we can derive that there exist symmetric matrices A and B such that

$$(q, p, A) \in cD^{+(1,2)}w(\bar{\theta}, \bar{x}, \alpha),$$

and

$$(\hat{q}, p, A) \in cD^{-(1,2)}v(\bar{\theta}, \bar{y}, \alpha),$$

where $p = 2\beta_1(\bar{x} - \bar{y})$ and $q - \hat{q} = \varphi_t(\bar{\theta}, \bar{x}, \bar{y}) = \beta_2$, with $\varphi(\theta, x, y) = \beta_1|x - y|^2 + \beta_2(\theta - 1)$, and

$$-6\beta_1 \begin{bmatrix} I & 0 \\ 0 & I \end{bmatrix} \leq \begin{bmatrix} A & 0 \\ 0 & -B \end{bmatrix} \leq 6\beta_1 \begin{bmatrix} I & 0 \\ 0 & I \end{bmatrix}. \tag{A1}$$

Furthermore, the viscosity properties of w and v imply that

$$-\bar{\theta}\rho q + H(\bar{\theta}, \bar{x}, \alpha, p, A) \geq 0,$$

and

$$-\bar{\theta}\rho\hat{q} + H(\bar{\theta}, \bar{y}, \alpha, p, B) \leq 0.$$

Recall that $q - \hat{q} = \beta_2$, and A, B satisfy (A1). Hence

$$\beta_2 = q - \hat{q} \leq \frac{1}{\bar{\theta}\rho}\big(H(\bar{\theta}, \bar{x}, \alpha, p, A) - H(\bar{\theta}, \bar{y}, \alpha, p, B)\big).$$

If we claim that $H(\bar{\theta}, \cdot, \alpha, p, \cdot)$ is continuous with respect to x, then we have

$$H(\bar{\theta}, \bar{x}, \alpha, p, A) - H(\bar{\theta}, \bar{y}, \alpha, p, B) \leq \epsilon,$$

for $|\bar{x} - \bar{y}| \leq \delta$. Since ϵ can be arbitrary small, it contradicts with the fact that $\beta_2 > 0$. Now it remains to verify that $H(\bar{\theta}, \cdot, \alpha, p, \cdot)$ is continuous with respect to x. Note that

$$\begin{aligned}
& H(\bar{\theta}, \bar{x}, \alpha, p, A) - H(\bar{\theta}, \bar{y}, \alpha, p, B) \\
\leq\ & \sup_{u\in\mathbb{U}}\{\theta c(\bar{x}, \alpha, u)\psi(\theta, \bar{x}, \alpha) - \theta c(\bar{y}, \alpha, u)\psi(\theta, \bar{y}, \alpha)\} \\
& + \sup_{u\in\mathbb{U}}\{(b(\bar{x}, \alpha, u) - b(\bar{y}, \alpha, u))2\beta_1(\bar{x} - \bar{y})\} \\
& + \frac{1}{2}\sup_{u\in\mathbb{U}}\{tr(\sigma(\bar{x}, \alpha)\sigma^T(\bar{x}, \alpha)A) - tr(\sigma(\bar{y}, \alpha)\sigma^T(\bar{y}, \alpha)B)\} \\
& + \sup_{u\in\mathbb{U}}\{\sum_{j=1}^{m}(q_{\alpha j}(\bar{x}, u)\psi(\theta, \bar{x}, j) - q_{\alpha j}(\bar{y}, u)\psi(\theta, \bar{y}, j))\}.
\end{aligned}$$

Note that $c, b, \psi, q_{\alpha j}$ are all continuous with respect to x. Therefore, we only need to verify that

$$tr(\sigma(\bar{x}, \alpha)\sigma^T(\bar{x}, \alpha)A) - tr(\sigma(\bar{y}, \alpha)\sigma^T(\bar{y}, \alpha)B)$$

is also continuous with respect to x. In fact, set $D(\bar{x}) := \sigma(\bar{x}, \alpha)$ and $D(\bar{y}) := \sigma(\bar{y}, \alpha)$, by (A1), we have

$$\begin{aligned}
& tr(\sigma(\bar{x}, \alpha)\sigma^T(\bar{x}, \alpha)A) - tr(\sigma(\bar{y}, \alpha)\sigma^T(\bar{y}, \alpha)B) \\
=\ & tr(D(\bar{x})D^T(\bar{x})A) - tr(D(\bar{y})D^T(\bar{y})B) \\
=\ & tr\left(\begin{bmatrix} D(\bar{x})D^T(\bar{x}) & D(\bar{x})D^T(\bar{y}) \\ D(\bar{y})D^T(\bar{x}) & D(\bar{y})D^T(\bar{y}) \end{bmatrix}\begin{bmatrix} A & 0 \\ 0 & -B \end{bmatrix}\right) \\
\leq\ & 6\beta_2 tr\left(\begin{bmatrix} D(\bar{x})D^T(\bar{x}) & D(\bar{x})D^T(\bar{y}) \\ D(\bar{y})D^T(\bar{x}) & D(\bar{y})D^T(\bar{y}) \end{bmatrix}\begin{bmatrix} I & -I \\ -I & I \end{bmatrix}\right) \\
=\ & 6\beta_2\|D(\bar{x}) - D(\bar{y})\|^2 \\
=\ & 6\beta_2\|\sigma(\bar{x}, \alpha) - \sigma(\bar{y}, \alpha)\|^2 \\
\leq\ & C|\bar{x} - \bar{y}|^2.
\end{aligned}$$

Thus, the result follows. □

References

1. Howard, R.A.; Matheson, J.E. Risk sensitive markov decision processes. *Manag. Sci.* **1972**, *18*, 356–369. [CrossRef]
2. Jacobson, D.H. Optimal stochastic linear systems with exponential performance criteria and their relation to deterministic differential games. *IEEE Trans. Automat. Control* **1973**, *18*, 124–131. [CrossRef]
3. Di Masi, G.B.; Stettner, Ł. Infinite horizon risk sensitive control of discrete time markov processes with small risk. *Syst. Control Lett.* **2000**, *40*, 15–20. [CrossRef]
4. Di Masi, G.B.; Stettner, Ł. Infinite horizon risk sensitive control of discrete time markov processes under minorization property. *SIAM J. Control Optim.* **2007**, *46*, 231–252. [CrossRef]
5. Ghosh, M.K.; Saha, S. Risk-sensitive control of continuous time markov chains. *Stochastics* **2014**, *86*, 655–675. [CrossRef]
6. Guo, X.; Liao, Z. Risk-sensitive discounted continuous-time markov decision processes with unbounded rates. *SIAM J. Control Optim.* **2019**, *57*, 3857–3883. [CrossRef]
7. Guo, X.; Zhang, J. Risk-sensitive continuous-time markov decision processes with unbounded rates and borel spaces. *Discrete Event Dyn. Syst.* **2019**, *29*, 445–471. [CrossRef]

8. Kumar, K.S.; Pal, C. Risk-sensitive control of pure jump process on countable space with near monotone cost. *Appl. Math. Optim.* **2013**, *68*, 311–331.
9. Huang, Y.; Lian, Z.; Guo, X. Risk-sensitive finite-horizon piecewise deterministic markov decision processes. *Oper. Res. Lett.* **2020**, *48*, 96–103. [CrossRef]
10. Arapostathis, A.; Biswas, A. Infinite horizon risk-sensitive control of diffusions without any blanket stability assumptions. *Stoch. Process. Appl.* **2018**, *128*, 1485–1524. [CrossRef]
11. Arapostathis, A.; Biswas, A. A variational formula for risk-sensitive control of diffusions in $\mathbb{R}^d$. *SIAM J. Control Optim.* **2020**, *58*, 85–103. [CrossRef]
12. Gauttam, S.K.; Kumar, K.S.; Pal, C. Risk-sensitive control of reflected diffusion processes on orthrant. *Pure Appl. Funct. Anal.* **2017**, *2*, 477–510.
13. Menaldi, J.; Robin, M. Remarks on risk-sensitive control problems. *Appl. Math. Optim.* **2005**, *52*, 297–310. [CrossRef]
14. Borkar, V.S. Q-learning for risk-sensitive control. *Math. Oper. Res.* **2002**, *27*, 294–311. [CrossRef]
15. Fleming, W.H.; Sheu, S.J. Risk-sensitive control and an optimal investment model II. *Ann. Appl. Probab.* **2002**, *12*, 730–767. [CrossRef]
16. Grandits, P.; Hubalek, F.; Schachermayer, W.; Žigo, M. Optimal expected exponential utility of dividend payments in a brownian risk model. *Scand. Actuatial J.* **2007**, *2*, 73–107. [CrossRef]
17. Speyer, J. An adaptive terminal guidance scheme based on an exponential cost criterion with application to homing missile guidance. *IEEE Trans. Autom. Control* **1976**, *21*, 371–375. [CrossRef]
18. Nguyen, D.H.; Yin, G.; Zhu, C. Certain properties related to well posedness of switching diffusions. *Stochastic Process. Appl.* **2017**, *127*, 3135–3158. [CrossRef]
19. Yin, G.; Zhu, C. Properties of solutions of stochastic differential equations with continuous-state-dependent switching. *J. Differ. Eqs.* **2010**, *249*, 2409–2439. [CrossRef]
20. Ghosh, M.K.; Arapostathis, A.; Marcus, S.I. Optimal control of switching diffusions with application to flexible manufacturing systems. *SIAM J. Control Optim.* **1993**, *31*, 1183–1204. [CrossRef]
21. Sethi, S.P.; Zhang, Q. *Hierarchical Decision Making in Stochastic Manufacturing Systems*; Birkhäuser Boston, Inc.: Boston, MA, USA, 1994.
22. Yin, G.; Dey, S. Weak convergence of hybrid filtering problems involving nearly completely decomposable hidden markov chains. *SIAM J. Control Optim.* **2003**, *41*, 1820–1842. [CrossRef]
23. Yin, G.; Liu, R.H.; Zhang, Q. Recursive algorithms for stock liquidation: A stochastic optimization approach. *SIAM J. Optim.* **2002** *13*, 240–263. [CrossRef]
24. Mao, X.; Yuan, C. *Stochastic Differential Equations with Markovian Switching*; Imperial Colledge Press: London, UK, 2006.
25. Yin, G.G.; Zhu, C. *Hybrid Switching Diffusions: Properties and Applications*; Springer: New York, NY, USA, 2010; Volume 63.
26. Zhu, C.; Yin, G. On competitive lotka-volterra model in random environments. *J. Math. Anal. Appl.* **2009** *357*, 154–170. [CrossRef]
27. Lu, X. Constrained optimality for controlled switching diffusions with an application to stock purchasing. *Quant. Financ.* **2019**, *19*, 2069–2085. [CrossRef]
28. Fleming, W.H.; Soner, H.M. *Controlled Markov Processes and Viscosity Solutions*, 2nd ed.; Springer: Berlin/Heidelberg, Germany, 2006.
29. Yong, J.; Zhou, X. *Stochastic Controls: Hamiltonian Systems and HJB Equations*; Springer: Berlin/Heidelberg, Germany, 1999.
30. Øksendal, B. *Stochastic Differential Equations*; Springer: New York, NY, USA, 1998.
31. Deng, Y.; Liang, Z. *Random Point Processes and Applications*; Science Press: Beijing, China, 1992. (In Chinese)
32. Ghosh, M.K.; Arapostathis, A.; Marcus, S.I. Ergodic control of switching diffusions. *SIAM J. Control Optim.* **1997**, *35*, 1952–1988. [CrossRef]
33. Crandall, M.G.; Ishii, H.; Lions, P.L. User's guide to viscosity solutions of second order partial differential equations. *Bull. New Ser. Am. Math. Soc.* **1992**, *27*, 1–67. [CrossRef]

mathematics

MDPI

Article

Optimal Control of SLBRS with Recovery Rates

Xiangqing Zhao [1,*] and Wanmei Hou [2]

[1] Department of Mathematics, Suqian University, Suqian 223800, China
[2] School of Marxism, Suqian University, Suqian 223800, China; 29008@squ.edu.cn
* Correspondence: 23139@squ.edu.cn

Abstract: In the information age, frequent information exchange has provided a breeding ground for the spread of computer viruses. The significant losses caused by computer virus attacks have long rung the alarm for information security. From academia to businesses, and even to government, everyone remains highly vigilant about information security. Researchers have put forward various approaches to combat computer viruses, involving innovative efforts in both the hardware and software aspects, as well as theoretical innovation and practical exploration. This article is dedicated to theoretical exploration, specifically investigating the stability of a computer virus model, known as SLBRS, from the perspective of optimal control. Firstly, a control system is introduced with the aim of minimizing the costs related to network detoxification and diminishing the percentage of computers impacted by the virus. Secondly, we employ the Pontryagin maximum principle to analyze the optimality of a control strategy for the proposed system. Thirdly, we validate the effectiveness of our theoretical analysis through numerical simulation. In conclusion, both theoretical analysis and numerical simulation reveal that the utilization of optimal control analysis to stabilize the SLBRS has been demonstrated to be advantageous in restoring contaminated computer network environments.

Keywords: computer virus; SLBRS; optimal control; Pontryagin principle; simulation

MSC: 49J15; 93-10; 93C15

1. Introduction

In the information age, frequent information exchange has become an integral part of our daily lives, greatly facilitating the transmission of computer viruses in the cyber environment. The proliferation of network computer viruses has posed significant global information security threats, leading to substantial losses in various sectors, including finance, education, and energy.

From 1987 to 1988, F. Cohen and W. Murray discovered certain similarities between computer viruses and biological infectious diseases [1,2]. Consequently, they suggested applying the principles of infectious disease dynamics and qualitative and quantitative analysis methods to study the patterns of computer virus transmission. Unfortunately, they did not propose specific models for the spread of computer viruses at that time. It was not until 1991 that J. O. Kephart and S. R. White adopted the recommendations of F. Cohen and W. Murray [3]. Based on the similarity between computer viruses and biological viruses, they introduced the SIS (susceptible–infected–susceptible) computer virus propagation model for the first time, pioneering the application of biological virus propagation models to the field of computer viruses. Since then, extensive research has been conducted on computer viruses; a rough summary is provided in the Table 1 below.

Table 1. Early computer virus transmission models.

Model	Year	Authors	Character	Reference
SIS	1991	Kephart, White	Susceptible, infected computers involved	[3]
SIR	2001	Tian, Zheng	Computers with permanent immunity	[4]
SIRS	2004	Chen, Carley	Computers with temporary immunity	[5]
SEIR	2006	Yuan, Chen	Computers in a dormant state	[6]
SEIRS	2007	Mishra, Saini	Computers with temporary immunity or in dormant state	[7]
SAIC	2008	Piqueira, Vasconcelos	The infected computers exhibit logarithmic growth	[8]
SAIR	2009	Piqueira, Araujo	Coexistence of multiple viruses	[9]
SEIQRS	2010	Mishra, Jha	Infected computers are isolated	[10]

The computer virus models described above are based on a common assumption borrowed from epidemiological virus modeling, where an infected computer that remains in latency will not infect other computers. However, in the context of computer viruses, it is a whole different story:

Difference 1: Upon infection, a computer typically gains the immediate capability to propagate the infection.

Difference 2: Computers that have recovered may develop temporary immunity.

Considering the differences between computer viruses and biological viruses (**Differences 1–2**), Yang and Wen [11] and Yang, Zhang, and Li [12] proposed a mathematical model with characteristics of computer viruses known as SLBRS. They categorize the computers in the system into four groups, namely, S(t), L(t), B(t), and R(t):

S(t)—susceptible computers: computers not yet infected by the virus but susceptible to being infected by latent or outbreak computers, subsequently transitioning into latent computers.

L(t)—latent computers: computers that have been infected by the virus but do not exhibit apparent destructive behavior yet retain the potential to spread the infection.

B(t)—outbreak computers: computers that are infected by the virus, exhibiting apparent destructive effects and having the potential to spread the infection.

R(t)—recovery computers: computers that have been cleared of the virus by third-party security software or firewall products, possessing temporary immunity.

For the convenience of mathematical calculations, we assume that S(t), L(t), B(t), and R(t) represent the proportions of susceptible, latent, outbreak, and recovered computers in the network, respectively. Therefore, S(t), L(t), B(t), and R(t) satisfy the following normalization condition:

$$S(t) + L(t) + B(t) + R(t) = 1.$$

The transition relationships among the different states S(t), L(t), B(t), and R(t) are determined by the following assumptions:

Assumption 1: susceptible computers S(t) are infected with a virus at a certain rate $\beta S(L + B)$ and transform into latent computers L(t).

Assumption 2: latent computers L(t) transition into outbreak computers B(t) at an outbreak rate α.

Assumption 3: outbreak computers B(t) are cured at an antivirus software recovery rate γ_1 and transform into recovery computers R(t).

Assumption 4: recovery computers R(t) lose immunity at a certain rate σ and transform back into susceptible computers S(t).

Assumption 5: newly added computers are all susceptible computers S(t) with an access rate p, and each state of computer has an exit rate μ.

Based on the above assumptions (**Assumptions 1–5**), the state transition relationships among computers in different states of SLBRS are illustrated in Figure 1:

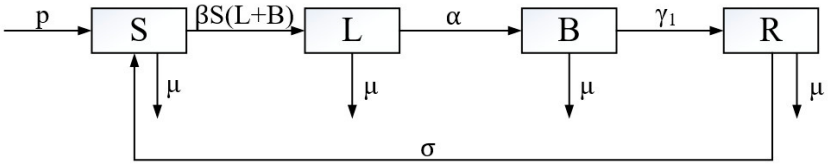

Figure 1. State transition diagram of SLBRS.

In reality, latent computers L(t) may recover due to users' virus prevention and control habits. Yang considered this factor in [13] and made the following additional assumption:

Assumption 6: latent computers L(t) are cured and transformed into recovery computers R(t) at a certain rate γ_2 due to third-party protective software or firewalls. Generally speaking, the possibility of clearing the virus by reinstalling the system is lower than using antivirus software, thus

$$\gamma_2 < \gamma_1.$$

Based on these assumptions (**Assumptions 1–6**), the state transition relationships among computers in different states of SLBRS can be illustrated in Figure 2:

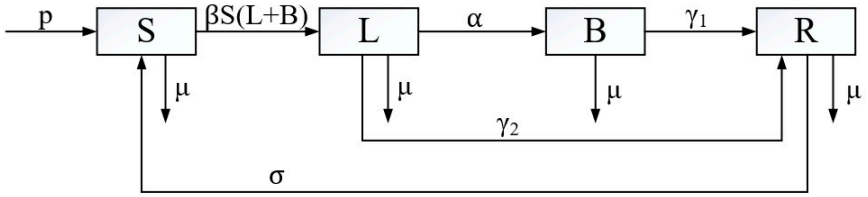

Figure 2. State transition diagram of SLBRS with graded recovery rates.

In consideration of various virus prevention and control measures that can be taken for outbreak computers B(t) in reality, the following assumption is further proposed:

Assumption 7: apart from using antivirus software, the virus can also be cleared by reinstalling the system, thereby transitioning the infected computer B(t) into a susceptible computer S(t) at a recovery rate of γ_3. Obviously, due to the numerical advantage of outbreak computers over latent computers, the probability of latent computers transitioning to the recovered state must be lower than the probability of outbreak computers transitioning to the recovered state. Therefore, the following assumption is also reasonable:

$$\gamma_3 < \gamma_2 < \gamma_1.$$

Under these assumptions (**Assumptions 1–7**), the state transition relationships of SLBRS are illustrated as follows:

Figure 3 can be formulated as:

$$\begin{cases} \frac{dS(t)}{dt} = p - \beta S(B+L) + \gamma_3 B + \sigma R - \mu S, \\ \frac{dL(t)}{dt} = \beta S(B+L) - \alpha L - \gamma_2 L - \mu L, \\ \frac{dB(t)}{dt} = \alpha L - \gamma_3 B - \mu B - \gamma_1 B, \\ \frac{dR(t)}{dt} = \gamma_2 L - \sigma R - \mu R + \gamma_1 B, \end{cases} \tag{1}$$

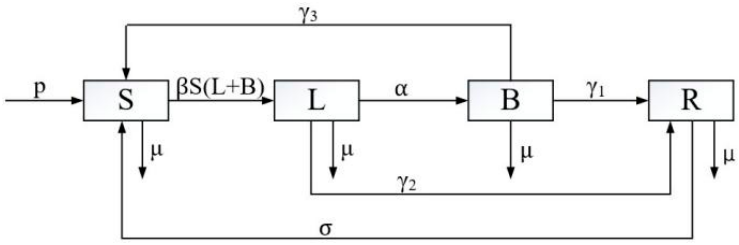

Figure 3. State transition diagram of SLBRS with constant recovery rates.

The fact is that the severity of computer virus attacks varies over time, and protective measures should be flexible and adaptable in response. Therefore, it is more reasonable to consider that recovery rates vary with time [14]. In this paper, as an example, the authors take the recovery rate γ_1 as a continuous function of time $\mu_1(t)$, representing the frequency of running antivirus software on outbreak computers at time t. Consequently, we propose SLBRS with variable recovery rates as follows:

Figure 4 can be reformulated by:

$$\begin{cases} \frac{dS(t)}{dt} = p - \beta S(B+L) + \gamma_3 B + \sigma R - \mu S, \\ \frac{dL(t)}{dt} = \beta S(B+L) - \alpha L - \gamma_2 L - \mu L, \\ \frac{dB(t)}{dt} = \alpha L - \gamma_3 B - \mu B - u_1(t)B, \\ \frac{dR(t)}{dt} = \gamma_2 L - \sigma R - \mu R + u_1(t)B. \end{cases} \tag{2}$$

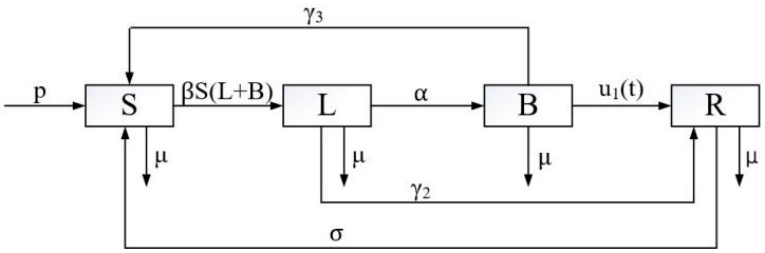

Figure 4. State transition diagram of SLBRS with time-variable recovery rate.

Following the introduction of the SLBRS model and its variations (1) and (2) in [4–13], the focus of analysis concerning them has primarily revolved around stability. This paper will delve further into studying the system's behavior from an optimal control perspective, aiming to explore the mechanisms of computer virus transmission and prevention. The organization of the remaining sections is as follows:

In Section 2, we will utilize the Hurwitz criterion to explore the stability conditions of both non-toxic and toxic equilibria of the SLBRS (1) and prove the stability of these two types of equilibrium.

In Section 3, we will focus on establishing the fundamental theoretical results concerning the optimal control of SLBRS. This will encompass the following key aspects: the existence of an optimal control strategy, the necessary conditions for optimal control, and the uniqueness of the optimal control system.

In Section 4, we will perform simulations to offer a numerical illustration of the practical implications of the theoretical discussions.

In Section 5, we will discuss the advantages of optimal control analysis in this paper and the necessity of multi-control input analysis.

In Section 6, we will conclude the paper by summarizing the progress made in the study of SLBRS.

2. The Stability of SLBRS

Before investigating the optimal control of SLBRS, let us first conduct a brief analysis of its stability. For the sake of convenience, under the normalization condition

$$S(t) + L(t) + B(t) + R(t) = 1,$$

the system of Equation (1) is transformed into:

$$\begin{cases} \frac{dL(t)}{dt} = \beta(1 - L - B - R)(L + B) - \alpha L - \gamma_2 L - \mu L, \\ \frac{dB(t)}{dt} = \alpha L - \gamma_1 B - \gamma_3 B - \mu B, \\ \frac{dR(t)}{dt} = \gamma_1 B + \gamma_2 L - \sigma R - \mu R, \end{cases} \tag{3}$$

2.1. Stability of the Non-Toxic Equilibrium

According to the definition of a non-toxic equilibrium, there are no infected computers in the system. By (3), we deduced that L = 0, B = 0, and R = 0. Furthermore, utilizing the normalization condition, we obtain the non-toxic equilibrium $E_0 = (1,\ 0,\ 0,\ 0)$. We define the basic reproduction number as follows:

$$R_0 = \frac{[(\alpha + \gamma_2 + \mu - \beta)(\gamma_1 + \gamma_3 + \mu) - \beta\alpha](\sigma + \mu)}{\{(\alpha + \gamma_1 + \gamma_2 + \gamma_3 + \sigma + 3\mu - \beta) * [(\alpha + \gamma_1 + \gamma_2 + \gamma_3 + 2\mu - \beta)(\sigma + \mu) + (\alpha + \gamma_2 + \mu - \beta)(\gamma_1 + \gamma_3 + \mu) - \beta\alpha]\}}$$

Theorem 1. *For system (1), when $R_0 < 1$, the non-toxic equilibrium E_0 is locally asymptotically stable; when $R_0 > 1$, the non-toxic equilibrium E_0 is unstable.*

Proof of Theorem 1. The Hurwitz criterion is as follows: If the coefficients of characteristic equation

$$D(s) = a_0 s^3 + a_1 s^2 + a_2 s + a_1 = 0,\ a_0 > 0.$$

of the Jacobian matrix of the linearized system are positive, and $a_1 a_2 - a_0 a_3 > 0$ then the linearized system is asymptotic stable. First, we linearize (3) at E_0. The Jacobian matrix of functions of the right-hand side of (3) is:

$$\begin{aligned} J_{(E_0)} &= \begin{bmatrix} \beta - 2\beta L - 2\beta B - \beta R - \alpha - \gamma_2 - \mu & \beta - 2\beta L - 2\beta B - \beta R & -\beta L - \beta B \\ \alpha & -\gamma_1 - \gamma_3 - \mu & 0 \\ \gamma_2 & \gamma_1 & -\sigma - \mu \end{bmatrix}_{(E_0)} \\ &= \begin{bmatrix} \beta - \alpha - \gamma_2 - \mu & \beta & 0 \\ \alpha & -\gamma_1 - \gamma_3 - \mu & 0 \\ \gamma_2 & \gamma_1 & -\sigma - \mu \end{bmatrix}, \end{aligned}$$

Then, the linearized equations of (3) at E0 are as follows:

$$\begin{cases} \frac{dL(t)}{dt} = (\beta - \alpha - \gamma_2 - \mu)L + \beta B, \\ \frac{dB(t)}{dt} = \alpha L - (\gamma_1 + \gamma_3 + \mu)B, \\ \frac{dR(t)}{dt} = \gamma_2 L + \gamma_1 B - (\sigma + \mu)R, \end{cases}$$

The characteristic equation of the Jacobian matrix $J_{(E_0)}$ is:

$$\begin{vmatrix} \lambda - \beta + \alpha + \gamma_2 + \mu & -\beta & 0 \\ -\alpha & \lambda + \gamma_1 + \gamma_3 + \mu & 0 \\ -\gamma_2 & -\gamma_1 & \lambda + \sigma + \mu \end{vmatrix} = 0,$$

Expressed as a polynomial, it is:

$$p_1(\lambda) = a_0\lambda^3 + a_1\lambda^2 + a_2\lambda + a_3 = 0,$$

where

$$a_0 = 1,$$

$$a_1 = \alpha + \gamma_1 + \gamma_2 + \gamma_3 + \sigma + 3\mu - \beta,$$

$$a_2 = (\alpha + \gamma_1 + \gamma_2 + \gamma_3 + 2\mu - \beta)(\sigma + \mu) + (\alpha + \gamma_2 + \mu - \beta)(\gamma_1 + \gamma_3 + \mu) - \beta\alpha,$$

$$a_3 = [(\alpha + \gamma_2 + \mu - \beta)(\gamma_1 + \gamma_3 + \mu) - \beta\alpha](\sigma + \mu).$$

when $R_0 < 1$, we have $a_1 > 0$, $a_2 > 0$, $a_3 > 0$ and $a_1a_2 - a_0a_3 > 0$. By the Hurwitz criterion, E_0 is locally asymptotically stable.

The proof is finished. □

2.2. Stability of the Toxic Equilibrium

According to the definition of a toxic equilibrium, there exist infected computers in the system. By (3), we deduced the toxic equilibrium

$$E_1 = (L_*, B_*, R_*),$$

where

$$L_* = \frac{(\gamma_1 + \gamma_3 + \mu)(\sigma + \mu)(\mu S_* - p)}{\sigma\gamma_2(\gamma_1 + \gamma_3 + \mu) + \alpha[(\sigma + \mu)\gamma_3 + \sigma\gamma_1] - \beta S_*(\gamma_1 + \gamma_3 + \alpha + \mu)(\sigma + \mu)},$$

$$B_* = \frac{\alpha L_*}{(\gamma_1 + \gamma_3 + \mu)},$$

$$R_* = \frac{[\alpha\gamma_1 + (\gamma_1 + \gamma_3 + \mu)\gamma_2]L_*}{(\gamma_1 + \gamma_3 + \mu)(\sigma + \mu)}.$$

Furthermore, by (1), we obtain

$$S_* = \frac{(\gamma_1 + \gamma_3 + \mu)(\alpha + \gamma_2 + \mu)}{\beta(\gamma_1 + \gamma_3 + \mu + \alpha)}.$$

We define the basic reproduction number as follows:

$$R_1 = \frac{\beta\alpha(L_* + B_*)\left[\frac{L_*}{B_*}(\sigma + \mu) + \gamma_1 + \frac{\gamma_2 L_*}{B_*} + (\sigma + \mu)\right]}{\left\{\left[\beta(L_* + B_* + \frac{S_* B_*}{L_*}) + (\gamma_1 + \gamma_3 + \sigma + 2\mu)\right] * \left[(\beta(L_* + B_* + \frac{S_* B_*}{L_*}) + \frac{\alpha L_*}{B_*})(\sigma + \mu) + \beta(L_* + B_*)(\frac{\alpha L_*}{B_*} + \gamma_2 + \alpha)\right]\right\}}$$

Theorem 2. *For system (1), when $R_1 < 1$, the toxic equilibrium E_1 is locally asymptotically stable; when $R_1 > 1$, the toxic equilibrium is unstable.*

Proof of Theorem 2. First, we linearize (3) at E_1. Then, the Jacobian matrix linearized system is

$$J_{(E_0)} = \begin{bmatrix} \beta - 2\beta L - 2\beta B - \beta R - \alpha - \gamma_2 - \mu & \beta - 2\beta L - 2\beta B - \beta R & -\beta L - \beta B \\ \alpha & -\gamma_1 - \gamma_3 - \mu & 0 \\ \gamma_2 & \gamma_1 & -\sigma - \mu \end{bmatrix}_{(E_1)}$$

$$= \begin{bmatrix} -\beta(L_* + B_* - S_*) - \alpha - \gamma_2 - \mu & -\beta(L_* + B_* - S_*) & -\beta(L_* + B_*) \\ \alpha & -\gamma_1 - \gamma_3 - \mu & 0 \\ \gamma_2 & \gamma_1 & -\sigma - \mu \end{bmatrix},$$

We simplify the characteristic equation $|\lambda E - J| = 0$ to obtain

$$p_2(\lambda) = a_0\lambda^3 + a_1\lambda^2 + a_2\lambda + a_3 = 0,$$

where

$$a_0 = 1,$$

$$a_1 = \beta(L_* + B_* + \frac{S_*B_*}{L_*}) + (\gamma_1 + \gamma_3 + \sigma + 2\mu),$$

$$a_2 = \left[\beta\left(L_* + B_* + \frac{S_*B_*}{L_*}\right) + \frac{\alpha L_*}{B_*}\right](\sigma + \mu) + \beta(L_* + B_*)\left(\frac{\alpha L_*}{B_*} + \gamma_2 + \alpha\right),$$

$$a_3 = \beta\alpha(L_* + B_*)\left[\frac{L_*}{B_*}(\sigma + \mu) + \gamma_1 + \frac{\gamma_2 L_*}{B_*} + (\sigma + \mu)\right].$$

When $R_1 < 1$,

$$\begin{aligned} R_1 &= \frac{\beta\alpha(L_* + B_*)\left[\frac{L_*}{B_*}(\sigma+\mu) + \gamma_1 + \frac{\gamma_2 L_*}{B_*} + (\sigma+\mu)\right]}{\left\{\left[\beta(L_* + B_* + \frac{S_*B_*}{L_*}) + (\gamma_1+\gamma_3+\sigma+2\mu)\right] * \left[(\beta(L_* + B_* + \frac{S_*B_*}{L_*}) + \frac{\alpha L_*}{B_*})(\sigma+\mu) + \beta(L_* + B_*)(\frac{\alpha L_*}{B_*} + \gamma_2 + \alpha)\right]\right\}} \\ &= \frac{a_3}{a_1 \cdot a_2} < 1, \end{aligned}$$

We have $a_1 > 0$, $a_2 > 0$, $a_3 > 0$ and $a_1a_2 - a_0a_3 > 0$. By the Hurwitz criterion, E_1 is locally asymptotically stable.

The proof is finished. □

3. Optimal Control of SLBRS

In the past, significant emphasis has been placed on mathematically modeling computer viruses and analyzing the stability of these models [3–13]. Comparatively, fewer studies have delved into the control strategies of computer virus models, as is evident in [14–17]. Nevertheless, these limited investigations have offered valuable insights to our understanding of restoration strategies of virus containment networks.

The focal point of this paper is to investigate the optimal control problem of SLBRS, aiming at diminishing the percentage of infected computers within a network and reducing network maintenance expenses.

3.1. The Formulation of the Optimal Control Problem

Now, let us establish an optimal control model based on SLBRS. Firstly, in Section 1, we transformed the constant recovery rate γ_1 into a time-varying function $u_1(t)$. The state transition relationships of S(t), L(t), B(t), and R(t) are illustrated in Figure 4, and the relevant mathematical model can be found in (2). Secondly, we will select an appropriate control set. Thirdly, we will choose a suitable objective function based on the intention of control.

Let us assume T is a predefined time. We stipulate the allowable control set as follows:

$$U = \left\{u_1(t) \in L^2(0,\ T) :\ 0 \le u_1(t) \le 1,\ 0 \le t \le T\right\}. \tag{4}$$

Our goal is to reduce the prevalence of virus-infected computers within the network while minimizing the system's maintenance expenses. Therefore, the objective function could be formulated as follows:

$$J(u_1) = \int_0^T \left[B(t) + \frac{\varepsilon u_1^2(t)}{2}\right] dt, \tag{5}$$

where ε is a positive constant.

Thus, the optimal control problem can be formulated as:

$$\min_{u_1 \in U} J(u_1)$$

Subject to the differential equations in (2).

In order to facilitate subsequent analysis of the problem and corresponding to the objective function, we introduce the following Lagrangian function:

$$L(B,\ u_1) = B(t) + \frac{\varepsilon u_1^2(t)}{2}$$

and the following Hamiltonian function:

$$\begin{aligned} H(t) = \quad & L(B,\ u_1) + \lambda_1[p - \beta S(L+B) + \gamma_3 B + \sigma R - \mu S] \\ & + \lambda_2[\beta S(L+B) - \alpha L - \gamma_2 L - \mu L] + \lambda_3[\alpha L - \gamma_3 B \\ & - \mu B - u_1(t)B] + \lambda_4[\gamma_2 L - \sigma R - \mu R + u_1(t)B]. \end{aligned} \tag{6}$$

3.2. Optimal Control Results and Their Proofs

In this section, we will establish the existence of an optimal control strategy, the necessary conditions for the existence of optimal control, and the uniqueness of the optimal control system. This will serve as the foundation for numerical simulations.

Theorem 3. *An optimal control input, denoted as* $u_1^*(t)$*, exists for the control system (5) with the given initial data:*

$$S(0) = S^0 \geq 0,\ L(0) = L^0 \geq 0,\ B(0) = B^0 \geq 0,\ R(0) = R^0 \geq 0,$$

such that

$$\min_{u_1 \in U} J(u_1) = J(u_1^*)$$

Proof of Theorem 3. According to [18], it is sufficient to verify the following four conditions:

Condition 1. $U = \left\{ u_1(t) \in L^2(0,\ T) :\ 0 \leq u_1(t) \leq 1,\ 0 \leq t \leq T \right\} \neq \Phi$;

Condition 2. $U = \left\{ u_1(t) \in L^2(0,\ T) :\ 0 \leq u_1(t) \leq 1,\ 0 \leq t \leq T \right\}$ is closed and convex set;

Condition 3. The right-hand side of state equations

$$\begin{cases} \frac{dS(t)}{dt} = p - \beta S(B+L) + \gamma_3 B + \sigma R - \mu S, \\ \frac{dL(t)}{dt} = \beta S(B+L) - \alpha L - \gamma_2 L - \mu L, \\ \frac{dB(t)}{dt} = \alpha L - \gamma_3 B - \mu B - u_1(t)B, \\ \frac{dR(t)}{dt} = \gamma_2 L - \sigma R - \mu R + u_1(t)B. \end{cases}$$

are restricted by linear functions in terms of $S,\ L,\ B,\ R$. We need only to show the condition for the first equation (the second is similar). Indeed, by the normalization condition

$$S(t) + L(t) + B(t) + R(t) = 1$$

we have $0 \leq B \leq 1$. Thus,

$$\begin{aligned} & p - \beta S(B+L) + \gamma_3 B + \sigma R - \mu S \\ & \leq p - \beta(L+B) + \gamma_3 B + \sigma R - \mu S \\ & = p - \beta L + (\gamma_3 - \beta)B + \sigma R - \mu S. \end{aligned}$$

Condition 4. The Lagrangian function $L(B,\ u_1)$ exhibits concavity over the set U, and there exists $\rho > 1$, $\eta_1 > 0$, and η_2 such that

$$L(B,\ u_1) \geq \eta_1(|u|)\rho + \eta_2.$$

The proof is completed. □

Next, through the utilization of the Pontryagin maximum principle, we will derive the essential condition for the optimal control input:

Theorem 4. *For the given optimal control input* $u_1^*(t)$ *and the related states* $S^*,\ L^*,\ B^*,\ R^*$ *of state Equation (2), there exist co-states* λ_1, λ_2, λ_3, *and* λ_4 *such that*

$$\frac{d\lambda_1}{dt} = \lambda_1[\beta(L+B)+\mu] - \lambda_2\beta(L+B), \tag{7}$$

$$\frac{d\lambda_2}{dt} = \lambda_1\beta S - \lambda_2(\beta S - \alpha - \gamma_2 - \mu) - \lambda_3\alpha - \lambda_4\gamma_2, \tag{8}$$

$$\frac{d\lambda_3}{dt} = -1 + \lambda_1(\beta S - \gamma_3) - \lambda_2\beta S + \lambda_3[\gamma_3 + \mu + u_1(t)] - \lambda_4 u_1(t), \tag{9}$$

$$\frac{d\lambda_4}{dt} = -\lambda_1\sigma + \lambda_4(\sigma + \mu), \tag{10}$$

with the transversal conditions

$$\lambda_1(T) = \lambda_2(T) = \lambda_3(T) = \lambda_4(T) = 0. \tag{11}$$

The optimal control is as follows:

$$u_1^*(t) = \max\left\{\min\left\{\frac{\lambda_3 - \lambda_4}{\varepsilon}B^*,\ 1\right\},\ 0\right\}.$$

Proof of Theorem 4. We differentiate the Hamiltonian function (6), and we obtain the following co-state system:

$$\frac{d\lambda_1}{dt} = -H_{S^*}(t), \frac{d\lambda_2}{dt} = -H_{L^*}(t), \frac{d\lambda_3}{dt} = -H_{B^*}(t), \frac{d\lambda_4}{dt} = -H_{R^*}(t),$$

which implies (7)–(10).

We deduce from the optimal conditions

$$\left.\frac{\partial H}{\partial u_1}\right|_{u_1(t)=u_1^*(t)} = \varepsilon u_1(t) - \lambda_3 B + \lambda_4 B.$$

and the admissible condition

$$U = \left\{u_1(t) \in L^2(0,\ T) :\ 0 \leq u_1(t) \leq 1,\ 0 \leq t \leq T\right\}$$

that

$$u_1^*(t) = \max\left\{\min\left\{\frac{\lambda_3 - \lambda_4}{\varepsilon}B^*,\ 1\right\},\ 0\right\}.$$

By assembling the state equations of (2), co-state Equations (7)–(10), and the transversal conditions of (11), we derive the optimal system as follows:

$$\begin{cases} \frac{dS(t)}{dt} = p - \beta S(B+L) + \gamma_3 B + \sigma R - \mu S, \\ \frac{dL(t)}{dt} = \beta S(B+L) - \alpha L - \gamma_2 L - \mu L, \\ \frac{dB(t)}{dt} = \alpha L - \gamma_3 B - \mu B - u_1(t)B, \\ \frac{dR(t)}{dt} = \gamma_2 L - \sigma R - \mu R + u_1(t)B, \end{cases} \tag{12}$$

and

$$\begin{cases} \frac{d\lambda_1}{dt} = \lambda_1[\beta(L+B)+\mu] - \lambda_2\beta(L+B), \\ \frac{d\lambda_2}{dt} = \lambda_1\beta S - \lambda_2(\beta S - \alpha - \gamma_2 - \mu) - \lambda_3\alpha - \lambda_4\gamma_2, \\ \frac{d\lambda_3}{dt} = -1 + \lambda_1(\beta S - \gamma_3) - \lambda_2\beta S + \lambda_3[\gamma_3 + \mu + u_1(t)] - \lambda_4 u_1(t), \\ \frac{d\lambda_4}{dt} = -\lambda_1\sigma + \lambda_4(\sigma + \mu), \end{cases} \tag{13}$$

with initial values

$$S^0 \geq 0,\ L^0 \geq 0,\ B^0 \geq 0,\ R^0 \geq 0 \tag{14}$$

and the transversal conditions

$$\lambda_1(T) = \lambda_2(T) = \lambda_3(T) = \lambda_4(T) = 0. \tag{15}$$

The proof is completed. □

Finally, we show the uniqueness of the optimal system (12)–(15):

Theorem 5. *Given control time T, the solution of the optimal system (12)–(15) is unique.*

Proof of Theorem 5. Assume that both $(S,\ L,\ B,\ R;\ \lambda_1,\ \lambda_2,\ \lambda_3,\ \lambda_4)$ and $(\overline{S},\ \overline{L},\ \overline{B},\ \overline{R};\ \overline{\lambda}_1,\ \overline{\lambda}_2,\ \overline{\lambda}_3,\ \overline{\lambda}_4)$ are solutions of (12)–(15). Let

$$S = e^{\lambda t}a,\ L = e^{\lambda t}b,\ B = e^{\lambda t}c,\ R = e^{\lambda t}d;$$

$$\lambda_1 = e^{-\lambda t}w,\ \lambda_2 = e^{-\lambda t}x,\ \lambda_3 = e^{-\lambda t}y,\ \lambda_4 = e^{-\lambda t}z$$

and

$$\overline{S} = e^{\lambda t}\overline{a},\ \overline{L} = e^{\lambda t}\overline{b},\ \overline{B} = e^{\lambda t}\overline{c},\ \overline{R} = e^{\lambda t}\overline{d};$$

$$\overline{\lambda}_1 = e^{-\lambda t}\overline{w},\ \overline{\lambda}_2 = e^{-\lambda t}\overline{x},\ \overline{\lambda}_3 = e^{-\lambda t}\overline{y},\ \overline{\lambda}_4 = e^{-\lambda t}\overline{z},$$

where λ is a constant that will be determined later.

From (11), we obtain

$$u_1(t) = \max\left\{\min\left\{\frac{(y-z)c}{\varepsilon},\ 1\right\},\ 0\right\},$$

$$\overline{u}_1(t) = \max\left\{\min\left\{\frac{(\overline{y}-\overline{z})\overline{d}}{\varepsilon},\ 1\right\},\ 0\right\}.$$

From (12), we obtain

$$\lambda e^{\lambda t}a + e^{\lambda t}a' = p - \beta e^{2\lambda t}a(b+c) + \gamma_3 e^{\lambda t}c + \sigma e^{\lambda t}d - \mu e^{\lambda t}a \tag{16}$$

and

$$\lambda e^{\lambda t}\overline{a} + e^{\lambda t}\overline{a'} = p - \beta e^{2\lambda t}\overline{a}(\overline{b}+\overline{c}) + \gamma_3 e^{\lambda t}\overline{c} + \sigma e^{\lambda t}\overline{d} - \mu e^{\lambda t}\overline{a}. \tag{17}$$

From (13), we obtain

$$w' - \lambda w = (w + x)\beta e^{\lambda t}(b + c) + w\mu,$$

and

$$\overline{w'} - \lambda \overline{w} = (\overline{w} + \overline{x})\beta e^{\lambda t}(\overline{b} + c) + \overline{w}\mu,$$

From (16) and (17), we obtain

$$\begin{aligned}\lambda(a - \overline{a}) + (a' - \overline{a'}) = \quad & -\beta e^{\lambda t}[a(b + c) - \overline{a}(\overline{b} + \overline{c})] \\ & +\gamma_3(\gamma - \overline{\gamma}) + \sigma(d - \overline{d}) - \mu(a - \overline{a}),\end{aligned}$$

We then integrate from 0 to T, and we obtain

$$\begin{aligned}&\tfrac{1}{2}(a(T) - \overline{a}(T))2 + \lambda \int_0^T (a - \overline{a})^2 dt \\ &= -\beta \int_0^T e^{\lambda t}[a(b + c) - \overline{a}(\overline{b} + \overline{c})](a - \overline{a})dt + \gamma_3 \int_0^T (\gamma - \overline{\gamma})(a - \overline{a})dt + \sigma \int_0^T (d - \overline{d})(a - \overline{a})dt - \mu \int_0^T (a - \overline{a})^2 dt \\ &= -\beta \int_0^T e^{\lambda t}(\overline{a}\overline{b} - ab + \overline{a}c - ac)(\overline{a} - a)dt + \gamma_3 \int_0^T (\overline{\gamma} - \gamma)(\overline{a} - a)dt \\ &\quad + \sigma \int_0^T (\overline{d} - d)(\overline{a} - a)dt - \mu \int_0^T (\overline{a} - a)^2 dt \\ &\leq C_1 e^{\lambda t} \int_0^T \left[(\overline{a} - a)^2 + (\overline{b} - b)^2 + (d - c)^2\right] dt + C_2 \int_0^T (\overline{a} - a)^2 + (\overline{b} - b)^2 + (\overline{c} - c)^2 + (\overline{d} - d)^2 \\ &\quad + (w - \overline{w})^2 + (x - \overline{x})^2 + (y - \overline{y})^2 + (z - \overline{z})^2 dt\end{aligned}$$

where C_1 and C_2 are constants.

Similarly, we estimate the following:

$$\frac{1}{2}(b - \overline{b})^2(T),\ \frac{1}{2}(c - \overline{c})^2(T),\ \frac{1}{2}(d - \overline{d})^2(T).$$

Finally, we obtain

$$\begin{aligned}&\tfrac{1}{2}(\overline{a} - a)^2(T) + \tfrac{1}{2}(\overline{b} - b)^2(T) + \tfrac{1}{2}(\overline{c} - c)^2(T) + \tfrac{1}{2}(\overline{d} - d)^2(T) + \tfrac{1}{2}(\overline{w} - w)^2(0) + \tfrac{1}{2}(\overline{x} - x)^2(0) + \tfrac{1}{2}(\overline{y} - y)^2(0) \\ &+ \tfrac{1}{2}(z - \overline{z})^2(0) + \lambda \int_0^T \left[(\overline{a} - a)^2 + (\overline{b} - b)^2 + (\overline{c} - c)^2 + (\overline{d} - d)^2\right] dt + \lambda \int_0^T \left[(\overline{x} - x)^2 + (\overline{y} - y)^2 + (\overline{z} - z)^2 + (\overline{w} - w)^2\right] dt \\ &\leq (C_3 + C_4^{3\lambda t}) \int_0^T \left[(\overline{a} - a)^2 + (\overline{b} - b)^2 + (\overline{c} - c)^2 + (\overline{d} - d)^2\right] dt + (C_3 + C_4^{3\lambda t}) \int_0^T \left[(\overline{w} - w)^2 + (\overline{x} - x)^2 + (\overline{y} - y)^2 + (\overline{z} - z)^2\right] dt.\end{aligned}$$

Taking λ such that

$$\lambda > (C_3 + C_4 e^{3\lambda T})$$

and

$$T < \frac{1}{3\lambda} \ln\left(\frac{\lambda - C_3}{C_4}\right)$$

then

$$\begin{aligned}&(\lambda - (C_3 + C_4 e^{3\lambda T})) \int_0^T \left[(\overline{a} - a)^2 + (\overline{b} - b)^2 + (c - \overline{d})^2 + (\overline{d} - d)^2\right] dt \\ &+ (\lambda - (C_3 + C_4 e^{3\lambda T})) \int_0^T \left[(\overline{x} - x)^2 + (\overline{y} - y)^2 + (\overline{z} - z)^2 + (\overline{w} - w)^2\right] dt \\ &\leq 0,\end{aligned}$$

which implies that

$$a = \overline{a}, b = \overline{b}, c = \overline{c}, d = \overline{d};$$

and

$$x = \overline{x}, y = \overline{y}, z = \overline{z}, w = \overline{w}.$$

Thus,

$$S = \overline{S}, L = \overline{L}, B = \overline{B}, R = \overline{R};$$

$$\lambda_1 = \overline{\lambda}_1,\ \lambda_2 = \overline{\lambda}_2,\ \lambda_3 = \overline{\lambda}_3,\ \lambda_4 = \overline{\lambda}_4.$$

The proof is completed. □

Remark 1. *The benefit of employing Pontryagin's maximum principle to prove Theorem 2 is that, alongside completing the proof, it sets the stage for our subsequent numerical simulations. In fact, the state equation, co-state equation, transversality condition, and initial values generated during the proof process serve as the very foundation for our upcoming numerical simulations.*

4. Numerical Simulation

In this section, we will conduct numerical simulations to examine the stability of (1) and the controllability of (2) separately. To facilitate a comparative analysis, we will use common initial values and parameter values for models (1) and (2) in the following section.

We take the initial value as follows:

$$S^0 = 0.4,\ L^0 = 0.3,\ B^0 = 0.2,\ R^0 = 0.1.$$

The parameter selection principle abides by the conditions specified in Theorems 1 and 2, ensuring that the basic reproduction number is less than 1. For detailed parameter selection, refer to Table 2.

Table 2. Values of parameters.

Parameters	Values	Parameters	Values
p	0.10	ε	2.00
α	0.60	β	0.90
γ_2	0.10	γ_1	0.15
σ	0.05	γ_3	0.05
μ	0.10		

4.1. Stability of SLBRS

Stability simulation is a relatively straightforward process. By utilizing the provided parameters and initial values, we write a simple code employing ODE45 and execute it. The outcomes of the simulation are illustrated in Figures 5 and 6.

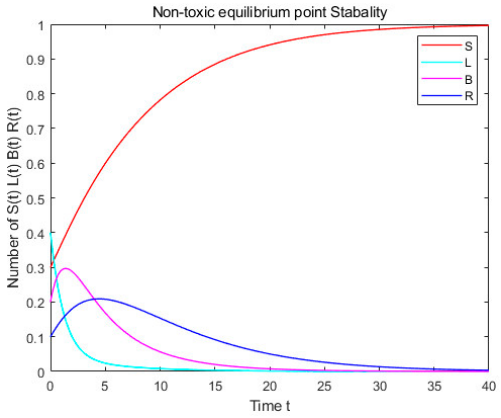

Figure 5. Stability of non-toxic equilibrium.

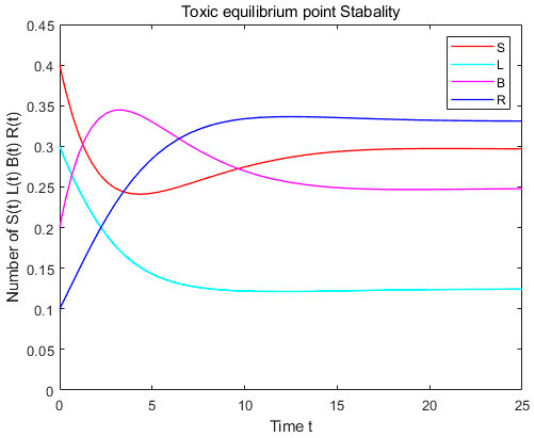

Figure 6. Stability of toxic equilibrium.

Figure 5 demonstrates that all the states S(t), L(t), B(t), and R(t) asymptotically stabilize to the non-toxic equilibrium, in line with the conclusion of Theorem 1. Similarly, from Figure 6, it is evident that all the states S(t), L(t), B(t), and R(t) asymptotically stabilize to the toxic equilibrium, consistent with the conclusion of Theorem 2.

4.2. Controllability of SLBRS

The simulation of optimal control is quite complex. On one hand, there are many equations that need to be solved (in fact, the optimal controllability simulation algorithm involves solving the state equations, co-state equations, and control input equation). On the other hand, for ensuring simulation accuracy, it is not only necessary to employ high-order differences but also to utilize a combination of forward and backward differences.

For clarity, let us briefly outline the algorithm:

Step 1. Initialization: determine the time step, set iteration termination conditions, and initialize the state, co-state, and control variables.

Step 2. Iteration Process: we solve the state equations using forward differences and the co-state equations using backward differences.

Step 2.1. **State Equation Solution**: use fourth-order forward Runge-Kutta difference to solve the state equation based on known control and initial value conditions.

Step 2.2. Co-state Equation Solution: employ fourth-order backward Runge-Kutta difference, solving the co-state equation backward from the final time.

Step 2.3. Control Update: update control variables based on the results of the state and co-state equations.

Step 2.4. Iterative Update: based on the updated control, repeat the solution of state and co-state equations until the termination conditions are met.

Step 3. Simulation Results: obtain the optimal control strategy, state trajectory, and other necessary numerical results.

The evolution trends of types S(t), L(t), B(t), and R(t) are presented in Figures 7–10. The simulation results align well with the theoretical analysis results (Theorems 3–5).

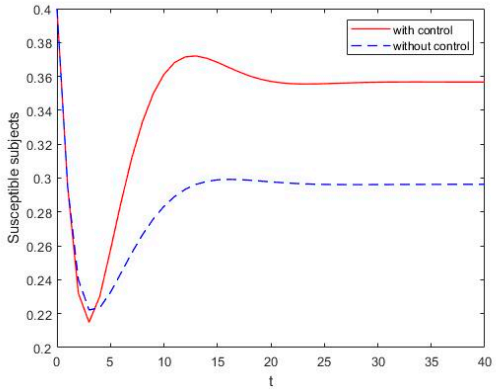

Figure 7. Evolution of susceptible computer S(t).

Figures 7 and 9 demonstrate that, under the effect of control, the proportion of uninfected computers (S(t) and R(t)) gradually increases and stabilizes. This indicates the restoration of the virus-contaminated network environment.

Figures 8 and 10 reveal that, under the influence of control, the proportion of infected computers (L(t) and B(t)) gradually decreases and stabilizes. This, from another perspective, reflects the ongoing restoration of the virus-infected network environment.

The evolution of control input is as follows.

The trend of the optimal control curve is consistent with reality (see Figure 11): Initially, the computer virus attack intensity is high, and the level of protection is correspondingly strong. However, as time passes, the intensity of the attack weakens, and the level of protection decreases in parallel.

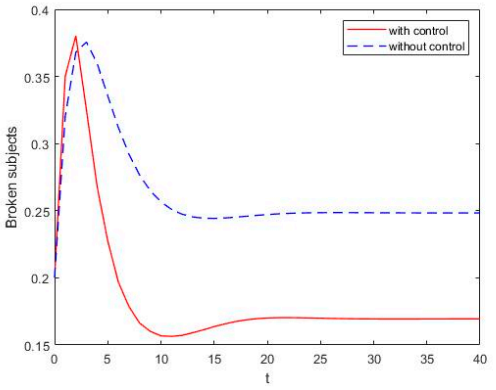

Figure 8. Evolution of outbreak computer B(t).

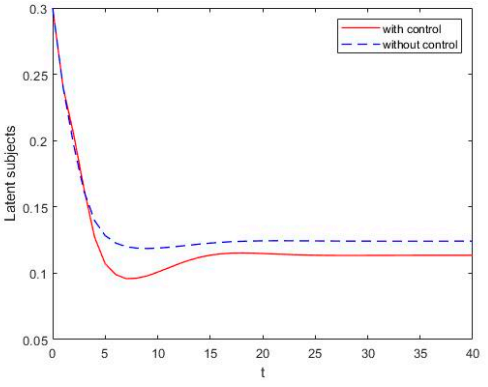

Figure 9. Evolution of latent computer L(t).

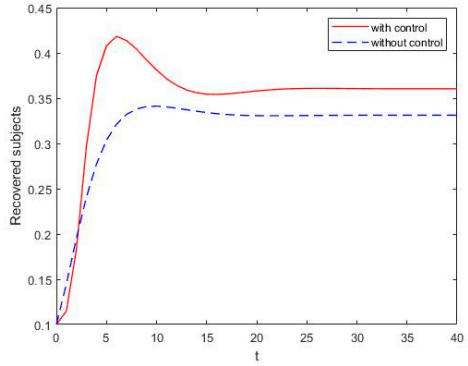

Figure 10. Evolution of recovered computer R(t).

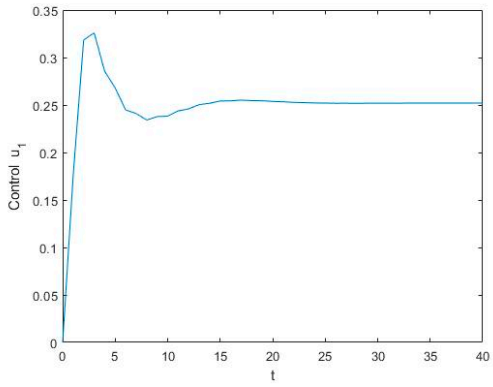

Figure 11. Optimal control function $u_1^*(t)$.

Remark 2. *We use the forward Runge-Kutta method to solve the state equations and the backward Runge-Kutta method to solve the co-state equations, and the simulation results are superior to simply using either forward or backward Runge-Kutta methods for solving them.*

5. Discussion

At this point in the paper, let us address a few issues for discussion.

Firstly, is it necessary to introduce control to SLBRS?

To address this question, we directly compare the stable values of SLBRS with and without control input (Equations (1) and (2)). Utilizing the same parameters and initial states, we calculate the stable values of each state variable in (1) and (2) (see Table 3 for details).

Table 3. The comparison of Equations (1) and (2).

Model	S*	L*	B*
Equation (1)	0.30	0.12	0.25
Equation (2)	0.36	0.11	0.17

Table 2 illustrates that toxicity-free nodes (S*, R*) increase, and toxic nodes (L*, B*) decrease. This observation strongly suggests that optimal control is beneficial for the restoration of a contaminated network.

Secondly, there are several issues regarding the selection of the optimal control input function:

(1) What if the recovery rate (γ_2 or γ_3) is used as the control input? It is similar to γ_1, so we omit the details.

(2) What if more than one recovery rate is utilized in the control inputs? The fact is that the more control inputs are employed, the greater the ability to control the system.

Thirdly, there are questions regarding model improvement.

The selected model in this paper does not account for time-delay factors. However, in reality, the transformation from latent to active computers and the recovery of virus-infected computers both take a certain amount of time. Therefore, in future work, consideration of time-delay factors can be introduced to establish an optimal computer virus control model with time-delay factors. This is expected to yield results that are more practically meaningful. Please refer to [15] for further details.

This paper employs optimal control theory to study the SLBRS model and has obtained research conclusions that align with expectations. Introducing current popular research directions such as stochastic control and adaptive control into the study of SLBRS would undoubtedly open up new possibilities. For more details, please refer to the latest literature [19–24].

6. Conclusions

In this paper, we have introduced the SLBRS computer virus model with triple recovery rates. Subsequently, we have investigated its stability through both linearization and optimal control. The primary findings are as follows.

Firstly, using the Hurwitz criterion, we have demonstrated the stability of both the non-toxic equilibrium point and the toxic equilibrium point. Furthermore, we have validated these findings through simulation.

Secondly, the existence and uniqueness of the optimal solution have been rigorously established and confirmed through the application of the Pontryagin maximum principle.

Thirdly, for numerical simulations, we have employed an iterative algorithm. The results of these simulations illustrate that the optimal control strategy can effectively minimize the outbreak of a virus in the network, all the while reducing network maintenance costs.

Author Contributions: Conceptualization, methodology, X.Z.; Simulation, W.H. All authors have read and agreed to the published version of the manuscript.

Funding: The authors are sponsored by the Qing-Lan Project of Jiangsu Province.

Data Availability Statement: Data are contained within the article.

Acknowledgments: Both authors would like to thank the referees for their suggestions which helped us to improve the quality of this paper greatly.

Conflicts of Interest: The authors declare no conflict of interest.

References

1. Cohen, F. Computer viruses: Theory and experiments. *Comput. Secur.* **1987**, *6*, 22–35. [CrossRef]
2. Murray, W. The application of epidemiology to computer viruses. *Comput. Secur.* **1988**, *7*, 139–150. [CrossRef]
3. Kephart, J.O.; White, S.R. Directed-graph Epidemiological Models of Computer Viruse. In Proceedings of the IEEE Computer Society Symposium on Research in Security and Privacy, Oakland, CA, USA, 20–22 May 1991; pp. 343–359.
4. Tian, C.; Zheng, S.R. The study of computer virus computational models. *J. Comput. Sci.* **2001**, *24*, 158–163. (In Chinese)
5. Chen, L.C.; Carley, K.M. The impact of countermeasure propagation on the prevalence of computer viruses. *IEEE Trans. Syst. Man Cybern. Part B* **2004**, *34*, 823–833. [CrossRef] [PubMed]
6. Yuan, H.; Chen, G.Q. Network virus-epidemic model with the point-to-group information propagation. *Appl. Math. Comput.* **2008**, *206*, 357–367. [CrossRef]
7. Mishra, B.K.; Saini, D.K. SEIRS epidemic model with delay for transmission of malicious objects in computer network. *Appl. Math. Comput.* **2007**, *1881476*, 1482. [CrossRef]
8. Piqueira, J.R.C.; de Vasconcelos, A.A. Dynamic models for computers viruses. *Comput. Secur.* **2008**, *27*, 355–359. [CrossRef]
9. Piqueira, J.R.C.; Araujo, V.O. A modified epidemiological model for computer viruses. *Appl. Math. Comput.* **2009**, *213*, 55–360. [CrossRef]
10. Mishra, B.K.; Jha, N. SEIQRS model for the transmission of malicious objects in computer network. *Appl. Math. Model.* **2010**, *34*, 710–715. [CrossRef]
11. Yang, L.X.; Yang, X.F.; Wen, L.S. A novel computer virus propagation model and its dynamics. *Int. J. Comput. Math.* **2012**, *89*, 2307–2314. [CrossRef]
12. Yang, M.; Yang, X.; Yang, L.-X.; Zhu, Q. A model of computer virus with recovery compartment. *J. Inf. Comput. Sci.* **2012**, *18*, 359–378.

13. Yang, L.X.; Yang, X.F.; Zhu, Q.Y.; Wen, L.S. A computer virus model with graded recovery rates. *Nonlinear Anal. Real World Appl.* **2013**, *14*, 414–422. [CrossRef]
14. Zhao, X.Q. Optimal Control of SLBRS with Two Control Inputs. *Mathematics* **2023**, *11*, 4036. [CrossRef]
15. Chen, L.; Hattaf, K.; Sun, J. Optimal control of a delayed SLBS computer virus model. *Phys. A. Stat. Mech. Its Appl.* **2015**, *42*, 244–250. [CrossRef]
16. Zhang, C.M.; Huang, H.T. Optimal control strategy for a novel computer virus propagation model on scale-free networks. *Phys. A. Stat. Mech. Its Appl.* **2016**, *451*, 251–265. [CrossRef]
17. Avcı, D.; Soytürk, F. Optimal control strategies for a computer network under virus threat. *J. Comput. Appl. Math.* **2023**, *419*, 114740. [CrossRef]
18. Birkhoff, G.; Rota, G.C. *Ordinary Differential Equations*, 4th ed.; John Wiley & Sons: New York, NY, USA, 1989.
19. Yang, X.; Wang, H.; Zhu, Q. Event-triggered predictive control of nonlinear stochastic systems with output delay. *Automatica* **2022**, *140*, 110230. [CrossRef]
20. Xue, Y.; Han, J.; Tu, Z.; Chen, X. Stability analysis and design of cooperative control for linear delta operator system. *AIMS Math.* **2023**, *8*, 12671–12693. [CrossRef]
21. Tang, Y.; Zhou, L.; Tang, J.; Rao, Y.; Fan, H.; Zhu, J. Hybrid impulsive pinning control for mean square synchronization of uncertain multi-link complex networks with stochastic characteristics and hybrid delays. *Mathematics* **2023**, *11*, 1697. [CrossRef]
22. Xiao, H.; Li, Z.; Lin, H.; Zhao, Y. A dual rumor spreading model with consideration of fans versus ordinary people. *Mathematics* **2023**, *11*, 2958. [CrossRef]
23. Fan, L.N.; Zhu, Q.X.; Zheng, W.X. Stability analysis of switched stochastic nonlinear systems with state-dependent delay. *IEEE Trans. Autom. Control.* **2023**. [CrossRef]
24. Xu, H.F.; Zhu, Q.X.; Zheng, W.X. Exponential stability of stochastic nonlinear delay systems subject to multiple periodic impulses. *IEEE Trans. Autom. Control.* **2023**. [CrossRef]

mathematics

MDPI

Article

Generalized Halanay Inequalities and Asymptotic Behavior of Nonautonomous Neural Networks with Infinite Delays

Dehao Ruan and Yao Lu *

School of Mathematics and Systems Science, Guangdong Polytechnic Normal University, Guangzhou 510665, China; mathhope@sina.com
* Correspondence: luyaomath@gpnu.edu.cn

Abstract: This paper focuses on the asymptotic behavior of nonautonomous neural networks with delays. We establish criteria for analyzing the asymptotic behavior of nonautonomous recurrent neural networks with delays by means of constructing some new generalized Halanay inequalities. We do not require to constructi any complicated Lyapunov function and our results improve some existing works. Lastly, we provide some illustrative examples to demonstrate the effectiveness of the obtained results.

Keywords: generalized Halanay inequalities; dissipativity; asymptotic behavior; recurrent neural networks

MSC: 34A40; 35B40; 92B20

1. Introduction

Recently, neural networks (NNs) have garnered significant attention and have found extensive applications across various domains, including image restoration [1], pattern recognition [2] and associative memory [3]. In practical applications, time delays are an unavoidable factor stemming from the finite switching speed of amplifiers. It's well-established that time delays can potentially induce oscillations and instability in systems. Consequently, the asymptotic behavior of NNs with delays has been a focal point of research for numerous authors.

The study of asymptotic behavior such as dissipativity [4–7] attracting sets [8], stabilization [9–11] and stability offers potent tools for addressing the problem of controlling dynamics systems. In the asymptotic behavior analysis, one powerful tool is Lyapunov function or functional. Wang and Zhu [12] used a novel Lyapunov–Krasovskill functional to consider the stability of discrete-time semi-Markov jump linear systems with time delay. Fan et al. [13] using multiple Lyapunov-Krasovskii functionals to investigate the stability of switched stochastic nonlinear systems. Xu et al. [14] used the improved Lyapunov Razumikhin method to consider exponential stability of stochastic nonlinear delay systems. Zhu and Zhu [15] constructed the Lyapunov-Krasovskii functional to the stability of stochastic Highly Nonlinear Systems.

Especially, Cao and Zhou [16], Cao [17], Mohanmad and Gopalsamy [18], Sun et al. [19], Zeng et al. [7], Zeng et al. [20], Zhang et al. [21], Zhang et al. [22], Zhao and Cao [23], Zheng and Zhang [24], and Zhou and Zhang [25] used the Lypunov functional to investigate the stability of delayed cellular NNs with constant coefficient, respectively. Jiang and Cao [26], Jiang and Teng [27,28], Long et al. [29], Rehim et al. [30], Song and Zhao [6], Yu et al. [31], Zhang et al. [32], Zhang et al. [33] investigated the stability of recurrent NNs with variable coefficient by constructing Lyapunov function or functional, respectively. Through the construction of Lyapunov functions or functionals, one can find some interesting results. Nevertheless, constructing an appropriate Lyapunov function or functional can

be a challenging task, particularly in the context of nonautonomous NNs with unbounded delays [34].

On the other hand, Halanay inequalities can be also used to consider the asymptotic behavior of NNs [5,29,34–38]. It should be noted that only [5,35,38] considered the unbounded coefficient functions, and unbounded delay functions. Hien et al. [35] considered the generalized exponential stability of one-dimensional Halalay inequalities and gave application to nonautonomous NNs. Later, Lu et al. [38] studied the global generalized exponential stability of nonautonomous NNs by multi-dimensional generalized Halanay inequalities which extended the results in [35]. However, when the coefficient functions are constants and the delay functions are infinite the works in [35,38] do not work. Hien et al. [5] considered the global dissipativity of nonautonomous NNs with delays. Howerer, their delay functions are required to be proportional.

Inspired by the preceding discussion, in this paper, we propose some generalized Halanay inequalities to investigate the asymptotic behaviour of neural networks with unbounded variable coefficients and infinite delay, and our assumptions are less restrictive than most of existing works. Our results not only enhance but also extend the results initially presented in [5,35,38].

The structure of this paper unfolds as follows. Section 2 provides an introduction to some preliminaries, definitions and model descriptions. Section 3 investigates the asymptotic behavior of NNs with delays by means of constructing some generalized Halanay inequalities. Section 4 offers some examples and simulations to exemplify the practical utility of our theoretical results. Finally, this paper concludes in the Section 5.

Notations: let $N_n = \{1, 2, \ldots, n\}$ and A^T denotes the transpose of matrix A. $\mathbb{R}^n$ is the n-dimensional Euclidean space equipped with the norm $\|q\| = \max_{i \in N_n}\{|q_i|\}$ for $q = (q_1, q_2, \ldots, q_n)^T \in \mathbb{R}^n$. For $t_0 \geq 0$, $BC((-\infty, t_0], \mathbb{R}^n)$ stands for the space of all bounded and continuous functions $\psi : (-\infty, t_0] \to \mathbb{R}^n$ equipped with the norm $\|\psi\|_\infty := \sup_{\theta \leq t_0} \|\psi(\theta)\|$. For any sets D and E, define $D - E := \{x | x \in D,\ x \notin E\}$. $b_+ = \max\{0, b\}$.

2. Preliminaries and Model Description

This paper investigates the following NNs with delays

$$\begin{cases} \frac{dq_i(t)}{dt} = -\alpha_i(t)q_i(t) + \sum_{j=1}^{n} [\beta_{ij}(t)f_j(q_j(t)) + \gamma_{ij}(t)g_j(q_j(t - \tau_{ij}(t)))] + h_i(t), \quad t \geq t_0, \\ q_i(t) = \psi_i(t), \quad t \in (-\infty, t_0], \quad i \in N_n, \end{cases} \tag{1}$$

where $q_i(t)$ is the neuron state variable of the neural network, $\psi(t) = (\psi_1(t), \ldots, \psi_n(t))$ is the initial value, $q(t, \psi) = (q_1(t), \ldots, q_n(t))^T \in BC((-\infty, t_0]$ denotes the solution (1) with initial value ψ, sometimes we write $q(t)$ for short. $\alpha_i(t)$ stands for self-feedback coefficient, $\beta_{ij}(t)$ and $\gamma_{ij}(t)$ stand for neuron connect weight. $\tau_{ij}(t) \geq 0$ represents the transmission delay. $h_i(t)$ is the external bias, f_j and g_j stand for the activation functions. If the initial value of $q_j(t)$ defined on $[\min_{t \geq t_0}\{t - \tau_{ij}(t)\}, t_0]$, define $q_j(t) = q_j(\min_{t \geq t_0}\{t - \tau_{ij}(t)\})$ for $t < \min_{t \geq t_0}\{t - \tau_{ij}(t)\}$, then (1) is clearly defined.

Now, we introduce four definitions of asymptotic behavior.

Definition 1 ([5]). *A compact set $\Omega \subset \mathbb{R}^n$ is called to be a global attracting set of (1), provided $\limsup_{t \to +\infty} d(q(t, \psi), \Omega) = 0$, where $d(q, \Omega) := \inf_{x \in \Omega} \|q - x\|$ represents the distance between q and Ω.*

Definition 2 ([5]). *A compact set $\Omega \subset \mathbb{R}^n$ is called to be a global generalized exponential attracting set of (1), provided there exists a $\rho(\psi) \geq 0$ satisfies that*

$$d(q(t, \psi), \Omega) \leq \rho(\psi)e^{-\lambda(t)}, \quad t \geq t_0, \tag{2}$$

where $\lambda(t) \geq 0$ is a nondecreasing function satisfies that $\lim_{t\to+\infty} \lambda(t) = +\infty$.

Remark 1. *Substituting $\lambda(t)$ with $\lambda(t-t_0)$, $\lambda \ln(t-t_0+1)$, and $\lambda \ln(\ln(t-t_0+e))$, $(\lambda > 0)$, respectively, results in Ω becoming a global exponential, polynomial as well as logarithmic attracting set of system (1), correspondingly.*

Definition 3 ([5])**.** *System (1) is called to be globally dissipative, provided there is a bounded set $\mathcal{B} \subset \mathbb{R}^n$ satisfies that for any bounded set $\Psi \subset \mathbb{R}^n$, there exists a time $t_B = t_B(\Psi)$ satisfies that for any initial value $\psi \in \Psi$, $q(t) = q(t,\psi) \in \mathcal{B}$ for $t \geq t_B(\Psi)$. Then $\mathcal{B}$ is called an absorbing set of (1).*

Remark 2. *If Ω is a global generalized exponential attracting set of (1), this implies (1) is globally dissipative. For any bounded set $\Psi \subset \mathbb{R}^n$, there exists an absorbing set of (1) such that $\mathcal{B}_\varepsilon = \{x \in \mathbb{R}^n : d(x,\Omega) \leq \varepsilon\}$.*

Definition 4 ([38])**.** *System (1) is called to be globally generalized exponential stable, provided for any two solutions $q^{(1)}(t) = (q_1^{(1)}(t), \ldots, q_n^{(1)}(t))^T$ and $q^{(2)}(t) = (q_1^{(2)}(t), \ldots, q_n^{(2)}(t))^T$, each having distinct initial values $\psi^{(1)}, \psi^{(2)} \in BC((-\infty, t_0], \mathbb{R}^n)$, there exists a non-negative function $\varrho(\psi^{(1)} - \psi^{(2)})$ and a non-decreasing function $\lambda(t) \geq 0$ with property $\lim_{t\to+\infty} \lambda(t) = +\infty$ such that*

$$|q^{(1)}(t) - q^{(2)}(t)| \leq \varrho(\psi^{(1)} - \psi^{(2)})e^{-\lambda(t)}, \quad t \geq t_0,$$

where $\lambda(t)$ represents the decay rate.

3. Main Results

In this section, the asymptotic behavior of (1) is discussed by means of generalized Halanay inequalities.

Theorem 1. *Let the following conditions hold*

(**C.1**) *For $i, j \in N_n$ and $t \geq t_0$, $\alpha_i(t) \geq 0, \beta_{ij}(t), \gamma_{ij}(t), h_i(t)$ are all integrable functions.*
(**C.2**) *For $j \in N_n$ and $q_1, q_2 \in \mathbb{R}$, there exist constants F_j, G_j such that*

$$|f_j(q_1) - f_j(q_2)| \leq F_j|q_1 - q_2|, \quad |g_j(q_1) - g_j(q_2)| \leq G_j|q_1 - q_2|.$$

(**C.3**) *For each $i \in N_n$, there exist positive constants $\eta_1, \eta_2, \ldots, \eta_n$, $(\max\{\eta_1, \eta_2, \ldots, \eta_n\} = 1)$ and non-negative constants μ_i such that*

$$\eta_i\alpha_i(t) - \sum_{j=1}^{n}(|\beta_{ij}(t)|F_j + |\gamma_{ij}(t)|G_j)\eta_j \geq 0, \quad t \geq t_0,$$

and

$$\sup_{\{t|t\geq t_0\}-D}\left\{\frac{\sum\limits_{j=1}^{n}(|\beta_{ij}(t)f_j(0)| + |\gamma_{ij}(t)g_j(0)|) + |h_i(t)|}{\eta_i\alpha_i(t) - \sum\limits_{j=1}^{n}(|\beta_{ij}(t)|F_j + |\gamma_{ij}(t)|G_j)\eta_j}\right\} := \mu_i,$$

where

$$D = \left\{t|\eta_i\alpha_i(t) - \sum_{j=1}^{n}(|\beta_{ij}(t)|F_j + |\gamma_{ij}(t)|G_j)\eta_j = \sum_{j=1}^{n}(|\beta_{ij}(t)f_j(0)| + |\gamma_{ij}(t)g_j(0)|) + |h_i(t)| = 0\right\},$$

$$\sum_{j=1}^{n}(|\beta_{ij}(t)f_j(0)| + |\gamma_{ij}(t)g_j(0)|) + |h_i(t)| := \mu_i(t).$$

Then systems (1) is globally dissipative and $\max\limits_{k\in N_n}\left\{\frac{\sup\limits_{t\le t_0}|\psi_k(\theta)|}{\eta_k},\mu_k\right\}$ *is an absorbing set of (1).*

Remark 3. *Conditions* (**C.1**)–(**C.3**) *imply the local Lipschitz condition and local linear growth condition. So the existence and uniqueness of solution can be guaranteed.*

Proof. Assume $q(t)=(q_1(t),\ldots,q_n(t))^T$ is the solution of (1) with initial value $\psi=(\psi_1,\ldots,\psi_n)^T$. Let

$$z(t)=(z_1(t),\ldots,z_n(t))^T=(\eta_1^{-1}q_1(t),\ldots,\eta_n^{-1}q_n(t))^T, \tag{3}$$

then

$$\begin{cases}\frac{dz_i(t)}{dt}=-\alpha_i(t)z_i(t)+\eta_i^{-1}\sum\limits_{j=1}^{n}[\beta_{ij}(t)f_j(q_j(t))+\gamma_{ij}(t)g_j(q_j(t-\tau_{ij}(t)))]+\eta_i^{-1}h_i(t), & t\ge t_0,\\ z_i(t)=\eta_i^{-1}\psi_i(t), & t\in(-\infty,t_0].\end{cases} \tag{4}$$

For each $i\in N_n$ and $t\ge t_0$, from (**C.2**), (3) and (4), we have

$$\begin{aligned}D^+|z_i(t)|&\le-\alpha_i(t)|z_i(t)|+\eta_i^{-1}\sum_{j=1}^{n}|\beta_{ij}(t)|(F_j\eta_j|z_j(t)|+|f_j(0)|)\\&\quad+\eta_i^{-1}\sum_{j=1}^{n}|\gamma_{ij}(t)|(\sup_{t-\tau_{ij}(t)\le s\le t}(G_j\eta_j|z_j(s)|+|g_j(0)|)+\eta_i^{-1}|h_i(t)|\\&=-\alpha_i(t)|z_i(t)|+\eta_i^{-1}\sum_{j=1}^{n}|\beta_{ij}(t)|F_j\eta_j|z_j(t)|+\eta_i^{-1}\sum_{j=1}^{n}|\gamma_{ij}(t)|G_j\eta_j\sup_{t-\tau_{ij}(t)\le s\le t}|z_j(s)|\\&\quad+\eta_i^{-1}\left[\sum_{j=1}^{n}(|\beta_{ij}(t)f_j(0)|+|\gamma_{ij}(t)g_j(0)|)+|h_i(t)|\right],\end{aligned} \tag{5}$$

where D^+ is the upper-right Dini derivative. Define $M:=\max\limits_{k\in N_n}\{\sup\limits_{t\le t_0}\frac{|\psi_k(\theta)|}{\eta_k},\mu_k\}$. It is clear that $|z_i(t)|\le M$ for $t\le t_0$ and $i\in N_n$. Suppose there exist $i_1\in N_n$, $\epsilon_1>0$ and $t_1>t_0$ such that $|z_{i_1}(t_1)|=M+\epsilon_1$, and $|z_j(t)|\le M+\epsilon_1$ for $t\le t_1$ and $j\in N_n$. Then we get $D^+|z_{i_1}(t)|\Big|_{t=t_1}>0$. In contrast

$$\begin{aligned}D^+|z_{i_1}(t)|\Big|_{t=t_1}&\le-\alpha_{i_1}(t_1)|z_{i_1}(t_1)|+\eta_{i_1}^{-1}\sum_{j=1}^{n}|\beta_{i_1j}(t_1)|F_j\eta_j|z_j(t_1)|\\&\quad+\eta_{i_1}^{-1}\sum_{j=1}^{n}|\gamma_{i_1j}(t_1)|G_j\eta_j\sup_{t_1-\tau_{i_1j}(t_1)\le s\le t_1}|z_j(s)|+\eta_i^{-1}\mu_{i_1}(t_1)\\&\le-\alpha_{i_1}(t_1)(M+\epsilon_1)+\eta_{i_1}^{-1}\sum_{j=1}^{n}|\beta_{i_1j}(t_1)|F_j\eta_j(M+\epsilon_1)+\eta_i^{-1}\sum_{j=1}^{n}|\gamma_{i_1j}(t_1)|G_j\eta_j(M+\epsilon_1)\\&\quad+\mu_{i_1}\left[\alpha_{i_1}(t_1)-\eta_i^{-1}\sum_{j=1}^{n}|\beta_{i_1j}(t_1)|F_j\eta_j-\eta_i^{-1}\sum_{j=1}^{n}|\gamma_{i_1j}(t_1)|G_j\eta_j\right]\\&=-\left[\alpha_{i_1}(t_1)-\eta_{i_1}^{-1}\sum_{j=1}^{n}|\beta_{i_1j}(t_1)|F_j\eta_j-\eta_i^{-1}\sum_{j=1}^{n}|\gamma_{i_1j}(t_1)|G_j\eta_j\right](M-\mu_{i_1}+\epsilon_1)\le0.\end{aligned}$$

This signifies a contradiction, implying that

$$|z_i(t)| \le \max_{k\in N_n}\left\{\frac{\sup_{t\le t_0}|\psi_k(\theta)|}{\eta_k}, \mu_k\right\}, \quad t \ge t_0, \quad i \in N_n.$$

So we get

$$|q_i(t)| \le \max_{k\in N_n}\left\{\frac{\sup_{t\le t_0}|\psi_k(\theta)|}{\eta_k}, \mu_k\right\}\eta_i, \quad t \ge t_0, \quad i \in N_n.$$

Then

$$\|q(t)\| \le \max_{k\in N_n}\left\{\frac{\sup_{t\le t_0}|\psi_k(\theta)|}{\eta_k}, \mu_k\right\}, \quad t \ge t_0.$$

This completes the proof. □

Remark 4. *Condition* $(\max\{\eta_1, \eta_2, \ldots, \eta_n\} = 1)$ *can be omitted, but in order to see our main results clearly, so we reserve it.*

Theorem 2. *Assume* (**C**.**1**)–(**C**.**3**) *and the following conditions hold:*

(**C**.**4**) *For* $i, j \in N_n$, *there exist constants* $\alpha_i > 0$ *and* $\alpha(t)$ *such that*

$$0 \le \alpha_i\alpha(t) \le \alpha_i(t) \text{ for } t \ge t_0, \quad \lim_{t\to+\infty}\int_{t_0}^{t}\alpha(s)ds \to +\infty, \quad \sup_{t\ge t_0}\left\{\int_{t-\tau_{ij}(t)}^{t}\alpha^*(s)ds\right\} := \tau_{ij} < +\infty,$$

where

$$\alpha^*(t) := \begin{cases} \alpha(t), & t \ge t_0, \\ 0, & t < t_0. \end{cases}$$

(**C**.**5**) *For* $i, j \in N_n$,

$$\sup_{\{t|t\ge t_0\}-\{t|\alpha_i(t)=|\beta_{ij}(t)|F_j=0\}}\left\{\frac{|\beta_{ij}(t)|F_j}{\alpha_i(t)}\right\} := \rho_{ij}^{(1)}, \quad \sup_{\{t|t\ge t_0\}-\{t|\alpha_i(t)=|\gamma_{ij}(t)|G_j=0\}}\left\{\frac{|\gamma_{ij}(t)|G_j}{\alpha_i(t)}\right\} := \rho_{ij}^{(2)},$$

and

$$-\eta_i + \sum_{j=1}^{n}(\rho_{ij}^{(1)} + \rho_{ij}^{(2)})\eta_j < 0,$$

where, $\eta_1, \eta_2, \ldots, \eta_n$ *were introduced in Theorem 1.*

Then we have the following assertions:

(**1**) *For* $i \in N_n$,

$$|q_i(t)| \le \left[\left(\max_{k\in N_n}\left\{\frac{\sup_{t\le t_0}|\psi_k(\theta)|}{\eta_k}\right\} - \max_{k\in N_n}\{\mu_k\}\right)_+ e^{-\lambda^*\int_{t_0}^{t}\alpha(s)ds} + \max_{k\in N_n}\{\mu_k\}\right]\eta_i, \quad t \ge t_0.$$

where λ^* *represents the smallest solution to the following equations*

$$\frac{\lambda}{\alpha_i} + \frac{\sum_{i=1}^{n}(\rho_{ij}^{(1)} + \rho_{ij}^{(2)}e^{\lambda\tau_{ij}})\eta_j}{\eta_i} - 1 = 0, \quad i \in N_n.$$

(**2**) *The set*

$$\Omega := \left\{u \in \mathbb{R}^n : \|u\| \le \max_{k\in N_n}\{\mu_k\}\right\}$$

is a global generalized exponential attracting set of (1).

(**3**) *System (1) is globally dissipative.*

Proof. When $\max\limits_{k\in N_n}\left\{\frac{\sup\limits_{t\le t_0}|\psi_k(\theta)|}{\eta_k}\right\}\le\max\limits_{k\in N_n}\{\mu_k\}$, the proof is deduce from Theorem (1). Now, suppose $\max\limits_{k\in N_n}\left\{\frac{\sup\limits_{t\le t_0}|\psi_k(\theta)|}{\eta_k}\right\}>\max\limits_{k\in N_n}\{\mu_k\}$ and define

$$K_i(\lambda):=\frac{\lambda}{\alpha_i}+\eta_i^{-1}\sum_{j=1}^{n}(\rho_{ij}^{(1)}+\rho_{ij}^{(2)}e^{\lambda\tau_{ij}})\eta_j-1,\quad\lambda\in[0,+\infty).$$

Note that, for each $i\in N_n$, $K_i(\lambda)$ is continuous on $[0,+\infty)$, $K_i(0)=\eta_i^{-1}\sum\limits_{j=1}^{n}(\rho_{ij}^{(1)}+\rho_{ij}^{(2)})\eta_j-1<0$,

$$K_i'(\lambda)=\frac{1}{\alpha_i}+\eta_i^{-1}\sum_{j=1}^{n}\tau_{ij}\eta_j\rho_{ij}^{(2)}e^{\lambda\tau_{ij}}>0,$$

and $\lim\limits_{\lambda\to+\infty}K_i(\lambda)=+\infty$. So for $i\in N_n$, equation $K_i(\lambda)=0$ has an unique solution $\lambda_i\in(0,+\infty)$. Define $\lambda^*:=\min\limits_{k\in N_n}\{\lambda_k\}$, then

$$\frac{\lambda^*}{\alpha_i}+\eta_i^{-1}\sum_{j=1}^{n}(\rho_{ij}^{(1)}+\rho_{ij}^{(2)}e^{\lambda^*\tau_{ij}})\eta_j-1\le0,\quad i\in N_n.\tag{6}$$

Multiply both sides of (6) by $\alpha_i(t)$, we get

$$\frac{\lambda^*\alpha_i(t)}{\alpha_i}+\eta_i^{-1}\sum_{j=1}^{n}(\rho_{ij}^{(1)}+\rho_{ij}^{(2)}e^{\lambda^*\tau_{ij}})\eta_j\alpha_i(t)-\alpha_i(t)\le0,\quad t\ge t_0,\quad i\in N_n.\tag{7}$$

From (**C**.**4**), (**C**.**5**) and (7), we have

$$\eta_i^{-1}\sum_{j=1}^{n}(\rho_{ij}^{(1)}+\rho_{ij}^{(2)}e^{\lambda^*\tau_{ij}})\eta_j\alpha_i(t)-\alpha_i(t)\le-\lambda^*\alpha(t),\quad t\ge t_0,\quad i\in N_n\tag{8}$$

and

$$\eta_i^{-1}\sum_{j=1}^{n}(|\beta_{ij}(t)|F_j+|\gamma_{ij}(t)|G_je^{\lambda^*\tau_{ij}})\eta_j-\alpha_i(t)\le-\lambda^*\alpha(t),\quad t\ge t_0,\quad i\in N_n.\tag{9}$$

For $t\in\mathbb{R}$, define

$$v(t):=\left(\max_{k\in N_n}\left\{\frac{\sup\limits_{t\le t_0}|\psi_k(\theta)|}{\eta_k}\right\}-\max_{k\in N_n}\{\mu_k\}\right)e^{-\lambda^*\int_{t_0}^{t}\alpha^*(s)ds}+\max_{k\in N_n}\{\mu_k\}.\tag{10}$$

Then

$$\begin{aligned}(v(s)-\max_{k\in N_n}\{\mu_k\})&=(v(t)-\max_{k\in N_n}\{\mu_k\})e^{\lambda^*\int_s^t\alpha^*(u)du}\\&\le(v(t)-\max_{k\in N_n}\{\mu_k\})e^{\lambda^*\int_{t-\tau_{ij}(t)}^{t}\alpha^*(u)du},\quad i,j\in N_n,\quad s\in[t-\tau_{ij}(t),t].\end{aligned}$$

Hence

$$\sup_{t-\tau_{ij}(t)\le s\le t}\{v(s)-\max_{k\in N_n}\{\mu_k\}\}\le(v(t)-\max_{k\in N_n}\{\mu_k\})e^{\lambda^*\int_{t-\tau_{ij}(t)}^{t}\alpha^*(u)du},\quad t\ge t_0,\quad i,j\in N_n.\tag{11}$$

By (11) and the definition of τ_{ij}, we get

$$\sup_{t-\tau_{ij}(t)\le s\le t}\{v(s)-\max_{k\in N_n}\{\mu_k\}\}\le (v(t)-\max_{k\in N_n}\{\mu_k\})e^{\lambda^*\tau_{ij}},\quad t\ge t_0,\quad i,j\in N_n. \tag{12}$$

Thus, for $t\ge t_0$ and $i\in N_n$, from (**C**.**3**)–(**C**.**5**), (8)–(10) and (12), we get

$$\begin{aligned}
\frac{dv(t)}{dt} &= -\lambda^*\alpha(t)\left(\max_{k\in N_n}\left\{\frac{\sup_{t\le t_0}|\psi_k(\theta)|}{\eta_k}\right\}-\max_{k\in N_n}\{\mu_k\}\right)e^{-\lambda^*\int_{t_0}^t\alpha^*(s)ds}\\
&= -\lambda^*\alpha(t)(v(t)-\max_{k\in N_n}\{\mu_k\})\\
&\ge -\left[1-\eta_i^{-1}\sum_{j=1}^n\left(\rho_{ij}^{(1)}+\rho_{ij}^{(2)}e^{\lambda^*\tau_{ij}}\right)\eta_j\right]\alpha_i(t)(v(t)-\max_{k\in N_n}\{\mu_k\})\\
&\ge -\alpha_i(t)v(t)+\eta_i^{-1}\sum_{j=1}^n\rho_{ij}^{(1)}\alpha_i(t)\eta_jv(t)+\eta_i^{-1}\sum_{j=1}^n\rho_{ij}^{(2)}\alpha_i(t)(t)e^{\lambda^*\tau_{ij}}\eta_jv(t)\\
&\quad+\left[\alpha_i(t)-\eta_i^{-1}\sum_{j=1}^n\left(|\beta_{ij}(t)|F_j\eta_j+|\gamma_{ij}(t)|G_j\eta_j\right)\right]\max_{k\in N_n}\{\mu_k\}\\
&\ge -\alpha_i(t)v(t)+\eta_i^{-1}\sum_{j=1}^n|\beta_{ij}(t)|F_j\eta_jv(t)+\eta_i^{-1}\sum_{j=1}^n|\gamma_{ij}(t)|G_j\eta_j\sup_{t-\tau_{ij}(t)\le s\le t}v(s)+\eta_i^{-1}\mu_i(t).
\end{aligned}\tag{13}$$

At last, we show when $\max\limits_{k\in N_n}\left\{\frac{\sup_{t\le t_0}|\psi_k(\theta)|}{\eta_k}\right\}>\max\limits_{k\in N_n}\{\mu_k\}$, $|z_i(t)|\le v(t)$ for $t\ge t_0$ and $i\in N_n$ by reduction to absurdity. Clearly, $|z_i(t)|\le v(t)$ for $t\in(-\infty,t_0]$. Suppose there exist $i_2\in N_n$, $\varepsilon_2>0$ and $t_2>t_0$ such that $|z_{i_2}(t_2)|=v(t_2)+\epsilon_2$, and $|z_j(t)|\le v(t)+\epsilon_2$ for $t\in(-\infty,t_2]$ and $j\in N_n$, then we get $D^+\left(|z_{i_2}(t)|-\frac{dv(t)}{dt}\right)\Big|_{t=t_2}>0$. In contrast, from (5) and (13), we get

$$\begin{aligned}
D^+\left(|z_{i_2}(t)|-\frac{dv(t)}{dt}\right)\Big|_{t=t_2} &\le -\alpha_{i_2}(t_2)(|z_{i_2}(t_2)|-v(t_2))+\eta_{i_2}^{-1}\sum_{j=1}^n|\beta_{i_2j}(t_2)|F_j\eta_j(|z_j(t_2)|-v(t_2))\\
&\quad+\eta_{i_2}^{-1}\sum_{j=1}^n|\gamma_{i_2j}(t_2)|G_j\eta_j\sup_{t_2-\tau_{i_2j}(t_2)\le s\le t_2}(|z_j(s)|-v(s))\\
&= -\left[\alpha_{i_2}(t_2)-\eta_{i_2}^{-1}\sum_{j=1}^n|\beta_{i_2j}(t_2)|F_j\eta_j-\eta_i^{-1}\sum_{j=1}^n|\gamma_{i_2j}(t_2)|G_j\eta_j\right]\epsilon_2\le 0.
\end{aligned}$$

This is a contradiction, the proof is completed. So for each $i\in N_n$, we get

$$|q_i(t)|\le\left[\left(\max_{k\in N_n}\left\{\frac{\sup_{t\le t_0}|\psi_k(\theta)|}{\eta_k}\right\}-\max_{k\in N_n}\{\mu_k\}\right)_+e^{-\lambda^*\int_{t_0}^t\alpha(s)ds}+\max_{k\in N_n}\{\mu_k\}\right]\eta_i,\quad t\ge t_0.$$

and

$$\|q(t)\|\le\left(\max_{k\in N_n}\left\{\frac{\sup_{t\le t_0}|\psi_k(\theta)|}{\eta_k}\right\}-\max_{k\in N_n}\{\mu_k\}\right)_+e^{-\lambda^*\int_{t_0}^t\alpha(s)ds}+\max_{k\in N_n}\{\mu_k\},\quad t\ge t_0. \tag{14}$$

Now, we proof the assertion (2). Define

$$\rho\left(\max_{k\in N_n}\left\{\frac{\sup_{t\le t_0}|\psi_k(\theta)|}{\eta_k}\right\}\right) := \begin{cases} \max\limits_{k\in N_n}\left\{\frac{\sup_{t\le t_0}|\psi_k(\theta)|}{\eta_k}\right\} - \max\limits_{k\in N_n}\{\mu_k\}, & \max\limits_{k\in N_n}\left\{\frac{\sup_{t\le t_0}|\psi_k(\theta)|}{\eta_k}\right\} \ge \max\limits_{k\in N_n}\{\mu_k\}, \\ 0, & \max\limits_{k\in N_n}\left\{\frac{\sup_{t\le t_0}|\psi_k(\theta)|}{\eta_k}\right\} < \max\limits_{k\in N_n}\{\mu_k\}. \end{cases}$$

By (14), we get

$$d(q(t),\Omega) \le \rho\left(\max_{k\in N_n}\left\{\frac{\sup_{t\le t_0}|\psi_k(\theta)|}{\eta_k}\right\}\right)e^{-\lambda^*\int_{t_0}^t \alpha(s)ds}, \quad t \ge t_0.$$

This means that $\Omega = \left\{u \in \mathbb{R}^n : \|u\| \le \max\limits_{k\in N_n}\{\mu_k\}\right\}$ is the global generalized exponential attracting set of (1). Now, we prove the assertion (3). Obvious, the ball $B(0, \max\limits_{k\in N_n}\{\mu_k\} + \varepsilon) := \left\{u \in \mathbb{R}^n : \|u\| \le \max\limits_{k\in N_n}\{\mu_k\} + \varepsilon\right\}$ is an absorbing set of (1) for any $\varepsilon > 0$. This completes the proof. □

Remark 5. *Hien et al. [5] investigated the dissipativity of the specific instance of the system (1), namely, the delay functions are proportional. Under condition* (**C**.**2**) *and the following conditions* (**C**.**4**′) *For $i, j \in N_n$, there exist constants $\alpha_i > 0$ and $\alpha(t)$ such that*

$$0 < \alpha_i\alpha(t) \le \alpha_i(t) \text{ for } t \ge 0, \quad \lim_{t\to+\infty}\int_0^t \alpha(s)ds \to +\infty, \quad \sup_{t\ge 0}\left\{\int_{q_{ij}t}^t \alpha(s)ds\right\} < +\infty.$$

(**C**.**5**′) *For $i, j \in N_n$, there exist constants $\hat{\beta}_{ij}$, $\hat{\gamma}_{ij}$ and $\hat{h}_i$ such that*

$$\frac{|\beta_{ij}(t)|}{\alpha_i(t)} \le \hat{\beta}_{ij}, \quad \frac{|\gamma_{ij}(t)|}{\alpha_i(t)} \le \hat{\gamma}_{ij}, \quad \frac{|h_i(t)|}{\alpha_i(t)} \le \hat{h}_i, \quad t \ge t_0.$$

and for each $i \in N_n$, there exist positive constants $\eta_1, \eta_2, \ldots, \eta_n$, $(\max\{\eta_1, \eta_2, \ldots, \eta_n\} = 1)$ such that

$$-\eta_i + \sum_{j=1}^n (F_j\hat{\beta}_{ij} + G_j\hat{\gamma}_{ij})\eta_j < 0.$$

They got the following results

$$|q_i(t)| \le \left[\left(\frac{\|\psi\|_\infty}{\min\{\eta_1,\ldots,\eta_n\}} - \frac{\hat{\gamma}}{\hat{m}}\right)_+ e^{\lambda^*\int_{t_0}^t \alpha(s)ds} + \frac{\hat{\gamma}}{\hat{m}}\right]\eta_i,$$

and the global generalized exponential attracting set is

$$\Omega_1 = \left\{q \in \mathbb{R}^n : \|q\| \le \frac{\hat{\gamma}}{\hat{m}}\right\},$$

where $\hat{\gamma} = \max\limits_{k\in N_n}\left\{\hat{h}_k + \sum\limits_{j=1}^n (\hat{b}_{kj}|f_j(0)| + \hat{c}_{kj}|g_j(0)|)\right\}$ *and* $\hat{m} = \min\limits_{k\in N_n}\left\{\eta_k - \sum\limits_{j=1}^n (\hat{b}_{kj}|f_j(0)| + \hat{c}_{kj}|g_j(0)|)\eta_j\right\}$.

We mention here that our conditions are less restrictive, i.e., $\alpha_i(t)$ can be zero at some time and the delay functions can be other types of delay functions. Besides our results also improve the results in [5]. Especially when condtions (**C**.**4**′) and (**C**.**5**′) hold, obvious,

$$\max_{k\in N_n}\left\{\frac{\sup_{t\le t_0}|\psi_k(\theta)|}{\eta_k}\right\}\le\frac{\|\psi\|_\infty}{\min\{\eta_1,\ldots,\eta_n\}},$$

and for each $i\in N_n$, we get

$$\begin{aligned}\sup_{\{t|t\ge t_0\}}\left\{\frac{\sum_{j=1}^{n}(|\beta_{ij}(t)f_j(0)|+|\gamma_{ij}(t)g_j(0)|)+|h_i(t)|}{\eta_i\alpha_i(t)-\sum_{j=1}^{n}(|\beta_{ij}(t)|F_j+|\gamma_{ij}(t)|G_j)\eta_j}\right\}&=\sup_{\{t|t\ge t_0\}}\left\{\frac{\sum_{j=1}^{n}\left(\frac{|\beta_{ij}(t)f_j(0)|}{\alpha_i(t)}+\frac{|\gamma_{ij}(t)g_j(0)|}{\alpha_i(t)}\right)+\frac{|h_i(t)|}{\alpha_i(t)}}{\eta_i-\sum_{j=1}^{n}\left(\frac{|\beta_{ij}(t)|F_j}{\alpha_i(t)}+\frac{|\gamma_{ij}(t)|G_j}{\alpha_i(t)}\right)\eta_j}\right\}\\&\le\frac{\hat{h}_i+\sum_{j=1}^{n}(\hat{\beta}_{ij}|f_j(0)|+\hat{\gamma}_{ij}|g_j(0)|)}{\eta_i-\sum_{j=1}^{n}(\hat{b}_{ij}|f_j(0)|+\hat{\gamma}_{ij}|g_j(0)|)\eta_j}\\&\le\frac{\hat{\gamma}}{\hat{m}}.\end{aligned}$$

So we have $\max_{k\in N_n}\{\mu_k\}\le\frac{\hat{\gamma}}{\hat{m}}$, this means that our estimate is sharper than [5]. The above discussion shows that this paper improves and extends the results in [5].

Theorem 3. *Let $q^{(1)}(t)=(q_1^{(1)}(t),\ldots,q_n^{(1)}(t))^T$ and $q^{(2)}(t)=(q_1^{(2)}(t),\ldots,q_n^{(2)}(t))^T$ denote two solutions of (1) with distinct initial values $\psi^{(1)},\psi^{(2)}\in BC((-\infty,t_0],\mathbb{R}^n)$. Assume that conditions* (**C**.**1**), (**C**.**2**), *and the following conditions are satisfied:*

(**C**.**6**) *For $i\in N_n$, there exist positive constants $\eta_1,\eta_2,\ldots,\eta_n$, $(\max\{\eta_1,\eta_2,\ldots,\eta_n\}=1)$ such that*

$$\sum_{j=1}^{n}(|\beta_{ij}(t)|F_j+|\gamma_{ij}(t)|G_j)\eta_j\le\eta_i\alpha_i(t),\quad t\in[t_0,+\infty),$$

and there exists $T\ge t_0$ such that

$$\sup_{\{t|t\ge T\}-\{t|\eta_i\alpha_i(t)=\sum_{j=1}^{n}(|\beta_{ij}(t)|F_j+|\gamma_{ij}(t)|G_j)\eta_j=0\}}\left\{\frac{\sum_{j=1}^{n}(|\beta_{ij}(t)|F_j+|\gamma_{ij}(t)|G_j)\eta_j}{\eta_i\alpha_i(t)}\right\}:=\rho<1.$$

(**C**.**7**) *For $i,j\in N_n$, there exist constants $\alpha_i>0$ and $\alpha(t)$ such that*

$$0\le\alpha_i\alpha(t)\le\alpha_i(t)\ \text{for}\ t\ge T,\quad\lim_{t\to+\infty}\int_T^t\alpha(s)ds\to+\infty,\quad\sup_{t-\tau_{ij}(t)\ge T}\left\{\int_{t-\tau_{ij}(t)}^{t}\alpha(s)ds\right\}:=\tau_{ij}<+\infty.$$

Then,

$$|q_i^{(1)}(t)-q_i^{(2)}(t)|\le\max_{k\in N_n}\left\{\frac{\sup_{t\le t_0}|\psi_k^{(1)}(\theta)-\psi_k^{(2)}(\theta)|}{\eta_k}\right\}\eta_i,\quad t\in[t_0,T],$$

and

$$|q_i^{(1)}(t)-q_i^{(2)}(t)|\le\max_{k\in N_n}\left\{\frac{\sup_{t\le t_0}|\psi_k^{(1)}(\theta)-\psi_k^{(2)}(\theta)|}{\eta_k}\right\}\eta_i e^{-\lambda^*\int_T^t\alpha(s)ds},\quad t\ge T.$$

Proof. For each $i \in N_n$ and $t \in \mathbb{R}$, define $l_i(t) := \left| \frac{q_i^{(1)}(t) - q_i^{(2)}(t)}{\eta_i} \right|$. Then for each $i \in N_n$ and $t \geq t_0$, we get

$$\begin{aligned} D^+ l_i(t) &\leq -\alpha_i(t) l_i(t) + \eta_i^{-1} \Bigg(\sum_{j=1}^{n} |\beta_{ij}(t)| F_j \eta_j l_j(t) + \sum_{j=1}^{n} |\gamma_{ij}(t)| G_j \eta_j \sup_{t-\tau_{ij}(t) \leq s \leq t} l_j(s) \Bigg) \\ &\leq -\alpha_i(t) l_i(t) + \eta_i^{-1} \sum_{j=1}^{n} (|\beta_{ij}(t)| F_j + |\gamma_{ij}(t)| G_j) \eta_j \sup_{t-\tau_{ij}(t) \leq s \leq t} l_j(s). \end{aligned} \tag{15}$$

Firstly, we prove

$$l_i(t) \leq \max_{k \in N_n} \left\{ \frac{\sup_{t \leq t_0} |\psi_k^{(1)}(\theta) - \psi_k^{(2)}(\theta)|}{\eta_k} \right\}, \quad t \geq t_0, \quad i \in N_n.$$

Obviously, $l_i(t) \leq \max\limits_{k \in N_n} \left\{ \frac{\sup_{t \leq t_0} |\psi_k^{(1)}(\theta) - \psi_k^{(2)}(\theta)|}{\eta_k} \right\}$ for $t \leq t_0$ and $i \in N_n$. Suppose there exist $i_3 \in N_n$, $\epsilon_3 > 0$ and $t_3 > t_0$ such that $l_{i_3}(t_3) = \max\limits_{k \in N_n} \left\{ \frac{\sup_{t \leq t_0} |\psi_k^{(1)}(\theta) - \psi_k^{(2)}(\theta)|}{\eta_k} \right\} + \epsilon_3$, and $l_j(t) \leq \max\limits_{k \in N_n} \left\{ \frac{\sup_{t \leq t_0} |\psi_k^{(1)}(\theta) - \psi_k^{(2)}(\theta)|}{\eta_k} \right\} + \epsilon_3$ for $t \in (-\infty, t_3]$ and $j \in N_n$, then $D^+ l_{i_3}(t)\Big|_{t=t_3} > 0$. In contrast

$$\begin{aligned} D^+ l_{i_3}(t)\Big|_{t=t_3} &\leq -\alpha_{i_3}(t_3) l_{i_3}(t_3) + \eta_{i_3}^{-1} \sum_{j=1}^{n} |\beta_{i_3 j}(t_3)| f_j \eta_j l_j(t_3) + \eta_{i_3}^{-1} \sum_{j=1}^{n} |\gamma_{i_3 j}(t_3)| G_j \eta_j \sup_{t_3 - \tau_{i_3 j}(t_3) \leq s \leq t_3} l_j(s) \\ &= -\alpha_{i_3}(t_3) \left(\max_{k \in N_n} \left\{ \frac{\sup_{t \leq t_0} |\psi_k^{(1)}(\theta) - \psi_k^{(2)}(\theta)|}{\eta_k} \right\} + \epsilon_3 \right) \\ &\quad + \eta_{i_3}^{-1} \sum_{j=1}^{n} |\beta_{i_3 j}(t_3)| F_j \eta_j \left(\max_{k \in N_n} \left\{ \frac{\sup_{t \leq t_0} |\psi_k^{(1)}(\theta) - \psi_k^{(2)}(\theta)|}{\eta_k} \right\} + \epsilon_3 \right) \\ &\quad + \eta_{i_3}^{-1} \sum_{j=1}^{n} |\gamma_{i_3 j}(t_3)| G_j \eta_j \left(\max_{k \in N_n} \left\{ \frac{\sup_{t \leq t_0} |\psi_k^{(1)}(\theta) - \psi_k^{(2)}(\theta)|}{\eta_k} \right\} + \epsilon_3 \right) \\ &= -\left[\alpha_{i_3}(t_3) - \eta_{i_3}^{-1} \sum_{j=1}^{n} (|\beta_{i_3 j}(t_3)| F_j + |\gamma_{i_3 j}(t_3)| G_j) \eta_j \right] \left(\max_{k \in N_n} \left\{ \frac{\sup_{t \leq t_0} |\psi_k^{(1)}(\theta) - \psi_k^{(2)}(\theta)|}{\eta_k} \right\} + \epsilon_3 \right) \leq 0, \end{aligned}$$

This is a contradiction. Then we get $l_i(t) \leq \max\limits_{k \in N_n} \left\{ \frac{\sup_{t \leq t_0} |\psi_k^{(1)}(\theta) - \psi_k^{(2)}(\theta)|}{\eta_k} \right\}$ for $t \geq t_0$ and $i \in N_n$. Construct the following inequalities:

$$\begin{cases} D^+ l_i(t) \leq -\alpha_i(t) l_i(t) + \eta_i^{-1} \sum\limits_{j=1}^{n} |\beta_{ij}(t)| F_j \eta_j l_j(t) + \eta_i^{-1} \sum\limits_{j=1}^{n} |\gamma_{ij}(t)| G_j \eta_j \sup\limits_{t-\tau_{ij}(t) \leq s \leq t} l_j(s), \quad t \geq T, \\ l_i(t) = l_i(t), \quad t \in (-\infty, T], \end{cases}$$

and define

$$\Gamma_i(\lambda) := \frac{\lambda}{\alpha_i} + \sum_{j=1}^{n} \rho e^{\lambda \tau_{ij}} - 1.$$

Similar to the proof of Theorem 2, one can find a $\lambda > 0$ such that

$$l_i(t) \le \max_{k\in N_n}\left\{\frac{\sup_{t\le t_0}|\psi_k^{(1)}(\theta)-\psi_k^{(2)}(\theta)|}{\eta_k}\right\}e^{-\lambda\int_T^t\alpha(u)du}, \quad t\in[T,+\infty).$$

then we have following estimates

$$|q_i^{(1)}(t)-q_i^{(2)}(t)| \le \max_{k\in N_n}\left\{\frac{\sup_{t\le t_0}|\psi_k^{(1)}(\theta)-\psi_k^{(2)}(\theta)|}{\eta_k}\right\}\eta_i, \quad t\in[t_0,T],$$

and

$$|q_i^{(1)}(t)-q_i^{(2)}(t)| \le \max_{k\in N_n}\left\{\frac{\sup_{t\le t_0}|\psi_k^{(1)}(\theta)-\psi_k^{(2)}(\theta)|}{\eta_k}\right\}\eta_i e^{-\lambda^*\int_T^t\alpha(s)ds}, \quad t\ge T.$$

This completes the proof. □

Remark 6. *Theorem 3 implies system (1) is globally generalized exponential stable. In fact that for $t\in[t_0,T)$, from the nonnegativity of $\alpha(u)$, we get*

$$\begin{aligned}\|q^{(1)}(t)-q^{(2)}(t)\| &\le \max_{k\in N_n}\left\{\frac{\sup_{t\le t_0}|\psi_k^{(1)}(\theta)-\psi_k^{(2)}(\theta)|}{\eta_k}\right\}e^{-\lambda\int_{t_0}^t\alpha(u)du}e^{\lambda\int_{t_0}^t\alpha(u)du}\\ &= C_T\max_{k\in N_n}\left\{\frac{\sup_{t\le t_0}|\psi_k^{(1)}(\theta)-\psi_k^{(2)}(\theta)|}{\eta_k}\right\}e^{-\lambda\int_{t_0}^t\alpha(u)du},\end{aligned}$$

where $C_T = e^{\lambda^*\int_{t_0}^T\alpha(s)ds}$. For $t\ge T$, we get

$$\begin{aligned}\|q^{(1)}(t)-q^{(2)}(t)\| &\le \max_{k\in N_n}\left\{\frac{\sup_{t\le t_0}|\psi_k^{(1)}(\theta)-\psi_k^{(2)}(\theta)|}{\eta_k}\right\}e^{-\lambda\int_{t_0}^t\alpha(u)du}e^{\lambda\int_{t_0}^T\alpha(u)du}\\ &= C_T\max_{k\in N_n}\left\{\frac{\sup_{t\le t_0}|\psi_k^{(1)}(\theta)-\psi_k^{(2)}(\theta)|}{\eta_k}\right\}e^{-\lambda\int_{t_0}^t\alpha(u)du}.\end{aligned}$$

So from the above, we get

$$\|q^{(1)}(t)-q^{(2)}(t)\| \le C_T\max_{k\in N_n}\left\{\frac{\sup_{t\le t_0}|\psi_k^{(1)}(\theta)-\psi_k^{(2)}(\theta)|}{\eta_k}\right\}e^{-\lambda\int_{t_0}^t\alpha(u)du}, \quad t\ge t_0.$$

Then system (1) is globally generalized exponential stable.

Remark 7. *Lu et al. [38] considered the globally generalized exponential stability of (1). Under condition* (**C.2**) *and the following conditions*

(**C.1′**) *For each $i,j\in N_n$, $\alpha_i(s)>0$, $\beta_{ij}(s)$, $\gamma_{ij}(s)$ and $I_i(s)$ are all continuous functions defined on $[t_0,+\infty)$.*

(**C.6′**) *For each $i\in N_n$,*

$$\sum_{j=1}^n(|\beta_{ij}(t)|F_j+|\gamma_{ij}(t)|G_j)\le\alpha_i(t), \quad t\in[t_0,+\infty),$$

and

$$\limsup_{t\to+\infty}\left\{\frac{\sum\limits_{j=1}^{n}(|\beta_{ij}(t)|F_j+|\gamma_{ij}(t)|G_j)}{\alpha_i(t)}\right\}<1.$$

(**C**.7′) *For $i,j\in N_n$, there exists a $l\in N_n$ such that*

$$\lim_{t\to+\infty}\int_0^t\alpha_l(s)ds\to+\infty,\quad \sup_{t-\tau_{ij}(t)\geq 0}\left\{\int_{t-\tau_{ij}(t)}^t\alpha_l(s)ds\right\}<+\infty,\quad \textit{and}\quad \sup_{t\geq t_0}\left\{\frac{\alpha_l(s)}{\alpha_i(s)}\right\}<\infty.$$

Then, system (1) is globally generalized exponential stable. We mention here that if we choose $\eta_1=\eta_2=\ldots=\eta_n=1$, then our condtions are similar to the conditions in [38], but less conservative, the results in [38] do not work if $\alpha_i(t)=0$ at some time, or $\sup\limits_{t-\tau_{ij}(t)\geq t_0}\left\{\int_{t-\tau_{ij}(t)}^t\alpha_i(s)ds\right\}=+\infty$ for all $i\in N_n$. Besides, $\sup\limits_{t-\tau_{ij}(t)\geq t_0}\left\{\int_{t-\tau_{ij}(t)}^t\alpha_i(s)ds\right\}=+\infty$ is quite restrictive. For instance, when $\alpha_i(t)=c>0$, and the delay functions are infinite, then the condition $\sup\limits_{t-\tau_{ij}(t)\geq t_0}\left\{\int_{t-\tau_{ij}(t)}^t\alpha_i(s)ds\right\}=+\infty$ is not satisfied. However, in such cases, we have the flexibility to select a suitable $\alpha(t)$ that aligns with our condtions. so this paper enhances and broadens the results in [38].

4. Examples

This section gives four illustrative examples to demonstrate the practical applicability of the theoretical results. To enhance the clarity of the obtained results, we employ a linear representation instead of a nonlinear one.

Example 1. *Consider the following NNs with proportional delays:*

$$\frac{dq_i(t)}{dt}=-\alpha_i(t)q_i(t)+\sum_{j=1}^{2}\left[\beta_{ij}(t)f_j(q_j(t))+\gamma_{ij}(t)g_j(q_j(0.5t))\right]+h_i(t),\quad i=1,2,\quad t\in[0,+\infty),\tag{16}$$

*where $\alpha_1(t)=6(t^2+3t+1)$, $\alpha_2(t)=4(t^2+4t+1)$, $\beta_{11}(t)=t^2+4t+1$, $\beta_{12}(t)=2(t^2+2t+1)$, $\beta_{21}(t)=t^2+6t+1$, $\beta_{22}(t)=t^2+5t+1$, $\gamma_{11}(t)=2(t^2+t+1)$, $\gamma_{12}(t)=t^2+5t+1$, $\gamma_{21}(t)=t^2+3t+1$, $\gamma_{22}(t)=t^2+1$, $h_1(t)=60t$, $h_2(t)=60t$, $\tau_{11}(t)=\tau_{21}(t)=\tau_{12}(t)=\tau_{22}(t)=0.5t$, $f_1(q_1)=f_2(q_1)=g_1(q_1)=g_2(q_1)=|q_1|$, $\psi(0)=(15,15)$. It can be verified that, $F_1=F_2=G_1=G_2=1$. Obviously, $\eta_1=\eta_2=1$, $\mu_1=20$ and $\mu_2=20$. we can find conditions (**C**.**1**)–(**C**.**3**) are satisfied, from Theorem 1, we get*

$$|q_1(t)|\leq 20,\ |q_2(t)|\leq 20,\ t\geq 0.$$

Then system (16) is dissipative, while the ball $B(0,20)$ serves as both a globally attracting and an absorbing set, as depicted in Figure 1.

Remark 8. *All the coefficient and delay functions of Example (1) are unbounded.*

Example 2. *Consider the following NNs with proportional delays:*

$$\frac{dq_i(t)}{dt}=-\alpha_i(t)q_i(t)+\sum_{j=1}^{2}\left[\beta_{ij}(t)f_j(q_j(t))+\gamma_{ij}(t)g_j(q_j(0.5t))\right]+h_i(t),\quad i=1,2,\quad t\in[0,+\infty),\tag{17}$$

where $\alpha_1(t)=8(t+1)$, $\alpha_2(t)=6(t+2)$, $\beta_{11}(t)=t+1$, $\beta_{12}(t)=4(t+1)$, $\beta_{21}(t)=0.5(t+2)$, $\beta_{22}(t)=t+2$, $\gamma_{11}(t)=t+1$, $\gamma_{12}(t)=2(t+1)$, $\gamma_{21}(t)=0.25(t+2)$, $\gamma_{22}(t)=t+2$, $h_1(t)=60(t+1)$, $h_2(t)=25(t+2)$, $\tau_{11}(t)=\tau_{21}(t)=\tau_{12}(t)=\tau_{22}(t)=0.5t$, $f_1(q_1)=f_2(q_1)=g_1(q_1)=g_2(q_1)=|q_1|$ and $\psi^{(1)}(0)=(40,20)$ and $\psi^{(2)}(0)=(10,10)$.

It can be verified that, $F_1 = F_2 = G_1 = G_2 = 1$, $\rho_{11}^{(1)} = \frac{1}{8}$, $\rho_{12}^{(1)} = \frac{1}{2}$, $\rho_{21}^{(1)} = \frac{1}{12}$, $\rho_{22}^{(1)} = \frac{1}{6}$, $\rho_{11}^{(2)} = \frac{1}{8}$, $\rho_{12}^{(2)} = \frac{1}{4}$, $\rho_{21}^{(2)} = \frac{1}{24}$, $\rho_{22}^{(2)} = \frac{1}{6}$.

Choose $\eta_1 = 1$, $\eta_2 = 0.5$ *and* $\alpha(t) = \frac{1}{t+1}$, *then* $\sup_{t\geq 0}\left\{\int_{0.5t}^{t} \frac{1}{s+1} ds\right\} = \ln 2$, $\alpha_1 = 8$ *and* $\alpha_2 = 6$. *One can find* $\lambda_1 = \lambda_2 = 1$, *and* $\mu_1 = \mu_2 = 20$. *Then conditions of* (**C.1**)–(**C.5**) *are satisfied, for different initial values* $\psi^{(1)}$ *and* $\psi^{(2)}$, *from Theorem 2, we get*

$$
\begin{aligned}
&|q_1^{(1)}(t)| \leq \frac{20}{t+1} + 20, \quad |q_2^{(1)}(t)| \leq \frac{10}{t+1} + 10,\\
&|q_1^{(2)}(t)| \leq 20, \quad |q_2^{(2)}(t)| \leq 10,\\
&|q_1^{(1)}(t) - q_1^{(2)}(t)| = \frac{30}{t+1}, \quad |q_2^{(1)}(t) - q_2^{(2)}(t)| = \frac{15}{t+1},
\end{aligned}
$$

which are shown in Figures 2–4, respectively.

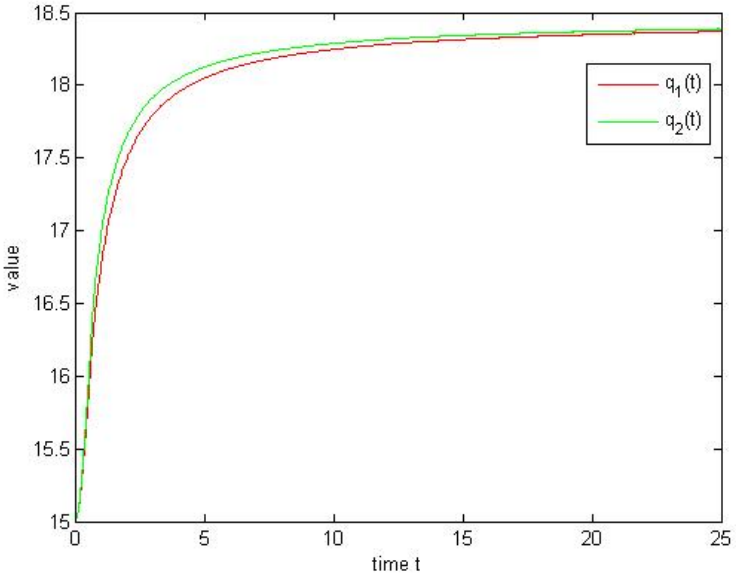

Figure 1. $q_1(t)$ and $q_2(t)$ of Example 1.

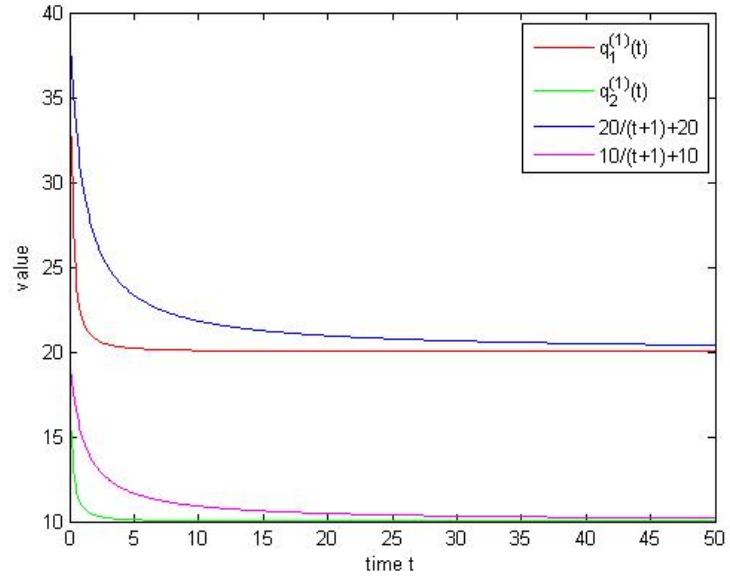

Figure 2. $q_1^{(1)}(t)$ and $q_2^{(1)}(t)$ of Example 2 and their estimates.

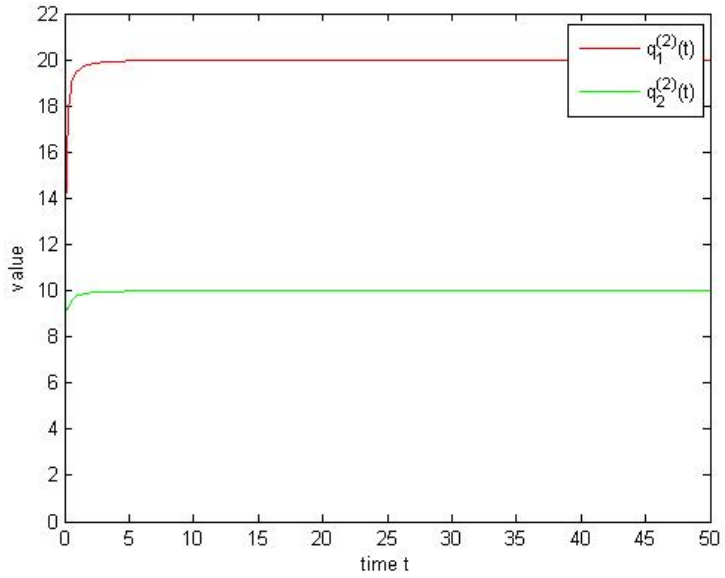

Figure 3. $q_1^{(2)}(t)$ and $q_2^{(2)}(t)$ of Example 2.

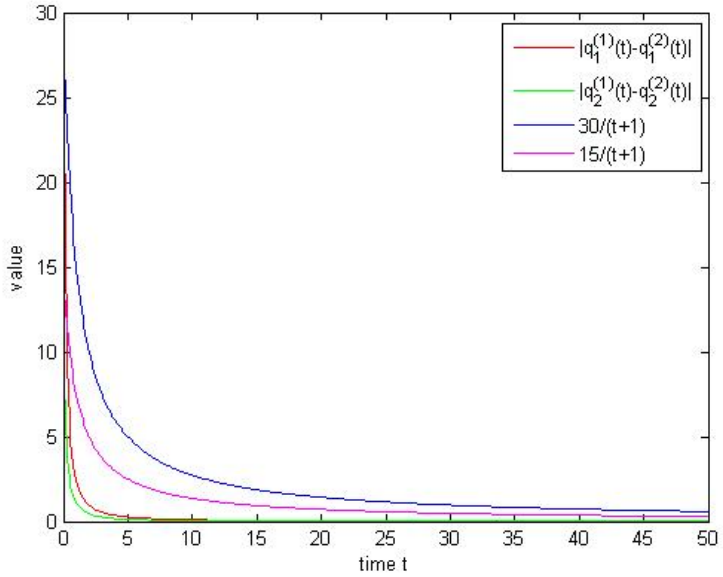

Figure 4. $|q_1^{(1)}(t) - q_1^{(2)}(t)|$ and $|q_2^{(1)}(t) - q_2^{(2)}(t)|$ of Example 2 and their estimates.

Remark 9. *All the coefficient, activation and delay functions in Example 2 are unbounded, and* $\sup_{t\geq 0} \int_{0.5t}^{t} \alpha_i(s)ds = +\infty$, *for* $i = 1, 2$, *which means that the results in [22,26,27,32,33,35–38] can not solve this case.*

Example 3. *Consider the following 2-dimensional NNs with time-varying delays:*

$$\frac{dq_i(t)}{dt} = -\alpha_i(t)q_i(t) + \sum_{j=1}^{2}\left[\beta_{ij}(t)f_j(q_j(t)) + \gamma_{ij}(t)g_j(q_j(t-\tau_{ij}(t)))\right] + h_i(t), \quad i = 1,2, \quad t \in [0,+\infty), \tag{18}$$

where, $\alpha_1(t) = 5(1-\sin t)$, $\alpha_2(t) = 7(1-\sin t)$, $\beta_{11}(t) = 1-\sin t$, $\beta_{12}(t) = 5(1-\sin t)$, $\beta_{21}(t) = 0.4(1-\sin t)$, $\beta_{22}(t) = 2(1-\sin t)$, $\gamma_{11}(t) = (1-\sin t)e^{-\pi-2}$, $\gamma_{12}(t) = 5(1-\sin t)e^{-\pi-2}$, $\gamma_{21}(t) = 0.4(1-\sin t)e^{-\pi-2}$, $\gamma_{22}(t) = (1-\sin t)e^{-\pi-2}$, $h_1(t) = 20(1-$

$\sin t)(3-2e^{-\pi-2})$, $h_2(t)=12(1-\sin t)(1-e^{-\pi-2})$, $\tau_{11}(t)=\tau_{21}(t)=\tau_{12}(t)=\tau_{22}(t)=\pi|\cos t|$, $f_1(q_1)=f_2(q_1)=g_1(q_1)=g_2(q_1)=|q_1|$, $\psi^{(1)}(0)=(40,8)$ *and* $\psi^{(2)}(0)=(1,1)$.

It can be verified that, $F_1=F_2=G_1=G_2=1$, $\rho_{11}^{(1)}=\frac{1}{5}$, $\rho_{12}^{(1)}=1$, $\rho_{21}^{(1)}=\frac{2}{35}$, $\rho_{22}^{(1)}=\frac{2}{7}$, $\rho_{11}^{(2)}=\frac{1}{5e^{\pi+2}}$, $\rho_{12}^{(2)}=\frac{1}{e^{\pi+2}}$, $\rho_{21}^{(2)}=\frac{2}{35e^{\pi+2}}$, $\rho_{22}^{(2)}=\frac{1}{7e^{\pi+2}}$.

Choose $\eta_1=1$, $\eta_2=0.2$ *and* $\alpha(t)=1-\sin t$, *then* $\sup\limits_{t\geq 0}\int_{t-\tau_{ij}(t)}^{t}\left(1-\sin s\right)^{*}ds=\pi+2$, $\alpha_1=5$ *and* $\alpha_2=7$. *We can find* $\lambda_1=\lambda_2=1$, *and* $\mu_1=\mu_2=20$. *Then conditions* (**C.1**)–(**C.5**) *are satisfied, for different initial values* $\psi^{(1)}$ *and* $\psi^{(2)}$, *from Theorem 2, we get*

$$|q_1^{(1)}(t)|\leq 20e^{-t+1-cost}+20,\quad |q_2^{(1)}(t)|\leq 4e^{-t+1-cost}+4,$$
$$|q_1^{(2)}(t)|\leq 20,\quad |q_2^{(2)}(t)|\leq 4,$$
$$|q_1^{(1)}(t)-q_1^{(2)}(t)|=39e^{-t+1-cost},\quad |q_2^{(1)}(t)-q_2^{(2)}(t)|=7.8e^{-t+1-cost},$$

which are shown by Figures 5–7, respectively.

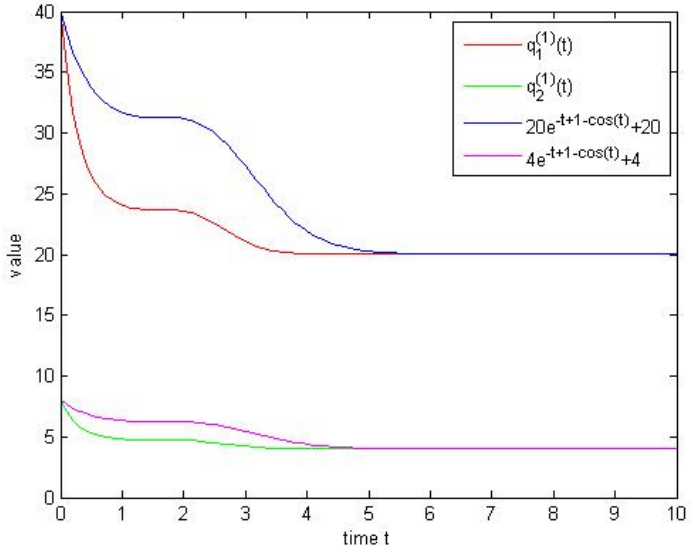

Figure 5. $q_1^{(1)}(t)$ and $q_2^{(1)}(t)$ of Example 3 and their estimates.

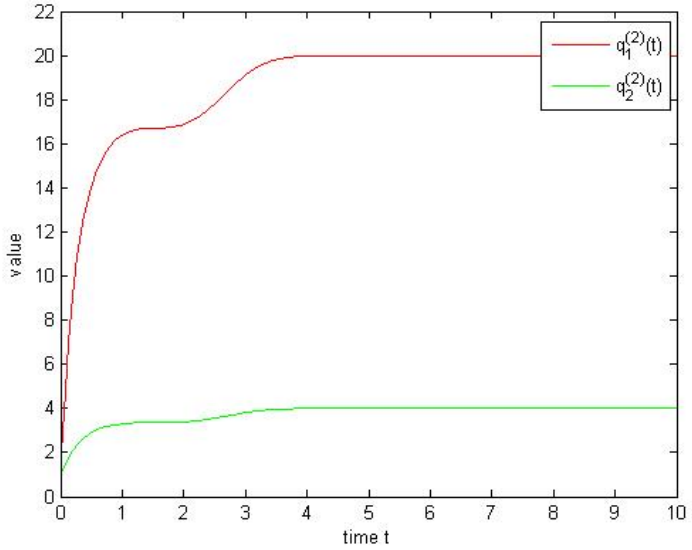

Figure 6. $q_1^{(2)}(t)$ and $q_2^{(2)}(t)$ of Example 3.

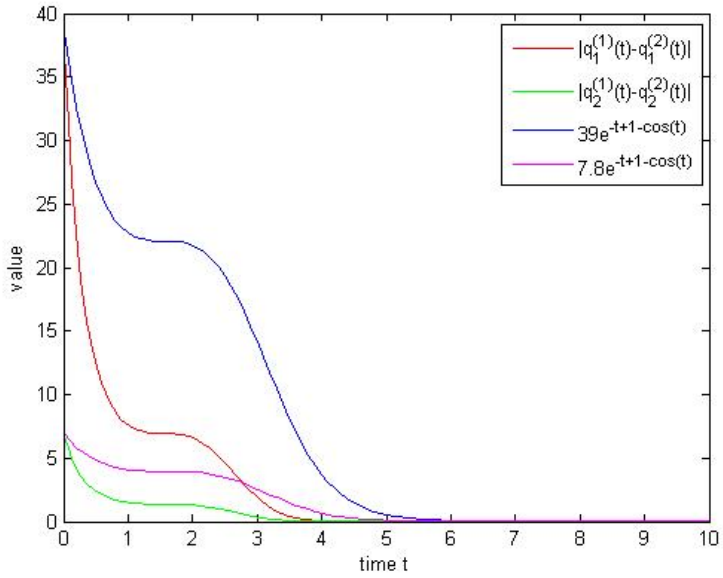

Figure 7. $|q_1^{(1)}(t) - q_1^{(2)}(t)|$ and $|q_2^{(1)}(t) - q_2^{(2)}(t)|$ of Example 3 and their estimates.

Remark 10. *It is worth noting that $\alpha_i(t) = 0$, for $t = \frac{\pi}{2} + 2k\pi$, $k \in \mathbb{N}$ and $i = 1, 2$ as well as the delay functions $\pi|\cos t|$ lack differentiability at points where $t = k\pi + \frac{\pi}{2}$ for $k \in \mathbb{N}$, which make the results in [22,26,28,32,33,36,37] be invalid.*

Example 4. *Consider the following 2-dimensional NNs with proportional delays:*

$$\frac{dq_i(t)}{dt} = -\alpha_i(t)q_i(t) + \sum_{j=1}^{2}\left[\beta_{ij}(t)f_j(q_j(t)) + \gamma_{ij}(t)g_j(q_j(t-\tau_{ij}(t)))\right] + h_i(t), \quad i = 1,2, \quad t \in [0,+\infty), \tag{19}$$

where $\alpha_1(t) = 8$, $\alpha_2(t) = 6$, $\beta_{11}(t) = \beta_{12}(t) = \beta_{21}(t) = \gamma_{11}(t) = \gamma_{12}(t) = \gamma_{21}(t) = 2$ for $t \in [0,5)$, $\beta_{11}(t) = \beta_{12}(t) = \beta_{21}(t) = \gamma_{11}(t) = \gamma_{12}(t) = \gamma_{21}(t) = 1$ for $t \geq 5$, $\beta_{12}(t) = \gamma_{22}(t) = 1$ for $t \in [0,5)$, $\beta_{12}(t) = \gamma_{22}(t) = 0.5$ for $t \geq 10$, $h_1(t) = 5$, $h_2(t) = 6$, $\tau_{11}(t) = \tau_{21}(t) = \tau_{12}(t) = \tau_{22}(t) = \sqrt{t+1}$, $f_1(q_1) = f_2(q_1) = g_1(q_1) = g_2(q_1) = |q_1|$, $\psi^{(1)}(t) = (40,8)$ and $\psi^{(2)}(t) = (1,1)$ for $t \in [-1,0]$.

It can be verified that, $F_1 = F_2 = G_1 = G_2 = 1$. Obviously, $\eta_1 = \eta_2 = 1$, then

$$\sum_{j=1}^{n}(|\beta_{ij}(t)|F_j + |\gamma_{ij}(t)|G_j) \leq \alpha_i(t), \quad t \in [0,+\infty),$$

and

$$\sup_{\{t|t\geq 5\}-\{t|\eta_i\alpha_i(t)=\sum_{j=1}^{n}(|\beta_{ij}(t)|F_j+|\gamma_{ij}(t)|G_j)\eta_j=0\}}\left\{\frac{\sum_{j=1}^{n}(|\beta_{ij}(t)|F_j + |\gamma_{ij}(t)|G_j)\eta_j}{\eta_i\alpha_i(t)}\right\} = 0.5 < 1.$$

Choose $\alpha(t) = \sqrt{\frac{5}{t}}$, $t \geq 5$, then $\alpha_1 = 8$, $\alpha_2 = 6$ and $\sup_{t-\sqrt{t+1}\geq 5}\left\{\int_{t-\sqrt{t+1}}^{t}\sqrt{\frac{5}{s}}\right\} = 4\sqrt{10} - 10$.
*We can find $\lambda^* \leq 0.245$. Then conditions of (**C.1**), (**C.2**), (**C.6**) and (**C.7**) are satisfied, from Theorem 3, we get the following estimate*

$$\|q^{(1)}(t) - q^{(2)}(t)\| \leq e_1(t) := \begin{cases} 20, & t \in [0,5], \\ 20e^{-0.245(2\sqrt{5t}-10)}, & t \in (5,+\infty), \end{cases}$$

which are illustrated by Figure 8.

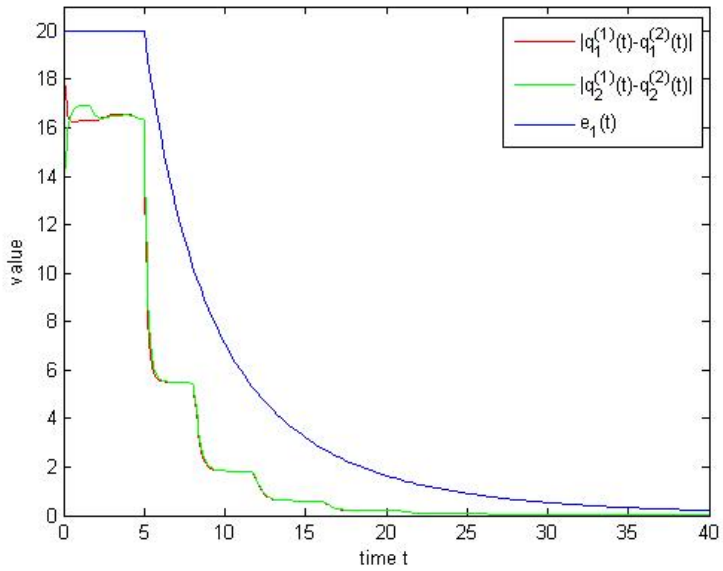

Figure 8. $q_1(t)$ and $q_2(t)$ of Example 4 and their estimate.

Remark 11. *We note that* $\sup_{t\geq 0}\int_{t-\sqrt{t+1}}^{t}\alpha_i(s)ds = +\infty$, *for* $i = 1, 2$, *which makes the results in [38] be invalid.*

5. Conclusions

In this paper, we obtained some criteria on dissipativity and globally generalized exponential stability of a class of NNs with delays by constructing some generalized Halanay inequalities. We mention here that our coefficient functions and delay functions can be all unbounded, and our results improve and generalize some existing works [5,35,38]. At last, four numerical examples have shown the effectiveness of our main results.

Our method has its limitations, when the $\alpha_i(t)$ is oscillation, such as $\alpha_i(t) = 0.5 + sint$, our method is invalid in this case. The author will investigate this case in the future.

Author Contributions: D.R.: Writing and original draft. Y.L.: Review and editing. All authors have read and agreed to the published version of the manuscript.

Funding: This research was funded by Talent Special Project of Guangdong Polytechnic Normal University (2021SDKYA053 and 2021SDKYA068), Guangzhou Basic and Applied Basic Research Foundation (2023A04J0031 and 2023A04J0032) and Young Innovative Talents Project of Guangdong Universities (2021KQNCX130).

Data Availability Statement: No data was used for the research described in the article.

Conflicts of Interest: The authors declare that they have no competing interests.

References

1. Hu, X.; Feng, G.; Duan, S.; Liu, L. Multilayer rtd-memristor-based cellular neural networks for color image processing. *Neurocomputing* **2015**, *162*, 150–162. [CrossRef]
2. Suganthan, P.N.; Teoh, E.K.; Mital, D.P. Pattern recognition by homomorphic graph matching using Hopfield neural networks. *Image Vis. Comput.* **2015**, *13*, 45–60. [CrossRef]
3. Liu, D.; Michel, A.N. Cellular neural networks for associative memories. *IEEE Trans. Circuits Syst. II Analog. Digit. Signal Process.* **1993**, *40*, 119–121. [CrossRef]
4. Feng, Z.; Lam, J. Stability and dissipativity analysis of distributed delay cellular neural networks. *IEEE Trans. Neural Netw.* **2011**, *22*, 976–981. [CrossRef]
5. Hien, L.V.; Phat, V.N.; Trinh, H. On global dissipativity of nonautonomous neural networks with multiple proportional delays. *IEEE Trans. Neural Netw. Learn. Syst.* **2018**, *29*, 225–231. [CrossRef] [PubMed]

6. Song, Q.; Zhao, Z. Global dissipativity of neural networks with both variable and unbounded delays. *Chaos Solitons Fractals* **2005**, *25*, 393–401. [CrossRef]
7. Zeng, H.; He, Y.; Shi, P.; Wu, M.; Xiao, S. Dissipativity analysis of neural networks with time-varying delays. *Neurocomputing* **2015**, *16*, 741–746. [CrossRef]
8. Chen, A.; Cao, J. Existence and attractivity of almost periodic solutions for cellular neural networks with distributed delays and variable coefficients. *Appl. Math. Comput.* **2003**, *134*, 125–140.
9. Ding, K.; Zhu, Q. Intermittent static output feedback control for stochastic delayed-switched positive systems with only partially measurable information. *IEEE Trans. Autom. Control* **2023**, *68*, 8150–8157. [CrossRef]
10. Xiao, Q.; Huang, T.; Zeng, Z. Stabilization of nonautonomous recurrent neural networks with bounded and unbounded delays on time scales. *IEEE Trans. Cybern.* **2019**, *50*, 4307–4317. [CrossRef]
11. Zhu, Q. Stabilization of stochastic nonlinear delay systems with exogenous disturbances and the event-triggered feedback control. *IEEE Trans. Autom. Control* **2019**, *64*, 3764–3771. [CrossRef]
12. Wang, B.; Zhu, Q. Stability analysis of discrete-time semi-Markov jump linear systems with time delay. *IEEE Trans. Autom. Control* **2023**, *68*, 6758–6765. [CrossRef]
13. Fan, L.; Zhu, Q.; Zheng, W. Stability analysis of switched stochastic nonlinear systems with state-dependent delay. *IEEE Trans. Autom. Control* **2023**. [CrossRef]
14. Xu, H.; Zhu, Q.; Zheng, W. Exponential stability of stochastic nonlinear delay systems subject to multiple periodic impulses. *IEEE Trans. Autom. Control* **2023**. [CrossRef]
15. Zhu, Z.; Zhu, Q. Adaptive event-triggered fuzzy control for stochastic highly nonlinear systems with time delay and non-triangular structure interconnections. *IEEE Trans. Fuzzy Syst.* **2023**. [CrossRef]
16. Cao, J.; Zhou, D. Stability analysis of delayed cellular neural networks. *Neural Netw.* **1998**, *11*, 1601–1605. [CrossRef]
17. Cao, J. New results concerning exponential stability and periodic solutions of delayed cellular neural networks. *Phys. Lett. A* **2003**, *307*, 136–147. [CrossRef]
18. Mohamad, S.; Gopalsamy, K. Exponential stability of continuous-time and discrete-time cellular neural networks with delays. *Appl. Math. Comput.* **2003**, *135*, 17–38. [CrossRef]
19. Sun, L.; Tang, Y.; Wang, W.; Shen, S. Stability analysis of time-varying delay neural networks based on new integral inequalities. *J. Frankl. Inst.* **2020**, *357*, 10828–10843. [CrossRef]
20. Zeng, Z.; Wang, J.; Liao, X. Global asymptotic stability and global exponential stability of neural networks with unbounded time-varying delays. *IEEE Trans. Neural Netw. Learn. Syst.* **2005**, *52*, 168–173.
21. Zhang, B.; Lam, J.; Xu, S. Stability analysis of distributed delay neural networks based on relaxed Lyapunov-Krasovskii functionals. *IEEE Trans. Neural Netw. Learn. Syst.* **2015**, *26*, 1480–1492. [CrossRef]
22. Zhang, Q.; Wei, X.; Xu, J. Delay-dependent exponential stability of cellular neural networks with time-varying delays. *Chaos Solitons Fractals* **2005**, *23*, 1363–1369. [CrossRef]
23. Zhao, H.; Cao, J. New conditions for global exponential stability of cellular neural networks with delays. *Neural Netw.* **2005**, *18*, 1332–1340. [CrossRef] [PubMed]
24. Zheng, C.; Zhang, H. New delay-dependent global exponential stability criterion for cellular-type neural networks with time-varying delays. *IEEE Trans. Neural Netw. Learn. Syst.* **2009**, *56*, 250–254.
25. Zhou, L.; Zhang, Y. Global exponential periodicity and stability of recurrent neural networks with multi-proportional delays. *ISA Trans.* **2016**, *60*, 89–95. [CrossRef]
26. Jiang, H.; Cao, J. Global exponential stability of periodic neural networks with time-varying delays. *Neurocomputing* **2006**, *70*, 343–350. [CrossRef]
27. Jiang, H.; Teng, Z. Global exponential stability of cellular neural networks with time-varying coefficients and delays. *Neural Netw.* **2004**, *17*, 1415–1425. [CrossRef]
28. Jiang, H.; Teng, Z. Boundedness and global stability for nonautonomous recurrent neural networks with distributed delays. *Chaos Solitons Fractals* **2006**, *30*, 83–93. [CrossRef]
29. Long, S.; Li, H.; Zhang, Y. Dynamic behavior of nonautonomous cellular neural networks with time-varying delays. *Neurocomputing* **2015**, *168*, 846–852. [CrossRef]
30. Rehim, M.; Jiang, H.; Li, Z.; Teng, Z. Boundedness and stability for nonautonomous cellular neural networks with delay. *Neural Netw.* **2004**, *17*, 1017–1025. [CrossRef]
31. Yu, T.; Cao, D.; Liu, S.; Chen, H. Stability analysis of neural networks with periodic coefficients and piecewise constant arguments. *J. Frankl. Inst.* **2016**, *353*, 409–425. [CrossRef]
32. Zhang, Q.; Wei, X.; Xu, J. Global exponential stability for nonautonomous cellular neural networks with delays. *Phys. Lett. A* **2006**, *351*, 153–160. [CrossRef]
33. Zhang, Q.; Wei, X.; Xu, J. Global exponential stability for nonautonomous cellular neural networks with unbounded delays. *Phys. Lett. A* **2009**, *39*, 1144–1151. [CrossRef]
34. Li, H.; Zhang, W.; Li, C.; Zhang, W. Global asymptotical stability for a class of non-autonomous impulsive inertial neural networks with unbounded time-varying delay. *Neural Comput. Appl.* **2019**, *31*, 6757–6766. [CrossRef]
35. Hien, L.V.; Son, D.T.; Trinh, H. New generalized Halanay inequalities with applications to stability of nonlinear non-autonomous time-delay systems. *Nonlinear Dyn.* **2015**, *82*, 563–575. [CrossRef]

36. Jiang, M.; Mu, J.; Huang, D. Globally exponential stability and dissipativity for nonautonomous neural networks with mixed time-varying delays. *Neurocomputing* **2016**, *205*, 421–429. [CrossRef]
37. Liu, B.; Lu, W.; Chen, T. Generalized Halanay inequalities and their applications to neural networks with unbounded time-varying delays. *IEEE Trans. Neural Netw.* **2011**, *22*, 1508–1513. [CrossRef]
38. Lu, B.; Jiang, H.; Abdurahman, A.; Hu, C. Global generalized exponential stability for a class of nonautonomous cellular neural networks via generalized Halanay inequalities. *Neurocomputing* **2016**, *214*, 1046–1052. [CrossRef]

mathematics

MDPI

Article

Synchronization for Reaction–Diffusion Switched Delayed Feedback Epidemic Systems via Impulsive Control

Ruofeng Rao [1,2,*] and Quanxin Zhu [3,*]

[1] College of Mathematics, Chengdu Normal University, Chengdu 611130, China
[2] School of Mathematical and Computational Science, Hunan University of Science and Technology, Xiangtan 411201, China
[3] School of Mathematics and Statistics, Hunan Normal University, Changsha 410081, China
* Correspondence: ruofengrao@cdnu.edu.cn (R.R.); zqx22@hunnu.edu.cn (Q.Z.)

Abstract: Due to the facts that epidemic-related parameters vary significantly in different stages of infectious diseases and are relatively stable within the same stage, infectious disease models should be switch-type models. However, research on switch-type infectious disease models is scarce due to the complexity and intricate design of switching rules. This scarcity has motivated the writing of this paper. By assuming that switching instants and impulse times occur at different moments, this paper proposes switch rules suitable for impulse control and derives synchronization criteria for reaction–diffusion switch-type infectious disease systems under impulse control. The effectiveness of this method is validated through numerical simulations. It is important to mention that, based on the information available to us, this paper is currently the sole study focusing on switch-type reaction–diffusion models for infectious diseases.

Keywords: reaction–diffusion; Lyapunov–Krasovskii functional; switched epidemic systems; impulsive control

MSC: 34K24; 34K45

1. Introduction

As is well known, infectious diseases exhibit significant diffusion effects, and, thus, reaction–diffusion epidemic models have been recently studied in the literature. Stability analysis and synchronization control of infectious disease models have theoretical implications in practical epidemic management [1,2]. For instance, in reference [3], the author explored the stability of the wavefront in a delayed monostable reaction–diffusion epidemic system. The motivation behind the extensive focus on the dynamical stability of infectious disease models is rooted in the inherent difficulty of completely eliminating such diseases. Achieving stability in the interaction between susceptible and infected populations is a crucial objective in the realm of infectious disease prevention and control [3–10]. Reference [4], for example, conducted research on susceptible–infected–recovered dynamics, taking into account the impact of the healthcare system. Their study considered a general incidence rate function and recovery rate dependent on the number of hospital beds, establishing the existence, uniqueness, and boundedness of the model. It extensively investigated all possible steady-state solutions and their stability. In another case, reference [5] explored an epidemic model incorporating an incubation period, newborns, and vaccination for susceptible individuals. Their study demonstrated global stability through Lyapunov functions. Reference [6] derived stability conditions for an infectious disease model with delays by constructing appropriate Lyapunov functionals. Reference [7] delved into an SIR epidemic model with nonlinear incidence and delay, discussing the local stability of equilibrium states, both disease-free and endemic, through the analysis of the corresponding characteristic equation. Moreover, synchronization control of infectious disease models

holds theoretical significance in practical epidemic management [1,2,11–15]. Reference [11] highlighted long-term spatiotemporal disease occurrence data indicating synchronization in many frequently occurring epidemics, especially childhood infections, between suburbs. The authors employed modeling techniques to elucidate the existence of synchronization phenomena. Reference [12] proposed a synchronization-based method for identifying parameters and estimating latent variables from real data in epidemic models. An adaptive synchronization method, based on an observer approach, was suggested, utilizing effective guiding parameters derived solely from real data. To validate identifiability and estimation results, a numerical simulation of a tuberculosis model was conducted using actual data from the central region of Cameroon. This study demonstrated that certain tools of nonlinear system synchronization can aid in addressing parameter and state estimation problems in the field of epidemiology. Reference [13] investigated synchronization between two identical susceptible–infected–recovered chaotic systems with fractional-order time derivatives.

The inclusion of a specific incubation period in infectious diseases necessitates the incorporation of models with delayed feedback in the mathematical modeling of these diseases. However, research in this field is very rare, which has motivated the writing of this article. Additionally, infectious diseases exhibit significant differences at different stages, and switch systems provide a good representation of infectious disease models. However, switch-type infectious disease models are seldom studied, providing another motivation for this article. Therefore, this article aims to investigate reaction–diffusion delayed feedback epidemic systems and intends to achieve synchronous control of infectious disease switch models through the use of pulse control techniques.

This article introduces innovations in three aspects:

- ◊ For the first time, this article introduces synchronous control of switch-type infectious disease models.
- ◊ For the first time, this article develops switching rules for infectious disease models.
- ◊ For the first time, this article successfully derives global exponential synchronization criteria specifically for impulse reaction–diffusion infectious disease models.

2. System Description

Recently, reaction–diffusion epidemic models have been studied in the literature. For instance, in the year 2020, reference [1] considered a reaction–diffusion epidemic model. In the year 2022, the authors of reference [2] investigated a delayed impulse reaction–diffusion epidemic model.

$$\begin{cases} \dfrac{\partial X(x,t)}{\partial t} = D\Delta X(x,t) + A(t)X(x,t) + \beta(t)f(t,X(x,t)), & x \in \Omega,\ t \geqslant t_0,\ t \neq t_k, \\ X(t_k^+,x) - X(t_k^-,x) = M_k X(t_k - v_k, x), & k \in \mathbb{N},\ x \in \Omega, \\ \dfrac{\partial X(x,t)}{\partial \nu} = 0, & x \in \partial\Omega,\ t \geqslant 0, \end{cases} \tag{1}$$

where $X(x,t) = (X_1(x,t), X_2(x,t), X_3(x,t))^T$, and the function $X_1(x,t)$ is the fraction of the susceptible population, $X_2(x,t)$ is the infected fraction, $X_3(x,t)$ is the recovered fraction, and $0 < X_i < 1$ for $i = 1,2,3$. In addition,

$$D = \begin{pmatrix} d_1 & 0 & 0 \\ 0 & d_2 & 0 \\ 0 & 0 & d_3 \end{pmatrix}, \quad A(t) = \begin{pmatrix} 0 & 0 & 0 \\ 0 & -\gamma(t) & 0 \\ 0 & \gamma(t) & 0 \end{pmatrix}, \quad f(t,X) = \begin{pmatrix} -X_1X_2 \\ X_1X_2 \\ 0 \end{pmatrix}, \tag{2}$$

Moreover, the disease transmission rate is denoted by $\beta(t)$, and the recovery rate is denoted by $\gamma(t)$. Taking into account the practical situation of delayed feedback in epidemic models, this paper considers the following delayed feedback epidemic model:

$$\begin{cases} \dfrac{\partial X(x,t)}{\partial t} = D_\sigma \Delta X(x,t) + A_\sigma X(x,t) + \beta_\sigma f(t, X(x,t)) + K_\sigma (X(x,t) - X(t - v(t), x)), \quad x \in \Omega,\ t \geqslant t_0,\ t \neq t_k, \\ X(t_k, x) = M_k X(t_k^-, x), \quad k \in \mathbb{N},\ x \in \Omega, \\ X(x,t) = 0, \quad x \in \partial\Omega,\ t \geqslant 0, \end{cases} \tag{3}$$

where K_σ is a family of positive definite diagonal matrices, which represents the delayed feedback parameters under the switching mode σ. Here, $\sigma \in \overline{N} \triangleq \{1, 2, \cdots, N\}$. t_k represents the moments of pulses, satisfying $0 < t_1 < t_2 < \cdots < t_k < t_{k+1} < \cdots$ with $\lim\limits_{k\to\infty} t_k = +\infty$. Assume that $X_i(t_k^+) = \lim\limits_{t\to t_k^+} X_i(t) = X_i(t_k)$, $i = 1, 2, 3$.

$$D_\sigma = \begin{pmatrix} d_{\sigma 1} & 0 & 0 \\ 0 & d_{\sigma 2} & 0 \\ 0 & 0 & d_{\sigma 3} \end{pmatrix}, \quad A_\sigma = \begin{pmatrix} 0 & 0 & 0 \\ 0 & -\gamma_\sigma & 0 \\ 0 & \gamma_\sigma & 0 \end{pmatrix}, \quad f(t, X) = \begin{pmatrix} -X_1 X_2 \\ X_1 X_2 \\ 0 \end{pmatrix}. \tag{4}$$

Here, β_σ and γ_σ are positive scalars for $\sigma \in \overline{N}$, and D_σ is the diffusion coefficient matrix.

System (3) is the drive system , and its response system can be considered as follows:

$$\begin{cases} \dfrac{\partial Y(x,t)}{\partial t} = D_\sigma \Delta Y(x,t) + A_\sigma Y(x,t) + \beta_\sigma f(t, Y(x,t)) + K_\sigma (Y(x,t) - Y(t - v(t), x)), \quad x \in \Omega,\ t \geqslant t_0,\ t \neq t_k, \\ Y(t_k, x) = M_k Y(t_k^-, x), \quad k \in \mathbb{N},\ x \in \Omega, \\ Y(x,t) = 0, \quad x \in \partial\Omega,\ t \geqslant 0, \end{cases} \tag{5}$$

Then, the error system is proposed as follows:

$$\begin{cases} \dfrac{\partial e(x,t)}{\partial t} = D_\sigma \Delta e(x,t) + A_\sigma e(x,t) + \beta_\sigma F(t, e(x,t)) + K_\sigma (e(x,t) - e(t - v(t), x)), \quad x \in \Omega,\ t \geqslant t_0,\ t \neq t_k, \\ e(t_k, x) = M_k e(t_k^-, x), \quad k \in \mathbb{N},\ x \in \Omega, \\ e(x,t) = 0, \quad t \geqslant 0,\ x \in \partial\Omega, \\ e(0, x) = \varphi(x), \quad x \in \Omega, \end{cases} \tag{6}$$

where $e = X - Y$, $v(t)$ is the time delay with $v(t) \in [-v, 0]$ and $v > 0$.

$$F(e(x,t)) = f(t, X(x,t)) - f(t, Y(x,t)) = \begin{pmatrix} -X_1 X_2 + Y_1 Y_2 \\ X_1 X_2 - Y_1 Y_2 \\ 0 \end{pmatrix} \tag{7}$$

Additionally, D_σ, A_σ, and f are defined in (4).

Obviously, $-1 < e_i < 1$.

Definition 1. *If the error system (6) is globally exponentially stable with a convergence rate of $\frac{\lambda}{2}$, then we say that system (5) globally exponentially synchronizes to system (3) with a synchronization rate of $\frac{\lambda}{2}$.*

Definition 2. *To establish the switching rule $\mathfrak{F}$:*

$$\sigma(t) = \arg\min \xi^T T_\sigma \xi. \tag{8}$$

($\mathfrak{F}_1$) Choose the initial mode $\sigma(t) = i_0$, if $\xi(t_0) \in \Gamma_{i_0}$.

($\mathfrak{F}_2$) For each $t > t_0$, if $\sigma(t^-) = i$ and $\xi \in \Gamma_i$, keep $\sigma(t) = i$. On the other hand, if $\sigma(t^-) = i$ but $\xi \notin \Gamma_i$, i.e., hitting a switching surface, choose the next mode by applying (8) and begin to switch.

Here, we assume that the switching moment and the impulse moment do not occur simultaneously and

$$\Gamma_i = \{\xi \in R^3, \xi^T T_i \xi < 0\}, i = 1, 2, \cdots, N, \tag{9}$$

$$T_\sigma \triangleq \frac{\lambda_{\max}(\Theta_\sigma)}{\lambda_{\min}(P)} P - (\varsigma - \lambda)P,$$

and

$$\Theta_\sigma = -\lambda_1(PD_\sigma + D_\sigma P) + PA_\sigma + A_\sigma^T P + PK_\sigma + K_\sigma P + 5\beta_\sigma E + PK_\sigma + \mu e^{\lambda v}\lambda_{\max}(K_\sigma)P,$$

where $\mu \geqslant 1$ is a scalar, E is an identity matrix, P is an undetermined positive definite symmetric matrix, and λ_1 is the smallest positive eigenvalue of the following eigenvalue problem:

$$\begin{cases} -\Delta\varphi(x) = \lambda\varphi(x), & x \in \Omega \subset \mathbb{R}^n, \\ \varphi(x) = 0, & x \in \partial\Omega. \end{cases}$$

Remark 1. *Firstly, from Figure 1, we can see that the pulse moment and the switching moment do not occur simultaneously. That is, the state transition curve does not exhibit a pulse burst shape. The dynamic indications caused by the pulse only show significant changes around the switching points. Secondly, the idea of state-dependent switching can be briefly described in Figure 1. The solutions initiate from different initial points within mode 1 (Ω_1). Subsequently, upon reaching the boundary of mode 1, where it intersects exclusively with mode 2 (Ω_2), the system transitions to mode 2, as illustrated by the blue curve in Figure 1. Similarly, when reaching the boundary of mode 1 that intersects exclusively with mode 3 (Ω_3), the system switches to mode 3, represented by the red curve in Figure 1. Lastly, upon reaching the boundary of mode 1, which intersects with both mode 2 and mode 3, the system undergoes a switch to the mode determined by the minimum of law (8), as depicted by the black curve in Figure 1.*

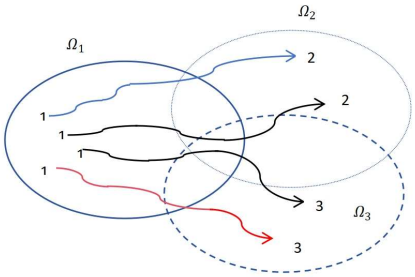

Figure 1. Switching behavior under impulse.

Lemma 1 ([16]). *Let $x \in R^n$, $y \in R^n$, and $\varepsilon > 0$. Then, we have*

$$x^T y + y^T x \leqslant \varepsilon x^T x + \varepsilon^{-1} y^T y.$$

Lemma 2 ([17]). *Suppose $V \in v_0$ and several positive scalars $p, c, k_1, k_2, \varsigma, \lambda > 0, \mu \geqslant 1$, and $\varsigma - \lambda \geqslant c$, satisfying:*

(i) $a_1\|x\|^p \leqslant V(t,x) \leqslant a_2\|x\|^p$, for any $t \in \mathbb{R}_+$ and $x \in \mathbb{R}^n$;

(ii) $\mathcal{D}^+V(t,\varphi(0)) \leqslant cV(t,\varphi(0))$, $t \in [t_{k-1}, t_k)$, $k \in \mathbb{N}$, whenever $qV(t,\varphi(0)) \geqslant V(t+s,\varphi(s))$ for $s \in [-v, 0]$, where $q \geqslant \mu e^{\lambda v}$ is a scalar;

(iii) $V(t_k, \varphi(0) + I_k(t_k,\varphi)) \leqslant d_k V(t_k^-, \varphi(0))$, where $0 < d_{k-1} \leqslant 1, \forall\, k \in \mathbb{N}$, are scalars;

(iv) $\varsigma \geqslant \frac{1}{d_{k-1}}$ and $\ln d_{k-1} < -(\varsigma + \lambda)(t_k - t_{k-1}), k \in \mathbb{N}$.

Then, the null solution of the delayed differential equation with impulse

$$\begin{cases} \dot{x}(t) = f(t, x_t), & t \neq t_k,\ t \geqslant t_0,\ k \in \mathbb{Z}_+; \\ \Delta x(t_k) = I_k(t_k, x_{t_k^-}) k \in \mathbb{Z}_+; \\ x_{t_0} = \varphi. \end{cases}$$

is globally exponentially stable with a convergent rate $\frac{\lambda}{p}$ *for any time delays* $v \in (0, \infty)$.

3. Main Results

Theorem 1. *System (5) globally exponentially asymptotically synchronizes with system (3), and its synchronization rate is* $\frac{\lambda}{2}$*, if the following conditions (a)–(c) are satisfied:*

(a) There is a scalar $m_0 > 0$ *such that*

$$0 < \lambda_{\max}(M_k) \leqslant m_0 < 1, \quad \forall\, k = 1, 2, \cdots \tag{10}$$

(b) There exist scalars $\varsigma > 0$ *and* $\lambda > 0$ *such that*

$$\varsigma \geqslant \frac{1}{m_0^2} \tag{11}$$

and

$$\ln m_0^2 < -(\varsigma + \lambda)(t_k - t_{k-1}), k \in \mathbb{N} \tag{12}$$

(c) There exist scalars $\alpha_i \geqslant 0$ *with* $\sum\limits_{i=1}^{N} \alpha_i = 1$ *such that*

$$\Lambda \triangleq \sum_{i=1}^{N} \alpha_i \frac{\lambda_{\max}(\Theta_i)}{\lambda_{\min}(P)} P - (\varsigma - \lambda)P < 0. \tag{13}$$

Proof. Consider the following Lyapunov–Krasovskii functional,

$$V(t) = \int_\Omega e^T(x,t) P e(x,t) dx. \tag{14}$$

Let $\|e(t)\|^2 = \int_\Omega e^T(x,t)e(x,t)dx$, where P is a positive definite symmetric matrix. Then, there are $k_1, k_2 > 0$ such that

$$k_1 \|e(t)\|^2 \leqslant V(t) \leqslant k_2 \|e(t)\|^2,$$

which satisfies condition (i) of Lemma 2.

Due to $0 < X_i < 1, 0 < Y_i < 1$, and (7), we can see this by using the differential along the trajectory of system (6) that

$$\begin{aligned}
\mathcal{D}^+ V &= 2\int_\Omega e^T(x,t) P \Big(D_\sigma \Delta e(x,t) + A_\sigma e(x,t) + \beta_\sigma F(t, e(x,t)) + K_\sigma (e(x,t) - e(t - v(t), x)) \Big) dx \\
&\leqslant \int_\Omega e^T(x,t) \Big(-\lambda_1 (P D_\sigma + D_\sigma P) + P A_\sigma + A_\sigma^T P + P K_\sigma + K_\sigma P \Big) e(x,t) dx + 2\beta_\sigma \int_\Omega e^T(t) F(t, e(t)) dx \\
&\quad - 2\int_\Omega e^T(t) P K_\sigma e(t - v(t)) dx \\
&\leqslant \int_\Omega e^T(x,t) \Big(-\lambda_1 (P D_\sigma + D_\sigma P) + P A_\sigma + A_\sigma^T P + P K_\sigma + K_\sigma P + 5\beta_\sigma E + P K_\sigma \Big) e(x,t) dx \\
&\quad + \int_\Omega e^T(t - v(t)) P K_\sigma e(t - v(t)) dx \\
&\leqslant \int_\Omega e^T(x,t) \Big(-\lambda_1 (P D_\sigma + D_\sigma P) + P A_\sigma + A_\sigma^T P + P K_\sigma + K_\sigma P + 5\beta_\sigma E + P K_\sigma \Big) e(x,t) dx \\
&\quad + \int_\Omega e^T(t - v(t)) P K_\sigma e(t - v(t)) dx
\end{aligned} \tag{15}$$

If there exists $\mu \geqslant 1$ such that $\mu e^{\lambda v} \int_\Omega e^T(x,t) P e(x,t) dx \geqslant \int_\Omega e^T(t - v(t), x) P e(t - v(t), x) dx$, by (15), we can obtain that

$$\begin{aligned}\mathcal{D}^+V &\leqslant \int_\Omega e^T(x,t)\Big(-\lambda_1(PD_\sigma + D_\sigma P) + PA_\sigma + A_\sigma^T P + PK_\sigma + K_\sigma P + 5\beta_\sigma E + PK_\sigma + \mu e^{\lambda v}\lambda_{\max}(K_\sigma)P\Big)e(x,t)dx \\ &\leqslant \int_\Omega e^T(x,t)\lambda_{\max}(\Theta_\sigma)e(x,t)dx \leqslant \frac{\lambda_{\max}(\Theta_\sigma)}{\lambda_{\min}(P)}\int_\Omega e^T(x,t)Pe(x,t)dx = \frac{\lambda_{\max}(\Theta_\sigma)}{\lambda_{\min}(P)}V(t)\end{aligned} \tag{16}$$

Next, we will derive the following inequlity based on the switching rule $\mathfrak{F}$ from (16).

$$\mathcal{D}^+V \leqslant (\varsigma - \lambda)\int_\Omega e^T(x,t)Pe(x,t)dx. \tag{17}$$

Firstly, we claim that

$$\bigcup_{i=1}^{N}\Gamma_i = R^3 \setminus \{0\} \tag{18}$$

Indeed, since there exist scalars $\alpha_i \geqslant 0$ with $\sum\limits_{i=1}^{N}\alpha_i = 1$ such that $\Lambda \triangleq \sum\limits_{i=1}^{N}\alpha_i\frac{\lambda_{\max}(\Theta_i)}{\lambda_{\min}(P)}P - (\varsigma - \lambda)P < 0$. Hence, utilizing proof by contradiction, it is not difficult to deduce the validity of equation (18). With the establishment of equation (18), we can now prove the validity of (17).

In fact, according to the switching law $\mathfrak{F}$, when $\sigma(t^-) = i$ and $e(x,t) \in \Gamma_i$, we can obtain, by the definition of T_i, that

$$0 > e(x,t)^T T_i e(x,t) = e(x,t)^T[\frac{\lambda_{\max}(\Theta_i)}{\lambda_{\min}(P)} - (\varsigma - \lambda)]e(x,t)^T$$

$$\mathcal{D}^+V \leqslant \frac{\lambda_{\max}(\Theta_i)}{\lambda_{\min}(P)}\int_\Omega e^T(x,t)Pe(x,t)dx \leqslant (\varsigma - \lambda)\int_\Omega e^T(x,t)Pe(x,t)dx$$

Note that the above expression also holds when $e(x,t) = 0$. Therefore, overall, we only need to consider the case where $e(x,t) \neq 0$.

When $\sigma(t^-) = i$ and $e(x,t) \notin \Gamma_i$, this means that the trajectory hits a switching surface. Due to (18), the minimum law (8) deduces that there must exist a Γ_j such that $e(x,t) \in \Gamma_j$ and

$$0 > e(x,t)^T T_j e(x,t) = e(x,t)^T[\frac{\lambda_{\max}(\Theta_j)}{\lambda_{\min}(P)} - (\varsigma - \lambda)]e(x,t)^T$$

$$\mathcal{D}^+V \leqslant \frac{\lambda_{\max}(\Theta_j)}{\lambda_{\min}(P)}\int_\Omega e^T(x,t)Pe(x,t)dx \leqslant (\varsigma - \lambda)\int_\Omega e^T(x,t)Pe(x,t)dx$$

To this end, we obtain $\mathcal{D}^+V \leqslant (\varsigma - \lambda)\int_\Omega e^T(x,t)Pe(x,t)dx$ if $\mu e^{\lambda v}V(t) \geqslant V(t - v(t))$, i.e.,

$$\mu e^{\lambda v}\int_\Omega e^T(x,t)Pe(x,t)dx \geqslant \int_\Omega e^T(t - v(t),x)Pe(t - v(t),x)dx$$

In other words, condition (ii) of Lemma 2 is satisfied.

Additionally,

$$V(t_k) = \int_\Omega e^T(t_k,x)Pe(t_k,x)dx = \int_\Omega e^T(t_k^-,x)M_k^T P M_k e(t_k^-,x)dx \leqslant m_0^2 V(t_k^-),$$

which implies that condition (iii) of Lemma 2 holds.

Furthermore, based on the conditions of Theorem 1, condition (iv) of Lemma 2 is satisfied.

Therefore, according to Lemma 2, error system (6) is globally exponentially stable with a convergence rate of $\frac{\lambda}{2}$. In other words, system (5) is globally exponentially synchronized with system (3), and its synchronization rate is $\frac{\lambda}{2}$. □

Remark 2. *Theorem 1 ingeniously addresses the challenges of synchronizing control that arise from the interplay of reaction–diffusion processes, time delays, and impulsive control. Specifically, it overcomes the mathematical difficulties induced by the diffusion term by employing Poincare inequalities, designs an appropriate Lyapunov function, sets suitable pulse intervals and pulse intensities, and, ultimately, achieves synchronization control through the utilization of the delayed-impulse inequalities lemma.*

Remark 3. *The switching rule of Theorem 1 is different from the switching rule in reference [18]. Meanwhile, synchronization control results for epidemic models have been achieved using impulse control. This is the first time that synchronization control has been obtained for a reaction–diffusion epidemic model under a switching rule.*

Discussion 1. *In epidemic prevention and control, the impulse moment is artificially determined and may not coincide with the switching moment. Therefore, this paper assumes that the impulse moment and switching moment do not occur simultaneously, which is reasonable. However, if one were to consider their simultaneous occurrence, the design of switching rules in this paper would need further consideration and discussion. This poses an interesting question worth exploring in more depth.*

Discussion 2. *Stochastic perturbations and stochastic models are widely employed in various fields, including infectious disease models ([6,19,20]). Exploring how to control the dynamics of infectious diseases through impulse control under stochastic perturbations is an intriguing question.*

4. Numerical Example

Now, we verify the effectiveness of Theorem 1 via the following numerical example.

Example 1. *Let* $\Omega = [0,1] \times [0,1] \subset R^2$. *Then,* $\lambda_1 = 2\pi^2 = 19.7392$ *([21], Remark 14). In addition, set* $N = 3$ *and* $\overline{N} = \{1,2,3\}$. *Then,* $\sigma \in \{1,2,3\}$. *Let* $\beta_1 = 0.1$, $\beta_2 = 0.15$, $\beta_3 = 0.2$, *and*

$$D_1 = \begin{pmatrix} 0.4 & 0 & 0 \\ 0 & 0.3 & 0 \\ 0 & 0 & 0.3 \end{pmatrix}, \quad A_1 = \begin{pmatrix} 0 & 0 & 0 \\ 0 & -0.1 & 0 \\ 0 & 0.1 & 0 \end{pmatrix}, \quad K_1 = \begin{pmatrix} 0.15 & 0 & 0 \\ 0 & 0.13 & 0 \\ 0 & 0 & 0.13 \end{pmatrix},$$

$$D_2 = \begin{pmatrix} 0.35 & 0 & 0 \\ 0 & 0.37 & 0 \\ 0 & 0 & 0.4 \end{pmatrix}, \quad A_2 = \begin{pmatrix} 0 & 0 & 0 \\ 0 & -0.15 & 0 \\ 0 & 0.15 & 0 \end{pmatrix}, \quad K_2 = \begin{pmatrix} 0.2 & 0 & 0 \\ 0 & 0.15 & 0 \\ 0 & 0 & 0.18 \end{pmatrix},$$

$$D_3 = \begin{pmatrix} 0.5 & 0 & 0 \\ 0 & 0.4 & 0 \\ 0 & 0 & 0.38 \end{pmatrix}, \quad A_3 = \begin{pmatrix} 0 & 0 & 0 \\ 0 & -0.2 & 0 \\ 0 & 0.2 & 0 \end{pmatrix}, \quad K_3 = \begin{pmatrix} 0.19 & 0 & 0 \\ 0 & 0.23 & 0 \\ 0 & 0 & 0.23 \end{pmatrix}.$$

Set $P = E$, $\mu = 1, v = 1, and \lambda = 1$. *Then,*

$$\Theta_1 = \begin{pmatrix} -14.4336 & 0 & 0 \\ 0 & -10.7458 & 0.1000 \\ 0 & 0.1000 & -10.5458 \end{pmatrix}, \quad \Theta_2 = \begin{pmatrix} -11.9238 & 0 & 0 \\ 0 & -13.1634 & 0.1500 \\ 0 & 0.1500 & -13.9577 \end{pmatrix},$$

$$\Theta_3 = \begin{pmatrix} -17.5340 & 0 & 0 \\ 0 & -13.9562 & 0.2000 \\ 0 & 0.2000 & -12.7366 \end{pmatrix}$$

$$\lambda_{\max}(\Theta_1) = -10.5044, \quad \lambda_{\max}(\Theta_2) = -11.9238, \quad \lambda_{\max}(\Theta_3) = -12.7046$$

$$\Theta_\sigma = -\lambda_1(PD_\sigma + D_\sigma P) + PA_\sigma + A_\sigma^T P + PK_\sigma + K_\sigma P + 5\beta_\sigma E + PK_\sigma + \mu e^{\lambda v}\lambda_{\max}(K_\sigma)P,$$

$$T_\sigma \triangleq \frac{\lambda_{\max}(\Theta_\sigma)}{\lambda_{\min}(P)} P - (\varsigma - \lambda)P,$$

Let

$$M_k = \begin{pmatrix} 0.9 & 0 & 0 \\ 0 & 0.89 & 0 \\ 0 & 0 & 0.88 \end{pmatrix}, k = 1, 2, \cdots$$

Then

$$m_0 = 0.9, \ \ m_0^2 = 0.81, \ \ \frac{1}{m_0^2} = 1.2346, \ \ \ln m_0^2 = -0.2107$$

Let $\varsigma = 1.3 > \frac{1}{m_0^2}$, $t_k - t_{k-1} \equiv 0.09$. *Then we obtain*

$$0 < \lambda_{\max}(M_k) \leqslant m_0 = 0.9 < 1, \quad \forall k = 1, 2, \cdots$$

$$\varsigma = 1.3 > \frac{1}{m_0^2}$$

and

$$\ln m_0^2 = -0.2107 < -0.2070 = -(\varsigma + \lambda)(t_k - t_{k-1}), \ k \in \mathbb{N}$$

Finally, let $\alpha_i = \frac{1}{3} \geqslant 0$ *with* $\sum_{i=1}^{3} \alpha_i = 1$. *We can see it that*

$$\Lambda = \sum_{i=1}^{3} \alpha_i \frac{\lambda_{\max}(\Theta_i)}{\lambda_{\min}(P)} P - (\varsigma - \lambda)P < 0.$$

Thus far, all conditions of Theorem 1 have been satisfied. Therefore, according to Theorem 1, error system (6) is globally exponentially stable with a convergence rate of $\frac{1}{2}$. *In other words, system (5) is globally exponentially asymptotically synchronized with system (3), and its synchronization rate is* $\frac{1}{2}$ *(see Figures 2–4).*

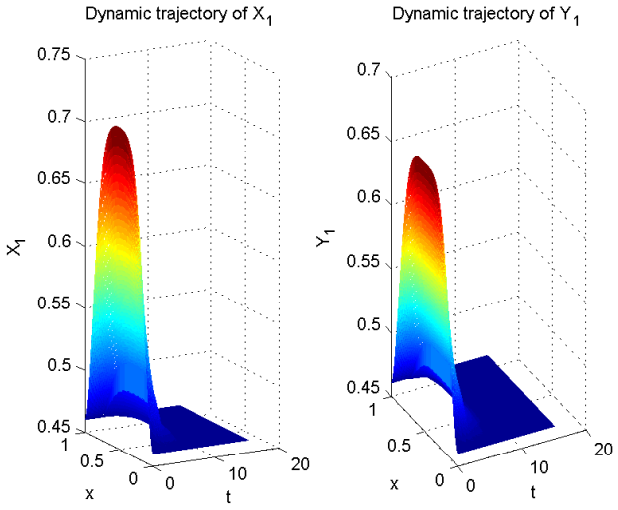

Figure 2. Numerical result of X_1 in (3) and Y_1 in (5).

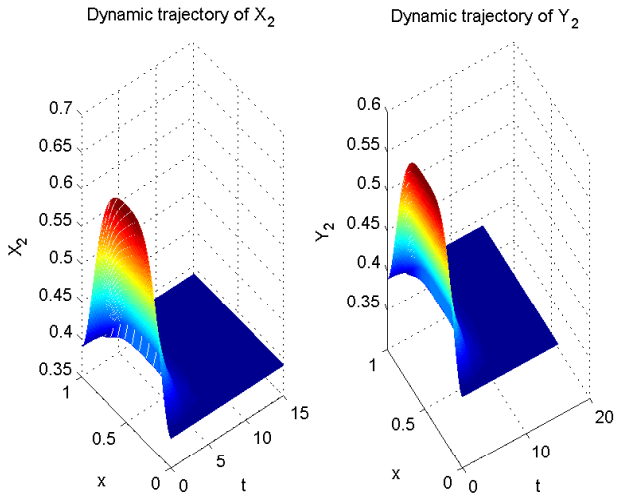

Figure 3. Numerical result of X_2 in (3) and Y_2 in (5).

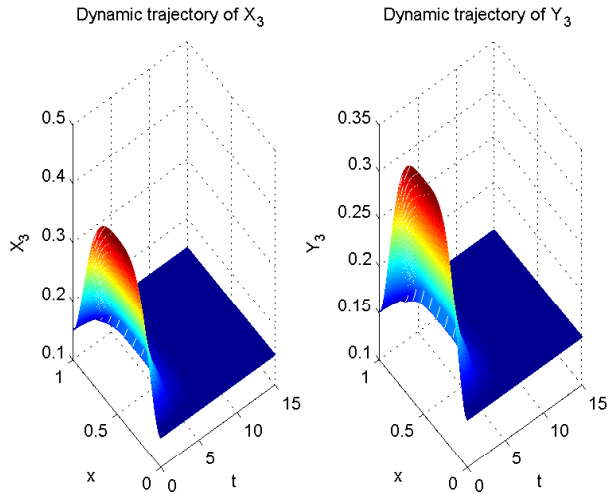

Figure 4. Numerical result of X_3 in (3) and Y_3 in (5).

Remark 4. *Numerical simulation results indicate that, despite the relatively small impulse strength, significant effectiveness in synchronizing control of the epidemic model can be achieved as long as an appropriate pulse interval is set. This validates the effectiveness of Theorem 1.*

Example 2. *In Example 1, let*

$$M_k = \begin{pmatrix} 0.5 & 0 & 0 \\ 0 & 0.5 & 0 \\ 0 & 0 & 0.49 \end{pmatrix}, k = 1, 2, \cdots$$

Then

$$m_0 = 0.5, \ \ m_0^2 = 0.25, \ \ \frac{1}{m_0^2} = 4, \ \ \ln m_0^2 = -1.3863$$

Let $\varsigma = 5$, $t_k - t_{k-1} \equiv 0.2$, *and other data of Example 1 hold unchanged. Then, we obtain* $\lambda = 1$ *and*

$$0 < \lambda_{\max}(M_k) \leqslant m_0 = 0.5 < 1, \quad \forall k = 1, 2, \cdots$$

$$\varsigma = 5 > 4 = \frac{1}{m_0^2}$$

and

$$\ln m_0^2 = -1.38637 < -1.2 = -(\varsigma + \lambda)(t_k - t_{k-1}),\ k \in \mathbb{N}$$

Finally, let $\alpha_i = \frac{1}{3} \geqslant 0$ *with* $\sum_{i=1}^{3} \alpha_i = 1$. *We can see it that*

$$\Lambda = \sum_{i=1}^{3} \alpha_i \frac{\lambda_{\max}(\Theta_i)}{\lambda_{\min}(P)} P - (\varsigma - \lambda)P < 0.$$

Thus far, all conditions of Theorem 1 have been satisfied. Therefore, according to Theorem 1, error system (6) is globally exponentially stable with a convergence rate of $\frac{1}{2}$. *In other words, system (5) is globally exponentially asymptotically synchronized with system (3), and its synchronization rate is* $\frac{1}{2}$ *(see Figures 5–7).*

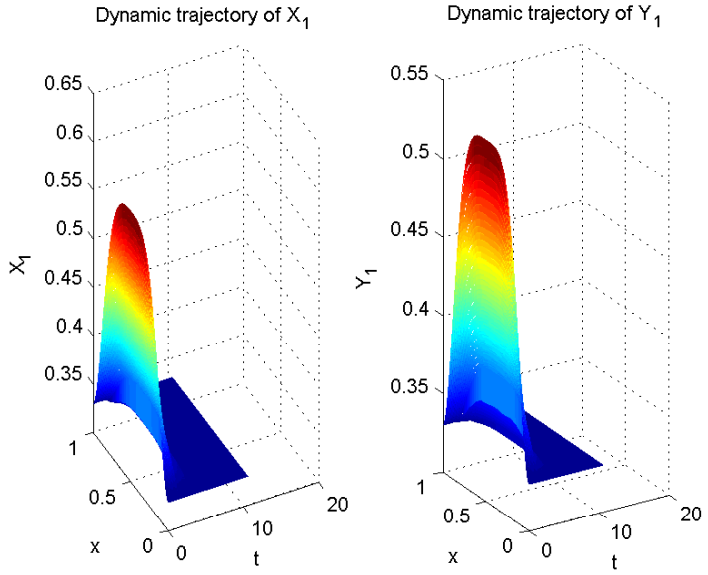

Figure 5. Numerical result of X_1 in (3) and Y_1 in (5).

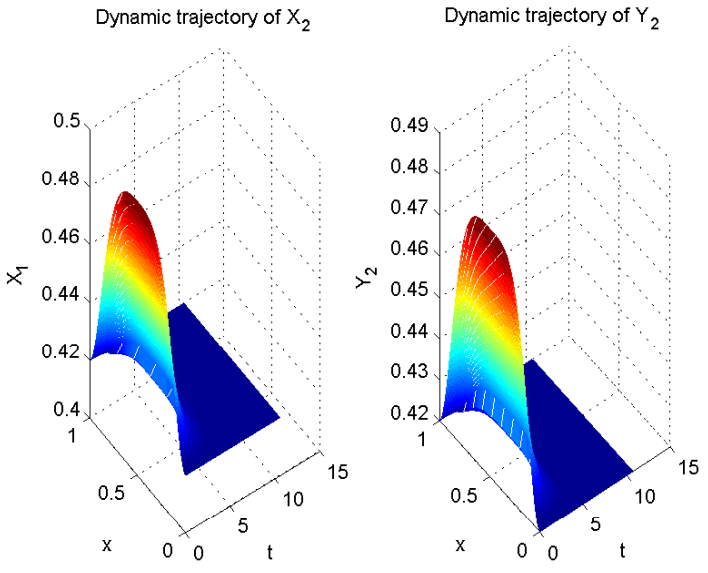

Figure 6. Numerical result of X_2 in (3) and Y_2 in (5).

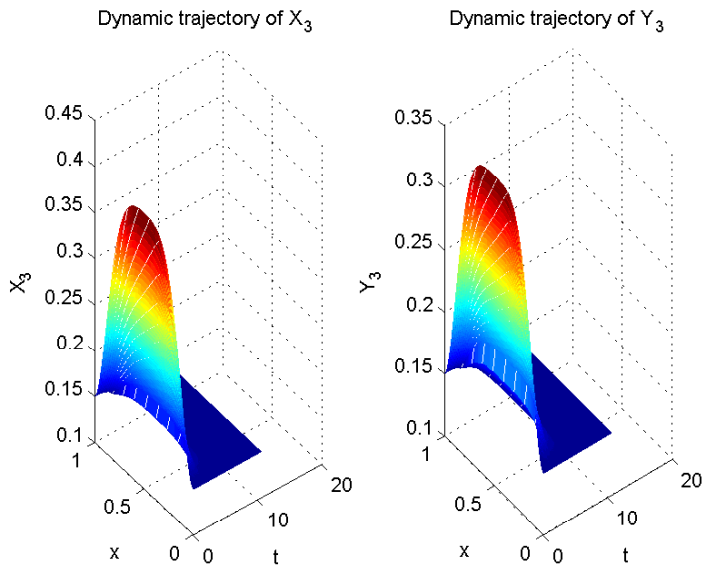

Figure 7. Numerical result of X_3 in (3) and Y_3 in (5).

Remark 5. *The numerical results indicate that, despite the enlargement of the impulse interval, as the impulse intensity increases, the convergence speed of synchronization still remains, which can be listed as Table 1:*

Table 1. Comparisons of Example 1 and Example 2.

	Impulse Interval	Impulse Frequency	Impulse Intensity	Intensity Degree	Convergent Rate
Example 1	0.09	↑	0.9	↓	1/2
Example 2	0.2	↓	0.5	↑	1/2

5. Conclusions

Synchronized control flow epidemic models have significant theoretical guidance, especially when there are substantial differences in the development stages of the epidemic. For instance, in the recent COVID-19 pandemic, various parameters, such as the number of infections and susceptible individuals, differ significantly across stages. The truth is that parameters related to different stages have notable distinctions. Impulse control, in essence, involves the momentary input intensity of artificial prevention measures and drug deployment treatment in different stages. Synchronized control under impulse measures allows for the gradual synchronization of heavily affected areas, where artificial measures are input in batches, in response to the evolving and fluctuating nature of the epidemic. This helps reduce the severity of the epidemic in heavily affected areas and gradually synchronize them with regions where the situation is improving. The synchronized control epidemic model offers significant theoretical guidance, especially when there are substantial differences in the development stages of the epidemic. Therefore, this paper considers a switching-type epidemic model. By establishing appropriate switching rules and utilizing impulse control techniques, global exponential synchronization criteria are obtained. Numerical examples demonstrate the effectiveness of the proposed methods. It is worth noting that this paper improves upon some existing methods in the literature and applies them for the first time to epidemic models, providing insights for a future series of related improvements.

Author Contributions: Conceptualization, R.R. and Q.Z.; methodology, R.R.; software, R.R.; validation, R.R. and Q.Z.; formal analysis, R.R. and Q.Z.; investigation, R.R.; resources, R.R.; data curation, R.R.; writing—original draft preparation, R.R.; writing—review and editing, R.R.; visualization, R.R.;

supervision, Q.Z.; project administration, Q.Z.; funding acquisition, Q.Z. All authors have read and agreed to the published version of the manuscript.

Funding: This research was funded by the Applied Basic Research Project of the Sichuan Provincial Department of Science and Technology (2020YJ0434).

Institutional Review Board Statement: Not applicable.

Informed Consent Statement: Not applicable.

Data Availability Statement: Data sharing is not applicable to this article.

Conflicts of Interest: The authors declare no conflict of interest.

References

1. Zhang, L.; Wang, Z.; Zhao, X. Time periodic traveling wave solutions for a Kermack-McKendrick epidemic model with diffusion and seasonality. *J. Evol. Equ*. **2020**, *20*, 1029–1059. [CrossRef]
2. Rao, R.; Lin, Z.; Ai, X.; Wu, J. Synchronization of Epidemic Systems with Neumann Boundary Value under Delayed Impulse. *Mathematics* **2022**, *10*, 2064. [CrossRef]
3. Yang, Y.; Li, W.; Wu, S. Exponential stability of traveling fronts in a diffusion epidemic system with delay. *Nonlinear Anal. RWA* **2011**, *12*, 1223–1234. [CrossRef]
4. Alqahtani, R. T. Mathematical model of SIR epidemic system (COVID-19) with fractional derivative: stability and numerical analysis. *Adv. Diff. Equ.* **2021**, *1*, 2. [CrossRef] [PubMed]
5. Li, J.; Yang, Y.; Zhou, Y. Global stability of an epidemic model with latent stage and vaccination. *Nonlinear Anal. RWA* **2011**, *12*, 2163–2173. [CrossRef]
6. Beretta, E.; Kolmanovskii, V.; Shaikhet, L. Stability of epidemic model with time delays influenced by stochastic perturbations. *Math. Comp. Simul.* **1998**, *45*, 269–277. [CrossRef]
7. Xu, R.; Ma, Z. Global stability of a SIR epidemic model with nonlinear incidence rate and time delay. *Nonlinear Anal. RWA* **2009**, *10*, 3175–3189. [CrossRef]
8. Khanafer, A.; Basar, T.; Gharesifard, B. Stability of epidemic models over directed graphs: A positive systems approach. *Automatica* **2016**, *74*, 126–134. [CrossRef]
9. Yi, N.; Zhang, Q.; Mao, K.; Yang, D.; Li, Q. Analysis and control of an SEIR epidemic system with nonlinear transmission rate. *Math. Comput. Model.* **2009**, *50*, 1498–1513. [CrossRef] [PubMed]
10. Zaman, G.; Kang, Y. H.; Jung, I. H. Stability analysis and optimal vaccination of an SIR epidemic model. *BioSystems* **2008**, *93*, 240–249. [CrossRef]
11. He, D.; Stone, L. Spatio-temporal synchronization of recurrent epidemics. *Proc. Royal Soc. Lond. Ser. B Biol. Sci.* **2003**, *270*, 1519–1526. [CrossRef] [PubMed]
12. Bowong, S., Kurths, J. Parameter estimation based synchronization for an epidemic model with application to tuberculosis in Cameroon. *Phys. Lett. A* **2010**, *374*, 4496–4505. [CrossRef]
13. Ansari, S. P.; Agrawal, S. K.; Das, S. Stability analysis of fractional-order generalized chaotic susceptible-infected-recovered epidemic model and its synchronization using active control method. *Pramana* **2015**, *84*, 23–32. [CrossRef]
14. Yan, G.; Fu, Z. Q.; Ren, J.; Wang, W. X. Collective synchronization induced by epidemic dynamics on complex networks with communities. *Phys. Rev. E* **2007**, *75*, 016108. [CrossRef]
15. Verma, T.; Gupta, A. K. Network synchronization, stability and rhythmic processes in a diffusive mean-field coupled SEIR model. *Commun. Nonlinear Sci. Numer. Simul.* **2021**, *102*, 105927 [CrossRef]
16. Wang, Z.; Liu, Y.; Yu, L.; Liu, X. Exponential stability of delayed recurrent neural networks with Markovian jumping parameters. *Phys. Lett. A* **2006**, *356*, 346–352. [CrossRef]
17. Wu, Q.; Zhou, J.; Xiang, L. Global exponential stability of impulsive differential equations with any time delays. *Appl. Math. Lett.* **2010**, *23*, 143–147. [CrossRef]
18. Yang, D.; Li, X.; Song, S. Design of state-dependent switching laws for stability of switched stochastic neural networks with time-delays. *IEEE Trans. Neural Netw. Learn. Syst.* **2020**, *31*, 1808–1819. [CrossRef]
19. Kumar, A. Light propagation through biological tissue: comparison between Monte Carlo simulation and deterministic models. *Int. J. Biomed. Eng. Technol.* **2009**, *2*, 344–351. [CrossRef]
20. Maini, D. S.; Aggarwal, A. K. Camera position estimation using 2D image dataset. *Int. J. Innov. Eng. Technol.* **2018**, *10*, 199–203.
21. Rao, R.; Huang, J.; Li, X. Stability analysis of nontrivial stationary solution and constant equilibrium point of reaction–diffusion neural networks with time delays under Dirichlet zero boundary value. *Neurocomputing* **2021**, *445*, 105–120. [CrossRef]

mathematics

MDPI

Article

Fractional-Order Model-Free Adaptive Control with High Order Estimation

Zhuo-Xuan Lv * and Jian Liao

School of Computer Science, Fudan University, Shanghai 200433, China; jliao@fudan.edu.cn
* Correspondence: lvzhuoxuan020309@outlook.com

Abstract: This paper concerns an improved model-free adaptive fractional-order control with a high-order pseudo-partial derivative for uncertain discrete-time nonlinear systems. Firstly, a new equivalent model is obtained by employing the Grünwald–Letnikov (G-L) fractional-order difference of the input in a compact-form dynamic linearization. Then, the pseudo-partial derivative (PPD) is derived using a high-order estimation algorithm, which provides more PPD information than the previous time. A discrete-time model-free adaptive fractional-order controller is proposed, which utilizes more past input–output data information. The ultimate uniform boundedness of the tracking errors are demonstrated through formal analysis. Finally, the simulation results demonstrate the effectiveness of the proposed method.

Keywords: model-free adaptive control; fractional-order; pseudo-partial derivative; discrete-time system

MSC: 37M15

1. Introduction

Recently, the model-free adaptive control (MFAC) method has attracted extensive attention; it does not need the specific dynamic characteristics of the control system, only input and output data [1]. Thanks to its fewer identification parameters and fewer calculations, as well as its wide range of applications, MFAC plays an important role in many fields and applications [2].

Different from the existing stability analysis for discrete-time (stochastic) systems [3–5], the main idea of MFAC is to use the concept of a pseudo-gradient to replace the general discrete-time nonlinear system with a series of dynamic linear time-varying models. In MFAC, the dynamic linear time-varying model has three main forms, namely, compact-form dynamic linearization (CFDL) [6], partial-form dynamic linearization (PFDL) [7], and full-form dynamic linearization (FFDL) [8]. In particular, by utilizing only input–output data information, equivalent models can be derived by means of the concept of a pseudo-partial derivative (PPD). Thus, the learning law can be established by treating the PPD as a time-varying parameter [9,10].

Using a virtual equivalent dynamic linearization data model, the time-varying PPD estimation algorithm was designed in [11], where the internal stability of the FFDL linearization-based MFAC scheme was rigorously presented. In [12], a new type of MFAC method based on an adaptive forgetting factor was proposed. In [13], by taking the affine structure of the ultra-local model and the extended state observer (ESO), a local PFDL-based ESO-MFAC was proposed to improve control performance. In order to make the MFAC scheme have a better performance, a PID-like MFAC with discrete (ESO) sparked interest in [14]. It is worth pointing out that the above-mentioned work did not consider high-order PPD estimation.

High-order MFAC is an important branch of MFAC which uses more information to further improve control performance. In [15], a high-order estimation algorithm was used

to estimate the value of PPD. An improved high-order MFAC method was proposed in [16], which not only considered more control knowledge than the previous time, but also used more information from the previous time in the estimation algorithm.

Fractional-order control is popular in controlling nonlinear systems [17]. In [18], a data driven model has been established and a discrete time fractional order reaching law was studied. In [19], a fractional order data-driven model was proposed, which related the first variation of the output signal with the fractional order variation of the input one. A fractional data-driven model was presented in [20], where the instantaneous gain from the fractional output variation to the input one was computed by means of a fuzzy inference system.

These observations motivate our current study. The main contributions of this paper can be summarized into two aspects: (1) both the error and its rate of change are introduced in the control input criterion function, which incorporates a fractional-order operator. Three weighting coefficients are executed to enhance the system capacity of track abrupt signals and mitigate sudden external disturbance; (2) by using the high-order PPD estimation scheme based on previous input and output data, a fractional-order MFAC with high order estimation to enhance convergence is developed.

The rest of this paper is organized as follows: some preliminaries and the problem formulation are presented in Section 2. The data-driven control algorithm is given in Section 3. A theoretical analysis of the enhanced convergent condition is derived in Section 4. Section 5 provides numerical simulations to illustrate the validity of the designed method. Finally, some conclusions are drawn in Section 6.

2. System Description

In this paper, we consider the following uncertain discrete-time nonlinear system:

$$y(k+1) = f(k, y(k), \ldots, y(k-n_y), u(k), \ldots, u(k-n_u)), \tag{1}$$

where $k \in \{0, 1 \cdots, T\}$ indexes the discrete time and T is the terminal time instant. $u(k) \in \mathbb{R}$ is the control input at time instant k and $y(k) \in \mathbb{R}$ is the system output at time instant k. $n_y, n_u \in \mathbb{N}$ are two unknown positive integers.

Definition 1 ([21])**.** *The fractional discrete approximation of the G-L derivative for $u(k)$ is defined as*

$$\Delta^n u(k) = \frac{1}{h^n} \sum_{v=0}^{k} (-1)^v \binom{n}{v} u(k-v), \tag{2}$$

where $n \in \mathbb{R}$ is the fractional order, $\mathbb{R}$ is the set of real numbers, h is set to 1 as a sampling time, and $k \in \mathbb{N}$ is a number of samples for which the approximation of the derivative is calculated.

The fractional binomial term in (2) can be obtained from the following relation:

$$\binom{n}{v} = \begin{cases} 1 & \text{for } v = 0 \\ \frac{n(n-1)\cdots(n-v+1)}{v!} & \text{for } v > 0 \end{cases} \tag{3}$$

The following assumptions are considered for the system (1).

Assumption 1. *There exist positive constants u_M and y_M such that $|\Delta^n u(k)| \leq u_M$ and $|y(k)| \leq y_M$.*

Assumption 2. *For any $k \in \{0, 1, \cdots, T\}$, the nonlinear function $f(\cdot, \cdots, \cdot)$ satisfies the Lipschitz condition, that is,*

$$|\Delta y(k+1)| \leq l |\Delta^n u(k)|, \tag{4}$$

where $\Delta y(k+1) = y(k+1) - y(k)$, l is a Lipschitz constant.

Remark 1. *The above assumptions are rather standard, and they are taken for granted by several schemes for the control of discrete-time systems. Assumption 1 gives a limit on the system input and output change rate. From a practical point of view, Assumption 2 implies that the output variation depends linearly on the input variation.*

By virtue of the second assumption, the dynamic model of (1) can be expressed as

$$\Delta y(k+1) = \phi(k)\Delta^n u(k), \tag{5}$$

where $\phi(k)$ satisfies $|\phi(k)| \leq l$. $\phi(k)$ establishes a dynamic relationship between the input and output data of the system. Therefore, the rapid identification of $\phi(k)$ becomes particularly crucial. This issue will be addressed in the next section. In this paper, we exclusively address the case of $n \in (0, 1]$.

Remark 2. *When $n = 1$, $\Delta u^n(k)$ degenerates to the conventional integer-order cases. $\phi(k)$ aligns with the standard pseudo-partial derivative in CFDL. For $n \in (0, 1)$, due to the short-memory characteristics of a fractional-order operator* [21]*, the controller compensates for more information from the previous time; therefore, the robustness of the system's equivalent model can be enhanced. This contributes to a smoother execution of dynamic linearization, enabling a faster convergence of the estimated $\hat{\phi}(k)$ to the desired $\phi(k)$.*

Assumption 3. *For any $k \in \{0, 1 \cdots, T\}$, the PPD satisfies $\varepsilon \leq \phi(k)$ (or $\phi(k) \leq -\varepsilon$), where ε is a relatively small positive constant.*

Remark 3. *Most of the plants, in practice, can satisfy Assumption 3. Its practical meaning is obvious, that is, the plant output should increase (or decrease) when the corresponding control input increases.*

3. Design of Model-Free Adaptive Fractional-Order Controller

The following improved calculation criteria are considered:

$$J(u(k)) = \begin{bmatrix} e^T(k+1) & \Delta e^T(k+1) \end{bmatrix} Q_e \begin{bmatrix} e(k+1) \\ \Delta e(k+1) \end{bmatrix} + \lambda \left| \Delta^n u(k) \right|^2, \tag{6}$$

where

$$e(k+1) = y_d(k+1) - y(k+1)$$

and

$$\Delta e(k+1) = e(k+1) - e(k)$$

represent the tracking error and its rate of change, respectively. $y_d(k)$ is the desired trajectory. Q_{e1} and $Q_{e2} \in \mathbb{R}$ are positive weight coefficients in $Q_e = diag\{Q_{e1},\ Q_{e2}\}$. $\lambda > 0$ is a penalty factor, which is used in order to limit the control input variation.

Remark 4. *In the input criterion function* (6)*, the first term is the square of the output error. The second term is the rate of change of the error at two adjacent moments. This is used to reduce the impact of excessive changes in the criterion function calculation by the output data.*

Substituting (5) into the criterion function (6), we can obtain

$$\begin{aligned} J(u(k)) &= Q_{e1} |y_d(k+1) - y(k) - \phi(k)\Delta^n u(k)|^2 + Q_{e2} |y_d(k+1) - y(k) - \phi(k)\Delta^n u(k) - e(k)|^2 \\ &+ \lambda \left| \Delta^n u(k) \right|^2. \end{aligned} \tag{7}$$

Through calculating, this yields

$$\begin{aligned}\frac{1}{2}\frac{\partial J(u(k))}{\partial u(k)} &= -Q_{e1}\phi(k)(y_d(k+1)-y(k)-\phi(k)\Delta^n u(k)) \\ &- Q_{e2}\phi(k)(y_d(k+1)-y(k)-\phi(k)\Delta^n u(k)-e(k))+\lambda\Delta^n u(k). \end{aligned} \quad (8)$$

Using the optimal technique, one can have

$$\Delta^n u(k) = \frac{\rho\phi(k)((Q_{e1}+Q_{e2})\Delta y_d(k+1)+Q_{e1}e(k))}{\lambda+|\sqrt{Q_{e1}+Q_{e2}}\phi(k)|^2},$$

where, as a step factor, ρ is designed to make the controller more universal [22].

Note that

$$\Delta^n u(k) = \sum_{v=1}^{k}(-1)^v\binom{n}{v}u(k-v)+u(k). \quad (9)$$

Thus, an improved model-free adaptive fractional-order controller (I-MFAFOC) can be expressed by

$$u(k) = \frac{\rho\phi(k)((Q_{e1}+Q_{e2})\Delta y_d(k+1)+Q_{e1}e(k))}{\lambda+|\sqrt{Q_{e1}+Q_{e2}}\phi(k)|^2} - \sum_{v=1}^{k}(-1)^v\binom{n}{v}u(k-v). \quad (10)$$

Remark 5. *Unlike other high-order algorithms designed based on the control input* [13,14,16]*, the I-MFAFOC algorithm* (10) *uses $y_d(k+1)$ to update the control input $u(k)$. On the other hand, compared to the algorithm in* [16]*, the improved algorithm does not need to set the weight coefficients for the previous control inputs $u(k-v), v=1,\cdots,k$.*

Since $\phi(k)$ is unknown, the following universal criteria function with the estimated parameter are defined:

$$J(\phi(k)) = |\Delta y(k)-\phi(k)\Delta^n u(k-1)|^2+\mu\left|\phi(k)-\hat{\phi}(k-1)\right|^2, \quad (11)$$

where μ is the weight factor. $\hat{\phi}(k)$ is the estimated value of $\phi(k)$. Equation (11) indicates that the target-constrained input should be minimized, while the tracking error converges to a minimum; this implies that $\hat{\phi}(k)$ will converge to $\phi(k)$.

In this paper, for enhancing tracking performance, a high-order parameter estimation algorithm for PPD (HOPPD) is proposed here by updating the criterion function (11) as follows:

$$J(\phi(k)) = |\Delta y(k)-\phi(k)\Delta^n u(k-1)|^2+\mu\left|\phi(k)-\sum_{j=1}^{m}\alpha_j\hat{\phi}(k-j)\right|^2, \quad (12)$$

where $m\in\mathbb{N}^+$ is the high-order degree and α_j are weighting coefficients with $\sum_{j=1}^{m}\alpha_j=1$.

Based on the derivation of (12), as below, and $\partial J(\phi(k))/\partial\phi(k)=0$, the estimation algorithm is expressed by (13)

$$\hat{\phi}(k) = \frac{\Delta^n u(k-1)\Delta y(k)}{\mu+|\Delta^n u(k-1)|^2}+\frac{\mu\eta}{\mu+|\Delta^n u(k-1)|^2}\sum_{j=1}^{m}\alpha_j\hat{\phi}(k-j), \quad (13)$$

where η is the step length to make the algorithm more flexible [22].

To ensure that the dynamic linearization model is always true, the following reset algorithm is applied:

$$\hat{\phi}(k)=\hat{\phi}(1), \text{if } \hat{\phi}(k)\le\varepsilon \text{ or } \left|\Delta^n u(k-1)\right|\le\varepsilon. \quad (14)$$

$$\begin{cases} \hat{\phi}(k) = \hat{\phi}(k-1) + \frac{\eta \Delta^n u(k-1)}{\mu + |\Delta^n u(k-1)|^2} (\Delta y(k) - \hat{\phi}(k-1)\Delta^n u(k-1)), & 2 \le k < m \\ \hat{\phi}(k) = \frac{\Delta^n u(k-1)\Delta y(k)}{\mu + |\Delta^n u(k-1)|^2} + \frac{\mu\eta}{\mu + |\Delta^n u(k-1)|^2} \sum_{j=1}^{m} \alpha_j \hat{\phi}(k-j), & k \ge m \end{cases} \tag{15}$$

$$u(k) = \frac{\rho \hat{\phi}(k)((Q_{e1} + Q_{e2})\Delta y_d(k+1) + Q_{e1} e(k))}{\lambda + |\sqrt{Q_{e1} + Q_{e2}}\hat{\phi}(k)|^2} - \sum_{v=1}^{k} (-1)^v \binom{n}{v} u(k-v). \tag{16}$$

Therefore, the overall control strategy of the proposed high-order PPD-based improved model-free adaptive fractional-order controller (HOPPD-I-MFAFOC) is delineated in Equations (14)–(16). The controller diagram is depicted in Figure 1 with the following two key points. (1) The PPD is derived using a high-order estimation algorithm. (2) The fractional-order controller is used to provide a better performance.

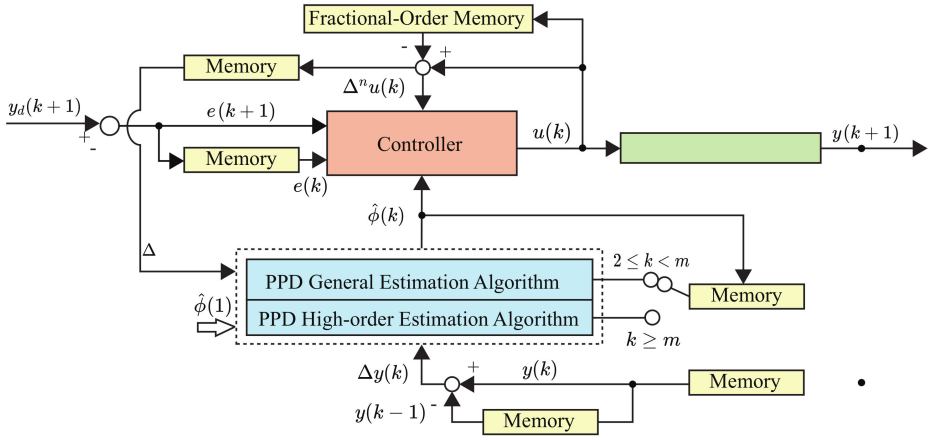

Figure 1. Block diagram of the proposed HOPPD-I-MFAFOC.

In comparison with traditional MFAC, HOPPD-I-MFAFOC incorporates more historical input and output data, enriching the gain parameters by involving $\hat{\phi}(k)$ due to the inclusion of a fractional-order and high-order algorithm.

Remark 6. *For practical realization, the number of samples taken into consideration has to be reduced to the predefined number* $L \in \{0, 1, \cdots, N\}$ *and* $N < T$ *in the experiment [23].*

Remark 7. *In the first instance, an initial value needs to be assigned to* $\hat{\phi}(1)$*. Since the calculation of* $\hat{\phi}(k)$ *relies on the previous m instances, it can only be computed when* $k \ge m$*. Therefore, the high-order estimation algorithm* (15) *is applied for* $k \ge m$*. However, in the case of* $2 \le k < m$*, where no previous instances are available, the original estimation algorithm in* (16) *is utilized.*

Remark 8. *The application of weighting coefficients* α_j *in the high-order estimation algorithm* (15) *is analogous to the use of a forgetting factor. Consequently, they can set* $\alpha_1 \ge \alpha_2 \ge \cdots \ge \alpha_m$*.*

4. Convergence Analysis

The following theorem can be obtained.

Theorem 1. *For system* (1)*, if Assumptions 1 and 2 hold, then for* $k \in \{0, 1, 2, \cdots, T\}$*,* $\hat{\phi}(k)$ *is bounded with* $\eta \in (0, 1]$*.*

Proof. When $2 \leq k < m$, the original estimation algorithm in (15) can be rewritten as

$$\hat{\phi}(k) = \left(1 - \eta \frac{|\Delta^n u(k-1)|^2}{\mu + |\Delta^n u(k-1)|^2}\right)\hat{\phi}(k-1) + \eta \frac{\Delta^n u(k-1)\Delta y(k)}{\mu + |\Delta^n u(k-1)|^2}. \tag{17}$$

From the assumptions of system (1), one has that

$$-\infty < \eta\left(\frac{\Delta^n u(k-1)\Delta y(k)}{\mu + |\Delta^n u(k-1)|^2}\right) < \infty, \tag{18}$$

whenever $|\Delta^n u(k-1)\Delta y(k)| < \infty$ since $0 < \mu < \mu + |\Delta^n u(k-1)|^2$. Thus, using the triangle inequality, we have

$$|\Delta^n u(k-1)\Delta y(k)| \leq l|\Delta^n u(k-1)|^2, \tag{19}$$

consequently, according to Assumption 2, we have

$$\left|\frac{\Delta^n u(k-1)\Delta y(k)}{\mu + |\Delta^n u(k-1)|^2}\right| \leq \frac{l|\Delta^n u(k-1)|^2}{\mu + |\Delta^n u(k-1)|^2} \leq la_1 < \infty. \tag{20}$$

It is worth noting that $\frac{|\Delta^n u(k-1)|^2}{\mu+|\Delta^n u(k-1)|^2}$ is monotonically increasing and bounded about $|\Delta^n u(k-1)|$. Set

$$a_1 = \sup_{k\in[0,T]}\left\{\frac{|\Delta^n u(k-1)|^2}{\mu + |\Delta^n u(k-1)|^2}\right\}. \tag{21}$$

Then, there is a relation that satisfies

$$0 \leq \left|1 - \eta \frac{|\Delta^n u(k-1)|^2}{\mu + |\Delta^n u(k-1)|^2}\right| \leq 1 - \eta a_2 < 1, \tag{22}$$

where

$$a_2 = \inf_{k\in[0,T]}\left\{\frac{|\Delta^n u(k-1)|^2}{\mu + |\Delta^n u(k-1)|^2}\right\}.$$

When $k \geq m$, by taking the absolute value on both sides, we obtain from (15) that

$$\begin{aligned} |\hat{\phi}(k)| &= \left|\frac{\Delta^n u(k-1)^2\Delta y(k)}{\mu + |\Delta^n u(k-1)|^2} + \frac{\mu\eta\sum_{j=1}^{m}\alpha_j\hat{\phi}(k-j)}{\mu + |\Delta^n u(k-1)|^2}\right| \leq la_1 + |\eta|\left|1 - \frac{|\Delta^n u(k-1)|^2}{\mu + |\Delta^n u(k-1)|^2}\right|\left|\sum_{j=1}^{m}\alpha_j\hat{\phi}(k-j)\right| \\ &\leq la_1 + (\eta - \eta^2 a_2)\left|\sum_{j=1}^{m}\alpha_j\hat{\phi}(k-j)\right|, \end{aligned} \tag{23}$$

where $(\eta - \eta^2 a_2) \in (0,1)$, since the boundedness of $\sum_{j=1}^{m}\alpha_j\hat{\phi}(k-j)$ has been demonstrated before. Therefore, $\hat{\phi}(k)$ is uniformly ultimately bounded, as demonstrated in the above proof. Given that $\phi(k)$ is bounded, it follows that $\hat{\phi}(k)$ is bounded as well. Additionally, the PPD estimation error $\tilde{\phi}(k) = \hat{\phi}(k) - \phi(k)$ is also bounded. The proof is completed. □

Theorem 2. *For system* (1) *with the help of the HOPPD-I-MFAFOC scheme* (15) *and* (16)*, if Assumptions 1 and 2 are satisfied and*

$$\sqrt{\lambda} > \frac{\varepsilon\rho Q_{e1}}{2\sqrt{Q_{e1} + Q_{e2}}},$$

then an error convergence rate $0 < M < 1$ *is introduced, ensuring that the tracking error* $e(k)$ *converges to zero as* $k \to \infty$ *with* $0 < \rho \leq 1$.

Proof. Using model (5), we have

$$|e(k+1)| = \left|\Delta y_d(k+1) - \hat{\phi}(k)\Delta^n u(k) + e(k)\right|. \tag{24}$$

Substituting Equation (9) into the Equation (25), this yields

$$\begin{aligned} |e(k+1)| &= |\Delta y_d(k+1) + e(k) \\ &- \frac{\rho\phi(k)\hat{\phi}(k)((Q_{e1}+Q_{e2})\Delta y_d(k+1) + Q_{e1}e(k))}{\lambda + |\sqrt{Q_{e1}+Q_{e2}}\hat{\phi}(k)|^2}| \\ &\leq \left|(1 - \frac{\rho Q_{e1}\phi(k)\hat{\phi}(k)}{\lambda + |\sqrt{Q_{e1}+Q_{e2}}\hat{\phi}(k)|^2})e(k)\right| \\ &\leq \left|1 - \frac{\rho Q_{e1}\phi(k)\hat{\phi}(k)}{\lambda + |\sqrt{Q_{e1}+Q_{e2}}\hat{\phi}(k)|^2}\right||e(k)|. \end{aligned} \tag{25}$$

From Assumption 2 and the reset algorithm (15), the inequality $\phi(k)\hat{\phi}(k) \geq 0$ is obtained. Furthermore, one has that

$$[\sqrt{\lambda} \pm \sqrt{Q_{e1}+Q_{e2}}\hat{\phi}(k)]^2 = \lambda + (Q_{e1}+Q_{e2})[\hat{\phi}(k)]^2 \pm 2\sqrt{\lambda(Q_{e1}+Q_{e2})}\hat{\phi}(k) \geq 0,$$

and consequently

$$2\sqrt{\lambda(Q_{e1}+Q_{e2})}|\hat{\phi}(k)| \leq \lambda + (Q_{e1}+Q_{e2})[\hat{\phi}(k)]^2.$$

Then,

$$\begin{aligned} &\left|1 - \frac{\rho Q_{e1}\phi(k)|\hat{\phi}(k)|}{\lambda + |\sqrt{Q_{e1}+Q_{e2}}\hat{\phi}(k)|^2}\right||e(k)| \\ \leq &\left|1 - \frac{\rho Q_{e1}\phi(k)}{2\sqrt{\lambda(Q_{e1}+Q_{e2})}}\right||e(k)| \\ \leq &(1-\varepsilon d)^2|e(k-1)| \leq (1-\varepsilon d)^3|e(k-2)| \\ \leq &\cdots \leq (1-\varepsilon d)^k|e(1)|, \end{aligned} \tag{26}$$

where

$$d = \frac{\rho Q_{e1}}{2\sqrt{\lambda_{min}(Q_{e1}+Q_{e2})}}$$

is a bounded constant. Therefore, there exists a constant

$$M = (1-\varepsilon d) = \sup_{k\in[0,T]}\left\{\left|1 - \frac{\rho Q_{e1}\phi(k)|\hat{\phi}(k)|}{\lambda_{min} + |\sqrt{Q_{e1}+Q_{e2}}\hat{\phi}(k)|^2}\right|\right\}$$

that represents the rate of error convergence. The proof is completed. □

Theorem 3. *For $k \in \{0, 1, 2, \cdots, T\}$, $u(k)$ and $y(k)$ are bounded, indicating that the closed-loop system is BIBO stable.*

Proof. The following equation is obtained from Equation (9):

$$\begin{aligned} \left|\Delta^n u(k)\right| &= \left|\frac{\rho\phi(k)((Q_{e1}+Q_{e2})\Delta y_d(k+1)+Q_{e1}e(k))}{\lambda+|\sqrt{Q_{e1}+Q_{e2}}\phi(k)|^2}\right| && (27)\\ &\leq \left|\frac{\rho Q_{e1}}{2\sqrt{\lambda(Q_{e1}+Q_{e2})}}\right||e(k)| \\ &\leq d|(e(k)|. && (28)\end{aligned}$$

Apply absolute values to both sides of Equation (2):

$$|\Delta^n u(k)| = \left|\sum_{v=0}^{k}(-1)^v\binom{n}{v}u(k-v)\right|. \tag{29}$$

Let

$$\psi(v) = (-1)^v\binom{n}{v}$$

be a function of v, where

$$-1 < \{\psi(1),\psi(2),\psi(3),\ldots,\psi(k)\} < 0.$$

The following relation can be derived from (27) and (29):

$$\begin{aligned} |\Delta^n u(k)| =& \left|\begin{bmatrix}\psi(0) & \psi(1) & \psi(2) & \cdots & \psi(k-1)\end{bmatrix}^\top\begin{bmatrix}u(k) & u(k-1) & u(k-2) & \cdots & u(1)\end{bmatrix}\right| \\ \leq& d|(e(k)|. \end{aligned} \tag{30}$$

Note that

$$\begin{aligned} |u(k)| =& |\psi(0)u(k)+\psi(1)u(k-1)-\psi(1)u(k-1)| \\ \leq& |\psi(0)u(k)+\psi(1)u(k-1)|+|\psi(1)u(k-1)| \\ \leq& |\psi(0)u(k)+\psi(1)u(k-1)+\psi(2)u(k-2)| \\ &+|\psi(1)u(k-1)|+|\psi(2)u(k-2)| \\ &\cdots \\ \leq& |\Delta^n u(k)|+|\psi(1)u(k-1)|+|\psi(2)u(k-2)| \\ &+\cdots+|\psi(k-1)u(1)| \\ \leq& d|(e(k)|+|\psi(1)u(k-1)|+|\psi(2)u(k-2)| \\ &+\cdots+|\psi(k-1)u(1)| \\ \leq& d|(e(k)|+|\psi(1)||u(k-1)|+|\psi(2)||u(k-2)| \\ &+\cdots+|\psi(k-1)||u(1)| \\ \leq& d|(e(k)|+\sum_{p=1}^{k-1}|u(k-p)|, \end{aligned} \tag{31}$$

where $\{|\psi(1)|,|\psi(2)|,\cdots,|\psi(k)|\} < 1$. This sequence, through a recursive relation, expresses $|u(k)|$ as a function of the input and error at previous time steps. According to Equation (31), the following sequence of inequalities is obtained at other times:

$$\begin{cases} |u(k-1)| \leq d|(e(k-1)|+\sum_{p=2}^{k-1}|u(k-p)| \\ |u(k-2)| \leq d|(e(k-2)|+\sum_{p=3}^{k-1}|u(k-p)| \\ \quad\cdots \\ |u(2)| \leq d|(e(2)|+|u(1)|. \end{cases} \tag{32}$$

By combining the inequality sequences (31) and (32), (31) can be reformulated as follows:

$$\begin{aligned}|u(k)| \leq & d|e(k)| + d|e(k-1)| + \sum_{p=2}^{k-1}|u(k-p)| \\ & \cdots \\ \leq & d|e(k)| + d|e(k-1)| + \cdots + d|e(1)| + |u(1)| \\ \leq & d(M^{k-1}|e(1)| + M^{k-2}|e(1)| + \cdots + M|e(1)| + |u(1)| \\ < & d\frac{M}{1-M}|e(1)| + |u(1)|.\end{aligned} \tag{33}$$

This implies that $u(k)$ is bounded.The proof is completed. □

5. Numerical Examples

In this section, to validate the effectiveness of the proposed method, two numerical examples are presented.

Example 1. *An unknown plant replaced by a differencing equation is represented as follows:*

$$y(k+1) = 0.3y(k) + 0.6y(k-1) + 0.6\sin(\pi u(k)) + 0.3\sin(3\pi u(k)) + 0.1\sin(5\pi u(k)). \tag{34}$$

The tracking trajectory is given as

$$y_d(k) = \begin{cases} 2, & 0 \leq k \leq 150 \\ 4, & 150 < k \leq 300 \end{cases}. \tag{35}$$

The controller parameters are $\lambda = 0.1$, $\rho = 0.2$, $\mu = 0.01$, and $\eta = 0.8$. The predefined number is fixed at $L = 100$. The fractional-order is set as $n = 0.8$. The high-order estimation is configured with $m = 3$, and the weighting coefficients are $\alpha_1 = 0.4$, $\alpha_2 = 0.4$, and $\alpha_3 = 0.2$. The high-order estimation algorithm commences at $k = 4$. The initial PPD is uniformly set as $\hat{\phi}(1) = 10$ for all controllers. Moreover, the weighting coefficients is chosen as $Q_e = diag\{1,\ 0.1\}$.

Figure 2 illustrates the tracking performance of each controller in response to the given reference signal. Table 1 presents a comparison of the Sum Square Error (SSE) and Sum Square Control (SSC) between fractional-order and tuned integer order. The results indicate that the I-MFAFOC method shortens the response time and reduces SSE to a certain extent, but requires an increased control effort. The HOPPD-MFAFOC method reduces the overshoot of the tracking signal and decreases SSC to a certain extent, but increases SSE. The HOPPD-I-MFAFOC method achieves a reduction in SSE and SSC, to a certain extent, simultaneously. Moreover, all three fractional-order control methods mentioned above significantly outperform the traditional MFAC method.

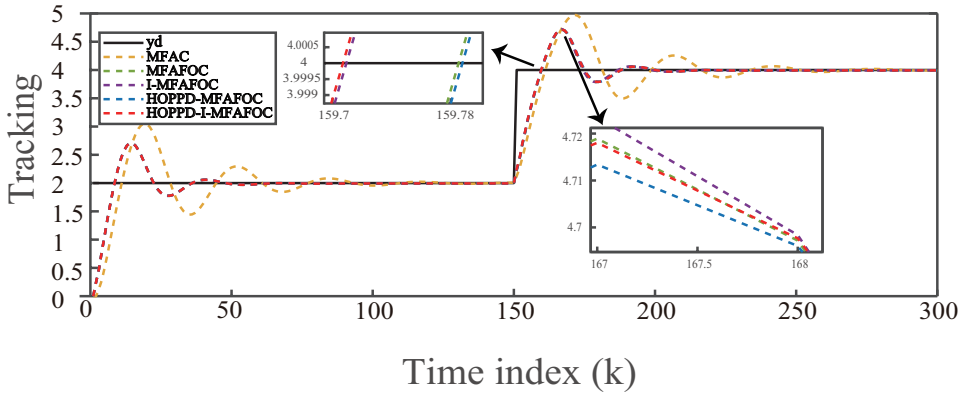

Figure 2. Comparison of the ability of different controllers to handle abrupt reference signals [16,20].

Table 1. A comparison of SSE and SSC among different controllers.

n	CONTROLLER	SSE	SSC
n = 1.0	MFAC	55.4360	1.2655
n = 0.8	MFAFOC	30.1095	1.2634
n = 0.8	I-MFAFOC	29.8452 ↓	1.2702 ↑
n = 0.8	HOPPD-MFAFOC	30.1924 ↑	1.2514 ↓
n = 0.8	HOPPD-I-MFAFOC	29.9294 ↓	1.2575 ↓

Example 2. *To demonstrate the effectiveness of the proposed control method in tracking smooth reference signals, a comparative experiment was conducted as follows. The system* (36) *contains time-varying parameters and uncertain disturbance* $\kappa(k)$*:*

$$y(k+1) = \sin(y(k)) + u(k)[5 + \cos(y(k)u(k))] + \kappa(k). \tag{36}$$

Define the desired trajectory as

$$y_d(k+1) = 0.5\sin(k/20) + 0.5\sin(k/40). \tag{37}$$

The HOPPD-I-MFAFOC method is applied to control the system (37) in simulation experiments. The controller parameters are $\lambda = 0.01, \rho = 0.9, \mu = 0.01$, and $\eta = 0.8$. The predefined number is set to $L = 100$. A comparison between fractional-order and tuned integer order with respect to SSE and SSC is presented in Table 2. The tracking performance of each controller is shown in Figure 3.

Table 2. A comparison of SSE and SSC for different orders using HOPPD-I-MFAFOC.

FRACTIONAL-ORDER	SSE	SSC
0.1	1.3256	0.0313
0.3	1.2478	0.0369
0.5	1.3961	0.0448
0.7	1.8542	0.0612
1.0	4.8235	0.0582

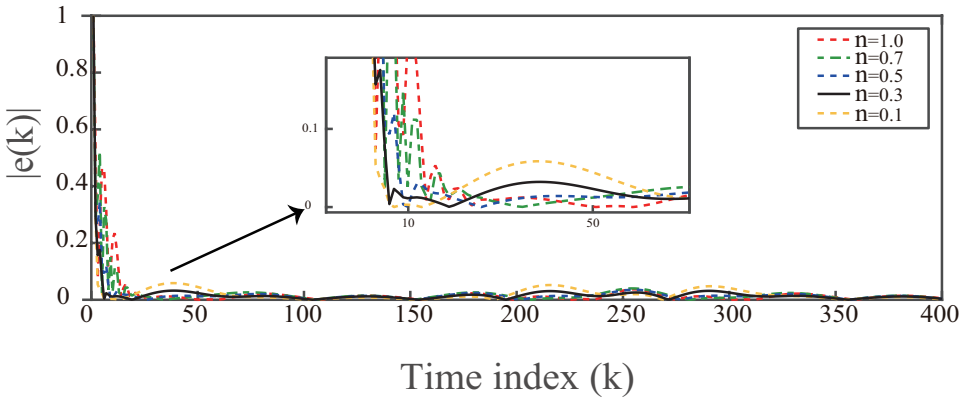

Figure 3. Comparison of different fractional orders when employing the HOPPD-I-MFAFOC method.

The fractional order is chosen as $n = 0.3$. The order of the high-order estimation is specified as $m = 3$, with weighting coefficients $\alpha_1 = 0.4, \alpha_2 = 0.4, and \alpha_3 = 0.2$. The high-order estimation algorithm commences at $k = 4$. The initial PPD is uniformly set as $\hat{\phi}(1) = 10$ for all controllers, and the weight factor is defined as $Q_e = diag\{1,\ 0.2\}$.

Figures 4 and 5 provide a trajectory tracking comparison among the MFAC, MFAFOC, and HOPPD-I-MFAFOC methods for the ideal case. The MFAC parameters are set to $\lambda = 0.01, \rho = 0.5, \mu = 0.01$, and $\eta = 0.5$, demonstrating superior performance. Additionally,

performance enhancements are evident when comparing SSE and SSC indices in Table 3. The results indicate that HOPPD-I-MFAFOC exhibits a 19.46% reduction in SSE and a 13.18% reduction in SSC compared to MFAFOC in tracking the target signal.

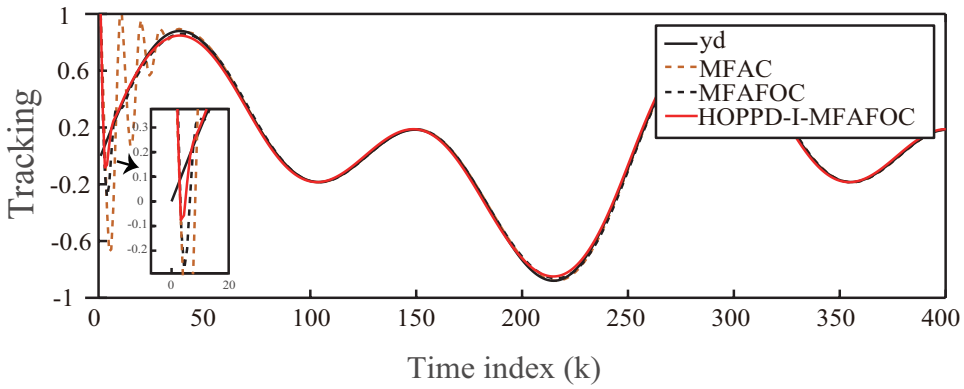

Figure 4. Trajectory tracking results for MFAC, MFAFOC, and HOPPD-I-MFAFOC [19,23].

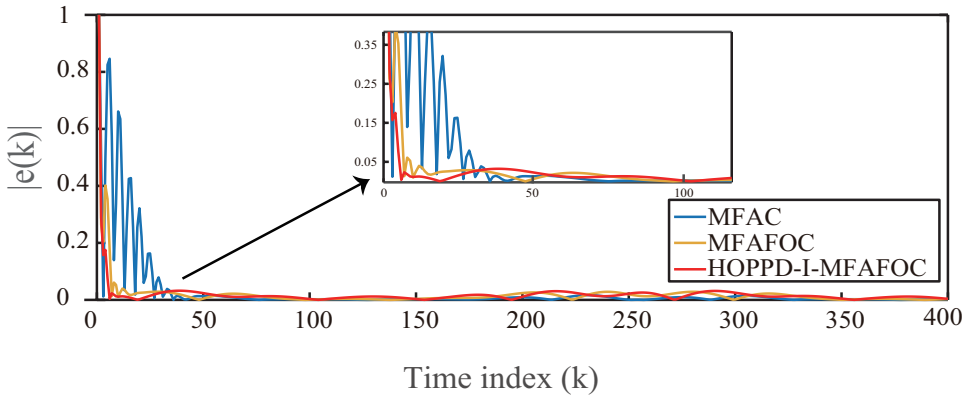

Figure 5. Comparison of the tracking error convergence among MFAC, MFAFOC, and HOPPD-I-MFAFOC [19,23].

Table 3. A comparison of SSE and SSC with different control methods. ($\kappa(k) = 0$).

CONTROLLER	SSE	SSC
MFAC	5.1984	0.0759
MFAFOC [19]	1.5492	0.0425
HOPPD-I-MFAFOC	1.2478 ↓	0.0369 ↓

Figures 6 and 7 demonstrate the robustness of the method, verified by introducing an uncertain disturbance based on repeating the experiment described above. The experiment illustrates the enhanced robustness of the new control method. Additionally, Table 4 provides a comparison between the MFAC, MFAFOC, and HOPPD-I-MFAFOC methods in terms of SSC and SSE for the case with a disturbance. The results show that HOPPD-I-MFAFOC exhibits a 26.43% reduction in SSE and a 9.71% reduction in SSC compared to MFAFOC in tracking the target signal.

Table 4. A comparison of SSE and SSC with different control methods. ($\kappa(k) \neq 0$).

CONTROLLER	SSE	SSC
MFAC	5.8112	0.0951
MFAFOC [19]	1.8500	0.0546
HOPPD-I-MFAFOC	1.3611 ↓	0.0493 ↓

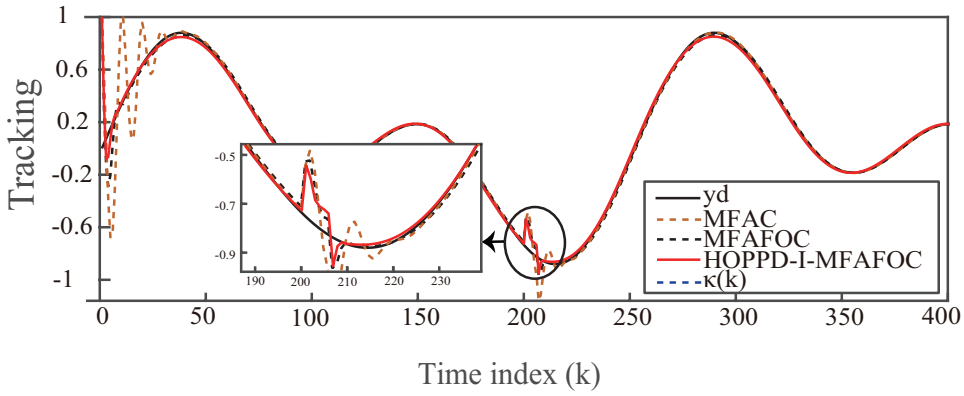

Figure 6. Tracking performance with disturbance $\kappa(k)$ [19,23].

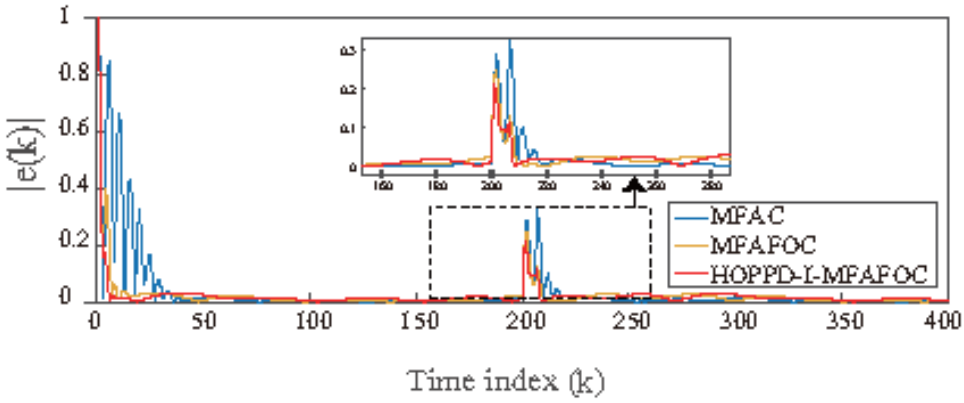

Figure 7. Tracking error convergence with disturbance $\kappa(k)$ [19,23].

6. Conclusions

In this paper, based on the compact-form fractional order dynamic linearization, an improved controller was applied to uncertain discrete-time nonlinear systems. Utilizing the fractional-order short-memory characteristics enhances the tracking performance of the output and the system's disturbance rejection capability. Additionally, the introduction of the tracking error rate of change and the incorporation of a high-order estimation algorithm for PPD complement each other, further improving the controller's performance. Our future work may focus on improving the MFAILC protocol, enabling the use of the fractional-order in the iterative axis and elsewhere in MFAC.

Author Contributions: Methodology, J.L.; Formal analysis, Z.-X.L. All authors have read and agreed to the published version of the manuscript.

Funding: This research received no external funding.

Data Availability Statement: Data is contained within the article.

Conflicts of Interest: The authors declare no conflicts of interest.

References

1. Hou, Z.S.; Han, Z.G. Parameter estimation algorithm of nonlinear systems and its dual adaptive control. *Acta Autom. Sin.* **1995**, *21*, 12–21.
2. Ma, Y.S.; Che, W.W.; Deng, C.; Wu, Z.G. Distributed model-free adaptive control for learning nonlinear MASs under DoS attacks. *IEEE Trans. Neural Netw. Learn. Syst.* **2021**, *34*, 1146–1155. [CrossRef] [PubMed]
3. Zhang, C.K.; Chen, W.H.; Zhu, C.; He, Y.; Wu, M. Stability analysis of discrete-time systems with time-varying delay via a delay-dependent matrix-separation-based inequality. *Automatica* **2023**, *156*, 1111922. [CrossRef]
4. Bao, W.; Zhu, Q.X. Stability analysis of discrete-time semi-Markov jump linear systems. *IEEE Trans. Autom. Control* **2020**, *65*, 5415–5421.

5. Bao, W.; Zhu, Q.X.; Li, S. Stabilization of discrete-time hidden semi-Markov jump linear systems with partly unknown emission probability matrix. *IEEE Trans. Autom. Control* **2023**, *99*, 1–8.
6. Zhang, B.; Zhang, W. Adaptive predictive functional control of a class of nonlinear systems. *ISA Trans.* **2006**, *45*, 175–183. [CrossRef] [PubMed]
7. Hou, Z.S.; Jin, S. Model-Free Adaptive Control for a Class of Nonlinear Discrete-Time Systems Based on the Partial Form Linearization. *IFAC Proc. Vol.* **2008**, *41*, 3509–3514. [CrossRef]
8. Li, Y.; Hou, Z.S.; Liu, X. Full form dynamic linearization based data-driven mfac for a class of discrete-time nonlinear systems. In Proceedings of the 2011 Chinese Control and Decision Conference (CCDC), Mianyang, China, 23–25 May 2011; pp. 127–132.
9. Treesatayapun, C. Model free adaptive control with pseudo partial derivative based on fuzzy rule emulated network. In Proceedings of the 2012 International Conference on Artificial Intelligence (ICAI), Las Vegas, NV, USA, 16–19 July 2012; pp. 257–269.
10. Chen, R.Z.; Li, Y.X.; Hou, Z.S. Distributed model-free adaptive control for multi-agent systems with external disturbances and DoS attacks. *Inf. Sci.* **2022**, *613*, 309–323. [CrossRef]
11. Hou, Z.S.; Xiong, S. On model-free adaptive control and its stability analysis. *IEEE Trans. Autom. Control* **2019**, *64*, 4555–4569. [CrossRef]
12. Liao, Y.; Du, T.; Jiang, Q. Model-free adaptive control method with variable forgetting factor for unmanned surface vehicle control. *Appl. Ocean. Res.* **2019**, *93*, 101945. [CrossRef]
13. Chi, R.; Hui, Y.; Zhang, S.; Huang, B.; Hou, Z.S. Discrete-time extended state observer-based model-free adaptive control via local dynamic linearization. *IEEE Trans. Ind. Electron.* **2020**, *67*, 8691–8701. [CrossRef]
14. Wang, C.; Huo, X.; Ma, K.; Ji, R. Pid-like model free adaptive control with discrete extended state observer and its application on an unmanned helicopter. *IEEE Trans. Ind. Inform.* **2023**, *19*, 11265–11274. [CrossRef]
15. Liu, F.; Wang, Z.; Gao, F. Improved high order model-free adaptive iterative learning control with disturbance compensation and enhanced convergence. *Comput. Model. Eng. Sci.* **2023**, *134*, 343–355.
16. Xu, J.; Lin, N.; Chi, R.; Li, X. High-order model-free adaptive iterative learning control. *Trans. Inst. Meas. Control* **2023**, *45*, 1886–1895. [CrossRef]
17. Podlubny, I. *Fractional Differential Equations*; Academic Press: San Diego, CA, USA, 1999.
18. Chidentree, T.; Aldo, J.M. Discrete-time fractional-order control based on data-driven equivalent model. *Appl. Soft Comput.* **2020**, *96*, 106633.
19. Aldo, J.; Chidentree, T. Fractional data-driven model for stabilization of uncertain discrete-time nonlinear systems. *J. Frankl. Inst.* **2022** *359*, 9690–9702.
20. Chidentree, T.; Aldo, J. Model-free adaptive control based on fractional input-output data model. *Appl. Sci.* **2022**, *12*, 11168.
21. Zieliński, A.; Sierociuk, D. Stability of discrete fractional order state space systems. *IFAC Proc. Vol.* **2006**, *39*, 505–510. [CrossRef]
22. Hou, Z. *Model Free Adaptive Control: Theory and Applications*; CRC Press: Boca Raton, FL, USA, 2013.
23. Wei, Y.H.; Chen, Y.Q.; Cheng, S.; Wang, Y. A note on short memory principle of fractional calculus. *Fract. Calc. Appl. Anal.* **2017**, *20*, 1382–1404. [CrossRef]

mathematics

MDPI

Article

Imputation-Based Variable Selection Method for Block-Wise Missing Data When Integrating Multiple Longitudinal Studies

Zhongzhe Ouyang, Lu Wang * and Alzheimer's Disease Neuroimaging Initiative †

Department of Biostatistics, University of Michigan, Ann Arbor, MI 48109, USA

* Correspondence: luwang@umich.edu

† Data used in preparation of this article were obtained from the Alzheimer's Disease Neuroimaging Initiative (ADNI) database (adni.loni.usc.edu). As such, the investigators within the ADNI contributed to the design and implementation of ADNI and/or provided data but did not participate in analysis or writing of this report. A complete listing of ADNI investigators can be found at: http://adni.loni.usc.edu/wp-content/uploads/how_to_apply/ADNI_Acknowledgement_List.pdf (accessed on 29 February 2024).

Abstract: When integrating data from multiple sources, a common challenge is block-wise missing. Most existing methods address this issue only in cross-sectional studies. In this paper, we propose a method for variable selection when combining datasets from multiple sources in longitudinal studies. To account for block-wise missing in covariates, we impute the missing values multiple times based on combinations of samples from different missing pattern and predictors from different data sources. We then use these imputed data to construct estimating equations, and aggregate the information across subjects and sources with the generalized method of moments. We employ the smoothly clipped absolute deviation penalty in variable selection and use the extended Bayesian Information Criterion criteria for tuning parameter selection. We establish the asymptotic properties of the proposed estimator, and demonstrate the superior performance of the proposed method through numerical experiments. Furthermore, we apply the proposed method in the Alzheimer's Disease Neuroimaging Initiative study to identify sensitive early-stage biomarkers of Alzheimer's Disease, which is crucial for early disease detection and personalized treatment.

Keywords: multiple imputation; correlated data; data integration

MSC: 62H99

1. Introduction

Multi-sources data are now attracting more attention in scientific research. A practical problem with multi-source data is block-wise missing. Our work is motivated by the existence of block-wise missingness in Alzheimer's Disease Neuroimaging Initiative (ADNI) data when investigating the biomarkers that are associated with Alzheimer's Disease (AD). In the ADNI study, healthy elderly subjects, as well as subjects with normal cognition (NC), mild cognitive impairment (MCI), or AD, were recruited to identify neuroimaging measures, cognitive measures and biomarkers that can effectively and timely detect cognitive and functional changes [1]. The ADNI data exhibit a block-wise missing structure along with the long duration of the study, and the high cost of certain measurements, etc. Besides the ADNI data, datasets with block-wise missing structure also exist across many other fields including environmental science, sociology, and economics. For example, a block-wise missing structure appears in human mortality data integrated from Italy and Switzerland [2] and in credit data collected from various institutions (Lan and Jiang [3]; Li et al. [4]).

Statistical analysis with missing covariates has been widely studied due to the prevalence of missing values in many datasets. Common methods for dealing with missing

data include complete case analysis, maximum likelihood, inverse probability weighting, and imputation. While complete case analysis is the easiest approach to implement, it has several drawbacks, such as potential bias in certain cases and a significant loss of information when the proportion of missingness is high. The maximum likelihood approach (e.g., Sabbe et al. [5]; Bondarenko and Raghunathan [6]; Audigier et al. [7]; von Hippel and Bartlett [8]) requires a specification on the distribution of variables, though this is unknown and unverifiable in practice. Inverse probability weighting (e.g., Chen et al. [9]; Creemers et al. [10]; Zubizarreta [11]; Hughes et al. [12]) heavily relies on the information from complete cases, which can be problematic when the fraction of completely observed subject is small.

Two big challenges with the above ADNI data are the high proportion of missingness and the large number of covariates, which make the complete case analysis and maximum likelihood approach inefficient. In addition to these two challenges, weighted methods cannot handle the problem in presence of multiple missing patterns. Compared to these methods with notable limitations, imputation methods are more appropriate for the ADNI data. Recently, multi-source data with block-wise missing, exemplified by the ADNI data, have drawn extensively attention in statistically research. Ref. [13] developed a classification framework, which was accomplished by three steps: feature selection, sample selection, and matrix completion. Ref. [2] proposed a dimension reduction method called generalized integrative principal component analysis (GIPCA). Under the assumption of identical type of distribution in the exponential family within each data source, GIPCA decomposed the overall effect into joint and individual effect across data sources. Ref. [14] imputed the missing data using a factor structure model, which considered the correlation between predictors and does not depend on missing mechanism. Ref. [15] developed a multiple block-wise imputation (MBI) approach by constructing estimating functions based on both complete and incomplete observation. Other related literature include those of [4,16,17].

However, these methods are not applicable to longitudinal studies. Using these methods on the ADNI data, they only select baseline measurement for each patient and simply delete the following measurements. Thus, these methods are inefficient for the ADNI data since they fail to take account of with-subject correlations. In this paper, we aim to develop a method for variable selection when integrating longitudinal data from multiple sources in the existing block-wise missing structure. We impute the block-wise missing data multiple times by using the information from both subjects with complete observation and subjects with missing values. We construct estimating equations based on imputed data and incorporate working correlation matrices to account for within-cluster correlation. With the generalized method of moment, we are capable of integrating data from multiple sources and identifying the relevant variables by introducing a penalty term.

This paper is organized as follows. Section 2 describes the setup and formalize the proposed method. In Section 3, we study the asymptotic properties of the proposed estimator. In Section 4, we develop an algorithm to implement the proposed method, followed by a simulation study conducted in Section 5 to evaluate the performance of the proposed method. In Section 6, we apply the proposed method to the ADNI study. Section 7 provides further discussions.

2. Methods

2.1. Setup

Suppose the dataset consists of n independent and identically distributed (*i.i.d.*) samples drawn from independent sources with disjoint covariates. Without loss of generality, we assume that the data are already sorted by missing patterns, and the total number of missing patterns is K with n_k samples in each pattern, where $\sum_{k=1}^{K} n_k = n$ and $k = 1, \ldots, K$. Within each missing pattern, all subjects have the same missing structure and the covariates from any specific source are either fully observed or fully missing. Let $\boldsymbol{Y}_{k,i} = (Y_{k,i1}, \ldots, Y_{k,im_i})^T$ be the response vector for the ith subject in the kth pattern with

m_i measurements. For ease of presentation, we assume that each sample has the same number of measurements m. Furthermore, let $\boldsymbol{X}_{k,i} = (\boldsymbol{X}_{k,i1}, \ldots, \boldsymbol{X}_{k,ip})$ be the corresponding covariate matrix for the ith subject in the kth pattern across all the measurements, where p is the number of covariates. We assume the underlying population-level model is as follows:

$$E(\boldsymbol{Y}_{k,i}|\boldsymbol{X}_{k,i}) = \mu(\boldsymbol{X}_{k,i}\boldsymbol{\beta}), \quad k = 1, \ldots, K,$$

where $\mu(\cdot)$ is a known monotonic link function and $\boldsymbol{\beta}$ is a p-dimentional vector in the parameter space. Let $O(k)$ and $M(k)$ denote the index of observed covariates and missing covariates in the kth pattern, respectively. Define $R_i = 1$ if $\boldsymbol{X}_{k,i}$ is fully observed, otherwise 0. We assume the missing mechanism of $\boldsymbol{X}_{k,i}$ is missing completely at random [18].

Figure 1 is an example illustrated what block-wise missing data look like, which consist of three sources with three missing patterns. Note that covariates in source 1 are completely observed in all three patterns, while covariates in source 2 are only observed in pattern 1 and 2, and covariates in source 3 are only observed in pattern 1 and 3. A similar structure also exists in the ADNI data. For example, variables in cerebrospinal fluid (CSF) are only measured in a subsample since CSF collection were mainly performed in phase II. Although complete cases analysis is feasible for ADNI data, it is inefficient especially the number of subjects with complete observation is limited. Thus, it is essential to leverage information from incomplete observation.

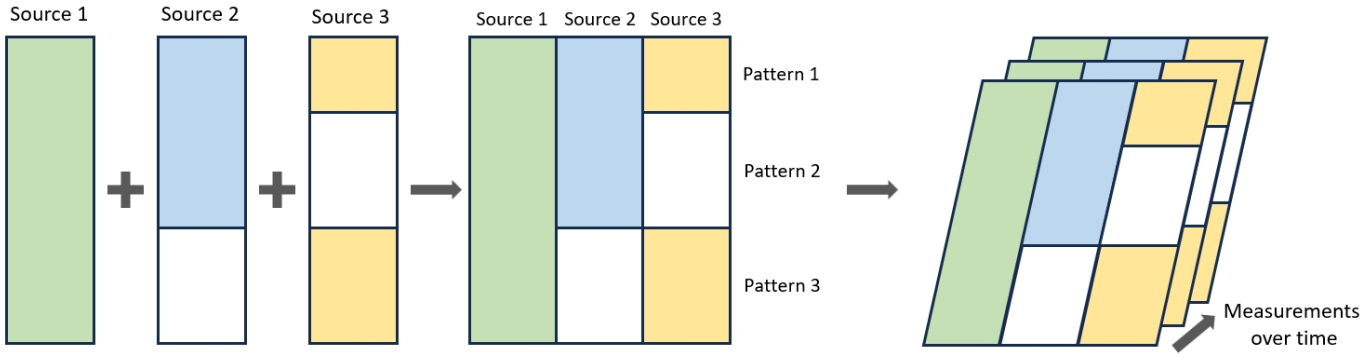

Figure 1. Example of block-wise missing data in longitudinal studies.

2.2. Proposed Method

One approach to utilizing incomplete data is by imputing missing values and performing statistical analysis based on the imputed dataset. Traditional methods impute missing values using information solely from complete cases. However, in scenarios involving block-wise missing data, the proportion of complete cases can be relatively small, resulting in unstable imputed values. To further illustrate how to incorporate information from subjects with partially observed values when imputing missing values, we continue to use the example given in Figure 1. Let $\boldsymbol{X}_{k,i(r)}$ be the rth imputed covariate vector for the ith subject from pattern k, $r = 1, \ldots, R_k$. For instance, the missing values of $\boldsymbol{X}_{2,i}$, i.e., the covariates of source 3 in pattern 2, can be imputed using the information of all sources in pattern 1, which we denoted as $\boldsymbol{X}_{2,i(1)}$. Additionally, these can also be imputed based on the covariates in source 1 and source 3 for subjects from pattern 1 and pattern 3, which we denoted as $\boldsymbol{X}_{2,i(2)}$. Figure 2 illustrate how the above procedures work. When all the covariates are observed, $\boldsymbol{X}_{k,i(r)} = \boldsymbol{X}_{k,i}$. Similarly, we can define $\boldsymbol{\mu}_{k,i(r)}(\boldsymbol{\beta})$ as the corresponding imputed conditional mean.

The intuition behind the proposed method stems from generalized estimating equations (GEE) and quadratic inference functions (QIF). Suppose $\boldsymbol{V}_{k,i}$ is the unknown true covariance matrix of $\boldsymbol{Y}_{k,i}$. Ref. [19] proposed that $\boldsymbol{V}_{k,i}$ can be estimated by $\boldsymbol{A}_{k,i}^{1/2}\boldsymbol{R}_{k,i}(\boldsymbol{\alpha})\boldsymbol{A}_{k,i}^{1/2}$, where $\boldsymbol{A}_{k,i}$ is the diagonal matrix of the conditional variance of $\boldsymbol{Y}_{k,i}$ and $\boldsymbol{R}_{k,i}$ is a working correlation matrix that fully specified by a vector of parameter α. Ref. [20] proposed the QIF using the fact that the inverse of the correlation matrix $\boldsymbol{R}_{k,i}^{-1}$ can be approximated

by $\sum_{j=1}^{J} a_{k,j}\boldsymbol{M}_j$, where $\boldsymbol{M}_1, \ldots, \boldsymbol{M}_J$ are some basis matrices. For example, if we assume the within-cluster correlation structure is exchangeable, $\boldsymbol{R}_{k,i}^{-1}$ can be approximated by $a_1\boldsymbol{M}_1 + a_2\boldsymbol{M}_2$, where $\boldsymbol{M}_1$ is the identity matrix and $\boldsymbol{M}_2$ is a matrix with elemtents in the diagonal to be 0 and elements in the off-diagonal to be 1. The estimation of inverse of correlation matrix using linear combination has been intensively studied by [21]. The advantage of this linear approximation is that the parameter $\boldsymbol{\alpha}$ can be treated as a nuisance parameter, leading to some improvement in computational efficiency. Then, the estimating function for the subject i in the kth pattern with the rth imputation is defined as:

$$\tilde{\mathbf{g}}_{k,i(r)}(\boldsymbol{\beta}) = \sum_{j=1}^{J} a_{k,j}\left\{\frac{\partial \boldsymbol{\mu}_{k,i}(\boldsymbol{\beta})}{\partial \boldsymbol{\beta}_{O(k)}}\right\}^T \boldsymbol{A}_{k,i}^{-1/2}\boldsymbol{M}_j\boldsymbol{A}_{k,i}^{-1/2}\{\boldsymbol{Y}_{k,i} - \boldsymbol{\mu}_{k,i(r)}(\boldsymbol{\beta})\}.$$

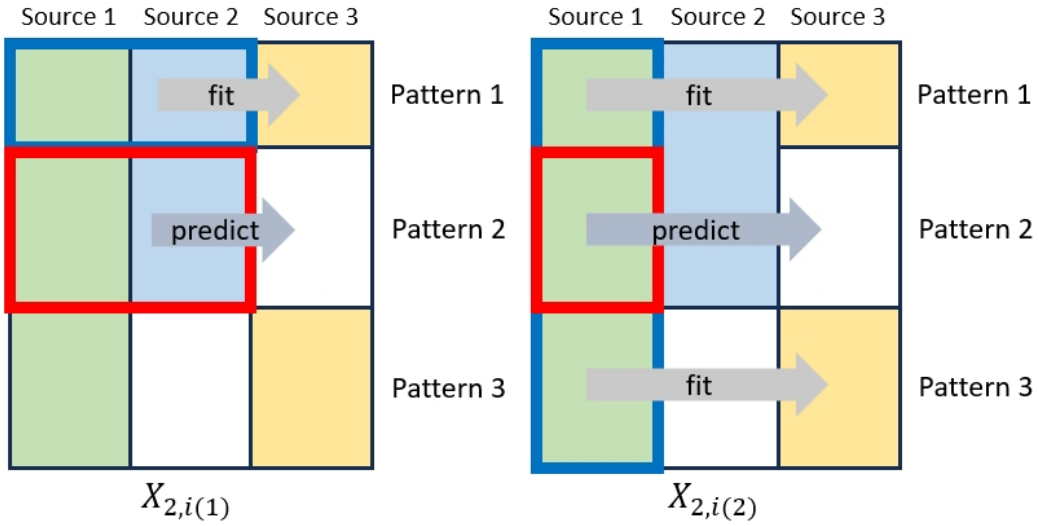

Figure 2. Two imputation approaches for missing covariates of source 3 in pattern 2. In the left figure, samples from pattern 1 and covariates in source 1 and source 2 are used to train the model, which is subsequently used to predict the missing covariates in pattern 2. Similarly, in the right figure, samples from pattern 1 and pattern 3 and covariates in source 1 are used to train the model.

Here, we only take derivative with respect to $\boldsymbol{\beta}_{O(k)}$ to enhance numerical stability. Recall that $a_{k,j}$ is a linear coefficient that used to approximate the inverse of correlation matrix, and thus, it is the nuisance parameter. To avoid estimating these nuisance parameters, we define the extended score vector:

$$\mathbf{g}_{k,i(r)}(\boldsymbol{\beta}) = \begin{pmatrix} \left\{\frac{\partial \boldsymbol{\mu}_{k,i}(\boldsymbol{\beta})}{\partial \boldsymbol{\beta}_{O(k)}}\right\}^T \boldsymbol{A}_{k,i}^{-1/2}\boldsymbol{M}_1\boldsymbol{A}_{k,i}^{-1/2}\{\boldsymbol{Y}_{k,i} - \boldsymbol{\mu}_{k,i(r)}(\boldsymbol{\beta})\} \\ \vdots \\ \left\{\frac{\partial \boldsymbol{\mu}_{k,i}(\boldsymbol{\beta})}{\partial \boldsymbol{\beta}_{O(k)}}\right\}^T \boldsymbol{A}_{k,i}^{-1/2}\boldsymbol{M}_J\boldsymbol{A}_{k,i}^{-1/2}\{\boldsymbol{Y}_{k,i} - \boldsymbol{\mu}_{k,i(r)}(\boldsymbol{\beta})\} \end{pmatrix}.$$

Similarly, we obtain extended score vectors for all imputed covariate vectors and subjects. To integrate all score vectors, we aggregate the information by stacking them into a long vector:

$$\mathbf{g}(\boldsymbol{\beta}) = \begin{pmatrix} \mathbf{g}_1(\boldsymbol{\beta}) \\ \vdots \\ \mathbf{g}_K(\boldsymbol{\beta}) \end{pmatrix} = \begin{pmatrix} \frac{1}{n_1}\sum_{i=1}^{n_1} \mathbf{g}_{1,i}(\boldsymbol{\beta}) \\ \vdots \\ \frac{1}{n_K}\sum_{i=1}^{n_K} \mathbf{g}_{K,i}(\boldsymbol{\beta}) \end{pmatrix},$$

where $\mathbf{g}_{k,i}(\boldsymbol{\beta}) = (\mathbf{g}^T_{k,i(1)}(\boldsymbol{\beta}), \ldots, \mathbf{g}^T_{k,i(R_k)}(\boldsymbol{\beta}))^T$. Note that this might be an overdetermined system because the number of equations can exceed the number of parameters. To overcome this difficulty, we adopt generalized method of moment [22] and add a penalty term. Therefore, the objective function becomes:

$$S(\boldsymbol{\beta}) = \mathbf{g}(\boldsymbol{\beta})^T \boldsymbol{C}(\boldsymbol{\beta})^{-1} \mathbf{g}(\boldsymbol{\beta}) + \sum_{j=1}^{p} p_{\lambda_n}(|\beta_j|), \tag{1}$$

where:

$$\boldsymbol{C}(\boldsymbol{\beta}) = \text{diag}\left\{ \frac{1}{n_1} \sum_{i=1}^{n_1} \mathbf{g}_{1,i}(\boldsymbol{\beta}) \mathbf{g}^T_{1,i}(\boldsymbol{\beta}), \ldots, \frac{1}{n_K} \sum_{i=1}^{n_K} \mathbf{g}_{K,i}(\boldsymbol{\beta}) \mathbf{g}^T_{K,i}(\boldsymbol{\beta}) \right\}$$

is a block-diagnoal matrix under the assumption of independence among samples from different missing patterns and $p_{\lambda_n}(\cdot)$ is an arbitrary, investigator's chosen, penalty function with a tuning parameter λ. Among many optional penalty functions, we adopt the non-convex smoothly clipped absolute deviation (SCAD) penalty [23]:

$$p_{\lambda_n}(|\beta|) = \lambda|\beta| I(|\beta| \leq \lambda) + \frac{2a\lambda|\beta| - \beta^2 - \lambda^2}{2(a-1)} I(\lambda < |\beta| \leq a\lambda) + \frac{\lambda^2(a+1)}{2} I(a\lambda < |\beta|)$$

for some $a > 2$, which possess desirable oracle property.

3. Asymptotic Properties

In this section, we investigate the asymptotic properties of the proposed estimator. In Section 3.1, we assume the sample size n is increasing while the number of parameters p is fixed, and demonstrate that the proposed estimator is $\sqrt{n}$-consistent and asymptotically normal. As sample size goes to infinity, the proposed method is capable of selecting out the relevant variables with probability goes to 1. We also show that the proposed estimator is asymptotically more efficient than single imputation method via incorporating information of samples with missing values. In Section 3.2, we suppose both the sample size n and the number of parameters p are increasing but n increases faster than p. We show that the consistency and sparsity still hold with diverging p. Without loss of generality, we assume $\hat{\boldsymbol{\beta}}$ can be partitioned into two parts, i.e., $\hat{\boldsymbol{\beta}} = (\hat{\boldsymbol{\beta}}^T_{\mathcal{A}}, \hat{\boldsymbol{\beta}}^T_{\mathcal{N}})^T$, where $\hat{\boldsymbol{\beta}}_{\mathcal{A}}$ corresponds to relevant variables with a non-zero true value, while $\hat{\boldsymbol{\beta}}_{\mathcal{N}}$ consists of coefficients of irrelevant variables with a zero true value. For any function $\boldsymbol{g}(\boldsymbol{\beta})$, we use $\dot{\boldsymbol{g}}(\boldsymbol{\beta})$ to denote the first derivative of $\boldsymbol{g}(\cdot)$ evaluated at $\boldsymbol{\beta}$. We use similar notation for its other order derivatives.

3.1. Fixed Number of Parameters

To establish the asymptotic properties of the proposed estimator in the setting of increasing sample sizes and fixed number of parameter, we require the following regularity conditions:

- C.1 $\mathrm{E}[\boldsymbol{X}_{k,j}]^4 < \infty$ and $\mathrm{E}[\mathrm{E}[\boldsymbol{X}_{k,j(r)}]]^4 < \infty$, for any $1 \leq k \leq K$, $1 \leq j \leq p$, and $1 \leq r$, where the inner expectation is with respect to the imputed values.
- C.2 All the variance matrix $\boldsymbol{A}_{k,i} \geq 0$ and $\|\boldsymbol{A}_{k,i}\| < \infty$, for any $1 \leq k \leq K$ and $1 \leq i \leq n_k$.
- C.3 Let $\boldsymbol{\varepsilon}_{k,i} = \boldsymbol{A}^{-1/2}_{k,i}(\boldsymbol{Y}_{k,i} - \boldsymbol{\mu}_{k,i}(\boldsymbol{\beta}_0))$. For any $1 \leq k \leq K$ and $1 \leq i \leq n_k$, $\mathrm{E}(\boldsymbol{\varepsilon}_{k,i}) = 0$ and the fourth moment of $\boldsymbol{\varepsilon}_{k,i}$ exists.
- C.4 $\|\boldsymbol{\mu}_{k,i}(\boldsymbol{\beta}_0) - \boldsymbol{\mu}_{k,i(r)}(\boldsymbol{\beta}_0)\| = o_p(n_k^{-1/2})$, for any $1 \leq k \leq K$ and $1 \leq i \leq n_k$.
- C.5 The penalty function satisfied:
  - (a) $\liminf_{n\to\infty} \inf_{\beta_j \to 0^+} p'_{\lambda_n}(\beta_j)/\lambda_n > 0$;
  - (b) $\max_{j\in\mathcal{A}}\{p'_{\lambda_n}(\beta_{0j})\} = o_p(n^{-1/2})$;
  - (c) $\max_{j\in\mathcal{A}}\{p''_{\lambda_n}(\beta_{0j})\} = o_p(1)$.

C.6 $\sqrt{n}\mathbf{g}(\boldsymbol{\beta}_0) \xrightarrow{d} N(\mathbf{0}, \boldsymbol{\Sigma}\boldsymbol{\Omega})$, where $\boldsymbol{\Sigma} = \text{diag}\{\boldsymbol{\Sigma}_1, \ldots, \boldsymbol{\Sigma}_K\}$ and $\boldsymbol{\Omega} = \text{diag}\{\boldsymbol{\Omega}_1, \ldots, \boldsymbol{\Omega}_K\}$, with $\boldsymbol{\Sigma}_k = \text{cov}(\mathbf{g}_{k,i}(\boldsymbol{\beta}_0))$ and $\boldsymbol{\Omega}_k$ to be a diagonal matrix with n_k dimension and each element equals to $\lim_{n\to\infty} n/n_k$.

C.1–C.3 are conditions that require the existence of the moment, which are easily satisfied. C.4 requires the imputed conditional mean converges to the true conditional mean in probability, which is satisfied as long as the imputed model is correctly specified and the missing mechanism is either missing completely at random. C.5 is a standard condition for SCAD penalty which is commonly used in variable selection method (Gao et al. [24]; Cho and Qu [25]; Tian et al. [26]). More specifically, (a) ensures the property of sparsity is satisfied, (b) and (c) ensure the property of consistency is satisfied, and (c) also guarantees that the objective function (1) is dominated by the first term. C.6 is used to establish the asymptotic normality of the proposed estimator.

Theorem 1. *Under C.1–C.5, there exists a local minimizer* $\hat{\boldsymbol{\beta}}$ *of* $S(\boldsymbol{\beta})$ *such that* $\|\hat{\boldsymbol{\beta}} - \boldsymbol{\beta}_0\| = O_p(n^{-1/2})$.

Theorem 1 states the existence of a minimizer of the objective function and the minimizer will converge to the true coefficients at a rate of $\sqrt{n}$ as the sample size increases. Next, we demonstrate that this estimator possesses the sparsity property and the estimator for the non-zero coefficient is asymptotically normal, as outlined in the following theorem.

Theorem 2. *Under C.1–C.5, if* $\lambda_n \to 0$ *and there exist a sequence such that* $\lambda_n\sqrt{n}/a_n \to \infty$ *as* $n \to \infty$, *where* $a_n = o_p(\sqrt{n})$, *then the proposed estimator* $\hat{\boldsymbol{\beta}} = (\hat{\boldsymbol{\beta}}_{\mathcal{A}}^T, \hat{\boldsymbol{\beta}}_{\mathcal{N}}^T)^T$ *satisfies the following properties:*

1. *(Sparsity)* $P(\hat{\boldsymbol{\beta}}_{\mathcal{N}} = \mathbf{0}) \to 1$;
2. *(Asymptotic Normality) Let* $\boldsymbol{H} = E\left[\partial \mathbf{g}^T(\boldsymbol{\beta}_0)/\partial \boldsymbol{\beta}_{\mathcal{A}}\right]$ *and* $\boldsymbol{V} = (\boldsymbol{H}\boldsymbol{\Sigma}^{-1}\boldsymbol{\Omega}^{-1}\boldsymbol{H}^T)^{-1}$ *and if C.6 holds, then* $\sqrt{n}(\hat{\boldsymbol{\beta}}_{\mathcal{A}} - \boldsymbol{\beta}_{0\mathcal{A}}) \xrightarrow{d} N(\mathbf{0}, \boldsymbol{V})$.

The sparsity of the proposed estimator guarantees that the probability of selecting the true model approaches 1. We also obtained in Theorem 2 the asymptotic normality of $\hat{\boldsymbol{\beta}}_{\mathcal{A}}$, the estimator of coefficients for the relevant variables, which allows us to estimate its variance if $\boldsymbol{H}$ and $\boldsymbol{\Sigma}$ are known. However, in practice, these are unknown to us. We can obtain the empirical variance covariance matrix of $\hat{\boldsymbol{\beta}}_{\mathcal{A}}$ by replacing $\boldsymbol{H}$ with $\widehat{\boldsymbol{H}}(\hat{\boldsymbol{\beta}}) = \partial \mathbf{g}^T(\hat{\boldsymbol{\beta}})/\partial \boldsymbol{\beta}_{\mathcal{A}}$ and replacing $\boldsymbol{\Sigma}$ with $\boldsymbol{C}(\hat{\boldsymbol{\beta}})$, i.e., $\widehat{\boldsymbol{V}} = (\widehat{\boldsymbol{H}}\boldsymbol{C}^{-1}\boldsymbol{\Omega}^{-1}\widehat{\boldsymbol{H}}^T)^{-1}$. Next, we compare the empirical variance of the proposed estimator with the empirical variance of the single imputation approach.

Theorem 3. *If a single imputation is used based on complete cases and denotes the asymptotic covariance matrix of* $\boldsymbol{\beta}_{\mathcal{A}}$ *as* $\widetilde{\boldsymbol{V}}$, *then under the conditions of Theorem 2,* $\widetilde{\boldsymbol{V}} - \boldsymbol{V}$ *is positive semi-definite.*

Theorem 3 claims that the proposed estimator is asymptotically more efficient than the single imputation approach, as it incorporates information from incomplete cases during imputation. The result of this Theorem is intuitive because the proposed method incorporates more samples into the imputation process.

3.2. Diverging Number of Parameters

In this subsection, we consider the setting where sample size n and number of coefficients p increase simultaneously. For certain properties to remain true, we require that n increases faster than p. We replace the notation p by p_n to indicate that the number of parameters also increases. We make the following assumptions:

D.1 For any i, j, k, $\dot{Q}_k(\boldsymbol{\beta}_0) = o_p(p_n^{1/2} n^{-1/2})$ and:

$$\left\| \frac{\partial^2 Q_k(\boldsymbol{\beta}_0)}{\partial \beta_i \partial \beta_j} - E\left\{ \frac{\partial^2 Q_k(\boldsymbol{\beta}_0)}{\partial \beta_i \partial \beta_j} \right\} \right\| = O_p(n^{-1/2}).$$

D.2 There exist an open ball of $\boldsymbol{\beta}_0$ and there exist a constant M such that each entries of $\ddot{Q}_k(\boldsymbol{\beta})$ is bounded by M, for any $\boldsymbol{\beta}$ in this open ball.

D.3 The penalty function satisfied:

(a) $\liminf_{n\to\infty} \inf_{\beta_j \to 0^+} p'_{\lambda_n}(\beta_j)/\lambda_n > 0$;

(b) $\max_{j\in\mathcal{A}}\{p'_{\lambda_n}(\beta_{0j})\} = o_p(p_n^{1/2} n^{-1/2})$;

(c) $\max_{j\in\mathcal{A}}\{p''_{\lambda_n}(\beta_{0j})\} = o_p(p_n^{1/2})$.

D.1 and D.2 are analogous to C.1–C.4. D.3 is the modification of C.5 for diverging number of parameters.

Theorem 4. *Under D.1–D.3, if $p_n = o(n^{1/4})$, there exists a local minimizer $\hat{\boldsymbol{\beta}}$ of $S(\boldsymbol{\beta})$ such that $\|\hat{\boldsymbol{\beta}} - \boldsymbol{\beta}_0\| = O_p(p_n^{1/2} n^{-1/2})$.*

From the result of Theorem 4, we find that the consistency still holds for the proposed estimator, even with a diverging number of parameters. Not surprisingly, the convergence rate is no longer $\sqrt{n}$, but $\sqrt{n/p_n}$. We also require that p_n does not increase faster than $n^{1/4}$ to ensure the model remains sparse. To be specific, the majority of the coefficients is zero.

Theorem 5. *Under D.1–D.3, if $p_n = o(n^{1/4})$, $\lambda_n \to 0$, and $\lambda_n \sqrt{n/p_n} \to \infty$ as $n \to \infty$, then with probability tending to 1, the estimator $\hat{\boldsymbol{\beta}} = (\hat{\boldsymbol{\beta}}_{\mathcal{A}}^T, \hat{\boldsymbol{\beta}}_{\mathcal{N}}^T)^T$ satisfies $P(\hat{\boldsymbol{\beta}}_{\mathcal{N}} = \mathbf{0}) \to 1$.*

Theorem 5 states the sparsity of the proposed estimator with a diverging number of parameters. This property guarantees that the proposed method can still select the true model with a probability approaching 1, even when the number of parameters is diverging.

4. Implementation

Since directly minimizing the objective function is difficult, we incorporate an iterative procedure inspired by the implementation in [27], where they combined the minorization–maximization algorithm [28] with the Newton–Raphson algorithm. Given the current estimate of $\boldsymbol{\beta}^{(t)}$ and tuning parameter λ_n, the objective function $S(\boldsymbol{\beta})$ can be locally approximated by (except a constant term):

$$Q(\boldsymbol{\beta}^{(t)}) + \dot{Q}(\boldsymbol{\beta}^{(t)})^T(\boldsymbol{\beta} - \boldsymbol{\beta}^{(t)}) + \frac{1}{2}(\boldsymbol{\beta} - \boldsymbol{\beta}^{(t)})^T \ddot{Q}(\boldsymbol{\beta}^{(t)})^T(\boldsymbol{\beta} - \boldsymbol{\beta}^{(t)}) + \frac{1}{2}\boldsymbol{\beta}^T \boldsymbol{D}_{\lambda_n}(\boldsymbol{\beta}^{(t)})\boldsymbol{\beta}, \quad (2)$$

where:

$$\boldsymbol{D}_{\lambda_n}(\boldsymbol{\beta}^{(t)}) = \operatorname{diag}\left\{ \frac{p'_{\lambda_n}(|\beta_1^{(t)}|)}{\epsilon + |\beta_1^{(t)}|}, \ldots, \frac{p'_{\lambda_n}(|\beta_p^{(t)}|)}{\epsilon + |\beta_p^{(t)}|} \right\}$$

and ϵ is a sufficiently small number (e.g., $\epsilon = 10^{-6}$). Thus, the search for estimator minimizing the objective function is equivalent to find an estimator that minimize (2). Notice that both $\ddot{Q}(\boldsymbol{\beta}^{(t)})$ and $\ddot{Q}(\boldsymbol{\beta}^{(t)})$ are unknown. Fortunately, from Lemma S2 in Supplementary Materials, $\dot{Q}(\boldsymbol{\beta}^{(t)})$ can be approximated by:

$$\boldsymbol{M}(\boldsymbol{\beta}^{(t)}) = 2\dot{\mathbf{g}}^T(\boldsymbol{\beta}^{(t)})\boldsymbol{C}(\boldsymbol{\beta}^{(t)})^{-1}\mathbf{g}(\boldsymbol{\beta}^{(t)}) \quad (3)$$

and $\ddot{Q}(\boldsymbol{\beta}^{(t)})$ can be approximated by:

$$\boldsymbol{F}(\boldsymbol{\beta}^{(t)}) = 2\dot{\mathbf{g}}^T(\boldsymbol{\beta}^{(t)})\boldsymbol{C}(\boldsymbol{\beta}^{(t)})^{-1}\dot{\mathbf{g}}(\boldsymbol{\beta}^{(t)}). \tag{4}$$

Plugging (3) and (4) into (2) and applying the Newton–Raphson algorithm, we obtain the following formula to update $\boldsymbol{\beta}^{(t+1)}$:

$$\boldsymbol{\beta}^{(t+1)} = \boldsymbol{\beta}^{(t)} - \left[\boldsymbol{F}(\boldsymbol{\beta}^{(t)}) + \boldsymbol{D}_{\lambda_n}(\boldsymbol{\beta}^{(t)})\right]^{-1}\left[\boldsymbol{M}(\boldsymbol{\beta}^{(t)}) + \boldsymbol{D}_{\lambda_n}(\boldsymbol{\beta}^{(t)})\boldsymbol{\beta}^{(t)}\right].$$

We repeat the above procedure until $\|\boldsymbol{\beta}^{(t+1)} - \boldsymbol{\beta}^{(t)}\|$ is smaller than a pre-specified threshold or reach a pre-specified maximum number of iteration.

It is known that the sampling covariance matrix $\boldsymbol{C}(\boldsymbol{\beta})$ may be singular in some cases [29]. To overcome the difficulty in computing the inverse of $\boldsymbol{C}(\boldsymbol{\beta})$, we adopt the Moore–Penrose generalized inverse, which exists and is unique for any matrix.

In the implementation of the proposed method, we select tuning parameter λ_n with extended Bayesian Information Criterion (EBIC) criteria proposed by [30]:

$$\text{EBIC}_\gamma = n\log(\text{RSS}/n) + df_{\lambda_n}\{\log(n) + 2\gamma\log(p)\}, \quad 0 \le \gamma \le 1,$$

where df_{λ_n} is the number of parameters of the model with tuning parameter λ_n and $\text{RSS} = \sum_{k=1}^{K}\text{RSS}_k$ is the residual sum of square of all the missing pattern with:

$$\text{RSS}_k = \frac{1}{R_k}\sum_{r=1}^{R_k}\sum_{i=1}^{n_k}\sum_{j=1}^{m}\left\{y_{k,ij} - \mu_{k,ij(r)}\right\}^2.$$

5. Simulation

In this section, we implement a simulation study to compare the performance of the proposed method in variable selection against complete case analysis (CC) with SCAD penalty, single imputation (SI) with SCAD penalty, and the penalized generalized estimating Equation (PGEE). We use the same data structure as shown in Figure 1, where we have three missing patterns and three sources. The number of measurement is set to be three throughout this section. We replicate the simulation 100 times and use false positive rate (FPR) and false negative rate (FNR) to evaluate the performance of each method, which reflect the proportion of covariates that are irrelevant but falsely selected and the proportion of covariates that are relevant but fail to be selected, respectively. In the tuning parameter selection procedure, the parameter γ was set to 0.5 in EBIC. At the end of the iterative algorithm in Section 4, the estimated coefficient is considered as zero, if its absolute value is smaller than 0.01.

In the first setting, we simulate a dataset with a small proportion of complete cases, where $n_1 = 40$, $n_2 = 120$, $n_3 = 120$, and the missing rate is around 87%. The data with continuous outcome are generated from the model:

$$Y_{ij} = \boldsymbol{X}_{ij}^T\boldsymbol{\beta} + \boldsymbol{\varepsilon}_i,$$

where $j = 1, \ldots, 3$, $\boldsymbol{X}_{ij} = (x_{ij,1}, \ldots, x_{ij,30})^T$ is a vector consisting of 30 covariates, and $\boldsymbol{\beta} = (1, 2, 0, \ldots, 0, 1, 2, 0, \ldots, 0, 1, 2, 0, \ldots, 0)^T$. Here, each source consists of 10 covariates with the first two covariates having non-zero coefficients. $x_{ij,1}$ is a time-fixed covariate and we generate it from the standard normal distribution, whereas other covariates are time-varying covariates and follow multivariate normal distribution with mean zero and exchangeable covariance matrix with marginal variance 1 and correlation coefficient 0.5. We generate random error $\boldsymbol{\varepsilon}_i$ from the multivariate normal distribution with mean 0 and exchangeable covariance matrix with marginal variance 1 and correlation coefficient ρ. We always assume the true within-cluster correlation structure is known and considered ρ to be 0.3, 0.5, and 0.7 in each setting, which corresponded to mild, moderate, and

strong within-cluster correlation. Let $\phi_i = 1/(1 + \exp\{1 + x_{i1,1} + \cdots + x_{i1,10}\})$. Then, n_1, n_2, and n_3 samples were sequentially drawn with probability proportional to the ϕ_i and assigned to the pattern 1, pattern 2, and pattern 3, respectively. Obviously, subjects with higher covariates value from source 1 at the baseline are more likely to be assigned to pattern 1, followed by pattern 2 and then pattern 3. This data generating process implies a MAR mechanism for the missing covariates. The results of Table 1 summarize the performance of each method for three different ρ. All of these methods effectively control the FNR. However, FPR of the proposed method is lower than the other three methods. In other words, the proposed method is able to select most of relevant variables while controlling the error of selecting irrelevant variables. In addition, we notice that the proposed method is more capable of utilizing within-cluster correlation compared with PGEE since the proposed method performs better as the within-cluster correlation becomes stronger. This result demonstrates the superiority of the proposed method when the percentage of complete cases is small in the block-missing data.

Table 1. Simulation scenario 1 with continuous outcomes: comparing the proposed method, complete cases analysis, single imputation method, and PGEE in terms of false positive rate (FPR), false negative rate (FNR), FPR + FNR, and computation time in seconds ($n_1 = 40$, $n_2 = 100$, $n_3 = 100$, $p_1 = 10$, $p_2 = 10$, $p_3 = 10$).

	Method	**FPR**	**FNR**	**FPR + FNR**	**Time**
$\rho = 0.3$	Proposed	0.083	<0.001	0.083	2.38
	CC	0.204	<0.001	0.204	0.26
	SI	0.118	0.002	0.120	1.22
	PGEE	0.085	<0.001	0.085	0.62
$\rho = 0.5$	Proposed	0.093	0.007	0.100	2.42
	CC	0.205	<0.001	0.205	0.27
	SI	0.146	<0.001	0.146	1.29
	PGEE	0.126	0.007	0.133	0.65
$\rho = 0.7$	Proposed	0.110	<0.001	0.110	2.50
	CC	0.198	0.005	0.203	0.28
	SI	0.141	<0.001	0.141	1.33
	PGEE	0.132	0.017	0.149	0.67

In the second setting, we continue to investigate the proposed method's performance with a continuous outcome, but we proportionally increase the sample size in each missing pattern to demonstrate the proposed method's effectiveness in larger samples, where $n_1 = 120$, $n_2 = 300$, $n_3 = 300$. The results are described in Table 2. Unsurprisingly, the FPR and FNR of all the methods decreased compared with the first setting. We observe that the performance of the PGEE is very close to that of the single imputation method while the proposed method has a much lower FPR. In the meanwhile, complete cases analysis is still the worst option since the improvement is minor as the sample size increase, and even negligible when the within-cluster correlation is strong. Therefore, the proposed method is still able to maintain an appealing performance in the large sample size. The results from this setting further verify the efficiency gain of the proposed method in incorporating more information from the missing data compared to the single imputation.

Table 2. Simulation scenario 2 with continuous outcomes: comparing the proposed method, complete cases analysis, single imputation method, and PGEE in terms of false positive rate (FPR), false negative rate (FNR), FPR + FNR, and computation time in seconds ($n_1 = 120$, $n_2 = 300$, $n_3 = 300$, $p_1 = 10$, $p_2 = 10$, $p_3 = 10$).

	Method	FPR	FNR	FPR + FNR	Time
$\rho = 0.3$	Proposed	0.003	<0.001	0.003	4.31
	CC	0.101	<0.001	0.101	0.58
	SI	0.018	<0.001	0.018	2.55
	PGEE	0.010	<0.001	0.010	1.55
$\rho = 0.5$	Proposed	0.005	<0.001	0.005	4.37
	CC	0.135	<0.001	0.135	0.61
	SI	0.025	<0.001	0.025	2.55
	PGEE	0.023	<0.001	0.023	1.52

Table 2. *Cont.*

	Method	FPR	FNR	FPR + FNR	Time
$\rho = 0.7$	Proposed	0.015	<0.001	0.015	4.29
	CC	0.190	<0.001	0.190	0.54
	SI	0.049	<0.001	0.049	2.47
	PGEE	0.078	<0.001	0.078	1.37

In the third setting, we consider a correlated binary outcome with $n_1 = 120$, $n_2 = 300$, and $n_3 = 300$. The data are generated from the model:

$$\log \frac{\pi_{ij}}{1 - \pi_{ij}} = \boldsymbol{X}_{ij}^T \boldsymbol{\beta} + \boldsymbol{\varepsilon}_i,$$

where $j = 1, \ldots, m$, $\boldsymbol{X}_{ij} = (x_{ij,1}, \ldots, x_{ij,15})^T$ is a vector consisting of 15 covariates, and $\boldsymbol{\beta} = (1, 0, \ldots, 0, -0.7, 0, \ldots, 0, 0.5, 0, \ldots, 0)^T$. Here, each source consists of five covariates, with the first covariate in each having non-zero coefficients. $x_{ij,1}$ is a time-fixed covariate and we generate it from the standard normal distribution, whereas other covariates are time-varying covariates and follow multivariate normal distribution with mean zero and exchangeable covariance matrix with marginal variance 1 and correlation coefficient 0.5. We generate random error $\boldsymbol{\varepsilon}_i$ from the multivariate normal distribution with mean 0 and exchangeable covariance matrix with marginal variance 1 and correlation coefficient 0.3. In this setting, $\phi_i = 1/(1 + \exp\{1 + x_{i1,11} + \cdots + x_{i1,15}\})$. The results are summarized in Table 3. Although the PGEE outperforms other methods in terms of FPR, its performance in FNR is poor. In contrast, the proposed method possesses a better balance between FPR and FNR. We still observed a better performance of the proposed method.

Table 3. Simulation scenario 3 with binary outcomes: comparison of the proposed method, complete cases analysis, single imputation method, and PGEE in terms of false positive rate (FPR), false negative rate (FNR), FPR + FNR, and computation time in seconds ($n_1 = 120$, $n_2 = 300$, $n_3 = 300$, $p_1 = 5$, $p_2 = 5$, $p_3 = 5$, $\rho = 0.3$).

Method	FPR	FNR	FPR + FNR	Time
Proposed	0.298	0.063	0.361	3.55
CC	0.334	0.218	0.552	0.32
SI	0.289	0.088	0.377	1.91
PGEE	0.071	0.537	0.608	0.74

6. Application

We apply our proposed method to the ADNI study. This study was launched in 2003 and has undertaken three different phases so far: ADNI 1, ADNI GO/2, and ADNI 3, which is designed to develop the effective treatment that can slow or stop the progression of AD. Our goal is to identify sensitive biomarkers of AD in the early stage from three data sources: magnetic resonance imaging (MRI), positron emission tomography (PET), and cerebrospinal fluid (CSF). We choose the mini-mental state examination (MMSE) [31] score as response variable, which has been widely used in the early diagnosis of AD [32]. The MRI data were analyzed by UCSF, who performed cortical reconstruction and volumetric segmentation with FreeSurfer. The processed MRI data primarly summarized average cortical thickness, standard deviation in cortical thickness, the volumes of cortical parcellations, the volumes of specific white matter parcellations, and the total surface area of the cortex [33]. The PET data were processed by UCB and quantities variables were obtained by standard uptake value ratio (SUVR) in amyloid florbetapir. The CSF data were acquired by ADNI Biomarker Core and Laboratory Medicine and Center for Neurodegenerative Diseases Research at UPENN. The block-wise missing emerged in this data. Less than half of patients lacked MRI measurements, few patients missed PET measurements, and only a small proportion of patients had CSF measurements. One of the reasons for the block-wise missing data is that obtaining CSF measurements requires more invasive procedures (such as lumbar puncture), which are refused by the majority of patients. The goal of this analysis is to identify biomarkers that are highly predictive of MMSE.

We only use the ADNI GO/2 dataset and consider measurements at baseline, month 24, and month 48, since the majority of patients have records at these time points. We also notice that there exist some low-quality data, such as those missed baseline measurement or belonged to a missing pattern with few patients. For simplicity of analysis, we discard these low-quality data, which leads us to a study cohort of 669 patients. Among them, 280 patients missed the measurement at month 24 and 487 patients missed the measurements at month 48. There are 340 features in MRI data, 229 features in PET data, and 3 features in CSF data. These three datasets and MMSE data are joined by a unique identifier "visit code" provided by the ADNI study. In total, we have three missing patterns. Table 4 describes the missing pattern of this dataset. The number of patients with fully observed variables is 63, with a missing rate around 90.6%. From this extremely high proportion of missing data, we will see how the proposed method can substantially improve the prediction ability by incorporating the information of related samples with missing values. To assess the predictive performance of the proposed method, data are randomly split into a test data with a sample size 30 (roughly 5%) and the remaining data as training data, where the test data are drawn from the data with fully observed variables (missing pattern 1). This random split process was replicated 30 times. A variable is marked as a potential predictor of AD if its absolute coefficient value is greater than 0.01.

Table 5 summarizes the average number of biomarkers selected by each method, along with the most frequently selected biomarkers. We also report the post-model-selection p-value. Our method successfully identifies biomarkers that align with findings reported in existing Alzheimer's Disease research literature. In comparison to PGEE, the other three methods consistently select amyloid-β as a biomarker of AD, whose accumulation in cells is an early event of AD [34]. Phosphorylated tau, another widely accepted biomarker, has been validated by multiple large-scale, multi-center studies [35]. Studies found that neurons in AD patients are more likely to loss the superior temporal sulcus [36]. Two distinct normalization methods of summary measures for the standardized uptake value ratio (SUVR) of the florbetapir tracer, in the composite reference region and the whole cerebellum reference region, may potentially serving as AD biomarkers [37]. Besides these biomarkers, the proposed method additionally identifies several well-established and potential biomarkers. The size of the region of interest (ROI) in the left and right hemisphere precuneus area of the cortex, as well as cortical volume of left precuneus, summarize the health status of

precuneus, which may be atrophy in the early stage of AD. The size and volume of the ROI in the left and right inferior lateral ventricle reflect disease progression (Bartos et al. [38]; Song et al. [39]). White matter changes in cerebral or subcortical areas can appear in other neurological conditions and normal aging, their connections with AD potentially make them useful biomarkers for distinguishing AD from normality, especially when considered along with other biomarkers in future investigations. While the surface area of the left caudal middle frontal and the cortical volume of the right caudal anterior cingulate are both associated with AD, more research is required to further explore these associations.

Table 4. Data composition and missing pattern for the subset of ADNI data; "O" denotes the observed data and "-" denotes the missing data.

Missing Pattern	MRI (340)	PET (229)	CSF (3)	Number of Patients
1	O	O	O	63
2	O	O	-	384
3	-	O	-	222

Table 5. Comparision of the mean of the number of selected biomarkers (MNSB) whose absolute value of coefficient is greater than 0.01 based on 30 replications in application to ADNI data. Time is the computation time in seconds.

Method	MNSB	Top Selected Biomarkers	Time
Proposed	16	ABETA, PTAU, ST30SV *, ST15SA ST89SV, ST151SV, ST52CV *, ST73CV, SUMMARYSUVR COMPOSITE REFNORM *, SUMMARYSUVR WHOLECEREBNORM *, CTX LH PRECUNEUS VOLUME, CTX RH PRECUNEUS SUVR, LEFT INF LAT VENT VOLUME, RIGHT INF LAT VENT VOLUME, CTX LH SUPERIORTEMPORAL SUVR *, LEFT CEREBRAL WHITE MATTER VOLUME	1550
CC	3	ABETA, TAU *, SUMMARYSUVR COMPOSITE REFNORM *	280
SI	9	ABETA *, TAU *, PTAU *, ST1SV, ST4SV *, ST52CV SUMMARYSUVR COMPOSITE REFNORM, SUMMARYSUVR WHOLECEREBNORM CC MID ANTERIOR VOLUME	1216
PGEE	1	ST52TA *	18

* Post-model-selection p-value < 0.05.

7. Discussion

It is well known that variable selection is a challenge for model robustness, estimator stableness and efficiency, as well as precise predictability. However, another non-negligible issue when integrating longitudinal studies is missingness in the covariate, especially in block-wise missing data. Specifically, with block-wise missing data, the percentage of complete observations is relatively small while traditional statistical methods heavily rely on information of complete cases. In this paper, we develop new methods to extend the MBI approach in a longitudinal study under the setting of block-wise missing data. Under certain regularity conditions, the desirable properties, consistency, sparsity, and asymptotic normality still hold. In addition, the proposed method demonstrates superior efficiency compared to the single imputation approach. It is worth noting that dropout missing data are also very common in longitudinal studies, which typically cause bias in many cases. In future work, it will be of great interest to develop methods to handle dropout missingness and incorporate inverse probability weighting in the proposed method.

One limitation of this paper is that we assume a homogeneous missing pattern across measurements within a single patient. Although this assumption may be restrictive in real data analysis, it is not hard to fulfill in multi-source data.

Supplementary Materials: The following supporting information can be downloaded at: https://www.mdpi.com/article/10.3390/math12070951/s1.

Author Contributions: Investigation, L.W. and Z.O.; methodology, Z.O.; software, Z.O.; formal analysis, Z.O.; data support, Alzheimer's Disease Neuroimaging Initiative. All authors have read and agreed to the published version of the manuscript.

Funding: This research is partially supported by the NIH Grants P50-DA-054039-02, P30-ES-017885-10-A1, R01-ES-033515-01, and CDC Grant R01-CE-003497-01.

Data Availability Statement: Data are publicly available (https://adni.loni.usc.edu, accessed on 29 February 2024).

Acknowledgments: Data collection and sharing for this project was funded by the Alzheimer's Disease Neuroimaging Initiative (ADNI) (National Institutes of Health Grant U01 AG024904) and DOD ADNI (Department of Defense award number W81XWH-12-2-0012). ADNI is funded by the National Institute on Aging, the National Institute of Biomedical Imaging and Bioengineering, and through generous contributions from the following: AbbVie, Alzheimer's Association; Alzheimer's Drug Discovery Foundation; Araclon Biotech; BioClinica, Inc.; Biogen; Bristol-Myers Squibb Company; CereSpir, Inc.; Cogstate; Eisai Inc.; Elan Pharmaceuticals, Inc.; Eli Lilly and Company; EuroImmun; F. Hoffmann-La Roche Ltd and its affiliated company Genentech, Inc.; Fujirebio; GE Healthcare; IXICO Ltd.; Janssen Alzheimer Immunotherapy Research & Development, LLC.; Johnson & Johnson Pharmaceutical Research & Development LLC.; Lumosity; Lundbeck; Merck & Co., Inc.; Meso Scale Diagnostics, LLC.; NeuroRx Research; Neurotrack Technologies; Novartis Pharmaceuticals Corporation; Pfizer Inc.; Piramal Imaging; Servier; Takeda Pharmaceutical Company; and Transition Therapeutics. The Canadian Institutes of Health Research is providing funds to support ADNI clinical sites in Canada. Private sector contributions are facilitated by the Foundation for the National Institutes of Health (www.fnih.org), accessed on 29 February 2024. The grantee organization is the Northern California Institute for Research and Education, and the study is coordinated by the Alzheimer's Therapeutic Research Institute at the University of Southern California. ADNI data are disseminated by the Laboratory for Neuro Imaging at the University of Southern California.

Conflicts of Interest: The authors declare no conflicts of interest.

References

1. Mueller, S.G.; Weiner, M.W.; Thal, L.J.; Petersen, R.C.; Jack, C.; Jagust, W.; Trojanowski, J.Q.; Toga, A.W.; Beckett, L. The Alzheimer's disease neuroimaging initiative. *Neuroimaging Clin.* **2005**, *15*, 869–877. [CrossRef] [PubMed]
2. Zhu, H.; Li, G.; Lock, E.F. Generalized integrative principal component analysis for multi-type data with block-wise missing structure. *Biostatistics* **2020**, *21*, 302–318. [CrossRef]
3. Lan, Q.; Jiang, S. A method of credit evaluation modeling based on block-wise missing data. *Appl. Intell.* **2021**, *51*, 6859–6880. [CrossRef]
4. Li, J.; Zhang, Q.; Chen, S.; Fang, K. Weighted multiple blockwise imputation method for high-dimensional regression with blockwise missing data. *J. Stat. Comput. Simul.* **2023**, *93*, 459–474. [CrossRef]
5. Sabbe, N.; Thas, O.; Ottoy, J.P. EMLasso: Logistic lasso with missing data. *Stat. Med.* **2013**, *32*, 3143–3157. [CrossRef]
6. Bondarenko, I.; Raghunathan, T. Graphical and numerical diagnostic tools to assess suitability of multiple imputations and imputation models. *Stat. Med.* **2016**, *35*, 3007–3020. [CrossRef]
7. Audigier, V.; Husson, F.; Josse, J. Multiple imputation for continuous variables using a Bayesian principal component analysis. *J. Stat. Comput. Simul.* **2016**, *86*, 2140–2156. [CrossRef]
8. von Hippel, P.T.; Bartlett, J.W. Maximum likelihood multiple imputation: Faster imputations and consistent standard errors without posterior draws. *Stat. Sci.* **2021**, *36*, 400–420. [CrossRef]
9. Chen, B.; Yi, G.Y.; Cook, R.J. Weighted generalized estimating functions for longitudinal response and covariate data that are missing at random. *J. Am. Stat. Assoc.* **2010**, *105*, 336–353. [CrossRef]
10. Creemers, A.; Aerts, M.; Hens, N.; Molenberghs, G. A nonparametric approach to weighted estimating equations for regression analysis with missing covariates. *Comput. Stat. Data Anal.* **2012**, *56*, 100–113. [CrossRef]
11. Zubizarreta, J.R. Stable weights that balance covariates for estimation with incomplete outcome data. *J. Am. Stat. Assoc.* **2015**, *110*, 910–922. [CrossRef]
12. Hughes, R.A.; Heron, J.; Sterne, J.A.; Tilling, K. Accounting for missing data in statistical analyses: Multiple imputation is not always the answer. *Int. J. Epidemiol.* **2019**, *48*, 1294–1304. [CrossRef] [PubMed]
13. Thung, K.H.; Wee, C.Y.; Yap, P.T.; Shen, D.; Initiative, A.D.N.; Alzheimer's Disease Neuroimaging Initiative. Neurodegenerative disease diagnosis using incomplete multi-modality data via matrix shrinkage and completion. *NeuroImage* **2014**, *91*, 386–400. [CrossRef] [PubMed]

14. Zhang, Y.; Tang, N.; Qu, A. Imputed factor regression for high-dimensional block-wise missing data. *Stat. Sin.* **2020**, *30*, 631–651. [CrossRef]
15. Xue, F.; Qu, A. Integrating multisource block-wise missing data in model selection. *J. Am. Stat. Assoc.* **2021**, *116*, 1914–1927. [CrossRef]
16. Yu, G.; Li, Q.; Shen, D.; Liu, Y. Optimal sparse linear prediction for block-missing multi-modality data without imputation. *J. Am. Stat. Assoc.* **2020**, *115*, 1406–1419. [CrossRef] [PubMed]
17. He, Y.; Feng, Y.; Song, X. Variable selection for high-dimensional generalized linear model with block-missing data. *Scand. J. Stat.* **2023**, *50*, 1279–1297. [CrossRef]
18. Rubin, D.B. Inference and missing data. *Biometrika* **1976**, *63*, 581–592. [CrossRef]
19. Liang, K.Y.; Zeger, S.L. Longitudinal data analysis using generalized linear models. *Biometrika* **1986**, *73*, 13–22. [CrossRef]
20. Qu, A.; Lindsay, B.G.; Li, B. Improving generalised estimating equations using quadratic inference functions. *Biometrika* **2000**, *87*, 823–836. [CrossRef]
21. Anderson, T.W. Asymptotically Efficient Estimation of Covariance Matrices with Linear Structure *Ann. Stat.* **1973**, *1*, 135–141. Available online: http://www.jstor.org/stable/2958164 (accessed on 29 February 2024).
22. Hansen, L.P. Large sample properties of generalized method of moments estimators. *Econom. J. Econom. Soc.* **1982**, pp. 1029–1054. [CrossRef]
23. Fan, J.; Li, R. Variable selection via nonconcave penalized likelihood and its oracle properties. *J. Am. Stat. Assoc.* **2001**, *96*, 1348–1360. [CrossRef]
24. Gao, X.; Pu, D.Q.; Wu, Y.; Xu, H. Tuning parameter selection for penalized likelihood estimation of Gaussian graphical model. *Stat. Sin.* **2012**, *22*, 1123–1146.
25. Cho, H.; Qu, A. Model selection for correlated data with diverging number of parameters. *Stat. Sin.* **2013**, *23*, 901–927. [CrossRef]
26. Tian, R.; Xue, L.; Liu, C. Penalized quadratic inference functions for semiparametric varying coefficient partially linear models with longitudinal data. *J. Multivar. Anal.* **2014**, *132*, 94–110. [CrossRef]
27. Johnson, B.A.; Lin, D.; Zeng, D. Penalized estimating functions and variable selection in semiparametric regression models. *J. Am. Stat. Assoc.* **2008**, *103*, 672–680. [CrossRef]
28. Hunter, D.R.; Li, R. Variable selection using MM algorithms. *Ann. Stat.* **2005**, *33*, 1617. [CrossRef]
29. Hu, Y.; Song, P.X.K. Sample size determination for quadratic inference functions in longitudinal design with dichotomous outcomes. *Stat. Med.* **2012**, *31*, 787–800. [CrossRef] [PubMed]
30. Wang, T.; Zhu, L. Consistent tuning parameter selection in high dimensional sparse linear regression. *J. Multivar. Anal.* **2011**, *102*, 1141–1151. [CrossRef]
31. Folstein, M.F.; Folstein, S.E.; McHugh, P.R. "Mini-mental state": A practical method for grading the cognitive state of patients for the clinician. *J. Psychiatr. Res.* **1975**, *12*, 189–198. [CrossRef] [PubMed]
32. Mendiondo, M.S.; Ashford, J.W.; Kryscio, R.J.; Schmitt, F.A. Modelling mini mental state examination changes in Alzheimer's disease. *Stat. Med.* **2000**, *19*, 1607–1616. [CrossRef]
33. Yuan, L.; Wang, Y.; Thompson, P.M.; Narayan, V.A.; Ye, J.; Alzheimer's Disease Neuroimaging Initiative. Multi-source feature learning for joint analysis of incomplete multiple heterogeneous neuroimaging data. *NeuroImage* **2012**, *61*, 622–632. [CrossRef] [PubMed]
34. LaFerla, F.M.; Green, K.N.; Oddo, S. Intracellular amyloid-β in Alzheimer's disease. *Nat. Rev. Neurosci.* **2007**, *8*, 499–509. [CrossRef] [PubMed]
35. Hampel, H.; Blennow, K.; Shaw, L.M.; Hoessler, Y.C.; Zetterberg, H.; Trojanowski, J.Q. Total and phosphorylated tau protein as biological markers of Alzheimer's disease. *Exp. Gerontol.* **2010**, *45*, 30–40. [CrossRef] [PubMed]
36. Gómez-Isla, T.; Hollister, R.; West, H.; Mui, S.; Growdon, J.H.; Petersen, R.C.; Parisi, J.E.; Hyman, B.T. Neuronal loss correlates with but exceeds neurofibrillary tangles in Alzheimer's disease. *Ann. Neurol. Off. J. Am. Neurol. Assoc. Child Neurol. Soc.* **1997**, *41*, 17–24. [CrossRef] [PubMed]
37. Wong, D.F.; Rosenberg, P.B.; Zhou, Y.; Kumar, A.; Raymont, V.; Ravert, H.T.; Dannals, R.F.; Nandi, A.; Brašić, J.R.; Ye, W.; et al. In vivo imaging of amyloid deposition in Alzheimer disease using the radioligand 18F-AV-45 (flobetapir F 18). *J. Nucl. Med.* **2010**, *51*, 913–920. [CrossRef]
38. Bartos, A.; Gregus, D.; Ibrahim, I.; Tintěra, J. Brain volumes and their ratios in Alzheimer s disease on magnetic resonance imaging segmented using Freesurfer 6.0. *Psychiatry Res. Neuroimaging* **2019**, *287*, 70–74. [CrossRef]
39. Song, M.; Jung, H.; Lee, S.; Kim, D.; Ahn, M. Diagnostic classification and biomarker identification of Alzheimer's disease with random forest algorithm. *Brain Sci.* **2021**, *11*, 453. [CrossRef]

mathematics

MDPI

Article

Stochastic Intermittent Control with Uncertainty

Zhengqi Ma [1], Hongyin Jiang [2], Chun Li [1], Defei Zhang [1,*] and Xiaoyou Liu [3]

[1] School of Mathematics and Statistic, Honghe University, Mengzi 661100, China
[2] School of Mathematics and Statistic, Puer University, Puer 665000, China
[3] School of Mathematics and Computing Sciences, Hunan University of Science and Technology, Xiangtan 411201, China
* Correspondence: defeizhang@uoh.edu.cn

Abstract: In this article, we delve into the exponential stability of uncertainty systems characterized by stochastic differential equations driven by G-Brownian motion, where coefficient uncertainty exists. To stabilize the system when it is unstable, we consider incorporating a delayed stochastic term. By employing linear matrix inequalities (LMI) and Lyapunov–Krasovskii functions, we derive a sufficient condition for stabilization. Our findings demonstrate that an unstable system can be stabilized with a control interval within $(\theta^*, 1)$. Some numerical examples are provided at the end to validate the correctness of our theoretical results.

Keywords: coefficient uncertainty; lyapunov-krasovskii function; LMI

MSC: 93E15

1. Introduction

In the domain of stability analysis for diverse stochastic differential equations (SDEs), substantial scholarly work has been undertaken [1–6]. These investigations primarily concentrate on methodologies to stabilize inherently unstable systems by incorporating randomness or implementing control strategies. Since Hasminskii's seminal work [7], which achieved stabilization of an unstable linear system using dual white noise, the focus on stabilizing and destabilizing stochastic systems has become a prominent area of research. The foundational work of Mao, as highlighted in [8,9], laid the groundwork with essential theorems for both the stabilization and destabilization of systems influenced by Brownian motion (BM). Following these pivotal contributions, the domain has seen an expansion through a wide range of significant investigations. These studies have delved into aspects such as exponential stabilization, stochastic stabilization, and guaranteed almost sure exponential stabilization, thereby broadening the scope of the field. Notably, the implementation of stochastic feedback control and state feedback control in both hybrid and stochastic systems, as discussed in [10], has provided insightful developments on how nonlinear systems behave in terms of stabilization and destabilization when subjected to stochastic effects. Notably, Mao et al. [11] have demonstrated mean square stability for hybrid systems through delayed feedback control (DFC). With the increasing complexity of industrial systems, hybrid stochastic systems have attracted considerable attention [12–18].

Intermittent control strategies are crucial for systems where continuous control is impractical due to resource limitations or inherent system constraints. Key strategies include sampled-data control, impulse control, event-triggered control, hybrid systems, reset control, and model predictive control [19–24]. These approaches enable efficient and effective control across various applications by balancing control performance with practical limitations. For example, reference [25] explores the use of adaptive control strategies to stabilize systems under parameter uncertainties.

Applications across fields, from ecological models to mechanical systems, demonstrate the practical implications of parameter sensitivity. For example, slight variations in

growth rate parameters can alter equilibrium point stability in ecological models, impacting population dynamics. Similarly, in mechanical systems, small changes in the damping coefficient critically affect oscillatory behavior. In real-world engineering, uncertainties like measurement noise, aging components, wear, unmodeled dynamics, and linearization errors challenge the accuracy of system models, affecting performance and stability [26]. To combat this, some studies have leveraged LMI and Lyapunov functions to define system stability criteria [27,28].

Acknowledging the challenges that traditional Brownian Motion (BM) faces in capturing the nuances of uncertainties in extreme scenarios, Peng [29,30] proposed the G-Brownian Motion (G-BM) as a refined model to more precisely simulate these uncertainties. Traditional BM models often assume normal distribution of noise, which may not accurately reflect the complexities and irregularities encountered in real-world systems, such as extreme financial risks, ecological changes, and nonlinear responses in engineering. The G-BM, inspired by the heat equation, offers a more flexible framework that relaxes the normal distribution assumption and accommodates a broader range of distribution forms through the G-expectation framework. G-BM not only broadens the scope of probabilistic measures but also equips researchers with robust tools for tackling G-martingale issues and exploring G-stochastic integrals. Based on Peng's groundwork, the stability of SDEs driven by G-BM has been thoroughly explored, revealing extensive properties and theorems [31–35].

The consideration of parameter uncertainties in control design is crucial for the robustness of the proposed methods. Ignoring these uncertainties can lead to suboptimal or even unstable control performance. By incorporating G-Brownian motion and parameter uncertainties, this paper aims to bridge the gap between theoretical models and practical applications, enhancing the robustness and applicability of the control methods. This study utilizes the generalized Itô formula, alongside Lyapunov functions and linear matrix inequality methods, to introduce new stability criteria, aiming to fill the existing research void by offering novel perspectives and methods for the stability analysis of stochastic systems

Consider the unstable systems:

$$dx(t) = A(t)x(t)dt. \tag{1}$$

In this paper, we investigate stochastic intermittent control strategies based on G-Brownian motion and parameter uncertainties. The incorporation of delay and intermittent control strategies is based on the following reasons:

1. Common Phenomena in Real Systems: In many practical systems, delays and intermittent phenomena are unavoidable. For example, in communication networks, signal transmission delays are inherent; in industrial control, intermittent control is often necessary for energy saving and resource limitations.
2. Enhancing Control Efficiency: Intermittent control strategies can maintain system stability while reducing the frequency of control inputs, thereby improving control efficiency. Thus, we consider the following form of stochastic system:

$$\begin{aligned} dx(t) = {} & [A(t)x(t) + u(x(t-\tau))I(t)]dt + B_{ij}(t)I(t)x(t-\tau)d\langle w^i, w^j\rangle_t \\ & + C_j(t)I(t)x(t-\tau)dw_t^j, \end{aligned} \tag{2}$$

where $A(t)$, $B_{ij}(t)$, $C_j(t)$, H, $Y(t)$, Z, Z_{ij}, $Z_j \in R^{\tilde{N}\times\tilde{N}}$; $u(x(t-\tau)) \in R^{\tilde{N}\times 1}$ is a control function with delayed feedback; $A(t) = A + \Delta A(t)$, $B_{ij}(t) = B_{ij} + \Delta B_{ij}(t)$, $C_j(t) = C_j + \Delta C_j(t)$, and $[A(t),\ B_{ij}(t),\ C_j(t)] = HY(t)[Z,\ Z_{ij},\ Z_j]$, and $Y^T(t)Y(t) \leq E$, and E is a unit matrix; $I(t)$ represent an indicator function defined by the summation $I(t) = \sum_{k=0}^{\infty} I_{[kh,kh+\theta h)}(t)$, where $h > 0$ denotes the control period, and $\theta h > 0$ specifies the duration of control; w_t stands for an $\tilde{N}$-dimensional G-Brownian motion defined in the G-expectation space.

2. Noation and Preliminaries

The symbol T signifies the transpose of either a matrix or a vector, whereas tr() represents the trace of the given matrix. If matrix A is a positive definite denoted as $A \succ 0$, (respectively, negative definite matrix is denoted as $A \prec 0$). $|x|$ denotes the Euclidean norm of a vector x and $\|\xi\| = \sup|\xi(t) : -\tau \leq t \leq 0|$, $\|x_{n\tau+T}\| = \sup|x(t) : n\tau + T \leq t \leq (n+1)\tau + T|$. $L^{P}_{\mathcal{F}_t}(R^n)$ is a set of $\mathcal{F}_t$ measurable random variables η, which are valued in R^n, and satisfy the condition $\hat{E}|\eta| < \infty$. $\lambda_{\max}(A)$ denotes the largest eigenvalue of A. Where $*$ denotes the transpose of a matrix on its diagonal. For convenience, $A(t)x(t) := f(x(t))$, $B_{ij}(t)x(t-\tau)I(t) := g_{ij}(x(t-\tau))$, $C_j(t)x(t-\tau)I(t) := h_j(x(t-\tau))$. Here, we employ the Einstein summation convention:

$$B_{ij}(t)I(t)x(t-\tau)d\langle w^i, w^i\rangle_t := \sum_{i,j=1}^{\tilde{N}} B_{ij}(t)I(t)x(t-\tau)d\langle w^i, w^i\rangle_t$$

$$C_j(t)I(t)x(t-\tau)dw_t^j := \sum_{j=1}^{\tilde{N}} C_j(t)I(t)x(t-\tau)dw_t^j.$$

Definition 1 ([29]). *Consider Ω as the collection of all continuous functions valued in R^n that start from $w_0 = 0$. This set is endowed with a metric defined by:*

$$\rho(w^1, w^2) = \sum_{i=1}^{\infty} \frac{1}{2^i}[(\max\left|w_t^1 - w_t^2\right|) \wedge 1].$$

Under this construction, (Ω, ρ) forms a metric space. We define H as a space comprising real-valued functions that operate over Ω.

Definition 2 ([30]). *A function $\hat{E} : H \to R$ called sublinear expectation, if $\forall X, Y \in H$, $C \in R$, it satisfies the following properties:*

(1) Monotonicity: If $X, Y \in H$ and $X \geq Y$, then $\hat{E}(X) \geq \hat{E}(Y)$.
(2) Maintaining of constants: $\hat{E}(C) = C$.
(3) Subadditivity: $\hat{E}(X+Y) \leq \hat{E}(X) + \hat{E}(Y)$.
(4) Positive homogeneity: $\hat{E}(\lambda X) = \lambda\hat{E}(X)$, $\lambda \geqslant 0$.

Definition 3 ([29]). *(G-normal distributions) Let $X = (X_1, X_2, \cdots X_{\tilde{N}})$ be an $\tilde{N}$-dimensional random vector in the sublinear expectation space $(\Omega, H, \hat{E})$, with $\tilde{X}$ independent of and identically distributed to X. If the distributions of $aX + b\tilde{X}$ and $\sqrt{a^2+b^2}X$ remain identical for any $a, b > 0$, then X is considered to follow a G-normal distribution, where G is a function defined in this space: $S^d(R) \to R$.*

$$G(A) = \hat{E}[\frac{1}{2}\langle AX, X\rangle], A \in S^d(R).$$

Here, $S^d(R)$ signifies the set of symmetric matrices of size $d \times d$. It is important to note the existence of a compact and bounded subset Y within $S^d_+(R)$, fulfilling the condition:

$$G(A) = \frac{1}{2}\sup_{\mathrm{O}\in\mathrm{Y}} tr[\mathrm{O}A], A \in S^d(R).$$

Definition 4 ([30]). *G-martingale is a stochastic process $\{X_t\}_{t\geq 0}$ defined on a G-expectation space that satisfies the following conditions:*

(1) Adaptivity: For all $t \geq 0$, X_t is $\mathcal{F}_t$-measurable.
(2) G-martingale condition: For all $0 \leq s \leq t$,

$$\hat{E}[X_t|\mathcal{F}_s] = X_s,$$

where $\hat{E}[\cdot|\mathcal{F}_s]$ *denotes the conditional G-expectation given* $\mathcal{F}_s$.

Remark 1. *Outlines the distinct properties of G.* A, B *are both symmetric matrices:*

Property 1: The function satisfies $G(A+B) \leq G(A) + G(B)$.
Property 2: For any non-negative scalar λ, *it holds that* $G(\lambda A) = \lambda G(A)$.
Property 3: Given two matrices where $A \prec B$, *then* $G(A) \leq G(B)$ *is guaranteed.*

Definition 5. *Define an operator L which is called a generalized G-Lyapunov function:*

$$\begin{aligned} LV(y(t),t) = {} & V_t(y(t),t) + \langle V_y(y(t),t), A(t)y(t) + u(y(t))I(t)\rangle \\ & + G(\langle V_y(y(t),t), B_{ij}(t)y(t) + B_{ji}(t)y(t)\rangle + \langle V_{yy}(y,t)C_j(t)y(t), C_i(t)y(t)\rangle), \end{aligned}$$

where $\langle V_y(y(t),t), B_{ij}(t)y(t) + B_{ji}(t)y(t)\rangle + \langle V_{yy}(y(t),t)C_j(t)y(t), C_i(t)y(t)\rangle$ *is a symmetric matrix in* $S^d(R)$, *with the form*

$$\begin{aligned} & \langle V_y(y(t),t), B_{ij}(t)y(t) + B_{ji}(t)y(t)\rangle + \langle V_{yy}(y(t),t)C_j(t)y(t), C_i(t)y(t)\rangle := \\ & [\langle V_y(y(t),t), B_{ij}(t)y(t) + B_{ji}(t)y(t)\rangle + \langle V_{yy}(y(t),t)C_j(t)y(t), C_i(t)y(t)\rangle]_{ij}^n. \end{aligned}$$

Lemma 1 ([32]). *For* $p \geq 0$ *and* $x(s) \in M_G^p([-\tau, T], R^{\tilde{N}})$, *we have*

(1) $\hat{\mathrm{E}}\Big(\Big|\int_{-\tau}^T x(s)d\langle w^i, w^j\rangle_s\Big|\Big) \leq \bar{\delta}^2\hat{\mathrm{E}}\Big(\int_{-\tau}^T |x(s)|ds\Big)$.

(2) $\hat{\mathrm{E}}\Big(\Big|\int_{-\tau}^T x(s)dw_s^j\Big|^2\Big) = \hat{\mathrm{E}}\Big(\int_{-\tau}^T |x(s)|^2 d\langle w\rangle_s\Big)$.

(3) $\hat{\mathrm{E}}\Big(\int_{-\tau}^T |x(s)|^p ds\Big) \leq \int_{-\tau}^T \hat{\mathrm{E}}|x(s)|^p ds$.

Lemma 2 ([32]). *For* $p \geq 0$, $a \in [0,t]$ *and* $x(s) \in M_G^p([-\tau, T], R^{\tilde{N}})$, *we have*

$$\hat{\mathrm{E}}\left(\sup_{a\leq b\leq t}\left|\int_a^b x(s)d\left\langle w^i, w^j\right\rangle_s\right|^p\right) \leq \bar{\delta}^{2p}|t-a|^P\hat{\mathrm{E}}\left(\int_a^b |x(s)|^p ds\right).$$

Lemma 3 ([33]). *For* $p \geq 2$, $a \in [0,t]$ *and* $x(s) \in M_G^p([-\tau, T], R^{\tilde{N}})$, *we have*

$$\hat{\mathrm{E}}\left(\sup_{a\leq b\leq t}\left|\int_{-\tau}^T x(s)dw_s^j\right|^p\right) \leq \bar{\delta}^{2p}|t-a|^p\hat{\mathrm{E}}\left(\int_a^b |x(s)|^p ds\right).$$

Lemma 4 ([36]). *(Schur complement) For known real matrices* $\Omega_1, \Omega_2, \Omega_3$, *where* $\Omega_1 = \Omega_1^T$, $\Omega_2 = \Omega_2^T$, *then the following conditions are equivalent to each other:*

(1) $\begin{bmatrix} \Omega_1 & \Omega_3 \\ \Omega_3^T & \Omega_2 \end{bmatrix} \prec 0$.

(2) $\Omega_1 \succ 0, \Omega_2 - \Omega_3^T\Omega_1^{-1}\Omega_3 \prec 0$.

(3) $\Omega_2 \succ 0, \Omega_1 - \Omega_3^T\Omega_2^{-1}\Omega_3 \prec 0$.

Lemma 5 ([36]). *For a symmetric matrix* Σ, *and real matrices* M, N, *we have upcoming matrix inequality holds:*

$$\Sigma + MYN + N^TY^TM^T \prec 0,$$

if and only if the upcoming matrix inequality is met:

$$\Sigma + \varepsilon MM^T + \varepsilon^{-1}N^TN \prec 0,$$

where $Y^TY \leq E$, *and given scalar* $\varepsilon > 0$.

Assumption 1. $B_{ij}(t) = B_{ij}^T(t)$, $C_i(t) = C_j(t)$.

Assumption 2. *There exist a constant* β_1, β_2, β_3, β_4, $\beta_5 > 0$, *such that*

(1) $|A(t)y_1(t) - A(t)y_2(t)| \leq \beta_1|y_1(t) - y_2(t)|$.
(2) $\left|B_{ij}(t)y_1(t) - B_{ij}(t)y_2(t)\right| \leq \beta_2|y_1(t) - y_2(t)|$.
(3) $\left|C_j(t)y_1(t) - C_j(t)y_2(t)\right| \leq \beta_3|y_1(t) - y_2(t)|$.
(4) $u^T(y(t))y(t) \leq -\beta_4|y(t)|^2$.
(5) $|u(y_1(t)) - u(y_2(t))| \leq \beta_5|y_1(t) - y_2(t)|$.

Assumption 3. *There are exists positive definite matrices* $P_{ij} = P_{ij}^T \succ 0$, $Q_{ij} = Q_{ij}^T \succ 0$ *and a scalar* $\forall\varepsilon > 0$, *for* $i, j = 1, \cdots, \tilde{N}$, *satisfying the following linear matrix inequality:*

$$\begin{pmatrix} B_{ij}P_{ij} + P_{ij}B_{ji}^T + \varepsilon^{-1}Z_{ij}^TZ_{ij} + Z_i^TZ_i & C_iP_{ij} & P_{ij}H \\ * & -P_{ij} & P_{ij}H \\ * & * & -\varepsilon Q_{ij} \end{pmatrix} \prec 0.$$

Remark 2. *According to [34], Assumption 2 ensures the existence and uniqueness of solutions (2) and (3). Assumptions 1 and 3 are crucial components of our work. They play a significant role in the subsequent proofs and represent our novel contributions to the field. However, these Assumptions also have their limitations. In Assumption 1, the system coefficients cannot always be presented in a symmetric form. In Assumption 3, the existence of a positive definite matrix is also challenging.*

3. Lemmas

To obtain the main conclusion, several lemmas were presented. First, let us consider the following auxiliary G-SDE:

$$dy(t) = [A(t)y(t) + u(y(t))I(t)]dt + B_{ij}(t)I(t)y(t)d\left\langle w^i, w^i\right\rangle_t + C_j(t)I(t)y(t)dw_t^j, \tag{3}$$

with initial value $y_0 \in L^p_{\mathcal{F}_t}(R^n)$.

Lemma 6. *Under Assumptions 1 and 3, with* $\theta \in (\theta^*, 1]$, *then (3) holds:*

$$\hat{E}|y(t; y_0)|^2 \leq C\hat{E}|y_0|^2e^{-\eta t},$$

for $t \geq 0$, *where* $C > 0$ *and* $\eta = max\{\eta_{ij}\} > 0$. *Here, the constant* $\theta^* = \max\left\{\theta_{ij}^*\right\}$, *and the* θ_{ij}^* *are given by*

$$\theta_{ij}^* = \frac{2\lambda_{\max}(A^TP_{ij}) + \eta_{ij}\lambda_{\max}(P_{ij})}{2\beta_4\lambda_{\max}(P_{ij}) - \min\limits_{1\leq i,j\leq\tilde{N}}\{\delta_{ij}\}\sum\limits_{i,j=1}^{\tilde{N}}\lambda_{\max}(\Lambda_{ij})}.$$

Proof. The Lyapunov function for $i, j = 1, \cdots, \tilde{N}$ are defined by

$$V_{ij}(y(t), t) = \frac{1}{\theta_{ij}^*}y^T(t)P_{ij}y(t),$$

obviously, there exist constants $C_1,\ C_2 > 0$, such that

$$C_1\ |y(t)|^2 \leq V_{ij}(y(t), t) \leq\ C_2|y(t)|^2. \tag{4}$$

We can choose constant $\eta_{ij} > 0$, such that

$$
\begin{aligned}
LV_{ij}(y(t),t) &= \left\langle \tfrac{2}{\theta_{ij}^*}P_{ij}y(t), A(t)y(t)+u(y(t))I(t)\right\rangle \\
&\quad + \tfrac{1}{\theta_{ij}^*}G(\langle 2P_{ij}y(t), B_{ij}(t)I(t)y(t)+B_{ji}(t)I(t)y(t)\rangle + \langle 2P_{ij}C_j(t)I(t)y(t), C_i(t)I(t)y(t)\rangle) \\
&\leq \tfrac{2}{\theta_{ij}^*}y^T(t)A^T(t)P_{ij}y(t) + \tfrac{2}{\theta_{ij}^*}u^T(y(t))P_{ij}y(t)I(t) + \eta_{ij}V_{ij}(y(t),t) \\
&\quad + \tfrac{2}{\theta_{ij}^*}G(y^T(t)[(B_{ij}(t)+B_{ji}(t))P_{ij}I(t) + C_j^T(t)P_{ij}C_i(t)I(t)]y(t)).
\end{aligned}
$$

We define $\Lambda_{ij} = (B_{ij}(t)+B_{ji}(t))P_{ij} + C_j^T(t)P_{ij}C_i(t)$. Consequently

$$
y^T(t)\Lambda_{ij}y(t) = tr(y^T(t)\Lambda_{ij}y(t)) = tr(y^T(t)[(B_{ij}(t)P_{ij} + P_{ij}B_{ji}^T(t) + C_i^T(t)P_{ij}^nC_i(t)]y(t)).
$$

It is important to note that $B_{ij}(t)P_{ij} + P_{ij}B_{ji}^T(t) + C_i^T(t)P_{ij}C_i(t) \prec 0$. Applying Lemma 4, this condition is equivalent to

$$
\begin{pmatrix} B_{ij}(t)P_{ij} + P_{ij}B_{ji}^T(t) & C_i(t)P_{ij} \\ * & -P_{ij} \end{pmatrix} \prec 0, \tag{5}
$$

utilizing Lemma 5, (5) corresponds to

$$
\Xi_1 + \Omega_1 Y(t)\Pi_1 + \Pi_1^T Y^T(t)\Omega_1^T \prec 0, \tag{6}
$$

where $\Xi_1 = \begin{pmatrix} B_{ij}P_{ij} + P_{ij}B_{ji}^T & C_iP_{ij} \\ * & -P_{ij}^n \end{pmatrix}, \Omega_1 = \begin{pmatrix} P_{ij}H & 0 \\ * & P_{ij}H \end{pmatrix}, \Pi_1 = \begin{pmatrix} Z_{ij} & 0 \\ Z_i & 0 \end{pmatrix}$. Thus, it follows that (6) is tantamount to

$$
\Xi_1 + \varepsilon\Omega_1\Omega_1^T + \varepsilon^{-1}\Pi_1^T\Pi_1 \prec 0,
$$

further equating to

$$
\begin{pmatrix} B_{ij}P_{ij} + P_{ij}B_{ji}^T + \varepsilon^{-1}Z_{ij}^TZ_{ij} + Z_i^TZ_i & C_iP_{ij} & P_{ij}H \\ * & -P_{ij} & P_{ij}H \\ * & * & -\varepsilon Q_{ij} \end{pmatrix} \prec 0.
$$

Following, based on the characteristics of the function G(·) and given that $\Lambda_{ij} \prec 0$, coupled with the understanding that $O(\delta_{ij})_{i,j=1}^{\tilde{N}}$ is a positive definite matrix, it follows that

$$
G(2[y^T(t)\Lambda_{ij}y(t)]_{i,j=1}^{\tilde{N}}) = \sup_{O\in\Psi} tr(O[y^T(t)\Lambda_{ij}y(t)]_{i,j=1}^{\tilde{N}}) \leq \min_{1\leq i,j\leq\tilde{N}}\{\delta_{ij}\}\sum_{i,j=1}^{\tilde{N}} y^T(t)\Lambda_{ij}y(t) < 0.
$$

So we have

$$
\begin{aligned}
LV_{ij}(y(t),t) &\leq \left\{\tfrac{2}{\theta_{ij}^*}\lambda_{\max}(A^TP_{ij}) - \tfrac{2}{\theta_{ij}^*}\beta_4\lambda_{\max}(P_{ij})I(t) + \tfrac{\eta_{ij}}{\theta_{ij}^*}\lambda_{\max}(P_{ij})\right\}|y(t)|^2 \\
&\quad + \tfrac{1}{\theta_{ij}^*}\min_{1\leq i,j\leq\tilde{N}}\{\delta_{ij}\}\sum_{i,j=1}^{\tilde{N}} y^T(t)\Lambda_{ij}y(t)I(t),
\end{aligned}
$$

for $t \in [lh, (l+\theta_{ij}^*)h)$ and $\xi_1 \in [lh, lh+\theta_{ij}^*h)$

$$
\begin{aligned}
\int_{lh}^{lh+\theta_{ij}^*}[LV_{ij}(y(s),s) + \eta_{ij}V_{ij}(y(s),s)]ds &\leq \left\{\tfrac{2}{\theta_{ij}^*}\lambda_{\max}(A^T(P_{ij}) - \tfrac{2}{\theta_{ij}^*}\beta_4\lambda_{\max}(P_{ij})\right. \\
&\quad \left. + \tfrac{\eta_{ij}}{\theta_{ij}^*}\lambda_{\max}(P_{ij}) + \tfrac{1}{\theta_{ij}^*}\min_{1\leq i,j\leq\tilde{N}}\{\delta_{ij}\}\sum_{i,j=1}^{\tilde{N}}\lambda_{\max}(\Lambda_{ij})\right\}\theta_{ij}^*h|y(\xi_1)|^2.
\end{aligned} \tag{7}
$$

Similarly, for $t \in [(l+\theta_{ij}^*)h, (l+1)h)$ and $\xi_2 \in [(l+\theta_{ij}^*)h, (l+1)h)$

$$\int_{lh+h\theta_{ij}^*}^{(l+1)h} [LV_{ij}(y(s),s) + \eta_{ij}V_{ij}(y(s),s)]ds \leq \left\{ \frac{2}{\theta_{ij}^*}\lambda_{\max}(A^TP_{ij}) + \frac{\eta_{ij}}{\theta_{ij}^*}\lambda_{\max}(P_{ij}) \right\}(1-\theta_{ij}^*)h|y(\xi_2)|^2, \tag{8}$$

merge (7) and (8), yield

$$\begin{aligned}\int_{lh}^{(l+1)h} [LV_{ij}(y(s),n) + \eta_{ij}V_{ij}(y(s),s)]ds \leq \Bigg\{ &\frac{2\lambda_{\max}(A^TP_{ij})+\eta_{ij}\lambda_{\max}(P_{ij})}{\theta_{ij}^*} - 2\beta_4\lambda_{\max}(P_{ij}) \\ &+ \min_{1\leq i,j\leq \tilde{N}}\{\delta_{ij}\}\sum_{i,j=1}^{\tilde{N}}\lambda_{\max}(\Lambda_{ij}) \Bigg\}|y(\xi_1)|^2 \vee |y(\xi_2)|^2 h.\end{aligned}$$

Applying the G-Itô formula, and take G-expectation

$$\begin{aligned}\hat{E}e^{\eta_{ij}t}V_{ij}y(t),t) &= \hat{E}V_{ij}(y_0,t) + \hat{E}\int_{kh}^{(k+1)h} e^{\eta_{ij}s}(LV_{ij}(y(s),s) + \eta_{ij}V_{ij}(y(s),s))ds + \hat{E}\mathrm{M}_t \\ &\quad + \hat{E}\int_{kh}^{(k+1)h} e^{\eta_{ij}s}\langle V_{ij}x(y(s),s), h(y(s),s)\rangle dw_s^j \\ &\leq EV_{ij}(y_0,t) + \Bigg\{ \frac{2\lambda_{\max}(A^TP_{ij})+\eta_{ij}\lambda_{\max}(P_{ij})}{\theta_{ij}^*} - 2\beta_4\lambda_{\max}(P_{ij}) \\ &\quad + \min_{1\leq i,j\leq \tilde{N}}\{\delta_{ij}\}\sum_{i,j=1}^{\tilde{N}}\lambda_{\max}(\Lambda_{ij}) \Bigg\}|y(\xi_1)|^2 \vee |y(\xi_2)|^2 h,\end{aligned}$$

where

$$\begin{aligned}M_t = &\int_{kh}^{(k+1)h} e^{\eta_{ij}s}[\langle V_{ij}y(y(s),s), g(y(s))\rangle + \tfrac{1}{2}\langle V_{ij}yy(y(s),s)h(y(s)), h(y(s))\rangle]d\langle w^i, w^j\rangle_s \\ &- \int_{kh}^{(k+1)h} e^{\eta_{ij}s}G(\langle V_{ij}y(y(s)), g(y(s))\rangle + \langle V_{ij}yy(y(s),s)h(y(s),s), h(y(s))\rangle)ds,\end{aligned}$$

note that

$$\hat{E}M_t \leq 0.$$

Due to $\theta \in (\theta^*, 1]$, leveraging the positive homogeneity characteristic of G, which yielded

$$\hat{E}e^{\eta_{ij}t}V_{ij}(y(t),t) \leq V_{ij}(y_0,t).$$

Subsequently, as elucidated by (4)

$$\hat{E}|y(t)|^2 \leq \frac{1}{C_1}e^{-\eta_{ij}t}V_{ij}(y_0,t),$$

thereby concluding the proof. □

Remark 3. *Based on the results of Lemma 6, the intermittent time θ is inversely proportional to the gain term β_4. To decrease the lower limit of the intermittent time, it is necessary to increase the feedback gain. However, due to the consideration of random terms to stabilize the system, in practical operation, besides increasing the feedback gain, system stability can also be enhanced by increasing the disturbance of random terms δ_{ij}. If the feedback gain cannot be further increased, the estimated lower limit of the random disturbance term δ_{ij} is as follows:*

$$\min_{1\leq i,j\leq \tilde{N}}\{\delta_{ij}\} \geq \frac{2\lambda_{\max}(A^TP_{ij}) + \eta_{ij}\lambda_{\max}(P_{ij}) - 2\beta_4\lambda_{\max}(P_{ij})}{-\sum_{i,j=1}^{\tilde{N}}\lambda_{\max}(\Lambda_{ij})}.$$

Remark 4. *This lemma primarily addresses the stability of the system under parameter uncertainty. By introducing a Lyapunov function and applying the G-expectation theory, it demonstrates that the system state remains stable even in the presence of uncertain parameters. This lemma lays the foundation for analyzing the behavior of systems with uncertain parameters and provides preliminary stability conditions for the main theorem.*

Lemma 7. *Under Assumptions 2 and* $\forall T > 0$*, then for* $[-\tau, T]$

$$\sup_{0\le t\le T+\tau} \hat{E}|x(t)|^2 \le 2\kappa_1 \hat{E}\|\xi\|^2, \tag{9}$$

$$\hat{E}(\sup_{0\le u\le \tau} |x(t+u)-x(t)|^2) \le \kappa_2 \hat{E}\|\xi\|^2, \tag{10}$$

where the constants κ_1 *and* κ_2 *are given by*

$$\kappa_1 = e^{[1+\beta_1^2+\beta_5^2+\bar{\delta}^2(\beta_2^2+\beta_3^2+1)](T+\tau)},$$

$$\kappa_2 = 6\tau^2(\beta_1^2+\beta_5^2+\bar{\delta}^4(\beta_2^2+4\beta_3^2))\kappa_1.$$

Proof. To utilize the G-Itô formula on $|x(t)|^2$, we proceed as follows:

$$\begin{aligned} |x(t)|^2 = |x_0|^2 &+ \textstyle\int_0^t 2[u^T(x(s-\tau))x(s)I(t) + f^T(x(s))x(s)]ds \\ &+ \textstyle\int_0^t [2g_{ij}^T(x(s-\tau),n)x(s) + h_j^T(x(s-\tau))h_i(x(s-\tau))d\langle w^i, w^j\rangle_s \\ &+ \textstyle\int_0^t 2h_j^T(x(s-\tau))x(s)dw_s^j, \end{aligned} \tag{11}$$

under Assumptions 2, (11) leads to the inference that

$$\begin{aligned} \hat{E}|x(t)|^2 \le |x_0|^2 &+ \textstyle\int_0^t [\hat{E}|x(s)|^2 + \beta_5^2\hat{E}|x(s-\tau)|^2 + \beta_1^2\hat{E}|x(s)|^2]ds \\ &+ \textstyle\int_0^t [\bar{\delta}^2(\beta_2^2\hat{E}|x(s-\tau)|^2 + \hat{E}|x(s)|^2) + \bar{\delta}^2\beta_3^2\hat{E}|x(s-\tau)|^2]ds, \end{aligned}$$

upon reorganizing the right-hand side of the above equation, we obtain

$$\hat{E}|x(t)|^2 \le |x_0|^2 + \int_0^t [(1+\beta_1^2+\bar{\delta}^2)\hat{E}|x(s)|^2 + (\beta_5^2+\bar{\delta}^2(\beta_2^2+\beta_3^2))\hat{E}|x(s-\tau)|^2]ds. \tag{12}$$

Noting that

$$\int_0^t \hat{E}|x(s-\tau)|^2 ds \le \tau\hat{E}\|\xi\|^2 + \int_0^t \sup_{0\le u\le s} \hat{E}|x(u)|^2 ds, \tag{13}$$

substitute (13) into (12) and merging them yields

$$\sup_{0\le u\le t} \hat{E}|x(u)|^2 \le [1+\beta_5^2+\bar{\delta}^2(\beta_2^2+\beta_3^2)]\hat{E}\|\xi\|^2 + [1+\beta_5^2+\bar{\delta}^2(1+\beta_2^2+\beta_3^2)]\int_0^t \sup_{0\le u\le s} \hat{E}|x(u)|^2 ds,$$

using Gronwall inequality yields (9).

Subsequently, employing the fundamental inequality $|x+y+z|^2 \le 3(x^2+y^2+z^2)$

$$\begin{aligned}\hat{E}(\sup_{0\le u\le\tau}|x(t+u)-x(t)|^2) &\le \hat{E}\Big|\int_t^{t+\tau}(f(x(s))+u(x(s-\tau))I(t))ds\\ &+\int_t^{t+\tau}g_{ij}(x(s-\tau))d\langle w^i,w^j\rangle_s+\int_t^{t+\tau}h_j(x(s-\tau))dw_s^j\Big|^2\\ &\le 3\hat{E}\Big|\int_t^{t+\tau}(f(x(s))+u(x(s-\tau))I(t))ds\Big|^2\\ &+3\hat{E}\Big|\int_t^{t+\tau}g_{ij}(x(s-\tau))d\langle w^i,w^j\rangle_s\Big|^2+3\hat{E}\Big|\int_t^{t+\tau}h_j(x(s-\tau))dw_s^j\Big|^2\\ &\le 3\tau\beta_1^2\int_t^{t+\tau}\hat{E}|x(s)|^2ds+(3\tau\beta_5^2+3\tau\bar{\delta}^4(\beta_2^2+4\beta_3^2))\int_t^{t+\tau}\hat{E}|x(s-\tau)|^2ds\\ &\le 3\tau^2\beta_1^2\sup_{0\le u\le T+\tau}\hat{E}|x(u)|^2+3\tau^2(\beta_5^2+\bar{\delta}^4(\beta_2^2+4\beta_3^2))\sup_{0\le u\le T+\tau}\hat{E}|x(u)|^2,\end{aligned}$$

again using Gronwall inequality yields (10). □

Remark 5. *This lemma focuses on the relationship between delayed and non-delayed systems. Specifically, it proves that even in the presence of system delays, the stability of the system can be ensured through appropriate control strategies. The significance of this lemma lies in its extension to more practical application scenarios, as delays are inevitable in many real-world systems.*

Lemma 8. *Under Assumptions 2 and* $\forall T>0$*, then for* $[-\tau,T]$

$$\hat{E}|x(t)-y(t)|^2\le\kappa_3(T+\tau)\hat{E}\|\xi\|^2,$$

where κ_3 *is given by*

$$\kappa_3=(12\beta_5+4\beta_1+2\beta_3^2+4\beta_3)(6\beta_5+2\beta_1+6\beta_2+\beta_3^2+6\beta_3)\kappa_2.$$

Proof. Applying the G-Itô formula, and take G-expectation

$$\begin{aligned}\hat{E}|x(t)-y(t)|^2 &= 2\hat{E}\int_0^t[(u(x(s-\tau))-u(y(s)))^T(x(s)-y(s))I(t)\\ &+(f(x(s))-f(y(s)))^T(x(s)-y(s))]ds\\ &+\hat{E}\int_0^t[2(g_{ij}(x(s-\tau))-g_{ij}(y(s)))^T(x(s)-y(s))\\ &+(h_j(x(s-\tau),n)-h_j(y(s)))^T(h_j(x(s-\tau))-h_j(y(s))]d\langle w^i,w^j\rangle_s\\ &+2\hat{E}\int_0^t(h_j(x(s-\tau))-h_j(y(s)))^T(x(s)-y(s))dw_s^j,\end{aligned}$$

under Assumption 2, we have

$$\begin{aligned}\hat{E}|x(t)-y(t)|^2 &\le 2\hat{E}\int_0^t[\beta_5|x(s-\tau)-y(s)||x(s)-y(s)|+\beta_1|x(s)-y(s)|^2]ds\\ &+\hat{E}\int_0^t[2\beta_2|x(s-\tau)-y(s)||x(s)-y(s)|+\beta_3|x(s-\tau)-y(s)|^2]d\langle w^i,w^j\rangle_s\\ &+2\beta_3\hat{E}\int_0^t|x(s-\tau)-y(s)||x(s)-y(s)|dw_s^j.\end{aligned}$$

By applying the Hölder inequality

$$\begin{aligned}\hat{E}|x(t)-y(t)|^2 &\le 2\hat{E}\int_0^t[\beta_5(3|x(s)-y(s)|^2+|x(s)-x(s-\tau)|^2)+\beta_1|x(s)-y(s)|^2]ds\\ &+2\hat{E}\int_0^t[\beta_2(6|x(s)-y(s)|^2+2|x(s)-x(s-\tau)|^2)\\ &+\beta_3^2(|x(s)-x(s-\tau)|^2+|x(s)-y(s)|^2)]ds\\ &+2\beta_3\hat{E}\int_0^t(3|x(s)-y(s)|^2+|x(s)-x(s-\tau)|^2)ds\\ &=(6\beta_5+2\beta_1+6\beta_2+\beta_3^2+6\beta_3)\hat{E}\int_0^t|x(s)-y(s)|^2ds\\ &+(2\beta_5+2\beta_1+\beta_3^2+2\beta_3)\hat{E}\int_0^t|x(s)-x(s-\tau)|^2ds.\end{aligned}$$

By virtue of Lemma 7 and Gronwall inequality, we can easily obtain

$$\hat{E}|x(t) - y(t)|^2 \leq \kappa_3(T+\tau)\hat{E}\|\xi\|^2.$$

□

4. Main Results

Here is the proof of our main theorem, which is based on the aforementioned three lemmas.

Theorem 1. *Under Assumptions 1–3, choose a constant* $\varsigma \in (0,1)$ *and* $T = \frac{1}{\eta}\log(\frac{4C}{\varsigma})$, τ^* *is the unique solution of (14), choose* $\tau \in [0, \tau^*)$

$$\varsigma + 4\kappa_3(T+\tau) + 2\kappa_2 = 1, \tag{14}$$

then (2) have

$$\hat{E}|x(t)|^2 \leq e^{-\eta t}.$$

Proof. Consider $t \in (\tau, 2\tau + T)$, by Lemma 6 we can obtain

$$\hat{E}|y(\tau+T)|^2 \leq C\hat{E}|y(\tau)|^2 e^{-\eta T},$$

moreover

$$\hat{E}|x(\tau+T)|^2 \leq 2\Big(\hat{E}|y(\tau+T)|^2 + \hat{E}|x(\tau+T) - y(\tau+T)|^2\Big),$$

using Lemma 8

$$\hat{E}|x(\tau+T)|^2 \leq 2\Big(Ce^{-\eta T}\hat{E}|y(\tau)|^2 + \kappa_3(T+\tau)\hat{E}\|\xi\|^2\Big) \leq 2\Big(Ce^{-\eta T} + \kappa_3(T+\tau)\Big)\hat{E}\|\xi\|^2. \tag{15}$$

On the other hand, by Lemma 7, we have

$$\begin{aligned}\hat{E}\|x(2\tau+T)\|^2 &\leq 2\hat{E}|x(\tau+T)|^2 + 2\hat{E}(\sup_{0\leq u\leq\tau}|x(\tau+T+u) - x(\tau+T)|^2) \\ &\leq 2\hat{E}|x(\tau+T)|^2 + 2\kappa_2\hat{E}\|\xi\|^2,\end{aligned} \tag{16}$$

together with (15) into (16), we have

$$\hat{E}\|x(2\tau+T)\|^2 \leq \Big(4Ce^{-\eta T} + 4\kappa_3(T+\tau) + 2\kappa_2\Big)\hat{E}\|\xi\|^2,$$

due to $\varsigma = 4Ce^{-\eta T}$ and $\tau \in (0, \tau^*)$, we have

$$\varsigma + 4\kappa_3(T+\tau) + 2\kappa_2 < 1.$$

There certainly exists a suitable constant α, such that

$$\varsigma + 4\kappa_3(T+\tau) + 2\kappa_2 = e^{-\alpha(T+\tau)},$$

obviously, we have

$$\hat{E}\|x(2\tau+T)\|^2 \leq e^{-\alpha(T+\tau)}\hat{E}\|\xi\|^2,$$

based on the homogeneity of time and repeating the iteration, we obtain

$$\hat{E}\|x(n\tau+T)\|^2 \leq e^{-\alpha(n-1)(T+\tau)}\hat{E}\|\xi\|^2. \tag{17}$$

hence, for $t \in (n\tau+T, (n+1)\tau+T)$, combining (9) and (17)

$$\sup_{n\tau+T\le t\le(n+1)\tau+T} \hat{E}|x(t)|^2 \le 2\kappa_1\hat{E}\|x_{n\tau+T}\|^2 \le 2\kappa_1 e^{-\alpha(n-1)(T+\tau)}\hat{E}\|\xi\|^2.$$

This proof is hereby completed. □

Remark 6. *The main theorem synthesizes the results of Lemmas 6–8, proving that the system remains stable under G-Brownian motion and parameter uncertainty, even when delays and intermittent control strategies are introduced. The main theorem relies on the stability conditions and analytical methods provided by the preceding lemmas, detailing the behavior of the system under these complex conditions and providing sufficient conditions for system stability.*

5. Numerical Examples

Example 1. *Now, we consider a two-dimensional numerical example. There are the given parameter matrices:*

$$A=\begin{pmatrix}0.1 & 0.5\\ 0.5 & 0.1\end{pmatrix}, B_{11}=\begin{pmatrix}-0.5 & 0\\ 0 & -0.5\end{pmatrix}, B_{12}=\begin{pmatrix}0 & 0\\ 0 & 0\end{pmatrix}, B_{21}=\begin{pmatrix}0 & 0\\ 0 & 0\end{pmatrix}, B_{22}=\begin{pmatrix}-0.5 & 0\\ 0 & -0.5\end{pmatrix}$$
$$C_1=\begin{pmatrix}0.1 & 0\\ 0 & 0.1\end{pmatrix}, C_2=\begin{pmatrix}0.1 & 0\\ 0 & 0.1\end{pmatrix}, Z_{11}=\begin{pmatrix}0.2 & 0\\ 0 & 0.2\end{pmatrix} Z_{12}=\begin{pmatrix}0 & 0\\ 0 & 0\end{pmatrix}, Z_{22}=\begin{pmatrix}0.2 & 0\\ 0 & 0.2\end{pmatrix}$$
$$Z_1=\begin{pmatrix}2 & 0\\ 0 & 2\end{pmatrix}, Z_2=\begin{pmatrix}2 & 0\\ 0 & 2\end{pmatrix}, H=\begin{pmatrix}0.5 & 0\\ 0 & 0.5\end{pmatrix}.$$

The values of the random term are given in the following matrix:

$$O=\left\{\Psi=\begin{pmatrix}\delta_{11} & \delta_{12}\\ \delta_{12} & \delta_{22}\end{pmatrix} : \delta_{11}\in[5,6], \delta_{12}\in[2,3], \delta_{22}\in[5,6]\right\}.$$

For convenience, let $\tau=0$. The design of the control functions $u(x(t))$ are as follows:

$$u(x)=\begin{pmatrix}-0.4x_1(t)\\ -0.4x_2(t)\end{pmatrix}.$$

Through the MATLAB LMI toolbox, we have:

$$P_{11}=\begin{pmatrix}0.345 & 0\\ 0 & 0.345\end{pmatrix}, P_{22}=\begin{pmatrix}0.505 & 0\\ 0 & 0.505\end{pmatrix}, Q_{11}=\begin{pmatrix}1.481 & 0\\ 0 & 1.481\end{pmatrix}, Q_{22}=\begin{pmatrix}1.744 & 0\\ 0 & 1.744\end{pmatrix}.$$

It can be easily verified that $A(t)$, $u(x(t))I(t)$, $B_{ij}(t)x(t)I(t)$, $C_{ij}(t)x(t)I(t)$ satisfy Assumption 1. From Lemma 6, we choose $\eta_{ij}=1$. After inserting these values into Lemma 6 and completing the calculations, we obtain $\theta^*=0.533$ and opt for $\theta=0.55$. Furthermore, with $C=2.898$ and choosing $\varsigma=0.001$, substituting the above into Theorem 1 and performing the calculations yields $T=9.951$.

Figures 1–3 both employ the Euler numerical method with $\Delta t=0.01$, and each selects a variance within the specified range to simulate graphically. Figure 1 elucidates that the system manifests instability when a smaller variance, denoted as $\delta^2=0.1$, is utilized. Conversely, stability is attained when the variance is augmented to $\delta^2=5$. Figure 2 delineates the impact of the control interval θ on system stability. Specifically, the system exhibits instability when $\theta=0.1$, a value that falls below the critical threshold. However, stability is restored when the control interval is set to a value that exceeds this critical threshold. These simulation figures substantiate the veracity of the theoretical proofs previously articulated, demonstrating the nuanced dependency of system stability on the parameters of variance and control interval.

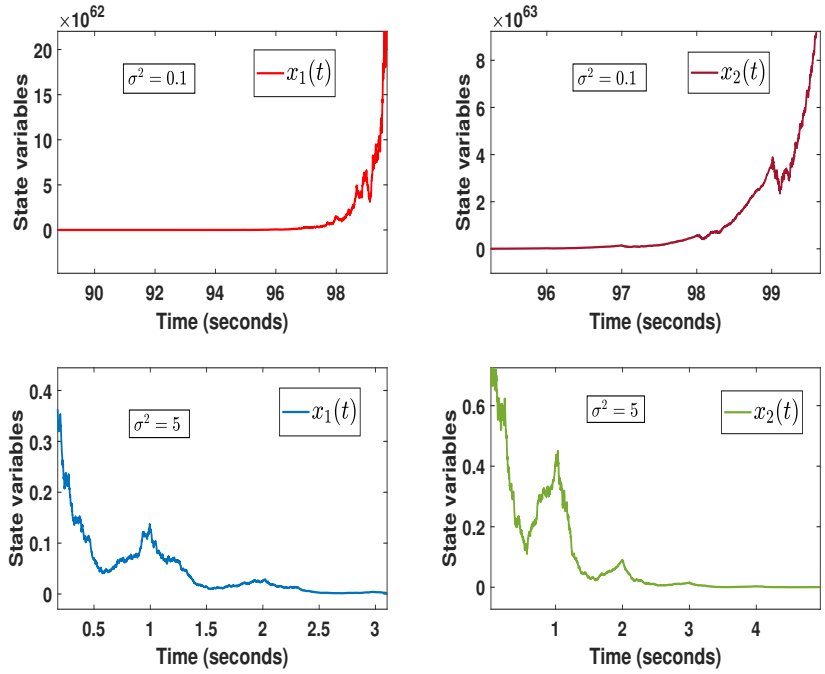

Figure 1. Intermittent Control and Dynamic Parameters.

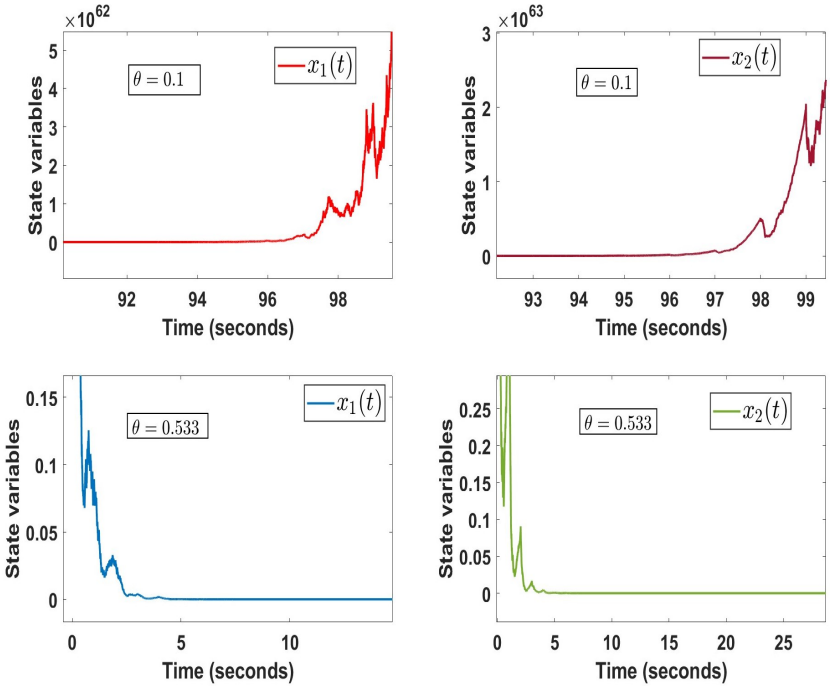

Figure 2. Intermittent Control and Dynamic Parameters.

Example 2. *Consider a two-dimensional system with delays:*

$$A = \begin{pmatrix} 0.2 & 0.1 \\ 0.1 & 0.2 \end{pmatrix}, B_{11} = \begin{pmatrix} -0.5 & 0 \\ 0 & -0.5 \end{pmatrix}, B_{12} = \begin{pmatrix} 0 & 0 \\ 0 & 0 \end{pmatrix}, B_{21} = \begin{pmatrix} 0 & 0 \\ 0 & 0 \end{pmatrix}, B_{22} = \begin{pmatrix} -0.5 & 0 \\ 0 & -0.5 \end{pmatrix}$$
$$C_1 = \begin{pmatrix} 0.1 & 0 \\ 0 & 0.1 \end{pmatrix}, C_2 = \begin{pmatrix} 0.1 & 0 \\ 0 & 0.1 \end{pmatrix}, Z_{11} = \begin{pmatrix} 0.2 & 0 \\ 0 & 0.2 \end{pmatrix} Z_{12} = \begin{pmatrix} 0 & 0 \\ 0 & 0 \end{pmatrix}, Z_{22} = \begin{pmatrix} 0.2 & 0 \\ 0 & 0.2 \end{pmatrix}$$
$$Z_1 = \begin{pmatrix} 2 & 0 \\ 0 & 2 \end{pmatrix}, Z_2 = \begin{pmatrix} 2 & 0 \\ 0 & 2 \end{pmatrix}, H = \begin{pmatrix} 0.5 & 0 \\ 0 & 0.5 \end{pmatrix}.$$

The design of the control functions $u(x(t-\tau))$ are as follows:

$$u(x) = \begin{pmatrix} -4x_1(t-\tau) \\ -4x_2(t-\tau) \end{pmatrix}.$$

The values of the random term are given in the following matrix:

$$O = \left\{ \Psi = \begin{pmatrix} \delta_{11} & \delta_{12} \\ \delta_{12} & \delta_{22} \end{pmatrix} : \delta_{11} \in [0.8, 1], \delta_{12} \in [0.5, 0.8], \delta_{22} \in [0.8, 1] \right\}.$$

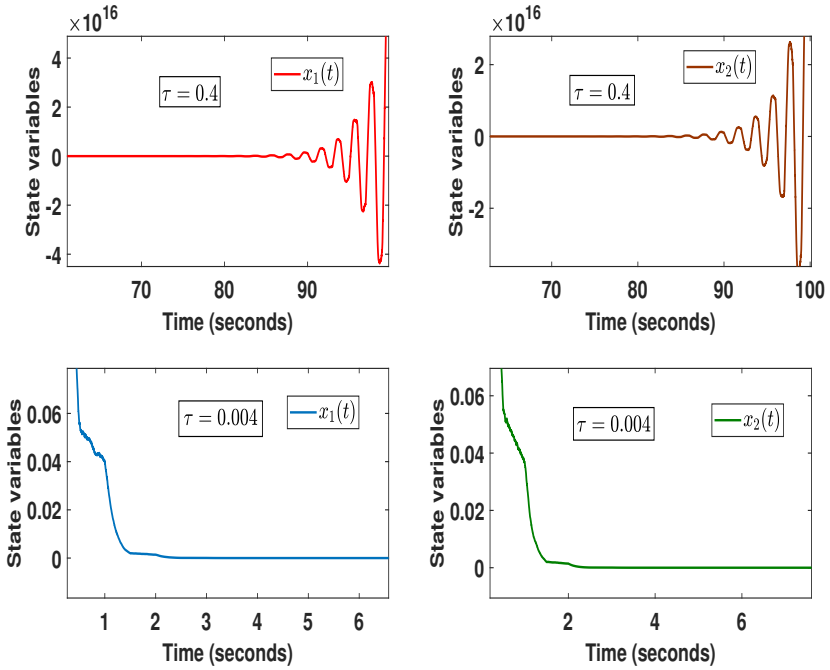

Figure 3. Intermittent Control and Dynamic Parameters.

Through the MATLAB LMI toolbox, we have:

$$P_{11} = \begin{pmatrix} 1.82 & 0 \\ 0 & 1.82 \end{pmatrix}, P_{22} = \begin{pmatrix} 1.82 & 0 \\ 0 & 1.82 \end{pmatrix}, Q_{11} = \begin{pmatrix} 2.9 & 0 \\ 0 & 2.9 \end{pmatrix}, Q_{22} = \begin{pmatrix} 2.9 & 0 \\ 0 & 2.9 \end{pmatrix},$$

after calculation, it is easy to obtain $\beta_1 = 0.31$, $\beta_2 = 0.35$, $\beta_3 = 0.14$, $\beta_4 = 0.4$, $\beta_5 = 0.56$, $T = 0.9$. Substituting the above values into Equation (14), we obtain $\tau = 0.0076$. The simulation in Figure 3 clearly shows that the system is stable when the delay $\tau < 0.0076$. When the delay $\tau > 0.0076$, the system becomes unstable.

6. Conclusions

In this paper, we have investigated stochastic intermittent control strategies based on G-Brownian motion and parameter uncertainties. The key contributions of our work can be summarized as follows: We demonstrated that the system remains stable even under parameter uncertainties by constructing appropriate Lyapunov functions and applying G-expectation theory, addressing a significant challenge in practical applications where parameters cannot always be precisely known. Additionally, we extended the analysis to systems with delays and intermittent control strategies, proving that stability can still be maintained, which is particularly relevant for real-world systems where delays and resource constraints necessitate intermittent control. Future research can build on this work by relaxing some of the assumptions made in this study, such as known system parameters and linear control functions, to enhance the applicability of the methods. Furthermore, implementing and validating the proposed methods in real-world systems, such as industrial

processes or networked control systems, would provide valuable insights and confirm their practical effectiveness. Lastly, investigating advanced control strategies, such as adaptive and robust control, in the context of G-Brownian motion and intermittent control could further improve system performance under uncertainty and resource constraints.

Author Contributions: Conceptualization, Z.M. and H.J.; methodology, Z.M. and D.Z.; software, X.L.; validation, D.Z.; formal analysis, C.L.; investigation, X.L.; resources, C.L.; data curation, Z.M. and H.J.; writing—original draft preparation, Z.M.; writing—review and editing, Z.M.; visualization, Z.M.; supervision, D.Z.; project administration, D.Z.; funding acquisition, D.Z. All authors have read and agreed to the published version of the manuscript.

Funding: This research was funded by YNWR-QNBJ (2019-169).

Data Availability Statement: Not applicable.

Conflicts of Interest: The authors declare no conflicts of interest.

References

1. Mao, X. *Stochastic Differential Equations and Applications*, 2nd ed.; Horwood: Chichester, UK, 2007.
2. Higham, D.; Mao, X.; Stuart, A. Strong convergence of Euler-type methods for nonlinear stochastic differential equations. *Siam J. Numer. Anal.* **2002**, *40*, 1041–1063. [CrossRef]
3. Zhu, Q. Stabilization of stochastic nonlinear delay systems with exogenous disturbances and the event-triggered feedback control. *IEEE Trans. Autom. Control* **2019**, *64*, 3764–3771. [CrossRef]
4. Yin, Z.; Zhu, Q. Stabilization of stochastic highly nonlinear delay systems with neutral term. *IEEE Trans. Autom. Control* **2023**, *68*, 2544–2551.
5. Hao, X.; Zhu, Q.; Xing, Z. Exponential stability of stochastic nonlinear delay systems subject to multiple periodic impulses. *IEEE Trans. Autom. Control* **2024**, *69*, 2621–2628.
6. Lina, F.; Zhu, Q.; Xing, Z. Stability analysis of switched stochastic nonlinear systems with state-dependent delay. *IEEE Trans. Autom. Control* **2024**, *69*, 2567–2574.
7. Hasminskii, R. *Stochastic Stability of Differential Equations*; Sijthoff and Noordhoff: Groningen, The Netherlands, 1981.
8. Mao, X. Stochastic stabilization and destabilization. *Syst. Control Lett.* **1994**, *23*, 279–290. [CrossRef]
9. Mao, X.; Yin, G.; Yuan, C. Stabilization and destabilization of hybrid systems stochastic differential equations. *Automatica* **2007**, *43*, 264–273. [CrossRef]
10. Nair, G.; Evans, R. Stabilizability of stochastic linear systems with finite feedback data rates. *Siam J. Control Optim.* **2004**, *43*, 413–436. [CrossRef]
11. Mao, X.; Lam, J.; Huang, L. Stabilisation of hybrid stochastic differential equations by delay feedback control. *Syst. Control Lett.* **2008**, *57*, 927–935. [CrossRef]
12. Mao, X. Almost sure exponential stabilization by discrete-time stochastic feedback control. *IEEE Trans. Autom. Control* **2016**, *61*, 1619–1624. [CrossRef]
13. Deng, F.; Luo, Q.; Mao, X. Stochastic stabilization of hybrid differential equations. *Automatica* **2012**, *48*, 2321–2328. [CrossRef]
14. Yu, K.; Zhai, D.-H.; Liu, G.-P.; Zhao, Y.-B.; Zhao, P. Stability analysis of a class of hybrid stochastic retarded systems under asynchronous switching. *IEEE Trans. Autom. Control* **2014**, *59*, 1511–1523
15. Lu, Z.; Hu, J.; Mao, X. Stabilisation by delay feedback control for highly nonlinear hybrid stochastic differential equations. *Discret. Contin. Dyn.-Syst.-Ser. B* **2019**, *24*, 4099–4116. [CrossRef]
16. Hu, J.; Liu, W.; Deng, W.; Mao, X. Advances in stabilization of hybrid stochastic differential equations by delay feedback control. *Siam J. Control Optim.* **2020**, *58*, 735–754. [CrossRef]
17. Zong, X.; Wu, F.; Yin, G. Stochastic regularization and stabilization of hybrid functional differential equations. In Proceedings of the IEEE Conference on Decision and Control (CDC), Osaka, Japan, 15–18 December 2015; Volume 54, pp. 1211–1216.
18. Zhu, Q.; Zhang, Q. Pth moment exponential stabilisation of hybrid stochastic differential equations by feedback controls based on discrete-time state observations with a time delay. *IET Control Theory Appl.* **2017**, *11*, 1992–2003. [CrossRef]
19. Astrom, K.; Wittenmark, B. *Computer-Controlled Systems: Theory and Design*, 3rd ed.; Prentice Hall: Upper Saddle River, HJ, USA, 1997.
20. Shevitz, D.; Paden, B. Lyapunov stability theory of nonsmooth systems. *IEEE Trans. Autom. Control* **1991**, *36*, 495–500.
21. Heemels, W.; Donkers, M.; Teel, A. Periodic event-triggered control for linear systems. *IEEE Trans. Autom. Control* **2013**, *58*, 847–861. [CrossRef]
22. Heydari, A. Optimal Switching with Minimum Dwell Time Constraint. *J. Frankl. Inst.* **2017**, *354*, 4498–4518. [CrossRef]
23. Nesic, D.; Teel, A. A framework for stabilization of nonlinear sampled-data systems based on their approximate discrete-time models. *IEEE Trans. Autom. Control* **2004**, *49*, 1103–1122. [CrossRef]
24. Mayne, D.; Rawlings, J.; Rao, C.; Scokaert, P. Constrained model predictive control: Stability and optimality. *Automatica* **2000**, *36*, 789–814. [CrossRef]

25. Chen, C. Robust self-organizing neural-fuzzy control with uncertainty observer for mi-mo nonlinear systems. *IEEE Trans. Fuzzy Syst.* **2011**, *19*, 694–706. [CrossRef]
26. Magdi, S. Passive Control Synthesis for Uncertain Time-delay Systems. In Proceedings of the American Conference on Decision and Control, Tampa, FL, USA, 18 December 1998; IEEE Press: Piscataway, NJ, USA, 1998; Volume 37, pp. 4139–4143.
27. Iwasaki, T.; Skelton, R. All controllers for the general H∞ control problem: LMI existence conditions and state space formulas. *Automatica* **1994**, *30*, 1307–1317. [CrossRef]
28. Ma, Z.; Yuan, S.; Meng, K.; Mei, S. Mean-square stability of uncertain delayed stochastic systems driven by G-Brownian motion. *Mathematics* **2023**, *11*, 2405. [CrossRef]
29. Peng, S. G-expectation, G-Brownian motion and related stochastic calculus of Itô type. *Stoch. Anal. Appl. Abel Symp.* **2007**, *2*, 541–567.
30. Peng, S. Multi-Dimensional G-Brownian motion and related stochastic calculus under G-Expectation. *Stoch. Process. Their Appl.* **2008**, *118*, 2223–2253. [CrossRef]
31. Ren, Y.; Jia, X.; Hu, L. Exponential stability of solutions to impulsive stochastic differential equations driven by G-Brownian motion. *Discret. Contin. Dyn. Syst. B* **2017**, *20*, 2157–2169. [CrossRef]
32. Zhu, Q.; Huang, T. Stability analysis for a class of stochastic delay nonlinear systems driven by G-Brownian motion. *Syst. Control Lett.* **2020**, *140*, 104699. [CrossRef]
33. Gao, F. Pathwise properties and homeomorphic flows for stochastic differential equations driven by G-Brownian motion. *Stoch. Process. Their Appl.* **2009**, *11*, 3356–3382. [CrossRef]
34. Li, X.; Lin, X.; Lin, Y. Lyapunov-type conditions and stochastic differential equations driven by G-Brownian motion. *J. Math. Anal. Appl.* **2016**, *439*, 235–255 [CrossRef]
35. Liu, Z.; Zhu, Q. Delay feedback control of highly nonlinear neutral stochastic delay differential equations driven by G-Brownian motion. *Syst. Control Lett.* **2023**, *181*, 105640. [CrossRef]
36. Boyd, S.; Ghaoui, L.; Feron, E.; Balakrishnan, V. *Linear Matrix Inequalities in System and Control Theory*; SIAM: Philadelphia, PA, USA, 1994.

mathematics

MDPI

Article

Exponential Synchronization of Coupled Neural Networks with Hybrid Delays and Stochastic Distributed Delayed Impulses

Gang Zhang [1], Yinfang Song [1,*] and Xiaoyou Liu [2]

[1] School of Information and Mathematics, Yangtze University, Jingzhou 434023, China; 2022710157@yangtzeu.edu.cn
[2] School of Mathematics and Computing Sciences, Hunan University of Science and Technology, Xiangtan 411201, China; xiaoyouliu@hnust.edu.cn
* Correspondence: yfs81@yangtzeu.edu.cn

Abstract: This paper is concerned with exponential synchronization for a class of coupled neural networks with hybrid delays and stochastic distributed delayed impulses. First of all, based on the average impulsive interval method, total probability formula and ergodic theory, several novel impulsive Halanay differential inequalities are established. Two types of stochastic impulses, i.e., stochastic distributed delayed impulses with dependent property and Markov property have been taken into account, respectively. Secondly, some criteria on exponential synchronization in the mean square of a class of coupled neural networks with stochastic distributed delayed impulses are acquired by combining the proposed lemmas and graph theory. The validity of the theoretical results is demonstrated by several numerical simulation examples.

Keywords: coupled neural networks; stochastic distributed delayed impulses; synchronization; Markov property

MSC: 93C27; 34K24

1. Introduction

In recent years, the dynamical properties of neural networks (NNs) have been extensively investigated due to NNs' high-nonlinearity and good fault tolerance. Various kinds of NNs including Hopfield NNs, Cohen-Grossber NNs, BAM NNs and inertial NNs have been proposed and examined. Moreover, coupled neural networks (CNNs) can be regarded as one kind of complicated NN composed of multiple interconnected nodes. In contrast to NNs with single nodes, CNNs possess more elaborate and unforeseeable characteristics. Recently, a considerable number of results with respect to the collective behavior of CNNs have been reported [1–4].

Synchronization is an interesting and important class of collective behavior and depicts that several systems adapt each other to a common trajectory that may be an equilibrium point, periodic solution, or chaotic attractor. Since Pecora and Carroll [5] introduced the synchronization of two identical chaotic systems, the synchronization issue has gained considerable attention because it can describe many natural phenomena and has many potential applications for image processing, secure communication, and neuronal synchronization. For instance, the theta rhythm related to the behavior of animals is produced by partial synchronization of neuronal activity in the hippocampal network, and an excessive synchronization of the neuronal activity over a wide area in the brain results in the epileptic rhythm [6]. Currently, various approaches to synchronization of CNNs have been developed including pinning control [7], adaptive control [8], event-triggered control [9], sampling control [10], periodic intermittent control [11], sliding control [12], impulsive control [13,14] and so on. Particularly, in [8], several criteria on exponential

synchronization in the mean square and the almost sure sense for a class of neutral stochastic CNNs have been provided by combining M-matrix theory and algebraic inequalities, and adaptive controllers have been designed. In the real environment, it is desirable to realize synchronization within a finite horizon. Consequently, finite-time and fixed-time synchronization [15] of CNNs have been examined which exhibit strong robustness and anti-interference capability.

In addition, some practical networks such as electronic networks and biological networks frequently encounter momentary disturbances and abrupt variations, which could be characterized as impulses. Generally, impulses can be categorized into stabilizing impulses, destabilizing impulses and hybrid impulses. Numerous achievements relevant to the dynamic behaviors of CNNs with impulsive effects have been published. For instance, asymptotic synchronization of CNNs with time delays and stabilizing impulses has been studied by utilizing the stability theory for impulsive functional differential equations in [16] while exponential synchronization issue of CNNs has been dealt with through destabilizing impulses in [17]. By referring to [16–18], unified synchronization criteria in an array of CNNs with hybrid impulses have been established, and several concepts on average impulsive interval and average impulsive gain have been put forward in [19]. Furthermore, by using the improved Razumikhin approach, several criteria on pth moment exponential stability of non-autonomous stochastic delayed systems with impulsive effects have been derived in [20,21]. Actually, time delays also exist at the moment of the impulses and affect the dynamic properties in some applicable systems including signal transmission processing and biology systems. Numerous studies about stability and synchronization of nonlinear systems with delayed impulses have been carried out [22–25]. In [22], by utilizing the impulsive control theory and some comparison principles, various stability of nonlinear systems with state-dependent impulses have been examined. In [25], in light of the average impulsive delay–gain approach, exponential synchronization of CNNs with hybrid delayed impulses has been analyzed. The aforementioned impulsive delays are constant delays or time-varying delays, and one new class of distributed-delay-dependent impulses [26–31] has also caught the researchers' attention. In [28,29], several impulsive Halanay differential inequalities have been presented and applied to the synchronization of network systems with distributed delayed impulses. Furthermore, the mean square stability of stochastic functional systems with distributed delayed impulses has been discussed based on the stochastic analysis technique and average dwell time method in [30,31]. Due to the existence of stochastic disturbances at the impulsive moment, stochastic impulses [32–38] have been introduced. In [34], under the circumstance that the impulse intensities were supposed to be random, the exponential synchronization problem of the neural networks (NNs) has been tackled, and the results have been further generalized to inertial network systems with stochastic delayed impulses [35,36].

It can be seen that the existing achievements in [26–31] are related to the deterministic distributed delayed impulses. Particularly, in [27], exponential synchronization of chaotic NNs with distributed delayed impulses has been examined, and the theoretical work has been extended to CNNs with time-varying delays of unknown bounded in [28]. However, so far, the synchronization issue of CNNs with hybrid delays and stochastic distributed delayed impulses has not been explored. Actually, when some factors such as hybrid delays and stochastic distributed delayed impulses are taken into account simultaneously, the approaches in [34–36] can not be directly applied to this case. How to overcome the difficulties that these factors bring is full of challenges. Additionally, the parameter c is limited to the condition $0 < c \leq 1$ in [34] and $c = 1$ in [35], and impulses can not have a positive impact on the synchronization realization of coupled inertial NNs with hybrid delays in [36]. Consequently, how to relax these constraints and reduce the conservativeness of the existing work [34–36] is of great significance.

Inspired by the above discussions, we aim to explore the exponential synchronization of a class of CNNs with hybrid delays and stochastic distributed delayed impulses. To begin with, we propose two novel impulsive Halanay differential inequalities, where two types of

stochastic impulses, i.e., stochastic distributed delayed impulses with dependent property and Markov property have been considered, respectively. Furthermore, combining the proposed lemmas and graph theory, some criteria on exponential synchronization in the mean square of a class of CNNs with stochastic distributed delayed impulses are obtained. The main contributions can be unfolded in three aspects.

(1) Different from the deterministic distributed delayed impulses in the literature [26–31], in this paper, the intensities of distributed delayed impulses are supposed to be random. Two types of stochastic impulses including stochastic distributed delayed impulses with independent property and Markov property have been explored, respectively.
(2) Based on the average impulsive interval method, total probability formula and ergodic theory, two novel impulsive Halanay differential inequalities are established, which generalize the findings in the literature [34,35] since time-varying delays, distributed delays and stochastic distributed delayed impulses are introduced simultaneously. Parameter c can be arbitrarily chosen. In view of invariant distribution theory, the stochastic impulses with Markov property are tackled.
(3) By utilizing the established inequalities and graph theory, some criteria for exponential synchronization of CNNs with stochastic distributed delayed impulses are derived. In [36], impulses can only be regarded as outer disturbances for coupled inertial NNs with hybrid delays. Compared with the work [36], in this paper, impulses may also be viewed as outer perturbations or stabilizing sources, and the case of stochastic impulses with Markov property is also discussed.

The remainder of this paper is arranged as follows. In Section 2, some necessary definitions and assumptions are given, and two novel impulsive Halanay differential inequalities are established. In Section 3, a class of coupled neural networks with stochastic distributed delayed impulses is presented and several criteria on exponential mean square synchronization are derived. In Section 4, two numerical simulation examples are provided to show the validity of the theoretical results. Conclusions are drawn in the last section.

Notations: Let $\mathbb{R}$ and $\mathbb{R}^+$ be the set of real numbers and the set of non-negative real numbers, respectively. $\mathbb{N}^+$ stands for the set of positive integer numbers. $C(\mathbb{R}^+, \mathbb{R})$ denotes the set of continuous functions $v : \mathbb{R}^+ \to \mathbb{R}$. $D^+v(t)$ represents the upper right Dini derivative of a function $v(t)$. $B = (b_{ij})_{m\times n}$ denotes an $m \times n$ matrix, and B^T denotes the transpose of matrix B. $\lambda_{\max}(B)$ denotes the maximal eigenvalue. For a random variable β, $E(\beta)$ and $D(\beta)$ denote the mathematical expectation and the variance, respectively. $\beta \sim U(a, b)$ and $\beta \sim E(c)$ indicate that β obeys the uniform distribution and the exponential distribution, respectively. $P(A)$ represents the probability of the random event A.

2. Preliminaries

In this section, we will propose some necessary definitions and assumptions. Meanwhile, based on the average impulsive interval method, total probability formula and ergodic theory, two novel impulsive Halanay differential inequalities with hybrid delays are given. Two types of stochastic impulses, i.e., stochastic distributed delayed impulses with dependent property and Markov property have been taken into account, respectively.

Definition 1. *Suppose that $\Theta = \{t_1, t_2, \cdots, t_n\}$ is the impulsive sequence and T_a is the average impulsive interval. If $T_a \in \mathbb{R}^+, N_0 \in \mathbb{N}^+$ satisfied*

$$\frac{T-t}{T_a} - N_0 \leq N_\Theta(T, t) \leq \frac{T-t}{T_a} + N_0, \forall T \geq t \geq 0, \tag{1}$$

let $N_\Theta(T, t)$ be the number of impulsive times and Θ be the impulsive sequence on the interval $[t, T]$.

Assumption 1. *Let $\{\beta_k\}_{k=1,2,\ldots}$ denote a sequence of independent and identically distributed random variables satisfying*

$$\begin{cases} E\beta_k = \alpha > 0, \\ D\beta_k \leq \gamma^2, \\ \beta_k \geq 0, \end{cases} \tag{2}$$

where γ is a determined non-negative constant.

Lemma 1. *Let $\Theta = \{t_1, t_2, \cdots, t_n\}$ denote the impulsive sequence and T_a denote the average impulsive interval. Suppose that Assumption 1 holds. Function $v(t) \in C(\mathbb{R}^+, \mathbb{R})$, $t \geq t_0 (t \neq t_k)$ satisfies the following differential inequality with stochastic distributed delayed impulses*

$$\begin{cases} D^+v(t) \leq -pv(t) + qv(t - \sigma_1(t)) + r\int_{t-\sigma_2}^{t} v(s)ds, t \neq t_k, \\ v(t_k) \leq \beta_k \int_{t-\rho_k}^{t} v(s)ds, t = t_k, k = 1, 2, \cdots, \\ v(t) = \Phi(t), t \in [t_0 - \tau_0, t_0], \end{cases} \tag{3}$$

where $v(t_k) = v(t_k^+)$, $0 \leq \rho_k \leq \rho$, $\sigma_2 \geq \rho_k$, $\sigma_1(t) \leq \sigma_1$, $\tau_0 = \max\{\sigma_1, \sigma_2\}$, $p \geq 0$, $q \geq 0$, $r \geq 0$ and $\|\Phi_{t_0}\|_{\tau_0} = \sup_{-\tau_0 \leq s \leq 0} \|\Phi(t_0 + s)\|$. Denote $M_1 = \max\left\{c^{-\frac{\sigma_1}{T_a} - N_0}, 1\right\}$ and $M_2 = \max\left\{c^{-\frac{\sigma_2}{T_a} - N_0}, 1\right\}$. If $p > qM_1 + rM_2\sigma_2 \geq 0$, then we have

$$Ev(t) \leq M_0 \|\Phi_{t_0}\|_{\tau_0} e^{-\left(\bar{\epsilon} - \frac{\ln \lambda}{T_a}\right)(t - t_0)}, \forall t \geq t_0, \tag{4}$$

where $\lambda \triangleq \min\left\{\alpha\rho_i e^{\bar{\epsilon}\rho_i} + \frac{c\rho_i^2 e^{2\bar{\epsilon}\rho_i}\gamma^2}{(\alpha\rho_i e^{\bar{\epsilon}\rho_i} - c)^2}, \alpha\rho_i e^{\bar{\epsilon}\rho_i} + c\right\}$, $M_0 \triangleq \max\{\lambda^{-N_0}, \lambda^{N_0}\}$, $c \neq \alpha\rho_i e^{\bar{\epsilon}\rho_i}$ and $\bar{\epsilon} > 0$ is the unique solution of $\Pi(\epsilon) = \epsilon - p + qM_1 e^{\sigma_1 \epsilon} + rM_2 \frac{1}{\epsilon}(e^{\sigma_2 \epsilon} - 1) = 0$.

Proof. Construct the following function

$$\Pi(\epsilon) = \epsilon - p + qM_1 e^{\epsilon\sigma_1} + rM_2 \frac{1}{\epsilon}(e^{\epsilon\sigma_2} - 1). \tag{5}$$

Noting that $\lim_{\epsilon \to 0^+} \Pi(\epsilon) = -p + qM_1 + rM_2\sigma_2 < 0$, $\lim_{\epsilon \to +\infty} \Pi(\epsilon) > 0$ and $\Pi'(\epsilon) > 0$, there exists a unique positive root $\bar{\epsilon}$ for equation $\Pi(\epsilon) = 0$. Subsequently, we will claim that

$$v(t) \leq \left(\prod_{i=1}^{k} \mu_i\right) \|\Phi_{t_0}\|_{\tau_0} e^{-\bar{\epsilon}(t - t_0)}, t \in [t_k, t_{k+1}), k = 0, 1, 2, \ldots, \tag{6}$$

where $\mu_i \triangleq \max\{\beta_i\rho_i e^{\bar{\epsilon}\rho_i}, c\}, i = 1, 2, \ldots,$ and $c > 0$. When $t \in [t_0 - \tau, t_0]$, obviously, $v(t) \leq \|\Phi_{t_0}\|_{\tau}$. Let $\Gamma > \|\Phi_{t_0}\|_{\tau_0}$. In order to show that assertion (5) holds, we need to prove that

$$v(t) < \Gamma\left(\prod_{i=1}^{k} \mu_i\right) e^{-\bar{\epsilon}(t - t_0)} = z_k(t), \forall t \in [t_k, t_{k+1}), k = 0, 1, 2, \ldots. \tag{7}$$

When $k = 0$, since the system is not influenced by impulse, we need to show that

$$v(t) < \Gamma e^{-\bar{\epsilon}(t - t_0)} \triangleq z_0(t), \forall t \in [t_0, t_1). \tag{8}$$

Assume that inequality (8) is not satisfied, there exists a $t^* \in [t_0, t_1)$ such that

$$v(t) < \Gamma e^{-\bar{\epsilon}(t - t_0)}, t \in [t_0, t_*), v(t^*) = \Gamma e^{-\bar{\epsilon}(t^* - t_0)}; D^+v(t^*) \geq D^+z_0(t^*). \tag{9}$$

It follows from (9) that

$$\begin{aligned} D^+v(t^*) \leq & -pv(t^*) + qv(t^* - \sigma_1(t)) + r\int_{t^*-\sigma_2}^{t^*} v(s)ds \\ < & -p\Gamma e^{-\bar{\epsilon}(t^*-t_0)} + q\Gamma e^{-\bar{\epsilon}(t^*-\sigma_1-t_0)} + r\int_{t*-\sigma_2}^{t*} \Gamma e^{-\bar{\epsilon}(s-t_0)}ds \\ < & \big[-p + qM_1e^{\sigma_1\bar{\epsilon}} + \frac{r}{\bar{\epsilon}}(e^{\sigma_2\bar{\epsilon}} - 1)M_2\big]z_0(t^*) \\ = & D^+z_0(t^*), \end{aligned} \tag{10}$$

which means that $D^+v(t^*) < D^+z(t^*)$. It yields a contradiction with (9). Hence, inequality (8) holds. Assume that inequality (7) holds for $k \leq m_0 - 1, m_0 \in \mathbb{N}^+$, i.e.,

$$v(t) < z_k(t), \forall t \in [t_k, t_{k+1}), k = 1, 2, \ldots, m_0 - 1. \tag{11}$$

In what follows, we need to prove that inequality (7) is true for $k = m_0$. Actually, when $t = t_{m_0}$, one has that $v(t_{m_0}) < \beta_{m_0}\int_{t-\rho_{m_0}}^{t_{m_0}} \Gamma\left(\prod_{i=1}^{m_0-1}\mu_i\right)e^{-\bar{\epsilon}(s-t_0)}ds \leq \Gamma\beta_{m_0}e^{\bar{\epsilon}\rho_{m_0}}\rho_{m_0}\left(\prod_{i=1}^{m_0-1}\mu_i\right)$ $e^{-\bar{\epsilon}(t_{m_0}-t_0)} \leq \Gamma\left(\prod_{i=1}^{m_0}\mu_i\right)e^{-\bar{\epsilon}(t_{m_0}-t_0)} \leq z_{m_0}(t_{m_0})$. If inequality (7) is incorrect for $t \in (t_{m_0}, t_{m_0+1})$, then there exists a $t_* \in (t_{m_0}, t_{m_0+1})$ such that

$$v(t) < z_{m_0}(t), t \in [t_{m_0}, t_*), v(t_*) = z_{m_0}(t_*); D^+v(t_*) \geq D^+z_{m_0}(t_*). \tag{12}$$

For $\forall t \in [t_* - \sigma_1, t_*)$, suppose $t \in [t_{b_t}, t_{b_t+1})$, where b_t is related to t. It follows from inequalities (11) and (12)

$$v(t) < z_{b_t}(t), \forall t \in [t_* - \sigma_1, t_*). \tag{13}$$

Noting that $\mu_i \geq c$, we may know that

$$v(t) < z_{b_t}(t) = \frac{1}{\mu_{b_t+1}\ldots\mu_{m_0}}\Big(\prod_{i=1}^{m_0}\mu_i\Big)\Gamma e^{\bar{\epsilon}(t_*-t)}e^{-\bar{\epsilon}(t_*-t_0)} \leq \frac{e^{\bar{\epsilon}(t_*-t)}}{c^{m_0-b_t}}z_{m_0}(t_*), \forall t \in [t_* - \sigma_1, t_*). \tag{14}$$

Let $t_* - \sigma_1 \in [t_{d_0}, t_{d_0+1})$; we can find that $b_t \in [d_0, m_0]$. According to Definition 1, we can derive that

$$0 \leq m_0 - b_t \leq m_0 - d_0 = N_\Theta(t_* - \sigma_1, t_*) \leq \frac{\sigma_1}{T_a} + N_0, \forall t \in [t_* - \sigma_1, t_*). \tag{15}$$

When $c \leq 1$, combining inequalities (14) and (15) yields

$$v(t) < c^{-\frac{\sigma_1}{T_a}-N_0}e^{\bar{\epsilon}(t_*-t)}z_{m_0}(t_*), \forall t \in [t_* - \sigma_1, t_*). \tag{16}$$

When $c > 1$, according to inequalities (14) and (15), we obtain that

$$v(t) < e^{\bar{\epsilon}(t_*-t)}z_{m_0}(t_*), \forall t \in [t_* - \sigma_1, t_*). \tag{17}$$

Since $z_{m_0}(t)$ is decreasing, it satisfies the following inequality

$$v(t_* - \sigma_1(t_*)) < \max\Big\{c^{-\frac{\sigma_1}{T_a}-N_0}, 1\Big\}e^{\sigma_1\bar{\epsilon}}z_{m_0}(t_*) = M_1e^{\sigma_1\bar{\epsilon}}z_{m_0}(t_*). \tag{18}$$

Similarly, when $s \in [t_* - \sigma_2, t_*]$, we also have that

$$v(s) < \max\Big\{c^{-\frac{\sigma_2}{T_a}-N_0}, 1\Big\}e^{\bar{\epsilon}(t_*-s)}z_{m_0}(t_*). \tag{19}$$

It follows from inequality (18) and inequality (19) that

$$\begin{aligned} D^+v(t_*) \leq & -pv(t_*) + qv(t_* - \sigma_1(t_*)) + r\int_{t_*-\sigma_2}^{t_*} v(s)ds \\ < & -pz_{m_0}(t_*) + qM_1e^{\sigma_1\bar{\epsilon}}z_{m_0}(t_*) + r\max\left\{c^{-\frac{\sigma_2}{T_a}-N_0}, 1\right\}z_{m_0}(t_*)\int_{t_*-\sigma_2}^{t_*} e^{\bar{\epsilon}(t_*-s)}ds \\ = & \big[-p + qM_1e^{\bar{\epsilon}\sigma_1} + rM_2\frac{1}{\bar{\epsilon}}(e^{\bar{\epsilon}\sigma_2}-1)\big]z_{m_0}(t_*) \\ = & D^+z_{m_0}(t_*), \end{aligned} \tag{20}$$

which means that $D^+v(t_*) < D^+z(t_*)$. It yields a contradiction with inequality (12). Hence, inequality (7) is true when $k = m_0$. Let $\Gamma \to \|\Phi_{t_0}\|_{\tau_0}$; we can infer that inequality (6) is satisfied. Since $\{\beta_i\}$ is an independent and identically distributed stochastic sequence, $\delta_i = \beta_i\rho_ie^{\bar{\epsilon}\rho_i}, (i = 1, 2, \dots)$ is also an independent and identically distributed stochastic sequence. Taking expectation on the both sides of inequality (6) gives that

$$\begin{aligned} Ev(t) \leq & E\left[\left(\prod_{i=1}^{k}\mu_i\right)\|\Phi_{t_0}\|_{\tau_0}e^{-\bar{\epsilon}(t-t_0)}\right] \\ = & \left(\prod_{i=1}^{k}E\mu_i\right)\|\Phi_{t_0}\|_{\tau_0}e^{-\bar{\epsilon}(t-t_0)}, \forall t \geq t_0, t \in [t_k, t_{k+1}). \end{aligned} \tag{21}$$

Subsequently, by estimating $E\mu_i$, we have that

$$E\mu_i = P(\delta_i \leq c)c + P(\delta_i > c)E(\delta_i|\delta_i > c) \leq P(\delta_i \leq c)c + E(\delta_i) \leq P(\delta_i \leq c)c + \alpha\rho_ie^{\bar{\epsilon}\rho_i}. \tag{22}$$

According to Assumption 1 $E\beta_i = \alpha \neq c, D\beta_i \leq \gamma^2$, by employing the Chebyshev inequality, we find that

$$P(\delta_i \leq c) \leq \min\left\{\frac{\rho_i^2e^{2\bar{\epsilon}\rho_i}\gamma^2}{(\alpha\rho_ie^{\bar{\epsilon}\rho_i}-c)^2}, 1\right\}. \tag{23}$$

Hence, we have that

$$E\mu_i \leq \min\left\{\alpha\rho_ie^{\bar{\epsilon}\rho_i} + \frac{c\rho_i^2e^{2\bar{\epsilon}\rho_i}\gamma^2}{(\alpha\rho_ie^{\bar{\epsilon}\rho_i}-c)^2}, \alpha\rho_ie^{\bar{\epsilon}\rho_i} + c\right\} \triangleq \lambda. \tag{24}$$

It follows from inequalities (21) and (24) that

$$\begin{aligned} Ev(t) \leq & \lambda^k\|\Phi_{t_0}\|_{\tau_0}e^{-\bar{\epsilon}(t-t_0)} \\ \leq & \lambda^{\frac{t-t_0}{T_a}}\max\left\{\lambda^{-N_0}, \lambda^{N_0}\right\}\|\Phi_{t_0}\|_{\tau_0}e^{-\bar{\epsilon}(t-t_0)} \\ \leq & M_0\|\Phi_{t_0}\|_{\tau_0}e^{-\left(\bar{\epsilon}-\frac{\ln\lambda}{T_a}\right)(t-t_0)}, \forall t \geq t_0. \end{aligned} \tag{25}$$

This completes the proof. □

Assumption 2. *Assume that the random impulsive intensity is satisfied:*

H1. $\{\psi(t_k)\}_{k\in\mathbb{N}^+}$ *is a discrete-time Markov chain and takes values from* $\Omega \triangleq \{1, 2, \dots, m\}$. *Let this Markov chain be irreducible and all states are positive recurrent. Denote that* $\Xi_1 = (\xi_1, \xi_2, \dots, \xi_\nu)$ *is a unique invariant distribution of this Markov chain.*

H2. *Let $\{\beta^{(i)}\}_{i\in\Omega}$ denote m kinds of different random variables independent each other and satisfy*

$$\begin{cases} E\beta^{(i)} = \alpha_i > 0, \\ D\beta^{(i)} \leq \gamma_i^2, \\ \beta^{(i)} \geq 0, i \in \Omega, \end{cases} \tag{26}$$

where γ_i are determined non-negative constant.

H3. *Let $\{\beta_k\}_{k=1,2,\ldots}$ denote a sequence of independent random variables. Furthermore, β_k has the same distribution with $\beta^{(\psi(t_k))}$.*

Lemma 2. *Let $\Theta = \{t_1, t_2, \cdots, t_k\}$ be the impulsive sequence and T_a be the average impulsive interval. Suppose that Assumption 2 holds. Function $v(t) \in C(\mathbb{R}^+, \mathbb{R})$, $t \geq t_0 (t \neq t_k)$ satisfies the following differential inequality with stochastic distributed delayed impulses*

$$\begin{cases} D^+v(t) \leq -pv(t) + qv(t-\sigma_1(t)) + r\int_{t-\sigma_2}^{t} v(s)ds, t \neq t_k, \\ v(t_k) \leq \beta_k \int_{t-\rho_k}^{t} v(s)ds, t = t_k, k = 1, 2, \cdots, \\ v(t) = \Phi(t), t \in [t_0 - \tau_0, t_0], \end{cases} \tag{27}$$

where $v(t_k) = v(t_k^+)$, $0 \leq \rho_k \leq \rho$, $\sigma_2 \geq \rho_k$, $\sigma_1(t) \leq \sigma_1$, $\tau_0 = \max\{\sigma_1, \sigma_2\}$, $p \geq 0, q \geq 0, r \geq 0$ and $\|\Phi_{t_0}\|_{\tau_0} = \sup_{-\tau_0 \leq s \leq 0} \|\Phi(t_0 + s)\|$. Denote $M_1 = \max\left\{c^{-\frac{\sigma_1}{T_a} - N_0}, 1\right\}$ and $M_2 = \max\left\{c^{-\frac{\sigma_2}{T_a} - N_0}, 1\right\}$. If $p > qM_1 + rM_2\sigma_2 \geq 0$; then, we have

$$Ev(t) \leq M_0^* \|\Phi_{t_0}\|_{\tau_0} e^{-\left(\bar{\epsilon} - \frac{\ln(\zeta+\epsilon_0)}{T_a}\right)(t-t_0)}, \forall t \geq t_0, \tag{28}$$

where $M_0^* = \max_{1\leq k\leq \bar{N}}\left\{\left(\frac{\kappa}{(\zeta+\epsilon_0)}\right)^k\right\} e^{N_0|\ln(\zeta+\epsilon_0)|}$, $\zeta = \sum_{i=1}^{m} \xi_i\lambda_i$, $\lambda_i \triangleq \min\left\{\alpha_i\rho e^{\bar{\epsilon}\rho} + \frac{c\rho^2 e^{2\bar{\epsilon}\rho}\gamma_i^2}{(\alpha_i\rho e^{\bar{\epsilon}\rho} - c)^2}, \alpha_i\rho e^{\bar{\epsilon}\rho} + c\right\} > 0$, $\kappa = \max_{i\in\Omega}\{\lambda_i\}$, $c \neq \alpha_i\rho e^{\bar{\epsilon}\rho}$, $\bar{N} > 0, \epsilon_0 > 0$ and $\bar{\epsilon} > 0$ is the unique solution of $\Pi(\epsilon) = \epsilon - p + qM_1 e^{\sigma_1\epsilon} + rM_2\frac{1}{\epsilon}(e^{\sigma_2\epsilon} - 1) = 0$.

Proof. Let $c > 0$, $\mu^{(i)} \triangleq \max\{\beta^{(i)}\rho e^{\bar{\epsilon}\rho}, c\}$, and $\mu_i \triangleq \max\{\beta_i\rho e^{\bar{\epsilon}\rho}, c\} \in \{\mu^{(1)}, \mu^{(2)}, \cdots, \mu^{(m)}\}, i \in \Omega$. Similar to the proof of Lemma 1, we can derive that

$$E\mu^{(i)} \leq \lambda_i, i = 1, 2, \ldots, m, \tag{29}$$

and

$$v(t) \leq \left(\prod_{i=1}^{k} \mu_i\right) \|\Phi_{t_0}\|_{\tau_0} e^{-\bar{\epsilon}(t-t_0)}, \forall t \geq t_0, t \in [t_k, t_{k+1})\ k = 0, 1, 2, \ldots. \tag{30}$$

Let $\mathcal{F}_k = \sigma(\psi(t_1), \psi(t_2), \ldots, \psi(t_k))$. $\{\mathcal{F}_t\}_{t\geq t_0}$ denotes the filtration in the probability space $(\Omega, \mathcal{F}, P)$. Accordingly, we have that

$$Ev(t) = E\Big[\big[Ev(t)\big]|\mathcal{F}_k\Big] \leq E\Big[E\big[\prod_{i=1}^{k} \mu_i\big]|\mathcal{F}_k\Big] \|\Phi_{t_0}\|_{\tau_0} e^{-\bar{\epsilon}(t-t_0)}, t \in [t_k, t_{k+1}). \tag{31}$$

On the other hand, we can obtain from Theorem 4.3.3 in [39] that

$$\lim_{k\to\infty} \sum_{j=1}^{m} P(\psi(t_k) = i|\psi(t_1) = j) = \pi_i, \tag{32}$$

which means that

$$\lim_{k\to\infty}\sum_{i=1}^{m}P(\psi(t_k)=i)=\pi_i. \tag{33}$$

By the total probability formula, we have that

$$E\mu_{\psi(t_k)}=\sum_{i=1}^{m}P(\psi(t_k)=i)E\mu^{(i)}, \tag{34}$$

Substituting Equation (33) to Equation (34) yields

$$\lim_{k\to\infty}E\mu_{\psi(t_k)}=\sum_{i=1}^{m}\pi_iE\mu^{(i)}\le\sum_{i=1}^{m}\pi_i\lambda_i=\zeta. \tag{35}$$

According to Equation (35), we can find one sufficient small positive constant ϵ_0 and one large enough positive constant $\bar{N}$ such that

$$E\mu_{\psi(t_k)}\le\zeta+\epsilon_0, k>\bar{N}. \tag{36}$$

Moreover, we may estimate that

$$\begin{aligned}E\Big[E[\prod_{j=1}^{k}\mu_j]|\mathcal{F}_k\Big]=&E\Big[[\prod_{j=1}^{k}E\mu^{(\psi(t_j))}]|\mathcal{F}_k\Big]\\&=\sum_{i_1=1}^{m}\sum_{i_2=1}^{m}\cdots\sum_{i_k=1}^{m}\Big((\prod_{j=1}^{k}E\mu^{(i_j)})\\&\quad\times P\big((\psi(t_1)=i_1,\psi(t_2)=i_2,\ldots,\psi(t_k)=i_k)\big)\Big),\end{aligned} \tag{37}$$

where $E\mu^{(\psi(t_j))}=E\mu^{(i_j)}, j\in\{1,2,\cdots,k\}, i_j\in\{1,2,\cdots,m\}$. If $k>\bar{N}$, we have

$$\begin{aligned}\sum_{i_1=1}^{m}\sum_{i_2=1}^{m}\cdots\sum_{i_k=1}^{m}\Big((\prod_{j=1}^{k}E\mu^{(i_j)})\times P\big((\psi(t_1)=i_1,\psi(t_2)=i_2,\ldots,\psi(t_k)=i_k)\Big)&\le\kappa^{\bar{N}}(\prod_{\bar{N}+1}^{k}E\mu^{(i_j)})\\&\le\kappa^{\bar{N}}(\zeta+\epsilon_0)^{k-\bar{N}},\end{aligned} \tag{38}$$

where $\kappa=\max_{i\in\Omega}\{\lambda_i\}$. On the other hand, if $k\le\bar{N}$, then we also acquire that

$$\sum_{i_1=1}^{m}\sum_{i_2=1}^{m}\cdots\sum_{i_k=1}^{m}\Big((\prod_{j=1}^{k}E\mu^{(i_j)})\times P\big((\psi(t_1)=i_1,\psi(t_2)=i_2,\ldots,\psi(t_k)\big)\Big)\le\kappa^k. \tag{39}$$

Furthermore, according to Definition 1, we can find that

$$\begin{aligned}E\Big[E[\prod_{j=1}^{k}\mu_j]|\mathcal{F}_k\Big]&\le\max_{1\le k\le\bar{N}}\Big\{\Big(\frac{\kappa}{(\zeta+\epsilon_0)}\Big)^k\Big\}(\zeta+\epsilon_0)^k\\&\le\max_{1\le k\le\bar{N}}\Big\{\Big(\frac{\kappa}{(\zeta+\epsilon_0)}\Big)^k\Big\}e^{N_0|\ln(\zeta+\epsilon_0)|}e^{\frac{\ln(\zeta+\epsilon_0)}{T_a}(t-t_0)}.\end{aligned} \tag{40}$$

It follows from inequalities (31) and (40) that

$$Ev(t)\le E\Big[E[\prod_{i=1}^{k}\mu_i]|\mathcal{F}_k\Big]\|\Phi_{t_0}\|_{\tau_0}e^{-\bar{\epsilon}(t-t_0)}\le M_0^*\|\Phi_{t_0}\|_{\tau_0}e^{-\left(\bar{\epsilon}-\frac{\ln(\zeta+\epsilon_0)}{T_a}\right)(t-t_0)}, \forall t\ge t_0, \tag{41}$$

where $M_0^*=\max\limits_{1\le k\le\bar{N}}\Big\{\Big(\frac{\kappa}{(\zeta+\epsilon_0)}\Big)^k\Big\}e^{N_0|\ln(\zeta+\epsilon_0)|}$. □

Remark 1. *In the literature [26–31], dynamic properties of various nonlinear systems with distributed delayed impulses have been investigated. It is worth pointing out that the considered distributed-delay-dependent impulses are deterministic, but in this paper, the intensities of distributed delayed impulses are supposed to be random. Two types of stochastic impulses including stochastic distributed delayed impulses with independent property and Markov property have been explored, respectively. Based on the average impulsive interval method, total probability formula and ergodic theory, two novel impulsive Halanay differential inequalities are established, which generalize the findings in the literature [34,35] since time-varying delays, distributed delays and stochastic distributed delayed impulses are introduced simultaneously. Parameter c can be arbitrarily chosen. In view of invariant distribution theory, the stochastic impulses with Markov property is tackled.*

3. Main Results

In this section, the exponential synchronization of coupled neural networks with stochastic distributed delayed impulses is investigated. Some sufficient conditions are attained based on the established lemmas and stochastic analysis technique.

Consider the following coupled neural networks model with hybrid delays and stochastic distributed delayed impulses composed of N nodes described by

$$\begin{cases} \dot{u}_i(t) = Du_i(t) + Ag(u_i(t)) + Bg(u_i(t-\sigma_1(t)) + C\int_{t-\sigma_2}^{t} g(u_i(s))ds \\ \quad + \theta\sum_{j=1}^{N} l_{ij}\Gamma u_j(t) + J(t), t \geq 0, t \neq t_k, k \in N^+, \\ u_j(t_k^+) - u_i(t_k^+) = \eta_k \int_{t-\rho_k}^{t} (u_j(s) - u_i(s))ds, k \in N^+, \\ u_i(t) = \phi_i(t), -\bar{\sigma} \leq t \leq 0, \end{cases} \tag{42}$$

where $u_i(\cdot)$ denotes the state vector of the ith neural network, and the initial value $\phi_i(t) \in \mathbb{C}([-\bar{\sigma}, 0], \mathbb{R}^n)$. $g(\cdot) \in \mathbb{R}^n$ denotes the activation function. $D, A, B, C \in \mathbb{R}^{n\times n}$ are connection weights matrices. Γ is the inner coupling matrix which is positive definite. Meanwhile, $L = (l_{ij})_{N\times N}$ denotes the outer coupling matrices, where $l_{ij} \geq 0, l_{ij} \neq 0$, if and only if there is a connection between nodes i and $j (j \neq i)$, and $l_{ii} = -\sum_{j=1, j\neq i}^{N} l_{ij}$. θ represents the coupling strength, and $J(t)$ is an external input vector. $\sigma_1(t)$ is the time-varying delay, and η_k is the stochastic impulsive intensity at t_k. In addition, the isolated node of the coupled neural networks is given as

$$\begin{cases} \dot{s}(t) = Ds(t) + Ag(s(t)) + Bg(s(t-\sigma_1(t)) + C\int_{t-\sigma_2}^{t} g(s(s))ds + J(t), t \geq 0, \\ s(t) = \phi(t), -\bar{\sigma} \leq t \leq 0. \end{cases} \tag{43}$$

Let error vector $z_i(t) = u_i(t) - s(t)$. Subtracting Equation (43) from Equation (42) yields that

$$\begin{cases} \dot{z}_i(t) = Dz_i(t) + A\bar{g}(z_i(t)) + B\bar{g}(z_i(t-\sigma_1(t)) + C\int_{t-\sigma_2}^{t} \bar{g}(z_i(s))ds \\ \quad + \theta\sum_{j=1}^{N} l_{ij}\Gamma z_j(t), t \geq 0, t \neq t_k, k \in N^+ \\ z_j(t_k^+) - z_i(t_k^+) = \eta_k \int_{t-\rho_k}^{t} (z_j(s) - z_i(s))ds, k \in N^+, \\ z_i(t) = \Phi_i(t), -\bar{\sigma} \leq t \leq 0, \end{cases} \tag{44}$$

where $\bar{g}(z_i(t)) = g(u_i(t)) - g(s(t))$, $\bar{g}(z_i(t-\sigma_1(t)) = g(u_i(t-\sigma_1(t)) - g(s(t-\sigma_1(t))$, $\bar{g}(z_i(s)) = g(u_i(s)) - g(s(s))$ and $\Phi_i(t) = \phi_i(t) - \phi(t)$. By introducing the Kronecker product, Equation (44) is turned into the following form

$$\begin{cases} \dot{z}(t) = (I_N \otimes D)z(t) + (I_N \otimes A)\bar{G}(z(t)) + (I_N \otimes B)\bar{G}(z(t-\sigma_1(t)) \\ + (I_N \otimes C)\int_{t-\sigma_2}^{t} \bar{G}(z(s))ds + \theta(\Gamma \otimes L)z(t), t \geq 0, t \neq t_k, \\ z_j(t_k^+) - z_i(t_k^+) = \eta_k \int_{t-\rho_k}^{t} (z_j(s) - z_i(s))ds, k \in N^+ \\ z_i(t) = \Phi_i(t), -\bar{\sigma} \leq t \leq 0, \end{cases} \tag{45}$$

where $z(t) = \left(z_1^T(t), z_2^T(t), \ldots, z_N^T(t)\right)^T$, $\bar{G}(z(t)) = (\bar{g}^T(z_1(t)), \bar{g}^T(z_2(t)), \ldots, \bar{g}^T(z_N(t)))^T$, $\bar{G}(z(t-\sigma_1(t)) = (\bar{g}^T(z_1(t-\sigma_1(t)), \bar{g}^T(z_2(t-\sigma_1(t), \ldots, \bar{g}^T(z_N(t-\sigma_1(t)))^T$ and $\bar{G}(z(s)) = (\bar{g}(z_1(s)), \bar{g}(z_2(s)), \ldots, \bar{g}(z_N(s)))$.

Assumption 3. *Assume that outer coupling matrix L is a irreducible matrix.*

Lemma 3 ([40])**.** *Under Assumption 3, the left eigenvector corresponding to the zero eigenvalue of matrix L is* $\xi = (\xi_1, \ldots, \xi_N)^T$ *and* $\sum_{i=1}^{N} \xi_i = 1, \xi_i \geq 0$*. Denote* $\Xi = \mathrm{diag}\{\xi_1, \ldots, \xi_N\}$*. Then,* $\bar{L} = \Xi L + L^T \Xi$ *is irreducible and symmetric, whose eigenvalues satisfy* $0 = \lambda_1(\bar{L}) > \lambda_2(\bar{L}) \geq \ldots \lambda_N(\bar{L})$.

Assumption 4. *For vector-valued function* $\bar{G}(\cdot)$ *in Equation (45), there exists a matrix* $Q \in \mathbb{R}^{n \times n}$ *such that*

$$\bar{G}(u_1) - \bar{G}(u_2)t^T\left[\bar{G}(u_1) - \bar{G}(u_2)\right] \leq (u_1 - u_2)^T QQ^T(u_1 - u_2), \tag{46}$$

where $u_1, u_2 \in \mathbb{R}^n$.

Definition 2. *If there are positive constants* $\bar{M}$ *and* ι *such that*

$$E\|z_i(t)\|^2 \leq \bar{M}e^{-\iota t}, \forall t \geq 0, i = 1, 2, \ldots, N, \tag{47}$$

then system (42) is said to be globally exponentially synchronized in mean square.

Based on the above assumptions, by utilizing the proposed lemmas in Section 2, we can derive the following criteria for exponential synchronization of CNNs with hybrid delays and stochastic distributed delayed impulses.

Theorem 1. *Let Assumptions 3 and 4 hold.* η_k *is the stochastic impulsive intensity with* $E(\eta_k) = \bar{\alpha}$, $D(\eta_k) = \bar{\gamma}^2, E(\eta_k^4) = \chi$*. Time delays* $\sigma_1(t), \sigma_2, \rho_k$ *satisfy* $\sigma_1(t) \leq \sigma_1$, $\sigma_2 \geq \rho \geq \rho_k \geq 0$, $\tau_0 = \max\{\sigma_1, \sigma_2\}$*. If the following conditions hold,*

(i) $p > qM_1 + rM_2\sigma_2 \geq 0$*, where* $W = \Xi - \xi\xi^T$, $b = -\frac{\lambda_2(\bar{L})}{\lambda_{\max}(W)}$, $p = -\lambda_{\max}\Big(D + D^T + AA^T + QQ^T + BB^T + CC^T - \theta b\Gamma\Big)$, $q = \lambda_{\max}(QQ^T)$, $r = \sigma_2\lambda_{\max}(QQ^T)$, $M_1 = \max\left\{c^{-\frac{\sigma_1}{T_a} - N_0}, 1\right\}$ *and* $M_2 = \max\left\{c^{-\frac{\sigma_2}{T_a} - N_0}, 1\right\}, c > 0$.

(ii) $\bar{\epsilon} - \frac{\ln\lambda}{T_a} > 0$*, where* $\lambda \triangleq \min\left\{\alpha\rho_i e^{\bar{\epsilon}\rho_i} + \frac{c\rho_i^2 e^{2\bar{\epsilon}\rho_i}\gamma^2}{(\alpha\rho_i e^{\bar{\epsilon}\rho_i} - c)^2}, \alpha\rho_i e^{\bar{\epsilon}\rho_i} + c\right\}$, $M_0 \triangleq \max\{\lambda^{-N_0}, \lambda^{N_0}\}$, $c \neq \alpha\rho_i e^{\bar{\epsilon}\rho_i}$, $\rho_k(\bar{\alpha}^2 + \bar{\gamma}^2) = \alpha$, $\rho_k^2(\chi - (\bar{\alpha}^2 + \bar{\gamma}^2)^2) = \gamma^2$ *and* $\bar{\epsilon} > 0$ *is the unique solution of* $\Pi(\epsilon) = \epsilon - p + qM_1e^{\sigma_1\epsilon} + rM_2\frac{1}{\epsilon}(e^{\sigma_2\epsilon} - 1) = 0$.

Then we have

$$E|z(t)|^2 \leq M_0\|\Phi_{t_0}\|_{\tau_0}e^{-\left(\bar{\epsilon} - \frac{\ln\lambda}{T_a}\right)t}, \forall t \geq 0, \tag{48}$$

which means that system (42) can achieve exponential synchronization in mean square.

Proof. Choose the Lyapunov function $V(t) = z^T(t)(W \otimes I_n)z(t)$, where $W = \Xi - \xi\xi^T$, Ξ and ξ are the same as Lemma 3. Since $W = (w_{ij})_{N\times N}$ is semi-positive definite and zero-row-sum, function $V(t)$ can be rewritten by $V(t) = -\frac{1}{2}\sum_{i=1}^{N}\sum_{j=1,j\neq i}^{N} w_{ij}(z_i(t) - z_j(t))^T(z_i(t) - z_j(t))$. For $t \in [t_{n-1}, t_n], n \in \mathbb{Z}_+$, calculating the time-derivative of V along the trajectories of the error system (45) yields that

$$\begin{aligned} D^+V(t) =& 2z^T(t)(W \otimes I_n)\dot{z}(t) \\ =& 2z^T(t)(W \otimes I_n)\Big[(I_N \otimes D)z(t) + (I_N \otimes A)\bar{G}(z(t)) + (I_N \otimes B)\bar{G}(z(t-\sigma_1(t)) \\ &+ (I_N \otimes C)\int_{t-\sigma_2}^{t}\bar{G}(z(s))ds + \theta(L \otimes \Gamma)z(t)\Big] \\ =& 2z^T(t)(W \otimes D)z(t) + 2z^T(t)(W \otimes A)\bar{G}(z(t)) + 2z^T(t)(W \otimes B)\bar{G}(z(t-\sigma_1(t)) \\ &+ 2z^T(t)(W \otimes C)\int_{t-\sigma_2}^{t}\bar{G}(z(s))ds + 2\theta z^T(t)((WL) \otimes \Gamma + \frac{b}{2}W \otimes \Gamma)z(t) \\ &- b\theta z^T(t)(W \otimes \Gamma)z(t), \end{aligned} \tag{49}$$

where $b = -\frac{\lambda_2(\bar{L})}{\lambda_{\max}(W)}$ and $\bar{L}$ is same as Lemma 3. Then, we have that

$$\begin{aligned} 2z^T(t)(W \otimes A)\bar{G}(z(t)) =& -\sum_{i=1}^{N}\sum_{j=1,j\neq i}^{N} w_{ij}(z_i(t) - z_j(t))^T A(\bar{G}(z_i(t)) - \bar{G}(z_j(t))) \\ \leq& -\frac{1}{2}\sum_{i=1}^{N}\sum_{j=1,j\neq i}^{N} w_{ij}\big[(z_i(t) - z_j(t))^T AA^T(z_i(t) - z_j(t)) \\ &+ (z_i(t) - z_j(t))^T QQ^T(z_i(t) - z_j(t))\big] \\ =& z^T(t)(W \otimes AA^T)z(t) + z^T(t)(W \otimes QQ^T)z(t). \end{aligned} \tag{50}$$

Similarly, it follows that

$$\begin{aligned} 2z^T(t)(W \otimes B)\bar{G}(z(t-\sigma_1(t)) \leq& z^T(t)(W \otimes BB^T)z(t) \\ &+ z^T(t-\sigma_1(t))(W \otimes QQ^T)z(t-\sigma_1(t)), \end{aligned} \tag{51}$$

$$\begin{aligned} 2z^T(t)(W \otimes C)\int_{t-\sigma_2}^{t}\bar{G}(z(s))ds \leq& z^T(t)(W \otimes CC^T)z(t) \\ &+ \sigma_2\int_{t-\sigma_2}^{t} z(s)^T(W \otimes QQ^T)z(s)ds. \end{aligned} \tag{52}$$

Noting that $\bar{L} = \Xi L + L^T\Xi$ is irreducible and symmetric, by the Perron–Frobenius theorem, we infer that the eigenvalues of $\bar{L}$ satisfy

$$0 = \lambda_1(\bar{L}) > \lambda_2(\bar{L}) \geq \ldots \lambda_N(\bar{L}). \tag{53}$$

Furthermore, since matrix $\bar{L}$ is symmetric, there exists a unitary matrix U such that $\bar{L} = U\Lambda U^T$, where $\Lambda = \mathrm{diag}\{0, \lambda_2(\bar{L}), \ldots, \lambda_N(\bar{L})\}$, $U = (U_1, U_2, \ldots, U_N)$ and $U_1 = (\frac{1}{\sqrt{N}}, \ldots, \frac{1}{\sqrt{N}})^T$. Let $y(t) = (y_1^T(t), y_2^T(t), \ldots, y_N^T(t))^T = (U^T \otimes I_n)z(t)$, which signifies $z(t) = (U \otimes I_n)y(t)$. It also can be verified that $WL + L^TW = (\Xi - \xi\xi^T)L + L^T(\Xi - \xi\xi^T) = \Xi L - \xi(\xi^T L) + L^T\Xi - (\xi^T L)^T\xi = \bar{L}$. Hence, we can acquire that

$$\begin{aligned}2\theta z^T(t)((WL)\otimes\Gamma+\frac{b}{2}W\otimes\Gamma))z(t) =&\theta z^T(t)((WL+L^TW)\otimes\Gamma+b(W\otimes\Gamma))z(t)\\ =&\theta y^T(t)(U^T\otimes I_n)((\bar{L}\otimes\Gamma)(U\otimes I_n)y(t)\\ &+\theta b y^T(t)((U^TWU)\otimes\Gamma)y(t)\\ \leq&\theta\Big(\sum_{i=2}^{N}\lambda_i(\bar{L})y_i^T(t)\Gamma y_i(t)+b\lambda_{\max}(W)\sum_{i=2}^{N}y_i^T(t)\Gamma y_i(t)\Big)\\ \leq&\theta(\lambda_2(\bar{L})+b\lambda_{\max}(W))\sum_{i=2}^{N}y_i^T(t)\Gamma y_i(t)=0.\end{aligned} \tag{54}$$

Substituting Equation (54) to Equation (49) yields that

$$\begin{aligned}D^+V(t) \leq&z^T(t)(W\otimes(D+D^T+AA^T+QQ^T+BB^T+CC^T-\theta b\Gamma)z(t)+\\ &z^T(t-\sigma_1(t))(W\otimes QQ^T)z(t-\sigma_1(t))+\sigma_2\int_{t-\sigma_2}^{t}z(s)^T(W\otimes QQ^T)z(s)ds\\ \leq&\lambda_{\max}(D+D^T+AA^T+QQ^T+BB^T+CC^T-\theta b\Gamma)V(t)\\ &+\lambda_{\max}(QQ^T)V(t-\sigma_1(t))+\sigma_2\lambda_{\max}(QQ^T)\int_{t-\sigma_2}^{t}V(s)ds\\ \triangleq&-pV(t)+qV(t-\sigma_1(t))+r\int_{t-\sigma_2}^{t}V(s)ds.\end{aligned} \tag{55}$$

Since the outer coupling matrix L is an irreducible matrix, then there always exists a path for any nodes j and i. In other words, there are $s_1, s_2, \ldots, s_m$ such that $l_{js_m}\geq 0, \ldots, l_{s_1 i}\geq 0$. Hence, we can find that

$$\begin{aligned}z_j(t_k^+)-z_i(t_k^+) =&u_j(t_k^+)-u_i(t_k^+)\\ =&\big(u_j(t_k^+)-u_{s_m}(t_k^+)\big)+\big(u_{s_m}(t_k^+)-u_{s_{m-1}}(t_k^+)\big)+\cdots+\big(u_{s_1}(t_k^+)-u_i(t_k^+)\big)\\ =&\eta_k\int_{t-\rho_k}^{t}(u_j(v)-u_{s_m}(v)+u_{s_m}(v)-u_{s_{m-1}}(v)+\cdots+u_{s_1}(v)-u_i(v))dv\\ =&\eta_k\int_{t-\rho_k}^{t}(z_j(s)-z_i(s))ds.\end{aligned} \tag{56}$$

According to Equation (56), one has that

$$\begin{aligned}V(t_k^+) =&-\frac{1}{2}\sum_{i=1}^{N}\sum_{j=1,j\neq i}^{N}w_{ij}(z_i(t_k^+)-z_j(t_k^+))^T(z_i(t_k^+)-z_j(t_k^+))\\ =&-\frac{\eta_k^2}{2}\sum_{i=1}^{N}\sum_{j=1,j\neq i}^{N}w_{ij}\Big[\int_{t-\rho_k}^{t}(z_j(s)-z_i(s))^Tds\int_{t-\rho_k}^{t}(z_j(s)-z_i(s))ds\Big]\\ \leq&-\frac{\eta_k^2\rho_k}{2}\sum_{i=1}^{N}\sum_{j=1,j\neq i}^{N}w_{ij}\Big[\int_{t-\rho_k}^{t}(z_j(s)-z_i(s))^T(z_j(s)-z_i(s))ds\Big]\\ \leq&\beta_k\int_{t-\rho_k}^{t}V(s)ds,\end{aligned} \tag{57}$$

where $\beta_k=\eta_k^2\rho_k$. Noting that $E(\eta_k)=\bar{\alpha}$, $D(\eta_k)=\bar{\gamma}^2$, $E(\eta_k^4)=\chi$, we can obtain that

$$E(\beta_k)=E(\eta_k^2\rho_k)=\rho_k(\bar{\alpha}^2+\bar{\gamma}^2)=\alpha, \tag{58}$$

and

$$D(\beta_k)=D(\eta_k^2\rho_k)=\rho_k^2(\chi-(\bar{\alpha}^2+\bar{\gamma}^2)^2)=\gamma^2. \tag{59}$$

Combining conditions (i) and (ii), by Lemma 1, we immediately obtain the following assertion

$$EV(t) \leq M_0 \|\Phi_{t_0}\|_{\tau_0} e^{-\left(\bar{\epsilon} - \frac{\ln \lambda}{T_a}\right)t}, \forall t \geq 0, \tag{60}$$

where $\lambda \triangleq \min\left\{\alpha\rho_i e^{\bar{\epsilon}\rho_i} + \frac{c\rho_i^2 e^{2\bar{\epsilon}\rho_i}\gamma^2}{(\alpha\rho_i e^{\bar{\epsilon}\rho_i} - c)^2}, \alpha\rho_i e^{\bar{\epsilon}\rho_i} + c\right\}$, $M_0 \triangleq \max\{\lambda^{-N_0}, \lambda^{N_0}\}$, $c \neq \alpha\rho_i e^{\bar{\epsilon}\rho_i}$ and $\bar{\epsilon} > 0$ is the unique solution of $\Pi(\epsilon) = \epsilon - p + qM_1 e^{\sigma_1 \epsilon} + rM_2 \frac{1}{\epsilon}(e^{\sigma_2 \epsilon} - 1) = 0$. According to the construction of $V(t)$, we can derive that

$$\begin{aligned} V(t) = z^T(t)(W \otimes I_n)z(t) =& -\frac{1}{2}\sum_{i=1}^{N}\sum_{j=1, j\neq i}^{N} w_{ij}(z_i(t) - z_j(t))^T(z_i(t) - z_j(t)) \\ \geq& \frac{1}{2}\sum_{i=1}^{N}\sum_{j=1, j\neq i}^{N} \xi_i\xi_j(z_i(t) - z_j(t))^T(z_i(t) - z_j(t)) \\ \geq& \frac{1}{2}\xi_1\xi_2\|z_1(t) - z_2(t)\|^2 \end{aligned} \tag{61}$$

which implies that $\|z_1(t) - z_2(t)\|^2 \leq \frac{2}{\xi_1\xi_2}V(t)$. Hence, we have

$$\begin{aligned} \|z_1(t)\|^2 \leq& (\|z_1(t) - z_2(t)\| + \|z_2(t)\|)^2 \\ \leq& 2\|z_1(t) - z_2(t)\|^2 + 2\|z_2(t)\|^2 \\ \leq& \frac{4}{\xi_1\xi_2}V(t) + 2\|z_2(t)\|^2. \end{aligned} \tag{62}$$

Additionally, similar to the matrix decomposition procedures before inequality (54), we can acquire that

$$V(t) = z^T(t)(W \otimes I_n)z(t) \geq \lambda_2(W)\sum_{l=2}^{N} z_l^T(t)z_l(t) = \lambda_2(W)\sum_{l=2}^{N}\|z_l(t)\|^2, \tag{63}$$

where $0 = \lambda_1(W) < \lambda_2(W) \leq \ldots \lambda_N(W)$ and $\lambda_i(W), (i = 1, 2, \cdots, N)$ denotes the eigenvalues of the matrix W. It implies that

$$\|z_l(t)\|^2 \leq \frac{1}{\lambda_2(W)}V(t), l = 2, 3, \cdots, N. \tag{64}$$

Combining Equations (62) and (64), we can obtain that

$$\|z_l(t)\|^2 \leq \left(\frac{4}{\xi_1\xi_2} + \frac{2}{\lambda_2(W)}\right)V(t) \triangleq \delta V(t), l = 1, 2, 3, \cdots, N, \tag{65}$$

It follows from inequalities (60) and (65) that

$$E\|z_l(t)\|^2 \leq \bar{M}\|\Phi_{t_0}\|_{\tau_0} e^{-\left(\bar{\epsilon} - \frac{\ln \lambda}{T_a}\right)t}, \forall t \geq 0, l = 1, \ldots, N, \tag{66}$$

where $\bar{M} = \delta M_0, \delta = \left(\frac{4}{\xi_1\xi_2} + \frac{2}{\lambda_2(W)}\right)$. Therefore, system (42) is mean square exponentially synchronized. □

Remark 2. *In Theorem 1, it can be seen that parameter p contains coupling strength θ. When coupling strength θ becomes larger, accordingly, parameter p also becomes larger. It is noted that parameter p satisfies the equation* $\Pi(\epsilon) = \epsilon - p + qM_1 e^{\sigma_1 \epsilon} + rM_2 \frac{1}{\epsilon}(e^{\sigma_2 \epsilon} - 1) = 0$. *Consequently, it can be inferred that the positive root* $\bar{\epsilon}$ *of the above equation will become larger when parameter p becomes larger, which implies that convergent rate becomes larger and error trajectories will converge to zero vector more quickly.*

Theorem 2. *Let Assumptions 3 and 4 hold. The impulsive sequence* $\{t_k\}, k \in \mathbb{Z}_+$ *satisfies Definition 1. Let* $\psi(t)$ *be a Markov chain satisfying Assumption 2.* $\{\eta^{(i)}\}_{i\in\Omega}$ *denotes m kinds of different independent random variables with* $E(\eta^{(i)}) = \mu^{(i)} > 0$, $D(\eta^{(i)}) = (\omega^{(i)})^2$ *and* $E(\eta^{(i)})^4 = \chi^{(i)}$, $i \in \Omega$, *and* η_k *has the same distributed with* $\{\eta^{(\psi(k))}\}$. *Time delays* $\sigma_1(t), \sigma_2, \rho_k$ *satisfy* $\sigma_1(t) \leq \sigma_1$, $\sigma_2 \geq \rho \geq \rho_k \geq 0$, $\tau_0 = \max\{\sigma_1, \sigma_2\}$. *If the following conditions hold,*

(i) $p > qM_1 + rM_2\sigma_2 \geq 0$, *where* $W = \Xi - \xi\xi^T$, $b = -\frac{\lambda_2(\bar{L})}{\lambda_{\max}(W)}$, $p = -\lambda_{\max}\Big(D + D^T + AA^T + QQ^T + BB^T + CC^T - \theta b\Gamma\Big)$, $q = \lambda_{\max}(QQ^T)$, $r = \sigma_2\lambda_{\max}(QQ^T)$, $M_1 = \max\Big\{c^{-\frac{\sigma_1}{T_a}-N_0}, 1\Big\}$ *and* $M_2 = \max\Big\{c^{-\frac{\sigma_2}{T_a}-N_0}, 1\Big\}, c > 0$;

(ii) $\bar{\epsilon} - \frac{\ln(\zeta+\epsilon_0)}{T_a} > 0$, *where* $\zeta = \sum_{i=1}^{m} \xi_i\lambda_i$, $\lambda_i \triangleq \min\Big\{\alpha_i\rho e^{\bar{\epsilon}\rho} + \frac{c\rho^2 e^{2\bar{\epsilon}\rho}\gamma_i^2}{(\alpha_i\rho e^{\bar{\epsilon}\rho}-c)^2}, \alpha_i\rho e^{\bar{\epsilon}\rho} + c\Big\}$, $c \neq \alpha_i\rho e^{\bar{\epsilon}\rho}$, $\rho\big[(\mu^{(i)})^2 + (\omega^{(i)})^2\big] = \alpha_i$, $\rho^2\big[\chi^{(i)} - ((\mu^{(i)})^2 + (\omega^{(i)})^2)^2\big] = \gamma_i^2$, $M_0^* = \max_{1\leq k\leq\bar{N}}\Big\{\Big(\frac{\kappa}{(\zeta+\epsilon_0)}\Big)^k\Big\}e^{N_0|\ln(\zeta+\epsilon_0)|}$, $\bar{N} > 0$, ϵ_0 *is a sufficient small positive constant and* $\bar{\epsilon} > 0$ *is the unique solution of* $\Pi(\epsilon) = \epsilon - p + qM_1e^{\sigma_1\epsilon} + rM_2\frac{1}{\epsilon}(e^{\sigma_2\epsilon} - 1) = 0$;

Then we have

$$E|z(t)|^2 \leq M_0^*\|\Phi_{t_0}\|_{\tau_0}e^{-\left(\bar{\epsilon}-\frac{\ln(\zeta+\epsilon_0)}{T_a}\right)t}, \forall t \geq 0, \tag{67}$$

which means that system (42) can achieve exponential synchronization in mean square.

Proof. Choose a Lyapunov function $V(t) = z^T(t)(W \otimes I_n)z(t)$ the same as Theorem 1. Similar to Theorem 1, by computing, we have that

$$D^+V(t) \leq -pV(t) + qV(t - \sigma_1(t)) + r\int_{t-\sigma_2}^{t} V(s)ds, \tag{68}$$

and

$$V(t_k^+) \leq \rho\eta_k^2\int_{t-\rho_k}^{t} V(s)ds. \tag{69}$$

Let $\beta_k = \rho\eta_k^2$ and $\beta^{(i)} = \rho(\eta^{(i)})^2, i \in \Omega$. Then, we can find that

$$E(\beta^{(i)}) = E(\rho(\eta^{(i)})^2) = \rho\big[(\mu^{(i)})^2 + (\omega^{(i)})^2\big] = \alpha_i, \tag{70}$$

and

$$D(\beta^{(i)}) = D(\rho(\eta^{(i)})^2) = \rho^2\big[\chi^{(i)} - ((\mu^{(i)})^2 + (\omega^{(i)})^2)^2\big] = \gamma_i^2. \tag{71}$$

Combining conditions (i) and (ii), by Lemma 2, we immediately have the following assertion

$$EV(t) \leq M_0^*\|\Phi_{t_0}\|_{\tau_0}e^{-\left(\bar{\epsilon}-\frac{\ln(\zeta+\epsilon_0)}{T_a}\right)t}, \forall t \geq 0, \tag{72}$$

where $M_0^* = \max_{1\leq k\leq\bar{N}}\Big\{\Big(\frac{\kappa}{(\zeta+\epsilon_0)}\Big)^k\Big\}e^{N_0|\ln(\zeta+\epsilon_0)|}$, $\bar{N} > 0$, $\zeta = \sum_{i=1}^{m}\xi_i\lambda_i$, $\lambda_i \triangleq \min\Big\{\alpha_i\rho_i e^{\bar{\epsilon}\rho_i} + \frac{c\rho_i^2 e^{2\bar{\epsilon}\rho_i}\gamma_i^2}{(\alpha_i\rho_i e^{\bar{\epsilon}\rho_i}-c)^2}, \alpha_i\rho_i e^{\bar{\epsilon}\rho_i} + c\Big\}$, $c \neq \alpha_i\rho_i e^{\bar{\epsilon}\rho_i}$ and $\bar{\epsilon} > 0$ is the unique solution of $\Pi(\epsilon) = \epsilon - p + qM_1e^{\sigma_1\epsilon} + rM_2\frac{1}{\epsilon}(e^{\sigma_2\epsilon} - 1) = 0$. It is easy to know that

$$\|z_l(t)\|^2 \leq \big(\frac{4}{\xi_1\xi_2} + \frac{2}{\lambda_2(W)}\big)V(t) \triangleq \delta V(t), l = 2, 3, \cdots, N, \tag{73}$$

According to Equations (72) and (73), we can find that

$$E\|z_l(t)\|^2 \leq \bar{M}\|\Phi_{t_0}\|_{\tau_0}e^{-\left(\bar{\epsilon}-\frac{\ln(\zeta+\epsilon_0)}{T_a}\right)t}, \forall t \geq 0, l = 1, \ldots, N, \tag{74}$$

where $\bar{M} = \delta M_0^*, \delta = \big(\frac{4}{\xi_1\xi_2} + \frac{2}{\lambda_2(W)}\big)$. Therefore, system (42) is mean square exponentially synchronized. □

Remark 3. *In [34], under the circumstance that the impulses intensities were supposed to be random, the exponential synchronization problem of the NNs has been tackled, and the results have been further generalized to inertial network systems with stochastic delays impulses [35,36]. Different from the findings in [34–36], by utilizing the proposed lemmas and graph theory, this paper acquires some novel criteria on exponential synchronization of CNNs with hybrid delays and stochastic distributed delayed impulses. In [36], impulses can only be regarded as outer disturbances for coupled inertial NNs with hybrid delays. Compared with [36], in this paper, impulses may also be viewed as outer perturbations or stabilizing sources, and the case of stochastic impulses with Markov property is also discussed.*

Remark 4. *The Razumikhin approach is one significant and effective tool for analyzing dynamic characteristics. Particularly, in [20,21], with the help of the improved Razumikhin method, several criteria on p th moment exponential stability of non-autonomous stochastic delayed systems with impulsive effects have been derived. It is noted that the impulsive sequences are deterministic impulses in [20,21], and non-autonomous stochastic systems with stochastic delayed impulses have not been examined by adopting the Razumikhin approach, which deserves further investigation. On the other hand, in [37], input-to-state stability for switched stochastic nonlinear systems with random impulses has been tackled. However, it is required that stochastic impulsive intensity ρ_{k,k_l} satisfy $1 < E\rho_{k,k_l} = \rho_i < +\infty$. In our paper, this restrictive condition is removed, and two types of stochastic impulses, i.e., stochastic distributed delayed impulses with dependent property and Markov property have been taken into account, respectively.*

Remark 5. *In [38], pth exponential stability of stochastic delayed semi-Markov jump systems with stochastic mixed impulses has been investigated. A new impulsive differential inequality with semi-Markov jump and stochastic mixed impulses has been established by virtue of stochastic theory, which is further applied to a kind of stochastic delayed semi-Markov jump oscillator systems. Compared with the work in [38], we consider the effects of hybrid delays and two types of stochastic distributed delayed impulses. In the future, our findings can be extended to stochastic delayed semi-Markov jump oscillator systems.*

Remark 6. *In [41], almost surely synchronization of directed CNNs via stochastic distributed delayed impulsive control has been studied by adopting graph theory, the Chebyshev inequality, the Borel–Cantelli Lemma and the stochastic Lyapunov functional method. It is noted that the distributed impulsive control is imposed from the perspective of the spatial structure while the distributed delayed impulses are considered here from the perspective of time delay. In this paper, stochastic intensities are not restricted to obeying the Gaussian distribution, and two types of stochastic impulses with independent property and Markov property have been explored.*

Remark 7. *Neuronal synchronization has appeared in real applications. For instance, the theta rhythm related to the behavior of animals is produced by partial synchronization of neuronal activity in the hippocampal network, and an excessive synchronization of the neuronal activity over a wide area in the brain results in the epileptic rhythm [6]. On the other hand, the results of exponential synchronization of CNNs in our paper can be further extended to coupled oscillators, multi-agent systems, and coupled unmanned aerial vehicles (UAV) communicating with each other. In the future, when random noise and stochastic impulses coexist, the dynamical properties of nonlinear coupled systems are worthy of further exploration.*

4. Examples

In this section, two numerical examples are provided to demonstrate the validity of the proposed findings.

Example 1. *Consider the following coupled neural networks model with hybrid delays and stochastic distributed delayed impulses*

$$\begin{cases} \dot{u}_i(t) = Du_i(t) + Ag(u_i(t)) + Bg(u_i(t-\sigma_1(t)) + C\int_{t-\sigma_2}^{t} g(u_i(s))ds \\ \quad + \theta\sum_{j=1}^{N} l_{ij}\Gamma u_j(t) + J(t), t \geq 0, t \neq t_k, k \in N^+, \\ u_j(t_k^+) - u_i(t_k^+) = \eta_k \int_{t-\rho_k}^{t} (u_j(s) - u_i(s))ds, k \in N^+, \\ u_i(t) = \phi_i(t), -\bar{\sigma} \leq t \leq 0, \end{cases} \tag{75}$$

where $u_i = (u_{i1}, u_{i2})^T, N = 5, \sigma_1(t) = 0.6\cos(t) \leq \sigma_1 = 0.6, \sigma_2 = 0.5, \theta = 1.8, J(t) = (0.4, 2.6)^T, 0 \leq \rho_k = 0.5 = \rho, g(u_i(t)) = 0.8(\tanh(u_{i1}(t), \tanh(u_{i2}(t)))^T, i = 1, \ldots, N$, *and the corresponding coefficient matrices and inner coupled matrix are selected below*

$$D = \begin{pmatrix} -4.8 & 0 \\ 0 & -5.2 \end{pmatrix}, \quad A = \begin{pmatrix} -1.7 & -1.4 \\ -1.6 & 1.12 \end{pmatrix}, \quad B = \begin{pmatrix} -1.7 & -2.6 \\ -2.54 & 1.1 \end{pmatrix},$$

$$C = \begin{pmatrix} 0.3 & -0.17 \\ 0.35 & 0.35 \end{pmatrix}, \quad \Gamma = \begin{pmatrix} 1.2 & 0 \\ 0 & 2.4 \end{pmatrix},$$

and the outer coupling matrix is

$$L = \begin{pmatrix} -4 & 2 & 0 & 0 & 2 \\ 0 & -3 & 2 & 1 & 0 \\ 1 & 0 & -5 & 0 & 4 \\ 2 & 0 & 1 & -3 & 0 \\ 0 & 1 & 0 & 1 & -2 \end{pmatrix}.$$

η_k is the stochastic impulsive intensity at t_k satisfying the uniform distribution U(0.6, 1.2). Figure 1 shows the stochastic impulsive sequence η_k with $T_a = 0.5$ and $N_0 = 1$. Let $c = 0.75$. The impulsive sequence is chosen as $t_k = 0.5k, k \in N^+$. Apparently, $T_a = 0.5, N_0 = 1$. By calculation, we can obtain that $Q = \mathrm{diag}\{0.8, 0.8\}$, $\bar{\alpha} = 0.9$, $\bar{\gamma}^2 = 0.03$, $\chi = 0.8035$, $b = -\frac{\lambda_2(\bar{L})}{\lambda_{\max}(W)} = 3.6227$, $p = -\lambda_{\max}\Big(D + D^T + AA^T + QQ^T + BB^T + CC^T - \theta b\Gamma\Big) = 1.5836$, $q = \lambda_{\max}(QQ^T) = 0.64$, $r = \sigma_2\lambda_{\max}(QQ^T) = 0.32$, $M_1 = \max\left\{c^{-\frac{\sigma_1}{T_a} - N_0}, 1\right\} = 1.8831$, $M_2 = \max\left\{c^{-\frac{\sigma_2}{T_a} - N_0}, 1\right\} = 1.7778$, $\alpha = \rho_k(\bar{\alpha}^2 + \bar{\gamma}^2) = 0.42$, and $\gamma^2 = \rho_k^2[\chi - (\bar{\alpha}^2 + \bar{\gamma}^2)^2] = 0.0244$. Since $p > qM_1 + rM_2\sigma_2 = 1.4896$, we can find that $\bar{\epsilon} = 0.052 > 0$ is the unique solution of equation $\epsilon - p + qM_1e^{\sigma_1\epsilon} + rM_2\frac{1}{\epsilon}(e^{\sigma_2\epsilon} - 1) = 0$. Furthermore, we can compute that $\lambda = \min\Big\{\alpha\rho_k e^{\bar{\epsilon}\rho_k} + \frac{c\rho_k^2 e^{2\bar{\epsilon}\rho_k}\gamma^2}{(\alpha\rho_k e^{\bar{\epsilon}\rho_k} - c)^2}, \alpha\rho_k e^{\bar{\epsilon}\rho_k} + c\Big\} = 0.2324$. Noting that $\bar{\epsilon} - \frac{\ln\lambda}{T_a} = 1.3195$, all the conditions in Theorem 1 are satisfied, which signifies that system (75) can be exponentially synchronized in mean square. Figure 2 shows the state trajectories of all nodes, and the error trajectories $z_{i1}, (i = 1, 2, 3, 4, 5)$ and $z_{i2}, (i = 1, 2, 3, 4, 5)$ are shown in Figures 3 and 4, respectively. It can be seen from Figures 2–4 that the state trajectories of different nodes tend to be consistent.

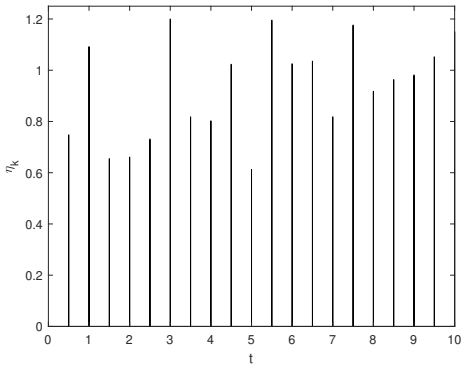

Figure 1. Stochastic impulsive sequence with $\eta_k \sim U(0.6, 1.2)$.

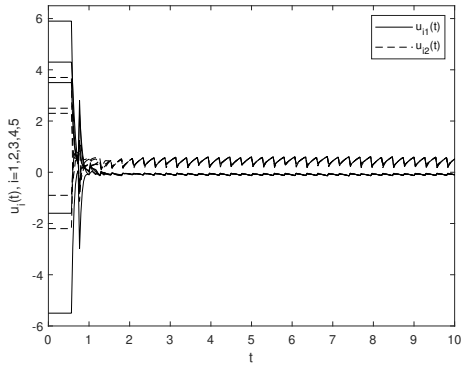

Figure 2. State trajectories of all the nodes.

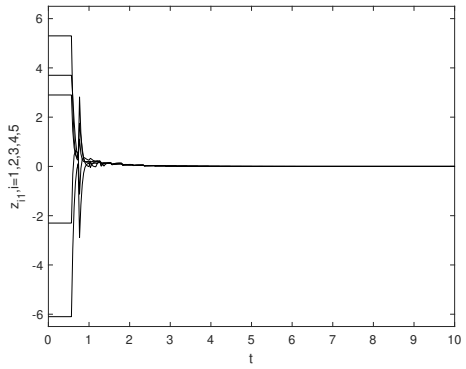

Figure 3. Error trajectories z_{i1}, $(i = 1, 2, 3, 4, 5)$ of Example 1.

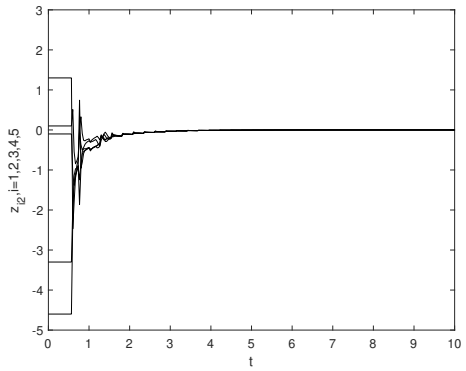

Figure 4. Error trajectories z_{i2}, $(i = 1, 2, 3, 4, 5)$ of Example 1.

Example 2. *Consider the coupled neural network system (75) with* $u_i = (u_{i1}, u_{i2})^T, N = 5$, $\sigma_1(t) = 0.6\cos(t) \le \sigma_1 = 0.6, \sigma_2 = 0.5, \theta = 1.8, J(t) = (1.2, 3.6)^T, 0 \le \rho_k = 0.5 = \rho$, $g(u_i(t)) = 0.9(\tanh(u_{i1}(t), \tanh(u_{i2}(t)))^T, i = 1, \ldots, N$. *Meanwhile, the corresponding coefficient matrices and inner coupled matrix are selected below.*

$$D = \begin{pmatrix} -3 & 0 \\ 0 & -3.6 \end{pmatrix}, \quad A = \begin{pmatrix} 1.9 & 1.5 \\ -1.6 & 1.2 \end{pmatrix}, \quad B = \begin{pmatrix} -1.9 & 1.2 \\ -1.6 & 1.7 \end{pmatrix}$$

$$C = \begin{pmatrix} 0.3 & -0.1 \\ 0.4 & 0.5 \end{pmatrix}, \quad \Gamma = \begin{pmatrix} 2.1 & 0 \\ 0 & 1.5 \end{pmatrix},$$

and the outer coupling matrix is

$$L = \begin{pmatrix} -3 & 0 & 1 & 2 & 0 \\ 1 & -2 & 1 & 0 & 0 \\ 0 & 0 & -4 & 2 & 2 \\ 0 & 1 & 0 & -3 & 2 \\ 1 & 1 & 0 & 0 & -2 \end{pmatrix}.$$

$\{\eta^{(i)}\}_{i\in\Omega}, \Omega \triangleq \{1, 2, 3\}$ *denotes three kinds of different independent random variables and satisfy* $\eta^{(1)} \sim U(0.2, 0.8), \eta^{(2)} \sim U(1.2, 1.8)$, *and* $\eta^{(3)} \sim E(1.6)$. *Figures 5–7 show the stochastic impulsive sequence* $\{\eta^{(i)}\}_{i\in\Omega}, \Omega \triangleq \{1, 2, 3\}$ *with* $T_a = 0.5$ *and* $N_0 = 1$, *respectively. A transition probability matrix is*

$$P = \begin{pmatrix} 0.2 & 0.5 & 0.3 \\ 0.4 & 0.3 & 0.3 \\ 0.3 & 0.6 & 0.1 \end{pmatrix},$$

and $\xi_1 = 0.3125, \xi_2 = 0.4375, \xi_3 = 0.25$. *Let* $c = 1$. *The impulsive sequence is chosen as* $t_k = 0.4k, k \in N^+$. *Apparently,* $T_a = 0.4, N_0 = 1$. *By calculation, we can obtain that* $Q = \mathrm{diag}\{0.9, 0.9\}$, $\mu_1^{(i)} = 0.5$, $(\omega_1^{(i)})^2 = 0.03$, $\chi_1^{(i)} = 0.1091$, $\mu_2^{(i)} = 1.5$, $(\omega_2^{(i)})^2 = 0.03$, $\chi_2^{(i)} = 5.4691$, $\mu_3^{(i)} = 0.625$, $(\omega_3^{(i)})^2 = 0.3906$, $\chi_3^{(i)} = 15$, $b = -\frac{\lambda_2(\bar{L})}{\lambda_{\max}(W)} = 3.8514$, $p = -\lambda_{\max}\Big(D + D^T + AA^T + QQ^T + BB^T + CC^T - \theta b\Gamma\Big) = 3.8202$, $q = \lambda_{\max}(QQ^T) = 0.81, r = \sigma_2\lambda_{\max}(QQ^T) = 0.4050$, $M_1 = \max\left\{c^{-\frac{\sigma_1}{T_a} - N_0}, 1\right\} = 1$, $M_2 = \max\left\{c^{-\frac{\sigma_2}{T_a} - N_0}, 1\right\} = 1$, $\alpha_1 = \rho\big[(\mu_1^{(i)})^2 + (\omega_1^{(i)})^2\big] = 0.1400$, *and* $\gamma_1^2 = \rho^2\big[\chi_1^{(i)} - ((\mu_1^{(i)})^2 + (\omega_1^{(i)})^2)^2\big] = 0.0077$, $\alpha_2 = \rho\big[(\mu_2^{(i)})^2 + (\omega_2^{(i)})^2\big] = 1.1400$, *and* $\gamma_2^2 = \rho^2\big[\chi_2^{(i)} - ((\mu_2^{(i)})^2 + (\omega_2^{(i)})^2)^2\big] = 0.0677$, $\alpha_3 = \rho\big[(\mu_3^{(i)})^2 + (\omega_3^{(i)})^2\big] = 0.3906$, *and* $\gamma_3^2 = \rho^2\big[\chi_3^{(i)} - ((\mu_3^{(i)})^2 + (\omega_3^{(i)})^2)^2\big] = 3.5974$. *Since* $p > qM_1 + rM_2\sigma_2 = 1.0125$, *we can find that* $\bar{\epsilon} = 1.5115 > 0$ *is the unique solution of equation* $\epsilon - p + qM_1e^{\sigma_1\epsilon} + rM_2\frac{1}{\epsilon}(e^{\sigma_2\epsilon} - 1) = 0$. *Furthermore, we can compute that* $\lambda_1 = \min\Big\{\alpha_1\rho e^{\bar{\epsilon}\rho} + \frac{c\rho^2e^{2\bar{\epsilon}\rho}\gamma_1^2}{(\alpha_1\rho e^{\bar{\epsilon}\rho} - c)^2}, \alpha_1\rho e^{\bar{\epsilon}\rho} + c\Big\} = 0.1610$, $\lambda_2 = \min\Big\{\alpha_2\rho e^{\bar{\epsilon}\rho} + \frac{c\rho^2e^{2\bar{\epsilon}\rho}\gamma_2^2}{(\alpha_2\rho e^{\bar{\epsilon}\rho} - c)^2}, \alpha_2\rho e^{\bar{\epsilon}\rho} + c\Big\} = 2.2136$, $\lambda_3 = \min\Big\{\alpha_3\rho e^{\bar{\epsilon}\rho} + \frac{c\rho^2e^{2\bar{\epsilon}\rho}\gamma_3^2}{(\alpha_3\rho e^{\bar{\epsilon}\rho} - c)^2}, \alpha_3\rho e^{\bar{\epsilon}\rho} + c\Big\} = 1.4216$. $\zeta = 1.3742$, $\epsilon_0 = 0.1$. *Noting that* $\bar{\epsilon} - \frac{\ln(\zeta + \epsilon_0)}{T_a} = 0.5412$, *all the conditions in Theorem 1 are satisfied, which signifies that system (75) can be exponentially synchronized in mean square. Figure 8 shows the state trajectories of all nodes, and the error trajectories* $z_{i1}, (i = 1, 2, 3, 4, 5)$ *and* $z_{i2}, (i = 1, 2, 3, 4, 5)$ *are shown in Figures 9 and 10, respectively. It can be seen from Figures 8–10 that the state trajectories of different nodes tend to be consistent.*

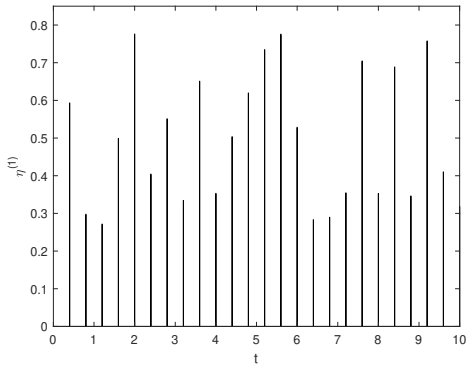

Figure 5. Stochastic impulsive sequence with $\eta^{(1)} \sim U(0.2, 0.8)$.

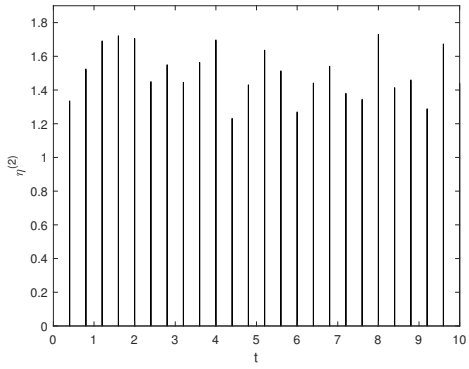

Figure 6. Stochastic impulsive sequence with $\eta^{(2)} \sim U(1.2, 1.8)$.

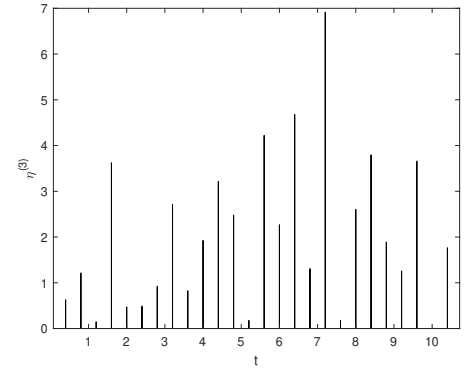

Figure 7. Stochastic impulsive sequence with $\eta^{(3)} \sim E(1.6)$.

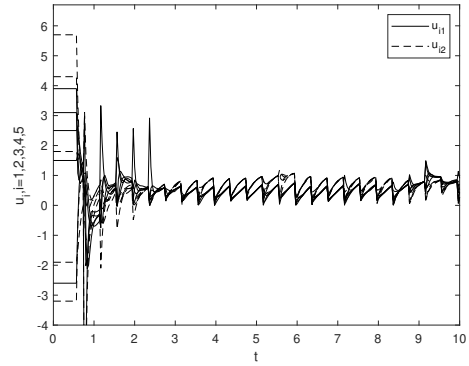

Figure 8. State trajectories of all the nodes.

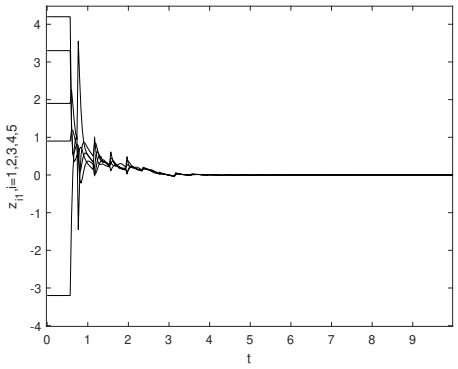

Figure 9. Error trajectories z_{i1}, $(i = 1, 2, 3, 4, 5)$ of Example 2.

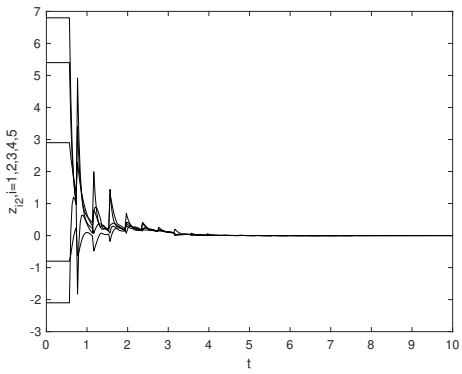

Figure 10. Error trajectories z_{i2}, $(i = 1, 2, 3, 4, 5)$ of Example 2.

Remark 8. *In Examples 1 and 2, apart from stochastic distributed impulsive sequence, hybrid delays and coupled strengthen have been considered and discussed simultaneously. Particularly, when coupled strengthen θ become large, error trajectories will converge to zero vector more quickly. In references [34–36], although stochastic impulses have been considered, hybrid delays, coupled structure and stochastic distributed impulses have been ignored. Therefore, those theoretical results in [34–36] can not be directly to Examples 1 and 2, and by utilizing Theorems 1 and 2, we can verified that the exponential synchronization in mean square of CNNs is realized in Examples 1 and 2.*

5. Conclusions

In this article, we have investigated the exponential synchronization of CNNs with hybrid delays and stochastic distributed delayed impulses. Some new criteria on the exponential synchronization in the mean square of CNNs are derived.

Firstly, two types of stochastic impulses, i.e., stochastic distributed delayed impulses with dependent property and Markov property have been taken into account, respectively. By utilizing the average impulsive interval method, total probability formula and ergodic theory, two novel Halanay differential inequalities with stochastic distributed delay impulses are established.

Secondly, based on the previous two novel impulsive Halanay differential inequalities, some sufficient conditions are acquired to guarantee the mean square exponential synchronization of CNNs.

Thirdly, the effectiveness of theoretical results is verified through two simulation examples, stochastic impulsive sequences, state trajectories of all the nodes and error trajectories have been shown through a series of figures.

However, semi-Markov jump CNNs or discrete CNNs with stochastic delayed impulses have not been investigated. Therefore, in the future, we can further explore the mean square exponential synchronization of semi-Markov jump CNNs or discrete CNNs with stochastic delayed impulses.

Author Contributions: Conceptualization, Y.S.; methodology, Y.S.; software, G.Z. and X.L.; formal analysis, G.Z.; investigation, G.Z.; writing—original draft preparation, G.Z.; writing—review and editing, X.L. and Y.S.; supervision, Y.S.; funding acquisition, Y.S. All authors have read and agreed to the published version of the manuscript.

Funding: This research is supported by the National Natural Science Foundation of China (62076039).

Data Availability Statement: Data are contained within the article.

Conflicts of Interest: The authors declare no conflict of interest.

References

1. Nishio, Y.; Ushida, A. Spatio-temporal chaos in simple coupled chaotic circuits. *IEEE Trans. Circuits Syst. I Fundam. Theory Appl.* **1995**, *42*, 678–686. [CrossRef]
2. Perez-Munuzuri, V.; Perez-Villar, V.; Chua, O.L. Autowaves for image processing on a two-dimensional CNN array of excitable nonlinear circuits:Flat and wrinkled labyrinths. *IEEE Trans. Circuits Syst. I Fundam. Theory Appl.* **1993**, *40*, 174–181. [CrossRef]
3. Xiu, R.; Zhang, W.; Zhou, Z. Synchronization issue of coupled neural networks based on flexible impulse control. *Neural Netw.* **2022**, *149*, 57–65. [CrossRef] [PubMed]
4. Mao, X.; Wang, Z. Stability switches and bifurcation in a system of four coupled neural networks with multiple time delays. *Nonlinear Dyn.* **2015**, *82*, 1551–1567. [CrossRef]
5. Pecora, L.M.; Carroll, T.L. Synchronization in chaotic systems. *Phys. Rev. Lett.* **1990**, *64*, 821–824. [CrossRef] [PubMed]
6. Liang, J.; Wang, Z.; Liu, Y.; Liu, X. Robust synchronization of an array of coupled stochastic discrete-time delayed neural networks. *IEEE Trans. Neural Netw.* **2008**, *19*, 1910–1921. [CrossRef] [PubMed]
7. Wang, J.L.; Wu, H.N.; Huang, T. Pinning control strategies for synchronization of linearly coupled neural networks with reaction-diffusion terms. *IEEE Trans. Neural Netw. Learn. Syst.* **2016**, *27*, 749–761. [CrossRef] [PubMed]
8. Chen, H.; Shi, P.; Lim, C.C. Exponential synchronization for Markovian stochastic coupled neural networks of neutral-type via adaptive feedback control. *IEEE Trans. Neural Netw. Learn. Syst.* **2017**, *28*, 1618–1632. [CrossRef]
9. Wen, S.; Zeng, Z.; Chen, M.Z.Q.; Huang, T. Synchronization of switched neural networks with communication delays via the event-triggered control. *IEEE Trans. Neural Netw. Learn. Syst.* **2017**, *28*, 2334–2343. [CrossRef]
10. Gao, C.; Wang, Z.; He, X.; Yue, D. Sampled-data-based fault-tolerant consensus control for multi-agent systems: A data privacy preserving scheme. *Automatica* **2021**, *133*, 109–847. [CrossRef]
11. Zhang, L.; Liu, J. Exponential synchronization for delayed coupled systems on networks via graph-theoretic method and periodically intermittent control. *Phys. A* **2020**, *545*, 123–733. [CrossRef]
12. Zhang, G.; Xia, Y.; Li, X.; He, S. Multievent-triggered sliding-Mode control for a class of complex dynamic network. *IEEE Trans. Control Netw. Syst.* **2022**, *9*, 835–844. [CrossRef]
13. Fan, H.; Rao, Y.; Shi, K.; Wen, H. Global synchronization of fractional-order multi-delay coupled neural networks with multi-link complicated structures via hybrid impulsive control. *Mathematics* **2023**, *11*, 3051. [CrossRef]
14. Rao, R.; Zhu, Q. Synchronization for reaction–diffusion switched delayed feedback epidemic systems via impulsive control. *Mathematics* **2024**, *12*, 447. [CrossRef]
15. Xiao, Q.; Liu, H.; Wang, Y. An improved finite-time and fixed-time stable synchronization of coupled discontinuous neural networks. *IEEE Trans. Neural Netw. Learn. Syst.* **2021**, *34*, 3516–3526. [CrossRef]
16. Li, P.; Cao, J.; Wang, Z. Robust impulsive synchronization of coupled delayed neural networks with uncertainties. *Phys. A* **2007**, *373*, 261–272. [CrossRef]
17. Lu, J.; Ho, D.W.; Cao, J.; Kurths, J. Exponential synchronization of linearly coupled neural networks with impulsive disturbances. *IEEE Trans. Neural Netw.* **2011**, *22*, 329–335. [CrossRef] [PubMed]
18. Yang, D.; Li, X.; Song, S. Finite-time synchronization for delayed complex dynamical networks with synchronizing or desynchronizing impulses. *IEEE Trans. Neural Netw. Learn. Syst.* **2022**, *33*, 736–746. [CrossRef]
19. Wang, N.; Li, X.; Lu, J.; Alsaadi, F.E. Unified synchronization criteria in an array of coupled neural networks with hybrid impulses. *Neural Netw.* **2018**, *101*, 25–32. [CrossRef]
20. Xu, H.; Zhu, Q.; Zheng, W.X. Exponential stability of stochastic nonlinear delay systems subject to multiple periodic impulses. *IEEE Trans. Autom. Control* **2023**, *69*, 2621–2628. [CrossRef]
21. Hu, W.; Zhu, Q.; Karimi, H.R. Some improved Razumikhin stability criteria for impulsive stochastic delay differential systems. *IEEE Trans. Autom. Control* **2019**, *64*, 5207–5213. [CrossRef]
22. Li, X.; Wu, J. Stability of nonlinear differential systems with state-dependent delayed impulses. *Automatica* **2016**, *64*, 63–69. [CrossRef]
23. Liu, X.; Zhang, K. Synchronization of linear dynamical networks on time scales: Pinning control via delayed impulses. *Automatica* **2016**, *72*, 147–152. [CrossRef]
24. Huang, Z.; Cao, J.; Li, J.; Bin, H. Quasi-synchronization of neural networks with parameter mismatches and delayed impulsive controller on time scales. *Nonlinear Anal. Hybri.* **2019**, *33*, 104–115. [CrossRef]

25. Gao, K.; Lu, J.; Zheng, W.X.; Chen, X. Synchronization in coupled neural networks with hybrid delayed impulses: Average impulsive delay-gain method. *IEEE Trans. Neural Netw. Learn. Syst.* 2024, *in press*. [CrossRef]
26. Liu, X.; Zhang, K. Stabilization of nonlinear time-delay systems: Distributed-delay dependent impulsive control. *Syst. Control Lett.* **2018**, *120*, 17–22. [CrossRef]
27. Xu, Z.; Peng, D.; Li, X. Synchronization of chaotic neural networks with time delay via distributed delayed impulsive control. *Neural Netw.* **2019**, *118*, 332–337. [CrossRef]
28. Zhang, X.; Li, C.; Li, H.; Cao, Z. Synchronization of uncertain coupled neural networks with time-varying delay of unknown bound via distributed delayed impulsive control. *IEEE Trans. Neural Netw. Learn. Syst.* **2021**, *34*, 3624–3635. [CrossRef] [PubMed]
29. Fang, Q.; Wang, M.; Li, X. Event-triggered distributed delayed impulsive control for nonlinear systems with applications to complex networks. *Chaos Soliton Fract.* **2023**, *175*, 113–943. [CrossRef]
30. Hu, W.; Zhu, Q. Stability criteria for impulsive stochastic functional differential systems with distributed-delay dependent impulsive effects. *IEEE Trans. Syst. Man, Cybern.* **2021**, *51*, 2027–2032. [CrossRef]
31. Li, J.; Zhu, Q. Stability of neutral stochastic delayed systems with switching and distributed-delay dependent impulses. *Nonlinear Anal. Hybri.* **2023**, *47*, 101–279. [CrossRef]
32. Tang, Y.; Wu, X.; Shi, P.; Qian, F. Input-to-state stability for nonlinear systems with stochastic impulses. *Automatica* **2020**, *113*, 108–766. [CrossRef]
33. Liu, J.; Zhu, Q. Finite time stability of time-varying stochastic nonlinear systems with random impulses. *Int. J. Control* **2023**. [CrossRef]
34. Sun, Y.; Li, L.; Liu, X. Exponential synchronization of neural networks with time-varying delays and stochastic impulses. *Neural Netw.* **2020**, *132*, 342–352. [CrossRef]
35. Cui, Q.; Li, L.; Cao, J. Stability of inertial delayed neural networks with stochastic delayed impulses via matrix measure method. *Neurocomputing* **2022**, *471*, 70–78. [CrossRef]
36. Li, L.; Cui, Q.; Cao, J.; Qiu, J.; Sun, Y. Exponential synchronization of coupled inertial neural networks with hybrid delays and stochastic impulses. *IEEE Trans. Neural Netw. Learn. Syst.* 2023, *in press*. [CrossRef]
37. Ling, G.; Liu, X.; Guan, Z.H.; Ge, M.F.; Tong, Y.H. Input-to-state stability for switched stochastic nonlinear systems with mode-dependent random impulses. *Inf. Sci.* **2022**, *596*, 588–607. [CrossRef]
38. Zhang, N.; Huang, S.; Li, W. Stability of stochastic delayed semi-Markov jump systems with stochastic mixed impulses: A novel stochastic impulsive differential inequality. *J. Franklin Inst. Eng. Appl. Math.* **2022**, *359*, 10785–10812. [CrossRef]
39. Ross, S.M. *Stochastic Processes*; John Wiley & Sons: New York, NY, USA, 1996.
40. Lu, J.; Ho, D.W.C.; Cao, J. A unified synchronization criterion for impulsive dynamical networks. *Automatica* **2010**, *46*, 1215–1221. [CrossRef]
41. Dong, S.; Shi, K.; Wen, S.; Shen, Y.; Zhong, S. Almost surely synchronization of directed coupled neural networks via stochastic distributed delayed impulsive control. *Chaos Soliton Fract.* **2023**, *174*, 113–742. [CrossRef]

mathematics

MDPI

Article

Command-Filtered Nussbaum Design for Nonlinear Systems with Unknown Control Direction and Input Constraints

Yuxuan Liu

School of Electronic and Electrical Engineering, University of Leeds, Leeds LS2 9IT, UK; el23yl@leeds.ac.uk

Abstract: This paper studies the problem of adaptive fuzzy control based on command filtering for a class of nonlinear systems characterized by an input dead zone, input saturation, and unknown control direction. First, this paper proposes a novel equivalent transformation technique that simplifies the design complexity of multiple input constraints by converting the input dead zone and saturation nonlinearities into a unified functional form. Subsequently, a fuzzy logic system is utilized to handle the unknown nonlinear functions, and the command-filtering method is employed to address the issue of complexity explosion, while the Nussbaum function is utilized to resolve the challenge of an unknown control direction. Based on Lyapunov stability, it is proven that the tracking error converges to a small neighborhood around the origin, and all closed-loop signals are bounded. Finally, a numerical simulation result and an actual simulation result of a pendulum are presented to verify the feasibility and effectiveness of the proposed control strategy.

Keywords: unknown control direction; adaptive fuzzy control; dead zone and saturation; command filter

MSC: 93-10; 93C10; 93C40; 93D21

1. Introduction

It is widely acknowledged that stability analysis and controller design for nonlinear systems have been subjects of ongoing research and interest for several decades [1–3]. This technology is often applied to robots [4], quadcopter UAVs [5], noise data classification [6], aerospace systems [7], etc. Recently, the combination of backstepping methodology with adaptive control techniques to address nonlinear systems has undergone significant development and practical application. In earlier studies, nonlinear terms of the system were often assumed to be known a priori or linearly parameterizable. However, for many practical systems, this assumption is considered unrealistic. To solve this problem, neural networks (NNs) and fuzzy logic systems (FLS) have been used to approximate unknown system dynamics [8,9]. For example, [10] introduced an adaptive fuzzy controller grounded in sliding mode control theory. In [11–13], the authors introduced several intelligent control methodologies for nonlinear systems featuring pure feedback structures by amalgamating neural networks or fuzzy logic systems with adaptive backstepping approaches.

However, the most common drawback of backstepping techniques is the complexity explosion caused by repeatedly differentiating the virtual controller. To address this issue, Ref. [14] proposed a dynamic surface control (DSC) scheme, which incorporated a first-order filter dynamic surface at each stage of the backstepping control design process, thereby obviating the need for calculating the derivatives of the virtual controller. Dynamic filtering technology was introduced by [15] to investigate event-triggered tracking control of a category of uncertain nonlinear systems. However, DSC technology failed to account for the error introduced by the filter, consequently diminishing the control performance of the system. Refs. [16–19] applied command-filtering technology to nonlinear systems under different constraints, which not only solved the problem of complexity explosion in the backstepping design process, but also established an error compensation system to make up for the shortcomings of DSC technology.

Despite the success of command-filter adaptive control in nonlinear systems, the presence of various constraints in practical engineering contexts, such as input dead zones, input saturation, unknown control direction, etc., can influence the system's stability. To solve the dead-zone problem, some related results are provided in [20–22]. Ref. [20] proposed an adaptive dead-zone inverse technology. Ref. [21] developed a corresponding disturbance observer for estimation based on the unknown approximation error and the impact of unknown dead zones and external disturbances. In [22], the system was converted into n-step predictors, and an adaptive compensation term was introduced to overcome the asymmetric dead zone existing in the system. Apart from the presence of dead zone input, the presence of input saturation can also cause performance degradation of nonlinear systems and signal delay or loss. The study of input saturated systems has also been an important topic in recent years [23,24].

On the other hand, when researching adaptive control of nonlinear systems, it is often necessary to know the control direction representing the direction of motion in advance [25,26]. However, the direction of controlling gain is mostly unknown in practical applications. The Nussbaum gain method is an effective tool for processing unknown signals. Characterized by its values and integral oscillating infinitely between positive and negative, the Nussbaum function allows the control system to adjust its strategy automatically, despite uncertainty about the sign of the control gain, ensuring that the system can stably achieve the desired state. Building upon this technology, numerous control strategies have been formulated [27–30]. Ref. [27] introduced the Nussbaum function to compensate for the impact of the unknown direction problem and designed an adaptive tracking controller based on a command filter. For systems featuring multiple unknown high-frequency gains, Ref. [28] introduced a novel command-filtered Nussbaum design. A novel Nussbaum function was devised by [29] to address the tracking problem encountered within a category ofstochastic strict feedback nonlinear systems. By using an improved Nussbaum function, [30] extended previous research results to cover a broader range of nonlinear systems, characterized by unknown variations in both the sign and magnitude of the control gain over time. However, to the best of our knowledge, there is a scarcity of papers that concurrently address nonlinear systems with input dead zones, input saturation, and uncertain control directions. This scarcity partly motivated the research presented in this paper.

Based on the previous discussion, the main contributions of this article, in contrast to existing research outcomes, can be encapsulated as follows:

1. Compared with the nonlinear systems studied in [25,26], where the control direction was known, this paper considers a broader situation in which the control direction is unknown, and it designs adaptive fuzzy control using the Nussbaum function.
2. This paper proposes a novel transformation method to eliminate the impact of the input dead zone and saturation on the system, and uses command-filtering technology to solve the problem of complexity explosion in traditional backstepping design.

2. Preliminary Knowledge and Problem Statement

2.1. System Model

Consider the following nonlinear system

$$\begin{cases} \dot{x}_i = f_i(\bar{x}_i) + \lambda_i g_i(\bar{x}_i) x_{i+1}, \ i = 1, \ldots, n-1, \\ \dot{x}_n = f_n(\bar{x}_n) + \lambda_n g_n(\bar{x}_n) u, \\ y = x_1, \end{cases} \tag{1}$$

where $x = [x_1, x_2, \ldots x_n]^T \in R^n$ represents the state vector with $\bar{x}_i = [x_1, x_2, \ldots x_i]^T \in R^i$, and $y \in R$ denotes the system output; $\lambda_i = 1$ (or -1) represents an unknown control direction; $g_i(\bar{x}_i)$ are bounded continuous functions with $0 < \hbar_i \leq g_i(\cdot) \leq \Theta_i$, $\hbar_i$ and Θ_i

represent two constants; and $f_i(\bar{x}_i)$ signifies the unknown smooth function. The control input $u \in R$ is specified as

$$u(t) = \begin{cases} u_h, & v(t) > u_h, \\ k_h(v(t) - m_h), & m_h \le v(t) < u_h, \\ 0, & -m_l < v(t) \le m_h, \\ k_l(v(t) + m_l), & -u_l < v(t) \le -m_l, \\ -u_l, & v(t) < -u_l, \end{cases} \tag{2}$$

where $v(t)$ is the input of the dead zone; u_h and u_l are positive parameters and represent unknown saturation values; $k_h > 0$, $k_l > 0$, $m_h > 0$, and $m_l > 0$ are the unknown zone parameters; and the dead-zone slopes in positive and negative region are same, i.e., $k_h = k_l = k$.

Assumption 1 ([22]). *The dead-zone parameters of m_h, m_l, and k are bounded. This implies that there are known parameters $m_{h\max}$, $m_{h\min}$, $m_{l\max}$, $m_{l\min}$, $k_{\max}$, and $k_{\min}$, such that $m_h \in [m_{h\min}, m_{h\max}]$, $m_l \in [m_{l\min}, m_{l\max}]$, and $k \in [k_{\min}, k_{\max}]$.*

For the development of a robust control scheme, (2) is reformulated as follows:

$$u(t) = \pi\big(v(t)\big)v(t) + \vartheta\big(v(t)\big). \tag{3}$$

Based on Assumption 1, one can conclude that $\vartheta\big(v(t)\big)$ is bounded, while satisfies $\big|\vartheta\big(v(t)\big)\big| \le L_p$, where L_p represents the upper bound.

Assumption 2 ([25]). *In this article, considering that the input signal v is limited in actual situations, $\pi\big(v(t)\big)$ satisfies the following inequality*

$$0 < \Im \le \min\left\{\frac{u_h}{v(t)_{\max}}, k\right\} \le \pi\big(v(t)\big) \le \max\{1, k\}, \tag{4}$$

2.2. Fuzzy Logic Systems

FLS consists of four primary components: the knowledge base, fuzzifier, fuzzy inference engine, and defuzzifier. The knowledge base houses a comprehensive set of fuzzy if-then rules, which are defined as follows:

R^l: IF x_1 is P_1^j, and x_2 is P_2^j, and x_n is P_n^j, then y is Q^j,$j = 1, 2, \ldots, \wp$, where $x = [x_1, x_2, \ldots, x_n]^T$, and y are the FLSs input and system output, respectively; P_m^j, Q^j denote the fuzzy sets for x and y, respecitvley; an equivalent expression of FLS can be obtained as

$$y(x) = \frac{\sum_{j=1}^{\wp} \bar{y}_j \prod_{m=1}^{n} \mu_{F_m^j}(x_m)}{\sum_{j=1}^{\wp}\left[\prod_{m=1}^{n} \mu_{F_m^j}(x_m)\right]}, \tag{5}$$

with $\bar{y}_j = \max_{y \in R} \mu_{Q^j}(y)$, where $\mu_{P_m^j}(x_m)$ and $\mu_{Q^j}(y)$ are the membership functions. Denote $W = [\bar{y}_1, \bar{y}_2, \ldots, \bar{y}_\wp]^T = [W_1, W_2, \ldots, W_\wp]^T$ and $\psi(x) = [\psi_1(x), \psi_2(x), \ldots, \psi_\wp(x)]^T$, the membership functions, which are defined as $\psi_j(x) = \frac{\prod_{m=1}^{n} \mu_{F_m^j}(x_m)}{\sum_{j=1}^{\wp}\left[\prod_{m=1}^{n} \mu_{F_m^j}(x_m)\right]}$. Consequently, FLS can be succinctly described as follows

$$y(x) = W^T \psi(x). \tag{6}$$

Lemma 1 ([27]). *The following inequality holds for any smooth function $f(x)$ defined on the compact set Ω if there is a sufficiently tiny positive scalar ε:*

$$\sup_{x\in\Omega}\left|f(x)-W^{\mathrm{T}}\psi(x)\right|\leq\varepsilon. \tag{7}$$

Definition 1 ([29]). *The Nussbaum function $N(\zeta):\mathbb{R}\to\mathbb{R}$ has the properties*

$$\begin{aligned}&\lim_{\ell\to\infty}\sup\frac{1}{\ell}\int_0^{\ell}N(\zeta)d\zeta=+\infty,\\&\lim_{\ell\to-\infty}\inf\frac{1}{\ell}\int_0^{\ell}N(\zeta)d\zeta=-\infty.\end{aligned} \tag{8}$$

Lemma 2 ([29]). *Consider $\zeta(t)$ and $V(t)\geq 0$ are smooth functions on $[0,t_f)$, and $N(\zeta(t))$ is an even smooth Nussbaum-type function. Suppose*

$$V(t)\leq e^{-\mathrm{Y}_1t}\int_0^t\big(w\big(\bar{x}(\tau)\big)N\big(\zeta(\tau)\big)+1\big)\dot{\zeta}(\tau)e^{\mathrm{Y}_1\tau}d\tau+D, \tag{9}$$

in which $D>0$ and $\mathrm{Y}_1>0$, and $V(t)$, $\zeta(t)$ and $\int_0^t w\big(\bar{x}(\tau)\big)N\big(\zeta(\tau)\big)\dot{\zeta}(\tau)d\tau$ remain bounded on $[0,t_f)$.

Lemma 3 ([25]). *The command filter is defined as*

$$\begin{cases}\dot{\omega}_i=\varpi\omega_{i,2},\\ \dot{\omega}_{i,2}=-2\varphi\varpi\omega_{i,2}-\varpi(\omega_i-\alpha_{i-1}),\end{cases} \tag{10}$$

where α_{i-1} and ω_i represent the input and output of the command filter, respectively, $\omega_i(0)=\alpha_{i-1}$ and $\omega_{i,2}(0)=0$, $\varphi\in(0,1]$, and $\varpi>0$.

Remark 1. *The command-filtering approach is a control strategy that simplifies the design and implementation of complex control systems. By incorporating a filter between the controller and actuator, it smooths the control signals, preventing performance degradation due to overly complex control strategies. This method effectively reduces system complexity and avoids "complexity explosion" caused by high-frequency control updates and excessive regulation.*

Assumption 3 ([26]). *The reference signal x_d and its first-order derivative $\dot{x}_d$ are continuous and bounded.*

3. Controller Design and Stability Analysis

3.1. Controller Design

In this section, an adaptive command-filter controller is designed for the nonlinear system (1) by integrating the Nussbaum function with the back-stepping technique. Coordinate changes are introduced to facilitate controller design:

$$\begin{cases}e_1=x_1-y_d,\\ e_i=x_i-\omega_i,\ \ i=1,\ldots,n,\end{cases} \tag{11}$$

where e_i represents the tracking error and ω_i denotes the output of the filter.

Remark 2. *It is noteworthy that the error induced by the command filter exacerbates the system error. To address this drawback, a compensation signal, denoted as β, is introduced to mitigate the adverse effects of the filter error $\omega_i-\alpha_{i-1}$ on the system.*

Design the compensation signal β_i to eliminate the error caused by the command filter as follows

$$\begin{cases} \dot{\beta}_i = -k_i\beta_i + g_i\beta_{i+1} + g_i(\omega_{i+1} - \alpha_i), \\ \dot{\beta}_n = -k_n\beta_n, \end{cases} \tag{12}$$

where k_i is a given positive constant and $\beta_i(0) = 0$.

Subsequently, the compensated tracking error signals can be expressed as follows

$$\xi_i = e_i - \beta_i, \quad i = 1, 2, \ldots, n. \tag{13}$$

Step 1: Taking the derivative of ξ_i as

$$\dot{\xi}_1 = \dot{e}_1 - \dot{\beta}_1 = \dot{x}_1 - \dot{y}_d - \dot{\beta}_1 = f_1 + \lambda_1 g_1 x_2 - \dot{y}_d - \dot{\beta}_1. \tag{14}$$

The Lyapunov function is chosen as

$$V_1 = \frac{1}{2}\xi_1^2 + \frac{1}{2\Gamma_1}\tilde{\theta}_1^2, \tag{15}$$

where Γ_1 represents the positive parameter to be constructed, and in order to solve the parameter estimation problem, the parameter estimation error is $\tilde{\theta}_1 = \theta_1 - \hat{\theta}_1$, and the constant is defined as $\theta_i = \|W_i\|^2$.

Based on (11), (13), (14) and (15) the time derivative of V_1 is shown as

$$\begin{aligned} \dot{V}_1 &= \xi_1\dot{\xi}_1 - \frac{1}{\Gamma_1}\tilde{\theta}_1\dot{\hat{\theta}}_1 \\ &= \xi_1\big(f_1 + \lambda_1 g_1(\omega_2 + \xi_2 + \beta_2) - \dot{y}_d - \dot{\beta}_1\big) - \frac{1}{\Gamma_1}\tilde{\theta}_1\dot{\hat{\theta}}_1 \\ &= \xi_1 f_1 + \lambda_1 g_1\xi_1\omega_2 + \lambda_1 g_1\xi_1\xi_2 + \lambda_1 g_1\xi_1\beta_2 - \xi_1\dot{y}_d - \xi_1\dot{\beta}_1 - \frac{1}{\Gamma_1}\tilde{\theta}_1\dot{\hat{\theta}}_1. \end{aligned} \tag{16}$$

As function $f_1(x)$ is unknown, the direct design of the virtual control signal α_1 is not feasible. Thus, according to Lemma 1, for any given number $\varepsilon_1 > 0$, there are

$$f_1(B_1) = W_1^T\psi_1 + \delta_1(B_1), \|\delta_1(B_1)\| < \varepsilon_1,$$

in which $\|\delta_1(B_1)\|$ denotes the estimation error.

By applying Young's inequality, the following formula can be derived

$$\xi_1 f_1 \leq \frac{\xi_1^2\theta_1 S_1^T S_1}{2a_1^2} + \frac{1}{2}a_1^2 + \frac{1}{2}\xi_1^2 + \frac{1}{2}\varepsilon_1^2, \tag{17}$$

where a_1 is a given positive scalar.

Consider a compensating signal $\dot{\beta}_1$ as

$$\dot{\beta}_1 = -k_1\beta_1 + g_1\beta_2 + g_1(\omega_2 - \alpha_1). \tag{18}$$

Next, after combining formulas (16)–(18), it can be easily obtained that

$$\begin{aligned} \dot{V}_1 \leq& \frac{\xi_1^2\theta_1 S_1^T S_1}{2a_1^2} + \frac{1}{2}a_1^2 + \frac{1}{2}\xi_1^2 + \frac{1}{2}\varepsilon_1^2 + \lambda_1 g_1\xi_1\omega_2 + \lambda_1 g_1\xi_1\xi_2 + \lambda_1 g_1\xi_1\beta_2 \\ &+ k_1\xi_1\beta_1 - g_1\xi_1\beta_2 - g_1\xi_1\omega_2 + g_1\xi_1\alpha_1 - \frac{1}{\Gamma_1}\tilde{\theta}_1\dot{\hat{\theta}}_1 - \xi_1\dot{y}_d \\ \leq& \frac{\xi_1^2\theta_1 S_1^T S_1}{2a_1^2} + \frac{1}{2}a_1^2 + \frac{1}{2}\xi_1^2 + \frac{1}{2}\varepsilon_1^2 + \lambda_1 g_1\xi_1\xi_2 + k_1\xi_1\beta_1 + g_1\xi_1\alpha_1 - \frac{1}{\Gamma_1}\tilde{\theta}_1\dot{\hat{\theta}}_1 \\ &+ (\lambda_1 - 1)g_1\xi_1(\beta_2 + \omega_2) - \xi_1\dot{y}_d. \end{aligned} \tag{19}$$

In this article, $\lambda_1 = 1(or-1)$ represents the unknown control direction. Applying Young's inequality, one can obtain

$$\begin{aligned}(\lambda_1-1)g_1\xi_1(\beta_2+\omega_2) = (\lambda_1-1)g_1\xi_1(x_2-\xi_2) = 0 \le 2g_1^2\xi_1^2 + x_2^2 + \xi_2^2, \quad \lambda_1 = 1,\\ (\lambda_1-1)g_1\xi_1(\beta_2+\omega_2) = (\lambda_1-1)g_1\xi_1(x_2-\xi_2) \le 2g_1^2\xi_1^2 + x_2^2 + \xi_2^2, \quad \lambda_1 = -1,\\ \lambda_1 g_1\xi_1\xi_2 \le \frac{1}{2}g_1^2\xi_1^2 + \frac{1}{2}\xi_2^2, \quad \lambda_1 = 1(or-1).\end{aligned} \tag{20}$$

Substituting (20) into (19) produces

$$\begin{aligned}\dot{V}_1 \le &\frac{\xi_1^2\theta_1\psi_1^T\psi_1}{2a_1^2} + \frac{1}{2}a_1^2 + \frac{1}{2}\xi_1^2 + \frac{1}{2}\varepsilon_1^2 + \frac{5}{2}g_1^2\xi_1^2 + \frac{3}{2}\xi_2^2\\ &+ k_1\xi_1\beta_1 + g_1\xi_1\alpha_1 - \frac{1}{\Gamma_1}\tilde{\theta}_1\dot{\hat{\theta}}_1 + x_2^2 - \xi_1\dot{y}_d.\end{aligned} \tag{21}$$

Next, the virtual control signal α_1 and the Nussbaum-type gain ζ_1 are developed as follows

$$\begin{cases}\alpha_1 = N(\zeta_1)\left(\frac{\xi_1\hat{\theta}_1 S_1^T S_1}{2a_1^2} + k_1e_1 + \frac{1}{2}\xi_1 + \frac{5}{2}g_1^2\xi_1 - \dot{y}_d\right),\\ \dot{\zeta}_1 = \xi_1\left(\frac{\xi_1\hat{\theta}_1 S_1^T S_1}{2a_1^2} + k_1e_1 + \frac{1}{2}\xi_1 + \frac{5}{2}g_1^2\xi_1 - \dot{y}_d\right).\end{cases} \tag{22}$$

By amalgamating the aforementioned equation, (21) can be reformulated as

$$\begin{aligned}\dot{V}_1 &\le \frac{\xi_1^2\theta_1\psi_1^T\psi_1}{2a_1^2} + \frac{1}{2}a_1^2 + \frac{1}{2}\xi_1^2 + \frac{1}{2}\varepsilon_1^2 + \frac{5}{2}g_1^2\xi_1^2 + \frac{3}{2}\xi_2^2 + k_1\xi_1\beta_1 + g_1\xi_1\alpha_1 - \frac{1}{\Gamma_1}\tilde{\theta}_1\dot{\hat{\theta}}_1 + x_2^2 - \xi_1\dot{y}_d\\ &\le -k_1\xi_1^2 + g_1N(\zeta_1)\dot{\zeta}_1 + \dot{\zeta}_1 + \frac{\tilde{\theta}_1}{\Gamma_1}\left(\frac{\Gamma_1\xi_1^2\psi_1^T\psi_1}{2a_1^2} - \dot{\hat{\theta}}_1\right) + \frac{1}{2}a_1^2 + \frac{1}{2}\varepsilon_1^2 + \frac{3}{2}\xi_2^2 + x_2^2.\end{aligned} \tag{23}$$

Next, the adaptive law $\dot{\hat{\theta}}_1$ is designed as $\dot{\hat{\theta}}_1 = \frac{\Gamma_1\xi_1^2\psi_1^T\psi_1}{2a_1^2} - \sigma_1\hat{\theta}_1$, and with the help of Young's inequality $\frac{\sigma_1\tilde{\theta}_1\hat{\theta}_1}{\Gamma_1} \le \frac{\sigma_1\theta_1^2}{2\Gamma_1} - \frac{\sigma_1\tilde{\theta}_1^2}{2\Gamma_1}$, one obtain

$$\dot{V}_1 \le -k_1\xi_1^2 + g_1N(\zeta_1)\dot{\zeta}_1 + \dot{\zeta}_1 - \frac{\sigma_1\tilde{\theta}_1^2}{2\Gamma_1} + N_1, \tag{24}$$

where $N_1 = \frac{1}{2}a_1^2 + \frac{1}{2}\varepsilon_1^2 + \frac{3}{2}\xi_2^2 + x_2^2 + \frac{\sigma_1\theta_1^2}{2\Gamma_1}$.

Step i: $(2 \le i \le n-1)$: According to the differential rules, the following expression is derived

$$\dot{\xi}_i = \dot{e}_i - \dot{\beta}_i = \dot{x}_i - \dot{\omega}_i - \dot{\beta}_i = f_i + \lambda_i g_i x_{i+1} - \dot{\omega}_i - \dot{\beta}_i. \tag{25}$$

Choose a Lyapunov function candidate function, as follows

$$V_i = V_{i-1} + \frac{1}{2}\xi_i^2 + \frac{1}{2\Gamma_i}\tilde{\theta}_i^2. \tag{26}$$

where $\tilde{\theta}_i = \theta_i - \hat{\theta}_i$.

By differentiating V_i, the following formula holds

$$\begin{aligned}\dot{V}_i &= \dot{V}_{i-1} + \xi_i\dot{\xi}_i - \frac{1}{\Gamma_i}\tilde{\theta}_i\dot{\hat{\theta}}_i\\ &= \dot{V}_{i-1} + \xi_i\left(f_i + \lambda_i g_i(\omega_{i+1} + \xi_{i+1} + \beta_{i+1}) - \dot{\omega}_i - \dot{\beta}_i\right) - \frac{1}{\Gamma_i}\tilde{\theta}_i\dot{\hat{\theta}}_i\\ &= \dot{V}_{i-1} + \xi_i f_i + \lambda_i g_i\xi_i\omega_{i+1} + \lambda_i g_i\xi_i\xi_{i+1} + \lambda_i g_i\xi_i\beta_{i+1} - \xi_i\dot{\omega}_i - \xi_i\dot{\beta}_i - \frac{1}{\Gamma_i}\tilde{\theta}_i\dot{\hat{\theta}}_i.\end{aligned} \tag{27}$$

According to Lemma 1 again, for any given number $\varepsilon_i > 0$, there are

$$f_i(B_i) = W_i^T \psi_i + \delta_i(B_i), \|\delta_i(B_i)\| < \varepsilon_i,$$

in which $\|\delta_i(B_i)\|$ denotes the estimation error.

By applying Young's inequality again, the following formula can be derived

$$\xi_i f_i \leq \frac{\xi_i^2 \theta_i \psi_i^T \psi_i}{2a_i^2} + \frac{1}{2}a_i^2 + \frac{1}{2}\xi_i^2 + \frac{1}{2}\varepsilon_i^2, \tag{28}$$

where a_i is a given positive scalar.

The compensation signal $\dot{\beta}_i$ is designed to be

$$\dot{\beta}_i = -k_i \beta_i + g_i \beta_{i+1} + g_i(\omega_{i+1} - \alpha_i). \tag{29}$$

Incorporating Equations (28) and (29) into (27), one can obtain

$$\begin{aligned}
\dot{V}_i \leq & \dot{V}_{i-1} + \frac{\xi_i^2 \theta_i \psi_i^T \psi_i}{2a_i^2} + \frac{1}{2}a_i^2 + \frac{1}{2}\xi_i^2 + \frac{1}{2}\varepsilon_i^2 + \lambda_i g_i \xi_i \xi_{i+1} + k_i \xi_i \beta_i + g_i \xi_i \alpha_i - \frac{1}{\Gamma_i}\tilde{\theta}_i \dot{\hat{\theta}}_i \\
& + \left[\lambda_i g_i \xi_i \omega_{i+1} + \lambda_i g_i \xi_i \beta_{i+1} - g_i \xi_i \beta_{i+1} - g_i \xi_i \omega_{i+1}\right] - \xi_i \dot{\omega}_i \\
\leq & \dot{V}_{i-1} + \frac{\xi_i^2 \theta_i \psi_i^T \psi_i}{2a_i^2} + \frac{1}{2}a_i^2 + \frac{1}{2}\xi_i^2 + \frac{1}{2}\varepsilon_i^2 + \lambda_i g_i \xi_i \xi_{i+1} + k_i \xi_i \beta_i + g_i \xi_i \alpha_i - \frac{1}{\Gamma_i}\tilde{\theta}_i \dot{\hat{\theta}}_i \\
& + (\lambda_i - 1) g_i \xi_i (\beta_{i+1} + \omega_{i+1}) - \xi_i \dot{\omega}_i.
\end{aligned} \tag{30}$$

Similar to (20), one can obtain

$$\begin{aligned}
\lambda_i g_i \xi_i \xi_{i+1} &\leq \frac{1}{2} g_i^2 \xi_i^2 + \frac{1}{2}\xi_{i+1}^2, \\
(\lambda_i - 1) g_i \xi_i (\beta_{i+1} + \omega_{i+1}) &\leq 2 g_i^2 \xi_i^2 + x_{i+1}^2 + \xi_{i+1}^2.
\end{aligned} \tag{31}$$

Then, (30) is rewritten as

$$\begin{aligned}
\dot{V}_1 \leq & \dot{V}_{i-1} + \frac{\xi_i^2 \theta_i \psi_i^T \psi_i}{2a_i^2} + \frac{1}{2}a_i^2 + \frac{1}{2}\xi_i^2 + \frac{1}{2}\varepsilon_i^2 + \frac{5}{2} g_i^2 \xi_i^2 + \frac{3}{2}\xi_{i+1}^2 \\
& + k_i \xi_i \beta_i + g_i \xi_i \alpha_i - \frac{1}{\Gamma_i}\tilde{\theta}_i \dot{\hat{\theta}}_i + x_{i+1}^2 - \xi_i \dot{\omega}_i.
\end{aligned} \tag{32}$$

The virtual control signal α_1 and the Nussbaum-type gain ζ_1 are designed as

$$\begin{cases}
\alpha_i = N(\zeta_i)\left(\frac{\xi_i \hat{\theta}_i \psi_i^T \psi_i}{2a_i^2} + k_i e_i + \frac{1}{2}\xi_i + \frac{5}{2} g_i^2 \xi_i - \dot{\omega}_i\right), \\
\dot{\zeta}_i = \xi_i \left(\frac{\xi_i \hat{\theta}_i \psi_i^T \psi_i}{2a_i^2} + k_i e_i + \frac{1}{2}\xi_i + \frac{5}{2} g_i^2 \xi_i - \dot{\omega}_i\right).
\end{cases} \tag{33}$$

Combining the above equation, (32) can be rewritten as

$$\dot{V}_i \leq \dot{V}_{i-1} - k_i \xi_i^2 + g_i N(\zeta_i)\dot{\zeta}_i + \dot{\zeta}_i + \frac{\tilde{\theta}_i}{\Gamma_i}\left(\frac{\Gamma_i \xi_i^2 \psi_i^T \psi_i}{2a_i^2} - \dot{\hat{\theta}}_i\right) + \frac{1}{2}a_i^2 + \frac{1}{2}\varepsilon_i^2 + \frac{3}{2}\xi_{i+1}^2 + x_{i+1}^2. \tag{34}$$

Next, the adaptive law $\dot{\hat{\theta}}_i$ is designed as $\dot{\hat{\theta}}_i = \frac{\Gamma_i \xi_i^2 \psi_i^T \psi_i}{2a_i^2} - \sigma_i \hat{\theta}_i$, and with the help of Young's inequality $\frac{\sigma_i \tilde{\theta}_i \hat{\theta}_i}{\Gamma_i} \leq \frac{\sigma_i \theta_i^2}{2\Gamma_i} - \frac{\sigma_i \tilde{\theta}_i^2}{2\Gamma_i}$, one obtain

$$\begin{aligned}\dot{V}_i \leq & \dot{V}_{i-1} - k_i \xi_i^2 + g_i N(\zeta_i)\dot{\zeta}_i + \dot{\zeta}_i - \frac{\sigma_i \tilde{\theta}_i^2}{2\Gamma_i} + \frac{1}{2}a_i^2 + \frac{1}{2}\varepsilon_i^2 + \frac{3}{2}\xi_{i+1}^2 + x_{i+1}^2 + \frac{\sigma_i \theta_i^2}{2\Gamma_i} \\ \leq & -\sum_{j=1}^{i} k_j \xi_j^2 - \sum_{j=1}^{i} \frac{1}{2}\frac{\sigma_j \tilde{\theta}_j^2}{\Gamma_j} + \sum_{j=1}^{i} g_j N(\zeta_j)\dot{\zeta}_j + \sum_{j=1}^{i} \dot{\zeta}_j \\ & + \frac{1}{2}\sum_{j=1}^{i}\left(a_j^2 + \varepsilon_j^2 + 3\xi_{j+1}^2 + \frac{\sigma_j \theta_j^2}{\Gamma_j}\right) + \sum_{j=1}^{i} {x_{j+1}}^2.\end{aligned} \tag{35}$$

Step n: Based on (1), (4), (11) and (13), one has

$$\begin{aligned}\xi_n &= \dot{e}_n - \dot{\beta}_n = \dot{x}_n - \dot{\omega}_n - \dot{\beta}_n = f_n + \lambda_n g_n u - \dot{\omega}_n - \dot{\beta}_n \\ &= f_n + \lambda_n g_n[\pi(v)v + \vartheta(v)] - \dot{\omega}_n - \dot{\beta}_n.\end{aligned} \tag{36}$$

Take a Lyapunov function V_n in the following form

$$V_n = V_{n-1} + \frac{1}{2}\xi_n^2 + \frac{1}{2\Gamma_n}\tilde{\theta}_n^2, \tag{37}$$

where $\tilde{\theta}_n = \theta_n - \hat{\theta}_n$.

Differentiating V_n, one can obtain

$$\begin{aligned}\dot{V}_n &= \dot{V}_{n-1} + \xi_n \dot{\xi}_n - \frac{1}{\Gamma_n}\tilde{\theta}_n \dot{\hat{\theta}}_n \\ &= \dot{V}_{n-1} + \xi_n\left(f_n + \lambda_n g_n(\pi(v)v + \vartheta(v)) - \dot{\omega}_n - \dot{\beta}_n\right) - \frac{1}{\Gamma_n}\tilde{\theta}_n \dot{\hat{\theta}}_n \\ &= \dot{V}_{n-1} + \xi_n f_n + \xi_n \lambda_n g_n \pi(v)v + \xi_n \lambda_n g_n \vartheta(v) - \xi_n \dot{\omega}_n - \xi_n \dot{\beta}_n - \frac{1}{\Gamma}\tilde{\theta}_n \dot{\hat{\theta}}_n.\end{aligned} \tag{38}$$

Similarly, according to Lemma 1 and Young's inequality, one can obtain

$$\xi_n f_n \leq \frac{\xi_n^2 \theta_n \psi_n^T \psi_n}{2a_n^2} + \frac{1}{2}a_n^2 + \frac{1}{2}\xi_n^2 + \frac{1}{2}\varepsilon_n^2, \tag{39}$$

where a_n is a given positive scalar.

$$\lambda_n g_n \xi_n \vartheta(v) \leq \lambda_n(\frac{1}{2}\xi_n^2 + \frac{1}{2}\Re^2), \tag{40}$$

where $|\vartheta(v)| < L_p$, $|g_i| < \Theta_i$, and $|g_n \vartheta(v)| < \Re$, with $\Re = \Theta_n L_p$.

Then, the compensation signal $\dot{r}_n$ is designed to be

$$\dot{\beta}_n = -k_n \beta_n. \tag{41}$$

Combined with the above formula, (38) is rewritten as

$$\begin{aligned}\dot{V}_n \leq & \dot{V}_{n-1} + \frac{\xi_n^2 \theta_n \psi_n^T \psi_n}{2a_n^2} + \frac{1}{2}a_n^2 + \frac{1}{2}\xi_n^2 + \frac{1}{2}\varepsilon_n^2 + \lambda_n g_n \xi_n \pi(v)v \\ & + \lambda_n\left(\frac{1}{2}\xi_n^2 + \frac{1}{2}\Re_n^2\right) + \xi_n k_n \beta_n - \frac{1}{\lambda_n}\tilde{\theta}_n \dot{\hat{\theta}} - \xi_n \dot{\omega}_n.\end{aligned} \tag{42}$$

The virtual control signal v and the Nussbaum-type gain ζ_n are designed as

$$\begin{cases} v = \frac{1}{\Im} N(\zeta_n)\Big(\frac{\xi_n \hat{\theta}_n \psi_n^T \psi_n}{2a_n^2} + k_n e_n + \xi_n - \dot{\omega}_n\Big), \\ \dot{\zeta}_n = \xi_n\Big(\frac{\xi_n \hat{\theta}_n \psi_n^T \psi_n}{2a_n^2} + k_n e_n + \xi_n - \dot{\omega}_n\Big). \end{cases} \tag{43}$$

Combining the above equation, (42) can be rewritten as

$$\dot{V}_n \leq \dot{V}_{n-1} - k_n \xi_n^2 + \lambda_n g_n N(\zeta_n)\dot{\zeta}_n + \dot{\zeta}_n + \frac{1}{2}\Re_n^2 + \frac{\tilde{\theta}_n}{\Gamma_n}\left(\frac{\Gamma_n \xi_n^2 \psi_n^T \psi_n}{2a_n^2} - \dot{\hat{\theta}}_n\right) + \frac{1}{2}a_n^2 + \frac{1}{2}\varepsilon_n^2. \tag{44}$$

Next, the adaptive law $\dot{\hat{\theta}}_n$ is designed as $\dot{\hat{\theta}}_n = \frac{\Gamma_n \xi_n^2 \psi_n^T \psi_n}{2a_n^2} - \sigma_n \hat{\theta}_n$, and with the help of Young's inequality $\frac{\sigma_n \tilde{\theta}_n \hat{\theta}_n}{\Gamma_n} \leq \frac{\sigma_n \theta_n^2}{2\Gamma_n} - \frac{\sigma_n \tilde{\theta}_n^2}{2\Gamma_n}$, one obtain

$$\begin{aligned} \dot{V}_n \leq & \dot{V}_{n-1} - k_n \xi_n^2 + \lambda_n g_n N(\zeta_n)\dot{\zeta}_n + \dot{\zeta}_n - \frac{\sigma_n \tilde{\theta}_n^2}{2\Gamma_n} + \frac{1}{2}a_n^2 + \frac{1}{2}\varepsilon_n^2 + \frac{\sigma_n \theta_n^2}{2\Gamma_n} + \frac{1}{2}\Re_n^2 \\ \leq & -\sum_{j=1}^{n} k_j \xi_j^2 - \sum_{j=1}^{n} \frac{1}{2}\frac{\sigma_j \tilde{\theta}_j^2}{\Gamma_j} + \sum_{j=1}^{n-1} g_j N(\zeta_j)\dot{\zeta}_j + \lambda_n g_n N(\zeta_n)\dot{\zeta}_n + \sum_{j=1}^{n} \dot{\zeta}_j \\ & + \frac{1}{2}\sum_{j=1}^{n}\left(a_j^2 + \varepsilon_j^2 + \frac{\sigma_j \theta_j^2}{\Gamma_j}\right) + \sum_{j=1}^{n-1} x_{j+1}^2 + \frac{3}{2}\sum_{j=1}^{n-1} \xi_{j+1}^2 + \frac{1}{2}\Re_n^2. \end{aligned} \tag{45}$$

3.2. Stability Analysis

Theorem 1. *Consider the nonlinear system* (1) *under Assumptions 1–3, utilizing the error compensation signals* (18), (29), (41), *virtual controllers* (22) *and* (33), *as well as the actual controller* (43) *designed in this study, and combining the constructed parameter adaptive law along with the provided signal xd, it is assured that all closed-loop signals remain bounded, and the tracking error is driven to the vicinity of the origin.*

Proof. Denote $D = \{2k_j\sigma_j, \ \forall j = 1, \ldots, n\}$, (45) can be rewritten as

$$\dot{V}_n \leq -DV_n + C + \sum_{i=1}^{n-1}(g_j N(\zeta_j) + 1)\dot{\zeta}_j + \dot{\zeta}_n(\lambda_n g_n N(\zeta_n) + 1), \tag{46}$$

where $C = \frac{1}{2}\sum_{j=1}^{n}\left(a_j^2 + \varepsilon_j^2 + \frac{\sigma_j \theta_j^2}{\Gamma_j}\right) + \sum_{j=1}^{n-1} x_{j+1}^2 + \frac{3}{2}\sum_{j=1}^{n-1} \xi_{j+1}^2 + \frac{1}{2}\Re_n^2$.

Thus, multiplying (46) by e^{Dt} results in

$$\frac{d}{dt}\Big(V_n e^{Dt}\Big) \leq e^{Dt}\sum_{j=1}^{n-1}\Big(g_j N(\zeta_j) + 1\Big)\dot{\zeta}_j + e^{Dt}\Big(\lambda_n g_n N(\zeta_n) + 1\Big)\dot{\zeta}_n + e^{Dt}C. \tag{47}$$

Integrating the above equation to the interval $[0, t)$, one can obtain

$$\begin{aligned} V_n(t) \leq & e^{-Dt}\int_0^t \sum_{j=1}^{n-1}(g_j N(\zeta_j) + 1)\dot{\zeta}_j e^{D\tau} d\tau + e^{-Dt}\int_0^t (\lambda_n g_n N(\zeta_n) + 1)\dot{\zeta}_n e^{D\tau} d\tau \\ & + \frac{C}{D} + e^{-Dt}V_n(0) - \frac{C}{D}e^{-Dt}. \end{aligned} \tag{48}$$

According to Lemma 2, it can be inferred that V_n, ζ_n and $\int_0^t(\lambda_n g_n N(\zeta_n) + 1)\dot{\zeta}_n d\tau$ are bounded. Thus, ξ_n and $\tilde{\theta}_n$ are bounded. In addition, similar to the previous derivation, it can be derived that V_{n-1}, ζ_{n-1}, ξ_{n-1} ,$\tilde{\theta}_{n-1}$ and V_i, ζ_i, ξ_i ,$\tilde{\theta}_i$ are all bounded, which derive

the boundedness of $\int_0^t \sum_{i=1}^{n-1}(g_j N(\zeta_j)+1)\zeta_j e^{D\tau}d\tau$ and $\int_0^t(\lambda_n g_n N(\zeta_n)+1)\dot{\zeta}_n e^{D\tau}d\tau$. Thus, the following formula holds

$$0 \le V_n \le \left[\Lambda_1 + \Lambda_2 + V_n(0) - \frac{C}{D}\right]e^{-Dt} + \frac{C}{D}, \tag{49}$$

where Λ_1 represents $\int_0^t \sum_{i=1}^{n-1}(g_j N(\zeta_j)+1)\zeta_j e^{D\tau}d\tau$, and Λ_2 denotes $\int_0^t(\lambda_n g_n N(\zeta_n)+1)\dot{\zeta}_n e^{D\tau}d\tau$.

According to (49), one can obtain

$$\lim_{t\to\infty} V_n(t) \le \frac{C}{D}. \tag{50}$$

Connecting Equations (37) and (49), the following equation is established

$$|\xi_n| \le \sqrt{2\left[(\Lambda_1 + \Lambda_2 + V(0) - \frac{C}{D})e^{-Dt} + \frac{C}{D}\right]}, \tag{51}$$

which implies that

$$\lim_{t\to\infty} |\xi_n| \le \sqrt{\frac{2C}{D}}. \tag{52}$$

this means ξ_n is bounded.

According to (13), it is evident that the boundedness of e_n correlates with β_n. According to the results in [31], it can be obtained that β_n is bounded. Then, the following formula holds

$$\lim_{t\to\infty}|e_n| \le \lim_{t\to\infty}(|\xi_n| + |\beta_n|) \le \sqrt{\frac{2C}{D}} + \Delta, \tag{53}$$

where Δ represents a positive constant that satisfies $|\beta_n| \le \Delta$.

This proves that e_n and ξ_n are bounded. Finally, all of the signals in (1) are all bounded. This completes the proof. □

Remark 3. *Even though the control strategy presented in this paper shows an outstanding control performance, it still has its limitations. For instance, the equivalent transformation technique depends on precise system models and parameters; large errors in parameter estimation might impact the control effectiveness. Furthermore, for extreme nonlinear effects, our method may need further refinement or combination with other techniques.*

Remark 4. *Refs. [27–30] investigated nonlinear systems with unknown control directions. However, these studies did not account for the error induced by the filter or the effects of an input dead zone and saturation. Unlike these studies, this paper employs command-filtering technology to address the complexity explosion issue and proposes a transformation method to mitigate the impact of an input dead zone and saturation on the system.*

4. Simulation Results

This section provides two illustrative examples to demonstrate the feasibility of the proposed approach.

Example 1. *The following second-order nonlinear system are considered*

$$\begin{cases} \dot{x}_1 = 0.1{x_1}^2 + \lambda_1 g_1(\bar{x}_1)x_2 \\ \dot{x}_2 = 0.2x_1x_2 + x_1 + \lambda_2 g_2(\bar{x}_2)u \\ y = x_1, \end{cases} \tag{54}$$

where $g_1(\bar{x}_1) = 4$, $g_2(\bar{x}_2) = 1$, $\lambda_1 = -1$, $\lambda_2 = 1$, *and u is defined as*

$$u = \begin{cases} 5, & v > 5 \\ 0.6(v - 0.6), & 0.6 < v < 5 \\ 0, & -0.6 < v < 0.6 \\ 0.6(v + 0.6), & -5 < v < 0.6 \\ -5, & v < -5. \end{cases} \tag{55}$$

The virtual controller α_1 *is designed as*

$$\begin{cases} \alpha_1 = N(\zeta_1)\left(\frac{\xi_1\hat{\theta}_1\psi_1^T\psi_1}{2a_1^2} + k_1e_1 + \frac{1}{2}\xi_1 + \frac{5}{2}g_1^2\xi_1 - \dot{y}_d\right), \\ \dot{\zeta}_1 = \xi_1\left(\frac{\xi_1\hat{\theta}_1\psi_1^T\psi_1}{2a_1^2} + k_1e_1 + \frac{1}{2}\xi_1 + \frac{5}{2}g_1^2\xi_1 - \dot{y}_d\right). \end{cases} \tag{56}$$

The controller v is designed as

$$\begin{cases} v = \frac{1}{\Im}N(\zeta_2)\left(\frac{\xi_2\hat{\theta}_2\psi_2^T\psi_2}{2a_2^2} + k_2e_2 + \xi_2 - \dot{\omega}_2\right), \\ \dot{\zeta}_2 = \xi_2\left(\frac{\xi_2\hat{\theta}_2\psi_2^T\psi_2}{2a_2^2} + k_2e_2 + \xi_2 - \dot{\omega}_2\right), \end{cases} \tag{57}$$

where the initial state variables of the system are $x_1(0) = 0.2$, $x_2(0) = -0.1$, $\hat{\theta}_1(0) = 0.5$, $\hat{\theta}_1(0) = 0.2$, *and the desired trajectory* $y_d = 0.5\sin(t)$. *The design parameters are given as* $k_1 = 2$, $k_2 = 1$, $\Im = 1$, $\sigma_1 = 0.08$, $\sigma_2 = 0.08$, $a_1 = 2$, $a_2 = 7$, $\Gamma_1 = 0.3$, $\Gamma_2 = 0.3$, $\varpi = 50$, *and* $\varphi = 1$ *and select* $N(\zeta_1) = \zeta_1^2\cos(\zeta_1)$ *and* $N(\zeta_2) = \zeta_2^2\cos(\zeta_2)$ *with* $\zeta_1(0) = 0$ *and* $\zeta_2(0) = 0$. *In addition, to handle nonlinear terms, one might choose the following fuzzy membership function* $\mu_{P_m^1} = e^{-\frac{\left(x_1 + x_j^0\right)^2}{2}}$, $\mu_{P_m^2} = e^{-\frac{\left(x_2 + x_j^0\right)^2}{2}}$, ${x_j}^0 = 3,\ 2,\ 1,\ 0\ , -1, -2, -3,\ j = 1, \ldots 7$.

The simulation results are illustrated in Figures 1–6. The trajectories of the system output y and the reference signal y_d, using the control strategy proposed in this paper and the control strategy with the same design parameters from reference [27], are shown in Figure 1. According to Figure 1, we can see that the system output y can effectively track the reference signal y_d, and the control method proposed in this paper, which accounts for input dead zones and saturation, achieves a higher tracking accuracy compared with the control method proposed in reference [27]. Figures 2 and 3 show states x_1 and x_2 of the system and the trajectories of the adaptive parameters $\hat{\theta}_1$ and $\hat{\theta}_2$, respectively. Figure 4 shows the evolution of signals u and v. Figures 5 and 6 describe the Nussbaum function signals ζ_1, ζ_2, $N(\zeta_1)$, and $N(\zeta_2)$. Based on the above simulation results, it is evident that the proposed scheme achieves an excellent tracking performance, and all of the signals within the closed-loop system are bounded. This demonstrates the effectiveness of the proposed control scheme.

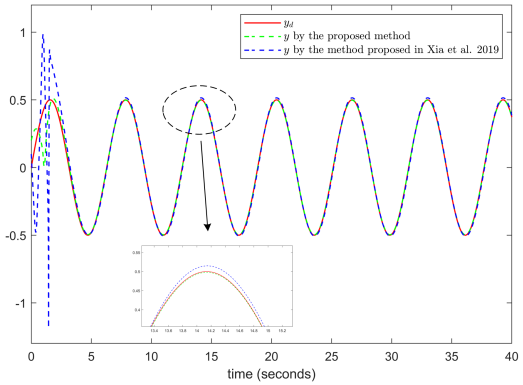

Figure 1. Trajectories of y_d and y [27].

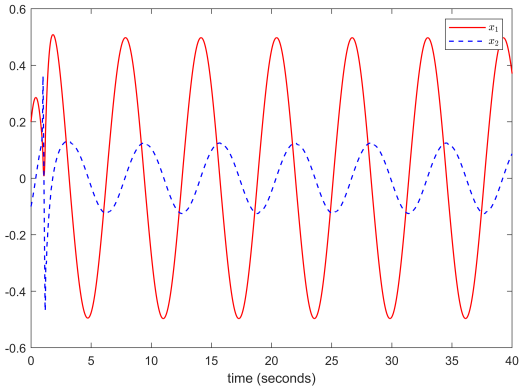

Figure 2. The trajectories of x_1 and x_2.

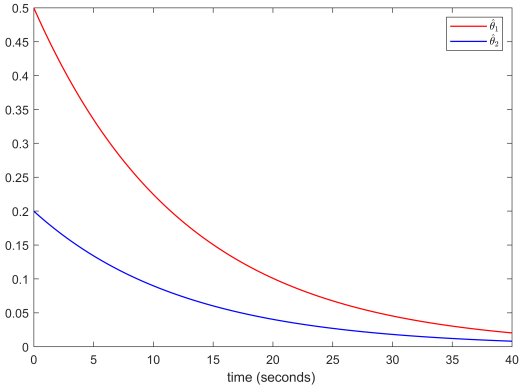

Figure 3. Adaptive parameters.

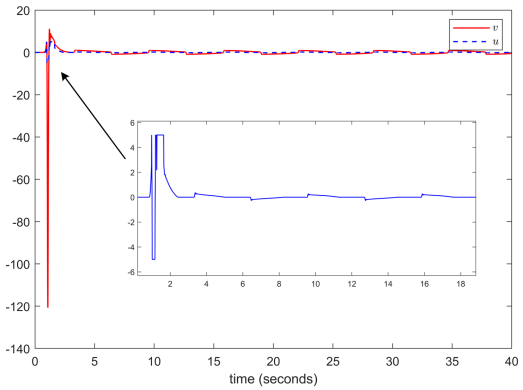

Figure 4. Trajectories of the control input.

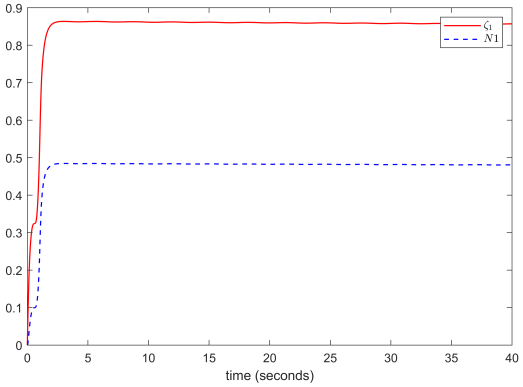

Figure 5. The trajectories of ζ_1 and $N(\zeta_1)$.

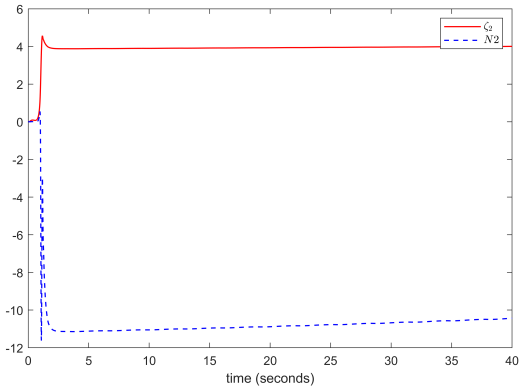

Figure 6. The trajectories of ζ_2 and $N(\zeta_2)$.

Example 2. *Consider the pendulum model shown in Figure 7.*

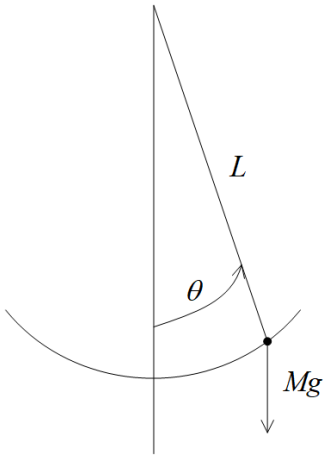

Figure 7. Pendulum.

Its equation of motion in the tangential direction can be written as

$$ML\ddot{\theta} + kL\dot{\theta} + Mg\sin\theta = u, \tag{58}$$

where $M = 1$ denotes the mass of the dot; θ is the angle subtended by the rod and the vertical axis through the pivot point; $k = 2$ represents the friction coefficient; $L = 1$ is the length of the rod; $g = 9.8$ represents the acceleration due to gravity; $\dot{\theta}$ and $\ddot{\theta}$ are angular velocity and angular acceleration, respectively.

Define $x_1 = \theta(t)$ and $x_2 = \dot{\theta}(t)$. Then, the state equations are

$$\begin{cases} \dot{x}_1 = \lambda_1 g_1(\bar{x}_1) x_2 \\ \dot{x}_2 = -2x_2 - 10\sin(x_1) + \lambda_2 g_2(\bar{x}_1) u \\ y = x_1, \end{cases} \tag{59}$$

where $\lambda_1 = 1$, $\lambda_2 = -1$, $g_1(\bar{x}_1) = 1$, $g_2(\bar{x}_1) = 1$, *and* u *is defined as*

$$u = \begin{cases} 20, & v > 20 \\ 0.5(v - 0.5), & 0.5 < v < 20 \\ 0, & -0.5 < v < 0.5 \\ 0.5(v + 0.5), & -20 < v < 0.5 \\ -20, & v < -20 \end{cases} \tag{60}$$

The virtual controller, controller, desired signal, Nussbaunm functions, and fuzzy membership function designs are similar to those in Example 1. The initial parameters are chosen as $x_1(0) = 0.2$, $x_2(0) = -0.1$, $\hat{\theta}_1(0) = 0.3$, and $\hat{\theta}_1(0) = 0.5$, and the desired trajectory is $y_d = 0.5\sin(t)$. The design parameters are $k_1 = 4$, $k_2 = 3$, $\Im = 1$, $\sigma_1 = 1$, $\sigma_2 = 1$, $a_1 = 10$, $a_2 = 10$, $\Gamma_1 = 0.7$, $\Gamma_2 = 0.7$, $\varpi = 50$, and $\varphi = 1$.

The simulation results are depicted in Figures 8–13. The above simulation results show that the developed adaptive command-filtered fuzzy control scheme achieves a satisfactory tracking performance, with all of the signals in the control system remaining bounded.

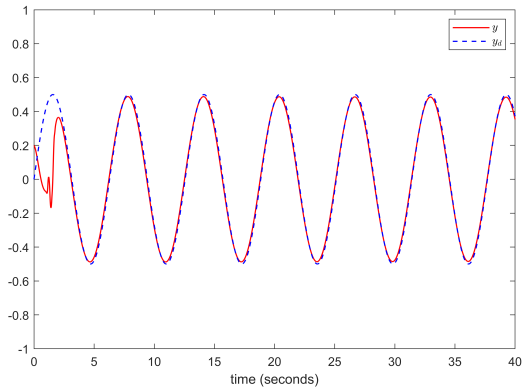

Figure 8. The trajectories of y_d and y.

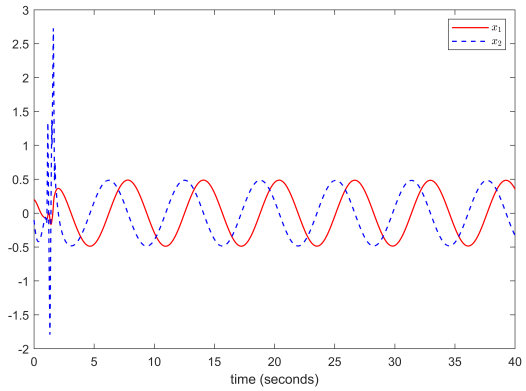

Figure 9. The trajectories of x_1 and x_2.

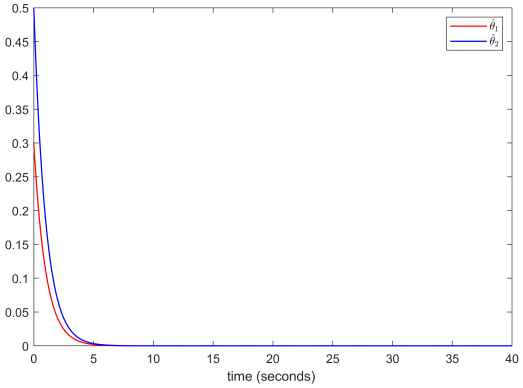

Figure 10. Adaptive parameters.

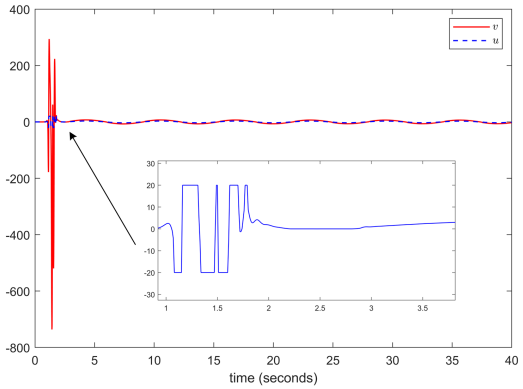

Figure 11. The trajectories of the control input.

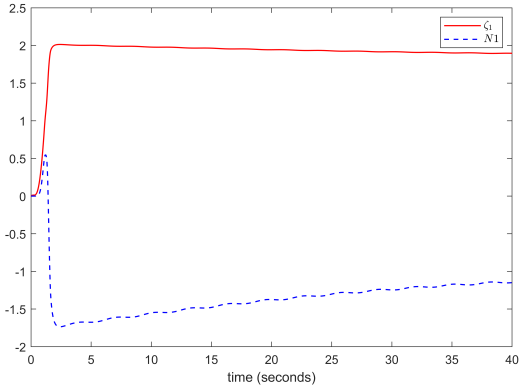

Figure 12. The trajectories of ζ_1 and $N(\zeta_1)$.

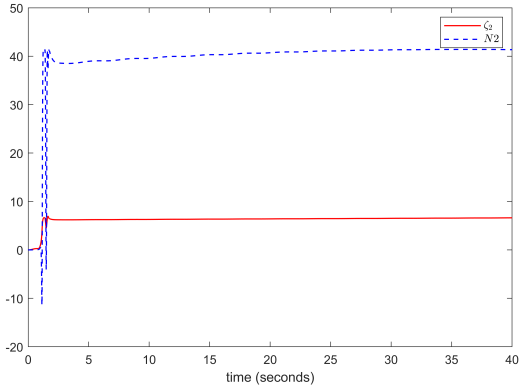

Figure 13. The trajectories of ζ_2 and $N(\zeta_2)$.

5. Conclusions

This paper proposes a command-filtering adaptive fuzzy tracking control strategy for nonlinear systems with unknown control directions, input dead zones, and saturation. A novel approach is applied to analyze the effects of input dead zone and saturation. By combining the fuzzy logic system and the command filter, an adaptive fuzzy logic controller is constructed to ensure that the error signal converges to a bounded compact set around the origin. The combination of the Nussbaum function and the backstepping method solves the difficulty caused by the unknown system control direction. Based on the adaptive tracking controller proposed in this article, the boundedness of all signals in the closed-loop system is guaranteed.

Funding: This research received no external funding.

Data Availability Statement: The original contributions presented in the study are included in the article, further inquiries can be directed to the corresponding author.

Conflicts of Interest: The author declares no conflicts of interest.

References

1. Xu, H.; Zhu, Q.; Zheng, W.X. Exponential stability of stochastic nonlinear delay systems subject to multiple periodic impulses. *IEEE Trans. Autom. Control* **2024**, *69*, 2621–2628. [CrossRef]
2. Fan, L.; Zhu, Q.; Zheng, W.X. Stability analysis of switched stochastic nonlinear systems with state-dependent delay. *IEEE Trans. Autom. Control* **2024**, *69*, 2567–2574. [CrossRef]
3. Zhao, Y.; Zhu, Q. Stabilization of stochastic highly nonlinear delay systems with neutral term. *IEEE Trans. Autom. Control* **2023**, *68*, 2544–2551. [CrossRef]
4. Do, K.D.; Pan, J. Nonlinear formation control of unicycle-type mobile robots. *Robot. Auton. Syst.* **2007**, *55*, 191–204. [CrossRef]
5. Merabti, H.; Bouchachi, I.; Belarbi, K. Nonlinear model predictive control of quadcopter. In Proceedings of the 2015 16th International Conference on Sciences and Techniques of Automatic Control and Computer Engineering (STA), Monastir, Tunisia, 21–23 December 2015; IEEE: Piscataway, NJ, USA, 2015; pp. 208–211.
6. Geng, X.; Zhan, D.; Zhou, Z. Supervised nonlinear dimensionality reduction for visualization and classification. *IEEE Trans. Syst. Man Cybern. Part B Cybern.* **2005**, *35*, 1098–1107. [CrossRef]
7. Goege, D.; Fuellekrug, U.; Sinapius, M.; Link, M.; Gaul, L. Advanced test strategy for identification and characterization of nonlinearities of aerospace structures. *AIAA J.* **2005**, *43*, 974–986. [CrossRef]
8. Liu, Y.; Zhao, W.; Liu, L.; Li, D.; Tong, S.; Chen, C.P. Adaptive neural network control for a class of nonlinear systems with function constraints on states. *IEEE Trans. Neural Netw. Learn. Syst.* **2021**, *34*, 2732–2741. [CrossRef]
9. Zhang, J.; Niu, B.; Wang, D.; Wang, H.; Duan, P.; Zong, G. Adaptive neural control of nonlinear nonstrict feedback systems with full-state constraints: A novel nonlinear mapping method. *IEEE Trans. Neural Netw. Learn. Syst.* **2021**, *34*, 999–1007. [CrossRef]
10. Al Mahturi, A.; Santoso, F.; Garratt, M.A.; Anavatti, S.G. A Robust Self-Adaptive Interval Type-2 TS Fuzzy Logic for Controlling Multi-Input–Multi-Output Nonlinear Uncertain Dynamical Systems. *IEEE Trans. Syst. Man Cybern. Syst.* **2020**, *52*, 655–666. [CrossRef]
11. Park, J.H.; Kim, S.H.; Park, T.S. Output-feedback adaptive neural controller for uncertain pure-feedback nonlinear systems using a high-order sliding mode observer. *IEEE Trans. Neural Netw. Learn. Syst.* **2018**, *30*, 1596–1601. [CrossRef]
12. Wu, J.; Wu, Z.; Li, J.; Wang, G.; Zhao, H.; Chen, W. Practical adaptive fuzzy control of nonlinear pure-feedback systems with quantized nonlinearity input. *IEEE Trans. Syst. Man Cybern. Syst.* **2018**, *49*, 638–648. [CrossRef]
13. Li, Y.; Yang, G. Adaptive neural control of pure-feedback nonlinear systems with event-triggered communications. *IEEE Trans. Neural Netw. Learn. Syst.* **2018**, *29*, 6242–6251. [CrossRef] [PubMed]
14. Swaroop, D.; Hedrick, J.K.; Yip, P.P.; Gerdes, J.C. Dynamic surface control for a class of nonlinear systems. *IEEE Trans. Autom. Control* **2000**, *45*, 1893–1899. [CrossRef]
15. Zhang, Z.; Wen, C.; Xing, L.; Song, Y. Event-triggered adaptive control for a class of nonlinear systems with mismatched uncertainties via intermittent and faulty output feedback. *IEEE Trans. Autom. Control* **2023**, *68*, 8142–8149. [CrossRef]
16. Huang, S.; Zong, G.; Wang, H.; Zhao, X.; Alharbi, K.H. Command filter-based adaptive fuzzy self-triggered control for MIMO nonlinear systems with time-varying full-state constraints. *Int. J. Fuzzy Syst.* **2023**, *25*, 3144–3161. [CrossRef]
17. Yang, Y.; Tang, L.; Zou, W.; Ding, D. Robust adaptive control of uncertain nonlinear systems with unmodeled dynamics using command filter. *Int. J. Robust Nonlinear Control* **2021**, *31*, 7764–7784. [CrossRef]
18. Wang, L.; Wang, H.; Liu, P.X.; Ling, S.; Liu, S. Fuzzy finite-time command filtering output feedback control of nonlinear systems. *IEEE Trans. Fuzzy Syst.* **2020**, *30*, 97–107. [CrossRef]
19. Yu, H.; Yu, J.; Wang, Q.; Lin, C. Time-varying BLFs-based adaptive neural network finite-time command-filtered control for nonlinear systems. *IEEE Trans. Syst. Man Cybern. Syst.* **2023**, *53*, 4696–4704. [CrossRef]

20. Tian, M.; Tao, G. Adaptive dead-zone compensation for output-feedback canonical systems. *Int. J. Control* **1997**, *67*, 791–812. [CrossRef]
21. Chen, M.; Tao, G. Adaptive fault-tolerant control of uncertain nonlinear large-scale systems with unknown dead zone. *IEEE Trans. Cybern.* **2015**, *46*, 1851–1862. [CrossRef]
22. Kumar, R.; Singh, U.P.; Bali, A.; Raj, K. Hybrid neural network controller for uncertain nonlinear discrete-time systems with non-symmetric dead zone and unknown disturbances. *Int. J. Control* **2023**, *96*, 2003–2011. [CrossRef]
23. Tang, F.; Wang, H.; Zhang, L.; Xu, N.; Ahmad, A.M. Adaptive optimized consensus control for a class of nonlinear multi-agent systems with asymmetric input saturation constraints and hybrid faults. *Commun. Nonlinear Sci. Numer. Simul.* **2023**, *126*, 107446. [CrossRef]
24. Zhao, N.; Tian, Y.; Zhang, H.; Herrera-Viedma, E. Learning-Based Adaptive Fuzzy Output Feedback Control for MIMO Nonlinear Systems With Deception Attacks and Input Saturation. *IEEE Trans. Fuzzy Syst.* **2024**, *32*, 2850–2862. [CrossRef]
25. Wang, H.; Kang, S.; Zhao, X.; Xu, N.; Li, T. Command filter-based adaptive neural control design for nonstrict-feedback nonlinear systems with multiple actuator constraints. *IEEE Trans. Cybern.* **2021**, *52*, 12561–12570. [CrossRef]
26. Lu, Y.; Liu, W.; Ma, B. Finite-time command filtered tracking control for time-varying full state-constrained nonlinear systems with unknown input delay. *IEEE Trans. Circuits Syst. II Express Briefs* **2022**, *69*, 4954–4958. [CrossRef]
27. Xia, J.; Zhang, J.; Feng, J.; Wang, Z.; Zhuang, G. Command filter-based adaptive fuzzy control for nonlinear systems with unknown control directions. *IEEE Trans. Syst. Man Cybern. Syst.* **2019**, *51*, 1945–1953. [CrossRef]
28. Yang, Y.; Tang, L.; Zou, W.; Ahn, C.K. Novel command-filtered Nussbaum design for continuous-time nonlinear dynamical systems with multiple unknown high-frequency gains. *Nonlinear Dyn.* **2023**, *111*, 4313–4323. [CrossRef]
29. Yang, Y.; Liu, G.; Li, Q.; Ahn, C.K. Multiple adaptive fuzzy Nussbaum-type functions design for stochastic nonlinear systems with fixed-time performance. *Fuzzy Sets Syst.* **2024**, *476*, 108767. [CrossRef]
30. Ye, H.; Zhao, K.; Wu, H.; Song, Y. Adaptive control with global exponential stability for parameter-varying nonlinear systems under unknown control gains. *IEEE Trans. Cybern.* **2023**, *53*, 7858–7867. [CrossRef]
31. Hu, J.; Zhang, H. Immersion and invariance based command-filtered adaptive backstepping control of VTOL vehicles. *Automatica* **2013**, *49*, 2160–2167. [CrossRef]

mathematics

MDPI

Article

The Dynamic Behavior of a Stochastic SEIRM Model of COVID-19 with Standard Incidence Rate

Yuxiao Zhao, Hui Wang * and Dongxu Wang *

School of Mathematics and Information Science, Shandong Technology and Business University, Yantai 264005, China; 18354264118@163.com

* Correspondence: 202113981@sdtbu.edu.cn (H.W.); 202013881@sdtbu.edu.cn (D.W.)

Abstract: This paper studies the dynamic behavior of a stochastic SEIRM model of COVID-19 with a standard incidence rate. The existence of global solutions for dynamic system models is proven by integrating stochastic process theory and the concept of stopping times, together with the contradiction method. Moreover, we construct appropriate Lyapunov functions to analyze system stability and apply Dynkin's formula and Fatou's lemma to handle stopping times and expectations of stochastic processes. Notably, the extinction study provides mathematical proof that under the given system dynamics, the total population does not grow indefinitely but tends to stabilize over time. The properties of the diffusion matrix are harnessed to guarantee the system's stationary distribution. Conclusively, numerical simulations confirm the model's extinction outcomes.

Keywords: SEIRM; standard incidence rate; dynamic behavior; extinction; stationary distribution

MSC: 34A37

1. Introduction

The Wuhan outbreak occurred from December 2019 to February 2020, primarily in the Huanan Seafood Market and its surrounding areas in Wuhan City, Hubei Province. The epidemic has attracted global attention and concern, leading to thousands of infections and deaths. Currently, the fight against the COVID-19 pandemic continues worldwide. The transmission of the virus is mainly through respiratory droplets. That is, when an infected person coughs, sneezes, or speaks, they produce droplets containing the virus, which can remain suspended in the air and be inhaled by others. Although the scientific community was racing to understand the epidemiological characteristics of COVID-19 to make a vaccine, because of the long and expensive manufacturing cycle, people could not be vaccinated in time in the early stages of the epidemic. The Government adopted various non-drug interventions, such as the wearing of masks, and the ban on gathering and working from home, which unfortunately also had undesirable social consequences, such as unemployment and economic decline. Classical epidemiological models of infectious diseases include SIR (susceptibility, infection and removal) and SEIR (susceptibility, exposure, infection and removal) models [1,2]. The adequate contact rate often takes two forms, bilinear incidence rate βIS and standard incidence rate $\frac{\beta IS}{N}$. The bilinear incidence rate takes into account the interaction between susceptible and infected individuals, better reflecting the nonlinear characteristics of disease transmission [3–5]. Bilinear incidence rates may not be applicable to all types of infectious diseases. The parameters of the standard incidence rate are easier to estimate and interpret from actual data [6–10]. To analyze and predict the dynamics of infectious diseases, especially those with high mortality rates, in order to accurately simulate the transmission process of diseases with significant fatality rates. This is particularly important for studying the spread of severe diseases such as

COVID-19 and Ebola. We have adjusted the SEIR model to better align with real-world scenarios. This modification aims to enhance the model's accuracy and applicability, thereby providing a better reflection of the disease's transmission dynamics as follows:

$$\begin{cases} \frac{dS}{dt} = \Lambda - \frac{\beta_1 SI}{N} - \frac{\beta_2 SI}{N}, \\ \frac{dE}{dt} = \frac{\beta_1 SI}{N} + \frac{\beta_2 SI}{N} - (\varepsilon + \gamma_2)E, \\ \frac{dI}{dt} = \varepsilon E - \gamma_1 I - \mu I \\ \frac{dR}{dt} = \gamma_1 I + \gamma_2 E - dR \\ \frac{dM}{dt} = \mu I \end{cases} \tag{1}$$

Table 1 illustrates the meaning of each parameter within the model. The parameters in the mathematical model of the infectious disease model SEIR are always affected by environmental noise [11–18]. The stochastic model can more accurately describe the infectious disease and establish the distribution of the predicted results [19–21]:

$$\begin{cases} dS = \left[\Lambda - \frac{\beta_1 SI}{N} - \frac{\beta_2 SI}{N}\right]dt + \sigma_1 S dB_1(t), \\ dE = \left[\frac{\beta_1 SI}{N} + \frac{\beta_2 SI}{N} - \varepsilon E - \gamma_2 E\right]dt + \sigma_2 E dB_2(t), \\ dI = [\varepsilon E - \gamma_1 I - \mu I]dt + \sigma_3 I dB_3(t), \\ dR = [\gamma_1 I + \gamma_2 E]dt + \sigma_4 R dB_4(t), \\ dM = \mu I dt + \sigma_5 I dB_5(t), \end{cases} \tag{2}$$

where S represents susceptible individuals, referring to those who are healthy but susceptible to infection. E represents exposed individuals, indicating those who have been infected but are not yet infectious. This typically denotes an incubation period during which an individual has been infected but does not show symptoms and is unable to transmit the virus to others. R represents removed or recovered individuals, indicating those who have recovered from the infection and gained immunity, or have died due to the disease. These individuals no longer participate in the transmission process. I represents infectious individuals, denoting those who are already infectious and capable of transmitting the pathogen to susceptible individuals. M represents mortality, referring to individuals who have died due to the disease. $\frac{\beta_1 IS}{N}$ and $\frac{\beta_2 IS}{N}$ represent the infection rates through direct and indirect contact transmission, respectively.

We began by introducing the essential foundational knowledge, followed by an exploration of the conditions for the existence of global positive solutions. Subsequently, we analyzed the extinction behavior of populations. After that, we studied the steady-state distribution of the system. Finally, numerical simulations were used to validate the accuracy of our theoretical analysis.

Table 1. Meaning of parameter.

Parameter	Description
Λ	Recruitment rate of the population
β_1	Transmission rate due to social contact
β_2	Transmission rate due to frontline contact
$\varepsilon(\varepsilon^{-1})$	Infection rate (Incubation rate)
$\gamma_1(\gamma_1^{-1})$	Recovery rate of infectious individuals (Recovery period)
$\gamma_2(\gamma_2^{-1})$	Immune recovery rate (Natural immune recovery period)

2. Preliminary

To facilitate subsequent calculations, we often express $\beta = \beta_1 + \beta_2$. Consider the stochastic differential equation

$$dX(t) = f(t, X(t))dt + g(t, X(t))dB(t).$$

The function $f(t; X(t))$ in $\mathbb{R}^d$ on $[t_0, \infty] \times \mathbb{R}^d$, whereas $g(t, X(t))$ constitutes a matrix of dimensions $d \times m$, $B(t)$ represents an m-dimensional standard Brownian motion defined on the complete probability space $(\Omega, \mathscr{F}_t, (\mathscr{F}_t)_{t\geq 0}, \mathbb{P})$. The class $C^{2,1}([t_0, \infty] \times \mathbb{R}^d; \mathbb{R}_+)$ includes all positive valued functions $V(t, x)$ that possess continuous second-order differentiability in x and first-order differentiability in t. The Lyapunov operator is defined as:

$$\mathcal{L}V = V_t(t, x_t) + V_x \boldsymbol{f}(t, x_t) + \frac{1}{2} trace[\boldsymbol{g}^\top(t, x_t) V_{xx} \boldsymbol{g}(t, x_t)]. \tag{3}$$

3. The Existence of Global Solutions

The significance of the existence of global positive solutions for COVID-19 models is to ensure the reliability and accuracy of the results obtained by the models. If a model does not have a global positive solution, then the model may have incorrect predictions or biases that lead to problems in real-life decision-making. Therefore, in order to ensure that the model can accurately predict the development trend of the COVID-19 epidemic, it needs to prove that its global positive solution exists.

Theorem 1. *For any initial value* $(S(0), E(0), R(0), I(0), M(0)) \in \mathbb{R}^5_+$, *if a unique solution to system (2) exists, then the values of* $(S(t), E(t), R(t), I(t), M(t)) \in \mathbb{R}^5_+$ *with probability one.*

Proof. Our proof method is inspired by Reference [1]. It is evident that the coefficients specified in the equations are locally Lipschitz continuous. For any initial approximation of the state variables $(S(0), E(0), I(0), R(0), M(0)) \in \mathbb{R}^5_+$, there is a unique local solution on $t \in [-\infty, \rho_e]$, where ρ_e denotes the explosion time, which is the moment an explosion occurs. To demonstrate that the solution is global, it suffices to show that $\rho_e = \infty$. Let $k_0 > 0$ be sufficiently large such that $\xi(0)$ falls within the interval $[\frac{1}{k_0}, k_0]$. For each integer $n > n_0$, we define the stopping time, a concept from probability theory that refers to a random variable determining when a stochastic process is halted or concluded based on specific conditions or events. This concept is frequently employed in the study of Markov processes, where understanding when a process reaches a certain state or enters a particular region is crucial:

$$\tau_n = \inf\{t \in [0, \rho_e) : \min\{S(t), E(t), I(t), R(t), M(t)\} \notin (\frac{1}{n}, n)\}$$

Clearly, ρ_n is increasing as $n \to \infty$, Let $\rho_\infty = \lim_{n\to\infty} \rho_n$. If this statement is incorrect, there exists a pair of constants $T > 0$ and $\varepsilon \in (0, 1)$ such that

$$p\{\tau_\infty \leq T\} > \varepsilon.$$

Consequently, there exists an integer $n_1 \geq n_0$ such that

$$p\{\tau_n \leq T\} > \varepsilon.$$

Define a C^2 function V: $\mathbb{R}^5_+ \to \mathbb{R}_+$. When $x - logx - 1 > 0$, the function V is non-negative. By applying Itô's formula,

$$\begin{aligned}
\mathcal{L}V = &(1 - \frac{1}{S})[\Lambda - \frac{\beta SI}{N}] + \frac{1}{2}\sigma_1^2 \\
&+(1 - \frac{1}{E})[\frac{\beta SI}{N} - \varepsilon E(t) - \gamma_2 E] + \frac{1}{2}\sigma_2^2 \\
&+(1 - \frac{1}{I})[\varepsilon E(t) - \gamma_1 I(t) - \mu I(t)] + \frac{1}{2}\sigma_3^2
\end{aligned}$$

$$
\begin{aligned}
&+(1-\frac{1}{R})[\gamma_1 I(t)+\gamma_2 E(t)]+\frac{1}{2}\sigma_4^2+(1-\frac{1}{M})\mu+\frac{1}{2}\sigma_5^2\\
&\leq \Lambda+\frac{\beta SI}{N}+\varepsilon+\gamma_2+r_1+\mu+\sum_{i=1}^{5}\frac{1}{2}\sigma_i^2:=K\\
&\mathbb{E}V(S(\tau_1\wedge T),E(\tau_1\wedge T),I(\tau_1\wedge T),R(\tau_1\wedge T),M(\tau_1\wedge T))\\
&\leq V(S(0),E(0),I(0),R(0),M(0))+k_1E(\tau_1\wedge T)\\
&\leq V(S(0),E(0),I(0),R(0),M(0))+k_1T.
\end{aligned}
$$

Let $\Omega_n=\{\tau_n\leq T\}$ for $n\geq n_1$, then we have $P(\Omega_n)\geq\varepsilon$ for $\varepsilon\in(0,1)$, we find that for $\forall\omega\in\Omega_n$, $S(\tau_n,\omega),E(\tau_n,\omega),I(\tau_n,\omega),R(\tau_n,\omega),M(\tau_n,\omega)$ equals either n or $\frac{1}{n}$.

$$
\begin{aligned}
&V(S(0),E(0),I(0),R(0),M(0))=k_1T\\
&\geq\mathbb{E}[I\Omega_n(S(\tau_n,\omega),E(\tau_n,\omega),I(\tau_n,\omega),R(\tau_n,\omega),M(\tau_n,\omega))]\\
&\geq\varepsilon[(S-\log S+E-\log E+I-\log I+R-\log R+M-\log M-6)\\
&\wedge(-S+\log S-E+\log E-I+\log I-R+\log R-M+\log M-6)],
\end{aligned}
$$

where $I\Omega_n$ is the indicator function of Ω_l, when taking $n\to\infty$, we obtain

$$\infty>V(S(0),E(0),I(0),R(0),M(0))+k_1T=\infty,$$

there exists a contradiction. Hence, we have $\tau_\infty=\infty$. *a.s*. So $P(\tau_\infty=\infty)=1$ is as required, indicating that the system has a global positive solution. □

4. Extinction

Research on the extinction of COVID-19 models has the following significance. Policy decisions: Understanding the likelihood and timing of extinction can help governments and health authorities develop appropriate policies and measures, including vaccination, isolation measures and social restrictions, to better manage and control outbreaks. Resource allocation: Extinction models can assist decision-makers in the rational allocation of resources, such as determining the need for vaccine supplies, medical equipment and human resources, to ensure effective suppression of virus transmission and the provision of appropriate medical services. By studying the likelihood of extinction, the long-term risks of an outbreak to social, economic, and health systems can be assessed to help develop targeted risk management and prevention measures. Public awareness: Understanding the prospect of pandemic extinction can increase public awareness and understanding of vaccination and protective behavior. The findings of extinction models can convey important information to the public and promote cooperation and participation in society. It should be noted that the study of epidemic extinction is a complex and dynamic process, and the prediction results of the model may be affected by a variety of factors, and may not be able to predict the extinction time with complete accuracy. Therefore, there is still a need to take into account the full range of scientific evidence and expert advice to contain the outbreak and protect public health.

Lemma 1. *If the solution* $(S(t),E(t),I(t),R(t),M(t))$ *of system (2) with initial values* $(S(0),E(0),I(0),R(0),M(0))\in\mathbb{R}_+^5$ *exists, then the sum of* $S(t)+E(t)+I(t)+R(t)+M(t)<\infty$ *a.s. Moreover,*

$$\lim_{t\to\infty}\frac{S(t)}{t}=0,\lim_{t\to\infty}\frac{E(t)}{t}=0,\lim_{t\to\infty}\frac{I(t)}{t}=0,\lim_{t\to\infty}\frac{R(t)}{t}=0,\lim_{t\to\infty}\frac{M(t)}{t}=0,\ a.s.$$

$$\lim_{t\to\infty}\frac{\ln S(t)}{t}=0,\lim_{t\to\infty}\frac{\ln E(t)}{t}=0,\lim_{t\to\infty}\frac{\ln I(t)}{t}=0,\lim_{t\to\infty}\frac{\ln R(t)}{t}=0,\lim_{t\to\infty}\frac{\ln M(t)}{t}=0,\ a.s.$$

and

$$\lim_{t\to\infty}\frac{\int_0^t S(u)dB_1(u)}{t}=0,\lim_{t\to\infty}\frac{\int_0^t E(u)dB_1(u)}{t}=0,\lim_{t\to\infty}\frac{\int_0^t I(u)dB_1(u)}{t}=0, \tag{4}$$

$$\lim_{t\to\infty}\frac{\int_0^t R(u)dB_1(u)}{t}=0,\lim_{t\to\infty}\frac{\int_0^t M(u)dB_1(u)}{t}=0. \tag{5}$$

Proof.

$$\begin{aligned}&d(S+E+I+R+M)\\&=\Lambda dt+\sigma_1SdB_1(t)+\sigma_2EdB_2(t)+\sigma_3IdB_1(t)+\sigma_4RdB_1(t)+\sigma_5MdB_1(t).\end{aligned}$$

From Theorem 3.9 in [22], we can obtain that

$$\lim_{t\to\infty}N(t)<\infty.$$

So, we can obtain the conclusion of Lemma 1. □

Remark 1. *The lemma guarantees that the total population* $(S+E+I+R+M)$ *remains bounded over time for any non-negative initial values. This ensures that the model does not predict infinite growth in the population size and suggests that there are mechanisms within the system that limit the spread or recovery of individuals.*

5. Stationary Distribution

Deterministic systems typically have one or more equilibrium points, of which the endemic equilibrium point is the focus of research because it represents the stable state of the disease in the population. By analyzing the stability of these equilibrium points (for example, whether they attract nearby trajectories), the demise or persistence of the disease can be inferred. Unlike deterministic systems, stochastic systems may not have an endemic equilibrium. Therefore, the traditional method of studying disease persistence through equilibrium stability is not applicable. Due to the lack of an endemic equilibrium point in a stochastic system, we turn to the existence and uniqueness of the stationary distribution of the system (2). A stationary distribution can be understood as the stable state of a system after long periods of operation, but it occurs as a probability distribution rather than a fixed point. If it can be shown that the random system has a unique stationary distribution, this somehow indicates that the system achieves a long-term behavior pattern that can indirectly indicate the persistence of the disease. To study the stationary distribution of random systems (2), we refer to the classical results of Hasminskii [18]. Hasminskii's work provided mathematical tools for analyzing and determining the stationary distribution of Markov processes. The process $Y(t)$ is a normal, time-homogeneous Markov process in $\mathbb{R}_+^n$ (the space of non-negative real numbers), characterized by the stochastic differential equation:

$$dZ(t)=c(Z)dt+\sum_l^k\sigma_l dB_l(t).$$

The diffusion matrix $A(Z)$ is composed of elements $a_{ij}(z)$, where each element $a_{ij}(z)$ is defined as:

$$a_{ij}(z)=\sum_{l=1}^k\sigma_{il}(z)\sigma_{lj}(z).$$

Here, $\sigma_{il}(z)$ and $\sigma_{lj}(z)$ are the coefficients of the diffusion terms, which are dependent on the state x. This process exhibits the Markov property, where the future state depends exclusively on the present state and is independent of the past states. Furthermore, the process is time-homogeneous, indicating that the probabilistic laws governing the evolution

of the system remain unchanged over time. In essence, as time progresses, the system's state transitions according to fixed probabilistic rules that do not vary with time. This consistency in the rules of state transitions allows for a clearer understanding and prediction of the system's behavior as it evolves over time.

The stationary distribution in stochastic infectious disease models can first help us assess the risk of disease transmission; second it is important for us to develop long-term prevention and control strategies, and finally compare the steady-state distribution with actual epidemic data to evaluate the effectiveness of these measures.

Lemma 2. *The process $X(t)$ possesses a unique stationary distribution, denoted as $m(\cdot)$, under certain conditions. These conditions are defined within a domain that has continuous boundaries. Specifically, there exists an open set U and its closure $\bar{U}$ in $\mathbb{R}^d$, where:*

(1). In the vicinity of the open set U and its surroundings, the smallest eigenvalue of the matrix $H(t)$ is bounded.

(2). For any point x outside of U in $\mathbb{R}^d$, the average time t required for a trajectory originating from x to reach the set U is finite. Additionally, the supremum of this time over any compact subset $K \in \mathbb{R}^n$ is also finite.

Furthermore, if there is an integrable function $f(\cdot)$ with respect to a measure π then for almost all points $z \in \mathbb{R}^d$, the long-term time average of $f(Z_z(t))$ converges to the space average with respect to the measure π. This can be expressed mathematically as:

$$P\{\lim_{t\to\infty}\frac{1}{T}\int_0^T f(Z_z(t))dt = \int_{R^d} f(z)\pi dz\} = 1.$$

This statement outlines the conditions necessary for a system to exhibit ergodic behavior, indicating that the system's long-term dynamics can be characterized by a single invariant measure. Let $R_0^s = \frac{\delta\beta_2\varepsilon}{A_1A_2A_3}$, where $A_1 = (\sigma + \frac{1}{2}\sigma_1^2)$, $A_2 = \varepsilon + \gamma + \sigma + \frac{1}{2}\sigma_2^2$, $A_3 = r_1(1 + u_2) + \mu + \sigma + \frac{1}{2}\sigma_3^2$.

Theorem 2. *When $R_0^s > 1$, the solution $(S(t), E(t), R(t), I(t), M(t))$ to system (2) is ergodic and is a stationary division $\pi(\cdot)$.*

Proof. Let $V_1 = S + E + R + I + M - \ln S - \ln E - \ln I$

$$\begin{aligned}
\mathcal{L}V_1 &= \Lambda - \sigma(S+E+R+I+M) - c_1\frac{\Lambda}{S} + \frac{c_1\beta I}{N} \\
&+ \frac{1}{2}c_1\sigma_1^2 + c_1\sigma - c_1\frac{\beta_2 SI}{EN} + c_2(\varepsilon+\gamma+\sigma) + \frac{1}{2}c_2\sigma_2^2 \\
&- c_3\frac{\varepsilon E}{I} + r_1 + c_1(\sigma + \frac{1}{2}\sigma_1^2) + c_2(\varepsilon+\gamma+\sigma+\frac{1}{2}\sigma_1^2) \\
&+ c_3[r_1(1+u_2) + \mu + \sigma + \frac{1}{2}\sigma_3^2] + \Lambda \\
&= -\sigma(S+E+R+I+M) - c_1\frac{\Lambda}{S} - c_3\frac{\varepsilon E}{I} - c_1\frac{\beta_2 SI}{EN} \\
&+ \frac{c_1\beta I}{N} + c_1(\sigma + \frac{1}{2}\sigma_1^2) + c_2(\varepsilon+\gamma+\sigma+\frac{1}{2}\sigma_1^2) \\
&+ c_3[r_1 + \mu + \sigma + \frac{1}{2}\sigma_3^2] + \Lambda \\
&\leq -4(\sigma N \times c_1\frac{\Lambda}{S} \times c_1\frac{\beta_2 SI}{EN} \times c_3\frac{\varepsilon E}{I})^{\frac{1}{4}} \\
&+ c_1(\beta_1(1-u_1) + \beta_2 + \sigma + \frac{1}{2}\sigma_1^2) + c_2(\varepsilon+\gamma+\sigma+\frac{1}{2}\sigma_1^2) \\
&+ c_3[r_1(1+u_2) + \mu + \sigma + \frac{1}{2}\sigma_3^2] + \Lambda.
\end{aligned}$$

Let

$$\begin{aligned}\Lambda &= c_1(\beta_1(1-u_1)+\beta_2+\sigma+\frac{1}{2}\sigma_1^2) = c_2(\varepsilon+\gamma+\sigma+\frac{1}{2}\sigma_1^2)\\ &= c_3[r_1(1+u_2)+\mu+\sigma+\frac{1}{2}\sigma_3^2].\end{aligned}$$

$$\mathcal{L}V_1 \le -4\left[\frac{\sigma\beta_2\varepsilon\Lambda^4}{m_1m_2m_3}\right]+4\Lambda \le -4\Lambda[(R_0^s)^{\frac{1}{4}}-1],$$

where $m_1 = c_1(\beta_1(1-u_1)+\beta_2+\sigma+\frac{1}{2}\sigma_1^2), m_2 = c_2(\varepsilon+\gamma+\sigma+\frac{1}{2}\sigma_1^2), m_3 = c_3[r_1(1+u_2)+\mu+\sigma+\frac{1}{2}\sigma_3^2$.

$$\begin{aligned}V_2 &= c_4(S+I+E+R+M-c_1\ln S-c_2\ln E-c_3\ln I)\\ &\quad -\ln S-\ln R-\ln M+S+E+I+R+M\\ &= (c_4+1)(S+I+E+R+M)-(c_1c_4+1)\ln E\\ &\quad -c_2c_4\ln E-c_3c_4\ln I-\ln R-\ln M.\end{aligned}$$

where fixed $c_4 > 0$ will be computed later. Proving this is easy.

$$\liminf_{(S,E,R,I,M)\in R_+^6\setminus U_k\ k\to\infty} V_2(S+E+R+I+M) = +\infty, \tag{6}$$

where $U_k = (\frac{1}{k},k)(\frac{1}{k},k)(\frac{1}{k},k)$. To prove that $V(S,E,R,I,M)$ has a unique minimum value $V(S(0),E(0),R(0),I(0),M(0))$, we need to consider the partial derivative of $V(S,E,R,I,M)$ and the Hesse matrix. The partial derivative given is as follows:

$$\begin{aligned}\frac{\partial V_2}{\partial S} &= 1+c_4-\frac{1+c_1c_4}{S},\\ \frac{\partial V_2}{\partial E} &= 1+c_4-\frac{1+c_2c_4}{E},\\ \frac{\partial V_2}{\partial R} &= 1+c_4-\frac{1+c_3c_4}{I},\\ \frac{\partial V_2}{\partial I} &= 1+c_4-\frac{1}{R},\\ \frac{\partial V_2}{\partial M} &= 1+c_4-\frac{1}{M}.\end{aligned}$$

From these partial derivatives, we can see that the function V_2 stagnates at point $V_0 = (S(0),E(0),R(0),I(0),M(0))$, since this is the point where all partial derivatives are zero. Then, the Hesse matrix of V_2 at $(S(0),E(0),R(0),I(0),M(0))$ is

$$\mathbf{B} = \begin{pmatrix} \frac{1+c_1c_4}{S^2(0)}+ & 0 & 0 & 0 & 0\\ 0 & \frac{c_2c_4}{E^2(0)} & 0 & 0 & 0\\ 0 & 0 & \frac{c_3c_4}{R^2(0)} & 0 & 0\\ 0 & 0 & 0 & \frac{1}{I^2(0)} & 0\\ 0 & 0 & 0 & 0 & \frac{1}{M^2(0)} \end{pmatrix}.$$

Since the Hesse matrix $\mathbf{B}$ is positively definite at $(S(0),E(0),R(0),I(0),M(0))$, we can conclude that V_2 has a unique minimum value $(S(0),E(0),R(0),I(0),M(0))$ at that point. Define the set

$$D = \left\{\epsilon_1 < S < \frac{1}{\epsilon_6}, \epsilon_2 < E < \frac{1}{\epsilon_7}, \epsilon_3 < R < \frac{1}{\epsilon_8}, \epsilon_4 < I < \frac{1}{\epsilon_9}, \epsilon_5 < M < \frac{1}{\epsilon_{10}}\right\}.$$

According to $Ito's$

$$\begin{aligned}\mathcal{L}V &= c_4c_6 + c_1\beta(1-u_1) + c_1\beta_2 - \frac{\Lambda}{S} + \frac{\beta_1 I}{N} \\ &+ \frac{\beta_2 I}{N} + \sigma + \frac{\sigma_1^2}{2} - \frac{\beta_2 SI}{EN} + \epsilon + \gamma_2 + \sigma + \frac{1}{2}\sigma_2^2 \\ &- \frac{I}{R}r_1(1+u_2) - \frac{\gamma_2 E}{R} + \sigma + \frac{1}{2}\sigma_4^2 \\ &- \frac{I}{M}\mu + \sigma + \frac{1}{2}\sigma_5^2 + \Lambda - \sigma N + \frac{\beta_1 I}{N} \\ &\leq c_4c_6 + c_1\beta + c_1\beta_2 + 2\frac{\beta_1 I}{N} + \frac{\beta_2 I}{N} + \varepsilon + \gamma_2 \\ &+ 3\sigma + \frac{1}{2}(\sigma_1^2 + \sigma_2^2 + \sigma_4^2 + \sigma_5^2) - \sigma N,\end{aligned}$$

where $c_6 = 4\Lambda[(R_0^s)^{\frac{1}{4}} - 1] > 0$.
Case 1. $V \in D_1 = \{(S,E,R,I,M) \in \mathbb{R}_+^5, 0 < S \leq \epsilon_1\}$, we obtain

$$\begin{aligned}\mathcal{L}V &= c_4c_6 - \frac{\Lambda}{S} + \frac{\beta_1 I}{N} \\ &+ \frac{\beta_2 I}{N} + \sigma + \frac{\sigma_1^2}{2} - \frac{\beta_2 SI}{EN} + \epsilon + \gamma_2 + \sigma + \frac{1}{2}\sigma_2^2 \\ &- \frac{I}{R}r_1 - \frac{\gamma_2 E}{R} + \sigma + \frac{1}{2}\sigma_4^2 \\ &- \frac{I}{M}\mu + \sigma + \frac{1}{2}\sigma_5^2 + \Lambda - \sigma N + \frac{\beta_1 I}{N} \\ &\leq c_4c_6 + 2\frac{\beta_1 I}{N} + \frac{\beta_2 I}{N} + \varepsilon + \gamma_2 \\ &+ 3\sigma + \frac{1}{2}(\sigma_1^2 + \sigma_2^2 + \sigma_4^2 + \sigma_5^2) - \frac{\Lambda}{\epsilon_1}.\end{aligned}$$

For arbitrarily small ϵ_1 such that $\mathcal{L}V < 0$ for every $(S,E,R,I,M) \in D_1$.
Case 2. $V \in D_2 = \{(S,E,R,I,M) \in \mathbb{R}_+^5, 0 < E \leq \epsilon_1, S > \epsilon_2\}$, we obtain

$$\begin{aligned}\mathcal{L}V &= c_4c_6 - \frac{\Lambda}{S} + \frac{\beta_1 I}{N} \\ &+ \frac{\beta_2 I}{N} + \sigma + \frac{\sigma_1^2}{2} - \frac{\beta_2 SI}{EN} + \epsilon + \gamma_2 + \sigma + \frac{1}{2}\sigma_2^2 \\ &- \frac{I}{R}r_1 - \frac{\gamma_2 E}{R} + \sigma + \frac{1}{2}\sigma_4^2 \\ &- \frac{I}{M}\mu + \sigma + \frac{1}{2}\sigma_5^2 + \Lambda - \sigma N + \frac{\beta_1 I}{N} \\ &\leq c_4c_6 + c_1\beta + c_1\beta_2 + 2\frac{\beta_1 I}{N} + \frac{\beta_2 I}{N} + \varepsilon + \gamma_2 \\ &+ 3\sigma + \frac{1}{2}(\sigma_1^2 + \sigma_2^2 + \sigma_4^2 + \sigma_5^2) - \frac{\Lambda}{\epsilon_1}.\end{aligned}$$

Case 3. $V \in D_3 = \{(S,E,R,I,M) \in \mathbb{R}_+^5, 0 < R \leq \epsilon_3, E > \epsilon_2\}$, we obtain

$$\begin{aligned}\mathcal{L}V &\leq c_4c_6 + 2\frac{\beta_1 I}{N} + \frac{\beta_2 I}{N} + \varepsilon + \gamma_2 \\ &+ 3\sigma + \frac{1}{2}(\sigma_1^2 + \sigma_2^2 + \sigma_4^2 + \sigma_5^2) - \frac{\gamma_2\epsilon_2}{\epsilon_3}.\end{aligned}$$

ϵ_3 is much less than ϵ_2 and ϵ_3 is arbitrarily small, which guarantees that the operator is less than 0.

Case 4. $V \in D_4 = \{(S, E, R, I, M) \in \mathbb{R}^5_+, 0 < I \leq \epsilon_4, R > \epsilon_3\}$, we obtain

$$\begin{aligned}
\mathcal{L}V &= c_4c_6 - \frac{\Lambda}{S} + \frac{\beta_1 I}{N} \\
&\quad + \frac{\beta_2 I}{N} + \sigma + \frac{\sigma_1^2}{2} - \frac{\beta_2 SI}{EN} + \epsilon + \gamma_2 + \sigma + \frac{1}{2}\sigma_2^2 \\
&\quad - \frac{I}{R}r_1 - \frac{\gamma_2 E}{R} + \sigma + \frac{1}{2}\sigma_4^2 \\
&\quad - \frac{I}{M}\mu + \sigma + \frac{1}{2}\sigma_5^2 + \Lambda - \sigma N + \frac{\beta_1 I}{N} \\
&\leq c_4c_6 + c_1\beta + c_1\beta_2 + 2\frac{\beta_1 I}{N} + \frac{\beta_2 I}{N} + \varepsilon + \gamma_2 \\
&\quad + 3\sigma + \frac{1}{2}(\sigma_1^2 + \sigma_2^2 + \sigma_4^2 + \sigma_5^2) - \frac{\epsilon_4}{\epsilon_3}r_1.
\end{aligned}$$

ϵ_3 is much less than ϵ_4 and ϵ_3 is arbitrarily small, which guarantees that the operator is less than 0.

Case 5 $V \in D_5 = \{(S, E, R, I, M) \in \mathbb{R}^5_+, 0 < M \leq \epsilon_5, R > \epsilon_4\}$, we obtain

$$\begin{aligned}
\mathcal{L}V &= c_4c_6 - \frac{\Lambda}{S} + \frac{\beta_1 I}{N} \\
&\quad + \frac{\beta_2 I}{N} + \sigma + \frac{\sigma_1^2}{2} - \frac{\beta_2 SI}{EN} + \epsilon + \gamma_2 + \sigma + \frac{1}{2}\sigma_2^2 \\
&\quad - \frac{I}{R}r_1 - \frac{\gamma_2 E}{R} + \sigma + \frac{1}{2}\sigma_4^2 \\
&\quad - \frac{I}{M}\mu + \sigma + \frac{1}{2}\sigma_5^2 + \Lambda - \sigma N + \frac{\beta_1 I}{N} \\
&\leq c_4c_6 + c_1\beta + c_1\beta_2 + 2\frac{\beta_1 I}{N} + \frac{\beta_2 I}{N} + \varepsilon + \gamma_2 \\
&\quad + 3\sigma + \frac{1}{2}(\sigma_1^2 + \sigma_2^2 + \sigma_4^2 + \sigma_5^2) - \sigma\epsilon_4.
\end{aligned}$$

Case 6 $V \in D_6 = \{(S, E, R, I, M) \in \mathbb{R}^5_+, S > \epsilon_6\}$, we obtain

$$\begin{aligned}
\mathcal{L}V &= c_4c_6 - \frac{\Lambda}{S} + \frac{\beta_1(1-u_1) I}{N} \\
&\quad + \frac{\beta_2 I}{N} + \sigma + \frac{\sigma_1^2}{2} - \frac{\beta_2 SI}{EN} + \epsilon + \gamma_2 + \sigma + \frac{1}{2}\sigma_2^2 \\
&\quad - \frac{I}{R}r_1(1+u_2) - \frac{\gamma_2 E}{R} + \sigma + \frac{1}{2}\sigma_4^2 \\
&\quad - \frac{I}{M}\mu + \sigma + \frac{1}{2}\sigma_5^2 + \Lambda - \sigma N + \frac{\beta_1 I}{N} \\
&\leq c_4c_6 + c_1\beta(1-u_1) + c_1\beta_2 + 2\frac{\beta_1 I}{N} + \frac{\beta_2 I}{N} + \varepsilon + \gamma_2 \\
&\quad + 3\sigma + \frac{1}{2}(\sigma_1^2 + \sigma_2^2 + \sigma_4^2 + \sigma_5^2) - \sigma\epsilon_6.
\end{aligned}$$

Case 7 $V \in D_7 = \{(S, E, R, I, M) \in \mathbb{R}^5_+, E > \epsilon_7\}$, we obtain

$$\begin{aligned}\mathcal{L}V &= c_4c_6 - \frac{\Lambda}{S} + \frac{\beta_1 I}{N} \\ &+ \frac{\beta_2 I}{N} + \sigma + \frac{\sigma_1^2}{2} - \frac{\beta_2 SI}{EN} + \epsilon + \gamma_2 + \sigma + \frac{1}{2}\sigma_2^2 \\ &- \frac{I}{R}r_1 - \frac{\gamma_2 E}{R} + \sigma + \frac{1}{2}\sigma_4^2 \\ &- \frac{I}{M}\mu + \sigma + \frac{1}{2}\sigma_5^2 + \Lambda - \sigma N + \frac{\beta_1 I}{N} \\ &\leq c_4c_6 + c_1\beta + c_1\beta_2 + 2\frac{\beta_1 I}{N} + \frac{\beta_2 I}{N} + \varepsilon + \gamma_2 \\ &+ 3\sigma + \frac{1}{2}(\sigma_1^2 + \sigma_2^2 + \sigma_4^2 + \sigma_5^2) - \sigma\epsilon_7.\end{aligned}$$

Case 8 $V \in D_8 = \{(S, E, R, I, M) \in \mathbb{R}^5_+, I > \epsilon_8\}$, we obtain

$$\begin{aligned}\mathcal{L}V &= c_4c_6 - \frac{\Lambda}{S} + \frac{\beta_1 I}{N} \\ &+ \frac{\beta_2 I}{N} + \sigma + \frac{\sigma_1^2}{2} - \frac{\beta_2 SI}{EN} + \epsilon + \gamma_2 + \sigma + \frac{1}{2}\sigma_2^2 \\ &- \frac{I}{R}r_1 - \frac{\gamma_2 E}{R} + \sigma + \frac{1}{2}\sigma_4^2 \\ &- \frac{I}{M}\mu + \sigma + \frac{1}{2}\sigma_5^2 + \Lambda - \sigma N + \frac{\beta_1 I}{N} \\ &\leq c_4c_6 + c_1\beta + c_1\beta_2 + 2\frac{\beta_1 I}{N} + \frac{\beta_2 I}{N} + \varepsilon + \gamma_2 \\ &+ 3\sigma + \frac{1}{2}(\sigma_1^2 + \sigma_2^2 + \sigma_4^2 + \sigma_5^2) - \sigma\epsilon_8.\end{aligned}$$

Case 9 $V \in D_9 = \{(S, E, R, I, M) \in \mathbb{R}^5_+, R > \epsilon_9\}$, we obtain

$$\begin{aligned}\mathcal{L}V &= c_4c_6 - \frac{\Lambda}{S} + \frac{\beta_1 I}{N} \\ &+ \frac{\beta_2 I}{N} + \sigma + \frac{\sigma_1^2}{2} - \frac{\beta_2 SI}{EN} + \epsilon + \gamma_2 + \sigma + \frac{1}{2}\sigma_2^2 \\ &- \frac{I}{R}r_1 - \frac{\gamma_2 E}{R} + \sigma + \frac{1}{2}\sigma_4^2 \\ &- \frac{I}{M}\mu + \sigma + \frac{1}{2}\sigma_5^2 + \Lambda - \sigma N + \frac{\beta_1 I}{N} \\ &\leq c_4c_6 + c_1\beta + c_1\beta_2 + 2\frac{\beta_1 I}{N} + \frac{\beta_2 I}{N} + \varepsilon + \gamma_2 \\ &+ 3\sigma + \frac{1}{2}(\sigma_1^2 + \sigma_2^2 + \sigma_4^2 + \sigma_5^2) - \sigma\epsilon_9.\end{aligned}$$

Case 10 $V \in D_{10} = \{(S, E, R, I, M) \in \mathbb{R}^5_+, M > \epsilon_{10}\}$, we obtain

$$\begin{aligned}
\mathcal{L}V &= c_4c_6 - \frac{\Lambda}{S} + \frac{\beta_1 I}{N} \\
&+ \frac{\beta_2 I}{N} + \sigma + \frac{\sigma_1^2}{2} - \frac{\beta_2 SI}{EN} + \epsilon + \gamma_2 + \sigma + \frac{1}{2}\sigma_2^2 \\
&- \frac{I}{R}r_1 - \frac{\gamma_2 E}{R} + \sigma + \frac{1}{2}\sigma_4^2 \\
&- \frac{I}{M}\mu + \sigma + \frac{1}{2}\sigma_5^2 + \Lambda - \sigma N + \frac{\beta_1 I}{N} \\
&\leq c_4c_6 + c_1\beta + c_1\beta_2 + 2\frac{\beta_1 I}{N} + \frac{\beta_2 I}{N} + \varepsilon + \gamma_2 \\
&+ 3\sigma + \frac{1}{2}(\sigma_1^2 + \sigma_2^2 + \sigma_4^2 + \sigma_5^2) - \sigma\epsilon_{10}.
\end{aligned}$$

There is a W,

$$\mathcal{L}V(S, E, R, I, M) \leq -W < 0,$$

Suppose $(S(0), E(0), R(0), I(0), M(0)) = x_0 \in \mathbb{R}^5_+ \backslash D$ is the initial state, representing the starting point of the system. The symbol τ^x is defined as the time for the path from x to the set D, i.e., τ^x is the stopping time of some random process of the system.

$$\tau_n = \inf\{t : |X(t)| = n\}.$$

This means that τ_n is the magnitude of the vector $X(t)$ (as a function of time t) equal to the first time of n.

$$\tau^{(n)}(t) = \min\{\tau^x, t, \tau_n\}.$$

By applying Dynkin's formula, we obtain

$$\begin{aligned}
&\mathbb{E}V(S(\tau^n(t)), E(\tau^n(t)), I(\tau^n(t)), R(\tau^n(t)), M(\tau^n(t))) - V(x) \\
&= \mathbb{E}\int_0^{\tau^{(n)}(t)} \mathcal{L}V du \\
&\leq \mathbb{E}\int_0^{\tau^{(n)}(t)} -W du \\
&= -W\mathbb{E}\tau^{(n)}(t).
\end{aligned}$$

Then,

$$\mathbb{E}\tau^{(n)}(t) \leq \frac{\mathbb{E}(x)}{W}.$$

$P\{\tau_e = \infty\} = 1$, which means that the probability that the event will never happen is 1, or that the event will almost certainly not happen. In other words, system (2) is regular. As time and sequence grow, the stop time $\tau^{(n)}(t)$ will almost certainly converge to some specific value τ_x.

According to Fatou's lemma, we obtain the following inequality for the expected value of the stopping time $\tau^{(n)}(t)$

$$\mathbb{E}\tau^{(n)}(t) \leq \frac{V(x)}{W} < \infty.$$

Furthermore, it is stated that for a compact subset K of $\mathbb{R}^5_+$, the supremum of the expected stopping time over all x in K is finite:

$$\sup_{x\in K} \mathbb{E}\tau^x < \infty,$$

this means that regardless of which point x within the compact set K we consider, the expected stopping time remains finite. The proof of these statements is claimed to be direct, utilizing result (ii) from Lemma 3. Therefore, given the diffusion matrix of system (2)

$$\mathbf{B} = \begin{pmatrix} \sigma_1^2 S^2 & 0 & 0 & 0 & 0 \\ 0 & \sigma_2^2 E^2 & 0 & 0 & 0 \\ 0 & 0 & \sigma_3^2 I^2 & 0 & 0 \\ 0 & 0 & 0 & \sigma_4^2 R^2 & 0 \\ 0 & 0 & 0 & 0 & \sigma_5^2 M^2 \end{pmatrix}.$$

Take M as the minimum value on the main diagonal of the matrix.

$$\sum_{i,j=1}^{5} a_{ij}(S,E,R,I,M)\xi_i\xi_j = \sum_{i,j=1}^{5} \xi^2 x_i^2 \zeta_i^2 \geq M \mid \xi \mid^2 .$$

where $\xi = (\zeta_1, \zeta_2, \zeta_3, \zeta_4, \zeta_5) \in \mathbb{R}^5_+$, $x_1 = S$, $x_2 = E$, $x_3 = R$, $x_4 = I$, $x_5 = M$. The text further implies that this inequality is a consequence of Lemma 5, which ensures that the diffusion model (2) is ergodic and has a unique stationary distribution. Ergodicity means that the system's statistical properties are the same over time and do not depend on the initial conditions. A stationary distribution is a stable probability distribution that the system converges to over time. □

6. An Example

Based on the transmission characteristics of the disease and the research objectives, initially estimate the parameters in the model or set a reasonable initial range. Collect relevant infectious disease outbreak data, and we use the Markov Chain Monte Carlo simulation as utilized in reference [23] to estimate the model parameters using the Wuhan outbreak data. Next, we give the extinction of the system. The initial value $(S_0, E_0, R_0, I_0, M_0) = (95503, 638, 129, 709, 11)$, $\beta_1 = 2.5$, $\gamma_1 = 14$, $\Lambda = 0.0234$, $\sigma_1 = 0.735$, $\sigma_2 = 0.022$, $\sigma_3 = 0.001$, $\sigma_4 = 0.001$, $\sigma_5 = 0.001$. The Figures 1–5 represent the simulation of progression of the number of individuals who are classified as susceptible, exposed, infectious, recovered, and deceased, plotted against the number of days.

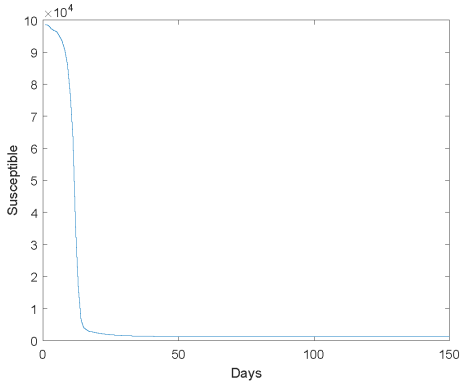

Figure 1. The susceptible go to extinction.

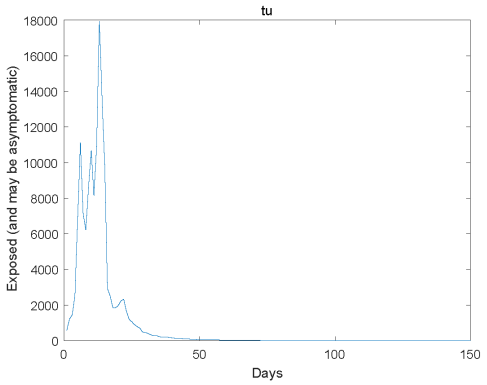

Figure 2. The exposed go to extinction.

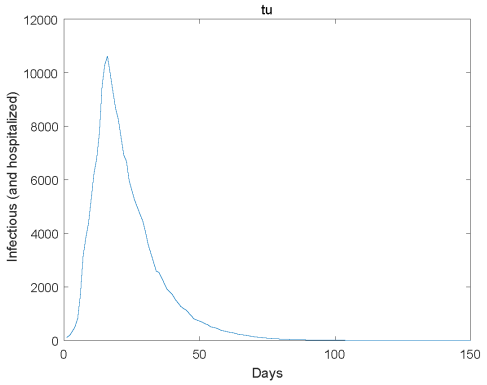

Figure 3. The infectious go to extinction.

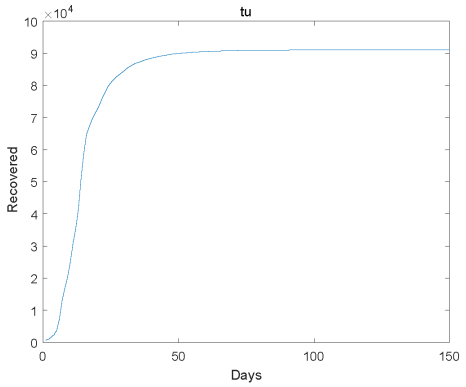

Figure 4. The recovered go to extinction.

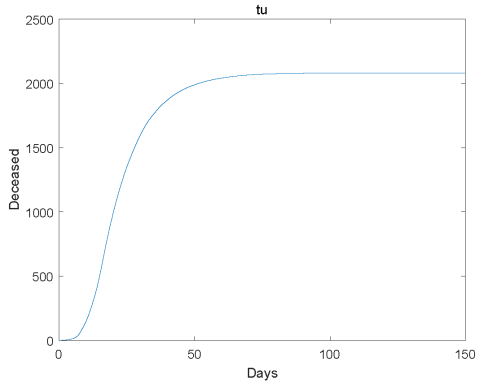

Figure 5. The deceased go to extinction.

Remark 2. *Under the current parameter settings, the disease cannot sustain transmission within the population and will eventually disappear. This may be due to a relatively high recovery rate or a relatively low infection rate, resulting in a transmission rate insufficient to maintain the disease's spread among people. The birth rate being relatively low may help reduce the number of new susceptible individuals, thereby slowing the transmission of the disease.*

Remark 3. *The first perturbation coefficient being relatively high might imply that the conversion of susceptible individuals to infected individuals occurs rapidly; however, due to the configuration of other parameters, this does not lead to sustained transmission of the disease. This information is significant for understanding and controlling the spread of infectious diseases.*

Remark 4. *It provides a mathematical proof that, given system dynamics, the total population does not grow indefinitely, but rather tends to stabilize over time. Although a disease control strategy is proposed in literature [12,13], this analysis of stability is not achieved by analyzing the ratio of each state in the system and the limit of the natural logarithm over time. Such stability analysis is crucial for understanding and predicting disease transmission and designing control strategies.*

7. Conclusions

This study provides a mathematical foundation and theoretical support for understanding and predicting the transmission dynamics of COVID-19. It proves the existence of global solutions for the stochastic SEIRM COVID-19 model with a standard incidence rate. System stability is analyzed by constructing Lyapunov functions and employing relevant mathematical tools. The properties of the diffusion matrix are utilized to ensure the steady-state distribution of the system. The potential limitations of the model and the scope for future work have been discussed in more detail:

Understand that you need to reorganize the language for the following content [24–28]:

a. Discuss whether the model assumes a uniform mixing of populations or fails to consider factors such as spatial distribution and varying contact rates among different demographic groups.
b. If the model assumes constant parameters, this may be a limitation because real-world scenarios often involve time-varying parameters due to interventions or behavioral changes.
c. Evaluate the model's capacity to predict long-term outcomes in dynamic environments.
d. Pandemics can be influenced by external factors such as policy changes, vaccine distribution, or the emergence of new variants.
e. Consider unreported cases as potential limitations of the model. Additionally, propose that future research could build on this work by integrating methods to estimate and account for unreported cases.

Author Contributions: Methodology, D.W.; software, D.W.; writing—original draft preparation, Y.Z.; visualization, H.W. All authors have read and agreed to the published version of the manuscript.

Funding: This work was supported by program for National Natural Science Foundation of China (No.11526046).

Data Availability Statement: The original contributions presented in the study are included in the article, further inquiries can be directed to the corresponding authors.

Conflicts of Interest: The authors declare no conflict of interest.

References

1. Kermack, W.O.; McKendrick, A.G. A contribution to the mathematical theory of epidemics. *Proc. R. Soc. Lond. Ser. Contain. Pap. Math. Phys. Character* **1927**, *115*, 700–721.
2. Brauer, F. Compartmental models in epidemiology. *Math. Epidemiol.* **2008**, 19–79.
3. Aybar, O. Biochemical models of SIR and SIRS: Effects of bilinear incidence rate on infection-free and endemic states. *Chaos* **2023**, *33*, 093120. [CrossRef]

4. Wang, J.; Zhang, J.; Jin, Z. Analysis of an SIR model with bilinear incidence rate. *Nonlinear Anal. Real World Appl.* **2010**, *14*, 2390–2402. [CrossRef]
5. Zhang, Q. On small-data solution of the chemotaxis-SIS epidemic system with bilinear incidence rate. *Nonlinear Anal. Real World Appl.* **2024**, *77*, 104063. [CrossRef]
6. Mahmood, P.; Majid, E. Global dynamics of an epidemic model with standard incidence rate and vaccination strategy. *Chaos Solitons Fractals* **2018**, *117*, 192–199.
7. Han, S.; Lei, C.; Zhang, X. Qualitative analysis on a diffusive SIRS epidemic model with standard incidence infection mechanism. *Z. Angew. Math. Phys.* **2021**, *71*, 190. [CrossRef]
8. Wu, Z.; Jiang, D. Dynamics and Density Function of a Stochastic SICA Model of a Standard Incidence Rate with Ornstein-Uhlenbeck Process. *Qual. Theory Dyn. Syst.* **2014**, *23*, 219. [CrossRef]
9. Guo, S.; Xue, Y.; Li, X. A novel analysis approach of uniform persistence for a COVID-19 model with quarantine and standard incidence rate. *Quant. Biol.* **2022**.
10. Guo, S.; He, M.; Cui, J. Global Stability of a Time-delayed Malaria Model with Standard Incidence Rate. *Acta Math. Appl.-Sin.-Engl. Ser.* **2023**, *39*, 211–221. [CrossRef]
11. He, B.; Peng, Y.; Sun, K. SEIR modeling of the COVID-19 and its dynamics. *Nonlinear Dyn.* **2020**, *101*, 1667–1680. [CrossRef] [PubMed]
12. Saroj, K.; Ahmed, N.U. Mathematical modeling and optimal intervention of COVID-19 outbreak. *Quatitative Biol.* **2021**, *9*, 84–92.
13. Shengjie, L. Effects of non-pharmaceutical interventions to contain COVID-19 in China. *Nature* **2020**, *585*, 410–413.
14. Zhao, Y.; Wang, L. Practical exponential stability of impulsive stochastic food chain system with time-varying delays. *Mathematics* **2023**, *11*, 147. [CrossRef]
15. Zhao, Y.; Lin, H.; Qiao, X. Persistence, extinction and practical exponential stability of impulsive stochastic competition models with varying delays. *AIMS Math.* **2023**, *8*, 22643–22661. [CrossRef]
16. Xu, H.; Zhu, Q.; Zheng, W. Exponential stability of stochastic nonlinear delay systems subject to multiple periodic impulses. *IEEE Trans. Autom. Control.* **2024**, *69*, 2621–2628. [CrossRef]
17. Zhao, Y.; Wang, L. Asymptotic behavior of a stochastic three-species food chain model with time-varying delays. *Period. Ocean. Univ. China* **2023**, *53*, 132–136.
18. Zhao, Y.; Wang, L.; Wang, Y. The Periodic Solutions to a Stochastic Two-Prey One-Predator Population Model with Impulsive Perturbations in a Polluted Environment. *Methodol. Comput. Appl. Probab.* **2021**, *23*, 859–872. [CrossRef]
19. Khan, A.; Ikram, R.; Din, A.; Humphries, U.W.; Akgul, A. Stochastic COVID-19 SEIQ epidemic model with time-delay. *Results Phys.* **2021**, *30*, 104775. [CrossRef]
20. Allen, L. *An Introduction to Stochastic Epidemic Models*; Springer: Berlin/Heidelberg, Germany, 2008.
21. Yang, Q.; Zhang, X.; Jiang, D. Dynamical behavior of a stochastic food chain system with ornstein uhlenbeck Process. *J. Nonlinear Sci.* **2022**, *32*, 34. [CrossRef]
22. Mao, X. *Stochastic Differential Equations and Their Applications*; Horwood: Chichester, UK, 1997.
23. He, S.; Tang, S.; Rong, C. A discrete stochastic model of the COVID-19 outbreak: Forecast and control. *Math. Biosci. Eng.* **2020**, *17*, 2792–2804. [CrossRef] [PubMed]
24. Pei, L.; Zhang, M. Long-Term Predictions of COVID-19 in Some Countries by the SIRD Model. *Complexity* **2021**, *1*, 6692678. [CrossRef]
25. Beghi, E.; Helbok, R.; Ozturk, S.; Karadas, O.; Lisnic, V.; Grosu, O.; Kovács, T.; Dobronyi, L.; Bereczki, D.; Cotelli, M.S.; et al. Short- and long-term outcome and predictors in an international cohort of patients with neuro-COVID-19. *Eur. J. Neurol.* **2022**, *29*, 1663–1684. [CrossRef] [PubMed]
26. El-Shabasy, R. Three waves changes, new variant strains, and vaccination effect against COVID-19 pandemic. *Int. J. Biol. Macromol.* **2022**, *204*, 161–168. [CrossRef] [PubMed]
27. Liu, Z. Predicting the number of reported and unreported cases for the COVID-19 epidemics in China, South Korea, Italy, France, Germany and United Kingdom. *J. Theor. Biol.* **2021**, *509*, 110501. [CrossRef]
28. Hamou, A. Analysis and dynamics of a mathematical model to predict unreported cases of COVID-19 epidemic in Morocco. *Comp. Appl. Math.* **2021**, *41*, 289. [CrossRef]

mathematics

MDPI

Article

Finite-Time Asynchronous H_∞ Control for Non-Homogeneous Hidden Semi-Markov Jump Systems

Qian Wang [1,*], Xiaojun Zhang [1,*], Yu Shao [2] and Kaibo Shi [3]

[1] School of Mathematics Sciences, University of Electronic Science and Technology of China, Chengdu 611731, China
[2] School of Automation, Southeast University, Nanjing 210096, China; yushao@njust.edu.cn
[3] School of Information Science and Engineering, Chengdu University, Chengdu 610106, China; skbs111@163.com
* Correspondence: qianwang11@yeah.net or 201911110408@std.uestc.edu.cn (Q.W.); sczhxj@uestc.edu.cn (X.Z.)

Abstract: This article explores the finite-time control problem associated with a specific category of non-homogeneous hidden semi-Markov jump systems. Firstly, a hidden semi-Markov model is designed to characterize the asynchronous interactions that occur between the true system mode and the controller mode, and emission probabilities are used to establish relationships between system models and controller modes. Secondly, a novel piecewise homogeneous method is introduced to tackle the non-homogeneous issue by taking into account the time-dependent transition rates for the jump rules between different modes of the system. Thirdly, an asynchronous controller is developed by applying Lyapunov theory along with criteria for stochastic finite-time boundedness, ensuring the specified H_∞ performance level is maintained. Finally, the effectiveness of this method is verified through two simulation examples.

Keywords: non-homogeneous hidden semi-Markov jump systems; stochastic finite-time boundedness; emission probabilities

MSC: 37M05; 37M10

1. Introduction

The Markov process (MP) is commonly utilized to analyze system state transitions in various fields such as finance, power systems, and robotics. Due to its ability to capture dynamic behavior, Markov jump systems (MJSs) have been extensively researched in recent years [1–5]. In continuous-time systems, the transition rates between different modes of an MP are influenced solely by the current mode in which the system resides. The dwell time (DT) follows an exponential distribution. In real systems, the DT distribution often follows different patterns, and new methods need to be explored to solve this problem. Unlike a traditional MP, semi-Markov processes (SMPs) consider historical data, and the DT is not constrained by an exponential distribution. As a result, researchers and practitioners may find semi-Markov jump systems (SMJSs) to be more suitable for modeling a variety of systems where the exponential assumption does not hold, thus enhancing their applicability in complex scenarios [6–12]. Regarding the stability analysis and synthesis of semi-Markov jump systems, Ref. [13] focused on the issues of stochastic stability and stabilization regarding a particular category of continuous-time semi-Markovian jump systems that feature mode transition-dependent sojourn time distributions. In [14], the author discussed the problem of H_∞ observer-based control for a class of continuous-time semi-Markovian jump systems with more detailed observational information.

A significant limitation in the majority of current research is the assumption that transition rates (TRs) are constant over time. This perspective overlooks the dynamic nature of many practical engineering applications. For instance, in contexts such as manufacturing

systems and voltage conversion circuitry, the conditions and factors affecting TRs frequently change, rendering the assumption of time invariance unrealistic. Therefore, it is important to consider non-homogeneous semi-Markov jump systems (NHSMJSs) in these scenarios. Ref. [15] proposed an SMP framework that is affected by deterministic high-order switching signals, and the Markov renewal process is non-homogeneous. The stabilization problem of a class of stochastic NHSMJSs is studied in [16]. To date, there is limited research on NHSMJSs, making it a fruitful area for exploration. This lack of existing literature is a key driving factor behind the current study.

On the other hand, the above research is based on the synchronization of the system mode and the controller mode. In fact, the asynchronous problem of SMJSs has attracted widespread attention from researchers. Given the potential misalignment of variables and modes between the filter and plant in real network environments, a double asynchronous phenomenon may occur. For this reason, Ref. [17] proposed a new fault detection filter which specifically targets fault detection in fuzzy SMJSs. Ref. [18] explored the issue of asynchronous control in two-dimensional SMJSs within the Roesser model. The interval type-2 fuzzy model was investigated in [19], which developed an asynchronous sliding mode control mechanism to achieve a quasi-sliding mode, effectively addressing the challenges posed by parameter uncertainties for nonlinear semi-Markov jump models. Hidden semi-Markov jump systems (HSMJSs) have emerged as a research area with the potential to overcome the limitations of the assumption that the system mode is consistent with the controller [20–24]. The hidden semi-Markov process (HSMP) can be understood as a parameter process characterized by two variables. The stochastic process, referred to as the SMP, is time-homogeneous and remains undisclosed to the controller, making it hidden. The observed modes within the underlying process are determined from the emission probabilities of the actual and observed system modes, which aids in the identification of hidden system modes. While there has been significant research on stability analysis and controller synthesis for HSMJSs, certain areas within this field have not been fully explored, leaving open questions that have inspired our current investigation.

Building upon this foundation, the examination of stability and control mechanisms for non-homogeneous hidden semi-Markov jump systems is undertaken. Ref. [25] addresses the analysis of stability for a class of discrete-time non-homogeneous hidden semi-Markov jump systems that operate with limited information regarding the sojourn time probability density functions. Ref. [26] explores the non-fragile asynchronous control challenge within discrete-time non-homogeneous hidden semi-Markov Lur'e systems, which face uncertainties related to the system mode and gain. However, the aforementioned studies are primarily based on discrete-time scenarios. To the best of the author's knowledge, the stability analysis of continuous-time non-homogeneous hidden semi-Markov jump systems remains unexplored. This gap in the literature serves as one of the primary motivations for this article.

Meanwhile, in numerous engineering applications, the performance during a transition phase of a system is evaluated within a restricted operational time frame, contrasting with the analysis of stability over an endless duration. The goal of finite-time stability is to guarantee that, within a specified time frame, the system's trajectories do not surpass a certain physical limit. Up to this point, significant interest has been directed towards finite-time stability [12,27,28].

This study examines the design challenges associated with asynchronous H_∞ controllers for non-homogeneous HSMJSs within a finite-time framework. The main contributions of this research can be outlined as follows:

(i) A hidden semi-Markov model is proposed to describe the asynchronous behavior observed between the mode of the actual system and that of the controller.

(ii) A novel piecewise homogeneous approach is suggested for addressing the non-homogeneous phenomenon by taking into account the time-dependent transition rates of the jump rules across different system modes.

(iii) An asynchronous controller is designed using Lyapunov theory to generate finite stochastic criteria with the prescribed H_∞ performance level.

Table 1 lists the notations used in this article.

Table 1. Common notations in this paper.

Notations	Meanings
$\mathbb{R}^n$	n-dimensional Euclidean space
$\|\cdot\|$	Euclidean norm
$U > 0$	U is a positive-definite symmetric matrix
U^{T}	the transpose of U
U^{-1}	the inverse of U
$\lambda_{\max}\{U\}, \lambda_{\min}\{U\}$	maximum and minimum eigenvalues of U
$\mathbf{He}\{U\}$	$U + U^{\mathrm{T}}$
$E(\cdot)$	the mathematical expectation
$*$	the elision for symmetry matrix
$\mathcal{M}_1$	1,2, … M_1
$\mathcal{M}_2$	1,2, … M_2
$\mathcal{N}$	1,2, … N

2. Materials and Methods

We consider a class of non-homogeneous HMJSs described by

$$\begin{cases} \dot{x}(t) = A_{r_t}x(t) + B_{r_t}u(t) + C_{r_t}\omega(t), \\ z(t) = D_{r_t}x(t) \end{cases} \tag{1}$$

where $x(t) \in \mathbb{R}^n$ represents the state vector of the system, $u(t) \in \mathbb{R}^m$ represents the control input, $z(t) \in \mathbb{R}^p$ represents the measured output, and $\omega(t) \in \mathbb{R}^q$ represents the external disturbance belonging to $L_2[0,\infty)$, $\forall t \geq 0$. r_t represents a continuous-time non-homogeneous semi-Markov process that assumes values within the set $\mathcal{M}_1$. The time-dependent TRs are indicated as follows:

$$\mathbf{Pr}\{r_{t+\Delta} = j \mid r_t = i\} = \begin{cases} \pi_{ij}^{\theta_t}(\delta)\Delta + o(\Delta), & j \neq i, \\ 1 + \pi_{ii}^{\theta_t}(\delta)\Delta + o(\Delta), & j = i. \end{cases} \tag{2}$$

with $\Delta > 0$, where δ means sojourn time, and $\lim_{\Delta\to 0} o(\Delta)/\Delta = 0$, $\pi_{ij}^{\theta_t}(\delta) > 0$ $(i, j \in \mathcal{M}_1, j \neq i)$ is the transition rate between the i mode at time t and the j mode at time $t + \Delta$, which satisfies

$$\pi_{ii}^{\theta_t}(\delta) = -\sum_{j\in\mathcal{M}_1\setminus\{i\}} \pi_{ij}^{\theta_t}(\delta), \forall i \in \mathcal{M}_1.$$

In this context, the variable θ_t represents a piecewise constant switching signal that assumes values from the set $\mathcal{N}$, and it determines the pattern of the transition probability matrix at each moment. For every potential value of the variable $r_t = i$, with $\theta_t = p$, the TRs, π_{ij}^p, are formulated as a function of the high-level switching signal, $\theta_t = p$.

This formulation underscores the fact that the TRs exhibit temporal variability. Additionally, when organized sequentially, the matrix representing the TRs is introduced as

$$\Pi^p(\delta) = \begin{bmatrix} \pi_{11}^p(\delta) & \pi_{12}^p(\delta) & \cdots \pi_{1m}^p(\delta) \\ \pi_{21}^p(\delta) & \pi_{22}^p(\delta) & \cdots \pi_{2m}^p(\delta) \\ \vdots & \vdots & \vdots \\ \pi_{m1}^p(\delta) & \pi_{m2}^p(\delta) & \cdots \pi_{mm}^p(\delta) \end{bmatrix}$$

Due to asynchronous phenomenon, we cannot assume that the controller has precise access to modal system information. This study aimed to discover the hidden controller modes by utilizing an observed mode analysis approach. Figure 1 can provide a clearer

depiction of the HSMP. $\{r_t, t \geq 0\}$ stands for the hidden system mode, and the observed mode $\{\sigma_t, t \geq 0\}$ assumes values from the set $\mathcal{M}_2$. A range of observed modes can be emitted by each hidden system mode. The emission probability matrix is

$$\mathbf{Pr}\{\sigma_t = m \mid r_t = i\} = \rho_{im}, \ \ \forall i \in \mathcal{M}_1, m \in \mathcal{M}_2, \tag{3}$$

with $\rho_{im} \in [0, 1]$ and $\sum_{m \in \mathcal{M}_2} \rho_{im} = 1$.

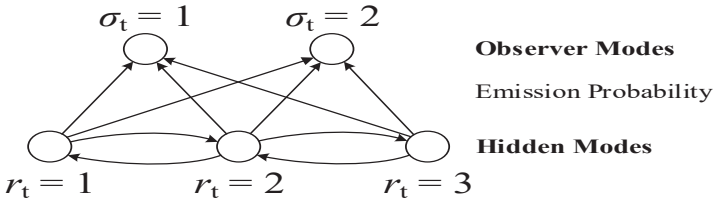

Figure 1. An example of a hidden semi-Markov process.

In this paper, for $r_t = i$, $\theta_t = p$, and $\sigma_t = m$, the parameter matrices A_i, B_i, C_i, and D_i possess suitable dimensions. We consider the following three-variable-dependent asynchronous controller for non-homogeneous HSMJSs (1):

$$u(t) = K_{i,m,p} x(t), \tag{4}$$

where $K_{i,m,p}$ means the feedback control gain matrix. The combination of (1) and (4) gives rise to an expression for non-homogeneous HSMJS as follows:

$$\begin{cases} \dot{x}(t) = (A_i + B_i K_{i,m,p}) x(t) + C_i \omega(t), \\ z(t) = D_i x(t). \end{cases} \tag{5}$$

Remark 1. *In practical application systems, the modal information acquired by the controller is often inaccurate, meaning that the true system model remains concealed from the controller. To address this issue, the variable σ_t is proposed to denote the mode of the controller, with the relationship between r_t and σ_t illustrated by Equation* (3).

Remark 2. *In actual systems, it is unrealistic to obtain the transition probability at each moment in real time. Therefore, it is difficult to study semi-Markov jump systems with time-varying transition probabilities, which also increases the difficulty of deriving the stability theory. Fortunately, in control practice, this type of system can usually be divided into a limited number of continuous homogeneous systems, hence the piecewise homogeneous system proposed in this article.*

Before we continue, here are the definitions, given below.

Assumption 1 ([27])**.** *Given the time interval $[0, \ T]$ and the constant $d \geq 0$, the unknown external disturbance $\omega(t)$ satisfies the following conditions:*

$$\int_0^T \omega^{\mathrm{T}}(t) \omega(t) \mathrm{d}t \leqslant d^2. \tag{6}$$

Definition 1 ([29])**.** *HSMJSs* (5) *are stochastically finite-time-bounded (SFTB) within a time interval $[0, \ T]$ concerning (d, T, R, c_1, c_2) if the following conditions hold:*

$$\begin{cases} \int_0^T \omega^{\mathrm{T}}(t) \omega(t) dt \leqslant d^2, \\ x^{\mathrm{T}}(0) R x(0) \leqslant c_1 \Rightarrow \mathrm{E}\{x^{\mathrm{T}}(t) R x(t) < c_2\}, \forall t \in \{0, T\}. \end{cases} \tag{7}$$

where c_1 and c_2 are positive scalars with $c_2 > c_1$, and $R > 0$ is a weighting matrix.

Definition 2 ([29]). *Given a scalar $\gamma \geq 0$, if there is an asynchronous controller* (4) *under zero initial conditions such that all $i \in \mathcal{M}_1$, $m \in \mathcal{M}_2$, and $p \in \mathcal{N}$, the HSMJS* (5) *is SFTB and satisfies the following:*

$$\int_0^T z^{\mathrm{T}}(t)z(t)dt < \gamma^2 \int_0^T \omega^{\mathrm{T}}(t)\omega(t)dt. \tag{8}$$

We say that the controller (4) *satisfies the H_∞ performance index γ.*

3. Results

Theorem 1. *For a given scalar $\alpha > 0$, the closed-loop non-homogeneous HSMJS* (5) *is SFTB and satisfies the H_∞ performance index γ concerning (d, T, R, c_1, c_2) if there exist symmetric matrices $P_{i,p} > 0$, such that the following conditions hold for every value of $i \in \mathcal{M}_1$, $m \in \mathcal{M}_2$, and $p \in \mathcal{N}$:*

$$e^{\alpha T}c_1\lambda_2 + \gamma^2 d^2 - c_2\lambda_1 < 0 \tag{9}$$

$$\Omega = \begin{bmatrix} \Xi_{11} & \Xi_{12} & \Xi_{13} \\ * & \Xi_{22} & 0 \\ * & * & \Xi_{33} \end{bmatrix} < 0 \tag{10}$$

with

$$\begin{aligned}
\lambda_1 &= \lambda_{\min}\{R^{-\frac{1}{2}}P_{i,p}R^{-\frac{1}{2}}\},\ \ \lambda_2 = \lambda_{\max}\{R^{-\frac{1}{2}}P_{i,p}R^{-\frac{1}{2}}\},\\
\Xi_{11} &= \mathbf{He}[P_{i,p}(A_i + \sum_{m\in\mathcal{M}_2}\rho_{im}B_iK_{i,m,p})] + \sum_{j\in\mathcal{M}_1}\overline{\pi}_{ij}^p P_{j,p} - \alpha P_{i,p}\\
\Xi_{12} &= P_{i,p}C_i, \quad \Xi_{13} = D_i^{\mathrm{T}},\\
\Xi_{22} &= -\gamma^2 e^{-\alpha T}, \quad \Xi_{33} = -I,\\
\overline{\pi}_{ij}^p &= E[\pi_{ij}^p(\delta)] = \int_0^\infty \pi_{ij}(\delta)d\mathcal{F}_i^p(\delta),
\end{aligned}$$

where $\mathcal{F}_i^p(\delta)$ represents the probability density function of DT with respect to δ.

Proof of Theorem 1. A stochastic Lyapunov functional candidate is chosen as follows:

$$V(x(t)) = x^{\mathrm{T}}P_{i,p}x(t). \tag{11}$$

Define $\mathcal{L}$ as a weak infinity operator, and for $\alpha > 0$, the auxiliary function is defined as follows:

$$J(t) = E\{\mathcal{L}V(x(t)) - \alpha V(x(t)) - \gamma^2 e^{-\alpha T}\omega^{\mathrm{T}}(t)\omega(t) + z^{\mathrm{T}}(t)z(t)\}. \tag{12}$$

By carrying out this calculation, we obtain

$$\begin{aligned}
J(t) &= E\{\mathcal{L}V(x(t)) - \alpha V(x(t)) - \gamma^2 e^{-\alpha T}\omega^{\mathrm{T}}(t)\omega(t) + z^{\mathrm{T}}(t)z(t)\}\\
&= E\{x^{\mathrm{T}}(t)(\sum_{j\in\mathcal{M}_1}\pi_{ij}^p P_{j,p})x(t) + 2[x^{\mathrm{T}}(t)P_{i,p}A_ix(t)\\
&+ x^{\mathrm{T}}(t)(\sum_{m\in\mathcal{M}_2}\rho_{im}P_{i,p}B_iK_{i,m,p})x(t) + \omega^{\mathrm{T}}(t)P_{i,p}C_i\omega(t)]\\
&- \alpha V(x(t)) - \gamma^2 e^{-\alpha T}\omega^{\mathrm{T}}(t)\omega(t) + z^{\mathrm{T}}(t)z(t)\}.
\end{aligned} \tag{13}$$

Thus, the following inequality can be obtained:

$$J(t) \leq \eta^{\mathrm{T}}(t)\Omega\eta(t) \tag{14}$$

where $\eta(t) = [x(t) \ \ \omega(t)]^{\mathrm{T}}$. From condition (10), we obtain

$$J(t) < 0. \tag{15}$$

According to (15), the equivalent inequality is obtained:

$$\mathcal{L}V(x(t)) - \alpha V(x(t)) - \gamma^2 e^{-\alpha T}\omega^{\mathrm{T}}(t)\omega(t) + z^{\mathrm{T}}(t)z(t) < 0. \tag{16}$$

Then, taking the expectation of (16), it follows that

$$E\{\mathcal{L}e^{-\alpha t}V(x(t))\} < \gamma^2 e^{-\alpha(t+T)}E\{\omega^{\mathrm{T}}(t)\omega(t)\}. \tag{17}$$

Integrating (17) over $t(t \in (0, T])$ yields

$$e^{-\alpha t}E\{V(x(t))\} < E\{V(x(0))\} + \gamma^2 E\Big\{\int_0^T e^{-\alpha(\tau+T)}\omega^{\mathrm{T}}(\tau)\omega(\tau)d\tau\Big\}. \tag{18}$$

Multiplying (18) by $e^{\alpha t}$ yields

$$E\{V(x(t))\} < e^{\alpha t}E\{V(x(0))\} + \gamma^2 d^2 < e^{\alpha T}\lambda_2 c_1 + \gamma^2 d^2.$$

Since

$$E\{V(x(t))\} \geq \lambda_1 E\{x^{\mathrm{T}}(t)Rx(t)\},$$

We can obviously obtain

$$E\{x^{\mathrm{T}}(t)Rx(t)\} < \frac{e^{\alpha T}\lambda_2 c_1 + \gamma^2 d^2}{\lambda_1}.$$

From (9), it follows that

$$E\{V(x(t))\} < \frac{e^{\alpha T}\lambda_2 c_1 + \gamma^2 d^2}{\lambda_1} < c_2.$$

Therefore, according to Definition 1, the closed-loop system (5) is SFTB. If we multiply (16) by $e^{\alpha t}$ and calculate the mathematical expectation, we obtain

$$E\{\mathcal{L}[e^{-\alpha t}V(x(t))]\} < E\{e^{-\alpha t}[\gamma^2 e^{-\alpha T}\omega^{\mathrm{T}}(t)\omega(t) - z^{\mathrm{T}}(t)z(t)]\}. \tag{19}$$

Integrating (19) over $t(t \in (0, t])$ under zero initial conditions, we obtain

$$E\Big\{\int_0^T e^{-\alpha\ell}[z^{\mathrm{T}}(\ell)z(\ell) - \gamma^2 e^{-\alpha T}\omega^{\mathrm{T}}(\ell)\omega(\ell)]d\ell\Big\} < 0.$$

Thus, for all $t(t \in (0, T])$, it follows that

$$E\Big\{\int_0^T z^{\mathrm{T}}(t)z(t)dt\Big\} < e^{-\alpha T}E\Big\{\int_0^T \gamma^2\omega^{\mathrm{T}}(t)\omega(t)dt\Big\} < \gamma^2 E\Big\{\int_0^T \omega^{\mathrm{T}}(t)\omega(t)\Big\}.$$

Returning to Definition 2, the closed-loop system (5) is SFTB and satisfies the H_∞ performance index γ. This completes the proof. □

The following theorem we solve for the three-variable-dependent asynchronous controller.

Theorem 2. *For a given scalar $\alpha > 0$, the closed-loop non-homogeneous HSMJS (5) is SFTB and satisfies the H_∞ performance index γ concerning (d, T, R, c_1, c_2) if there exist symmetric matrices $P_{i,p} > 0$ such that the following conditions hold for every value of $i \in \mathcal{M}_1$, $m \in \mathcal{M}_2$, and $p \in \mathcal{N}$:*

$$\begin{bmatrix} (\gamma^2 d^2 - c_2\lambda_1)e^{-\alpha T} & \sqrt{c_1} \\ * & -\lambda_2 \end{bmatrix} < 0 \tag{20}$$

$$\tilde{\Omega} = \begin{bmatrix} \tilde{\Xi}_{11} & \tilde{\Xi}_{12} & \tilde{\Xi}_{13} \\ * & \Xi_{22} & 0 \\ * & * & \Xi_{33} \end{bmatrix} < 0, \tag{21}$$

with

$$\begin{aligned} \tilde{\lambda}_1 &= \lambda_{\min}\{R^{-\frac{1}{2}} X_{i,p} R^{-\frac{1}{2}}\},\ \tilde{\lambda}_2 = \lambda_{\max}\{R^{-\frac{1}{2}} X_{i,p} R^{-\frac{1}{2}}\}, \\ \tilde{\Xi}_{11} &= \mathbf{He}[A_i X_{i,p} + \sum_{m\in\mathcal{M}_2} \rho_{im} B_i N_{i,m,p}] + \sum_{j\in\mathcal{M}_1} \overline{\pi}_{ij}^p X_{i,p}^{\mathrm{T}} P_{j,p} X_{i,p} - \alpha X_{i,p}, \\ \tilde{\Xi}_{12} &= C_i,\ \tilde{\Xi}_{13} = X_{i,p}^{\mathrm{T}} D_i^{\mathrm{T}}. \end{aligned}$$

The other parameters are consistent with Theorem 1. Then, the three-variable-dependent controller's gain matrices are given as $K_{i,m,p} = N_{m,p} X_{i,p}^{-1}$.

Proof of Theorem 2. Define

$$X_{i,p} = P_{i,p}^{-1},\ N_{i,m,p} = K_{i,m,p} X_{m,p},$$

$diag\{X_{i,p}; I; I\}$, and its transposition; then, (10) is equivalent to (21), and, obviously, (9) is equivalent to (20). Proof completed. □

Remark 3. *In contrast to the asynchronous controllers commonly found in the existing literature, the asynchronous controller presented in this paper is defined by three variables. This approach leverages the characteristics of the system state more effectively, thereby significantly reducing conservatism.*

4. Illustrative Example

Example 1. *Consider a non-homogeneous hidden semi-Markov jump system with two subsystems:*

$$\left[\begin{array}{c|c} A_1 & A_2 \end{array}\right] = \left[\begin{array}{cc|cc} -1 & 2 & -2 & -3 \\ -3 & -2 & 4 & -1 \end{array}\right],$$

$$B_1 = B_2 = R = \begin{bmatrix} 1 & 0 \\ 0 & 1 \end{bmatrix},$$

$$\left[\begin{array}{c|c} C_1 & C_2 \end{array}\right] = \left[\begin{array}{c|c} 0.001 & -0.001 \\ -0.001 & -0.001 \end{array}\right],\ \left[\begin{array}{c|c} D_1 & D_2 \end{array}\right] = \left[\begin{array}{c|c} 0.2 & 0.2 \\ 0.4 & 0.1 \end{array}\right],$$

The transition rate matrix $\Pi^p(\delta)$ is described by

$$\Pi^1(\delta) = \begin{bmatrix} -3(\delta)^2 & 3(\delta)^2 \\ 4(\delta)^3 & -4(\delta)^3 \end{bmatrix},\ \Pi^2(\delta) = \begin{bmatrix} -4(\delta)^3 & 4(\delta)^3 \\ 3(\delta)^2 & -3(\delta)^2 \end{bmatrix}.$$

The semi-Markov chain dwell time for each mode is assumed to follow a Weibull distribution. $\mathcal{F}_i^p(\delta)$ refers to the probability density functions of DT with respect to δ, where $d\mathcal{F}_1^1(\delta) = 3(\delta)^2 e^{-(\delta)^3} d\delta$, $d\mathcal{F}_2^1(\delta) = 4(\delta)^3 e^{-(\delta)^4} d\delta$, $d\mathcal{F}_2^2(\delta) = 3(\delta)^2 e^{-(\delta)^3} d\delta$, and $d\mathcal{F}_1^2(\delta) = 4(\delta)^3 e^{-(\delta)^4} d\delta$. Further, the mathematical expectation can be calculated:

$$[\bar{\pi}_{ij}]^1 = \begin{bmatrix} -2.7082 & 2.7082 \\ 3.6763 & -3.6763 \end{bmatrix}, \quad [\bar{\pi}_{ij}]^2 = \begin{bmatrix} -3.6763 & 3.6763 \\ 2.7082 & -2.7082 \end{bmatrix}.$$

Case I: Asynchronous case: we define the emission probability matrix.

$$[\rho_{im}] = \begin{bmatrix} 0.5 & 0.5 \\ 0.2 & 0.8 \end{bmatrix}.$$

By choosing $\alpha = 1$, $\gamma = 0.1$, $c_1 = 0.4$, $c_2 = 20$, $T = 4$, $d = 2$, $x_0 = [1, -1]^{\mathrm{T}}$, *and* $\omega(t) = e^{-2t}sin(0.5t)$ *and solving Theorem 2, we obtain the three-variable-dependent asynchronous feedback control gain matrix:*

$$\left[\begin{array}{c|c} K_{111} & K_{121} \end{array}\right] = \left[\begin{array}{cc|cc} 0.2312 & 1.0238 & 0.2216 & 1.0135 \\ -4.8556 & -12.6636 & -4.8641 & -12.6847 \end{array}\right],$$

$$\left[\begin{array}{c|c} K_{211} & K_{221} \end{array}\right] = \left[\begin{array}{cc|cc} 0.2227 & 1.0148 & 0.2323 & 1.0252 \\ -4.8704 & -12.7001 & -4.8619 & -12.6791 \end{array}\right],$$

$$\left[\begin{array}{c|c} K_{112} & K_{122} \end{array}\right] = \left[\begin{array}{cc|cc} -2.4428 & -1.1474 & -2.4407 & -1.1465 \\ 1.1370 & 1.1520 & 1.1371 & 1.1521 \end{array}\right],$$

$$\left[\begin{array}{c|c} K_{212} & K_{221} \end{array}\right] = \left[\begin{array}{cc|cc} -9.7750 & -4.5913 & -9.7755 & -4.5916 \\ 4.5435 & 4.6040 & 4.5435 & 4.6040 \end{array}\right].$$

The trajectories of the state response are shown in Figure 2. It can be clearly seen from Figure 3 that the evolution of $x^{\mathrm{T}}(t)Rx(t)$ tends to zero in finite time, and the designed asynchronous controllers can make non-homogeneous HSMJSs (5) become SFTB. Figure 4 and Figure 5 show the system mode and controller mode, which both have two modes. Figure 6 shows a possible evolution of the switching signal θ_t.

Case II: Synchronous case: we define the emission probability matrix.

$$[\rho_{im}] = \begin{bmatrix} 1.0 & 0.0 \\ 0.0 & 1.0 \end{bmatrix}.$$

The other parameters are the same as in case I.

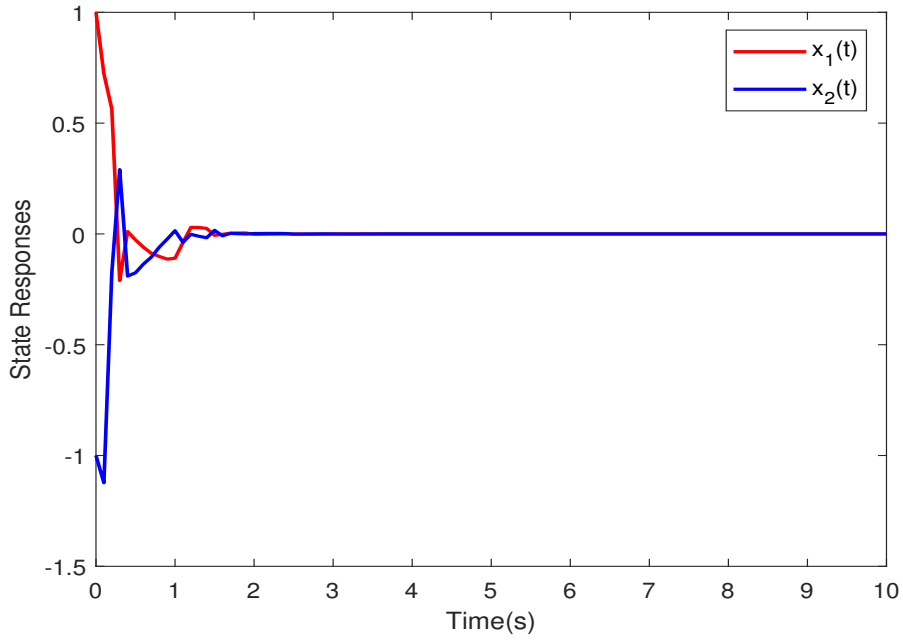

Figure 2. State response of closed-loop system.

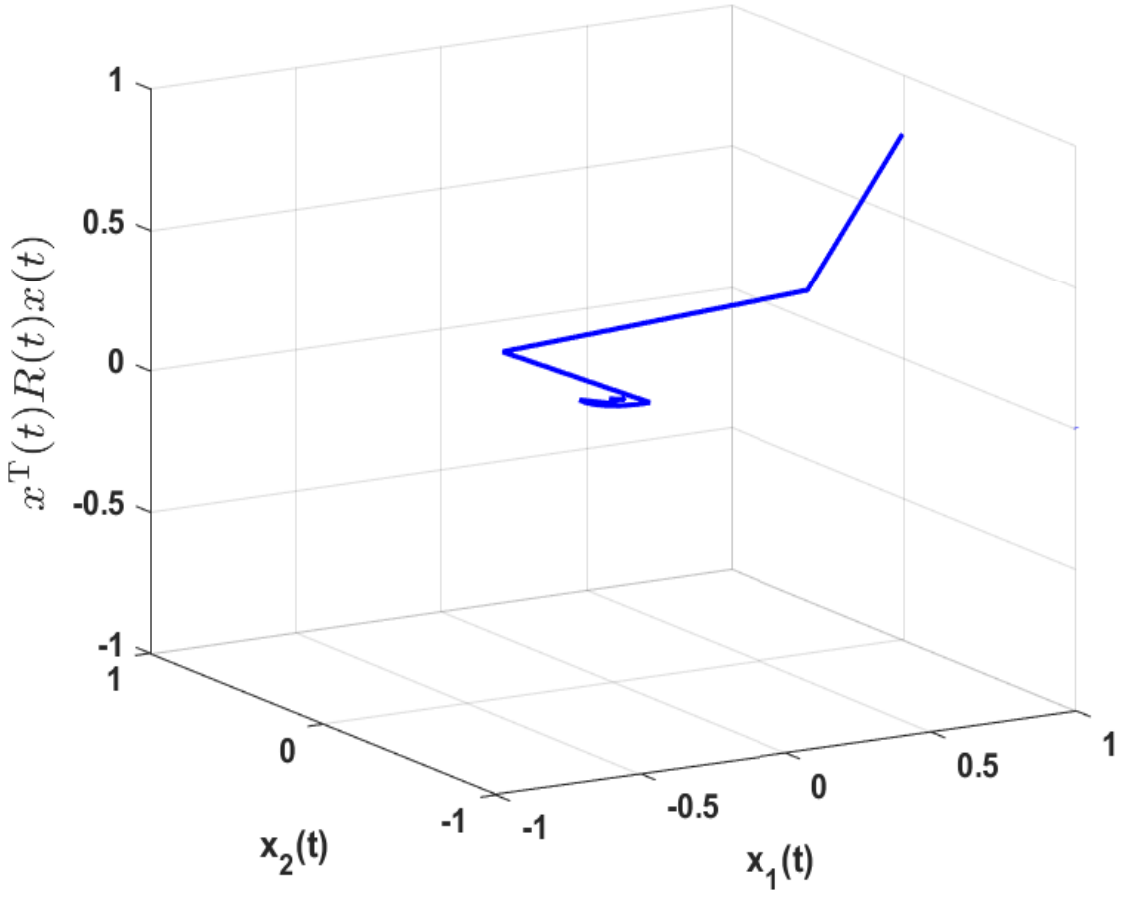

Figure 3. The evolution of $x^{\mathrm{T}}(t)Rx(t)$.

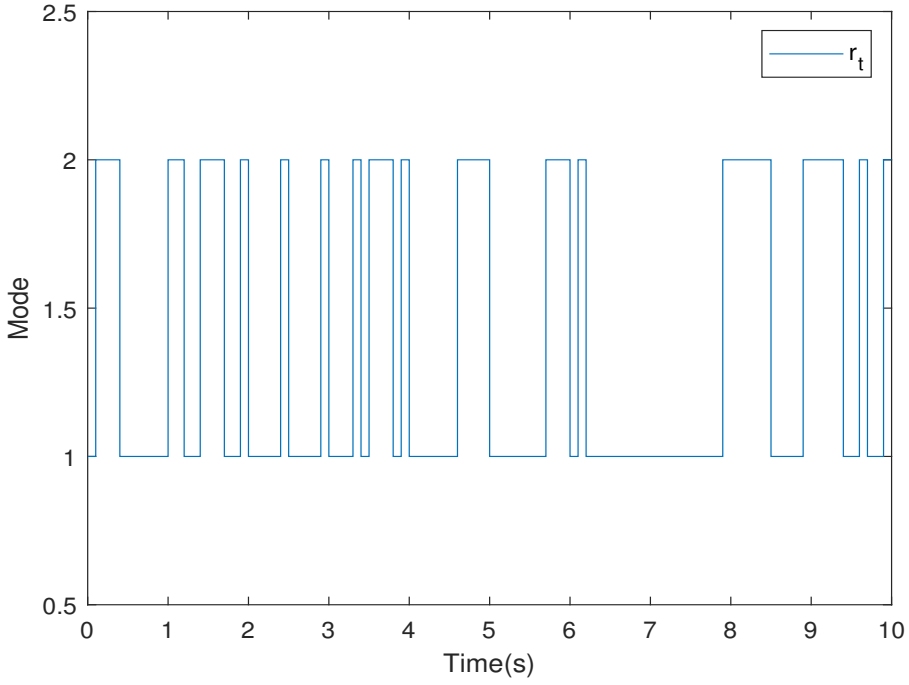

Figure 4. The system mode r_t.

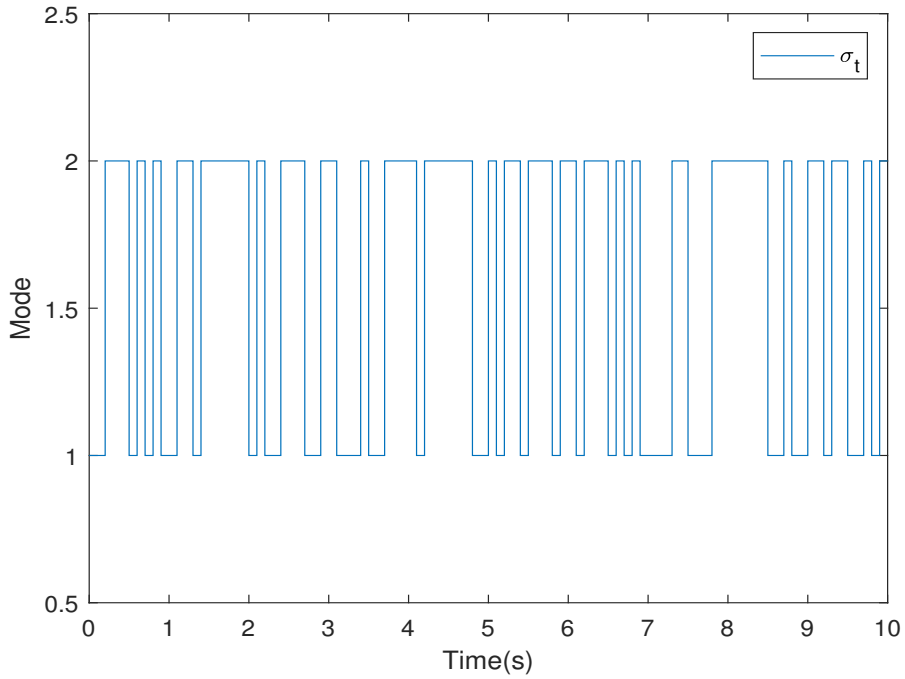

Figure 5. The controller mode σ_t.

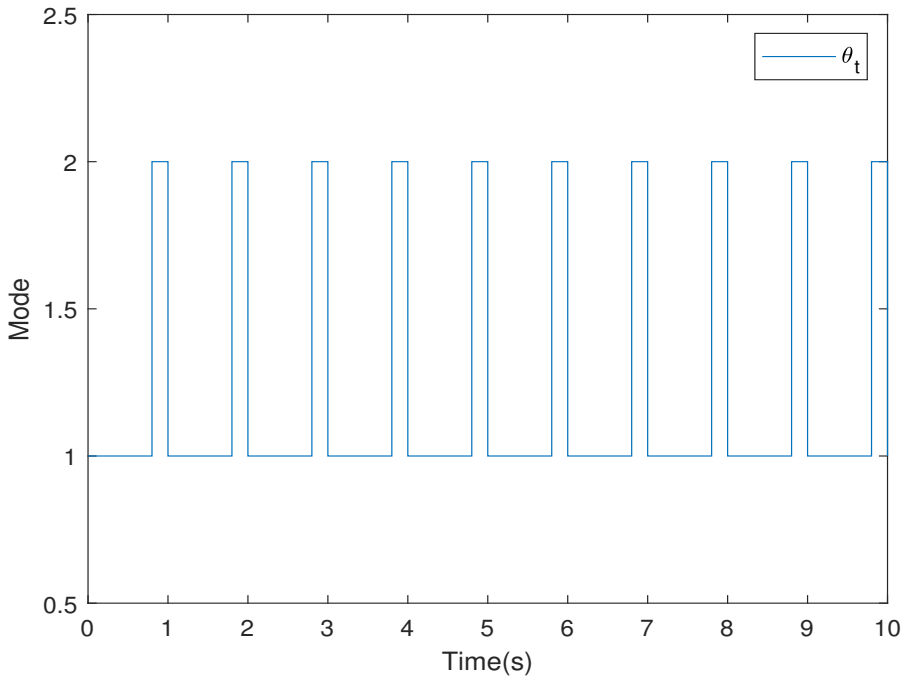

Figure 6. Value of θ_t .

The trajectories of the state response are shown in Figure 7. It can be clearly seen from Figure 8 that the evolution of $x^{\mathrm{T}}(t)Rx(t)$ tends to zero in finite time, and the designed synchronous controllers can make non-homogeneous HSMJSs (5) become SFTB. These figures fully demonstrate the effectiveness of the method presented in this paper.

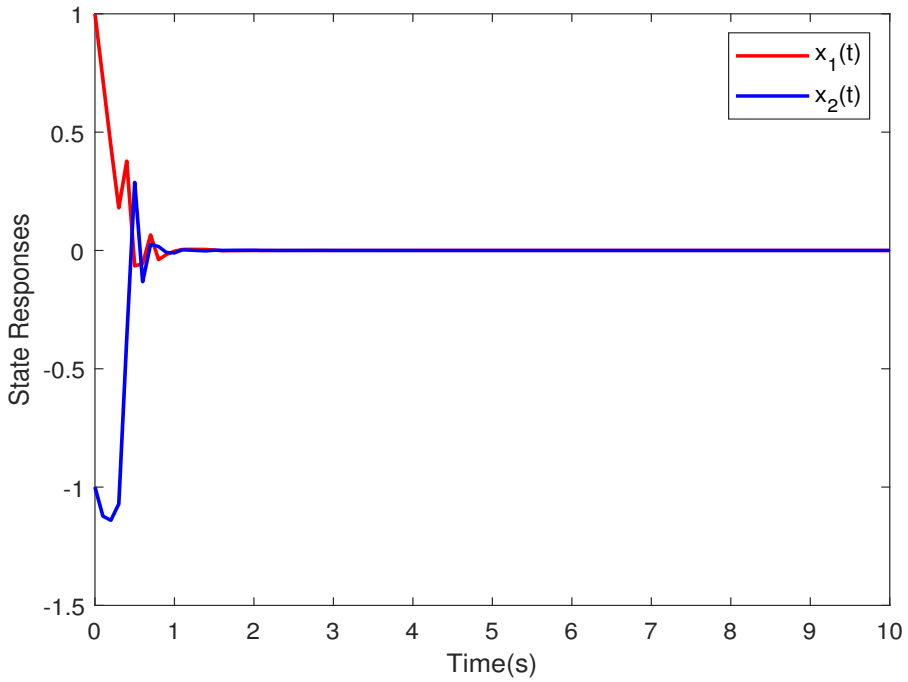

Figure 7. State response of closed-loop system.

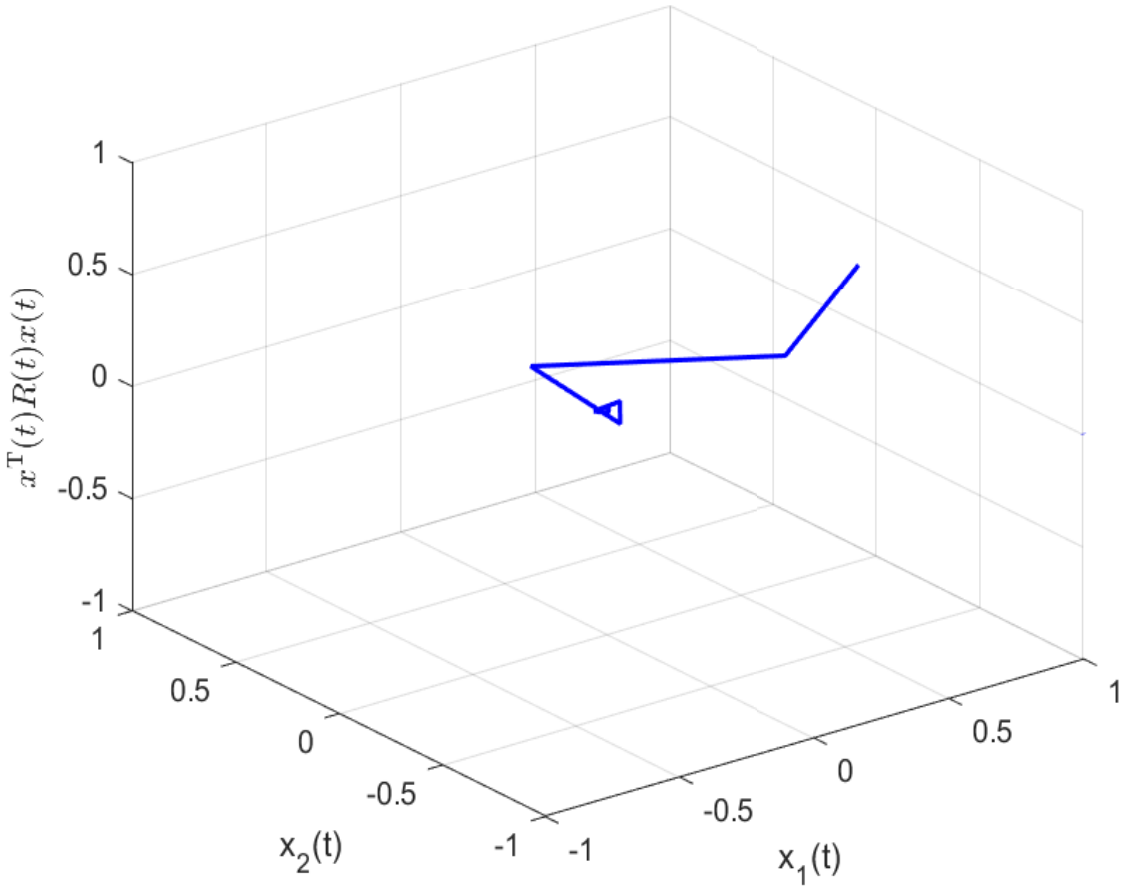

Figure 8. The evolution of $x^{\mathrm{T}}(t)Rx(t)$.

Remark 4. *From case I and case II, it can be seen that, differing from the existing literature [30,31], the method adopted in this paper can not only deal with the stochastic finite-time boundedness problem in the case of an asynchronous controller and system mode but also with the stochastic*

finite-time boundedness problem in the case of a synchronous controller and system mode, so the method in this paper has wider practicability and generality.

Example 2. *Next, we consider a single-link robot arm system from [28], which can be expressed as*

$$\ddot{\psi}(t) = -\frac{M_{r_t} g L}{J_{r_t}} \sin(\psi(t)) - \frac{W}{J_{r_t}} \dot{\psi}(t) + \frac{1}{J_{r_t}} u(t),$$

in which $\psi(t)$, $\dot{\psi}(t)$, and $\ddot{\psi}(t)$ separately stand for the angle, angular velocity, and angular acceleration, J_{r_t} represents the moment of inertia, M_{r_t} and L are the total mass and the length of the arm, respectively, g denotes the gravitational acceleration, and W is the coefficient of viscous friction. The robot runs under different payloads that obey the SMP $\{r_t, t \geq 0\}$ in $\mathcal{M}_1$, and $\{\sigma_t, t \geq 0\}$ in $\mathcal{M}_2$ is the asynchronous controller mode. Define $x(t) = [x_1^{\mathrm{T}}(t) \;\; x_2^{\mathrm{T}}(t)]^{\mathrm{T}}$, where $x_1(t) = \psi(t)$ and $x_2(t) = \dot{\psi}(t)$. Thus, when $r_t = i$, one has the linearized system

$$\dot{x}(t) = \begin{bmatrix} 0 & 1 \\ -\frac{M_i g L}{J_i} & -\frac{W}{J_i} \end{bmatrix} x(t) + \begin{bmatrix} 0 \\ \frac{1}{J_i} \end{bmatrix} u(t).$$

For every single-link robot arm, let $J_1 = 0.15$, $J_2 = 0.25$, $M_1 = 0.5$, $M_2 = 1$, $L = 0.5$, $W = 2$, $g = 9.81$, $x_0 = [2, -1]^{\mathrm{T}}$, and $\omega(t) = sin(t)$. The other parameters are the same as in Example 1 Case I. Solving Theorem 2, we obtain the three-variable-dependent asynchronous feedback control gain matrix:

$$\begin{aligned}
\left[\begin{array}{c|c} K_{111} & K_{121} \end{array}\right] &= \left[\begin{array}{cc|cc} 1.7565 & 0.5955 & 1.7306 & 0.5424 \end{array}\right], \\
\left[\begin{array}{c|c} K_{211} & K_{221} \end{array}\right] &= \left[\begin{array}{cc|cc} 2.6850 & 0.7930 & 0.6636 & 0.1921 \end{array}\right], \\
\left[\begin{array}{c|c} K_{112} & K_{122} \end{array}\right] &= \left[\begin{array}{cc|cc} 1.7636 & 0.5599 & 1.7808 & 0.5968 \end{array}\right], \\
\left[\begin{array}{c|c} K_{212} & K_{221} \end{array}\right] &= \left[\begin{array}{cc|cc} 2.4764 & 0.6709 & 0.6141 & 0.1638 \end{array}\right].
\end{aligned}$$

The trajectories of the state response are shown in Figure 9. It can be clearly seen from Figure 10 that the evolution of $x^{\mathrm{T}}(t)Rx(t)$ tends to zero in finite time, and the designed asynchronous controllers can make non-homogeneous HSMJSs (5) *become SFTB.*

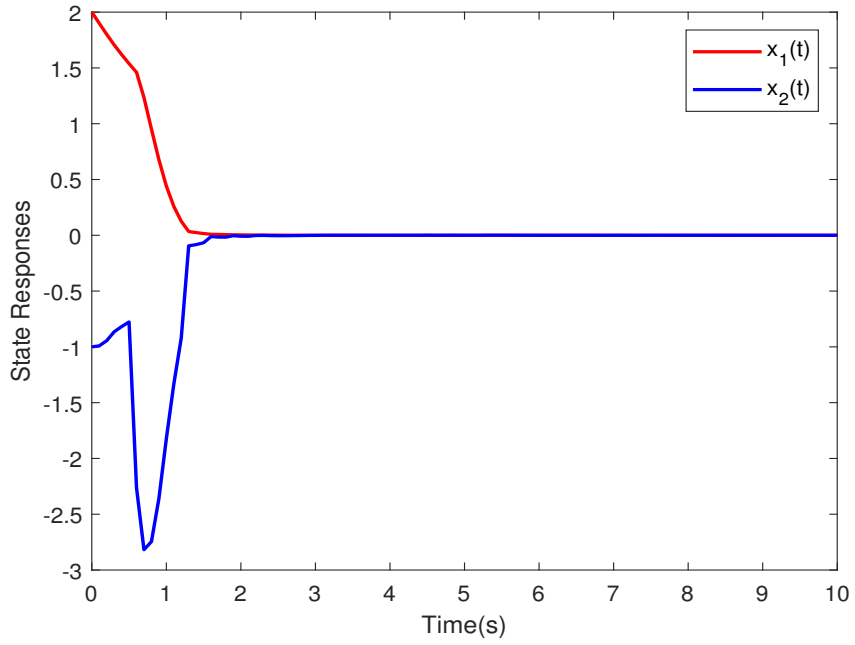

Figure 9. State response of closed-loop system.

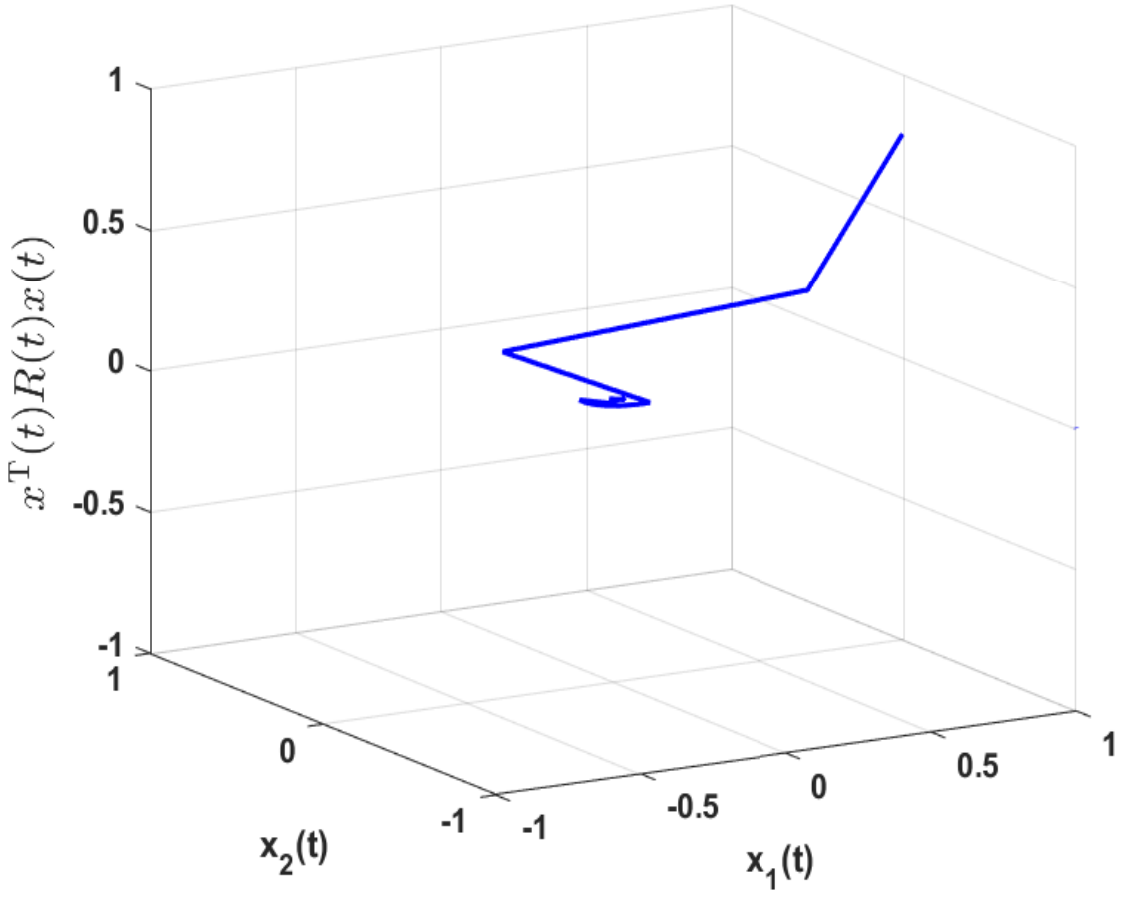

Figure 10. The evolution of $x^{\mathrm{T}}(t)Rx(t)$.

5. Conclusions

This article explores the finite-time control problem associated with a specific category of non-homogeneous hidden semi-Markov jump systems. A novel piecewise homogeneous strategy is presented to adequately address the challenges posed by the non-homogeneous nature of the system. Furthermore, based on Lyapunov theory, the closed-loop non-homogeneous HSMJSs can be stochastically finite-time-bounded and satisfy the H_∞ performance. To demonstrate the practical applicability and effectiveness of the proposed method, two simulation examples were employed. The issue of cyber attacks targeting network control systems has emerged as a significant concern this year, prompting us to investigate it further in our upcoming research. This study will investigate the finite-time stability of non-homogeneous hidden semi-Markov jump systems within the context of complex cyber attack environments.

Author Contributions: Conceptualization, Q.W.; methodology, Q.W.; writing—original draft preparation, Q.W.; writing—review and editing, Q.W.; supervision, Y.S. and K.S.; funding acquisition, X.Z. All authors have read and agreed to the published version of the manuscript.

Funding: This research was supported by the National Natural Science Foundation of China under Grant No. 62371094.

Data Availability Statement: Dataset available upon request from the authors.

Conflicts of Interest: The authors declare no conflicts of interest.

References

1. Wu, Z.; Shi, P.; Shu, Z.; Su, H.; Lu, R. Passivity-Based Asynchronous Control for Markov Jump Systems. *IEEE Trans. Autom. Control* **2017**, *62*, 2020–2025. [CrossRef]
2. Wang, Y.; Zhuang, G.; Chen, X.; Wang, Z.; Chen, F. Dynamic event-based finite-time mixed H_∞ and passive asynchronous filtering for T-S fuzzy singular Markov jump systems with general transition rates. *Nonlinear Anal.-Hybrid Syst.* **2020**, *36*, 100874. [CrossRef]
3. Cheng, J.; Wu, Y.; Yan, H.; Wu, Z.; Shi, K. Protocol-based filtering for fuzzy Markov affine systems with switching chain. *Automatica* **2022**, *141*, 110321. [CrossRef]
4. Wang, H.; Luan, X.; Stojanovic, V.; Liu, F. Self-triggered finite-time control for discrete-time Markov jump systems. *Inf. Sci.* **2023**, *634*, 101–121.
5. Shen, H.; Hu, X.; Wang, J.; Cao, J.; Qian, W. Non-Fragile H_∞ Synchronization for Markov Jump Singularly Perturbed Coupled Neural Networks Subject to Double-Layer Switching Regulation. *IEEE Trans. Neural Netw. Learn. Syst.* **2023**, *34*, 2682–2692. [CrossRef]
6. Li, F.; Wu, L.; Shi, P.; Lim, C. State estimation and sliding mode control for semi-Markovian jump systems with mismatched uncertainties. *Automatica* **2015**, *51*, 385–393. [CrossRef]
7. Shen, H.; Park, J.; Wu, Z.; Zhang, Z. Finite-time H_∞ synchronization for complex networks with semi-Markov jump topology. *Commun. Nonlinear Sci. Numer. Simul.* **2015**, *24*, 40–51. [CrossRef]
8. Wang, B.; Zhu, Q. Stability analysis of semi-Markov switched stochastic systems. *Automatica* **2018**, *94*, 72–80. [CrossRef]
9. Wang, J.; Hu, X.; Wei, Y.; Wang, Z. Sampled-data synchronization of semi-Markov jump complex dynamical networks subject to generalized dissipativity property. *Appl. Math. Comput.* **2019**, *346*, 853–864. [CrossRef]
10. Zhang, L.; Lam, H.; Liang, Y.S.H. Fault Detection for Fuzzy Semi-Markov Jump Systems Based on Interval Type-2 Fuzzy Approach. *IEEE Trans. Fuzzy Syst.* **2020**, *28*, 2375–2388. [CrossRef]
11. Yang, J.; Zhu, Y.; Zhang, L.; Duan, G. Smooth control with flexible duration for semi-Markov jump linear systems. *Automatica* **2024**, *164*, 111612. [CrossRef]
12. Wang, Q.; Zhang, X.; Zhang, R. Finite-time H_∞ control for continuous-time non-homogeneous semi-Markov jump systems. In Proceedings of the 2023 IEEE 11th International Conference on Information, Communication and Networks, Xi'an, China, 17–20 August 2023.
13. Kim, S. Stochastic stability and stabilization conditions of semi-Markovian jump systems with mode transition-dependent sojourn-time distributions. *Inf. Sci.* **2017**, *385–386*, 314–324. [CrossRef]
14. Nguyen, K.; Kim, S. Observer-based control design of semi-Markovian jump systems with uncertain probability intensities and mode-transition-dependent sojourn-time distribution. *Appl. Math. Comput.* **2020**, *372*, 124968. [CrossRef]
15. Cheng, J.; Xie, L.; Park, J.; Yan, H. Protocol-Based Output-Feedback Control for Semi-Markov Jump Systems. *IEEE Trans. Autom. Control* **2022**, *67*, 4346–4353. [CrossRef]
16. Wang, D.; Wu, F.; Lian, J.; Li, S. Observer-Based Asynchronous Control for Stochastic Nonhomogeneous Semi-Markov Jump Systems. *IEEE Trans. Autom. Control* **2024**, *69*, 2559–2566. [CrossRef]
17. Zhang, L.; Sun, Y.; Li, H.; Liang, H.; Wang, J. Event-triggered fault detection for nonlinear semi-Markov jump systems based on double asynchronous filtering approach. *Automatica* **2022**, *138*, 110144. [CrossRef]
18. Men, Y.; Sun, J. Asynchronous Control of 2-D Semi-Markov Jump Systems Under Actuator Saturation. *IEEE Trans. Circuits Syst. II-Express Briefs* **2023**, *70*, 4118–4122. [CrossRef]
19. Li, R.; Qi, W.; Park, J.; Cheng, J.; Shi, K. Sliding mode control for discrete interval type-2 fuzzy semi-Markov jump models with delay in controller mode switching. *Fuzzy Sets Syst.* **2024**, *483*, 108915. [CrossRef]
20. Liu, Y.; Wu, H.; Zhang, X. Stability and H_∞ performance of human-in-the-loop control systems through hidden semi-Markov human behavior modeling. *Appl. Math. Model.* **2023**, *116*, 799–815. [CrossRef]
21. Cai, B.; Zhang, L.; Shi, Y. Control Synthesis of Hidden Semi-Markov Uncertain Fuzzy Systems via Observations of Hidden Modes. *IEEE Trans. Cybern.* **2020**, *50*, 3709–3718. [CrossRef] [PubMed]
22. Men, Y.; Sun, J. H_∞ control of singularly perturbed systems using deficient hidden semi-Markov model. *Nonlinear Anal.-Hybrid Syst.* **2024**, *52*, 101453. [CrossRef]
23. Wu, E.; Zhu, L.; Li, G.; Li, H. Nonparametric Hierarchical Hidden Semi-Markov Model for Brain Fatigue Behavior Detection of Pilots during Flight. *IEEE Trans. Intell. Transp. Syst.* **2022**, *23*, 5245–5256. [CrossRef]
24. Li, F.; Zheng, W.; Xu, S. Stabilization of Discrete-Time Hidden Semi-Markov Jump Singularly Perturbed Systems with Partially Known Emission Probabilities. *IEEE Trans. Autom. Control* **2022**, *67*, 4234–4240. [CrossRef]
25. Zhang, L.; Cai, B.; Tan, T. Stabilization of non-homogeneous hidden semi-Markov Jump systems with limited sojourn-time information. *Automatica* **2020**, *117*, 108963. [CrossRef]
26. Shen, H.; Zhang, Z.; Li, F.; Yan, H. Non-Fragile H_∞ Control for Piecewise Homogeneous Hidden Semi-Markov Lur'e Systems. *IEEE Trans. Circuits Syst. II-Express Briefs* **2024**, *71*, 306–310. [CrossRef]
27. He, S.; Song, J.; Liu, F. Robust Finite-Time Bounded Controller Design of Time-Delay Conic Nonlinear Systems Using Sliding Mode Control Strategy. *IEEE Trans. Syst. Man Cybern.* **2018**, *48*, 1863–1873. [CrossRef]
28. Qi, W.; Zong, G.; Ahn, C. Input-Output Finite-Time Asynchronous SMC for Nonlinear Semi-Markov Switching Systems with Application. *IEEE Trans. Syst. Man Cybern.* **2022**, *52*, 5344–5353. [CrossRef]

29. Xia, Z.; He, S. Finite-time asynchronous H_∞ fault-tolerant control for nonlinear hidden markov jump systems with actuator and sensor faults. *Appl. Math. Comput.* **2022**, *428*, 127212. [CrossRef]
30. Wang, J.; Ru, T.; Xia, J. Finite-time synchronization for complex dynamic networks with semi-Markov switching topologies: An H_∞ event-triggered control scheme. *Appl. Math. Comput.* **2019**, *356*, 235–251. [CrossRef]
31. Zhong, S.; Zhang, W.; Li, K. Finite-time stability and asynchronous resilient control for Itô stochastic semi-Markovian jump systems. *J. Frankl. Inst.* **2022**, *359*, 1531–1557. [CrossRef]

mathematics

MDPI

Article

Wave Speeds for a Time-Periodic Bistable Three-Species Lattice Competition System

Chaohong Pan [1], Jiali Zhan [2] and Hongyong Wang [2,*]

[1] School of Mathematics and Statistics, Hunan First Normal University, Changsha 410205, China; chaohongpan2020@163.com
[2] School of Mathematics and Physics, University of South China, Hengyang 421001, China; zhanjiali0000@163.com
* Correspondence: uscwanghy@163.com

Abstract: In this paper, we consider propagation direction (which can be used to predict which species will occupy the habitat or win the competition eventually) of a bistable wave for a three-species time-periodic lattice competition system with bistable nonlinearity, aiming to address an open problem. As a first step, by transforming the competition system to a cooperative one, we study the asymptotic behavior for the bistable wave profile and then prove the uniqueness of the bistable wave speed. Secondly, we utilize comparison principle and build up two couples of upper and lower solutions to judge the sign of the bistable wave speed which partially provides the answer to the open problem. As an application, we reduce the time-periodic system to a space–time homogeneous system, we obtain the corresponding criteria and carry out numerical simulations to illustrate the availability of our results. Moreover, an interesting phenomenon we have found is that the two weak competitors can wipe out the strong competitor under some circumstances.

Keywords: propagation direction; bistable wave; lattice system

MSC: 35A01; 35C07; 35K57

1. Introduction

This paper is devoted to the propagation direction, which is determined by the sign of wave speed, of traveling wave solutions (TWSs) for the following bistable lattice system

$$\begin{cases} u_j'(t) = d_1(t)\mathcal{D}_2[u_j](t) + u_j(t)(r_1(t) - a_{11}(t)u_j(t) - a_{12}(t)v_j(t)), \\ v_j'(t) = d_2(t)\mathcal{D}_2[v_j](t) + v_j(t)(r_2(t) - b_{11}(t)v_j(t) - b_{12}(t)u_j(t) - b_{13}(t)w_j(t)), \\ w_j'(t) = d_3(t)\mathcal{D}_2[w_j](t) + w_j(t)(r_3(t) - c_{11}(t)w_j(t) - c_{12}(t)v_j(t)), \ j \in \mathbb{Z}, t > 0. \end{cases} \tag{1}$$

In model (1) and in the sense of biology, one can interpret $u_j(t), v_j(t)$ and $w_j(t)$ as the population densities of three species at position j and time t, respectively, $d_i(t)$ as the diffusivity coefficient and $r_i(t)$ as the growth rate of the species. Here, the coefficients $a_{1i}(t), c_{1i}(t), i = 1, 2$ and $d_k(t), b_{1k}(t), k = 1, 2, 3$ are assumed to be positive T-periodic functions with T being a positive number. Biologically speaking, $a_{1i}(t), b_{1k}(t), c_{1i}(t)$ are the intra-specific competitive coefficients as $i = k = 1$, while $i = 2$ or $k = 2, 3$, they represent the inter-specific competitive coefficients. The term $\mathcal{D}_2[s_j](t)$ appearing in (1) is the second-order central difference and is defined as $\mathcal{D}_2[s_j](t) := s(t, j+1) + s(t, j-1) - 2s(t, j)$ for $s = u, v, w$. Evidently, system (1) is a competitive system and models such a relationship between three species: v competes with u and w for common resources, while there is no competition between u and w. The biological interpretation is that species u and w have different preferences for food resources, while species v has the same food preferences as u and w.

As we all know, nature is a constantly changing and relatively stable system, in which competition for survival between species is a common phenomenon. Therefore, to study the dynamic behavior between different species, it is necessary to study the phenomenon of competition between species and establish a reasonable model. The Lotka–Volterra competitive diffusion system is one of the classical biological models to describe inter- and intra-specific interactions. When the environment is assumed to be homogenous, the general form of the three-species Lotka–Volterra competition diffusion model in the above biological context is as follows:

$$\begin{cases} u_t = d_1 u_{xx} + r_1 u(1 - u - a_1 v), \\ v_t = d_2 v_{xx} + r_2 v(1 - v - a_2 u - a_3 w), \\ w_t = d_3 w_{xx} + r_3 w(1 - w - a_4 v), t \in \mathbb{R}^+, x \in \mathbb{R}, \end{cases} \tag{2}$$

where $d_k, r_k, k = 1, 2, 3$ and $a_l, l = 1, 2, 3, 4$ are positive constants. As a matter of fact, system (2) can be regarded as an extension of the classic two-species Lotka–Volterra system which has been studied extensively in past decades; see, for example, [1–7] and references therein. Due to the benefit from the classic Lotka–Volterra system in the application of ecology, more and more works have also been devoted to system (2). For instance, we refer the readers to [8,9] for the selection mechanism of minimum wave speed in the monostable model; [10] for the stability of monotone traveling wave solutions; ref. [11] for the exact traveling wave solutions of (2) with nontrivial three components; ref. [12] for the uniqueness of traveling wavefronts; and ref. [13,14] for the sign of wave speed in the bistable model. Related to the present paper, we particularly mention that Guo et al. [13] studied two different cases for system (2): (1) the case where two species are weakly competitive and one species is strongly competitive, and (2) the case where all three species are very strong competitors. They obtained some new observations in contrast with the two-species Lotka–Volterra model. In addition to system (2), we further refer the readers to [15–19] for a discrete three-species competition system; refs. [20,21] for a three-component competition system with nonlocal dispersal; and refs. [22,23] for a competitive–cooperative Lotka–Volterra system of three species.

In their recent paper, besides model (2), Guo et al. [13] also proposed a discrete version of (2), as follows:

$$\begin{cases} u_j'(t) = d_1 \mathcal{D}_2[u_j](t) + r_1[u_j(1 - u_j - b_2 v_j)](t), \\ v_j'(t) = d_2 \mathcal{D}_2[v_j](t) + r_2[v_j(1 - b_1 u_j - v_j - b_3 w_j)](t), \\ w_j'(t) = d_3 \mathcal{D}_2[w_j](t) + r_3[w_j(1 - b_2 v_j - w_j)](t), t \in \mathbb{R}^+, j \in \mathbb{Z}, \end{cases} \tag{3}$$

where the parameters d_k, r_k and $b_k, k = 1, 2, 3$ are positive numbers and can be interpreted as the ones in system (2). In (3), although the sign of wave speed of (2) has been addressed for certain special cases, it is still largely left open for the discrete case (3). One of the reasons is that their method used on system (2) relies on the integration of the corresponding wave profile system, so it seems that such a method cannot be applied to system (3) directly due to the central difference involved in (3). Another reason might be that the combination of patchy environments and periodicity can make the corresponding analysis more difficult. In this paper, we try to make some progress in this direction and this is our main motivation. Our strategy is to use the upper/lower solution method to investigate the sign of the bistable wave speed of (1). As a matter of fact, this method has been proved to be valid in this subject for several diffusion systems; see, for instance, [4,6,9,24].

In recent years, an increasing number of scholars are attracted to traveling wave solutions that have advantages in describing the development, migration and invasion of biological populations. In particular, the sign of wave speed of traveling wave solutions can be used to explain the outcome of competition between different species, which makes it a meaningful topic. In this paper, we will study the propagation direction of traveling wave solutions for (1) which is a lattice competition system. To the best of our knowledge, the

research of lattice dynamical systems, which are more in line with nature, originated from Bunimovich and Sinai [25] in 1988. After that, lattice dynamical models have widely been used in biological issues; see, for example, [6,26–30]. Generally speaking, these models are more effective in the case of species living in patchy environments.

Evidently, the corresponding space-homogenous ordinary differential system of (1) is as follows:

$$\begin{cases} u'(t) = u(t)[r_1(t) - a_{11}(t)u(t) - a_{12}(t)v(t)], \\ v'(t) = v(t)[r_2(t) - b_{11}(t)v(t) - b_{12}(t)u(t) - b_{13}(t)w(t)], \\ w'(t) = w(t)[r_3(t) - c_{11}(t)w(t) - c_{12}(t)v(t)], t \in \mathbb{R}^+. \end{cases} \tag{4}$$

It is easy to see that system (4) at least has three nonnegative T-periodic solutions, which are the equilibrium points of (1). We denote them by $e_0 := (0,0,0), e_1 := (0,q(t),0)$, $e_2 := (p(t),0,r(t))$, respectively, in which $p(t), q(t), r(t)$ can be expressed as

$$p(t) = \frac{p_0 e^{\int_0^t r_1(s)ds}}{p_0 \int_0^t a_{11}(s) e^{\int_0^s r_1(\theta)d\theta} ds + 1}, p_0 = \frac{e^{\int_0^T r_1(s)ds} - 1}{\int_0^T a_{11}(s) e^{\int_0^s r_1(\theta)d\theta} ds},$$

$$q(t) = \frac{q_0 e^{\int_0^t r_2(s)ds}}{q_0 \int_0^t b_{11}(s) e^{\int_0^s r_2(\theta)d\theta} ds + 1}, \; q_0 = \frac{e^{\int_0^T r_2(s)ds} - 1}{\int_0^T b_{11}(s) e^{\int_0^s r_2(\theta)d\theta} ds},$$

$$r(t) = \frac{r_0 e^{\int_0^t r_3(s)ds}}{r_0 \int_0^t c_{11}(s) e^{\int_0^s r_3(\theta)d\theta} ds + 1}, r_0 = \frac{e^{\int_0^T r_3(s)ds} - 1}{\int_0^T c_{11}(s) e^{\int_0^s r_3(\theta)d\theta} ds}.$$

It is straightforward to check that $p(t), q(t)$ and $r(t)$ are T-periodic functions and satisfy $p(t+T) = p(t), q(t+T) = q(t)$ and $r(t+T) = r(t)$ for all $t \in \mathbb{R}^+$.

Since our main focus is on bistable waves of (1), we have to make the following assumption throughout this paper:

(A) $\int_0^T r_1(t)dt < \int_0^T a_{12}(t)q(t)dt, \int_0^T r_2(t)dt < \int_0^T b_{12}(t)p(t) + b_{13}(t)r(t)dt$ and $\int_0^T r_3(t)dt < \int_0^T c_{12}(t)q(t)dt$,

so that e_1 and e_2 are linearly stable equilibrium points.

As mentioned above, we are concerned with the periodic traveling wave of system (1), which bears the form of

$$\begin{pmatrix} u_j(t) \\ v_j(t) \\ w_j(t) \end{pmatrix} = \begin{pmatrix} U(t, j+ct) \\ V(t, j+ct) \\ W(t, j+ct) \end{pmatrix} =: \begin{pmatrix} U(t,z) \\ V(t,z) \\ W(t,z) \end{pmatrix}, \; z = j + ct, \tag{5}$$

satisfying

$$\begin{pmatrix} U(t+T,z) \\ V(t+T,z) \\ W(t+T,z) \end{pmatrix} = \begin{pmatrix} U(t,z) \\ V(t,z) \\ W(t,z) \end{pmatrix},$$

and is subject to the boundary conditions

$$(U,V,W)(t,-\infty) = (0,0,0), (U,V,W)(t,+\infty) = (1,1,1), \tag{6}$$

where c is the wave speed. The limits in (6) hold uniformly in $t \in \mathbb{R}^+$.

After a substitution of (5), (1) can be rewritten as a wave profile system

$$\begin{cases} U_t + cU_z = d_1(t)\mathcal{D}_2[U](t,z) + U(r_1(t) - a_{11}(t)U - a_{12}(t)V), \\ V_t + cV_z = d_2(t)\mathcal{D}_2[V](t,z) + V(r_2(t) - b_{11}(t)V - b_{12}(t)U - b_{13}(t)W), \\ W_t + cW_z = d_3(t)\mathcal{D}_2[W](t,z) + W(r_3(t) - c_{11}(t)W - c_{12}(t)V), \end{cases} \tag{7}$$

where $\mathcal{D}_2[S](t,z) = S(t,z+1) + S(t,z-1) - 2S(t,z)$ for $S = U, V, W$. Via the following changes

$$\Phi(t,z) = \frac{p(t) - U(t,z)}{p(t)}, \Psi(t,z) = \frac{V(t,z)}{q(t)}, \Theta(t,z) = \frac{r(t) - W(t,z)}{r(t)},$$

system (7) can be converted into a cooperative system

$$\begin{cases} d_1(t)\mathcal{D}_2[\Phi](t,z) - c\Phi_z + (1-\Phi)[a_{12}(t)q(t)\Psi - a_{11}(t)p(t)\Phi] = \Phi_t, \\ d_2(t)\mathcal{D}_2[\Psi](t,z) - c\Psi_z + \Psi[b_{11}(t)q(t)(1-\Psi) - b_{12}(t)p(t)(1-\Phi) - b_{13}(t)r(t)(1-\Theta)] = \Psi_t, \\ d_3(t)\mathcal{D}_2[\Theta](t,z) - c\Theta_z + (1-\Theta)[c_{12}(t)q(t)\Psi - c_{11}(t)r(t)\Theta] = \Theta_t, \end{cases} \tag{8}$$

with periodic conditions and boundary conditions (6) becoming

$$\begin{cases} (\Phi,\Psi,\Theta)(t,z) = (\Phi,\Psi,\Theta)(t+T,z), \\ (\Phi,\Psi,\Theta)(t,-\infty) = (0,0,0), (\Phi,\Psi,\Theta)(t,+\infty) = (1,1,1). \end{cases}$$

For the sake of convenience, we shall call the first equation of (8) Φ-equation, the second equation Ψ-equation and the last one Θ-equation throughout this paper. Note that the existence of a bistable periodic traveling wave solution of (1) can be proved by following the ideas in [16,31], or by the abstract theory established in [32].

The remainder of this paper is organized as follows. In Section 2, we investigate the asymptotic behaviors of $\Phi(t,z), \Psi(t,z)$ and $\Theta(t,z)$ as the co-moving coordinate z tends to infinity, upon which the uniqueness of bistable wave speed is considered. In Section 3, we derive two crucial theorems concerning the determination of the sign of the bistable wave speed by employing the comparison principle. We construct suitable upper/lower solutions to obtain explicit conditions in Section 4, and the results of numerical simulation are shown in Section 5.

2. Uniqueness of Bistable Wave-Speed

To facilitate the forthcoming calculation and statement, we define some mathematical notations as follows:

$$\begin{aligned} &\overline{f(t)} := \frac{1}{T}\int_0^T f(t)dt, \quad \Delta_1(t) := b_{11}(t)q(t) - b_{12}(t)p(t) - b_{13}(t)r(t), \\ &\Delta_2(t) := a_{11}(t)p(t) - a_{12}(t)q(t), \quad \Delta_3(t) := c_{11}(t)r(t) - c_{12}(t)q(t), \\ &\Gamma_1(t,\mu) := d_1(t)(e^{\mu} + e^{-\mu} - 2) - c\mu - a_{11}(t)p(t), \\ &\Gamma_2(t,\mu) := d_3(t)(e^{\mu} + e^{-\mu} - 2) - c\mu - c_{11}(t)r(t), \\ &\Gamma_3(t,\mu) := d_2(t)(e^{\mu} + e^{-\mu} - 2) + c\mu - b_{11}(t)q(t). \end{aligned}$$

To investigate the asymptotic behavior of the bistable wave profile, we denote the unique positive solutions of the following equations

$$\begin{aligned} &\overline{d_2(t)}(e^{\mu} + e^{-\mu} - 2) - c\mu + \overline{\Delta_1(t)} = 0, \\ &\overline{d_1(t)}(e^{\mu} + e^{-\mu} - 2) - c\mu - \overline{a_{11}(t)p(t)} = 0, \\ &\overline{d_3(t)}(e^{\mu} + e^{-\mu} - 2) - c\mu - \overline{c_{11}(t)r(t)} = 0, \end{aligned}$$

by $\mu_1(c), \mu_2(c), \mu_3(c)$, respectively. Moreover, by a simple analysis, it is not hard to find that $\mu_1(c)$, $\mu_2(c)$ and $\mu_3(c)$ are increasing functions in c. Meanwhile, we denote $\mu_4(c)$, $\mu_5(c)$ and $\mu_6(c)$, respectively, by the unique positive roots of the following equations

$$\begin{aligned} &\overline{d_1(t)}(e^{\mu} + e^{-\mu} - 2) + c\mu + \overline{\Delta_2(t)} = 0, \\ &\overline{d_3(t)}(e^{\mu} + e^{-\mu} - 2) + c\mu + \overline{\Delta_3(t)} = 0, \\ &\overline{d_2(t)}(e^{\mu} + e^{-\mu} - 2) + c\mu - \overline{b_{11}(t)q(t)} = 0. \end{aligned}$$

Here, $\mu_4(c)$, $\mu_5(c)$, $\mu_6(c)$ are decreasing functions in c.

Based on the above notations, we are already to give the following lemma.

Lemma 1. *As $z \to -\infty$, the wave profile $(\Phi, \Psi, \Theta)(t,z)$ behaves like*

$$\begin{pmatrix}\Phi(t,z)\\ \Psi(t,z)\\ \Theta(t,z)\end{pmatrix} \sim A_1 \begin{pmatrix}\phi^*_{01}(t)\\ \psi_{01}(t)\\ \theta^*_{01}(t)\end{pmatrix} e^{\mu_1 z} + A_2 \begin{pmatrix}\phi_{01}(t)\\ 0\\ 0\end{pmatrix} e^{\mu_2 z} + A_3 \begin{pmatrix}0\\ 0\\ \theta_{01}(t)\end{pmatrix} e^{\mu_3 z}, \tag{9}$$

where $\mu_1 \neq \mu_2 \neq \mu_3$ and it holds uniformly in $t \in \mathbb{R}^+$. As $z \to \infty$, the wave profile $(\Phi, \Psi, \Theta)(t,z)$ behaves like

$$\begin{pmatrix}\Phi(t,z)\\ \Psi(t,z)\\ \Theta(t,z)\end{pmatrix} \sim \begin{pmatrix}1\\ 1\\ 1\end{pmatrix} - B_1 \begin{pmatrix}\phi_{11}(t)\\ \psi^*_{11}(t)\\ 0\end{pmatrix} e^{-\mu_4 z} - B_2 \begin{pmatrix}0\\ \psi^{**}_{11}(t)\\ \theta_{11}(t)\end{pmatrix} e^{-\mu_5 z} - B_3 \begin{pmatrix}0\\ \psi_{11}(t)\\ 0\end{pmatrix} e^{-\mu_6 z}, \tag{10}$$

where $\mu_4 \neq \mu_5 \neq \mu_6$ and it holds uniformly in $t \in \mathbb{R}^+$. In the above formulas, A_i, B_i, $i = 1,2,3$ are nonnegative numbers. The functions $\psi_{01}(t), \phi_{01}(t), \theta_{01}(t), \phi^*_{01}(t), \theta^*_{01}(t)$ are defined as (14), (18), (19), (21) and (22), respectively; and $\phi_{11}(t), \theta_{11}(t), \psi_{11}(t), \psi^*_{11}(t), \psi^{**}_{11}(t)$ are defined as (25), (26), (29), (30) and (31), respectively.

Proof. Firstly, we are concerned about the situation of $z \to -\infty$. It is clear that the linear system of (8) around the equilibrium $(0,0,0)$ can be represented by

$$\begin{cases} d_1(t)\mathcal{D}_2[\widehat{\Phi}](t,z) - c\widehat{\Phi}_z + a_{12}(t)q(t)\widehat{\Psi} - a_{11}(t)p(t)\widehat{\Phi} - \widehat{\Phi}_t = 0,\\ d_2(t)\mathcal{D}_2[\widehat{\Psi}](t,z) - c\widehat{\Psi}_z + [b_{11}(t)q(t) - b_{12}(t)p(t) - b_{13}(t)r(t)]\widehat{\Psi} - \widehat{\Psi}_t = 0,\\ d_3(t)\mathcal{D}_2[\widehat{\Theta}](t,z) - c\widehat{\Theta}_z + c_{12}(t)q(t)\widehat{\Psi} - c_{11}(t)r(t)\widehat{\Theta} - \widehat{\Theta}_t = 0. \end{cases} \tag{11}$$

Substituting $\widehat{\Psi} = \psi_{01}(t)e^{\mu z}$ into the second equation of (11), we can obtain the corresponding characteristic equation

$$d_2(t)(e^{\mu} + e^{-\mu} - 2) - c\mu + \Delta_1(t) - \frac{\psi'_{01}(t)}{\psi_{01}(t)} = 0, \tag{12}$$

where $\psi_{01}(t) > 0$ is a T-periodic function. Integrating both sides of Equation (12) from 0 to T gives

$$\overline{d_2(t)}(e^{\mu} + e^{-\mu} - 2) - c\mu + \overline{\Delta_1(t)} = 0. \tag{13}$$

Noticing $\int_0^T r_2(t)dt = \int_0^T b_{11}(t)q(t)dt$, and recalling assumption (**A**), it can be obtained that $\overline{\Delta_1(t)} < 0$. Thereby, Equation (13) has a unique positive root $\mu_1 := \mu_1(c)$. By putting $\mu = \mu_1$ into (12), $\psi_{01}(t)$ then can be calculated as

$$\psi_{01}(t) = \psi_{01} \exp\left(\int_0^t \Big(d_2(s)(e^{\mu_1} + e^{-\mu_1} - 2) - c\mu_1 + \Delta_1(s) \Big) ds \right), \tag{14}$$

with $\psi_{01}(0) = \psi_{01} > 0$. Thus, the asymptotic behavior of $\Psi(t,z)$ as $z \to -\infty$ can be expressed as

$$\Psi(t,z) \sim A_1 \psi_{01}(t) e^{\mu_1 z}. \tag{15}$$

Using the same approach, ignoring $a_{12}(t)q(t)\widehat{\Psi}$ and $c_{12}(t)q(t)\widehat{\Psi}$, it is clear that the linear equations for $\widehat{\Phi}$ and $\widehat{\Theta}$ of (11), respectively, are as follows

$$\begin{cases} d_1(t)\mathcal{D}_2[\widehat{\Phi}](t,z) - c\widehat{\Phi}_z - a_{11}(t)p(t)\widehat{\Phi} - \widehat{\Phi}_t = 0,\\ d_3(t)\mathcal{D}_2[\widehat{\Theta}](t,z) - c\widehat{\Theta}_z - c_{11}(t)r(t)\widehat{\Theta} - \widehat{\Theta}_t = 0. \end{cases} \tag{16}$$

Setting $\widehat{\Phi} = \phi_{01}(t)e^{\mu z}$ and $\widehat{\Theta} = \theta_{01}(t)e^{\mu z}$, (16) can be simplified as

$$\begin{cases} d_1(t)(e^{\mu} + e^{-\mu} - 2) - c\mu - a_{11}(t)p(t) - \dfrac{\phi'_{01}(t)}{\phi_{01}(t)} = 0, \\ d_3(t)(e^{\mu} + e^{-\mu} - 2) - c\mu - c_{11}(t)r(t) - \dfrac{\theta'_{01}(t)}{\theta_{01}(t)} = 0. \end{cases} \tag{17}$$

Likewise, we can obtain

$$\phi_{01}(t) = \phi_{01} \exp\left(\int_0^t \Gamma_1(s, \mu_2) ds \right), \tag{18}$$

$$\theta_{01}(t) = \theta_{01} \exp\left(\int_0^t \Gamma_2(s, \mu_3) ds \right). \tag{19}$$

In the first and third equation of (11), if the terms containing $\widehat{\Psi}$ are not considered, the asymptotic behaviors of $\widehat{\Phi}$ and $\widehat{\Theta}$ when $z \to -\infty$ can be expressed as $A_2\phi_{01}(t)e^{\mu_2 z}$ and $A_3\theta_{01}(t)e^{\mu_3 z}$. Next, we consider (11). Replacing $\widehat{\Psi}$ with $A_1\psi_{01}(t)e^{\mu_1 z}$, we obtain

$$\begin{cases} d_1(t)\mathcal{D}_2[\widehat{\Phi}](t,z) - c\widehat{\Phi}_z - a_{11}(t)p(t)\widehat{\Phi} - \widehat{\Phi}_t = -A_1 a_{12}(t)q(t)\psi_{01}(t)e^{\mu_1 z}, \\ d_3(t)\mathcal{D}_2[\widehat{\Theta}](t,z) - c\widehat{\Theta}_z - c_{11}(t)r(t)\widehat{\Theta} - \widehat{\Theta}_t = -A_1 c_{12}(t)r(t)\psi_{01}(t)e^{\mu_1 z}. \end{cases}$$

A simple calculation yields

$$\begin{cases} \Phi(t,z) \sim A_1\phi^*_{01}(t)e^{\mu_1 z} + A_2\phi_{01}(t)e^{\mu_2 z}, \\ \Theta(t,z) \sim A_1\theta^*_{01}(t)e^{\mu_1 z} + A_3\theta_{01}(t)e^{\mu_3 z}. \end{cases} \tag{20}$$

Here,

$$\phi^*_{01}(t) = \exp\left(\int_0^t \Gamma_1(s, \mu_1) ds \right) \cdot \left[\int_0^t a_{12}(s)q(s)\psi_{01}(s) \exp\left(-\int_0^s \Gamma_1(\tau, \mu_1) d\tau \right) ds + \phi^*_{01}(0) \right], \tag{21}$$

$$\theta^*_{01}(t) = \exp\left(\int_0^t \Gamma_2(s, \mu_1) ds \right) \cdot \left[\int_0^t c_{12}(s)r(s)\psi_{01}(s) \exp\left(-\int_0^s \Gamma_2(\tau, \mu_1) d\tau \right) ds + \theta^*_{01}(0) \right], \tag{22}$$

with

$$\phi^*_{01}(0) = \frac{\int_0^T a_{12}(s)q(s)\psi_{01}(s) \exp\left(-\int_0^s \Gamma_1(\tau, \mu_1) d\tau \right) ds}{\exp\left(-\int_0^T \Gamma_1(s, \mu_1) ds \right) - 1},$$

$$\theta^*_{01}(0) = \frac{\int_0^T c_{12}(s)r(s)\psi_{01}(s) \exp\left(-\int_0^s \Gamma_2(\tau, \mu_1) d\tau \right) ds}{\exp\left(-\int_0^T \Gamma_2(s, \mu_1) ds \right) - 1}.$$

By making use of the method of successive approximation (see, e.g., [33]), we conclude that (15) and (20) lead to (9).

Next, we intend to consider the asymptotic behavior of $(\Phi, \Psi, \Theta)(t,z)$ as $z \to \infty$. The linear system of (8) around the equilibrium $(1,1,1)$ can be expressed as follows

$$\begin{cases} d_1(t)\mathcal{D}_2[\widehat{\Phi}](t,z) - c\widehat{\Phi}_z + [a_{11}(t)p(t) - a_{12}(t)q(t)]\widehat{\Phi} - \widehat{\Phi}_t = 0, \\ d_2(t)\mathcal{D}_2[\widehat{\Psi}](t,z) - c\widehat{\Psi}_z - b_{11}(t)q(t)\widehat{\Psi} + b_{12}(t)p(t)\widehat{\Phi} + b_{13}(t)r(t)\widehat{\Theta} - \widehat{\Psi}_t = 0, \\ d_3(t)\mathcal{D}_2[\widehat{\Theta}](t,z) - c\widehat{\Theta}_z + [c_{11}(t)r(t) - c_{12}(t)q(t)]\widehat{\Theta} - \widehat{\Theta}_t = 0. \end{cases} \tag{23}$$

In a similar way, the characteristic equations of the first and last equations of (23) are given by

$$\begin{cases} d_1(t)(e^{-\mu}+e^{\mu}-2)+c\mu+\Delta_2(t)-\dfrac{\phi_{11}'(t)}{\phi_{11}(t)}=0, \\ d_3(t)(e^{-\mu}+e^{\mu}-2)+c\mu+\Delta_3(t)-\dfrac{\theta_{11}'(t)}{\theta_{11}(t)}=0, \end{cases} \tag{24}$$

where $\phi_{11}(t)>0, \theta_{11}(t)>0$ are T-periodic functions. From (24), we can solve that

$$\phi_{11}(t)=\phi_{11}\exp\left(\int_0^t\Big(d_1(s)(e^{\mu_4}-e^{-\mu_4}-2)+c\mu_4+\Delta_2(s)\Big)ds\right), \tag{25}$$

$$\theta_{11}(t)=\theta_{11}\exp\left(\int_0^t\Big(d_3(s)(e^{\mu_5}-e^{-\mu_5}-2)+c\mu_5+\Delta_3(s)\Big)ds\right), \tag{26}$$

with $\phi_{11}:=\phi_{11}(0)>0, \theta_{11}:=\theta_{11}(0)>0$. The asymptotic behaviors of $\Phi(t,z)$ and $\Theta(t,z)$ as $z\to\infty$ are given by

$$\begin{cases} \Phi(t,z)\sim 1-B_1\phi_{11}(t)e^{-\mu_4 z}, \\ \Theta(t,z)\sim 1-B_2\theta_{11}(t)e^{-\mu_5 z}. \end{cases} \tag{27}$$

Following a similar argument for (20), we can obtain

$$\Psi(t,z)\sim 1-B_1\psi_{11}^*(t)e^{-\mu_4 z}-B_2\psi_{11}^{**}(t)e^{-\mu_5 z}-B_3\psi_{11}(t)e^{-\mu_6 z}, \text{ as } z\to\infty. \tag{28}$$

Here,

$$\psi_{11}(t)=\psi_{11}(0)\exp\left(\int_0^t\Gamma_3(s,\mu_6)ds\right), \tag{29}$$

$$\psi_{11}^*(t)=\exp\left(\int_0^t\Gamma_3(s,\mu_4)ds\right)\cdot\left[\int_0^t b_{12}(s)p(s)\phi_{11}(s)\exp\left(-\int_0^s\Gamma_3(\tau,\mu_4)d\tau\right)ds+\psi_{11}^*(0)\right], \tag{30}$$

$$\psi_{11}^{**}(t)=\exp\left(\int_0^t\Gamma_3(s,\mu_5)ds\right)\cdot\left[\int_0^t b_{13}(s)r(s)\theta_{11}(s)\exp\left(-\int_0^s\Gamma_3(\tau,\mu_5)d\tau\right)ds+\psi_{11}^{**}(0)\right], \tag{31}$$

with

$$\psi_{11}^*(0)=\frac{\int_0^T b_{12}(s)p(s)\phi_{11}(s)\exp\left(-\int_0^s\Gamma_3(\tau,\mu_4)d\tau\right)ds}{\exp\left(-\int_0^T\Gamma_3(s,\mu_4)ds\right)-1},$$

$$\psi_{11}^{**}(0)=\frac{\int_0^T b_{13}(s)r(s)\theta_{11}(s)\exp\left(-\int_0^s\Gamma_3(\tau,\mu_5)d\tau\right)ds}{\exp\left(-\int_0^T\Gamma_3(s,\mu_5)ds\right)-1}.$$

Again, by the method of successive approximation, we can infer (10) from (27) and (28). The proof is thus complete. □

Remark 1. *We make some explanations for the symbol "$\sim$" appearing in (9) and (10). Let us take the first element, namely $\Phi(t,z)$, in (9) as an example. In the case of $\mu_2<\mu_1<\mu_3$ or $\mu_2<\mu_3<\mu_1$, we mean $\Phi(t,z)=A_2\phi_{01}(t)e^{\mu_2 z}+o(e^{\mu_2 z})$ uniformly in $t\in\mathbb{R}^+$ where the symbol o comes from the classic asymptotic definition.*

The uniqueness of the wave speed of the bistable wave solutions of (8) is presented in the following theorem. Instead of using the global stability of traveling wave front to prove the uniqueness, we employ the idea from [3].

Theorem 1. *Suppose that (8) has two bistable traveling wave solutions* $(c_1, \Phi_1(t,z), \Psi_1(t,z), \Theta_1(t,z))$ *with* $z = x + c_1 t$ *and* $(c_2, \Phi_2(t,z), \Psi_2(t,z), \Theta_2(t.z))$ *with* $z = x + c_2 t$, *then* $c_1 = c_2$.

Proof. To prove the theorem, we use a contradiction argument. Suppose that $c_2 > c_1$. Combining the monotonicity of $\mu_i(c), i = 1,2,3,4,5,6$ and asymptotic behavior established in Lemma 1, we know that there exists a suitable positive constant z_0 (might be sufficiently large) such that

$$(\Phi_2, \Psi_2, \Theta_2)(t, z - z_0) < (\Phi_1, \Psi_1, \Theta_1)(t,z),\ (t,z) \in \mathbb{R}^+ \times \mathbb{R}.$$

Specifically, when $t = 0$, the initial data satisfy

$$(\Phi_2, \Psi_2, \Theta_2)(0, j - z_0) < (\Phi_1, \Psi_1, \Theta_1)(0,j),\ j \in \mathbb{Z}.$$

By the comparison principle, we have

$$(\Phi_2, \Psi_2, \Theta_2)(t, j + c_2 t - z_0) \leq (\Phi_1, \Psi_1, \Theta_1)(t, j + c_1 t).$$

In particular, there holds

$$\Psi_2(t, j + c_2 t - z_0) \leq \Psi_1(t, j + c_1 t).$$

Setting $\bar{z} = j + c_1 t$ so that $\Psi_1(t, \bar{z}) = \frac{1}{3}$, we obtain

$$\frac{1}{3} = \Psi_1(t, \bar{z}) \geq \Psi_2(t, \bar{z} + (c_2 - c_1)t - z_0) \to 1, \text{as } t \to \infty,$$

and a contradiction then follows, thus $c_2 \leq c_1$. By a similar manner, it yields $c_2 \geq c_1$. In summary, $c_1 = c_2$. The proof is complete. □

3. The Determination of the Sign of Bistable Wave Speed

In this section, we aim at establishing two results so that the sign of bistable wave speed can be determined by comparison. To this end, we first make the following change

$$\widetilde{u}_j(t) = 1 - \frac{u_j(t)}{p(t)}, \widetilde{v}_j(t) = \frac{v_j(t)}{q(t)}, \widetilde{w}_j(t) = 1 - \frac{w_j(t)}{r(t)}, t \in \mathbb{R}^+, j \in \mathbb{Z},$$

such that system (1) can be rewritten as

$$\begin{cases} \widetilde{u}_j'(t) = d_1(t)\mathcal{D}_2[\widetilde{u}_j](t) + f(\widetilde{u}_j(t), \widetilde{v}_j(t), \widetilde{w}_j(t)), \\ \widetilde{v}_j'(t) = d_2(t)\mathcal{D}_2[\widetilde{v}_j](t) + g(\widetilde{u}_j(t), \widetilde{v}_j(t), \widetilde{w}_j(t)), \\ \widetilde{w}_j'(t) = d_3(t)\mathcal{D}_2[\widetilde{w}_j](t) + h(\widetilde{u}_j(t), \widetilde{v}_j(t), \widetilde{w}_j(t)), t \in \mathbb{R}^+, j \in \mathbb{Z}, \end{cases} \tag{32}$$

where

$$\begin{aligned} f(\widetilde{u}_j(t), \widetilde{v}_j(t), \widetilde{w}_j(t)) &:= (1 - \widetilde{u}_j(t))[a_{12}(t)q(t)\widetilde{v}_j(t) - a_{11}(t)p(t)\widetilde{u}_j(t)], \\ g(\widetilde{u}_j(t), \widetilde{v}_j(t), \widetilde{w}_j(t)) &:= \widetilde{v}_j(t)[b_{11}(t)q(t)(1 - \widetilde{v}_j(t)) - b_{12}(t)p(t)(1 - \widetilde{u}_j(t)) \\ &\qquad - b_{13}(t)r(t)(1 - \widetilde{w}_j(t))], \\ h(\widetilde{u}_j(t), \widetilde{v}_j(t), \widetilde{w}_j(t)) &:= (1 - \widetilde{w}_j(t))[c_{12}(t)q(t)\widetilde{v}_j(t) - c_{11}(t)r(t)\widetilde{w}_j(t)]. \end{aligned}$$

To proceed, we investigate two eigen-problems of the ODE system of (32) around $(0,0,0)$ and $(1,1,1)$. Denote λ_0, λ_1 by the eigenvalues of the following systems, respectively,

$$\begin{cases} \dfrac{d\phi}{dt} - a_{12}(t)q(t)\psi(t) + a_{11}(t)p(t)\phi(t) = \lambda\phi(t), \\ \dfrac{d\psi}{dt} - [b_{11}(t)q(t) - b_{12}(t)p(t) - b_{13}(t)r(t)]\psi(t) = \lambda\psi(t), \\ \dfrac{d\theta}{dt} - c_{12}(t)q(t)\psi(t) + c_{11}(t)r(t)\theta(t) = \lambda\theta(t), \\ \phi(t+T) = \phi(t),\ \psi(t+T) = \psi(t),\ \theta(t+T) = \theta(t), \end{cases}$$

and

$$\begin{cases} \dfrac{d\phi}{dt} - [a_{11}(t)p(t) - a_{12}(t)q(t)]\phi(t) = \lambda\phi(t), \\ \dfrac{d\psi}{dt} + b_{11}(t)q(t)\psi(t) - b_{12}(t)p(t)\phi(t) - b_{13}(t)r(t)\theta(t) = \lambda\psi(t), \\ \dfrac{d\theta}{dt} - [c_{11}(t)r(t) - c_{12}(t)q(t)]\theta(t) = \lambda\theta(t), \\ \phi(t+T) = \phi(t),\ \psi(t+T) = \psi(t),\ \theta(t+T) = \theta(t). \end{cases}$$

Let $(\phi_0(t), \psi_0(t), \theta_0(t))$ and $(\phi_1(t), \psi_1(t), \theta_1(t))$ be the eigenfunctions corresponding to λ_0 and λ_1, respectively. It is easy to calculate that

$$\begin{cases} \phi_0(t) = (a_0(t) + \phi_0(0)) \exp\left(\lambda_0 t - \displaystyle\int_0^t a_{11}(s)p(s)ds\right), \\ \psi_0(t) = \exp\left(\displaystyle\int_0^t (b_{11}(s)q(s) - b_{12}(s)p(s) - b_{13}(s)r(s))ds + \lambda_0 t\right), \\ \theta_0(t) = (b_0(t) + \theta_0(0)) \exp\left(\lambda_0 t - \displaystyle\int_0^t c_{11}(s)r(s)ds\right), \end{cases}$$

where

$$\lambda_0 = -\overline{\Delta_1(t)},\ \ \psi_0(0) = 1,$$

$$\phi_0(0) = \frac{\int_0^T a_{12}(t)q(t)\psi_0(t)\exp(\int_0^t a_{11}(\tau)p(\tau)d\tau) - \lambda_0 t)dt}{\exp\left(\int_0^T a_{11}(t)q(t)dt - \lambda_0 T\right) - 1},$$

$$\theta_0(0) = \frac{\int_0^T c_{12}(t)q(t)\psi_0(t)\exp(\int_0^t c_{11}(\tau)r(\tau)d\tau) - \lambda_0 t)dt}{\exp\left(\int_0^T c_{11}(t)r(t)dt - \lambda_0 T\right) - 1},$$

$$a_0(t) = \int_0^t a_{12}(s)q(s)\psi_0(s)\exp\left(\int_0^s a_{11}(\tau)p(\tau)d\tau - \lambda_0 s\right)ds,$$

$$b_0(t) = \int_0^t c_{12}(s)q(s)\psi_0(s)\exp\left(\int_0^s c_{11}(\tau)r(\tau)d\tau - \lambda_0 s\right)ds,$$

and

$$\begin{cases} \phi_1(t) = \exp\left(\displaystyle\int_0^t (a_{11}(s)p(s) - a_{12}(s)q(s))ds + \lambda_1 t\right), \\ \psi_1(t) = (c_1(t) + \psi_1(0)) \exp\left(\lambda_1 t - \displaystyle\int_0^t b_{11}(s)q(s)ds\right), \\ \theta_1(t) = \exp\left(\displaystyle\int_0^t (c_{11}(s)r(s) - c_{12}(s)q(s))ds + \lambda_1 t\right), \end{cases}$$

where

$$\lambda_1 = -\overline{\Delta_2(t)} = -\overline{\Delta_3(t)},\ \ \phi_0(0) = \theta_0(0) = 1,$$
$$\psi_1(0) = \frac{\int_0^T (b_{12}(t)p(t)\phi_1(t) + b_{13}(t)r(t)\theta_1(t)) \exp(\int_0^t b_{11}(s)q(s)ds - \lambda_1 t)dt}{\exp\left(\int_0^T b_{11}(t)q(t)dt - \lambda_1 T\right) - 1},$$
$$c_1(t) = \int_0^t (b_{12}(s)p(s)\phi_1(s) + b_{13}(s)r(s)\theta_1(s)) \exp\left(\int_0^s b_{11}(\tau)q(\tau)d\tau - \lambda_1 s\right)ds.$$

Next, to construct a pair of crucial upper and lower solutions, we define the transition functions as follows

$$p_1(t,x) = \zeta(x)\phi_1(t) + (1-\zeta(x))\phi_0(t),$$
$$p_2(t,x) = \zeta(x)\psi_1(t) + (1-\zeta(x))\psi_0(t),$$
$$p_3(t,x) = \zeta(x)\theta_1(t) + (1-\zeta(x))\theta_0(t),$$

where $\zeta(x)$ is a smooth function with $\zeta(x) = 0$ for $x \le -2$ and $\zeta(x) = 1$ for $x \ge 2$.

In order to discuss the sign of bistable wave speed, we give the following two lemmas.

Lemma 2. *For any $\xi^{\pm} \in \mathbb{R}$, there exist positive numbers β, σ, δ such that $(u_j^+, v_j^+, w_j^+)(t)$ and $(u_j^-, v_j^-, w_j^-)(t)$ defined as*

$$\begin{cases} u_j^{\pm}(t) = \Phi(t, j+ct+\xi^{\pm} \pm \sigma\delta(1-e^{-\beta t})) \pm \delta p_1(t, j+ct+\xi^{\pm} \pm \sigma\delta(1-e^{-\beta t}))e^{-\beta t}, \\ v_j^{\pm}(t) = \Psi(t, j+ct+\xi^{\pm} \pm \sigma\delta(1-e^{-\beta t})) \pm \delta p_2(t, j+ct+\xi^{\pm} \pm \sigma\delta(1-e^{-\beta t}))e^{-\beta t}, \\ w_j^{\pm}(t) = \Theta(t, j+ct+\xi^{\pm} \pm \sigma\delta(1-e^{-\beta t})) \pm \delta p_3(t, j+ct+\xi^{\pm} \pm \sigma\delta(1-e^{-\beta t}))e^{-\beta t}, \end{cases} \tag{33}$$

form a generalized upper/lower solution of the system (32).

Proof. The proof is similar to the ideas in Lemma 3.1 in article [34]. Thus, we omit it for simplicity here. □

Noting that the nonlinear terms in (8) are quasi-monotone, then an application of contracting mapping theorem arguments (see [35]) ensures that the following lemma holds.

Lemma 3. *Suppose that the initial data $(\widetilde{u}_j(0), \widetilde{v}_j(0), \widetilde{w}_j(0))$ satisfy*

$$0 < \widetilde{u}_j(0) < 1, 0 < \widetilde{v}_j(0) < 1, 0 < \widetilde{w}_j(0) < 1,$$

and

$$u_j^-(0) \le \widetilde{u}_j(0) \le u_j^+(0), v_j^-(0) \le \widetilde{v}_j(0) \le v_j^+(0), w_j^-(0) \le \widetilde{w}_j(0) \le w_j^+(0),$$

then the solution $(\widetilde{u}_j(t), \widetilde{v}_j(t), \widetilde{w}_j(t))$ of (32) fulfills

$$u_j^-(t) \le \widetilde{u}_j(t) \le u_j^+(t), v_j^-(t) \le \widetilde{v}_j(t) \le v_j^+(t), w_j^-(t) \le \widetilde{w}_j(t) \le w_j^+(t)$$

for all $t \in \mathbb{R}^+, j \in \mathbb{Z}$.

Next, we use the comparison principle based on the above two lemmas to establish the two crucial theorems.

Theorem 2. *Assume that (8) has a nonnegative non-decreasing upper solution $(\overline{\Phi}(t,z), \overline{\Psi}(t,z), \overline{\Theta}(t,z))$ with speed $\bar{c} < 0$ and $\overline{\Phi}(t,z), \overline{\Psi}(t,z)$ and $\overline{\Theta}(t,z)$ are T-periodic functions relative to t, satisfying*

$$(\overline{\Phi}, \overline{\Psi}, \overline{\Theta})(t, -\infty) < (1,1,1),\ (\overline{\Phi}, \overline{\Psi}, \overline{\Theta})(t, \infty) \ge (1,1,1), \tag{34}$$

then

$$c \le \bar{c} < 0.$$

Proof. For contradiction, we assume that $c > \bar{c}$ on the contrary and choose the initial datum $(\widetilde{u}_j(0), \widetilde{v}_j(0), \widetilde{w}_j(0))$ of (32) which is continuous, nondecreasing and satisfies

$$\widetilde{u}_j(0) = \widetilde{v}_j(0) = \widetilde{w}_j(0) = 0, \quad \text{for } j \le -J,$$

and

$$\widetilde{u}_j(0) = \widetilde{v}_j(0) = \widetilde{w}_j(0) = 1 - \eta, \quad \text{for } j \ge J,$$

for a sufficiently large positive integer J and a small enough number $\eta > 0$. This, together with (34), enables us to further suppose that

$$\widetilde{u}_j(0) \le \overline{\Phi}(0, j), \widetilde{v}_j(0) \le \overline{\Psi}(0, j), \widetilde{w}_j(0) \le \overline{\Theta}(0, j), \quad \text{for } j \in \mathbb{Z}.$$

Then, by the comparison principle, we have

$$\widetilde{u}_j(t) \le \overline{\Phi}(t, z) = \overline{\Phi}(t, j + \bar{c}t), \widetilde{v}_j(t) \le \overline{\Psi}(t, z) = \overline{\Psi}(t, j + \bar{c}t), \widetilde{w}_j(t) \le \overline{\Theta}(t, z) = \overline{\Theta}(t, j + \bar{c}t) \tag{35}$$

for all $(t, j) \in \mathbb{R}^+ \times \mathbb{Z}$. On the other hand, by Lemma 3, we particularly have that

$$\widetilde{u}_j(t) \ge \Phi(t, j + ct + \xi^- - \sigma\delta(1 - e^{-\beta t})) - \delta p_1(t, j + ct + \xi^- - \sigma\delta(1 - e^{-\beta t}))e^{-\beta t}. \tag{36}$$

Again, in view of (34), we know that there exists a number $z_0 = j + \bar{c}t$ such that $\overline{\Phi}(t, z_0) < 1$. Combining (35) and (36), we can derive

$$1 > \overline{\Phi}(t, z_0) \ge \Phi(t, z_0 + (c - \bar{c})t + \xi^- - \sigma\delta(1 - e^{-\beta t})) - \delta p_1(t, j + ct + \xi^- - \sigma\delta(1 - e^{-\beta t}))e^{-\beta t} \to 1,$$

as $t \to \infty$, which gives a contradiction. Hence, $c \le \bar{c} < 0$. The proof is complete. □

Theorem 3. *Suppose that (8) has a nonnegative non-decreasing lower solution* $(\underline{\Phi}(t, z), \underline{\Psi}(t, z), \underline{\Theta}(t, z))$ *with speed* $\underline{c} > 0$ *and* $\underline{\Phi}(t, z), \underline{\Psi}(t, z)$ *and* $\underline{\Theta}(t, z)$ *are T-periodic functions relative to t, satisfying*

$$(\underline{\Phi}, \underline{\Psi}, \underline{\Theta})(t, -\infty) = (0, 0, 0) < (\underline{\Phi}, \underline{\Psi}, \underline{\Theta})(t, \infty) \le (1, 1, 1), \tag{37}$$

then

$$c \ge \underline{c} > 0.$$

Proof. The proof is similar to that of Theorem 2. By choosing proper initial data (depending on (37)) and assume $c < \underline{c}$ for contradiction, we can obtain

$$\underline{\Phi}(t, j + \underline{c}t) \le \Phi(t, j + ct + \xi^+ + \sigma\delta(1 - e^{-\beta t})) + \delta p_1(t, j + ct + \xi^+ + \sigma\delta(1 - e^{-\beta t}))e^{-\beta t}.$$

On the plane $z = z_1 := j + \underline{c}t$, we set $\underline{\Phi}(t, z_1) = \frac{1}{3}$. Hence,

$$\frac{1}{3} = \underline{\Phi}(t, z_1) \le \Phi(t, z_1 + (c - \underline{c})t + \xi^+ + \sigma\delta(1 - e^{-\beta t})) + \delta p_1(t, j + ct + \xi^+ + \sigma\delta(1 - e^{-\beta t}))e^{-\beta t} \to 0,$$

as $t \to \infty$. Thus, we reach a contradiction. In short, $c \ge \underline{c} > 0$. The proof is complete. □

4. Sign of Bistable Wave Speed with Specific Conditions

Although Theorems 2 and 3 provide two criteria about how to predict the sign of bistable wave speed, the explicit condition expressed by the model-parameter is not presented. This part aims to gain some of such conditions via constructing explicit upper and lower solutions which seems to be nontrivial in contrast with the classic constructions, namely, the joint of a constant function and an exponential function.

Theorem 4. *The speed c of the bistable traveling wave solution of (8) is negative, if there exist constants k_1, k_2 such that*

$$-2d_2(t)\tau_{10} + d_2(t)\tau_{10}^2\chi_{10} + b_{12}(t)q(t)k_1 + b_{13}(t)r(t)k_2 \le 0, \tag{38}$$

and

$$1 < \frac{a_{12}(t)q(t)}{a_{11}(t)p(t) + \Delta_1(t) + [d_2(t) - d_1(t)]\tau_{10}} < k_1 < \min_{t\in[0,T]}\left\{\frac{d_1(t)\tau_{10}(2-\tau_{10}\chi_{10})}{[d_1(t)-d_2(t)]\tau_{10} - \Delta_1(t)}\right\}, \tag{39}$$

$$1 < \frac{c_{12}(t)q(t)}{c_{11}(t)r(t) + \Delta_1(t) + [d_2(t) - d_3(t)]\tau_{10}} < k_2 < \min_{t\in[0,T]}\left\{\frac{d_3(t)\tau_{10}(2-\tau_{10}\chi_{10})}{[d_3(t)-d_2(t)]\tau_{10} - \Delta_1(t)}\right\}, \tag{40}$$

where

$$\tau_{10} = e^{\mu_1(0)} + e^{-\mu_1(0)} - 2, \chi_{10} = \frac{1}{\tau_{10} + 4 + 2\sqrt{\tau_{10}+4}}.$$

Proof. To make the sign of the bistable wave speed negative, by Theorem 2, we only need to construct an upper solution to (8). Let

$$\overline{\Psi}(t,z) = \frac{\psi_{01}(t)}{\psi_{01}(t) + e^{-\mu_1(-\epsilon)z}},$$

and redefine $\overline{\Phi}(t,z), \overline{\Theta}(t,z)$, which are continuous functions, as follows

$$\overline{\Phi}(t,z) = \min\{1, k_1\overline{\Psi}(t,z)\} = \begin{cases} k_1\overline{\Psi}(t,z), & z \le z_1(t), \\ 1, & z > z_1(t), \end{cases} \tag{41}$$

$$\overline{\Theta}(t,z) = \min\{1, k_2\overline{\Psi}(t,z)\} = \begin{cases} k_2\overline{\Psi}(t,z), & z \le z_2(t), \\ 1, & z > z_2(t). \end{cases}$$

Here, $0 < \epsilon \ll 1$. For any fixed $t \in \mathbb{R}^+$, $z_1(t)$ and $z_2(t)$ are uniquely determined by $k_1\overline{\Psi}(t, z_1(t)) = 1$ and $k_2\overline{\Psi}(t, z_2(t)) = 1$, respectively. Without loss of generality, we may assume that $k_1 > k_2$, which implies that $z_1(t) < z_2(t), t \in \mathbb{R}^+$, according to the monotonicity of $\overline{\Psi}(t,z)$ in z.

To proceed, we note that $\mathcal{D}_2[\overline{\Psi}]$ can be reduced to

$$\mathcal{D}_2[\overline{\Psi}] = \tau_1\overline{\Psi}(1-\overline{\Psi})(1-2\overline{\Psi}) + \tau_1^2\overline{\Psi}^2(1-\overline{\Psi})H_1(t,z), \tag{42}$$

where

$$\tau_1 = e^{\mu_1(-\epsilon)} + e^{-\mu_1(-\epsilon)} - 2,\ H_1(t,z) = \frac{e^{-\mu_1(-\epsilon)z}/\psi_{01}(t)(1 - e^{-\mu_1(-\epsilon)z}/\psi_{01}(t))}{(1 + e^{-\mu_1(-\epsilon)(z+1)}/\psi_{01}(t))(1 + e^{-\mu_1(-\epsilon)(z-1)}/\psi_{01}(t))}.$$

It is easy to check that $H_1(t,z) \le \chi_1$ with

$$\chi_1 = \frac{1}{\tau_1 + 4 + 2\sqrt{\tau_1+4}}.$$

We first concentrate on the Ψ-equation. Substituting

$$\overline{\Psi}_z = \mu_1\overline{\Psi}(1-\overline{\Psi}), \quad \overline{\Psi}_t = \frac{\psi_{01}'(t)}{\psi_{01}(t)}\overline{\Psi}(1-\overline{\Psi})$$

and (42) into the $\overline{\Psi}$-equation, we have

$$
\begin{aligned}
&d_2(t)\mathcal{D}_2[\overline{\Psi}](t,z)+\epsilon\overline{\Psi}_z+\overline{\Psi}[b_{11}(t)q(t)(1-\overline{\Psi})-b_{12}(t)p(t)(1-\overline{\Phi})-b_{13}(t)r(t)(1-\overline{\Theta})]-\overline{\Psi}_t\\
&\le \overline{\Psi}(1-\overline{\Psi})\Big\{d_2(t)\tau_1+\epsilon\mu_1+\Delta_1(t)-\frac{\psi_{01}'(t)}{\psi_{01}(t)}+\overline{\Psi}\Big(-2d_2(t)\tau_1+d_2(t)\tau_1^2\chi_1+\Upsilon(t,z)\Big)\Big\}\\
&\le \overline{\Psi}^2(1-\overline{\Psi})\Big\{-2d_2(t)\tau_1+d_2(t)\tau_1^2\chi_1+\Upsilon(t,z)\Big\},
\end{aligned}
$$

where

$$\Upsilon(t,z)=\frac{b_{12}(t)p(t)(\overline{\Phi}-\overline{\Psi})+b_{13}(t)r(t)(\overline{\Theta}-\overline{\Psi})}{\overline{\Psi}(1-\overline{\Psi})}.$$

Next, we have to discuss the maximum of $\Upsilon(t,z)$ in the following cases.

(1) When $z>z_2(t)$, it is easy to realize that $\overline{\Phi}(t,z)=1,\overline{\Theta}(t,z)=1,\frac{1}{k_2}\le\overline{\Psi}(t,z)\le 1$. Then,

$$\Upsilon(t,z)=\frac{b_{12}(t)p(t)+b_{13}(t)r(t)}{\overline{\Psi}}\le k_2\Big(b_{12}(t)p(t)+b_{13}(t)r(t)\Big). \tag{43}$$

(2) When $z\le z_1(t)$, it follows that $\overline{\Phi}(t,z)=k_1\overline{\Psi}(t,z)$ and $\overline{\Theta}(t,z)=k_2\overline{\Psi}(t,z)$. From (41), we can infer that $\overline{\Psi}\le\frac{1}{k_1}$. Therefore, $\Upsilon(t,z)$ can be rewritten as

$$\Upsilon(t,z)=\frac{b_{12}(t)p(t)(k_1-1)+b_{13}(t)r(t)(k_2-1)}{1-\overline{\Psi}}\le\frac{b_{12}(t)p(t)(k_1-1)+b_{13}(t)r(t)(k_2-1)}{1-\frac{1}{k_1}}. \tag{44}$$

(3) When $z_1(t)<z\le z_2(t)$, we have $\overline{\Phi}(t,z)=1$ and $\overline{\Theta}(t,z)=k_2\overline{\Psi}(t,z)$. Then,

$$\Upsilon(t,z)=\frac{b_{12}(t)p(t)}{\overline{\Psi}}+\frac{b_{13}(t)r(t)(k_2-1)}{1-\overline{\Psi}}.$$

It is easy to check that $\frac{1}{k_1}\le\overline{\Psi}\le\frac{1}{k_2}$, which results in

$$\Upsilon(t,z)\le b_{12}(t)q(t)k_1+b_{13}(t)r(t)k_2. \tag{45}$$

By comparing (43) and (44) with (45), we find the maximum among them is $b_{12}(t)q(t)k_1$ $+b_{13}(t)r(t)k_2$. Thus, by assumption (38), we have

$$-2d_2(t)\tau_1+d_2(t)\tau_1^2\chi_1+\Upsilon(t,z)\le-2d_2(t)\tau_1+d_2(t)\tau_1^2\chi_1+b_{12}(t)q(t)k_1+b_{13}(t)r(t)k_2\le 0. \tag{46}$$

Next, we consider the Φ-equation. There are four subcases that need to be discussed.

(i) When $z\ge z_1(t)+1$, we obtain $\overline{\Phi}(t,z)=1$ and hence

$$d_1(t)\mathcal{D}_2[\overline{\Phi}](t,z)+\epsilon\overline{\Phi}_z+(1-\overline{\Phi})[a_{12}(t)q(t)\overline{\Psi}-a_{11}(t)p(t)\overline{\Phi}]-\overline{\Phi}_t=0.$$

(ii) When $z_1(t)<z<z_1(t)+1$, we notice that $\overline{\Phi}(t,z-1)=k_1\overline{\Psi}(t,z-1),\overline{\Phi}(t,z+1)=\overline{\Phi}(t,z)=1$. Therefore, the Φ-equation can be evaluated by

$$d_1(t)\mathcal{D}_2[\overline{\Phi}](t,z)+\epsilon\overline{\Phi}_z+(1-\overline{\Phi})[a_{12}(t)q(t)\overline{\Psi}-a_{11}(t)p(t)\overline{\Phi}]-\overline{\Phi}_t=d_1(t)[k_1\overline{\Psi}(t,z-1)-1]\le 0,$$

using $k_1\overline{\Psi}(t,z-1)\le 1$.

(iii) The case $z_1(t)-1<z\le z_1(t)$ can be discussed together with the last case.

(iv) When $z \le z_1(t) - 1$, it follows from (41) that $\overline{\Phi}(t,z) = k_1\overline{\Psi}(t,z)$. Thus,

$$\begin{aligned}
&d_1(t)\mathcal{D}_2[\overline{\Phi}](t,z) + \epsilon\overline{\Phi}_z + (1-\overline{\Phi})[a_{12}(t)q(t)\overline{\Psi} - a_{11}(t)p(t)\overline{\Phi}] - \overline{\Phi}_t \\
&\le k_1\overline{\Psi}\Bigg\{(1-\overline{\Psi})\left[\tau_1(1-2\overline{\Psi})d_1(t) + \tau_1^2\chi_1\overline{\Psi}d_1(t) + \epsilon\mu_1 - \frac{\psi_{01}'(t)}{\psi_{01}(t)}\right] \\
&\qquad + (1-k_1\overline{\Psi})\left[\frac{a_{12}(t)q(t)}{k_1} - a_{11}(t)p(t)\right]\Bigg\} \\
&\le k_1\overline{\Psi}F_1(\overline{\Psi}),
\end{aligned}$$

where

$$\begin{aligned}
F_1(\overline{\Psi}) := (1-\overline{\Psi})&\left[\tau_1(1-2\overline{\Psi})d_1(t) + \tau_1^2\chi_1\overline{\Psi}d_1(t) + \epsilon\mu_1 - \frac{\psi_{01}'(t)}{\psi_{01}(t)}\right] \\
&+ (1-k_1\overline{\Psi})\left[\frac{a_{12}(t)q(t)}{k_1} - a_{11}(t)p(t)\right].
\end{aligned}$$

It is obvious that $F_1''(\overline{\Psi}) = 2d_1(t)\tau_1(2-\tau_1\chi_1) \ge 0$ (using $\tau_1\chi_1 < 1$), where the derivative is with respect to the variable $\overline{\Psi}$. Therefore, $F_1(\overline{\Psi})$ is concave for $\overline{\Psi} \in [0, \frac{1}{k_1}]$. It can be easily calculated that

$$\begin{aligned}
F_1(0) &= d_1(t)\tau_1 + \epsilon\mu_1 - \frac{\psi_{01}'(t)}{\psi_{01}(t)} + \frac{a_{12}(t)q(t)}{k_1} - a_{11}(t)p(t) \\
&= [d_1(t) - d_2(t)]\tau_1 - \Delta_1(t) + \frac{a_{12}(t)q(t)}{k_1} - a_{11}(t)p(t),
\end{aligned} \tag{47}$$

$$F_1(\frac{1}{k_1}) = (1-\frac{1}{k_1})\left[d_1(t)\tau_1 + \frac{1}{k_1}(\tau_1^2\chi_1 - 2\tau_1)d_1(t) + \epsilon\mu_1 - \frac{\psi_{01}'(t)}{\psi_{01}(t)}\right].$$

For the purpose of proving $F_1(\overline{\Psi}) < 0$ for $\overline{\Psi} \in [0, \frac{1}{k_1}]$, we only need to check that $F_1(0) < 0$ and $F_1(\frac{1}{k_1}) < 0$, which are ensured by (39) as $\epsilon \to 0^+$. To sum up cases (i)–(iv), we have

$$d_1(t)\mathcal{D}_2[\overline{\Phi}](t,z) + \epsilon\overline{\Phi}_z + (1-\overline{\Phi})[a_{12}(t)q(t)\overline{\Psi} - a_{11}(t)p(t)\overline{\Phi}] - \overline{\Phi}_t \le 0.$$

By a similar manner, we can infer from (40) that

$$d_3(t)\mathcal{D}_2[\overline{\Theta}](t,z) + \epsilon\overline{\Theta}_z + (1-\overline{\Theta})[c_{12}(t)q(t)\overline{\Psi} - c_{11}(t)r(t)\overline{\Theta}] - \overline{\Theta}_t \le 0.$$

As such, it is proved that $(\overline{\Phi}, \overline{\Psi}, \overline{\Theta})(t,z)$ is an upper solution of (8). By Theorem 2, the proof is complete. □

Theorem 5. *The speed c of the bistable traveling wave solution of (8) satisfies $c \ge \epsilon > 0$ provided that*

$$\max\{\Pi_1(t), \Pi_2(t)\} < \min_{t\in[0,T]}\left\{1 - \frac{d_2(t)(2\tau_{20} + \tau_{20}^2)}{b_{11}(t)q(t)}\right\}. \tag{48}$$

where

$$\Pi_1(t) := \frac{a_{11}(t)p(t) + [d_1(t) + d_1(t)\tau_{20} + d_2(t)]\tau_{20} + \Delta_1(t)}{a_{12}(t)q(t)},$$

$$\Pi_2(t) := \frac{c_{11}(t)r(t) + [d_3(t) + d_3(t)\tau_{20} + d_2(t)]\tau_{20} + \Delta_1(t)}{c_{12}(t)q(t)},$$

and

$$\tau_{20} = e^{\mu_1(0)} + e^{-\mu_1(0)} - 2.$$

Proof. We intend to construct a lower solution to show that the wave speed c is positive. Define

$$\underline{\Psi}(t,z)=\frac{\underline{k}\psi_{01}(t)}{\psi_{01}(t)+e^{-\mu_1(\epsilon)z}},\ \underline{\Phi}(t,z)=\underline{\Theta}(t,z)=\frac{\underline{\Psi}(t,z)}{\underline{k}}$$

with $0<\epsilon\ll 1$ and $\underline{k}$ satisfying

$$\max\{\Pi_1(t),\Pi_2(t)\}<\underline{k}<\min_{t\in[0,T]}\left\{1-\frac{d_2(t)(2\tau_2+\tau_2^2)}{b_{11}(t)q(t)}\right\}. \tag{49}$$

By a similar computation with (42), we obtain

$$\mathcal{D}_2[\underline{\Psi}]=\tau_2\underline{\Psi}(1-\frac{\underline{\Psi}}{\underline{k}})(1-\frac{2\underline{\Psi}}{\underline{k}})+\tau_2^2\frac{\underline{\Psi}^2}{\underline{k}}(1-\frac{\underline{\Psi}}{\underline{k}})H_2(t,z)$$

with

$$\tau_2=e^{\mu_1(\epsilon)}+e^{-\mu_1(\epsilon)}-2,\ H_2(t,z)=\frac{e^{-\mu_1(\epsilon)z}/\psi_{01}(t)(1-e^{-\mu_1(\epsilon)z}/\psi_{01}(t))}{(1+e^{-\mu_1(\epsilon)(z+1)}/\psi_{01}(t))(1+e^{-\mu_1(\epsilon)(z-1)}/\psi_{01}(t))}.$$

On account of the lower bound of $H_2(t,z)$ being -1, we have

$$\begin{aligned}&d_2(t)\mathcal{D}_2[\underline{\Psi}](t,z)-\epsilon\underline{\Psi}_z+\underline{\Psi}[b_{11}(t)q(t)(1-\underline{\Psi})-b_{12}(t)p(t)(1-\underline{\Phi})-b_{13}(t)r(t)(1-\underline{\Theta})]-\underline{\Psi}_t\\&\geq\frac{\underline{\Psi}^2}{\underline{k}}(1-\frac{\underline{\Psi}}{\underline{k}})\left\{-2d_2(t)\tau_2-d_2(t)\tau_2^2+b_{11}(t)q(t)(1-\underline{k})\right\}.\end{aligned}$$

Thanks to (49), we obtain

$$d_2(t)\mathcal{D}_2[\underline{\Psi}](t,z)-\epsilon\underline{\Psi}_z+\underline{\Psi}[b_{11}(t)q(t)(1-\underline{\Psi})-b_{12}(t)p(t)(1-\underline{\Phi})-b_{13}(t)r(t)(1-\underline{\Theta})]-\underline{\Psi}_t\geq 0.$$

As for the Φ-equation and Θ-equation, we have the following estimation:

$$\begin{aligned}&d_1(t)\mathcal{D}_2[\underline{\Phi}](t,z)-\epsilon\underline{\Phi}_z+(1-\underline{\Phi})[a_{12}(t)q(t)\underline{\Psi}-a_{11}(t)p(t)\underline{\Phi}]-\underline{\Phi}_t\\&\qquad\geq\underline{\Phi}(1-\underline{\Phi})\left\{-d_1(t)\tau_2-d_1(t)\tau_2^2-d_2(t)\tau_2-\Delta_1(t)+a_{12}(t)q(t)\underline{k}-a_{11}(t)p(t)\right\},\end{aligned}$$

and

$$\begin{aligned}&d_3(t)\mathcal{D}_2[\underline{\Theta}](t,z)-\epsilon\underline{\Theta}_z+(1-\underline{\Theta})[c_{12}(t)q(t)\underline{\Psi}-c_{11}(t)r(t)\underline{\Theta}]-\underline{\Theta}_t\\&\qquad\geq\underline{\Theta}(1-\underline{\Theta})\left\{-d_3(t)\tau_2-d_3(t)\tau_2^2-d_2(t)\tau_2-\Delta_1(t)+c_{12}(t)q(t)\underline{k}-c_{11}(t)r(t)\right\},\end{aligned}$$

in which assumption (49) is used. Let $\epsilon\to 0^+$; we can derive that

$$d_1(t)\mathcal{D}_2[\underline{\Phi}](t,z)-\epsilon\underline{\Phi}_z+(1-\underline{\Phi})[a_{12}(t)q(t)\underline{\Psi}-a_{11}(t)p(t)\underline{\Phi}]-\underline{\Phi}_t\geq 0,$$

and

$$d_3(t)\mathcal{D}_2[\underline{\Theta}](t,z)-\epsilon\underline{\Theta}_z+(1-\underline{\Theta})[c_{12}(t)q(t)\underline{\Psi}-c_{11}(t)r(t)\underline{\Theta}]-\underline{\Theta}_t\geq 0.$$

Thus, we proved that $(\underline{\Phi},\underline{\Psi},\underline{\Theta})(t,z)$ is a lower solution of (8). By Theorem 3, the proof is complete. □

As applications of Theorems 4 and 5, we want to partially provide the answer to the open problem proposed in [13], associated to the following constant coefficient system of (1)

$$\begin{cases} u_j'(t) = d_1\mathcal{D}_2[u_j](t) + u_j(t)(r_1 - a_{11}u_j(t) - a_{12}v_j(t)), \\ v_j'(t) = d_2\mathcal{D}_2[v_j](t) + v_j(t)(r_2 - b_{11}v_j(t) - b_{12}u_j(t) - b_{13}w_j(t)), \\ w_j'(t) = d_3\mathcal{D}_2[w_j](t) + w_j(t)(r_3 - c_{11}w_j(t) - c_{12}v_j(t)),\ j \in \mathbb{Z}, t > 0. \end{cases} \tag{50}$$

More precisely, in [13], it was stated that nothing is known about the sign of wave speed in the discrete lattice dynamical system (50). For system (50), the equilibrium points and bistable condition (**A**) become, respectively,

$$e_0 := (0,0,0), e_1 := (0, \frac{r_2}{b_{11}}, 0), e_2 := (\frac{r_1}{a_{11}}, 0, \frac{r_3}{c_{11}}),$$

and

$$b_{11}r_1 < a_{12}r_2, a_{11}c_{11}r_2 < b_{12}c_{11}r_1 + a_{11}b_{13}r_3, b_{11}r_3 < c_{12}r_2. \tag{51}$$

Applying Theorems 4 and 5 to (50), we have the following two corollaries:

Corollary 1. *The speed c of the bistable traveling wave solution of (50) is negative, if there exist positive constants k_1, k_2 such that*

$$-2d_2\tau_{10} + d_2\tau_{10}^2\chi_{10} + b_{12}\frac{r_2}{b_{11}}k_1 + b_{13}\frac{r_3}{c_{11}}k_2 \le 0, \tag{52}$$

and

$$1 < \frac{a_{12}\frac{r_2}{b_{11}}}{r_1 + r_2 - \frac{b_{12}r_1}{a_{11}} - \frac{b_{13}r_3}{c_{11}} + (d_2 - d_1)\tau_{10}} < \frac{d_1\tau_{10}(2 - \tau_{10}\chi_{10})}{(d_1 - d_2)\tau_{10} - r_2 + \frac{b_{12}r_1}{a_{11}} + \frac{b_{13}r_3}{c_{11}}}, \tag{53}$$

$$1 < \frac{c_{12}\frac{r_2}{b_{11}}}{r_3 + r_2 - \frac{b_{12}r_1}{a_{11}} - \frac{b_{13}r_3}{c_{11}} + (d_2 - d_3)\tau_{10}} < \frac{d_3\tau_{10}(2 - \tau_{10}\chi_{10})}{(d_3 - d_2)\tau_{10} - r_2 + \frac{b_{12}r_1}{a_{11}} + \frac{b_{13}r_3}{c_{11}}}. \tag{54}$$

Corollary 2. *The speed c of the bistable traveling wave solution of (50) is positive provided that*

$$\begin{aligned} \max\Big\{ &\frac{r_1 + [d_1 + d_1\tau_{20} + d_2]\tau_{20} + r_2 - \frac{b_{12}r_1}{a_{11}} - \frac{b_{13}r_3}{c_{11}}}{a_{12}\frac{r_2}{b_{11}}}, \\ &\frac{r_3 + [d_3 + d_3\tau_{20} + d_2]\tau_{20} + r_2 - \frac{b_{12}r_1}{a_{11}} - \frac{b_{13}r_3}{c_{11}}}{c_{12}\frac{r_2}{b_{11}}}\Big\} \\ < \min_{t\in[0,T]} &\Big\{1 - \frac{d_2(2\tau_{20} + \tau_{20}^2)}{r_2}\Big\}. \end{aligned} \tag{55}$$

We can learn from Corollaries 1 and 2 that almost all of the parameters appearing in (50) should be taken into account in the determination of bistable wave speed sign. Hence, one can analyze the effect of different coefficients on this determination. For instance, if one of the diffusivity coefficients $d_i, i = 1, 2, 3$ is sufficiently small, then one of conditions (52), (53) and (54) would no longer be valid. While we fixed d_1 and d_3 and let d_3 be sufficiently large, condition (55) is not true.

5. Numerical Simulation

We can derive that the bistable wave speed is negative in Theorem 4, which implies that the bistable wave speed propagates to the right and u and w will win the competition. On the contrary, Theorem 5 ensures that the bistable wave speed is positive, which means that the bistable wave speed propagates to the left and v will win the competition.

In order to illustrate our theoretical results from Corollaries 1 and 2, we choose the initial data in the form of

$$u_j(0) = \begin{cases} 0, & 1 \le j \le N_j, \\ 1, & N_j + 1 \le j \le N_L, \end{cases}$$
$$v_j(0) = \begin{cases} 1, & 1 \le j \le N_j, \\ 0, & N_j + 1 \le j \le N_L, \end{cases}$$
$$w_j(0) = \begin{cases} 0, & 1 \le j \le N_j, \\ 1, & N_j + 1 \le j \le N_L, \end{cases}$$

with the boundary conditions

$$\begin{cases} u_1(t) - u_2(t) = u_{N_L}(t) - u_{N_{L-1}}(t) = 0, \\ v_1(t) - v_2(t) = v_{N_L}(t) - v_{N_{L-1}}(t) = 0, \\ w_1(t) - w_2(t) = w_{N_L}(t) - w_{N_{L-1}}(t) = 0, \end{cases}$$

where N_j and N_L are two integers. In what follows, we will set $x \in [-100, 100]$ and $t \in [0, 60]$, and the step we take here is $\Delta x = 1$ and $\Delta t = 0.05$. All of the following simulation of the CPU time is about one second.

In (50), we choose

$$\begin{aligned} &a_{11} = b_{11} = c_{11} = 1,\ a_{12} = 1.2,\ b_{12} = 0.8,\ b_{13} = 0.7, \\ &c_{12} = 1.2,\ d_1 = 1,\ d_2 = 2,\ d_3 = 1.3,\ r_1 = r_2 = r_3 = 1. \end{aligned} \tag{56}$$

From this, we can compute $\tau_{10} = 0.250, \chi_{10} = 0.119$. It is easy to see that the set of such chosen parameters make (51)–(54) valid. As a result, one may accept the bistable wave speed to be negative. This fact is exactly verified by the numerical results; see Figure 1.

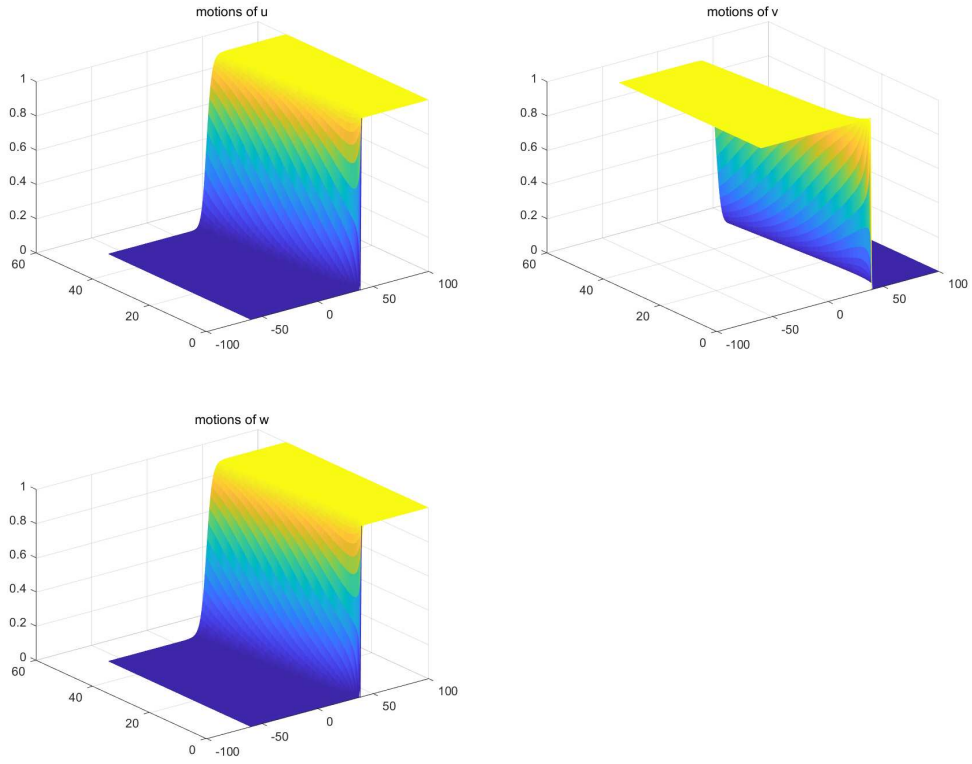

Figure 1. The simulation of (50) for the setting of (56).

In (50), we choose

$$\begin{aligned} &a_{11} = b_{11} = c_{11} = 1,\ a_{12} = 10,\ b_{12} = 1.2,\ b_{13} = 1.2,\\ &c_{12} = 8,\ d_1 = 1,\ d_2 = 0.5,\ d_3 = 1.2,\ r_1 = r_2 = r_3 = 1. \end{aligned} \tag{57}$$

For the above set of parameters, one can derive that $\tau_{20} = 2.800$. Meanwhile, they fulfill (51) and (55), so the bistable wave speed would be positive according to Corollary 2. This is demonstrated in Figure 2.

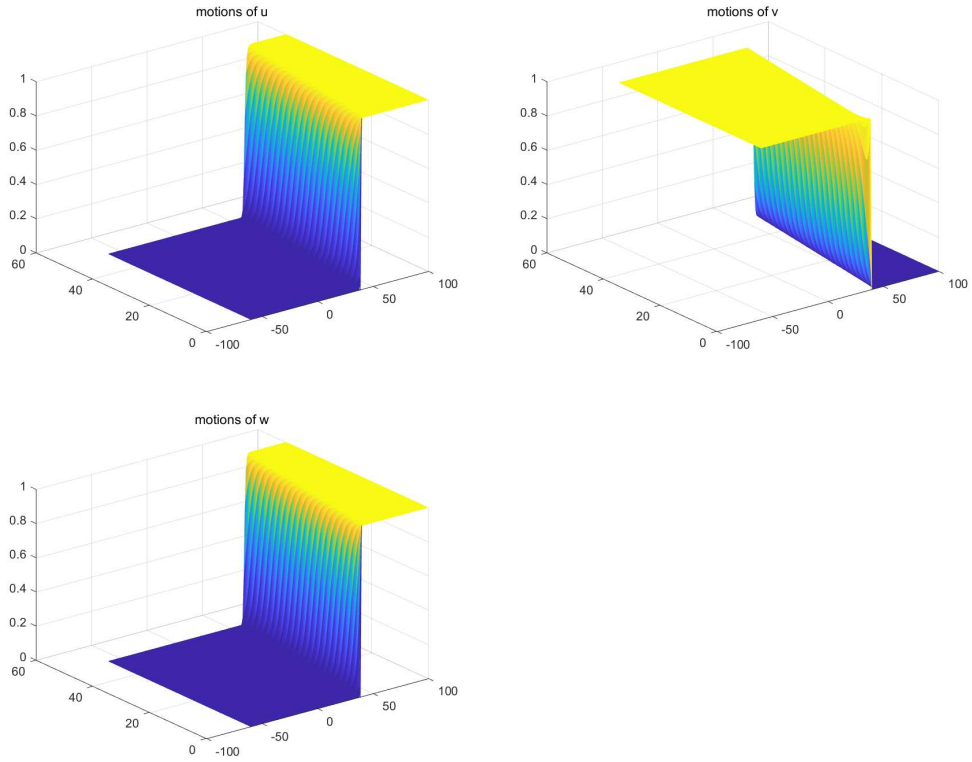

Figure 2. The simulation of (50) for the setting of (57).

We all know that the competitive ability of a strong species will be greater than that of a weak species, indicating that the strong species can wipe out the weak one. However, when more than two species are involved, the outcome may not be that simple. Indeed, Theorem 3.4 in Guo [13] proves that it is possible for two weak species to outcompete a strong species in model (2) under certain conditions. Naturally, we wonder whether the same phenomenon can be observed in model (50). To this end, we choose

$$\begin{aligned} &a_{11} = b_{11} = c_{11} = 1,\ a_{12} = c_{12} = 1.1,\ b_{12} = b_{13} = 0.9,\\ &r_1 = r_2 = r_3 = 1,\ d_1 = d_2 = d_3 = 1. \end{aligned} \tag{58}$$

Figure 3 tells us that such a phenomenon still exists.

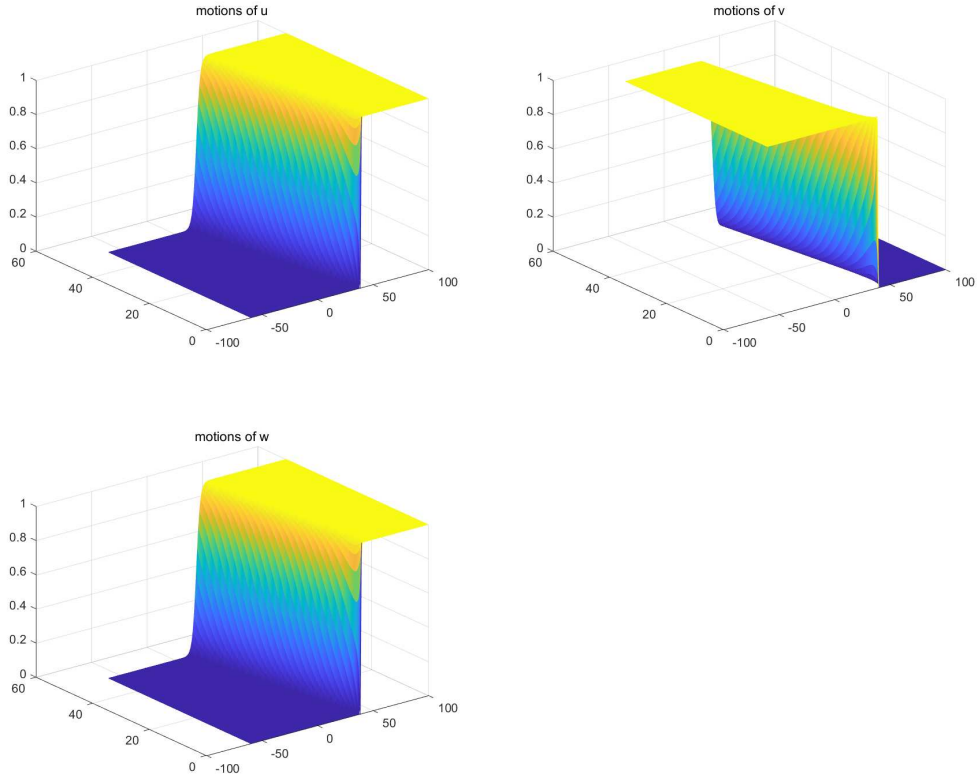

Figure 3. The simulation of (50) for the setting of (58).

6. Conclusions

We investigate a time-periodic lattice system modeling the evolution of three competing species in the case that one of the species competes with the other two species for common resources, while there is no competition between these other two species. The focus of the paper is the determination of the sign of bistable traveling wave solution, for which it is a challenging task to find the corresponding sufficient and necessary condition. Noting that the system is monotone, we apply the upper/lower solution method and the comparison principle to successfully establish several sufficient conditions so that one can confirm that the sigh is positive or negative. The results that we obtained here reveal how the periodic fluctuation caused by the season or other factors can have an impact on the competitive outcome for the three species. In particular, we addressed an open problem arose by Guo [13] since the integral method used for a continuous system there cannot be used for a discrete system. To confirm the validity of our results, a numerical simulation was also carried out.

Author Contributions: Investigation, C.P.; writing—review and editing, J.Z.; supervision, H.W. All authors have read and agreed to the published version of the manuscript.

Funding: This work is partially supported by CSC, the Scientific Research Fund of the Hunan Provincial Education Department (grant 23A0342) and the Graduate Research Innovation Project of the Hunan Provincial Education Department (grant CX20240820).

Data Availability Statement: The codes generated during the current study are available from the corresponding author on reasonable request.

Acknowledgments: The first and third authors would like to express their appreciations to C. Ou for his help and guidance, and their gratitude to the Memorial University of Newfoundland for its kind service, since most of the current paper was finished during the period of their overseas study.

Conflicts of Interest: The authors declare no conflicts of interest.

References

1. Alhasanat, A.; Ou, C. Minimal-speed selection of traveling waves to the Lotka-Volterra competition model. *J. Differ. Equ.* **2019**, *266*, 7357–7378. [CrossRef]
2. Guo, J.-S.; Lin, Y.-C. The sign of the wave speed for the Lotka-Volterra competition-diffusion system. *Comm. Pure Appl. Anal.* **2013**, *12*, 2083–2090. [CrossRef]
3. Ma, M.; Yue, J.; Huang, Z.; Ou, C. Propagation dynamics of bistable traveling wave to a time-periodic Lotka-Volterra competition model arising in strong competition model: Effect of seasonality. *J. Dyn. Differ. Equ.* **2022**, *35*, 1745–1767. [CrossRef]
4. Ma, M.; Yue, J.; Ou, C. Propagation direction of the bistable travelling wavefront for delayed non-local reaction diffusion equations. *Proc. Math. Phys. Eng. Sci.* **2019**, *475*, 20180898. [CrossRef]
5. Ma, M.; Zhang, Q.; Yue, J.; Ou, C. Bistable wave speed of the Lotka-Volterra competition model. *J. Biol. Dyn.* **2020**, *14*, 608–620. [CrossRef]
6. Wang, H.; Ou, C. Propagation direction of the traveling wave for the Lotka-Volterra competitive lattice system. *J. Dyn. Differ. Equ.* **2021**, *33*, 1153–1174. [CrossRef]
7. Zhang, G.-B.; Zhao, X.-Q. Propagation phenomena for a two-species Lotka-Volterra strong competition system with nonlocal dispersal. *Calc. Var. Partial Differ. Equ.* **2020**, *33*, 1–34. [CrossRef]
8. Guo, J.-S.; Wang, Y.; Wu, C.-H.; Wu, C.-C. The minimal speed of traveling wave solutions for a diffusive three species competition system. *Taiwanese J. Math.* **2015**, *19*, 1805–1829. [CrossRef]
9. Pan, C.; Wang, H.; Ou, C. Invasive speed for a competition-diffusion system with three Species. *Discrete Contin. Dyn. Syst. B* **2022**, *27*, 3515–3532. [CrossRef]
10. Chang, C.-H. The stability of traveling wave solutions for a diffusive competition system of three species. *J. Math. Anal. Appl.* **2018**, *459*, 564–576. [CrossRef]
11. Chen, C.-C.; Hung, L.-C.; Mimura, M.; Ueyama, D. Exact travelling wave solutions of three-species competition–diffusion systems. *Discrete Contin. Dyn. Syst. B* **2012**, *17*, 2653–2669. [CrossRef]
12. Meng, Y.-L.; Zhang, W.-G. Properties of traveling wave fronts for three species Lotka-Volterra system. *Qual. Theory Dyn. Syst.* **2020**, *19*, 1–28. [CrossRef]
13. Guo, J.-S.; Nakamura, K.I.; Ogiwara, T.; Wu, C.-H. The sign of traveling wave speed in bistable dynamics. *Discrete Contin. Dyn. Syst.* **2020**, *40*, 3451–3466. [CrossRef]
14. Zheng, J.-P. The wave speed signs for bistable traveling wave solutions in three species competition-diffusion systems. *Appl. Math. Mech.* **2021**, *42*, 1296–1305.
15. Gao, P.; Wu, S.-H. Qualitative properties of traveling wavefronts for a three-component lattice dynamical system with delay. *Electron. J. Differ. Equ.* **2019**, *34*, 1–19.
16. Guo, J.-S.; Wu, C.-C. The existence of traveling wave solutions for a bistable three-component lattice dynamical system. *J. Differ. Equ.* **2016**, *260*, 1445–1455. [CrossRef]
17. Guo, J.-S.; Nakamura, K.-I.; Ogiwara, T.; Wu, C.-C. Stability and uniqueness of traveling waves for a discrete bistable 3-species competition system. *J. Math. Anal. Appl.* **2019**, *472*, 1534–1550. [CrossRef]
18. Su, T.; Zhang, G.-B. Stability of traveling wavefronts for a three-component Lotka-Volterra competition system on a lattice. *Electron. J. Differ. Equ.* **2018**, *57*, 1–16.
19. Wu, H.-C. A general approach to the asymptotic behavior of traveling waves in a class of three-component lattice dynamical systems. *J. Dyn. Differ. Equ.* **2016**, *28*, 317–338. [CrossRef]
20. Dong, F.-D.; Wang, W.-T.; Wang, J.-B. Asymptotic behavior of traveling waves for a three-component system with nonlocal dispersal and its application. *Discrete Contin. Dyn. Syst.* **2017**, *37*, 2150058. [CrossRef]
21. He, J.; Zhang, G.-B. The minimal speed of traveling wavefronts for a three-component competition system with nonlocal dispersal. *Int. J. Biomath.* **2021**, *14*, 2150058. [CrossRef]
22. Hung, L.-C. Traveling wave solutions of competitive-cooperative Lotka-Volterra systems of three species. *Nonlinear Anal. Real World Appl.* **2011**, *12*, 3691–3700. [CrossRef]
23. Ma, Z.-H.; Wu, X.; Rong, Y. Nonlinear stability of traveling wavefronts for competitive-cooperative Lotka-Volterra systems of three species. *Appl. Math. Comput.* **2017**, *315*, 331–346. [CrossRef]
24. Ma, M.; Huang, Z.; Ou, C. Speed of the traveling wave for the bistable Lotka-Volterra competition Model. *Nonlinearity* **2019**, *32*, C3143–C3162. [CrossRef]
25. Bunimovich, L.A.; Sinai, Y.G. Spacetime chaos in coupled map lattices. *Nonlinearity* **1988**, *1*, 491. [CrossRef]
26. Chow, S.N. Lattice dynamical systems. In *Dynamical Systems*; Lecture Notes in Mathematics; Macki, J.W., Zecca, P., Eds.; Springer: Berlin, Germany, 2003; Volume 1822, pp. 1–102.
27. Fife, P.C. *Mathematical Aspects of Reacting and Diffusing Systems*; Lecture Notes in Biomathematics; Springer: Berlin, Germany, 1979; Volume 28.
28. Guo, J.-S.; Wu, C.-H. Wave propagation for a two-component lattice dynamical system arising in strong competition models. *J. Differ. Equ.* **2011**, *250*, 3504–3533. [CrossRef]
29. Vukusic, P.; Sambles, J.R. Photonic structures in biology. *Nature* **2003**, *424*, 852–855. [CrossRef]
30. Wang, H.; Pan, C. Spreading speed of a lattice time-periodic Lotka-Volterra competition system with bistable nonlinearity. *Appl. Anal.* **2022**, *102*, 4757–4778. [CrossRef]

31. Chen, X.; Guo, J.-S.; Wu, C.-C. Traveling waves in discrete periodic media for bistable dynamics. *Arch. Ration. Mech. Anal.* **2008**, *189*, 189–236. [CrossRef]
32. Fang, J.; Zhao, X.-Q. Bistable traveling waves for monotone semiflows with applications. *J. Eur. Math. Soc.* **2011**, *17*, 2243–2288. [CrossRef]
33. Ma, M.; Ou, C. Asymptotic analysis of the perturbed Poisson-Boltzmann equation on un bounded domains. *Asymptot. Anal.* **2015**, *91*, 125–146.
34. Bao, X.; Wang, Z.-C. Existence and stability of time periodic traveling waves for a periodic bistable Lotka-Volterra competition system. *J. Differ. Equ.* **2013**, *255*, 2402–2435. [CrossRef]
35. Thieme, H.R. Asymptotic estimates of the solutions of nonlinear integral equations and asymptotic speeds for the spread of populations. *J. Reine Ang. Math.* **1979**, *306*, 94–121.

mathematics

MDPI

Article

Attack-Dependent Adaptive Event-Triggered Security Fuzzy Control for Nonlinear Networked Cascade Control Systems Under Deception Attacks

Xi-Ming Liu, Xiao-Heng Chang * and Li-Wei Hou

School of Control Science and Engineering, Bohai University, Jinzhou 121013, China;
2022008006@qymail.bhu.edu.cn (X.-M.L.)
* Correspondence: changxiaoheng@wust.edu.cn

Abstract: This article investigates the issue of H_∞ security output feedback control for a nonlinear networked cascade control system with deception attacks. First, to further reduce the amount of communication data, reasonably schedule network resources, and alleviate the impact of multi-channel deception attacks, an attack-dependent adaptive event-triggered mechanism is introduced into the primary network channel, and its adaptive triggered threshold can be adjusted according to the random attack probability. Secondly, the output dynamic quantization of the secondary network channel is considered. Then, a novel security cascade output feedback controller design framework based on the Takagi–Sugeno (T-S) fuzzy networked cascade control system under deception attacks is established. In addition, by introducing the Lyapunov–Krasovskii stability theory, the design conditions of the controller are given. Finally, the effectiveness and superiority of the proposed design strategies are verified by two simulation examples of power plant boiler–turbine system and power plant boiler power generation control system.

Keywords: nonlinear networked cascade control system; attacks-dependent adaptive event-triggered mechanism; dynamic quantization; deception attacks

MSC: 93B70; 93C42

1. Introduction

Since the cascade control strategy was proposed [1], it has become an effective means to optimize the control system performance. Especially in the presence of external disturbances, the performance improvement effect is remarkable. The cascade control systems are composed of two subsystems in series, which are divided into the primary loop and the secondary loop. Since the secondary loop has a faster response speed than the primary loop, the secondary loop can effectively suppress the system disturbance, and the primary loop is responsible for adjusting the steady-state performance of the system [2]. It is precisely because the cascade control system has the advantages of reducing the disturbance of the secondary loop and improving the control quality, that the cascade control strategy is widely used in many industrial production process controls such as heat exchange systems [3] and cyber-physical systems [4].

In recent years, networked control systems (NCSs) have been widely used in intelligent transportation, intelligent manufacturing, and daily life due to their advantages of low cost, space saving, and easy maintenance [5–7]. Compared with the cascade control systems that do not transmit signal through the network, the networked cascade control systems (NCCSs) of signals transmission through the network combine the advantages of cascade control systems and NCSs. Based on this, many studies related to NCCSs have been published; for example, in [8], a passivity-based H_∞ controller design method for NCCSs was proposed and verified by a boiler–turbine system. The issue of H_∞ control for NCCSs with

uncertain time-delay was considered in [9]. However, the open network environment may lead to many important data being eavesdropped or maliciously attacked, which will lead to unreliable or unavailable communication data, and even serious security incidents [10]. Therefore, the problem of security controller design for NCCSs in practical engineering applications has attracted the attention of many scholars, and some results have been published. For example, in [11], a novel design method of networked cascade controller based on event-triggered control was proposed under stochastic nonlinear constraints and actuator faults. Considering the denial-of-service (DoS) attacks and the possible saturation problem of the actuator, the event-triggered controller of the NCCS was investigated in [12]. By proposing a switching method, the H_∞ stabilization problem of event-triggered NCCSs under DoS attacks was proposed in [13].

However, in the cascade security control strategy studied above, only the threat of DoS attacks to the system was concerned. Unlike the purpose of DoS attacks to block data transmission by occupying network bandwidth, deception attacks mainly achieve the purpose of attack by destroying the integrity and availability of transmitted data. At the same time, it is more covert and sensitive than DoS attacks. After the transmitted data are tampered with by the attacker, it is difficult for the data receiver to detect [14]. Furthermore, deception attacks can also be subdivided into: (1) false data injection attacks [15–17]; that is, the attacker knows the system state information, and (2) replay attacks [18]; that is, the attacker is unknown to the system state information. In addition, it is worth noting that stealth attacks can also be regarded as a kind of covert false data injection attacks with better concealment [19].

In this article, we focus on the study of random deception attacks in which the attacker knows the system state information in advance, such as [20], considering the influence of primary loop random deception attacks and actuator saturation, and the H_∞ control problem of NCCSs based on hybrid drive mechanism was studied. However, most of the existing literature only focuses on the threat of deception attacks on a single channel, and the research on deception attacks on any multi-channel is not sufficient [21,22], especially the security control problem of NCCSs under the threat of multi-channel deception attacks. Malicious adversaries that launch deception attacks on any multi-channel will seriously damage the integrity of the data transmitted by the main loop and the secondary loop of the NCCSs, thus affecting the adjustment of the entire NCCSs and affecting the performance and stability of the NCCSs. Therefore, the security cascade control strategy under the threat of arbitrary multi-channel deception attacks deserves further study.

In addition, we review the existing cascade control strategies based on event-triggered mechanism (ETM) under the influence of network attacks [8,13,14,20]. The design of event-triggered conditions or triggered thresholds only considers system-related information and ignores the impact of network attack sequences on event-triggered results. How to design the attacks-dependent adaptive ETM (ADAETM), obtain more stringent triggered conditions, and enhance the non-vulnerability of the triggered mechanism is a proposition worth exploring. On the other hand, the secondary network channel of the NCCSs also needs attention due to the transmission delay, packet disorder, and other threats caused by bandwidth constraints. Therefore, it is necessary to dynamically quantify the transmission signal of the secondary network channel. In recent years, many results on the controller and filter design of NCCSs under the joint framework of event-triggered and quantizer strategies have been published [23–27]. This inspires us to further explore the joint design method of ADAETM and dynamic quantization for NCCSs.

As an effective modeling method for nonlinear systems, the T-S fuzzy model is based on the principle of fuzzy logic. By setting appropriate membership functions (MFs), a series of local subsystems were smoothly connected to approximate the nonlinear systems [28]. Due to the advantages of the T-S fuzzy model, the related research results based on T-S fuzzy systems are remarkable, especially the control synthesis and filter design of nonlinear NCCSs in recent years [27,29–33]. For instance, the security fuzzy controller design problem of nonlinear NCCSs based on event-triggered and quantization strategy was studied in

the network attacks environment [27]. The reachable set control problem for the T-S fuzzy singular Markov jump system was studied in [31]. Considering the DC microgrid system based on T-S fuzzy model, the security fuzzy control strategy under the influence of time-constrained DoS attacks was given in [32]. Moreover, considering the unmeasurable or unavailable state variables in NCCs, the output feedback control strategy is more reasonable than the state feedback control strategy and closer to the practical application background. The excellent results of NCSs output feedback have been reported in [34–37]. For example, in [34], the quantized output feedback security tracking controller design problem was studied, and a novel design framework was given. Considering the problem of time delay and packet loss, ref. [36] designed a output feedback controller under finite-time stability for NCCS. However, it is found that the output feedback control problem of nonlinear NCCS based on the T-S fuzzy model has not been solved in the existing literature, which inspires this work.

On the basis of the above existing research works, we will consider the design of fuzzy security cascade output feedback controller (SCOFC) based on ADAETM for the nonlinear NCCSs under the multi-channel deception attacks and secondary-loop signal dynamic quantization. The contributions of the proposed design strategy are as follows:

1. Different from the results of single-channel deception attacks in [20,27], this article focuses on the multi-channel deception attacks from the primary sensor to the primary controller communication link and from the secondary controller to the actuator communication link.
2. A novel ADAETM is proposed. Its adaptive law can flexibly adjust the adaptive triggered threshold by random deception attacks probability, which further alleviates the impact of deception attacks on the NCCS.
3. Compared with [8,9,11–13,20,26,27], the signal dynamic quantization of the secondary loop channel is considered for the first time. The data transmission amount of the secondary network channel is reduced, and the network channel burden is further reduced.
4. A novel SCOFC design strategy is proposed under the framework of ADAETM, dynamic quantization, and deception attacks. Based on this framework, the theoretical results of the developed security fuzzy controller are expressed by linear matrix inequalities (LMIs), and the mean square asymptotically stable with H_∞ performance is ensured for the resulting system.

The structure of the follow-up research content of this article is as follows. The problem formulation of SCOFC is given in Section 2. In Section 3, the novel SCOFC design strategy and design results are given by LMIs. In Section 4, two simulation examples of power plant boiler–turbine system (PPBTS) and power plant boiler power generation control system (PPBPGCS) are shown the effectiveness of the proposed design strategy. The main conclusion of the article is concluded in Section 5.

Notations: Let $\mathbb{R}^n$ and $\mathbb{R}^{m\times n}$ represent the n-dimensional Euclidean space and the $m \times n$ real matrices sets, respectively. The matrices $\mathcal{N}^T$ and $\mathcal{N}^{-1}$ denote the matrix $\mathcal{N}$ transposition and inverse, respectively. diag$\{\cdot\}$ stands for the block-diagonal matrix and $\mathbf{I}_n$, $\mathbf{0}_n$ represent the n columns identity matrices and zero matrices with appropriate dimensions, respectively. Let $\mathcal{H}_e\{\mathcal{N}\}$ denotes $\mathcal{N} + \mathcal{N}^T$, and $l_2[0,\infty)$ stands for the square-integrable function space. The symbol $i \in \langle r\rangle$ means that $i = 1, 2, 3, \ldots, r$.

2. Problem Formulation

This article is concerned with security control for nonlinear NCCSs. As shown in Figure 1, the nonlinear NCCS is described by the T-S fuzzy model, which is mainly composed of primary and secondary systems in series. The primary loop consists of primary plant–Plant^1, primary sensor–Sensor^1, primary controller–Controller^1, and actuator. The secondary loop consists of secondary plant–Plant^2, secondary sensor–Sensor^2, secondary controller–Controller^2, and actuator.

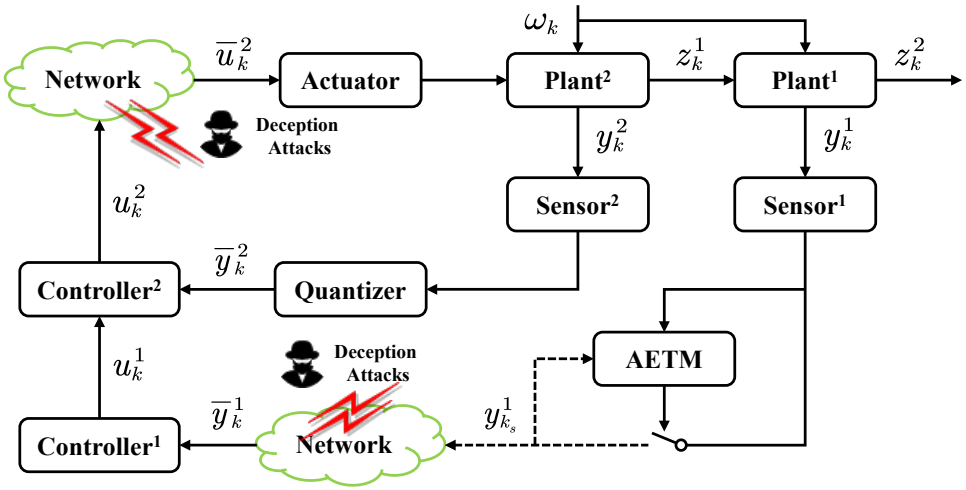

Figure 1. Framework of an NCCS under deception attacks.

Combining the advantages of NCCSs and traditional cascade control systems, the definition of NCCSs is mainly reflected in the sensor–controller, and the data between the controller and actuator are transmitted through the wireless network. Considering the characteristics of the NCCS, a dynamic quantizer is introduced in the secondary loop, and an ADAETM is introduced in the primary loop. At the same time, the risk of deception attacks from primary sensor–Sensor^1 to primary controller–Controller^1 and from secondary sensor–Sensor^2 to actuator is considered.

2.1. System Description

In the nonlinear NCCS, the discrete-time T-S fuzzy primary system–Plant^1 is described as follows:

Plant^1 Rule i: **IF** $d_1(x_k^1)$ is $\mathscr{D}_1^i, \ldots,$ and $d_p(x_k^1)$ is $\mathscr{D}_p^i$, **THEN**

$$\begin{cases} x_{k+1}^1 = A_{1i}x_k^1 + B_{1i}z_k^2 \\ z_k^1 = C_{1i}x_k^1 + D_{1i}\omega_k \\ y_k^1 = E_{1i}x_k^1 \end{cases} \tag{1}$$

where $\mathscr{D}_l^i (i \in \langle r \rangle, l \in \langle p \rangle)$ denotes the fuzzy sets, $d_l(x_k^1)$ is premise variable and $d(x_k^1) = [d_1(x_k^1) \ldots d_p(x_k^1)]$; $x_k^1 \in \mathbb{R}^{n_{x^1}}$, $z_k^1 \in \mathbb{R}^{n_{z^1}}$, $y_k^1 \in \mathbb{R}^{n_{y^1}}$ and $z_k^2 \in \mathbb{R}^{n_{z^2}}$ denote the state vector, measured output, regulated output of Plant^1, and the measurement output of Plant^2, respectively; $\omega_k \in \mathbb{R}^{n_\omega}$ belongs to $l_2[0, \infty)$ and represents the exogenous disturbances. A_{1i}, B_{1i}, C_{1i}, D_{1i}, and E_{1i} are the known system matrices of the appropriate dimensions.

By using a standard fuzzy inference approach, the fuzzy primary system (1) is inferred as follows:

$$\begin{cases} x_{k+1}^1 = \sum\limits_{i=1}^{r} g_i^1(d(x_k^1))[A_{1i}x_k^1 + B_{1i}z_k^2] \\ z_k^1 = \sum\limits_{i=1}^{r} g_i^1(d(x_k^1))[C_{1i}x_k^1 + D_{1i}\omega_k] \\ y_k^1 = \sum\limits_{i=1}^{r} g_i^1(d(x_k^1))E_{1i}x_k^1 \end{cases} \tag{2}$$

where $g_i^1(d(x_k^1))$ are the normalized MFs satisfying that $g_i^1(d(x_k^1)) = \frac{w_i(x_k^1)}{\sum_{i=1}^r w_i(x_k^1)} \geq 0$, $\sum_{i=1}^r g_i^1(d(x_k^1)) = 1$ with $w_i(x_k^1) = \prod_{l=1}^q \mathscr{D}_l^i(d_l(x_k^1))$ which denotes the MFs of the primary system with premise variable $d_l(x_k^1)$.

In addition, the introduction of event-triggered strategy in the network channel will lead to the problem of asynchronous signal transmission. And the asynchrony and mismatch of premise variables of the fuzzy primary controller–Controller^1 are considered.

Controller^1 Rule j: **IF** $d_1(\bar{x}_k^1)$ is $\mathscr{O}_1^j, \ldots,$ and $d_p(\bar{x}_k^1)$ is $\mathscr{O}_p^j$, **THEN**

$$u_k^1 = K_{1j}\bar{y}_k^1 \tag{3}$$

where K_{1j} are the Controller^1 gains, $\bar{y}_k^1$ is the final input of the Controller^1 after event-triggered and deception attacks, and $u_k^1 \in \mathbb{R}^{n_{u1}}$ denote control input of Plant^1. $\mathscr{O}_l^j (j \in \langle r \rangle$, $l \in \langle p \rangle)$ denotes the fuzzy sets, $d_l(\bar{x}_k^1)$ is premise variable, and $d(\bar{x}_k^1) = [d_1(\bar{x}_k^1) \ldots d_p(\bar{x}_k^1)]$.

By using single-point fuzzification, product reasoning, and the central weighted average defuzzification method, the output form of the fuzzy Controller^1 is as follows:

$$u_k^1 = \sum_{j=1}^{r} g_j^1(d(\bar{x}_k^1))K_{1j}\bar{y}_k^1 \tag{4}$$

where $g_j^1(d(\bar{x}_k^1))$ are the normalized MFs satisfying that $g_j^1(d(\bar{x}_k^1)) = \frac{w_j(\bar{x}_k^1)}{\sum_{j=1}^r w_j(\bar{x}_k^1)} \geq 0$, $\sum_{j=1}^r g_j^1(d(\bar{x}_k^1)) = 1$ with $w_j(\bar{x}_k^1) = \prod_{l=1}^p \mathscr{O}_l^j(d_l(\bar{x}_k^1))$ which denotes the MFs of the Controller^1 with premise variable $d_l(\bar{x}_k^1)$.

Based on the reconstruction strategy in [22], the asynchronous problem of MFs caused by event-triggered strategy was effectively solved. Suppose the minimum values of $g_j^1(d(x_k^1)) > 0$ and $g_j^1(d(\bar{x}_k^1)) > 0$, the relationship between $g_j^1(d(x_k^1))$ and $g_j^1(d(\bar{x}_k^1))$ is interpreted as

$$|g_j^1(d(\bar{x}_k^1)) - g_j^1(d(x_k^1))| \leq \Lambda_j$$

where $g_j^1(d(\bar{x}_k^1)) = \varrho_j g_j^1(d(x_k^1))$, Λ_j are some positive constants, $\varrho_j = \varrho_j(d(x_k^1), d(\bar{x}_k^1))$ is a parameter related with $g_j^1(d(x_k^1))$, and $g_j^1(d(\bar{x}_k^1))$.

Based on the conditions mentioned above, one obtains

$$\underline{\varrho}_j = 1 - \frac{\Lambda_j}{g_j^1(d(x_k^1))} \leq \varrho_j \leq 1 + \frac{\Lambda_j}{g_j^1(d(x_k^1))} = \bar{\varrho}_j \tag{5}$$

where $\underline{\varrho}_j$ and $\bar{\varrho}_j$ denote the known lower bound and upper bound of ϱ_j, which yields that

$$\frac{\underline{\varrho}_j}{\bar{\varrho}_j} \triangleq \frac{\min\{\varrho_i\}}{\max\{\varrho_j\}} \leq \frac{\varrho_i}{\varrho_j} \leq \frac{\max\{\varrho_i\}}{\min\{\varrho_j\}} \triangleq \frac{\bar{\varrho}_j}{\underline{\varrho}_j}.$$

Setting $\varrho_{\min} = \min\{\underline{\varrho}_j\}$ and $\varrho_{\max} = \max\{\bar{\varrho}_j\}$ for $i, j \in \langle r \rangle$, one has

$$\vartheta_1 \triangleq \frac{\varrho_{\min}}{\varrho_{\max}} \leq \frac{\varrho_i}{\varrho_j} \leq \frac{\varrho_{\max}}{\varrho_{\min}} \triangleq \vartheta_2. \tag{6}$$

In the nonlinear NCCS, the discrete-time T-S fuzzy secondary system–Plant^2 is described as follows:

Plant^2 Rule q: **IF** $f_1(x_k^2)$ is $\mathscr{F}_1^q, \ldots,$ and $f_p(x_k^2)$ is $\mathscr{F}_p^q$, **THEN**

$$\begin{cases} x_{k+1}^2 = A_{2q}x_k^2 + B_{2q}\bar{u}_k^2 + B_{3q}\omega_k \\ z_k^2 = C_{2q}x_k^2 + D_{2q}\omega_k \\ y_k^2 = E_{2q}x_k^2 \end{cases} \tag{7}$$

where $\mathscr{F}_l^q (q \in \langle r \rangle, l \in \langle p \rangle)$ denotes the fuzzy sets, $f_l(x_k^2)$ are fuzzy premise variables and $f(x_k^2) = [f_1(x_k^2) \dots f_p(x_k^2)]$; $x_k^2 \in \mathbb{R}^{n_{x^2}}$ and $\bar{u}_k^2 \in \mathbb{R}^{n_{u^2}}$ denote the state vector and the final control input of Plant^2, respectively; The remaining parameters are defined with reference to Plant^1. A_{2q}, B_{2q}, B_{3q}, C_{2q}, D_{2q}, and E_{2q} are the known system matrices of the appropriate dimensions.

Then, based on fuzzy inference approach, the secondary system–Plant^2 (7) is inferred as follows:

$$\begin{cases} x_{k+1}^2 = \sum\limits_{q=1}^{r} g_q^2(f(x_k^2))[A_{2q}x_k^2 + B_{2q}\bar{u}_k^2 + B_{3q}\omega_k] \\ z_k^2 = \sum\limits_{q=1}^{r} g_q^2(f(x_k^2))[C_{2q}x_k^2 + D_{2q}\omega_k] \\ y_k^2 = \sum\limits_{q=1}^{r} g_q^2(f(x_k^2))E_{2q}x_k^2 \end{cases} \tag{8}$$

where $g_q^2(f(x_k^2))$ are the normalized MFs satisfying that $g_q^2(f(x_k^2)) = \frac{w_q(x_k^2)}{\sum_{q=1}^{r} w_q(x_k^2)} \geq 0$, $\sum_{q=1}^{r} g_q^2(f(x_k^2)) = 1$ with $w_q(x_k^2) = \prod_{l=1}^{p} \mathscr{F}_l^q(f_l(x_k^2))$ denotes the MFs of the system with premise variable $f_l(x_k^2)$.

The model of secondary controller–Controller^2 considering quantization in network channel is given as follows:

$$u_k^2 = K_2\bar{y}_k^2 + u_k^1 \tag{9}$$

where K_2 is the Controller^2 gain and $\bar{y}_k^2$ is the quantized system measurement output.

2.2. Dynamic Quantizer

In this article, consider the following form of dynamic quantizer:

$$q_\mu(\nu_k) = \mu_k q\left(\frac{\nu_k}{\mu_k}\right), \mu_k > 0 \tag{10}$$

where μ_k is the dynamic parameter and suppose that the dynamic quantizer (10) satisfies the following constraints:

$$\|q(\nu_k) - \nu_k\| \leq \Delta, \text{ if } \|\nu_k\| \leq M \tag{11a}$$

$$\|q(\nu_k)\| > M - \Delta, \text{ if } \|\nu_k\| > M \tag{11b}$$

where $M > 0$ and $\Delta > 0$ represent the quantization range and quantization error bound of dynamic quantizer, respectively.

Then, the quantized measurement output signal of Plant^2 is in the following form:

$$\bar{y}_k^2 = q_\mu(y_k^2) = \mu_k q\left(\frac{y_k^2}{\mu_k}\right) = h_k^\mu + y_k^2 \tag{12}$$

where $q_\mu(*)$ is a dynamic quantizer defined by (10), and $h_k^\mu = \mu_k(q(\frac{y_k^2}{\mu_k}) - \frac{y_k^2}{\mu_k})$. The measurement output signal quantization process and parameter update of dynamic quantizer are shown in Algorithm 1.

Remark 1. *Due to the introduction of network in cascade control systems, it is necessary to consider the network phenomenon of each loop. Different from the existing literature [8,9,11–13,20,26,27], this article considers the signal quantization problem of the secondary loop for the first time. In addition, in order to balance the number of packets and quantization error in the network signal, based on the method proposed in [34], the quantization error term can be well processed.*

Algorithm 1 Calculation of μ_k and $\bar{y}_k^2$ in dynamic quantizer

Input: Δ, M, and $\hbar$
Output: μ_k, h_k^μ and $\bar{y}_k^2$
Step 1: At the sampling instant k, the dynamic quantizer receives y_k^2.
if $\|y_k^2/\mu_k\| \leq M$ **then**
$\|q(y_k^2/\mu_k) - (y_k^2/\mu_k)\| \leq \Delta$
else
$\|q(y_k^2/\mu_k)\| > M - \Delta$
end if
Step 2: Update dynamic parameter μ_k and quantization data $\bar{y}_k^2$.
$\mu_k = (\hbar/M)\|y_k^2\|$, $h_k^\mu = [(\hbar\Delta)/M]\sin(y_k^2)$, $\bar{y}_k^2 = h_k^\mu + y_k^2$
Step 3: Let $k = k + 1$ and go to Step 1.
return μ_k, h_k^μ and $\bar{y}_k^2$.
The dynamic quantizer parameter μ_k and quantization data $\bar{y}_k^2$ are obtained.

2.3. Multi-Channel Deception Attacks

The deception attacks in the NCCSs mainly inject the wrong data into the communication channel intermittently, and replace the real data at the same time, which affect the stability and performance of the systems. Therefore, the security problem of NCCSs interfered by multi-channel deception attacks cannot be ignored.

Considering the characteristics of the deception attacks signals $\mathfrak{f}_k^1 \in \mathbb{R}^{n_{y^1}}$ and $\mathfrak{f}_k^2 \in \mathbb{R}^{n_{u^2}}$, which assumes that the following constraints are satisfied:

$$\|\mathfrak{f}_k^1\|_2 \leq \|\mathcal{F}_1\hat{y}_k^1\|_2, \|\mathfrak{f}_k^2\|_2 \leq \|\mathcal{F}_2 u_k^2\|_2 \tag{13}$$

where $\mathcal{F}_1$ and $\mathcal{F}_2$ are constant matrices denoting the upper bound of the error data function with nonlinear characteristics. Bernoulli variables α_{1k} and α_{2k} are used to describe the probabilistic characteristics of deception attacks, satisfying

$$\mathbb{E}\{\alpha_{\iota k}\} = \bar{\alpha}_\iota, \mathbb{E}\{(\alpha_{\iota k} - \bar{\alpha}_\iota)^2\} = \rho_\iota^2, \iota \in \langle 2 \rangle.$$

Then, the signals $\bar{y}_k^1$ and $\bar{u}_k^2$ transmitted to the communication network after being deception attacks are expressed as follows:

$$\begin{aligned} \bar{y}_k^1 &= \alpha_{1k}\mathfrak{f}_k^1 + (1 - \alpha_{1k})\hat{y}_k^1 \\ \bar{u}_k^2 &= \alpha_{2k}\mathfrak{f}_k^2 + (1 - \alpha_{2k})u_k^2. \end{aligned} \tag{14}$$

Remark 2. *Different from [20,27], this article also considers the impact of deception attacks between the primary loop Sensor^1 to Controller^1 network channel and Controller^2 to actuator network channel. Compared with [20,27], the controller design method proposed in this article under multi-channel deception attacks is closer to the actual situation and more meaningful.*

Remark 3. *It is worth noting that the success of network attacks is random, which is determined by the built-in hardware and software protection in the device, the data transmitted based on the network protocol, and the network conditions with random fluctuation characteristics; that is, network congestion, network load, and so on [17,20]. Therefore, this article discusses random multi-channel deception attacks, and assumes that the deception attacks occur in the primary loop Sensor^1 to Controller^1 network channel and Controller^2 to actuator network channel. At the same time, the way deception attacks destroy data integrity is to completely replace real data with false data attack signals [15] (refer to (14)).*

Remark 4. *It should be further pointed out that the attack signal of the network attacks is generated by the attacker's strategy formulation of the attack object, so the network attacks may be difficult to detect or undetectable, and the attack signal may be associated with the systems state data, output*

data, control data, and other information [14]. Referring to the description of the attack signal in [20], the two deception attack signals considered in this article are modeled as nonlinear functions related to the output data of Plant[1] *and the control signal of Controller*[2]*, respectively, and satisfy the constraints in (13).*

2.4. Attacks-Dependent Adaptive Event-Triggered Mechanism

In order to alleviate the impact of deception attacks on the triggered effect and system performance, the following form of ADAETM is given:

$$k_{s+1} = \inf_{k}\left\{k > k_s | e_{sk}^T \Omega e_{sk} > \delta_k y_{k_s}^{1T} \Omega y_{k_s}^1 \right\} \tag{15}$$

where $e_{sk} = y_{k_s}^1 - y_k^1$, y_k^1 is the current sampled measurement output and $y_{k_s}^1$ is the latest measurement output signal that satisfies the triggered condition, $\Omega > 0$ is the event-triggered weighting matrix to be designed, and δ_k is an adaptive parameter and satisfies the following adaptive law:

$$\delta_k = \delta_1 - \delta_2 \frac{2\bar{\alpha}_1}{\pi} \text{atan}(\epsilon_1 \|y_{k_s}^1\|^{\epsilon_2}) + \delta_3 \exp(-\epsilon_3 \|\Omega^{\frac{1}{2}} e_{sk}\|^{\epsilon_4})$$

where atan$(*)$ is the inverse-tangent function. ϵ_1, ϵ_2, ϵ_3, and ϵ_4 are the event-triggered threshold adjustment positive parameters. δ_1, δ_2, and δ_3 are known constant thresholds. Then, the ADAETM operating mechanism is shown in Algorithm 2.

Remark 5. *Considering the influence of deception attacks, attack probability $\bar{\alpha}_1$ is introduced to design the random adaptive law δ_k. It is obvious that the expression $\delta_2 \frac{2\bar{\alpha}_1}{\pi} atan(\epsilon_1 \|y_{k_s}^1\|^{\epsilon_2})$ is always greater than 0. When the attack intensity increases, that is, the attack probability $\bar{\alpha}_1$ becomes larger, then the term $-\delta_2 \frac{2\bar{\alpha}_1}{\pi} atan(\epsilon_1 \|y_{k_s}^1\|^{\epsilon_2})$ makes the adaptive law δ_k smaller, the triggered condition is easier to meet, so that more sampling data are transmitted to compensate for the impact of the deception attacks. On the other hand, when the communication channel data are transmitted normally, the δ_k will degrade into $\delta_1 + \delta_3 \exp(-\epsilon_3 \|\Omega^{\frac{1}{2}} e_{sk}\|^{\epsilon_4})$; thus, δ_k will relatively increase. Such changes can make the triggered condition more stringent, help to further reduce the triggered data, and improve resource utilization. The detailed operation process can be understood by Algorithm 2.*

Consider the network induced delay η_{k_s} satisfying $\eta_{k_s} \in [0, \eta_M)$, where η_M is a positive integer. Based on the analysis process in [29], define the following:

$$\hat{y}_k^1 = y_{k_s}, k \in [k_s + \eta_{k_s}, k_{s+1} + \eta_{k_s+1} - 1]. \tag{16}$$

Then, the introduced time-varying delay variable τ_k and output data error e_{sk} are expressed as

$$\tau_k = \begin{cases} k - k_s, & k \in \mathscr{S}_0 \\ k - k_s - \ell, & k \in \mathscr{S}_\ell \\ k - k_s - \bar{\ell}, & k \in \mathscr{S}_{\bar{\ell}} \end{cases} \tag{17}$$

$$e_{sk} = \begin{cases} 0, & k \in \mathscr{S}_0 \\ y_{k_s}^1 - y_{k_s+\ell}^1, & k \in \mathscr{S}_\ell \\ y_{k_s}^1 - y_{k_s+\bar{\ell}}^1, & k \in \mathscr{S}_{\bar{\ell}} \end{cases} \tag{18}$$

where $\mathscr{S}_0 = [k_s + \eta_{k_s}, k_s + \eta_M + 1]$, $\mathscr{S}_\ell = [k_s + \eta_M + \ell, k_s + \eta_M + \ell + 1]$, $\mathscr{S}_{\bar{\ell}} = [k_s + \eta_M + \bar{\ell}, k_{s+1} + \eta_{k_s+1} - 1]$, $\ell = 1, 2, \ldots, \bar{\ell} - 1$.

Then, the range of τ_k is as follows:

$$0 < \eta_{k_s} \leq \tau_k \leq 1 + \eta_M = \bar{\tau} \tag{19}$$

where $\bar{\tau}$ is a constant, which is the upper bound of event-triggered data transmission delay. Then, the signal $\hat{y}_k^1$ transmitted to the Controller^1 can be obtained as

$$\hat{y}_k^1 = y_{k-\tau_k} + e_{sk}. \tag{20}$$

Algorithm 2 Calculation of δ_k and (k, y_k^1) in ADAETM

Input: Ω, $\bar{\alpha}_1$, δ_1, δ_2, δ_3, ϵ_1, ϵ_2, ϵ_3, and ϵ_4. Initial set $k_0 = 0$, $y_{k_0}^1 = 0$, $k = 1$, $s = 0$.
Output: δ_k and (k, y_k^1).
Step 1: At the sampling instant k, the network channel receives y_k^1.
if attack probability $\bar{\alpha}_1 = 0$ **then**
the term $-\delta_2 \frac{2\bar{\alpha}_1}{\pi} \text{atan}(\epsilon_1 \|y_{k_s}^1\|^{\epsilon_2}) = 0$, $\delta_1 + \delta_3 \exp(-\epsilon_3 \|\Omega^{\frac{1}{2}} e_{sk}\|^{\epsilon_4}) \Rightarrow \delta_k \uparrow$
else if attack probability $\bar{\alpha}_1 \uparrow$ **then**
the term $\delta_2 \frac{2\bar{\alpha}_1}{\pi} \text{atan}(\epsilon_1 \|y_{k_s}^1\|^{\epsilon_2}) \uparrow \Rightarrow \delta_k \downarrow$
else
the term $\delta_2 \frac{2\bar{\alpha}_1}{\pi} \text{atan}(\epsilon_1 \|y_{k_s}^1\|^{\epsilon_2}) \downarrow \Rightarrow \delta_k \uparrow$
end if
Step 2: Update attacks dependent adaptive law δ_k and data packet
if $e_{sk}^T \Omega e_{sk} > \delta_k y_{k_s}^{1T} \Omega y_{k_s}^1$ **then**
the buffer stores the data packet (k, y_k^1) with $k_0 = k$, $y_{k_0}^1 = y_k^1$, releases the data packet to the communication channel
else
the data packet is not transmission
end if
Step 3: Let $k = k + 1$ and go to Step 1.
return k_s, $y_{k_s}^1$, and δ_k.
The attacks-dependent adaptive law δ_k and latest output data packet (k, y_k^1) are obtained.

2.5. System Formulation

By combining (2), (4), (8), (9), (12), (14), (20), and defining $g_i^1 = g_i^1(d(x_k^1))$, $g_j^1 = g_j^1(d(\bar{x}_k^1))$, $g_q^2 = g_q^2(f(x_k^2))$, it can yield a new model for NCCSs as follows:

$$\begin{aligned}
x_{k+1}^1 &= \sum_{i=1}^{r} \sum_{j=1}^{r} g_i^1 g_q^2 [A_{1i} x_k^1 + B_{1i} C_{2q} x_k^2 + B_{1i} D_{2q} \omega_k] \\
x_{k+1}^2 &= \sum_{i=1}^{r} \sum_{j=1}^{r} \sum_{q=1}^{r} g_i^1 g_j^1 g_q^2 [(A_{2q} + (1-\alpha_{2k}) B_{2q} K_2 E_{2q}) x_k^2 \\
&\quad + (1-\alpha_{1k})(1-\alpha_{2k}) B_{2q} K_{1j} E_{1i} x_{k-\tau_k}^1 \\
&\quad + (1-\alpha_{1k})(1-\alpha_{2k}) B_{2q} K_{1j} e_{sk} \\
&\quad + (1-\alpha_{2k}) \alpha_{1k} B_{2q} K_{1j} \mathfrak{f}_k^1 + \alpha_{2k} B_{2q} \mathfrak{f}_k^2 \\
&\quad + (1-\alpha_{2k}) B_{2q} K_2 h_k^{\mu} + B_{3q} \omega_k] \\
z_k^1 &= \sum_{i=1}^{r} g_i^1 [C_{1i} x_1(k) + D_{1i} \omega_k].
\end{aligned} \tag{21}$$

The nonlinear NCCS is considered in this article, and under the influence of multi-channel deception attacks, the ADAETM and dynamic quantizer are introduced, so that the designed SCOFC satisfies the following objectives:

1. The system (21) is mean square asymptotically stable in the absence of external disturbances, i.e., $\omega_k = 0$;
2. Under zero initial conditions, for all $\omega_k \neq 0$, there exists a positive scalar $\gamma > 0$, such that the following condition holds: $\sum_{k=0}^{\infty} z_k^{1T} z_k^1 \leq \gamma^2 \sum_{k=0}^{\infty} \omega_k^T \omega_k$.

3. Main Results

In this section, the design conditions that guarantee the mean square asymptotically stable and H_∞ performance of the system (21) are given. Then, the design results of the security fuzzy controller gains under event-triggered and dynamic quantization strategy are given.

Theorem 1. *For given scalars $\bar{\alpha}_1 > 0$, $\bar{\alpha}_2 > 0$, $\delta_1 > 0$, $\delta_2 > 0$, $\delta_3 > 0$, $\Delta > 0$, $M > 0$, $\tau > 0$, $\bar{\tau} > 0$, and $\vartheta_\jmath > 0$ ($\jmath \in \langle 2 \rangle$), the system (21) is mean square asymptotically stable and satisfies the predetermined H_∞ performance index γ if there exist positive definite symmetric matrices P_1, P_2, Q_1, Q_2, Q_3, R_1, R_2, Ω, and slack matrix R_3 with appropriate dimensions, such that the following inequalities hold for $i < j$:*

$$\begin{bmatrix} R_2 & * \\ R_3 & R_2 \end{bmatrix} > 0 \tag{22}$$

$$\begin{bmatrix} \Pi_i^{11} & * \\ \Pi_{iiq}^{21} & \Pi_{22} \end{bmatrix} < 0 \tag{23}$$

$$\begin{bmatrix} \Pi_i^{11} + \vartheta_\jmath \Pi_j^{11} & * & * \\ \Pi_{ijq}^{21} & \Pi_{22} & * \\ \sqrt{\vartheta_2}\Pi_{jiq}^{21} & 0 & \Pi_{22} \end{bmatrix} < 0,\ i, j, q \in \langle r \rangle \tag{24}$$

where

$$\Pi_i^{11} = \begin{bmatrix} \Pi_i^1 & * \\ \Pi_i^3 & \Pi_2 \end{bmatrix},\ \Pi_i^1 = diag\{-\Pi_1,\ \bar{\Pi}_i^1,\ -P_2\}$$

$$\bar{\Pi}_i^1 = \begin{bmatrix} Q_2 - Q_1 - R_2 & * & * \\ R_2 - R_3 & -\Pi_{3i} & * \\ R_1 + R_3 & R_2 - R_3 & -\Pi_4 \end{bmatrix}$$

$$\Pi_1 = P_1 + R_1 - Q_1 - Q_3,\ \Pi_4 = Q_2 + Q_3 + R_1 + R_2$$

$$\Pi_{3i} = 2R_1 - \mathcal{H}_e\{R_3\} - \delta E_{1i}^T \Omega E_{1i},\ \delta = \delta_1 + \delta_2 + \delta_3$$

$$\Pi_i^3 = [\Pi_{1i}^{3T}\ 0\ 0\ 0\ 0]^T,\ \Pi_{1i}^3 = [\mathbf{0}_2\ \delta\Omega E_{1i}\ \mathbf{0}_2]$$

$$\Pi_2 = diag\left\{(\delta - 1)\Omega,\ -\frac{M^2}{\Delta^2}I,\ -\bar{\alpha}_1,\ -\bar{\alpha}_2,\ -\gamma^2 I\right\}$$

$$\Pi_{ijq}^{21T} = [\Pi_{ijq}^{211T}, \Pi_{ijq}^{212T}, \Pi_{ijq}^{213T}],\ \Pi_{ijq}^{211} = [\Sigma_{ijq}^3\ \Sigma_{ijq}^4]$$

$$\Sigma_{ijq}^3 = \mathcal{E}_1[\Sigma_i^{31T}\ \Sigma_q^{32T}\ \Sigma_i^{33T}\ \Sigma_{ijq}^{34T}\ \Sigma_{ij}^{35T}]^T$$

$$\Sigma_{ijq}^4 = \mathcal{E}_1[\Sigma_i^{41T}\ 0\ \Sigma^{43T}\ \Sigma_j^{44T}\ \Sigma_j^{45T}]^T$$

$$\Pi_{ijq}^{212} = \mathcal{E}_2[\Sigma_{iq}^{5T}\ \Sigma_{iq}^{6T}\ \Sigma_{iq}^{6T}]^T,\ \Pi_{ijq}^{213} = \mathcal{E}_3[\Sigma_{ijq}^7\ \Sigma_{ijq}^8]$$

$$\Sigma_i^{31} = [C_{1i}\ \mathbf{0}_4],\ \Sigma_q^{32} = [\mathbf{0}_4\ E_{2q}],\ \Sigma_i^{33} = [\mathbf{0}_2\ \mathcal{F}_1 E_{1i}\ \mathbf{0}_2]$$

$$\Sigma_{ijq}^{34} = [\mathbf{0}_2\ \vec{\alpha}_1 \mathcal{F}_2 K_{1j} E_{1i}\ 0\ \mathcal{F}_2 K_2 E_{2q}]$$

$$\Sigma_{ij}^{35} = [\mathbf{0}_2\ -K_{1j}E_{1i}\ \mathbf{0}_2],\ \Sigma_i^{41} = [\mathbf{0}_4\ D_{1i}],\ \Sigma^{43} = [\mathcal{F}_1\ \mathbf{0}_4]$$

$$\Sigma_j^{44} = [\vec{\alpha}_1 \mathcal{F}_2 K_{1j}\ 0\ \bar{\alpha}_1 \mathcal{F}_2 K_{1j}\ \mathbf{0}_2],\ \Sigma_j^{45} = [-K_{1j}\ 0\ K_{1j}\ \mathbf{0}_2]$$

$$\Sigma_{iq}^5 = [A_{1i}\ \mathbf{0}_3\ B_{1i}C_{2q}\ \mathbf{0}_4\ B_{1i}D_{2q}]$$

$$\Sigma_{iq}^6 = [A_{1i} - I\ \mathbf{0}_3\ B_{1i}C_{2q}\ \mathbf{0}_4\ B_{1i}D_{2q}]$$

$$\Sigma_{ijq}^7 = \begin{bmatrix} \mathbf{0}_2 & \vec{\alpha}_1\vec{\alpha}_2\mathcal{B}_{ijq}^1 & 0 & \vec{\alpha}_2\mathcal{B}_q^2 & \vec{\alpha}_1\vec{\alpha}_2\mathcal{B}_{jq}^3 \\ \mathbf{0}_2 & -\vec{\alpha}_2\mathcal{B}_{ijq}^1 & 0 & 0 & -\vec{\alpha}_2\mathcal{B}_{jq}^3 \\ \mathbf{0}_2 & -\vec{\alpha}_1\mathcal{B}_{ijq}^1 & 0 & -\mathcal{B}_q^2 & -\vec{\alpha}_1\mathcal{B}_{jq}^3 \\ \mathbf{0}_2 & \mathcal{B}_{ijq}^1 & 0 & -\mathcal{B}_q^2 & \mathcal{B}_{jq}^3 \end{bmatrix}$$

$$\Sigma_{ijq}^{8} = \begin{bmatrix} \vec{\alpha}_2 B_{2q} K_2 & \vec{\alpha}_2 \bar{\alpha}_1 \mathcal{B}_{jq}^{3} & \bar{\alpha}_2 B_{2q} & B_{3q} \\ 0 & \vec{\alpha}_2 \mathcal{B}_{jq}^{3} & 0 & 0 \\ -B_{2q} K_2 & -\bar{\alpha}_1 \mathcal{B}_{jq}^{3} & B_{2q} & 0 \\ -B_{2q} K_2 & -\mathcal{B}_{jq}^{3} & B_{2q} & 0 \end{bmatrix}$$

$$\Pi_{22} = diag\{\Pi_{22}^{1}, \Pi_{22}^{2}, \Pi_{22}^{3}\}, \vec{\alpha}_\iota = 1 - \bar{\alpha}_\iota$$

$$\Pi_{22}^{1} = diag\{-I, -I, -I, -I, -I\}$$

$$\Pi_{22}^{2} = diag\{-P_1^{-1}, -R_1^{-1}, -R_2^{-1}\}$$

$$\Pi_{22}^{3} = diag\{-P_2^{-1}, -P_2^{-1}, -P_2^{-1}, -P_2^{-1}\}$$

$$\mathcal{B}_{ijq}^{1} = B_{2q} K_{1j} E_{1i}, \mathcal{B}_{q}^{2} = B_{2q} K_2 E_{2q}, \mathcal{B}_{jq}^{3} = B_{2q} K_{1j}$$

$$\mathcal{E}_1 = diag\{I, \hbar, \sqrt{\bar{\alpha}_1}, \sqrt{\bar{\alpha}_2}, \sqrt{\bar{\alpha}_2}\rho_1\}$$

$$\mathcal{E}_2 = diag\{I, \bar{\tau} I, \tau I\}, \mathcal{E}_3 = diag\{I, \rho_1 I, \rho_2 I, \rho_1 \rho_2 I\}.$$

Proof. Consider the discrete-time piecewise Lyapunov–Krasovskii functional in the following form:

$$V_k = V_{1k} + V_{2k} + V_{3k} \tag{25}$$

where

$$V_{1k} = x_k^{1T} P_1 x_k^1 + x_k^{2T} P_2 x_k^2$$

$$V_{2k} = \sum_{v=k-\underline{\tau}}^{k-1} x_v^{1T} Q_1 x_v^1 + \sum_{v=k-\bar{\tau}}^{k-\underline{\tau}-1} x_v^{1T} Q_2 x_v^1 + \sum_{v=k-\bar{\tau}}^{k-1} x_v^{1T} Q_3 x_v^1$$

$$V_{3k} = \bar{\tau} \sum_{l=-\bar{\tau}}^{-1} \sum_{v=k+l}^{k-1} \varrho_v^{1T} R_1 \varrho_v^1 + \tau \sum_{l=-\bar{\tau}}^{-\underline{\tau}-1} \sum_{v=k+l}^{k-1} \varrho_v^{1T} R_2 \varrho_v^1$$

$$\varrho_k^1 = x_{k+1}^1 - x_k^1, \tau = \bar{\tau} - \underline{\tau}.$$

Then, defining $\Delta V_k = V_{k+1} - V_k$, the piecewise Lyapunov–Krasovskii functional difference equation under the mathematical expectation can be obtained as

$$\mathbb{E}\{\Delta V_{1k}\} = \sum_{i=1}^{r} \sum_{j=1}^{r} \sum_{q=1}^{r} g_i^1 g_j^1 g_q^2 \left\{ x_{k+1}^{1T} P_1 x_{k+1}^1 - x_k^{1T} P_1 x_k^1 + \mathbb{E}\{x_{k+1}^{2T} P_2 x_{k+1}^2\} - x_k^{2T} P_2 x_k^2 \right\}$$

$$\mathbb{E}\{\Delta V_{2k}\} = x_k^{1T}(Q_1 + Q_3) x_k^1 + x_{k-\underline{\tau}}^{1T}(Q_2 - Q_1) x_{k-\underline{\tau}}^1 - x_{k-\bar{\tau}}^{1T}(Q_2 + Q_3) x_{k-\bar{\tau}}^1$$

$$\mathbb{E}\{\Delta V_{3k}\} = \sum_{i=1}^{r} \sum_{j=1}^{r} \sum_{q=1}^{r} g_i^1 g_j^1 g_q^2 \left\{ \varrho_k^{1T}(\bar{\tau}^2 R_1 + \tau^2 R_2) \varrho_k^1 - \bar{\tau} \sum_{v=k-\bar{\tau}}^{k-1} \varrho_v^{1T} R_1 \varrho_v^1 \right.$$
$$\left. - \tau \sum_{v=k-\bar{\tau}}^{k-\underline{\tau}-1} \varrho_v^{1T} R_2 \varrho_v^1 \right\}. \tag{26}$$

According to (21) and (26), one has

$$\mathbb{E}\{x_{k+1}^{2T} P_2 x_{k+1}^2\} = \sum_{i=1}^{r} \sum_{j=1}^{r} \sum_{q=1}^{r} g_i^1 g_j^1 g_q^2 \{\mathcal{A}^T P_2 \mathcal{A} + \rho_1^2 \mathcal{B}^T P_2 \mathcal{B} + \rho_2^2 \mathcal{C}^T P_2 \mathcal{C} + \rho_1^2 \rho_2^2 \mathcal{D}^T P_2 \mathcal{D}\} \tag{27}$$

where

$$\mathcal{A} = A_{2q} x_k^2 + \vec{\alpha}_2 B_{2q} K_2 E_{2q} x_k^2 + \vec{\alpha}_1 \vec{\alpha}_2 B_{2q} K_{1j} E_{1i} x_{k-\tau_k}^1 + \vec{\alpha}_1 \vec{\alpha}_2 B_{2q} K_{1j} e_{sk} + \vec{\alpha}_2 \bar{\alpha}_1 B_{2q} K_{1j} \mathfrak{f}_k^1$$
$$+ \bar{\alpha}_2 B_{2q} \mathfrak{f}_k^2 + \vec{\alpha}_2 B_{2q} K_2 h_k^{\mu} + B_{3q} \omega_k$$

$$\mathcal{B} = -\vec{\alpha}_2 B_{2q} K_{1j} E_{1i} x_{k-\tau_k}^1 - \vec{\alpha}_2 B_{2q} K_{1j} e_{sk} + \vec{\alpha}_2 B_{2q} K_{1j} \mathfrak{f}_k^1$$

$$\mathcal{C} = -B_{2q} K_2 E_{2q} x_k^2 - \vec{\alpha}_1 (B_{2q} K_{1j} E_{1i} x_{k-\tau_k}^1 + B_{2q} K_{1j} e_{sk}) - \bar{\alpha}_1 B_{2q} K_{1j} \mathfrak{f}_k^1 - B_{2q} \mathfrak{f}_k^2 - B_{2q} K_2 h_k^{\mu}$$

$$\mathcal{D} = -B_{2q}K_2E_{2q}x_k^2 + B_{2q}K_{1j}E_{1i}x_{k-\tau_k}^1 + B_{2q}K_{1j}(e_{sk} - \mathfrak{f}_k^1) + B_{2q}\mathfrak{f}_k^2 - B_{2q}K_2h_k^\mu$$
$$\vec{\alpha}_1 = 1 - \bar{\alpha}_1,\ \vec{\alpha}_2 = 1 - \bar{\alpha}_2.$$

Considering $\underline{\tau} \le \tau_k \le \bar{\tau}$, one has

$$\begin{aligned} &-\bar{\tau}\sum_{v=k-\bar{\tau}}^{k-1}\varrho_v^{1T}R_1\varrho_v^1 - \tau\sum_{v=k-\bar{\tau}}^{k-\underline{\tau}-1}\varrho_v^{1T}R_2\varrho_v^1 \\ &\le -[x_k^1 - x_{k-\bar{\tau}}^1]^TR_1[x_k^1 - x_{k-\bar{\tau}}^1] - \theta_k^{13T}\begin{bmatrix}R_2 & * \\ R_3 & R_2\end{bmatrix}\theta_k^{13} \end{aligned} \tag{28}$$

where $\theta_k^{13} = [x_{k-\underline{\tau}}^{1T} - x_{k-\tau_k}^{1T}\ x_{k-\tau_k}^{1T} - x_{k-\bar{\tau}}^{1T}]^T$.

Without loss of generality, the dynamic parameters for the dynamic quantizer considered in this article are defined as $\mu_k = \frac{\hbar}{M}|y_k^2|$ with $\hbar \ge 1$. Then, as in [35], according to the definition of the dynamic quantizer given in (11) and the homogeneity property of Euclidean norm, it can be obtained that

$$h_k^{\mu T}h_k^\mu \le \frac{\hbar^2\Delta^2}{M^2}y_k^{2T}y_k^2. \tag{29}$$

Considering the constraint of nonlinear deception attack signals $\mathfrak{f}_k^1$ and $\mathfrak{f}_k^2$, we obtain

$$\begin{aligned} \bar{\alpha}_1(y_{k-\tau_k}^1 + e_{sk})^T\mathcal{F}_1^T\mathcal{F}_1(y_{k-\tau_k}^1 + e_{sk}) - \bar{\alpha}_1\mathfrak{f}_k^{1T}\mathfrak{f}_k^1 \ge 0 \\ \bar{\alpha}_2(K_2\bar{y}_k^2 + u_k^1)^T\mathcal{F}_2^T\mathcal{F}_2(K_2\bar{y}_k^2 + u_k^1) - \bar{\alpha}_2\mathfrak{f}_k^{2T}\mathfrak{f}_k^2 \ge 0. \end{aligned} \tag{30}$$

Based on the event-triggered condition (15), one has

$$e_{sk}^T\Omega e_{sk} \le \delta_k(y_{k-\tau_k}^1 + e_{sk})^T\Omega(y_{k-\tau_k}^1 + e_{sk}). \tag{31}$$

Combining (26)–(31), by defining $\zeta_k = [x_k^{1T}\ x_{k-\underline{\tau}}^{1T}\ x_{k-\tau_k}^{1T}\ x_{k-\bar{\tau}}^{1T}\ x_k^{2T}\ e_{sk}^T\ \mathfrak{f}_k^{1T}\ \mathfrak{f}_k^{2T}\ h_k^{\mu T}\ \omega_k^T]^T$, we can deduce that

$$\begin{aligned} &\mathbb{E}\{\Delta V_k\} + z_k^{1T}z_k^1 - \gamma^2\omega_k^T\omega_k \\ &\le \sum_{i,j,q=1}^{r}g_i^1g_j^1g_q^2\varrho_j\zeta_k^T(\Pi_{ijq}^{11} + \Pi_{ijq}^{21T}\Pi_{22}^{-1}\Pi_{ijq}^{21})\zeta_k \\ &= \sum_{i,q=1}^{r}\varrho_i^2(g_i^1)^2g_q^2\zeta^T(k)(\Pi_{iiq}^{11} + \Pi_{iiq}^{21T}\Pi_{22}^{-1}\Pi_{iiq}^{21})\zeta_k \\ &= \sum_{i,q=1}^{r}\sum_{i<j}^{r}g_i^1g_j^1g_q^2\varrho_j\zeta_k^T\left(\Pi_{ijq}^{11} + \frac{\varrho_i}{\varrho_j}\Pi_{ijq}^{11} + \Pi_{ijq}^{21T}\Pi_{22}^{-1}\Pi_{ijq}^{21} + \frac{\varrho_i}{\varrho_j}\Pi_{jiq}^{21T}\Pi_{22}^{-1}\Pi_{jiq}^{21}\right)\zeta_k. \end{aligned} \tag{32}$$

Then, it is obtained from conditions (23) and (24) that

$$\begin{aligned} \Pi_{iiq}^{11} + \Pi_{iiq}^{21T}\Pi_{22}^{-1}\Pi_{iiq}^{21} < 0 \\ \Pi_{ijq}^{11} + \vartheta_\jmath\Pi_{jiq}^{11} + \Pi_{ijq}^{21T}\Pi_{22}^{-1}\Pi_{ijq}^{21} + \vartheta_\jmath\Pi_{jiq}^{21T}\Pi_{22}^{-1}\Pi_{jiq}^{21} < 0,\ \jmath \in \langle 2\rangle. \end{aligned}$$

Due to $(\vartheta_2 - [\varrho_i/\varrho_j])\Pi_{jiq}^{21T}\Pi_{22}^{-1}\Pi_{jiq}^{21} > 0$, we have

$$\Pi_{ijq}^{11} + \frac{\varrho_i}{\varrho_j}\Pi_{jiq}^{11} + \Pi_{ijq}^{21T}\Pi_{22}^{-1}\Pi_{ijq}^{21} + \frac{\varrho_i}{\varrho_j}\Pi_{jiq}^{21T}\Pi_{22}^{-1}\Pi_{jiq}^{21} < 0.$$

Then, the following result can be obtained:

$$\mathbb{E}\{\Delta V_k\} + z_k^{1T}z_k^1 - \gamma^2\omega_k^T\omega_k < 0. \tag{33}$$

The sum of the two sides of the inequality (33) from $k = 0$ to $k = \infty$ can have

$$\mathbb{E}\{V_\infty - V_0\} + \sum_{k=0}^{\infty}\{z_k^{1T} z_k^1 - \gamma^2 \omega_k^T \omega_k\} < 0. \tag{34}$$

Considering the fact that $V_\infty > 0$ and $V_0 = 0$, the following conclusions can be obtained:

$$\sum_{k=0}^{\infty} z_k^{1T} z_k^1 - \gamma^2 \sum_{k=0}^{\infty} \omega_k^T \omega_k < 0 \tag{35}$$

which implies the system is mean square asymptotically stable without disturbance and satisfies the H_∞ performance index γ. The proof is completed. □

Remark 6. *Through the proof of Theorem 1, the sufficient conditions that the system satisfies H_∞ performance and mean square asymptotic stability are obtained. Specifically, this article considers the impact of event-triggered, dynamic quantization, and deception attacks on the system. To reduce the conservatism of the design results, the artificial time delay caused by event-triggered control is introduced, and the performance and stability of the system are analyzed by constructing the Lyapunov–Krasovskii functional. In the mean square sense, the inequality (22) and integral inequality (28) are used to reduce the inevitable time-delay summation term, and the inequality constraints (29)–(31) is introduced in a targeted manner. The preliminary inequality result is obtained in (32). Furthermore, the related design conditions of MFs are considered. Due to the introduction of ETM, the asynchronous phenomenon of MFs are inevitable. Through the method in [12] and Schur complement lemma, the final sufficient design conditions (23) and (24) are obtained.*

Remark 7. *It should be noted that, if the assumptions of cascade controller gain, dynamic quantizer parameters, and event-triggered weight matrix are removed, there will be some nonlinear terms and coupling terms in inequality conditions (23) and (24). This makes the inequality difficult to solve. In Theorem 2, this difficulty can be solved by some variable substitutions, basic inequalities, and matrix decoupling techniques.*

Theorem 2. *For given $\bar{\alpha}_1 > 0$, $\bar{\alpha}_2 > 0$, $\delta_1 > 0$, $\delta_2 > 0$, $\delta_3 > 0$, $\Delta > 0$, $M > 0$, $\tau > 0$, $\bar{\tau} > 0$, and $\vartheta_J > 0$ ($J \in \langle 2 \rangle$), the system (21) is mean square asymptotically stable and satisfies the H_∞ performance index γ if there exist positive definite symmetric matrices P_1, P_2, Q_1, Q_2, Q_3, R_1, R_2, Ω, and slack matrix R_3 with appropriate dimensions, such that (22) and the following inequalities hold for $i < j$:*

$$\begin{bmatrix} \vec{\Pi}_{iiq}^1 & * \\ \vec{\Pi}_{iiq}^{21} & \vec{\Pi}_i^3 \end{bmatrix} < 0 \tag{36}$$

$$\begin{bmatrix} \vec{\Pi}_{ijq}^{\vartheta_J} & * & * \\ \vec{\Pi}_{ijq}^{21} & \vec{\Pi}_i^3 & * \\ \sqrt{\vartheta_2}\vec{\Pi}_{jiq}^{31} & 0 & \vec{\Pi}_j^3 \end{bmatrix} < 0, i, j, q \in \langle r \rangle \tag{37}$$

where

$$\vec{\Pi}_i^1 = \begin{bmatrix} \Pi_{iiq}^{11} & * \\ \hat{\Pi}_{iiq}^{21} & \hat{\Pi}_{22} \end{bmatrix}, \vec{\Pi}_{iiq}^{21} = \varsigma\vec{\Pi}_{iq}^2 + \vec{\Pi}_{iiq}^3$$

$$\vec{\Pi}_{ijq}^{\vartheta_J} = \begin{bmatrix} \Pi_i^{11} + \vartheta_J\Pi_j^{11} & * & * \\ \hat{\Pi}_{ijq}^{21} & \hat{\Pi}_{22} & * \\ \sqrt{\vartheta_2}\hat{\Pi}_{jiq}^{21} & 0 & \hat{\Pi}_{22} \end{bmatrix}, \vec{\Pi}_{ijq}^{21} = \varsigma\vec{\Pi}_{iq}^4 + \vec{\Pi}_{ijq}^5$$

$$\vec{\Pi}_{jiq}^{31} = \varsigma\vec{\Pi}_{jq}^6 + \vec{\Pi}_{jiq}^7, \hat{\Pi}_{22} = diag\{\Pi_{22}^1, \hat{\Pi}_{22}^2, \hat{\Pi}_{22}^3\}$$

$$\hat{\Pi}^2_{22} = diag\{-P_1,\ -2\varepsilon P_1 + \varepsilon^2 R_1,\ -2\varepsilon P_1 + \varepsilon^2 R_2\}$$
$$\hat{\Pi}^3_{22} = diag\{-P_2,\ -P_2,\ -P_2,\ -P_2\}$$

in which $\hat{\Pi}^{21}_{iiq}(\hat{\Pi}^{21}_{ijq})$ *is obtained from* $\Pi^{21}_{iiq}(\Pi^{21}_{ijq})$ *by substituting* $P_2B_{2q}K_{1j}E_{1i}$, $P_2B_{2q}K_{1j}$, $P_2B_{2q}K_2E_{2q}$, $P_2B_{2q}K_2$, $P_1\mathcal{F}_2K_{1j}E_{1i}$, $P_1K_{1j}E_{1i}$, *and* $P_2\mathcal{F}_2K_2E_{2q}$ *with* $B_{2q}J_{1j}E_{1i}$, $B_{2q}J_{1j}$, $B_{2q}J_2E_{2q}$, $B_{2q}J_2$, $\mathcal{F}_2J_{1j}E_{1i}$, $J_{1j}E_{1i}$, *and* $\mathcal{F}_2J_2E_{2q}$, *and*

$$\vec{\Pi}^2_{iq} = [\vec{\Pi}^{21}_i\ \vec{\Pi}^{22}_{iq}],\ \vec{\Pi}^3_{iiq} = [\vec{\Pi}^{31}_{iiq}\ \vec{\Pi}^{32}_i],\ \vec{\Pi}^4_{iq} = [\vec{\Pi}^{21}_i\ \vec{\Pi}^{22}_{iq}\ 0]$$
$$\vec{\Pi}^5_{ijq} = [\vec{\Pi}^{31}_{ijq}\ \vec{\Pi}^{32}_j\ 0],\ \vec{\Pi}^6_{jq} = [\vec{\Pi}^{21}_j\ 0\ \vec{\Pi}^{22}_{jq}],\ \vec{\Pi}^7_{jiq} = [\vec{\Pi}^{31}_{jiq}\ 0\ \vec{\Pi}^{32}_j]$$
$$\vec{\Pi}^3_i = \mathcal{H}_e\{-\varsigma\mathbb{N}_i\},\ \vec{\Pi}^3_j = \mathcal{H}_e\{-\varsigma\mathbb{N}_j\}$$
$$\mathbb{N}_j = diag\{N_{1j},\ N_2,\ N_{1j},\ N_2,\ N_{1j}\}.$$

In addition, the gains of Controller^1 *and Controller*^{2} *are given as follows:*

$$K_{1j} = N_{1j}^{-1}J_{1j},\ K_2 = N_2^{-1}J_2. \tag{38}$$

Proof. Perform congruence transformation to (23) by $diag\{\mathbf{I}_{10}, \mathcal{P}\}$ with $\mathcal{P} = \text{diag}\{\mathbf{I}_5, P_1, P_1, P_1, P_2, P_2, P_2, P_2\}$, the inequality (23)–(25) can be rewritten as

$$\begin{bmatrix} \Pi^{11}_i & * \\ \tilde{\Pi}^{21}_{iiq} & \hat{\Pi}_{22} \end{bmatrix} < 0 \tag{39}$$

$$\begin{bmatrix} \Pi^{11}_i + \vartheta_j\Pi^{11}_j & * & * \\ \tilde{\Pi}^{21}_{ijq} & \hat{\Pi}_{22} & * \\ \sqrt{\vartheta_2}\tilde{\Pi}^{21}_{jiq} & 0 & \hat{\Pi}_{22} \end{bmatrix} < 0 \tag{40}$$

where $\tilde{\Pi}^{21T}_{ijq} = \mathcal{P}[\Pi^{211T}_{ijq}\ \Pi^{212T}_{ijq}\ \Pi^{213T}_{ijq}\ \Pi^{214T}_{ijq}]$.

Defining $J_{1j} = N_{1j}K_{1j}$, $J_2 = N_2K_2$. Then, the condition (39), (40) can be reexpressed as

$$\vec{\Pi}^1_{iiq} + \mathcal{H}_e\{\vec{\Pi}^{2T}_{iq}\mathbb{N}_i^{-1}\vec{\Pi}^3_{iiq}\} < 0 \tag{41}$$

$$\vec{\Pi}^{\vartheta_j}_{ijq} + \mathcal{H}_e\{\vec{\Pi}^{4T}_{iq}\mathbb{N}_i^{-1}\vec{\Pi}^5_{ijq} + \sqrt{\vartheta}_2\vec{\Pi}^{6T}_{jq}\mathbb{N}_j^{-1}\vec{\Pi}^7_{jiq}\} < 0 \tag{42}$$

the definitions of $\vec{\Pi}^2_{iq}$, $\vec{\Pi}^3_{iiq}$, $\vec{\Pi}^4_{iq}$, $\vec{\Pi}^5_{ijq}$, $\vec{\Pi}^6_{jq}$, $\vec{\Pi}^7_{jiq}$, and $\mathbb{N}_j$ are shown in Theorem 2, and

$$\vec{\Pi}^{21}_j = [\vec{\Upsilon}^{1T}_j\ \vec{\Upsilon}^{2T}\ \vec{\Upsilon}^{1T}_j\ 0\ \vec{\Upsilon}^{3T}_j]^T$$
$$\vec{\Pi}^{22}_{jq} = [\vec{\Upsilon}^{4T}_{jq}\ \vec{\Upsilon}^{5T}_q\ \vec{\Upsilon}^{4T}_{jq}\ \vec{\Upsilon}^{6T}_q\ \vec{\Upsilon}^{7T}_{jq}]^T$$
$$\vec{\Upsilon}^1_j = [\mathbf{0}_{13}\ \vec{\alpha}_1\hat{\mathbb{N}}_{1j}\ -\hat{\mathbb{N}}_{3j}\ \mathbf{0}_3],\ \vec{\Upsilon}^2_j = [\mathbf{0}_{13}\ \hat{\mathbb{N}}_2\ 0\ \mathbf{0}_3]$$
$$\vec{\Upsilon}^3_j = [\mathbf{0}_{13}\ \vec{\alpha}_1\hat{\mathbb{N}}_{1j}\ \hat{\mathbb{N}}_{3j}\ \mathbf{0}_3]$$
$$\vec{\Upsilon}^4_{jq} = [\vec{\alpha}_1\vec{\alpha}_2\hat{\mathbb{N}}_{5jq}\ -\vec{\alpha}_2\hat{\mathbb{N}}_{6jq}\ -\vec{\alpha}_1\hat{\mathbb{N}}_{7jq}\ \vec{\alpha}_1\hat{\mathbb{N}}_{8jq}]$$
$$\vec{\Upsilon}^5_q = [\vec{\alpha}_1\hat{\mathbb{N}}_{4q}\ 0\ -\hat{\mathbb{N}}_{4q}\ -\hat{\mathbb{N}}_{4q}]$$
$$\vec{\Upsilon}^6_q = [\vec{\alpha}_2\hat{\mathbb{N}}_{4q}\ 0\ -\hat{\mathbb{N}}_{4q}\ -\hat{\mathbb{N}}_{4q}]$$
$$\vec{\Upsilon}^7_{jq} = [\vec{\alpha}_2\bar{\alpha}_1\hat{\mathbb{N}}_{5jq}\ \vec{\alpha}_2\hat{\mathbb{N}}_{6jq}\ -\bar{\alpha}_1\hat{\mathbb{N}}_{7jq}\ -\hat{\mathbb{N}}_{8jq}]$$
$$\vec{\Pi}^{31}_{ijq} = \begin{bmatrix} \vec{\Upsilon}^8_{ij} & \vec{\Upsilon}^9_q \\ 0 & 0 \end{bmatrix},\ \vec{\Pi}^{32}_j = \begin{bmatrix} 0 & 0 \\ \vec{\Upsilon}^{10}_j & 0 \end{bmatrix},\ \vec{\Upsilon}^8_{ij} = \begin{bmatrix} \mathbf{0}_2 & J_{1j}E_{1i} \\ \mathbf{0}_2 & 0 \end{bmatrix}$$
$$\vec{\Upsilon}^9_q = \text{diag}\{0,\ J_2E_{2q}\},\ \vec{\Upsilon}^{10}_j = \text{diag}\{J_{1j},\ J_2,\ J_{1j}\}$$
$$\hat{\mathbb{N}}_{1j} = \sqrt{\bar{\alpha}_2}(\mathcal{F}_2 - \mathcal{F}_2N_{1j})^T,\ \hat{\mathbb{N}}_2 = \sqrt{\bar{\alpha}_2}(\mathcal{F}_2 - \mathcal{F}_2N_2)^T$$

$$\hat{\mathbb{N}}_{3j} = \sqrt{\bar{\alpha}_2}\rho_1(I - N_{1j})^T, \hat{\mathbb{N}}_{4q} = (P_2B_{2q} - B_{2q}N_2)^T$$
$$\hat{\mathbb{N}}_{5jq} = (P_2B_{2q} - B_{2q}N_{1j})^T, \hat{\mathbb{N}}_{6jq} = \rho_1\hat{\mathbb{N}}_{5jq}$$
$$\hat{\mathbb{N}}_{7jq} = \rho_2\hat{\mathbb{N}}_{5jq}, \hat{\mathbb{N}}_{8jq} = \rho_1\rho_2\hat{\mathbb{N}}_{5jq}.$$

It is easy to know that (41), (42) can hold if the conditions (36), (37) are satisfied by applying Lemma 2 in [34]. The proof is completed. □

Remark 8. *Through the proof of Theorem 2, the sufficient conditions for solving the cascade controller gain, quantizer parameter, and ADAETM weighting matrix are obtained. In the proof process, the nonlinear terms and coupling terms that affect the inequality solution are eliminated by congruence transformation, basic inequality transformation, and matrix decoupling technology, such as $P_2B_{2q}K_{1j}E_{1i}$, $P_2B_{2q}K_{1j}$, $P_2B_{2q}K_2E_{2q}$, and so on. Then, the solution of LMIs is a convex optimization problem. Many existing optimization methods and numerical tools, such as the YALMIP toolbox in MATLAB, can be used to solve convex optimization problems. Based on Theorem 2 and the existing solving tools, the design results can be more easily obtained by off-line execution. The detailed solution process is given by Algorithm 3.*

Remark 9. *The computational complexity $\mathscr{C} = \mathscr{N}^3\mathscr{L}$ of the LMIs in Theorem 2 is determined by the number of decision variables $\mathscr{N}$ and the dimension $\mathscr{L}$ of the LMIs. Based on Theorem 2, we have $\mathscr{N} = 3n_{x^1} \times (n_{x^1} + 1) + \frac{1}{2}n_{x^2}(n_{x^2} + 1) + \frac{1}{2}n_{y^1}(n_{y^1} + 1) + n_{x^1} \times n_{x^1} + n_{u^1} \times (n_{y^1} + n_{u^1}) + n_{u^2} \times (n_{y^2}n_{u^2}) + 1$ and $\mathscr{L} = 2n_{x^1} + \frac{1}{2}r^2(r + 1)(7n_{x^1} + 5n_{x^2} + 4n_{y^1} + n_{y^2} + n_\omega + 5n_{u^1} + 3n_{u^2}) + \frac{1}{2}r^2(r + 1)(10n_{x^1} + 4n_{x^2} + 4n_{y^1} + n_{y^2} + n_\omega + 8n_{u^1} + 5n_{u^2})$.*

Algorithm 3 Solve the control gains, quantizer parameter, and ADAETM weighting matrix

Input: parameter matrices A_{1i}, B_{1i}, C_{1i}, D_{1i}, E_{1i}, A_{2q}, B_{2q}, B_{3q}, C_{2q}, D_{2q}, E_{2q}, and parameter scalars δ_1, δ_2, δ_3, $\bar{\alpha}_1$, $\bar{\alpha}_2$, Δ, M, $\bar{\tau}$, τ, γ, ϑ_1, and ϑ_2.
Output: K_{1j}, K_2, $\hbar$, and Ω.
YALMIP toolbox in MATLAB is used to solve LMIs (22), (36)–(37).
if sum(checkset(LMIs)<0)=size(checkset(LMIs),1) **then**
go to Input adjust given parameters.
else
solve J_{1j}, J_2, N_{1j}^{-1}, N_2^{-1}, $\hbar$, and Ω with LMIs (22), (36)–(37) and substitute them into $K_{1j} = N_{1j}^{-1}J_{1j}$, $K_2 = N_2^{-1}J_2$.
end if
The gains K_{1j}, K_2, quantizer parameter $\hbar$, and ADAETM weighting matrix Ω are obtained.

4. Simulation Results

4.1. Design Example with PPBTS

By constructing the NCCS shown in Figure 2, the problem of excessive temperature deviation during the operation of the power PPBTS will be solved. Sensor[1] measures the steam temperature value of the secondary superheater. After the ADAETM and the influence of the deception attacks, the measurement data are fed back to Controller[1]. Controller[1] compares the measured data with the expected data, and then the output signal of Controller[1] is transmitted to Controller[2] as the expected data. Controller[2] compares the expected data with the quantized steam temperature measurement data at the Desuperheater end, and transmits the control output signal to the Desuperheater spray valve. The Desuperheater spray valve will be attacked during the adjustment of the Desuperheater. Through the proposed controller design strategy, we can ensure the stability and controllability of the steam temperature in the PPBTS under the network environment where the whole system is threatened by deception attacks.

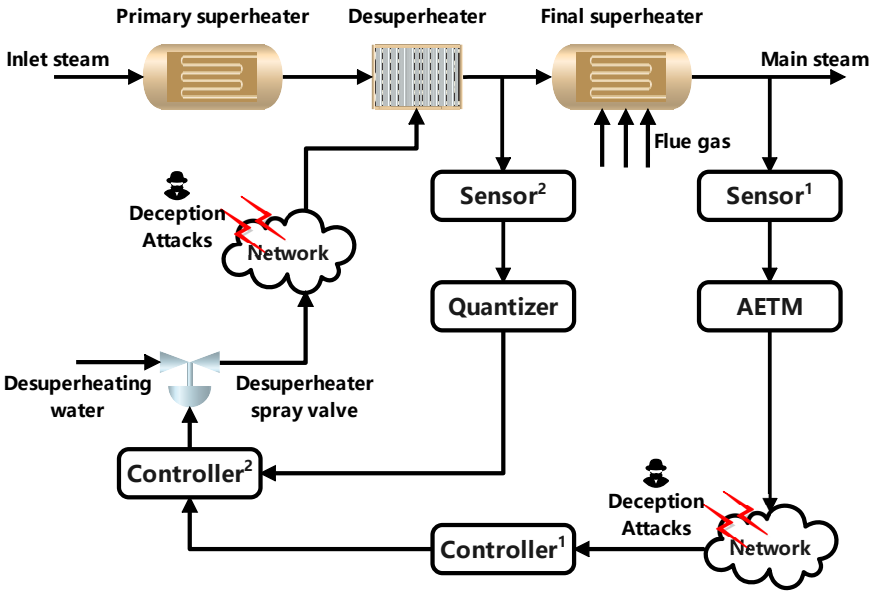

Figure 2. Structure diagram of an NCCS for a nonlinear PPBTS.

The discrete nonlinear networked PPBTS [9] parameters considered in the article are given as follows:

$$A_{11} = \begin{bmatrix} 0.6887 & -0.0093 \\ 0.8356 & 0.9951 \end{bmatrix}, B_{11} = \begin{bmatrix} 0.8356 \\ 0.4437 \end{bmatrix}, D_{11} = 0.1$$

$$A_{12} = \begin{bmatrix} 0.6908 & -0.0093 \\ 0.4182 & 0.9975 \end{bmatrix}, B_{12} = \begin{bmatrix} 0.8364 \\ 0.2219 \end{bmatrix}, D_{12} = 0.1$$

$$C_{11} = C_{12} = E_{11} = E_{12} = \begin{bmatrix} 0 & 0.0111 \end{bmatrix}$$

$$A_{21} = \begin{bmatrix} -0.0342 & -0.4364 & -0.0342 \\ 0.3425 & 0.6849 & -0.0254 \\ 0.2542 & 0.8762 & 0.9899 \end{bmatrix}, B_{21} = \begin{bmatrix} 0.3425 \\ 0.2542 \\ 0.1008 \end{bmatrix}$$

$$A_{22} = \begin{bmatrix} -0.0572 & -0.5285 & -0.1676 \\ 0.3352 & 0.6468 & -0.1262 \\ 0.2525 & 0.8654 & 0.9497 \end{bmatrix}, B_{22} = \begin{bmatrix} 0.3352 \\ 0.2525 \\ 0.1005 \end{bmatrix}$$

$$B_{31} = \begin{bmatrix} -0.0104 \\ 0.0483 \\ 0.0851 \end{bmatrix}, B_{32} = \begin{bmatrix} -0.0185 \\ 0.0453 \\ 0.0844 \end{bmatrix}, D_{21} = D_{22} = 0.2$$

$$C_{21} = C_{22} = \begin{bmatrix} 0 & 0 & 0.1 \end{bmatrix}, E_{21} = E_{22} = \begin{bmatrix} 0 & 0 & 0.2 \end{bmatrix}.$$

Moreover, the MFs are chosen by $d_1(x_k^1) = \frac{1-\sin^2(x_k^{11})}{2}$, $d_2(x_k^1) = 1 - d_1(x_k^1)$, $f_1(x_k^2) = \frac{1-0.5\sin^2(x_k^{21})}{2}$, and $f_2(x_k^2) = 1 - f_1(x_k^2)$. The initial states of the Plant^1 and Plant^2 are given as $x_0^1 = [-0.5\ 1.0]^T$, $x_0^2 = [0.2\ -0.1\ -0.3]^T$ and the external disturbance is given as follows: $\omega_k = 0.5e^{-0.05k}\sin(0.5k)$, $12 < k \leq 45$; otherwise, $\omega_k = 0$.

Selecting $\mathfrak{f}_k^1 = 0.005\tanh(\hat{y}_k^1)$, $\mathfrak{f}_k^2 = 0.005\tanh(u_k^2)$, $\gamma = 0.5$, $\underline{\tau} = \underline{\theta} = 1.0$, $\bar{\tau} = \bar{\theta} = 4$, $\bar{\alpha}_1 = \bar{\alpha}_2 = 0.3$, $\delta_1 = 0.05$, $\delta_2 = 0.02$, $\delta_3 = 0.03$, $\epsilon_1 = \epsilon_3 = 1$, $\epsilon_2 = \epsilon_4 = 0.5$, $\Delta = 0.001$, $M = 1$, and $\vartheta_1 = 0.75 < \vartheta_2 = 1.25$. By the design results in Theorem 2, the quantization parameter, security fuzzy controller gains, and the ADAETM weighting matrix are obtained as $\hbar = 27.2294$, $K_{11} = 0.0069$, $K_{12} = 0.0026$, $K_2 = -0.5940$, and $\Omega = 3.2766 \times 10^8$. The state responses of Plant^1 and Plant^2 are shown in Figure 3. The change trajectory of control signals u_k^1 and $\bar{u}_k^2$ are demonstrated on the left in Figure 4. The release instants, the release intervals, and the adaptive law δ_k are shown on the right in Figure 4.

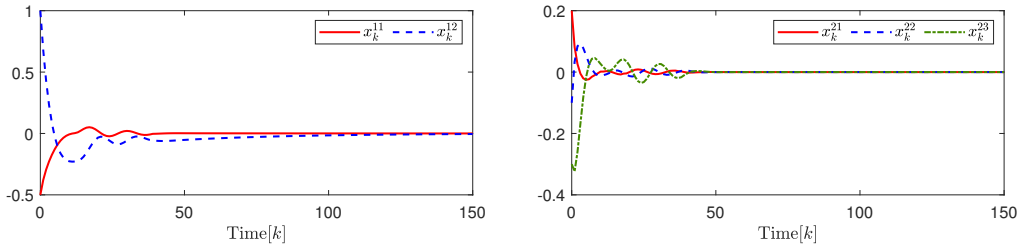

Figure 3. (**Left**). The response of system state x_k^1; (**Right**). The response of system state x_k^2.

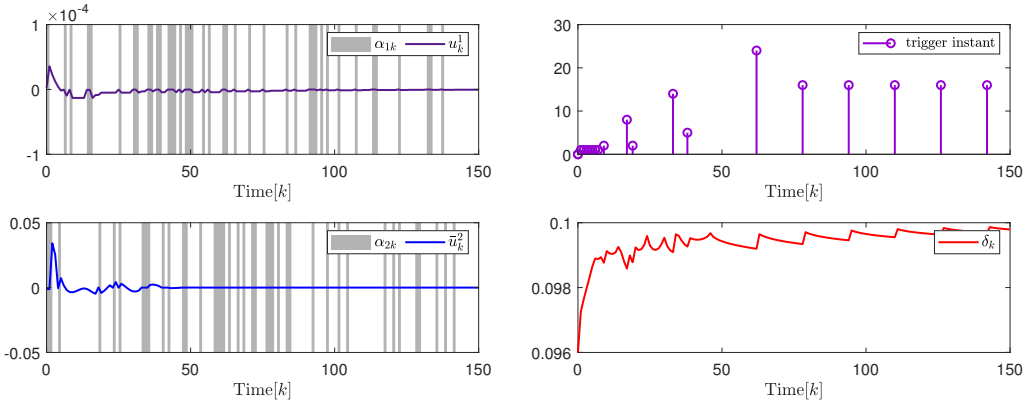

Figure 4. (**Left**). The control input u_k^1 and $\bar{u}_k^2$ with $\bar{\alpha}_1 = 0.3$; (**Right**). The release instants and the release intervals and the adaptive law δ_k with $\bar{\alpha}_1 = 0.3$.

In addition, to further illustrate the impact of the attack probability $\bar{\alpha}_1$ on packet transmission rate adjustment and system performance, Figures 5 and 6, and Table 1 give the analysis results under different attack probability $\bar{\alpha}_1$. By the design results in Theorem 2, the quantization parameter, security fuzzy controller gains, and the ADAETM weighting matrix are obtained as follows: $\hbar = 27.3840$, $K_{11} = 0.0098$, $K_{12} = 0.0038$, $K_2 = -0.3536$, $\Omega = 2.2361 \times 10^8$ with $\bar{\alpha}_1 = 0.5$. $\hbar = 48.2277$, $K_{11} = 0.0158$, $K_{12} = 0.0092$, $K_2 = -0.3027$, $\Omega = 2.2917 \times 10^8$ with $\bar{\alpha}_1 = 0.7$.

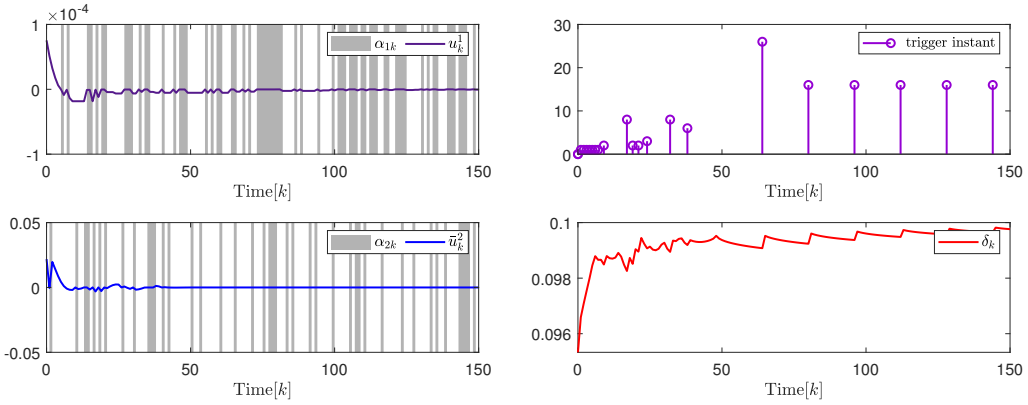

Figure 5. (**Left**). The control input u_k^1 and $\bar{u}_k^2$ with $\bar{\alpha}_1 = 0.5$; (**Right**). The release instants and the release intervals and the adaptive law δ_k with $\bar{\alpha}_1 = 0.5$.

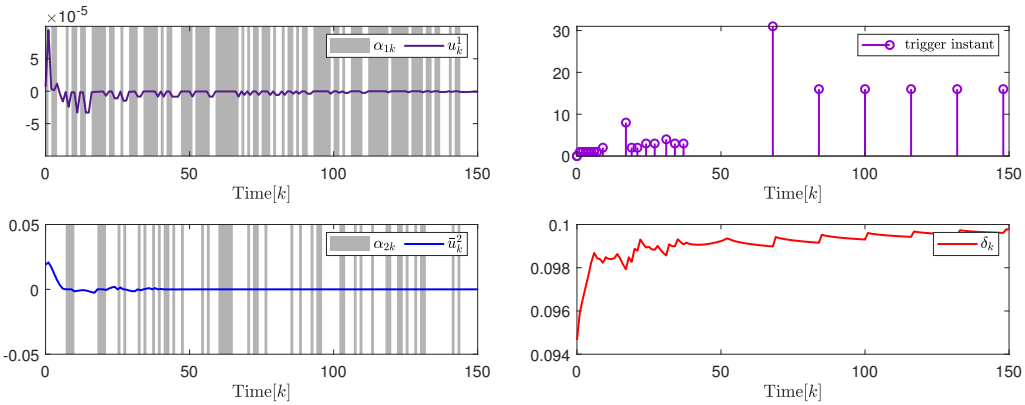

Figure 6. (**Left**). The control input u_k^1 and $\bar{u}_k^2$ with $\bar{\alpha}_1 = 0.7$; (**Right**). The release instants and the release intervals and the adaptive law δ_k with $\bar{\alpha}_1 = 0.7$.

Based on the above calculation results under different attack probability $\bar{\alpha}_1$, Figure 5 on the left and Figure 6 on the left show that the trajectory changes of the control input converge to 0 under $\bar{\alpha}_1 = 0.5$ and $\bar{\alpha}_1 = 0.7$, respectively, and the release instants, and the release intervals, the adaptive law δ_k are shown on the right in Figure 5 and Figure 6, respectively, which indicates the effectiveness of the designed security cascade controller for multi-channel deception attacks. Moreover, to further verify the superiority of the proposed ADAETM, it is compared with the triggered mechanism in [27], and the system performance γ under different attack probability $\bar{\alpha}_1$ is calculated. Through the transmission number (TN) and transmission rate $R_{e/k}$ in Figure 5 on the right and Figure 6 on the right, and Table 1, it can be seen that the ADAETM designed in this article has great advantages. With the increase in attack probability, the number of triggers will also increase, and the system performance index γ will decrease, which explains the rationality of the design of ADAETM to a certain extent. In addition, to further strengthen the demonstration of the superiority of the proposed control design, quantitative performance index analysis under different attack probabilities, such as system convergence time, network channel bandwidth utilization, and optimal H_∞ performance index, is presented in Table 2. It can be seen that the increase in attack probability will affect the convergence time of the system and the number of triggered packets to a certain extent, but the design strategy proposed in this article can balance the relationship between attack probability and the number of triggered packets, and maintain the optimal H_∞ performance index.

Table 1. Data transmission with different ETMs in Example with PPBTS.

Different ETMs	TN	$R_{e/k}$	γ
Triggered mechanism in [27]	47	31.3%	0.1056
$\bar{\alpha}_1 = 0.3, \delta_1 = 0.07, \delta_2 = 0.05, \delta_3 = 0.03$	20	13.3%	0.1064
$\bar{\alpha}_1 = 0.5, \delta_1 = 0.07, \delta_2 = 0.05, \delta_3 = 0.03$	22	14.7%	0.1058
$\bar{\alpha}_1 = 0.7, \delta_1 = 0.07, \delta_2 = 0.05, \delta_3 = 0.03$	24	16.0%	0.1056

Table 2. Quantitative performance index with different attack probabilities in Example with PPBTS.

Different Attack Probability	System Stability Time	$R_{e/k}$	γ
$\bar{\alpha}_1 = 0.3, \bar{\alpha}_2 = 0.3$	133/52	17.3%	0.1073
$\bar{\alpha}_1 = 0.5, \bar{\alpha}_2 = 0.5$	140/55	18.6%	0.1069
$\bar{\alpha}_1 = 0.7, \bar{\alpha}_2 = 0.7$	145/57	19.3%	0.1067

4.2. Comparison Example with PPBPGCS

In order to further verify the superiority of the derived results of Theorem 2, a nonlinear PPBPGCS based on fuzzy model is given. The structure of the NCCS is shown in Figure 7. In the main control loop, Sensor^1 is used to measure the output power supply voltage of the power control system. After the influence of ADAETM and deception attacks, the measurement data are fed back to Controller^1 and compared with the expected data. The output signal of Controller^1 is transmitted to Controller^2 as the expected data. In the secondary control loop, Controller^2 compares the boiler liquid level data, valve parameters measured by the quantized Sensor^2 with the expected data, and transmits the control output signal to the valve that controls the inlet to control the main steam temperature.

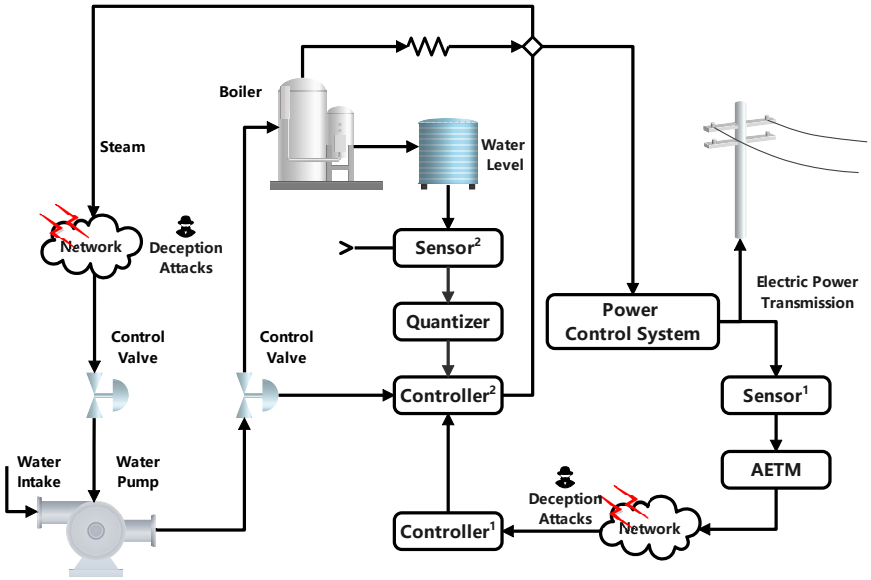

Figure 7. Structure diagram of an NCCS for a nonlinear PPBPGCS.

Suppose that the discrete nonlinear networked PPBPGCS parameters considered in this article are as follows:

$$A_{11} = \begin{bmatrix} 0.3443 & -0.1768 \\ 0.6398 & 0.8966 \end{bmatrix}, B_{11} = \begin{bmatrix} 0.6398 \\ 0.3743 \end{bmatrix}$$

$$A_{12} = \begin{bmatrix} 0.3304 & -0.2078 \\ 0.6343 & 0.8779 \end{bmatrix}, B_{12} = \begin{bmatrix} 0.6343 \\ 0.3278 \end{bmatrix}$$

$$C_{11} = C_{12} = \begin{bmatrix} 0 & 0.45 \end{bmatrix}, D_{11} = D_{12} = 0.1$$

$$E_{11} = E_{12} = \begin{bmatrix} 0 & 0.45 \end{bmatrix}$$

$$A_{21} = \begin{bmatrix} -0.1474 & -0.6879 & -0.1888 & -0.0165 \\ 0.0106 & -0.0835 & -0.5780 & -0.1157 \\ 0.0741 & 0.4579 & 0.6853 & -0.0662 \\ 0.0424 & 0.3300 & 0.8977 & 0.9781 \end{bmatrix}$$

$$A_{22} = \begin{bmatrix} -0.1465 & -0.6812 & -0.1733 & -0.0144 \\ 0.0109 & -0.0809 & -0.5684 & -0.0981 \\ 0.0741 & 0.4586 & 0.6885 & -0.0561 \\ 0.0424 & 0.3301 & 0.8985 & 0.9814 \end{bmatrix}$$

$$B_{21} = \begin{bmatrix} 0.0106 & 0.0741 & 0.0424 & 0.0140 \end{bmatrix}^T$$

$$B_{22} = \begin{bmatrix} 0.0109 & 0.0741 & 0.0424 & 0.0140 \end{bmatrix}^T$$

$$B_{31} = \begin{bmatrix} -0.1073 & 0.0532 & 0.0372 & 0.0141 \end{bmatrix}^T$$

$$B_{32} = \begin{bmatrix} -0.1070 & 0.0533 & 0.0372 & 0.0141 \end{bmatrix}^T$$

$$C_{21} = C_{22} = \begin{bmatrix} 0 & 0 & 0 & 1 \end{bmatrix}, D_{21} = D_{22} = 0.1$$
$$E_{21} = E_{22} = \begin{bmatrix} 0 & 0 & 0 & 1 \end{bmatrix}.$$

Moreover, the MFs are chosen by $d_1(x_k^1) = \cos^2(x_k^{12})$, $d_2(x_k^1) = 1 - d_1(x_k^1)$, $f_1(x_k^2) = \exp(\frac{-(x_k^{24})^2}{3})$, and $f_2(x_k^2) = 1 - f_1(x_k^2)$. The initial states of the Plant^1 and Plant^2 are given as $x_0^1 = [1\ 1]^T$, $x_0^2 = [1\ 1\ 1\ 1]^T$ and the external disturbance is given as follows: $\omega_k = 10e^{-0.01k}\sin_k$, $0 < k \leq 15$; Otherwise, $\omega_k = 0$.

Selecting $\mathfrak{f}_k^1 = 0.1\tanh(\hat{y}_k^1)$, $\mathfrak{f}_k^2 = 0.1\tanh(u_k^2)$, $\gamma = 1$, $\underline{\tau} = \underline{\theta} = 1$, $\bar{\tau} = \bar{\theta} = 4$, $\bar{\alpha}_1 = \bar{\alpha}_2 = 0.7$, $\delta_1 = 0.6$, $\delta_2 = 0.4$, $\delta_3 = 0.1$, $\epsilon_1 = \epsilon_3 = 1$, $\epsilon_2 = \epsilon_4 = 0.5$, $\Delta = 0.1$, $M = 10$, and $\vartheta_1 = 0.75 < \vartheta_2 = 1.25$. By the design results in Theorem 2, the quantization parameter, security fuzzy controller gains, and the ADAETM weighting matrix are obtained as $\hbar = 109.0809$, $K_{11} = 0.0025$, $K_{12} = 0.0014$, $K_2 = 0.5201$, and $\Omega = 7.1494 \times 10^5$.

The state responses of Plant^1 and Plant^2 are shown in Figure 8. The change trajectory in the control signals u_k^1 and $\bar{u}_k^2$ are demonstrated on the left in Figure 9. The release instants, the release intervals, and the adaptive law δ_k are shown on the right in Figure 9.

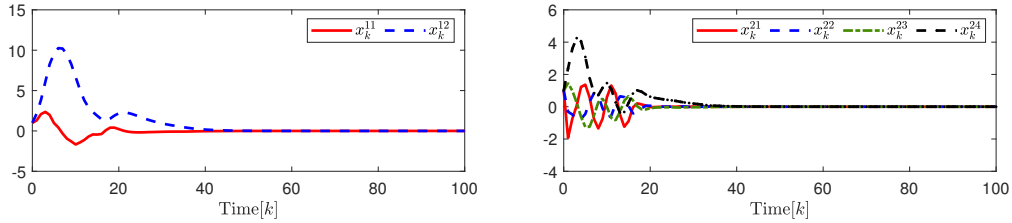

Figure 8. (**Left**). The response of system state x_k^1; (**Right**). The response of system state x_k^2.

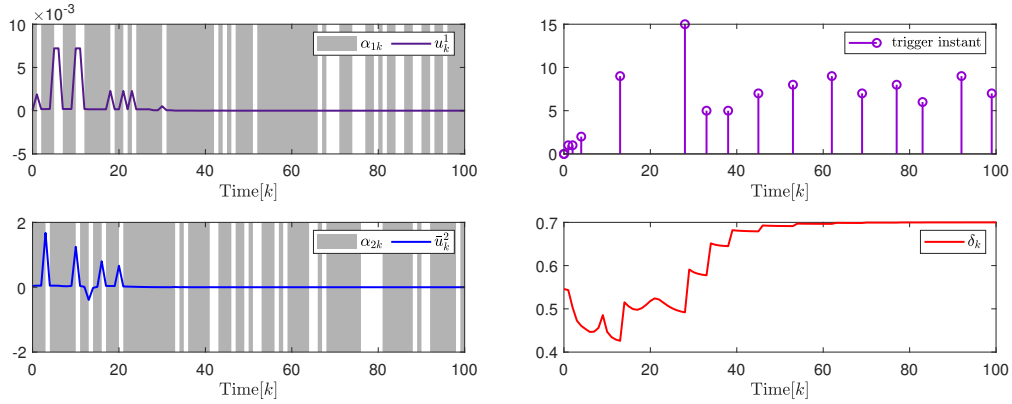

Figure 9. (**Left**). The control input u_k^1 and $\bar{u}_k^2$ with $\bar{\alpha}_1 = 0.7$; (**Right**). The release instants and the release intervals and the adaptive law δ_k with $\bar{\alpha}_1 = 0.7$.

In addition, to further illustrate the impact of the attack probability $\bar{\alpha}_1$ on packet transmission rate adjustment and system performance, Figures 10 and 11, and Table 2 give the analysis results under different attack probability $\bar{\alpha}_1$. By the design results in Theorem 2, the quantization parameter, security fuzzy controller gains, and the ADAETM weighting matrix are obtained as follows: $\hbar = 114.1739$, $K_{11} = 0.0022$, $K_{12} = 0.0012$, $K_2 = 0.5048$, $\Omega = 7.4453 \times 10^5$ with $\bar{\alpha}_1 = 0.6$. $\hbar = 121.9136$, $K_{11} = 0.0024$, $K_{12} = 0.0013$, $K_2 = 0.4041$, $\Omega = 1.1506 \times 10^6$ with $\bar{\alpha}_1 = 0.8$.

Based on the above calculation results under different attack probability $\bar{\alpha}_1$, the left in Figures 10 and 11 are show the trajectory changes of the control input converge to 0 under $\bar{\alpha}_1 = 0.6$ and $\bar{\alpha}_1 = 0.8$, respectively, which indicates the effectiveness of the designed security cascade controller for multi-channel deception attacks. Similar to the analysis of Example with PPBTS, the data in Figures 10 and 11, and Table 3 also show the effectiveness of the designed security cascade controller design algorithm against

multi-channel deception attacks. Similar to the analysis results in Section 4.1, Table 4 also gives quantitative performance analysis under different attack probabilities, which further verifies the superiority of the control design.

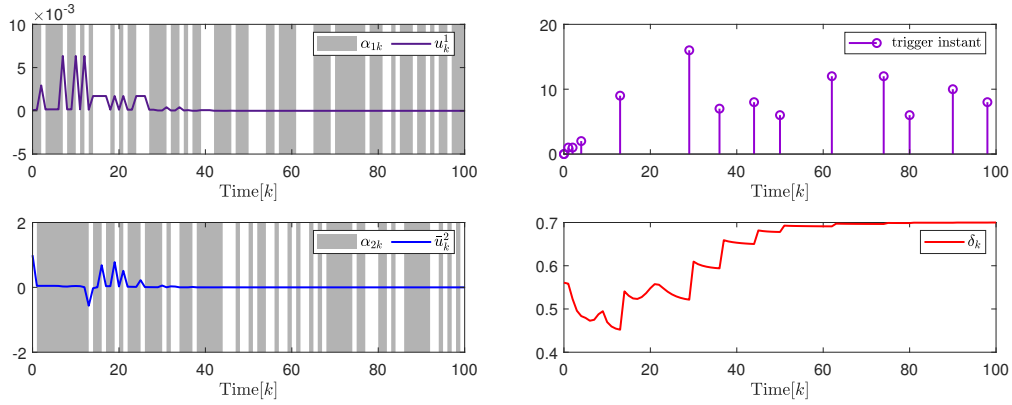

Figure 10. (**Left**). The control input u_k^1 and $\bar{u}_k^2$ with $\bar{\alpha}_1 = 0.6$; (**Right**). The release instants and the release intervals and the adaptive law δ_k with $\bar{\alpha}_1 = 0.6$.

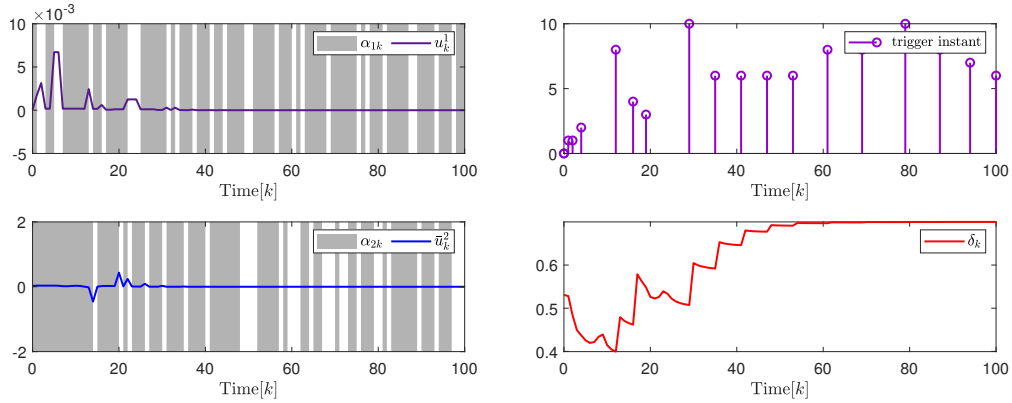

Figure 11. (**Left**). The control input u_k^1 and $\bar{u}_k^2$ with $\bar{\alpha}_1 = 0.8$; (**Right**). The release instants and the release intervals and the adaptive law δ_k with $\bar{\alpha}_1 = 0.8$.

Table 3. Data transmission with different ETMs in Example with PPBPGCS.

Different ETMs	TN	$R_{e/k}$	γ
Triggered mechanism in [27]	37	37.0%	0.4608
$\bar{\alpha}_1 = 0.6, \delta_1 = 0.6, \delta_2 = 0.4, \delta_3 = 0.1$	15	15.0%	0.4593
$\bar{\alpha}_1 = 0.7, \delta_1 = 0.6, \delta_2 = 0.4, \delta_3 = 0.1$	17	17.0%	0.4575
$\bar{\alpha}_1 = 0.8, \delta_1 = 0.6, \delta_2 = 0.4, \delta_3 = 0.1$	19	19.0%	0.4483

Table 4. Quantitative performance index with different attack probability in Example with PPBPGCS.

Different Attack Probability	System Stability Time	$R_{e/k}$	γ
$\bar{\alpha}_1 = 0.6, \bar{\alpha}_2 = 0.6$	55/47	29.0%	0.4671
$\bar{\alpha}_1 = 0.7, \bar{\alpha}_2 = 0.7$	57/48	31.0%	0.4603
$\bar{\alpha}_1 = 0.8, \bar{\alpha}_2 = 0.8$	60/50	35.0%	0.4533

5. Conclusions

This article mainly explores the SCOFC design problem of nonlinear NCCSs based on ADAETM and dynamic quantization under multi-channel deception attacks interference. The adaptive function of ADAETM can flexibly adjust the triggered threshold according to the state of deception attacks, and further alleviate the impact of deception attacks on system performance and stability. By using Lyapunov–Krasovskii stability theory, matrix decoupling lemma, and relaxation matrix technique, sufficient conditions for the mean square asymptotically stable and prescribed performance of the system are obtained. The criteria for the joint design of event-triggered weight matrix, dynamic quantizer parameters and controller are given in terms of a set of LMIs. Finally, the proposed SCOFC design strategy is verified by simulation of PPBTS and PPBPGCS.

The ADAETM proposed in this article is designed under the assumption that the attack probability is known in advance. Such assumptions inevitably make the design results have certain limitations. In an open network environment, complex, hybrid, and multiple attacks caused by various types of network attacks and a variety of network attack combinations often occur. Therefore, based on the existing work and literature, the future research focus of the security controller design and attack signal observer design problem of NCCSs under multi-channel complex attacks is considered. In addition, the controller design problem of NCCSs affected by internal time-varying delays and other network-induced factors is also a common problem in practical industrial engineering, which also stimulates future research work.

Author Contributions: Conceptualization, X.-M.L. and X.-H.C.; methodology, X.-M.L. and X.-H.C.; software, X.-M.L.; formal analysis, X.-M.L.; investigation, X.-M.L., X.-H.C. and L.-W.H.; writing—original draft preparation, X.-M.L., X.-H.C. and L.-W.H.; writing—review and editing, X.-M.L., X.-H.C. and L.-W.H.; funding acquisition, X.-H.C. All authors have read and agreed to the published version of the manuscript.

Funding: This research was supported by the Basic scientific research project of colleges and universities of Liaoning Province Education Department under Grant LJ212410167048.

Data Availability Statement: The raw data supporting the conclusions of this article will be made available by the authors upon request.

Conflicts of Interest: The authors declare no conflicts of interest.

Abbreviations

The following abbreviations are used in this manuscript:

T-S	Takagi–Sugeno
NCSs	Networked control systems
NCCSs	Networked cascade control systems
DoS	Denial of service
ETM	Event-triggered mechanism
ADAETM	Attack-dependent adaptive event-triggered mechanism
MFs	Membership functions
SCOFC	Security cascade output feedback controller
LMIs	Linear matrix inequalities
PPBTS	Power plant boiler–turbine system
PPBPGCS	Power plant boiler power generation control system
TN	Transmission number

References

1. Franks, R.G.; Worley, C.W. Quantitive analysis of cascade control. *Ind. Eng. Chem.* **1956**, *48*, 1074–1079. [CrossRef]
2. Raja, G.L.; Ali, A. Enhanced tuning of Smith predictor based series cascaded control structure for integrating processes. *ISA Trans.* **2021**, *114*, 191–205. [CrossRef] [PubMed]
3. Jia, Y.; Chai, T.; Wang, H.; Su, C.-Y. A signal compensation based cascaded PI control for an industrial heat exchange system. *Control Eng. Pract.* **2020**, *98*, 104372. [CrossRef]

4. Du, Z.; Zhang, C.; Yang, X.; Ye, H.; Li, J. Discrete-time event-triggered H-infinity stabilization for three closed-loop cyber-physical system with uncertain delay. *Appl. Math. Comput.* **2025**, *488*, 129127. [CrossRef]
5. Zhu, H.; Liu, G.; Yu, Z.; Li, Z. Detectability in discrete event systems using unbounded Petri nets. *Mathematics* **2023**, *11*, 3862. [CrossRef]
6. Song, J.; Chang, X.-H.; Li, Z.-M. Secure P2P nonfragile sampled-data controller design for nonlinear networked system under sensor saturation and DoS attack. *IEEE Trans. Netw. Sci. Eng.* **2023**, *10*, 1575–1585. [CrossRef]
7. Liu, Y.; Wei, Y.; Wang, C.; Wu, H. Trajectory optimization for adaptive deformed wheels to overcome steps using an improved hybrid genetic algorithm and an adaptive particle swarm optimization. *Mathematics* **2024**, *12*, 2077. [CrossRef]
8. Mathiyalagan, K.; Park, J.H.; Sakthivel, R. New results on passivity-based H_∞ control for networked cascade control systems with application to power plant boiler–turbine system. *Nonlinear Anal. Hybrid Syst.* **2015**, *17*, 56–69. [CrossRef]
9. Huang, C.; Bai, Y.; Liu, X. H-infinity state feedback control for a class of networked cascade control systems with uncertain delay. *IEEE Trans. Ind. Inform.* **2010**, *6*, 62–72. [CrossRef]
10. Pang, Z.-H.; Fan, L.-Z.; Guo, H.; Shi, Y.; Chai, R.; Sun, J.; Liu, G.-P. Security of networked control systems subject to deception attacks: A survey. *Int. J. Syst. Sci.* **2022**, *53*, 3577–3598. [CrossRef]
11. Gu, Z.; Zhang, T.; Yang, F.; Zhao, H.; Shen, M. A novel event-triggered mechanism for networked cascade control system with stochastic nonlinearities and actuator failures. *J. Frankl. Inst.* **2019**, *356*, 1955–1974. [CrossRef]
12. Zhao, N.; Shi, P.; Xing, W.; Agarwal, R.K. Resilient event-triggered control for networked cascade control systems under denial-of-service attacks and actuator saturation. *IEEE Syst. J.* **2022**, *16*, 1114–1122. [CrossRef]
13. Fallahnejad, M.; Kazemy, A.; Shafiee, M. Event-triggered H_∞ stabilization of networked cascade control systems under periodic DoS attack: A switching approach. *Int. J. Electr. Power Energy Syst.* **2023**, *153*, 109278. [CrossRef]
14. An, L.; Yang, G.-H. Improved adaptive resilient control against sensor and actuator attacks. *Inf. Sci.* **2018**, *423*, 145–156. [CrossRef]
15. Ding, D.; Wei, G.; Zhang, S.; Liu, Y.; Alsaadi, F.E. On scheduling of deception attacks for discrete-time networked systems equipped with attack detectors. *Neurocomputing* **2016**, *219*, 99–106. [CrossRef]
16. Wang, X.; Cao, Y.; Niu, B.; Song, Y. A novel bipartite consensus tracking control for multiagent systems under sensor deception attacks. *IEEE Trans. Cybern.* **2023**, *53*, 5984–5993. [CrossRef]
17. Ding, D.; Wang, Z.; Ho, D.W.C.; Wei, G. Distributed recursive filtering for stochastic systems under uniform quantizations and deception attacks through sensor networks. *Automatica* **2017**, *78*, 231–240. [CrossRef]
18. Guo, H.; Pang, Z.-H.; Sun, J.; Li, J. An output-coding-based detection scheme against replay attacks in cyber-physical systems. *IEEE Trans. Circuits Syst. II Express Briefs* **2021**, *68*, 3306–3310. [CrossRef]
19. Xie, J.; Zhu, S.; Zhang, D. Distributed interval state estimation with l_∞-gain optimization for cyber-physical systems subject to bounded disturbance and random stealthy attacks. *ISA Trans.* **2022**, *127*, 22–31. [CrossRef]
20. Liu, J.; Gu, Y.; Xie, X.; Yue, D.; Park, J.H. Hybrid-driven-based H_∞ control for networked cascade control systems with actuator saturations and stochastic cyber attacks. *IEEE Trans. Syst. Man Cybern. Syst.* **2019**, *49*, 2452–2463. [CrossRef]
21. Hu, Z.; Chen, K.; Deng, F.; Luo, S.; Hu, S. H_∞ controller design for networked systems with two-channel packet dropouts and FDI attacks. *IEEE Trans. Cybern.* **2024**, *54*, 1661–1670. [CrossRef] [PubMed]
22. Zhang, H.; Zhao, N.; Wang, S.; Agarwal, R.K. Improved event-triggered dynamic output feedback control for networked T-S fuzzy systems with actuator failure and deception attacks. *IEEE Trans. Cybern.* **2023**, *53*, 7989–7999. [CrossRef] [PubMed]
23. Wang, X.-Y.; Chang, X.-H. Nonlinear continuous-time system H_∞ control based on dynamic quantization and event-triggered mechanism. *Neural Process. Lett.* **2023**, *55*, 12223–12238. [CrossRef]
24. Xie, Y.; Ding, S.; Jing, Y.; Xie, X. Distributed set-membership estimation over sensor networks via an event-driven dynamic quantization scheme. *IEEE Syst. J.* **2024**, *18*, 1151–1161. [CrossRef]
25. Zhu, Q. Event-triggered sampling problem for exponential stability of stochastic nonlinear delay systems driven by Le´vy processes. *IEEE Trans. Autom. Control* 2024, *in press*. Available online: https://ieeexplore.ieee.org/document/10643716 (accessed on 22 August 2024). [CrossRef]
26. Du, Z.; Yuan, W.; Hu, S. Discrete-time event-triggered H-infinity stabilization for networked cascade control systems with uncertain delay. *J. Frankl. Inst.* **2019**, *356*, 9524–9544. [CrossRef]
27. Liu, J.; Wang, Y.; Zha, L.; Yan, H. Event-based control for networked T-S fuzzy cascade control systems with quantization and cyber attacks. *J. Frankl. Inst.* **2019**, *356*, 9451–9473. [CrossRef]
28. Takagi, T.; Sugeno, M. Fuzzy identification of systems and its applications to modeling and control. *IEEE Trans. Syst. Man Cybern.* **1985**, *SMC-15*, 116–132. [CrossRef]
29. Tan, Y.; Wang, K.; Su, X.; Xue, F.; Shi, P. Event-triggered fuzzy filtering for networked systems with application to sensor fault detection. *IEEE Trans. Fuzzy Syst.* **2021**, *29*, 1409–1422. [CrossRef]
30. Zhu, Z.; Zhu, Q. Adaptive event-triggered fuzzy control for stochastic highly nonlinear systems with time delay and nontriangular structure interconnections. *IEEE Trans. Fuzzy Syst.* **2024**, *32*, 27–37. [CrossRef]
31. Zhang, L.; Zong, G.; Zhao, X.; Zhao, N.; Sharaf, S. Reachable set control for discrete-time takagi–sugeno fuzzy singular Markov jump system. *IEEE Trans. Fuzzy Syst.* **2023**, *31*, 3173–3184. [CrossRef]
32. Yang, F.; Hu, S.; Xie, X.; Yue, D.; Sun, J. Resilient fuzzy control synthesis of nonlinear DC microgrid via a time-constrained DoS attack model. *IEEE Trans. Autom. Sci. Eng.* **2024**, *21*, 5270–5279. [CrossRef]

33. Zhao, X.-Y.; Chang, X.-H. H_∞ filtering for nonlinear discrete-time singular systems in encrypted state. *Neural Process. Lett.* **2023**, *55*, 2843–2866. [CrossRef]
34. Liu, X.-M.; Chang, X.-H. Adaptive event-triggered tracking control for nonlinear networked systems with dynamic quantization and deception attacks. *Int. J. Robust Nonlinear Control* **2024**, *34*, 8311–8333. [CrossRef]
35. Zha, L.; Liao, R.; Liu, J.; Xie, X.; Tian, E.; Cao, J. Dynamic event-triggered output feedback control for networked systems subject to multiple cyber attacks. *IEEE Trans. Cybern.* **2022**, *52*, 13800–13808. [CrossRef]
36. Elahi, A.; Alfi, A. Finite-time stabilisation of discrete networked cascade control systems under transmission delay and packet dropout via static output feedback control. *Int. J. Syst. Sci.* **2020**, *51*, 87–101. [CrossRef]
37. Zhu, Q. Stabilization of stochastic nonlinear delay systems with exogenous disturbances and the event-triggered feedback control. *IEEE Trans. Autom. Control* **2019**, *9*, 3764–3771. [CrossRef]

mathematics

MDPI

Article

An Improved Non-Monotonic Adaptive Trust Region Algorithm for Unconstrained Optimization

Mingming Xu [1], Quanxin Zhu [2] and Hongying Xiao [1,*]

[1] School of Mathematics and Physics, Yibin University, Yibin 644000, China; 2021070027@yibinu.edu.cn
[2] School of Mathematics and Statistics, Hunan Normal University, Changsha 410081, China; zqx22@hunnu.edu.cn
* Correspondence: 2020080001@yibinu.edu.cn

Abstract: The trust region method is an effective method for solving unconstrained optimization problems. Incorrectly updating the rules of the trust region radius will increase the number of iterations and affect the calculation efficiency. In order to obtain an effective radius for the trust region, an adaptive radius updating criterion is proposed based on the gradient of the current iteration point and the eigenvalue of the Hessian matrix which avoids calculating the inverse of the Hessian matrix during radius updating. This approach reduces the computation time and enhances the algorithm's performance. On this basis, we apply adaptive radius and non-monotonic techniques to the trust region algorithm and propose an improved non-monotonic adaptive trust region algorithm. Under proper assumptions, the convergence of the algorithm is analyzed. Numerical experiments confirm that the suggested algorithm is effective.

Keywords: non-monotonic technology; adaptive radius; trust region algorithm

MSC: 49M37; 65K05; 90C30

1. Introduction

Consider the following unconstrained optimization problem:

$$\min h(x), x \in R^n, \tag{1}$$

where $h : R^n \to R$ is twice continuously differentiable. There are two types of optimization problems: confined optimization and unconstrained optimization. Constrained optimization problems are typically addressed by being converted into unconstrained optimization problems. Unconstrained optimization problems can be solved using various techniques, including the conjugate gradient approach [1,2], the trust region method [3,4], and the Newton method [5,6]. The conjugate gradient method requires that the coefficient matrix is not only symmetric but also positive definite, which may not be applicable in the case of matrices with non-positive definite coefficients [7]. The Newton method needs to calculate the inverse of the Hessian matrix, and selection of the initial points is difficult in practice [8]. The trust region algorithm has strong convergence and robustness, and it has become one of the effective methods for solving unconstrained optimization problems [9,10].

Many practical application problems which arise in applied mathematics, economics, and engineering can be translated into Equation (1) to be solved [11]. As one of the effective algorithms for solving unconstrained optimization problems, the trust region has many applications in real life. For example, it can be extended to deal with constrained optimization problems, variational inequality problems, and nonlinear complementary problems [12]. Of course, the trust region algorithm can also be extended to reinforcement learning [13] and support vector machines [14] in machine learning, the electrical impedance tomography problem [15], and solving the inverse problem related to seismic spectrum analysis of Pn waves [16] as well as combined with the epitaxial implicit method [17]. Therefore, it is

necessary to propose a trust region algorithm which can effectively solve unconstrained optimization problems.

The underlying principle of trust region (TR) methods is that a trial step t_k is obtained at each iterate point x_k by solving the following subproblem:

$$\begin{aligned} \min \varpi_k(t) =& \mathrm{g}_k^T t + \frac{1}{2} t^T B_k t, \\ & s.t. \|t\| \leq \Delta_k, \end{aligned} \tag{2}$$

where $\|\cdot\|$ is the Euclidean norm, $\mathrm{g}_k = \nabla h(x_k)$, $B_k \approx \nabla^2 h(x_k)$, and Δ_k is the TR radius [18]. Next, the TR ratio r_k is used to compute the agreement between the predicted and actual reductions. It has the definition

$$r_k = \frac{Aret_k}{Pret_k} = \frac{h(x_k) - h(x_k + t_k)}{\varpi_k(0) - \varpi_k(t_k)},$$

where the predicted reduction $Pret_k$ and the actual reduction $Aret_k$ are given by

$$Aret_k = h(x_k) - h(x_k + t_k),$$

$$Pret_k = \varpi_k(0) - \varpi_k(t_k).$$

The iteration form of the TR is described below:

$$x_{k+1} = \begin{cases} x_k + t_k, & \text{if } r_k \geq \mu, \\ x_k, & \text{otherwise.} \end{cases}$$

If $r_k \geq \mu$ for a specified $0 < \mu < 1$, then the trial step t_k is approved, and $x_{k+1} = x_k + t_k$. The TR radius is adjusted correctly in this instance. In contrast, the t_k is rejected, and the current point is held constant for the following iteration if $r_k < \mu$. The TR radius is suitably decreased in this instance. This procedure is continued until the convergence requirements hold.

In the traditional TR algorithm, it is essential to select the appropriate initial value and update criteria for the TR radius. If the initial radius or radius updating criteria are not selected correctly, then the number of iterations of the trust region algorithm will be increased. Based on this, Sartenaer [19] proposed a criterion that can automatically determine the initial radius which uses gradient information (i.e., $\triangle_0 = \|\mathrm{g}_0\|$). Later, Lin et al. [20] proposed a better criterion for selecting the initial radius, which is set to be $\triangle_0 = \gamma\|\mathrm{g}_0\|$, where $\gamma > 0$ is an adjustable constant.

It can be noted that when the sequence $\{x_k\}$ generated by the traditional TR algorithm converges to the approximate best point x^*, the TR ratio r_k may converge to one. Therefore, according to the iterative steps of the algorithm, once k is big enough , $\triangle_k$ may be larger than the normal number. Moreover, the information of g_k and B_k generated at the current iteration point x_k is not used to revise the radius $\triangle_k$, which greatly increases the number of subproblems (Equation (2)) to be solved, thus reducing the calculation rate of the algorithm. To avoid the above problems, Zhang [21] proposed some variations of the adaptive TR method based on the following updated formula:

$$\triangle_k = \frac{q^\ell \|\mathrm{g}_k\|}{b_k},$$

in which $b_k = \min\{\|B_k\|, 1\}$, $0 < q < 1$ is a constant and $\ell \in \mathbf{N}$. Subsequently, Zhang et al. [22] proposed an adaptive radius formula containing g_k and B_k as follows:

$$\triangle_k = q^\ell \|\mathrm{g}_k\| \|\hat{B_k}^{-1}\|,$$

with ℓ and q as defined above and $\hat{B}_k = B_k + iI$ for some nonnegative integer i and the Hessian approximation B_k as a positive definite matrix. To avoid calculating $\hat{B}_k{}^{-1}$ at each iteration point x_k, Shi and Wang [23] proposed

$$\triangle_k = q^\ell \frac{\|g_k\|^3}{g_k^T \hat{B}_k g_k},$$

with ℓ, q, and $\hat{B}_k$ as defined above. To avoid counting $\hat{B}_k$, Sheng et al. [24] proposed a variant:

$$\triangle_k = q^\ell \frac{\|t_{k-1}\|}{\|y_{k-1}\|} \|g_k\|,$$

where $y_{k-1} = g_k - g_{k-1}$, $0 < q < 1$, and $\ell \in \mathbf{N}$. Recently, Wang et al. [25] employed the new radius updating criterion $\triangle_k = v_k \|g_k\|^\gamma$, where $\gamma \in (0,1)$ is a constant and the updating of v_k depends on the value of the ratio r_k. Building an adaptive TR radius which can speed up the solving of subproblems is vital since the TR algorithm heavily relies on the choice for the TR radius.

Each iteration in the monotone trust region method requires objective function h_k to have a certain reduction. However, it can be seen from some numerical experimental results that the monotonicity of forced h_k may significantly reduce the convergence rate, especially for the objective functions with highly eccentric level curves [26–28]. Therefore, allowing function values to increase to some extent while maintaining global convergence is advantageous. Non-monotonic methods are characterized by the fact that they do not enforce strict monotonicity of the value of the objective function over successive iterations. It has been shown that using non-monotonic techniques can improve the likelihood of finding global optimal values and the rate of convergence of the algorithm [26, 29]. Therefore, many researchers combined non-monotonic techniques with trust regions to form a new method for solving optimization problems [28,30–33]. Chamberlain et al. [34] proposed watchdog technology, which belongs to a non-monotonic line search technology. Next, Grippo et al. [26] extended Newton's method with another non-monotonic line search methodology and used it to solve unconstrained optimization problems. The idea of this non-monotonic line search technique is that for a given $0 < \zeta < 1$, one should select the step length α_k such that the following conditions are true:

$$h(x_k + \alpha_k t_k) \leq h_{l(k)} + \zeta \alpha_k g_k^T t_k,$$

where non-monotonic technology $h_{l(k)}$ is defined as

$$h_{l(k)} = h(x_{l(k)}) = \max_{0 \leq j \leq p(k)} \{h_{k-j}\}, \tag{3}$$

where $0 \leq p(k) \leq \min\{p(k-1)+1, M\}$ and M are positive integers. However, some numerical experiment results indicate that there are still certain issues with Grippo's non-monotonic method [35]. For instance, the current function value cannot be fully used. Moreover, the traditional non-monotonic technique is highly dependent on the selection of parameter M, and thus the numerical results of the algorithm may vary greatly with different selections of M values. To address these shortcomings of non-monotonic techniques, Zhang and Hager [29] proposed another non-monotonic technique as follows:

$$C_k = \begin{cases} h_0, & k = 0, \\ \frac{v_{k-1} Q_{k-1} C_{k-1} + h_k}{Q_k}, & k \geq 1, \end{cases}$$

and

$$Q_k = \begin{cases} 1, & k = 0, \\ v_{k-1} Q_{k-1} + 1, & k \geq 1, \end{cases}$$

where $\nu_{k-1} \in [\nu_{\min}, \nu_{\max}]$, $\nu_{\min} \in [0, 1)$, and $\nu_{\max} \in [\nu_{\min}, 1)$. Because the non-monotonic technique C_k needs to update ν_{k-1} and Q_k in each iteration, which affects the computation rate, Ahookhosh and Amini [35] combined h_k and $h_{l(k)}$ in a convex manner to form another efficient non-monotonic technique R_k:

$$R_k = \vartheta_k h_{l(k)} + (1 - \vartheta_k) h_k, \tag{4}$$

where $\vartheta_{k-1} \in [\vartheta_{\min}, \vartheta_{\max}]$, $\vartheta_{\min} \in [0, 1)$. Compared with $h_{l(k)}$, R_k has the following advantages. It can not only make full use of the current objective function value but also retain the current optimal operation value to a certain extent. Finally, better convergence can be achieved by selecting different parameters. Since the non-monotonic algorithm does not require the objective function to be strictly monotonic during continuous iteration, application of the non-monotonic technique to the trust region algorithm can increase both the likelihood of finding the global optimal solution and the algorithm's computation rate [30,36,37].

Because the convergence rate of the trust region algorithm depends on the renewal of the trust region radius, this paper aims to construct a new formula for the trust region radius. Combined with the non-monotonic technique, a new non-monotonic adaptive trust region algorithm is proposed to solve unconstrained optimization problems.

In this paper, in order to fully utilize the gradient and Hessian matrix of the current iteration points, we propose an improved adaptive radius updating criterion. In the improved adaptive radius-updating formula, the upper bound of the eigenvalue of matrix B_k is solved instead of the inverse of matrix B_k.

The rest of this article is organized as follows. In Section 2, we present a new adaptive trust region radius and propose a non-monotonic adaptive trust region algorithm. In Section 3, we demonstrate this algorithm's global convergence. In Section 4, numerical experiments are carried out, and the new method's effectiveness is demonstrated by the numerical results. Finally, we conclude the paper in Section 5 with a few closing thoughts.

2. The New Algorithm

In this section, an adaptive radius-updating formula is proposed. The improved adaptive radius updating criterion is described in detail below.

At the iterate point x_k, we set λ_{ki} to be the ith eigenvalue of the Hessian matrix B_k. According to the Geršgorin circle theory [12,38], we obtain

$$\lambda_{ki} \leq \sum_{j=1}^{n} |b_{ij}| \triangleq \bar{\lambda}_{ki}, \quad (i \in \mathbf{N}^*) \tag{5}$$

where $\bar{\lambda}_{ki}$ can be thought of as an upper bound on the ith eigenvalue of B_k and the element b_{ij} is the one which is placed at the ith row and jth column in matrix B_k.

Let

$$\lambda_k = \sum_{i=1}^{n} \omega_i \bar{\lambda}_{ki}^{-1}, \tag{6}$$

where $\omega_i > 0$ and $\sum_{i=1}^{n} \omega_i = 1$.

Based on this, the new adaptive trust region radius proposed in this paper is as follows:

$$\Delta_{k+1} = c_{k+1} \|g_{k+1}\| \lambda_{k+1}, \tag{7}$$

where

$$c_{k+1} = \begin{cases} t_1 c_k, & \tilde{r}_k < \mu_1, \\ c_k, & \mu_1 \leq \tilde{r}_k < \mu_2, \\ t_2 c_k, & \tilde{r}_k \geq \mu_2, \end{cases} \tag{8}$$

and $0 < t_1 < 1 < t_2$. Obviously, we adjust the size of c_{k+1} using the trust region ratio $\tilde{r}_k$, which can better use the information of the function to adjust the radius of the trust region so as to effectively decrease the number of solutions for Equation (2).

The adaptive radius updating criterion proposed in this paper not only makes full use of the first- and second-order information of the objective function but also avoids solving the inverse matrix B_k. Based on the non-monotonic technique and the new adaptive trust region radius (Equation (7)), we propose an improved non-monotonic adaptive trust region algorithm (NATR). In our algorithm, the non-monotone technique is defined by R_k, where R_k is given by Equation (4) and the ratio of the trust region $\tilde{r}_k$ is determined by

$$\tilde{r}_k = \frac{R_k - h(x_k + t_k)}{\varpi_k(0) - \varpi_k(t_k)}, \tag{9}$$

where t_k is the trial step to be calculated by Equation (2).

The procedure of NATR is described by Algorithm 1 .

Algorithm 1 An improved non-monotonic adaptive trust region algorithm (NATR).

Step 0. (Initialization) Start with $x_0 \in R^n$ and the symmetric matrix $B_0 \in R^{n \times n}$. The constants $0 \leq \vartheta_{\min} \leq \vartheta_{\max} \leq 1$, $\vartheta_k \in [\vartheta_{\min}, \vartheta_{\max}]$, $0 < t_1 < 1 < t_2$, $0 < \mu_1 < \mu_2 < 1$, $\varepsilon > 0$, $\theta > 0$, $\Delta_{\max} > 0$, $c_0 > 0, \omega > 0$, and $\Delta_0 > 0$ are also given. Set $k = 0$.
Step 1. If $\|g_k\| \leq \varepsilon$, then stop.
Step 2. Solve the subproblems of Equation (2) to find the trial step t_k.
Step 3. Compute R_k and $\tilde{r}_k$. If $\tilde{r}_k < \mu_1$, then go to Step 2. If $\tilde{r}_k \geq \mu_1$, then set $x_{k+1} = x_k + t_k$, and go to Step 4.
Step 4. Compute λ_{k+1}. If $\lambda_{k+1} \leq \omega$ or $\lambda_{k+1} \geq \frac{1}{\omega}$, then set $\lambda_{k+1} = \theta$; Update $\Delta = c_{k+1}\|g_{k+1}\|\lambda_{k+1}$, where c_{k+1} is given by Equation (8), and set $\Delta_{k+1} = \min\{\Delta, \Delta_{\max}\}$.
Step 5. Update B_k by using a modified quasi-Newton formula. Set $k = k + 1$, and go to Step 1.

From Step 4 of the NATR algorithm, it can be seen that sequence $\{\lambda_k\}$ is bounded; in other words, we have

$$0 < \min\{\omega, \theta\} \leq \lambda_k \leq \max\{\frac{1}{\omega}, \theta\} \tag{10}$$

for any $k \in \mathbf{N}$.

Remark 1. *It can be noted that in this paper, the non-monotone adaptive trust region algorithm uses the gradient and B_k matrix eigenvalues when the radius Δ_k is updated. Compared with [30,39] and [22], the radius in this paper avoids solving B_k^{-1} and makes full use of the ratio of the trust region $\tilde{r}_k$ in each iteration to automatically adjust the radius Δ_k, which can make better use of the information of the current iteration point of the objective function.*

Throughout this paper, we consider the following assumptions in order to analyze the convergence of the new algorithm:

H1: The level set $\tilde{L}(x_0) = \{x \in R^n | h(x) \leq h(x_0)\}$ is a bounded closed set.

H2: There exist constants $M_B > 0$, $M_g > 0$, and $M_G > 0$ such that $\|B_k\| \leq M_B$, $\|g_k\| \leq M_g$, and $\|\nabla^2 h(x)\| \leq M_G$.

H3: Suppose that there is a constant $\bar{c} > 0$ such that $\forall k \in \mathbf{N}$, and $c_k \leq \bar{c}$ is true.

Remark 2. *Similar to [10], for a solution t_k to the subproblem in Equation* (2)*, we have*

$$Pret_k = \varpi_k(0) - \varpi_k(t_k) \geq \delta \|g_k\| \min\{\Delta_k, \frac{\|g_k\|}{\|B_k\|}\},\ \delta \in (0,1). \tag{11}$$

3. Convergence Analysis

In order to analyze the convergence properties of Algorithm 1, we also need to present the following lemmas:

Lemma 1. *Based on H1 and H2, suppose that t_k is the solution to Equation* (2)*. Then, we have*

$$h(x_k) - h(x_k + t_k) - [\varpi_k(0) - \varpi_k(t_k)] \leq o(\|t_k\|^2).$$

Proof. See [31] for the proof of Lemma 1. □

Lemma 2. *Assume that the NATR algorithm produced the sequence $\{x_k\}$. Then, the sequence $\{h_{l(k)}\}$ is a decreasing sequence.*

Proof. See the proof of Lemma 4 in [35]. □

Lemma 3. *Suppose that the sequence $\{x_k\}$ is generated by the NATR algorithm. Then, we have*

$$h_k \leq R_k, \tag{12}$$

and

$$x_k \in \tilde{L}(x_0),$$

for each $k \in \mathbf{N}$.

Proof. From Equaitons (3) and (4), we have

$$h_k = \vartheta_k h_k + (1 - \vartheta_k) h_k \leq \vartheta_k h_{l(k)} + (1 - \vartheta_k) h_k = R_k.$$

Hence, Equation (12) holds. Now let us prove by induction that $x_k \in \tilde{L}(x_0)$ for each $k \in \mathbf{N}$. Obviously, the result holds for $k = 0$. We demonstrate that $x_{k+1} \in \tilde{L}(x_0)$, assuming that $x_k \in \tilde{L}(x_0)$. Based on Lemma 2, we have

$$h_{k+1} \leq h_{l(k+1)} \leq h_{l(k)} \leq h_0,$$

i.e., $x_{k+1} \in \tilde{L}(x_0)$. This completes the proof. □

Lemma 4. *Assume that the NATR algorithm produced the sequence $\{x_k\}$ and $\|g_k\| \geq \varepsilon > 0$. Then, $\forall k \in \mathrm{N}, \exists \varrho \in \mathbf{N}$ such that $x_{k+\varrho+1}$ is a successful iteration (i.e., $\tilde{r}_{k+\varrho} \geq \mu_1$).*

Proof. Assume that there exists an integer constant k such that the point $x_{k+\varrho+1}$ is not a successful point for any ϱ. Hence, we have that $\tilde{r}_{k+\varrho+1} < \mu_1$ for any constant $\varrho = 0, 1, 2, \cdots$. From H2 and Remark 1, we obtain

$$\begin{aligned} \varpi_{k+\varrho}(0) - \varpi_{k+\varrho}(d_{k+\varrho}) &\geq \delta \|g_{k+\varrho}\| \min\{\Delta_{k+\varrho}, \frac{\|g_{k+\varrho}\|}{\|B_{k+\varrho}\|}\} \\ &\geq \delta\varepsilon \min\{\Delta_{k+\varrho}, \frac{\varepsilon}{M_B}\}. \end{aligned} \tag{13}$$

Thus, from Lemma 1 and Equation (13), we have

$$\begin{aligned} \left| \frac{h(x_{k+\varrho}) - h(x_{k+\varrho} + t_{k+\varrho})}{\varpi_{k+\varrho}(0) - \varpi_{k+\varrho}(t_{k+\varrho})} - 1 \right| &= \left| \frac{h(x_{k+\varrho}) - h(x_{k+\varrho} + t_{k+\varrho}) - [\varpi_{k+\varrho}(0) - \varpi_{k+\varrho}(t_{k+\varrho})]}{\varpi_{k+\varrho}(0) - \varpi_{k+\varrho}(t_{k+\varrho})} \right| \\ &\leq \frac{o(\|t_{k+\varrho}\|^2)}{\delta\varepsilon \min\{\Delta_{k+\varrho}, \frac{\varepsilon}{M_B}\}}. \end{aligned} \tag{14}$$

When $\varrho \to \infty$, we have $\|t_{k+\varrho}\|^2 \to 0$, and subsequently

$$\lim_{\varrho \to \infty} \frac{h(x_{k+\varrho}) - h(x_{k+\varrho} + t_{k+\varrho})}{\varpi_{k+\varrho}(0) - \varpi_{k+\varrho}(t_{k+\varrho})} = 1. \tag{15}$$

From Lemma 3 and Equation (15), we obtain

$$\begin{aligned} \tilde{r}_{k+\varrho} &= \frac{R_{k+\varrho} - h(x_{k+\varrho} + t_{k+\varrho})}{\varpi_{k+\varrho}(0) - \varpi_{k+\varrho}(t_{k+\varrho})} \\ &\geq \frac{h(x_{k+\varrho}) - h(x_{k+\varrho} + t_{k+\varrho})}{\varpi_{k+\varrho}(0) - \varpi_{k+\varrho}(t_{k+\varrho})} \\ &\geq \mu_2. \end{aligned} \tag{16}$$

Therefore, when ϱ is sufficiently large, $\tilde{r}_{k+\varrho} \geq \mu_2 > \mu_1$. This contradicts the assumption that

$$\tilde{r}_{k+\varrho} < \mu_1,$$

and thus the hypothesis is not valid. □

Lemma 5. *Assuming that H3 is true, then there exists a constant $c_1 > 0$ such that t_k satisfies:*

$$\|t_k\| \leq c_1 \|g_k\|.$$

Proof. From H3 and Equations (7) and (10), we obtain

$$\Delta_k \leq \bar{c}\|g_k\| \max\{\frac{1}{\omega}, \theta\},$$

and subsequently, through $\|t_k\| \leq \Delta_k$ we have

$$\|t_k\| \leq \bar{c}\|g_k\| \max\{\frac{1}{\omega}, \theta\}.$$

Set $c_1 = \bar{c} \max\{\frac{1}{\omega}, \theta\}$. Then, we have

$$\|t_k\| \leq c_1 \|g_k\|. \tag{17}$$

□

Lemma 6. *Assume that H1 and H2 are true and the sequence $\{x_k\}$ is generated by the NATR algorithm. Then, we have*

$$\lim_{k \to \infty} h_{l(k)} = \lim_{k \to \infty} h(x_k). \tag{18}$$

Proof. See Lemma 7 in [35]. □

Lemma 7. *Assume that the sequence $\{x_k\}$ is generated by the NATR algorithm. Then, we have*

$$\lim_{k \to \infty} R_k = \lim_{k \to \infty} h(x_k). \tag{19}$$

Proof. Using Equations (3) and (4) and Lemma 3, we obtain

$$h_k \leq R_k = \vartheta_k h_{l(k)} + (1-\vartheta_k)h_k \leq \vartheta_k h_{l(k)} + (1-\vartheta_k)h_{l(k)} = h_{l(k)}.$$

According to Lemma 6, we obtain

$$\lim_{k\to\infty} R_k = \lim_{k\to\infty} h(x_k).$$

□

Theorem 1. *(Global Convergence) Assume that H1, H2, and H3 are true, and the sequence* $\{x_k\}$ *is generated by the NATR algorithm. Then, we have*

$$\liminf_{k\to\infty} \|g_k\| = 0. \tag{20}$$

Proof. By contradiction, we assume that there exists a constant $\varepsilon > 0$ such that

$$\|g_k\| \geq \varepsilon, \tag{21}$$

for any integer k.

When k is sufficiently large, with Equation (9), Lemma 3, and Lemma 4, we have

$$R_k - h(x_k + t_k) \geq \mu_1 Pret_k. \tag{22}$$

Using Equations (11) and (22), we obtain

$$h_{k+1} = h(x_k + t_k) \leq R_k - \mu_1 Pret_k \leq R_k - \mu_1\delta\|g_k\| \min\{\Delta_k, \frac{\|g_k\|}{\|B_k\|}\}. \tag{23}$$

From H2, Equation (23), Lemma 3, and the definition of R_k, it follows that

$$\begin{aligned}
h_{k+1} \leq R_{k+1} &= \vartheta_{k+1}h_{l(k+1)} + (1-\vartheta_{k+1})h_{k+1} \\
&\leq \vartheta_{k+1}h_{l(k)} + (1-\vartheta_{k+1})[R_k - \mu_1\delta\|g_k\| \min\{\Delta_k, \frac{\|g_k\|}{\|B_k\|}\}] \\
&\leq \vartheta_{k+1}h_{l(k)} + (1-\vartheta_{k+1})[h_{l(k)} - \mu_1\delta\|g_k\| \min\{\Delta_k, \frac{\|g_k\|}{\|B_k\|}\}] \\
&= \vartheta_{k+1}h_{l(k)} + (1-\vartheta_{k+1})h_{l(k)} - (1-\vartheta_{k+1})\mu_1\delta\|g_k\| \min\{\Delta_k, \frac{\|g_k\|}{\|B_k\|}\} \\
&= h_{l(k)} - (1-\vartheta_{k+1})\mu_1\delta\|g_k\| \min\{\Delta_k, \frac{\|g_k\|}{\|B_k\|}\} \\
&\leq h_{l(k)} - (1-\vartheta_{k+1})\mu_1\delta\varepsilon \min\{\Delta_k, \frac{\varepsilon}{M_B}\}.
\end{aligned} \tag{24}$$

This implies that

$$h_{l(k)} - h_{k+1} \geq (1-\vartheta_{k+1})\mu_1\delta\varepsilon \min\{\Delta_k, \frac{\varepsilon}{M_B}\}. \tag{25}$$

Based on Equation (25) and Lemma 6, we write

$$\lim_{k\to\infty} \min\{\Delta_k, \frac{\varepsilon}{M_B}\} = 0, \tag{26}$$

and subsequently, $\lim_{k\to\infty} \Delta_k = 0$; in other words, we have

$$\lim_{k\to\infty} \Delta_k = \lim_{k\to\infty} c_k\|g_k\|\lambda_k = 0. \tag{27}$$

If $\tilde{r}_k \geq \mu_2$—that is, x_{k+1} is a successful iteration point—then there exists a constant $c^+ > 0$ such that

$$c_k \geq c^+,$$

for sufficiently large k values. This information and Equation (10) suggest that

$$\Delta_k = c_k \|g_k\| \lambda_k \geq \varepsilon \min\{\omega, \theta\} c_k. \tag{28}$$

With Equations (27) and (28), we can deduce that

$$\lim_{k \to \infty} c_k = 0,$$

which contradicts the assumption that $c_k \geq c^+ > 0$.

Hence, the proof is completed. □

Remark 3. *It can be seen in Theorem 1 that the NATR algorithm has global convergence; that is, the algorithm is feasible theoretically.*

4. Preliminary Numerical Experiments

In this section, we test and compare the NATR algorithm with the traditional trust region algorithm in [8] (TTR) and the non-monotonic trust region algorithm proposed by Ahookhoosh et al. in [35] (NTR). All unconstrained optimization test problems were selected from [40], and all of the numerical experiments were carried out in the Matlab 2018 environment.

In all algorithms, we set $\Delta_0 = 2, B_0 = I$, $\mu_1 = 0.25$, $\mu_2 = 0.75$, $t_1 = 0.5$, $t_2 = 1.5$, $c_0 = 1$, $M = 5$, $\omega = 10^{-6}$, $\Delta_{\max} = 200$, and $\varepsilon = 10^{-6}$. If $\lambda_{k+1} \leq \omega$, then we set $\theta = \omega$, or if $\lambda_{k+1} \geq \frac{1}{\omega}$, then we set $\theta = \frac{1}{\omega}$. Moreover, we set $\vartheta_k = \begin{cases} \frac{\vartheta_0}{2}, & k = 1, \\ \frac{\vartheta_{k-1} + \vartheta_{k-2}}{2}, & k \geq 2, \end{cases}$ $\vartheta_0 = 0.85$ [35]. The matrix B_k is updated by the BFGS formula in [41], as follows:

$$B_{k+1} = \begin{cases} B_k + \frac{y_k y_k^T}{y_k^T s_k} - \frac{B_k s_k s_k^T B_k}{s_k^T B_k s_k}, & s_k^T y_k > 0, \\ B_k, & s_k^T y_k \leq 0, \end{cases}$$

where $y_k = g_{k+1} - g_k$ and $s_k = x_{k+1} - x_k$. Furthermore, we declare that an algorithm will fail if it has more than 10,000 iterations. All of the algorithms are stopped when $\|g_k\| \leq 10^{-6}$.

In Table 1, the name of the test function is denoted as "function", the dimension of the test function is denoted as "n", the number of iterations of the algorithm is denoted as "k", and the time used by the algorithm to solve the test function is denoted as "Cpu" (in seconds). If the algorithm is iterated more than 10,000 times, then it fails and is marked with "F".

According to the numerical results in Table 1, we can find that when the NATR algorithm was applied to solve these unconstrained optimization problems, it required fewer iterations than the TTR and NTR methods. Especially for the perturbed quadratic diagonal function and diagonal 2 function, our NATR algorithm could solve the problem in fewer iterations. However, the iteration times of the NTR algorithm and TTR algorithm both exceeded 10,000, which means that they could not effectively solve these problems. For the POWER function (CUTE), the CPU time required by the NATR algorithm was only 1/30 and 1/3 of that needed by the NTR and TTR methods, respectively. This is because neither the NTR nor TTR method can correctly adjust the radius of the confidence region, while the radius of the trust region of the NATR algorithm is automatically adjusted according to the gradient of the current iteration point and the eigenvalue of the Hessian matrix, thus reducing the number of iterations and reducing the calculation cost. For most test functions, the three algorithms ended up with the same function value results. For some functions, such as the POWER function (CUTE), the NATR algorithm not only had fewer iterations and fewer iterations, but the function value was also smaller.

Table 1. Numerical results.

Function	n	NATR (k/cpu/h)	NTR (k/cpu/h)	TTR (k/cpu/h)
POWER function (CUTE)	10	$21/0.030242/1.1308 \times 10^{-16}$	$634/0.133546/2.2135 \times 10^{-13}$	$71/24.828385/1.0899 \times 10^{-13}$
Quadratic QF1 function	10	$28/0.033207/-5.0000$	$43/0.040731/-5.0000$	$31/21.791012/-5.0000$
Raydan 1 function	10	21/0.018676/5.5000	59/0.020833/5.5000	87/16.056837/5.5000
Extended DENSCHNB function (CUTE)	10	12/0.035049/5.0000	15/0.031511/5.0000	12/23.596389/5.0000
Diagonal 2 function	100	$95/0.168606/1.5741 \times 10$	$496/0.270396/1.5741 \times 10$	$1364/ 21.161857/1.5741 \times 10$
QUARTC function(CUTE)	100	$27/0.07209/6.3426 \times 10^{-9}$	$39/0.032488/4.7396 \times 10^{-9}$	F/F/F
HIMMELBG function	100	$21/0.10308/4.5453 \times 10^{-6}$	$32/0.159167/4.5453 \times 10^{-6}$	F/F/F
Diagonal 2 function	500	$193/4.646668/2.6037 \times 10$	$2056/7.205046/2.6037 \times 10$	$6410/257.345146/2.6037 \times 10$
Perturbed quadratic diagonal function	500	$3/0.234107/4.3812 \times 10^{6}$	F/F/F	F/F/F
Diagonal 7 function	500	$8/0.141167/-4.0842 \times 10^{2}$	$17/0.164094/-4.0842 \times 10^{2}$	$8/19.918756/-4.0842 \times 10^{2}$
Diagonal 4 function	900	$9/0.769483/2.2052 \times 10^{2}$	$15/0.831553/2.2052 \times 10^{2}$	$9/23.19987/2.2052 \times 10^{2}$
Diagonal 2 function	1000	$260/44.791428/3.1275 \times 10^{1}$	F/F/F	F/F/F
QUARTC function	1000	$29/3.777523/6.6878 \times 10^{-9}$	$44/0.677226/1.4397 \times 10^{-8}$	F/F/F
Raydan 2 function	1000	$8/1.035779/1.0000 \times 10^{3}$	$23/1.317213/1.0000 \times 10^{3}$	$9/29.141964/1.0000 \times 10^{3}$
Diagonal 5 function	1000	$6/0.642228/6.9315 \times 10^{2}$	$12/0.749363/6.9315 \times 10^{2}$	$7/19.115579/6.9315 \times 10^{2}$
Diagonal 8 function	1000	$10/1.33452/-4.8045 \times 10^{2}$	$12/1.302234/-4.8045 \times 10^{2}$	$10/73.357103/-4.8045 \times 10^{2}$
Raydan 2 function	2000	$8/11.038501/2.0000 \times 10^{3}$	$25/12.024056/2.0000 \times 10^{3}$	$9/72.307226/2.0000 \times 10^{3}$
HIMMELBG function	3000	$24/46.598187/1.5727 \times 10^{-5}$	$47/38.713961/2.2028 \times 10^{-5}$	F/F/F
QUARTC function	3000	$29/41.807088/2.0063 \times 10^{-8}$	$37/24.486504/9.8927 \times 10^{-9}$	F/F/F
Diagonal 5 function	3000	$6/9.334939/2.0794 \times 10^{3}$	$9/4.407844/2.0794 \times 10^{3}$	$7/41.826252/2.0794 \times 10^{3}$
Perturbed quadratic diagonal function	5000	$3/61.283901/3.2506 \times 10^{8}$	F/F/F	F/F/F

For higher-dimension problems, such as the 3000 dimensional test functions of the HIMMELBG function and QUARTC function (CUTE) and the 5000 dimensional test functions of the perturbed quadratic diagonal function, the NATR algorithm could solve them effectively, but the TTR algorithm failed to solve them. This shows that the NATR algorithm has a certain effect when solving higher-dimension problems.

Overall, our new algorithm was effective for most test problems and took fewer iterations, as demonstrated by these numerical findings for both high- and low-dimensional test issues. In general, we can infer that the NATR algorithm is more efficient than the traditional trust region (TTR) algorithm and the non-monotonic trust region (NTR) algorithm in terms of the number of iterations and running time. Therefore, the NATR algorithm can effectively solve unconstrained optimization problems.

5. Conclusions

In this paper, based on the current iteration point gradient g_k and the eigenvalues of the Hessian matrix B_k, we proposed a new improved adaptive radius updating criterion which reduces the effort and computation time and improves the performance of an algorithm. Then, we proposed an improved non-monotonic adaptive trust region (NATR) algorithm by combining the adaptive radius updating criterion with the non-monotonic technique. Under certain common assumptions, the global convergence of the NATR algorithm was demonstrated. Finally, in the same environment, the test function was used to conduct numerical experiments on the three algorithms. The numerical experiments show that the NATR algorithm can effectively solve unconstrained problems, and for some test functions, the iteration time and iteration times of the NATR algorithm were less than those of the NTR algorithm and TTR algorithm, demonstrating an effective algorithm.

In the NATR algorithm, when the trust region ratio did not meet the requirements, the subproblem was recalculated to find the test step d_k which met the conditions. In the future, we will consider combining the trust region algorithm with the line search method to avoid double-computation subproblems. Secondly, the application of the non-monotonic trust region method will be studied further, such as by applying it to nonlinear fractional-order multi-agent systems [42] and cooperative control for linear delta operator systems [43].

Author Contributions: Writing—original draft, M.X.; Writing—review & editing, Q.Z.; Visualization, H.X.; Supervision, H.X. All authors contributed equally to this paper. All authors have read and agreed to the published version of the manuscript.

Funding: This work was supported by the specialized research fund of YiBin University (Grant No. 412-2021QH027).

Data Availability Statement: The data that support the findings of this study are available on request from the corresponding author, upon reasonable request.

Acknowledgments: The authors would like to thank the Editor and the anonymous referees for their helpful comments and valuable suggestions regarding this article.

Conflicts of Interest: The authors declare no conflict of interest.

References

1. Andrei, N. Another hybrid conjugate gradient algorithm for unconstrained optimization. *Numer. Algorithms* **2008**, *47*, 143–156. [CrossRef]
2. Fatemi, M. A new efficient conjugate gradient method for unconstrained optimization. *J. Comput. Appl. Math.* **2016**, *300*, 207–216. [CrossRef]
3. Kimiaei, M.; Ghaderi, S. A new restarting adaptive trust-region method for unconstrained optimization. *J. Oper. Res. Soc. China* **2017**, *5*, 487–507. [CrossRef]
4. Xue, Y.; Liu, H.; Liu, Z. An improved nonmonotone adaptive trust region method. *Appl. Math.* **2019**, *64*, 1–16. [CrossRef]
5. Gao, H.; Zhang, H.B.; Li, Z.B. A nonmonotone inexact Newton method for unconstrained optimization. *Optim. Lett.* **2017**, *11*, 947–965. [CrossRef]

6. Wei, Z.; Li, G.; Qi, L. New quasi-Newton methods for unconstrained optimization problems. *Appl. Math. Comput.* **2006**, *175*, 1156–1188. [CrossRef]
7. Fletcher, R. Conjugate gradient methods for indefinite systems. In *Numerical Analysis: Proceedings of the Dundee Conference on Numerical Analysis, 1975*; Springer: Berlin/Heidelberg, Germany, 2006; pp. 73–89.
8. Ma, C.F. *Optimization Method and Matlab Program Design*; Science Press: Beijing, China, 2010.
9. Mo, J.; Zhang, K.; Wei, Z. A nonmonotone trust region method for unconstrained optimization. *Appl. Math. Comput.* **2005**, *171*, 371–384. [CrossRef]
10. Nocedal, J.; Yuan, Y. Combining trust region and line search techniques. In *Advances in Nonlinear Programming: Proceedings of the 96 International Conference on Nonlinear Programming*; Springer: New York, NY, USA, 1998; pp. 153–175.
11. Jiang, X.; Huang, Z. An accelerated relaxed-inertial strategy based CGP algorithm with restart technique for constrained nonlinear pseudo-monotone equations to image de-blurring problems. *J. Comput. Appl. Math.* **2024**, *447*, 115887. [CrossRef]
12. Liu, J.; Xu, X.; Cui, X. An accelerated nonmonotone trust region method with adaptive trust region for unconstrained optimization. *Comput. Optim. Appl.* **2018**, *69*, 77–97. [CrossRef]
13. Xu, H.; Xuan, J.; Zhang, G.; Lu, J. Trust region policy optimization via entropy regularization for Kullback CLeibler divergence constraint. *Neurocomputing* **2024**, *589*, 127716. [CrossRef]
14. Yu, Z.; Yuan, Y.; Tian, P. An efficient trust region algorithm with bounded iteration sequence for unconstrained optimization and its application in support vector machine. *J. Comput. Appl. Math.* **2024**, *449*, 115956. [CrossRef]
15. Goharian, M.; Soleimani, M.; Jegatheesan, A.; Moran, G.R. *Regularization of EIT Problem Using Trust Region SubProblem Method*; Springer: Berlin/Heidelberg, Germany, 2007.
16. Weiping, W.; Hongchun, W.; Haofeng, Z.; Xiong, X. A Pn-wave spectral inversion technique based on trust region reflective algorithm. *J. Appl. Geophys.* **2024**, *230*, 105525. [CrossRef]
17. Ceng, L.; Yuan, Q. On a General Extragradient Implicit Method and Its Applications to Optimization. *Symmetry* **2020**, *12*, 124. [CrossRef]
18. Sun, W.; Yuan, Y. *Optimization Theory and Methods: Nonlinear Programming*; Springer: New York, NY, USA, 2006.
19. Sartenaer, A. Automatic Determination Of An Initial Trust Region In Nonlinear Programming. *Siam J. Sci. Comput.* **1997**, *18*, 1788–1803. [CrossRef]
20. Lin, C.; Mor, J. Newton's method for large bound-constrained optimization problems. *Siam J. Optim.* **1999**, *9*, 1100–1127. [CrossRef]
21. Zhang, X. NN models for general nonlinear programming. In *Neural Networks in Optimization*; Springer: Boston, MA, USA, 2000; pp. 273–288.
22. Zhang, X.; Zhang, J.; Liao, L. An adaptive trust region method and its convergence. *Sci. China Ser. Math.* **2002**, *45*, 620–631. [CrossRef]
23. Shi, Z.; Wang, S. Nonmonotone adaptive trust region method. *Eur. J. Oper. Res.* **2011**, *208*, 28–36. [CrossRef]
24. Sheng, Z.; Gonglin, Y.; Zengru, C. A new adaptive trust region algorithm for optimization problems. *Acta Math. Sci.* **2018**, *38*, 479–496. [CrossRef]
25. Wang, X.; Ding, X.; Qu, Q. A new filter nonmonotone adaptive trust region method for unconstrained optimization. *Symmetry* **2020**, *12*, 208. [CrossRef]
26. Grippo, L.; Lampariello, F.; Lucidi, S. A nonmonotone line search technique for Newton's method. *Siam J. Numer. Anal.* **1986**, *23*, 707–716. [CrossRef]
27. Grippo, L.; Lampariello, F.; Lucidi, S. A truncated Newton method with nonmonotone line search for unconstrained optimization. *J. Optim. Theory Appl.* **1989**, *60*, 401–419. [CrossRef]
28. Toint, P.L. Non-monotone trust-region algorithms for nonlinear optimization subject to convex con-straints. *Math. Progr.* **1997**, *77*, 69–94. [CrossRef]
29. Zhang, H.; Hager, W. A nonmonotone line search technique and its application to unconstrained optimization. *Siam J. Optim.* **2004**, *14*, 1043–1056. [CrossRef]
30. Cui, Z.; Wu, B. A new modified nonmonotone adaptive trust region method for unconstrained optimization. *Comput. Optim. Appl.* **2012**, *53*, 795–806. [CrossRef]
31. Reza Peyghami, M.; Ataee Tarzanagh, D. A relaxed nonmonotone adaptive trust region method for solving unconstrained optimization problems. *Comput. Optim. Appl.* **2015**, *61*, 321–341. [CrossRef]
32. Rezaee, S.; Babaie-Kafaki, S. An adaptive nonmonotone trust region algorithm. *Optim. Methods Softw.* **2019**, *34*, 264–277. [CrossRef]
33. Zhang, J.L.; Zhang, X.S. A nonmonotone adaptive trust region method and its convergence. *Comput. Math. Appl.* **2003**, *45*, 1469–1477. [CrossRef]
34. Chamberlain, R.M.; Powell, M.J.D.; Lemarechal, C.; Pedersen, H.C. The watchdog technique for forcing convergence in algorithms for constrained optimization. In *Algorithms for Constrained Minimization of Smooth Nonlinear Functions*; Springer: Berlin/Heidelberg, Germany, 1982; pp. 1–17.
35. Ahookhosh, M.; Amini, K. An efficient nonmonotone trust-region method for unconstrained optimization. *Numer. Algorithms* **2012**, *59*, 523–540. [CrossRef]

36. Ahookhosh, M.; Amini, K. A Nonmonotone trust region method with adaptive radius for unconstrained optimization problems. *Comput. Math. Appl.* **2010**, *60*, 411–422. [CrossRef]
37. Fu, J.; Sun, W. Nonmonotone adaptive trust-region method for unconstrained optimization problems. *Appl. Math. Comput.* **2005**, *163*, 489–504. [CrossRef]
38. Varga, R.S. *Geršgorin and His Circles*; Springer: Berlin/Heidelberg, Germany, 2010; Volume 36.
39. Sang, Z.; Sun, Q. Aself-adaptive trust region method with linesearch based on a simple subproblem model. *J. Comput. Appl. Math.* **2009**, *232*, C514–C522. [CrossRef]
40. Andrei, N. An unconstrained optimization test functions collection. *Adv. Model. Optim.* **2008**, *10*, 147–161.
41. Nocedal, J.; Wright, S.J. *Numerical Optimization*; Springer: New York, NY, USA, 2006.
42. Yang, Y.; Qi, Q.; Hu, J.; Dai, J.; Yang, C. Adaptive Fault-Tolerant Control for Consensus of Nonlinear Fractional-Order Multi-Agent Systems with Diffusion. *Fractal Fract.* **2023**, *7*, 760. [CrossRef]
43. Xue, Y.; Han, J.; Tu, Z.; Chen, X. Stability analysis and design of cooperative control for linear delta operator system. *Aims Math.* **2023**, *8*, 12671–12693. [CrossRef]

mathematics

MDPI

Article

Adaptive Fault-Tolerant Tracking Control for Continuous-Time Interval Type-2 Fuzzy Systems

Ming-Yang Qiao and Xiao-Heng Chang *

School of Information Science and Engineering, Wuhan University of Science and Technology, Wuhan 430081, China; qiaomingyang@wust.edu.cn

* Correspondence: changxiaoheng@wust.edu.cn

Abstract: This paper investigated the tracking problem of mixed $\mathcal{H}_\infty$ and $L_2 - L_\infty$ adaptive fault-tolerant control (FTC) for continuous-time interval type-2 fuzzy systems (IT2FSs). For the membership function mismatch and uncertainty between the modules of the nonlinear system, the IT2 fuzzy model is applied to linearly approximate it. The observer can sensitively estimate the system state, and the adaptive fault estimation functions can estimate adaptively the fault signals, which enables the designed adaptive FTC scheme to ensure the asymptotic stability of the closed-loop control system and achieve the desired mixed $\mathcal{H}_\infty$ and $L_2 - L_\infty$ tracking performance. The designed adaptive control law can achieve the purpose of dynamic compensation for faults and disturbances, and the introduced lemmas further reduce the design conservatism by adjusting the slack parameters and matrices. Finally, a mass-spring-damping system is used to illustrate the effectiveness of the designed method.

Keywords: interval type-2 fuzzy systems (IT2FSs); adaptive fault-tolerant control; mixed $\mathcal{H}_\infty$ and $L_2 - L_\infty$ performance; tracking control

MSC: 93C40

1. Introduction

As the automatic control systems tend to be large scale, randomized and complicated, the probability of faults caused by the long-term operation of system components or improper human operation is increasing greatly. Therefore, how to quickly detect a fault and repair it, or design a fault tolerance scheme to make the practical system able to tolerate a certain degree and type of fault, to achieve the purpose of fault tolerance control, has always been a hot research spot in the control field [1]. Among these, model-based fault detection makes full use of the deep knowledge inside the system and determines whether the fault occurs by residual error [2]. Then, to ensure the automatic control system is stable and reduce the impact of faults on the system performance, some targeted FTC strategies are studied [3–10]. Considering that active FTC relies too much on the fault detection module, it is easy to cause delay when reconstructing a controller according to detection results, which affects system performance [4–6]. Passive FTC is widely used because of its simple design, easy implementation and good real-time performance [7–10]. However, due to its conservative design and low tolerance to unknown faults, adaptive FTC can adjust its own characteristic feedback control system in real time and intelligently according to the specific fault affecting the system so that the system can work in the optimal state according to some set standards [11–19]. For example, ref. [13] proposed a kind of robust adaptive FTC circuit design and converted to analog control circuit implementation. The adaptive FTC strategy for an actuator fault in [12,18] has a good fault-tolerant effect. For unexpected fault situations in multi-agent systems, ref. [15] designed an compensation protocol and $\mathcal{H}_\infty$ resilient control scheme to adaptively achieve optimal control results. By designing the tracking controller, the adaptive optimal tracking problem with the FTC method of a

multi-agent system and active FTC tracking problem with input constraint are embodied in [19,20], respectively. However, there are few achievements on adaptive FTC for IT2 nonlinear systems with sensor and actuator faults.

Tracking control is used to achieve the purpose of tracking the desired trajectory or path through the control system [19–25]. At present, attitude tracking in aerospace [22], trajectory tracking in robotics [23] and path tracking in the field of automatic driving [24,25] have a wide range of applications. Therefore, in these real-environmental applications, when the sensor or actuator failure occurs, the tracking control effect will be greatly reduced and the system may even be unstable or collapse. The adaptive fault-tolerant tracking control can realize the tracking control under the fault condition, and the control signal can be adjusted adaptively to achieve a better tracking effect. In order to achieve a better tracking effect, we generally define some quantitative indicators to describe the system performance and give their characterization and calculation methods. Examples include peak-to-peak, energy-to-energy ($\mathcal{H}_\infty$), energy-to-peak ($L_2 - L_\infty$ [26,27]), and so on. Among them, $\mathcal{H}_\infty$ can ensure the robust stability of the system, and $L_2 - L_\infty$ is suitable for the scenario where the energy of the external interference signal is bounded and the peak value of the practical system output signal is bounded. These two kinds of performance indicators have their own application background, so if the tracking controller is designed to meet the performance requirements at the same time, it will have a wider application prospect [28,29]. For a memory neural networks system, there exist state estimation problems caused by delay and bounded perturbation. Based on the protocol, ref. [28] proposed a finite horizon mixed performance estimation method. Ref. [29] studied the hybrid control problem of measuring outliers in observer-based IT2FSs. But at present, there exist few such achievements, especially on the fuzzy system of fault-tolerant control, which is the original intention of this paper.

Note that system nonlinearity is inevitable in practical engineering in addition to other forms of nonlinear description ([30,31]). The T–S fuzzy model [32], as an effective tool, can approximate nonlinear systems through some local linear time-invariant systems, thus introducing traditional linear system theory into the study of nonlinear systems [33]. However, the type-1 T–S fuzzy model only has a good effect on dealing with system nonlinearity; if the membership function in the T–S fuzzy model contains uncertain information [9], the type-1 fuzzy model will be overwhelmed.

Based on this, the IT2 fuzzy model proposed in [34] effectively solves the above problems by defining upper and lower bound membership functions. Inspired by this, many interesting and meaningful research results have appeared successively, enriching the relevant achievements of fuzzy control and fuzzy filtering [9,25,35–40]. For example, by establishing the IT2 fuzzy model, ref. [25] effectively approximated the tire dynamic nonlinearity and speed variation in the path tracking control system and studied the path tracking control problem of autonomous ground vehicles under handover trigger and sensor attack. Ref. [36] studied the sampling exponential stability and nonlinear control of IT2 fuzzy systems. Based on event-driven faults, ref. [37] discussed the FD problem for IT2 fuzzy systems. Ref. [38] proposed an event-based control method for IT2FSs with fading channels. Ref. [39] studied a multistep model predictive control problem for IT2FSs subject to event-triggered faults. In this kind of research, FTC is indispensable in the study of fault handling, especially the membership function mismatch caused by many modules in adaptive FTC. In an IT2 fuzzy system, refs. [9,40] obtained appropriate FTC schemes for finite-time dynamic event-triggered and adaptive sliding mode control, respectively. However, the research content of other FTC problems of IT2 fuzzy systems is relatively small, which is the driving force of this paper.

Driven by the above considerations, this paper studies the tracking problem of mixed $\mathcal{H}_\infty$ and $L_2 - L_\infty$ adaptive FTC for continuous-time IT2FSs. Fully considering the mismatch and uncertainty of the membership function between systems, the faults estimate functions in observer and adaptive law in the controller, ensuring stricter system stability and performance requirements. The main innovations are summarized:

- Considering the membership function mismatch and uncertainty of each part in the practical system, the proposed design scheme is aimed at the tracking problem of a mixed $\mathcal{H}_\infty$ and $L_2 - L_\infty$ adaptive FTC for continuous-time IT2FSs.
- Compared with the general adaptive FTC scheme in [11,13], the adaptive control function is improved in this paper, which is simultaneously tolerant of the sensor and the actuator faults. Based on the adaptive signal, the dynamic parameters in the disturbance compensation term can be dynamically adjusted to achieve a better FTC effect.
- Mixed $\mathcal{H}_\infty$ and $L_2 - L_\infty$ performance is considered in the design of the fuzzy tracking controller and observer to meet a wider range of practical requirements. Based on the matrix inequality transformation technique in the lemmas, the designed algorithm reduces conservatism by introducing suitable slack variables and matrices in the theorem.

The rest of this paper is organized as follows. The problem statement and preliminary is formulated in Section 2. The main results about adaptive FTC system performance analysis and the design control strategy are presented in Sections 3 and 4, respectively. In Section 5, a mass-spring-damping system is used to illustrate the effectiveness of the designed method. Finally, Section 6 summarizes this paper.

2. Problem Statement and Preliminarie

In the real-environment application, due to the membership function mismatch and uncertainty between the modules of the fuzzy system, as well as the possible sensor and actuator faults in the system, this paper uses the IT2FSs to model the system, observer and controller. Moreover, in order to realize tracking control, a reference system is introduced.

2.1. Continuous-Time IT2FSs

In this section, similar to [9,37], the continuous-time IT2FSs with m fuzzy rules are expressed as

Rule i: If $\phi_1(x(t))$ is $\mathcal{M}_1^i$, $\cdots$, and $\phi_\iota(x(t))$ is $\mathcal{M}_\iota^i$, then

$$\begin{aligned} \dot{x}(t) &= A_i x(t) + B_i u_f(t) + E_i w(t) + F_i f_a(t) \\ y(t) &= C_i x(t) + G_i f_s(t) \end{aligned} \tag{1}$$

where $\mathcal{M}_\alpha^i$ is an IT2 fuzzy set of the i-th fuzzy rule with the function $\phi_\alpha(x(t))$ where $i = 1, 2, \cdots, m$ and $\alpha = 1, 2, \cdots, \iota$. m and ι are the positive integers; $x(t) \in R^{n_x}$, $u_f(t) \in R^{n_u}$, $y(t) \in R^{n_y}$ are the state variable, the control input after the system faults, and the measurement output, respectively. $w(t) \in R^{n_w}$ is the external disturbance signal in $L_2[0, \infty)$. $f_a(t) \in R^{n_f}$ and $f_s(t) \in R^{n_f}$ are the stuck fault signals from the actuator and sensor, respectively; The matrices A_i, B_i, E_i, F_i, C_i, G_i are known proper dimensional matrices.

The firing strength of the i-th fuzzy rule satisfies

$$\tilde{\alpha} = [\underline{\alpha}_i, \overline{\alpha}_i]$$

where

$$\begin{aligned} \underline{\alpha}_i &= \prod_{\alpha=1}^{\iota} \underline{\epsilon}_{\mathcal{M}_\alpha^i}(\phi_\alpha),\ \underline{\epsilon}_{\mathcal{M}_\alpha^i}(\phi_\alpha) \in [0,1] \\ \overline{\alpha}_i &= \prod_{\alpha=1}^{\iota} \overline{\epsilon}_{\mathcal{M}_\alpha^i}(\phi_\alpha),\ \overline{\epsilon}_{\mathcal{M}_\alpha^i}(\phi_\alpha) \in [0,1] \\ & \underline{\epsilon}_{\mathcal{M}_\alpha^i}(\phi_\alpha) \le \overline{\epsilon}_{\mathcal{M}_\alpha^i}(\phi_\alpha),\ \underline{\alpha}_i \le \overline{\alpha}_i \end{aligned}$$

with $\underline{\epsilon}_{\mathcal{M}_\alpha^i}(\phi_\alpha)$ and $\underline{\alpha}_i$ representing the lower grade and function of membership, $\overline{\epsilon}_{\mathcal{M}_\alpha^i}(\phi_\alpha)$ and $\overline{\alpha}_i$ representing the upper grade and function of membership, respectively. The global dynamic fuzzy model can be described as

$$\begin{aligned} \dot{x}(t) &= \sum_{i=1}^{m} g_i[A_i x(t) + B_i u_f(t) + E_i w(t) + F_i f_a(t)] \\ y(t) &= \sum_{i=1}^{m} g_i[C_i x(t) + G_i f_s(t)] \end{aligned} \tag{2}$$

where $g_i = \underline{p}_i\underline{\alpha}_i + \overline{p}_i\overline{\alpha}_i$, $\sum_{i=1}^{m} g_i = 1$, while the nonlinear functions have $0 \le \underline{p}_i \le \overline{p}_i \le 1$ and satisfy $\underline{p}_i + \overline{p}_i = 1$.

In addition to the additive bounded faults existing in the system, the system may also have partially degenerate multiplicative faults expressed as

$$\varsigma_f(t) = d_\varsigma \varsigma(t) \tag{3}$$

where $d_\varsigma \in (0, 1]$ with $\varsigma = y, u$ are the fault parameters of a partially degenerate incident.

For brevity, $\tilde{\alpha}$, $\underline{\alpha}_i$, $\overline{\alpha}_i$, $\underline{\epsilon}_{\mathcal{M}_\alpha^i}(\phi_\alpha)$, $\overline{\epsilon}_{\mathcal{M}_\alpha^i}(\phi_\alpha)$, $\underline{p}_i$, $\overline{p}_i$, and g_i are used to stand for $\tilde{\alpha}(x(t))$, $\underline{\alpha}_i(x(t))$, $\overline{\alpha}_i(x(t))$, $\underline{\epsilon}_{\mathcal{M}_\alpha^i}(\phi_\alpha(x(t)))$, $\overline{\epsilon}_{\mathcal{M}_\alpha^i}(\phi_\alpha(x(t)))$, $\underline{p}_i(x(t))$, $\overline{p}_i(x(t))$, and $g_i(x(t))$ in the IT2 fuzzy system. By the same token, the following symbols $\tilde{\vartheta}$, $\underline{\vartheta}_l$, $\overline{\vartheta}_l$, $\underline{v}_{\mathcal{H}_\vartheta^l}(\psi_\vartheta)$, $\overline{v}_{\mathcal{H}_\vartheta^l}(\psi_\vartheta)$, s_l, $\underline{r}_l$, $\overline{r}_l$, $\tilde{\beta}$, $\underline{\beta}_j$, $\overline{\beta}_j$, $\underline{\varepsilon}_{\mathcal{N}_\beta^j}(\varphi_\beta)$, $\overline{\varepsilon}_{\mathcal{N}_\beta^j}(\varphi_\beta)$, h_j, $\underline{q}_j$, and $\overline{q}_j$ are also abbreviations in the IT2 fuzzy observer and controller.

2.2. Reference Model

To reflect the control effect under the fault condition and to realize the tracking control, the following reference system is adopted in this paper

$$\begin{aligned} \dot{x}_r(t) &= A_r x_r(t) + B_r i_r(t) \\ y_r(t) &= C_r x_r(t) \end{aligned} \tag{4}$$

where $x_r(t) \in R^{n_r}$, $y_r(t) \in R^{n_y}$, and $i_r(t) \in R^{n_i}$ are the state, the reference output and reference input of the reference model, respectively. To verify the tracking effect of the controller, A_r is designed as a Hurwitz matrix. Moreover, B_r and C_r are known proper dimensional matrices.

2.3. IT2 Fuzzy Observer

Considering the practical engineering, the observer is nonlinear and does not match the membership function of other parts in the system. Similar to [9], to design the appropriate adaptive controller, the sensor/actuator fault values and system state are necessary to be estimated, so an IT2 fuzzy observer in the following form is designed as

Rule l: If $\psi_1(\hat{x}(t))$ is $\mathcal{H}_1^l, \cdots$, and $\psi_\ell(\hat{x}(t))$ is $\mathcal{H}_\ell^l$, then

$$\begin{aligned} \dot{\hat{x}}(t) = \sum_{i=1}^{m}\sum_{l=1}^{m} g_i s_l [&A_i\hat{x}(t) + B_i u_f(t) + E_i w(t) \\ &+ F_i\hat{f}_a(t) + L_l r(t)] \\ \hat{y}(t) = \sum_{i=1}^{m} g_i[&C_i\hat{x}(t) + G_i\hat{f}_s(t)] \end{aligned} \tag{5}$$

where $\mathcal{H}_\vartheta^l$ is an IT2 fuzzy set of the l-th fuzzy rule with the function $\psi_\vartheta(\hat{x}(t))$ where $l = 1, 2, \cdots, m$ and $\vartheta = 1, 2, \cdots, \ell$. m and ℓ are the positive integers; $\hat{x}(t) \in R^{n_x}$, $\hat{y}(t) \in R^{n_y}$, and $r(t) \in R^{n_y}$ are the state, the output, and the residual vector estimated by the IT2 fuzzy

observer, respectively. L_l is the designed observer gain matrix. In a similar way, the firing strength of the l-th rule satisfies

$$\tilde{\vartheta} = [\underline{\vartheta}_l, \overline{\vartheta}_l]$$

where

$$\underline{\vartheta}_l = \prod_{\vartheta=1}^{\ell} \underline{v}_{\mathcal{H}_\vartheta^l}(\psi_\vartheta),\ \underline{v}_{\mathcal{H}_\vartheta^l}(\psi_\vartheta) \in [0,1]$$
$$\overline{\vartheta}_l = \prod_{\vartheta=1}^{\ell} \overline{v}_{\mathcal{H}_\vartheta^l}(\psi_\vartheta),\ \overline{v}_{\mathcal{H}_\vartheta^l}(\psi_\vartheta) \in [0,1]$$
$$\underline{v}_{\mathcal{H}_\vartheta^l}(\psi_\vartheta) \le \overline{v}_{\mathcal{H}_\vartheta^l}(\psi_\vartheta),\ \underline{\vartheta}_l \le \overline{\vartheta}_l$$

where $\underline{v}_{\mathcal{H}_\vartheta^l}(\psi_\vartheta)$ and $\underline{\vartheta}_l$ are the lower grade and function of membership, and $\overline{v}_{\mathcal{H}_\vartheta^l}(\psi_\vartheta)$ and $\overline{\vartheta}_l$ are the upper grade and function of membership, respectively; $s_l = \frac{\underline{r}_l\underline{\vartheta}_l + \overline{r}_l\overline{\vartheta}_l}{\sum_{j=1}^{m}(\underline{r}_l\underline{\vartheta}_l + \overline{r}_l\overline{\vartheta}_l)}$, $\sum_{l=1}^{m} s_l = 1$, $\underline{r}_l \in [0,1]$ and $\overline{r}_l \in [0,1]$ are the nonlinear functions and satisfy $\underline{r}_l + \overline{r}_l = 1$.

Moreover, the adaptive fault information estimation functions are

$$\begin{aligned} \dot{\hat{f}}_s(t) &= s\|\xi^T(t)P\mathcal{L}\| \\ \dot{\hat{f}}_a(t) &= a\|\zeta(t)\| \end{aligned} \tag{6}$$

where $\zeta(t) = \xi^T(t)P\mathcal{B}$ and $r(t) = y_f(t) - \hat{y}(t)$, while the estimated values of state and fault information are represented by $\hat{x}(t)$, $\hat{f}_s(t)$, and $\hat{f}_a(t)$, respectively. s, a are any positive constants.

2.4. IT2 Fuzzy Adaptive Tracking Controller

Based on this, an observer-based adaptive tracking controller can be proposed.

Rule j: If $\varphi_1(\hat{x}(t))$ is $\mathcal{N}_1^j, \cdots$, and $\varphi_J(\hat{x}(t))$ is $\mathcal{N}_J^j$, then

$$u(t) = \sum_{j=1}^{o} h_j[K_j\hat{y}(t) + K_{rj}y_r(t) + K_a(t)] \tag{7}$$

where $\mathcal{N}_\beta^j$ is an IT2 fuzzy set of the j-th fuzzy rule with the function $\varphi_\beta(\hat{x}(t))$ where $j = 1, 2, \cdots, o$ and $\beta = 1, 2, \cdots, J$. m and J are the positive integers; $K_a(t)$ is the adaptive control function. K_j and K_{rj} are the controller gain matrices. In a similar way, the firing strength of the j-th rule satisfies

$$\tilde{\beta} = [\underline{\beta}_j, \overline{\beta}_j]$$

where

$$\underline{\beta}_j = \prod_{\beta=1}^{J} \underline{\varepsilon}_{\mathcal{N}_\beta^j}(\varphi_\beta),\ \underline{\varepsilon}_{\mathcal{N}_\beta^j}(\varphi_\beta) \in [0,1]$$
$$\overline{\beta}_j = \prod_{\beta=1}^{J} \overline{\varepsilon}_{\mathcal{N}_\beta^j}(\varphi_\beta),\ \overline{\varepsilon}_{\mathcal{N}_\beta^j}(\varphi_\beta) \in [0,1]$$
$$\underline{\varepsilon}_{\mathcal{N}_\beta^j}(\varphi_\beta) \le \overline{\varepsilon}_{\mathcal{N}_\beta^j}(\varphi_\beta),\ \underline{\beta}_j \le \overline{\beta}_j$$

where $\underline{\varepsilon}_{\mathcal{N}_\beta^j}(\varphi_\beta)$ and $\underline{\beta}_j$ are the lower grade and function of membership, while $\overline{\varepsilon}_{\mathcal{N}_\beta^j}(\varphi_\beta)$ and $\overline{\beta}_j$ are the upper grade and function of membership, respectively; $h_j = \frac{q_j\underline{\beta}_j + \overline{q}_j\overline{\beta}_j}{\sum_{j=1}^{m}(q_j\underline{\beta}_j + \overline{q}_j\overline{\beta}_j)}$, $\sum_{j=1}^{o} h_j = 1$, $\underline{q}_j \in [0,1]$ and $\overline{q}_j \in [0,1]$ are the nonlinear functions and satisfy $\underline{q}_j + \overline{q}_j = 1$.

The adaptive control function is defined as

$$K_a(t) = -\zeta^T(t)\frac{a(t)}{\|\zeta(t)\|^2 d_{\min}}$$

where

$$d_{\min} = \min\{\min\{d_y\}, \min\{d_u\}\}$$
$$a(t) = \|\xi^T(t)P\mathcal{L}\|\hat{f}_s(t) + \|\zeta(t)\|\hat{f}_a(t) + \|\zeta(t)\|\rho(t)\int_{t_0}^{t}\|\xi(\tau)\|d\tau.$$

There has $\rho(t) \geq 0$ in the compensation term $\rho(t)\int_{t_0}^{t}\|\xi(\tau)\|d\tau$ to achieve the compensation effect to the system fault and disturbance.

Assumption 1. *Similar to [13], sensor/actuator faults and disturbances can be expressed in the relevant segmented bounded functions, and it can be assumed that there exist matrices $\bar{E}_i$, $\bar{F}_i$, $\bar{G}_i$ and unknown constants $\bar{\omega}_1$, $\bar{\omega}_2$ such that the following inequality conditions were established*

$$\|\omega_1(t)\| = \|\bar{E}_i w(t) + \bar{F}_i f_a(t)\| \leq \|\xi(t)\|^{\alpha} + \bar{\omega}_1$$
$$\|\omega_2(t)\| = \|\bar{G}_i f_s(t)\| \leq \bar{\omega}_2$$

where $E_i = B_i\bar{E}_i$, $F_i = B_i\bar{F}_i$ and $G_i = C_i\bar{G}_i$.

Remark 1. *Different from other papers ([11,13]), the adaptive control strategy for the faults from the sensor and actuator is considered in the adaptive function, and in the compensation part of external disturbance and faults, the parameter*

$$\rho(t) = \begin{cases} \rho & when\ \xi(t) \neq 0 \\ 0 & when\ \xi(t) = 0 \end{cases}$$

with a large enough constant ρ, which will be changed according to the compensation situation. When the influence of faults and disturbances on the IT2FSs ends, the compensation can be quickly compensated, and the compensation item is 0 after the influence ends. In this way, better control can be achieved.

2.5. Adaptive FTC System

Based on the above description and definition, the constructed augmented closed-loop adaptive FTC system (in Figure 1) gives

$$\begin{aligned}\dot{\xi}(t) = \sum_{i=1}^{m}\sum_{l=1}^{m}\sum_{j=1}^{o} g_i s_l h_j[(\mathcal{A} + d_u\mathcal{B}\mathcal{K})\xi(t) + \mathcal{E}_s e_s(t) \\ + \mathcal{E}_a e_a(t) + d_u\mathcal{B}K_a(t) + \mathcal{B}\omega_1(t) + \mathcal{L}\omega_2(t) \\ + \mathcal{B}_r i_r(t)] \\ e_y(t) = \sum_{i=1}^{m} g_i[\mathcal{C}\xi(t) + G_i e_s(t)]\end{aligned} \tag{8}$$

where

$$\mathcal{A} = \begin{bmatrix} A_i - \bar{d}_y L_l C_i & -d_y L_l C_i & 0 \\ -\bar{d}_y L_l C_i & A_i - d_y L_l C_i & 0 \\ 0 & 0 & A_r \end{bmatrix}, \mathcal{B} = \begin{bmatrix} B_i \\ 0 \\ 0 \end{bmatrix}$$

$$\mathcal{C} = \begin{bmatrix} C_i & 0 & -C_r \end{bmatrix}, \mathcal{K} = \begin{bmatrix} K_j C_i & 0 & K_{rj} C_r \end{bmatrix}, \bar{d}_y = 1 - d_y$$

$$\mathcal{L} = \begin{bmatrix} d_u B_i K_j C_i - \bar{d}_y L_l C_i \\ -\bar{d}_y L_l C_i \\ 0 \end{bmatrix}, \mathcal{E}_s = \begin{bmatrix} d_u B_i K_j G_i - L_l G_i \\ -L_l G_i \\ 0 \end{bmatrix}$$

$$\mathcal{E}_a = \begin{bmatrix} 0 \\ F_i \\ 0 \end{bmatrix}, \mathcal{B}_r = \begin{bmatrix} 0 \\ 0 \\ B_r \end{bmatrix}, \xi(t) = \begin{bmatrix} \hat{x}(t) \\ e_x(t) \\ x_r(t) \end{bmatrix}$$

with $e_y(t) = \hat{y}(t) - y_r(t)$, $e_x(t) = \hat{x}(t) - x(t)$, $e_s(t) = \hat{f}_s(t) - f_s(t)$, and $e_a(t) = \hat{f}_a(t) - f_a(t)$.

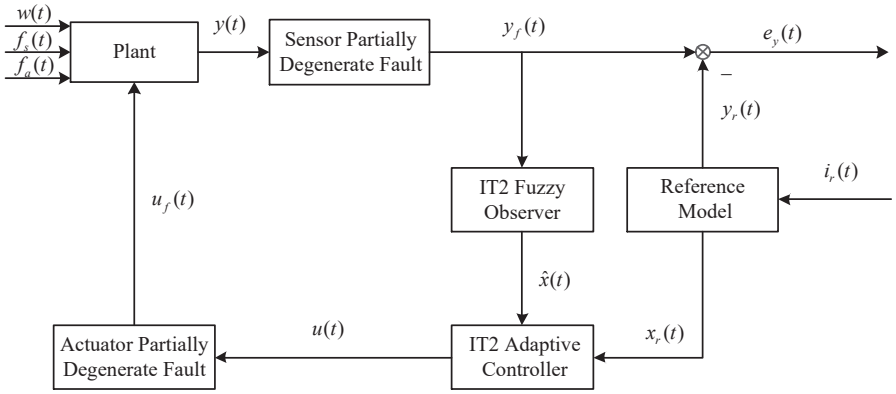

Figure 1. Framework of closed-loop adaptive FTC system.

Definition 1 ([29]). *The adaptive FTC system (8) is said to be asymptotically stable when $\bar{w}(t) = 0$, and it has the mixed $\mathcal{H}_\infty$ and $L_2 - L_\infty$ performances if under the zero initial condition, with the existed matrices $\Xi_1 \leq 0, \Xi_2 > 0, \Xi_3 \geq 0$, the following inequality holds*

$$\int_0^{t_a} J(t)dt \geq \sup_{0 \leq t \leq t_a} \{e_y^T(t) \Xi_3 e_y(t)\} \tag{9}$$

with $J(t) = e_y^T(t)\Xi_1 e_y(t) + \bar{w}^T(t)\Xi_2 \bar{w}(t)$. With the different selection of matrices, system (8) has different performance:

(1) The adaptive FTC system (8) has the $\mathcal{H}_\infty$ performance if $\Xi_1 = -I, \Xi_2 = \gamma^2 I, \Xi_3 = 0$.

(2) The adaptive FTC system (8) has the $L_2 - L_\infty$ performance if $\Xi_1 = 0, \Xi_2 = \gamma^2 I, \Xi_3 = I$.

Lemma 1 ([41]). *For the real matrices $\mathbb{T}_0$, $\mathbb{T}_1$, $\mathbb{T}_2$ and $\mathbb{T}_3$ with the proper dimensions and scalar β, the inequality $\mathbb{T}_0 + \mathbb{T}_3^T \mathbb{T}_1 \mathbb{T}_3 < 0$ holds if there exists the following situation*

$$\begin{bmatrix} \mathbb{T}_0 & * \\ \mathbb{T}_2 \mathbb{T}_3 & -He\{\beta \mathbb{T}_2\} + \beta^2 \mathbb{T}_1 \end{bmatrix} < 0.$$

Lemma 2 ([33]). *For the real matrices $\mathbb{X}_1$, $\mathbb{X}_2$, and real symmetric matrix $\mathbb{X}_0$ with the proper dimension and scalar $\wp$, the inequality $\mathbb{X}_0 + He\{\mathbb{X}_1 \mathbb{X}_2\} < 0$ holds if there exists matrix $\mathbb{S}$ satisfying*

$$\begin{bmatrix} \mathbb{X}_0 & * \\ \wp \mathbb{X}_1^T + \mathbb{S}\mathbb{X}_2 & -He\{\wp \mathbb{S}\} \end{bmatrix} < 0.$$

3. Adaptive FTC System Performance Analysis

In the following, the sufficient conditions of asymptotic stability with the mixed $\mathcal{H}_\infty$ and $L_2 - L_\infty$ performances for the adaptive FTC system (8) are provided.

Theorem 1. *Consider the adaptive FTC system (8). If there exist matrices $P > 0$ and $\Psi = \Psi^T$ with the given performance index γ and parameters η_i such that the inequalities hold with $i = 1, 2, \cdots, m; l = 1, 2, \cdots, m; j = 1, 2, \cdots, o$*

$$\Lambda_{ilj} - \Psi < 0 \tag{10}$$

$$\eta_i \Lambda_{ili} - \eta_i \Psi + \Psi < 0 \tag{11}$$

$$\eta_j \Lambda_{ilj} + \eta_i \Lambda_{jli} - \eta_j \Psi - \eta_i \Psi + 2\Psi < 0 \tag{12}$$

$$\sum_{i=1}^{m} g_i \Gamma \leq 0 \tag{13}$$

where

$$\begin{aligned}
\Lambda_{ilj} &= \begin{bmatrix} \Lambda_1 + \mathcal{C}^T\mathcal{C} & * \\ \Lambda_2 + \mathcal{G}_1^T\mathcal{C} & \Lambda_3 + \mathcal{G}_1^T\mathcal{G}_1 \end{bmatrix} \\
\Gamma &= \begin{bmatrix} \mathcal{C}^T\mathcal{C} - P & * \\ \mathcal{G}_2^T\mathcal{C} & -diag\{s^{-1}I, a^{-1}I\} + \mathcal{G}_2^T\mathcal{G}_2 \end{bmatrix} \\
\Lambda_1 &= (\mathcal{A} + d_u\mathcal{B}\mathcal{K})^T P + P(\mathcal{A} + d_u\mathcal{B}\mathcal{K}) \\
\Lambda_2^T &= \begin{bmatrix} P\mathcal{E}_s & P\mathcal{E}_a & P\mathcal{B}_r \end{bmatrix}, \mathcal{G}_2 = \begin{bmatrix} G_i & 0 \end{bmatrix} \\
\Lambda_3 &= -diag\{\gamma^2 I, \gamma^2 I, \gamma^2 I\}, \mathcal{G}_1 = \begin{bmatrix} G_i & 0 & 0 \end{bmatrix}.
\end{aligned}$$

Then, the fuzzy observer (5) and controller (7) can ensure the adaptive FTC system (8) is asymptotically stable and meets the mixed $\mathcal{H}_\infty$ and $L_2 - L_\infty$ performances.

Proof. Consider a Lyapunov function as

$$V(t) = \xi^T(t) P \xi(t) + s^{-1} e_s^2(t) + a^{-1} e_a^2(t). \tag{14}$$

Then, since $f_s(t)$ and $f_a(t)$ are the stuck faults, i.e., there has $\dot{f}_s(t) = \dot{f}_a(t) = 0$. The difference equation of $V(t)$ can be obtained

$$\begin{aligned}
\dot{V}(t) &= \dot{\xi}^T(t)P\xi(t) + \xi^T(t)P\dot{\xi}(t) + 2s^{-1}e_s(t)\dot{e}_s(t) \\
&\quad + 2a^{-1}e_a(t)\dot{e}_a(t) \\
&= \xi^T(t)[(\mathcal{A} + d_u\mathcal{B}\mathcal{K})^T P + P(\mathcal{A} + d_u\mathcal{B}\mathcal{K})]\xi(t) \\
&\quad + 2\xi^T(t)P\mathcal{E}_s e_s(t) + 2\xi^T(t)P\mathcal{E}_a e_a(t) + 2\xi^T(t)P\mathcal{B}\varpi_1(t) \\
&\quad + 2\xi^T(t)P\mathcal{L}\varpi_2(t) + 2\xi^T(t)P\mathcal{B}_r i_r(t) \\
&\quad + 2d_u\zeta(t)K_a(t) + 2s^{-1}e_s(t)\dot{e}_s(t) + 2a^{-1}e_a(t)\dot{e}_a(t) \\
&= \xi^T(t)[(\mathcal{A} + d_u\mathcal{B}\mathcal{K})^T P + P(\mathcal{A} + d_u\mathcal{B}\mathcal{K})]\xi(t) \\
&\quad + 2\xi^T(t)P\mathcal{E}_s e_s(t) + 2\xi^T(t)P\mathcal{E}_a e_a(t) + 2\xi^T(t)P\mathcal{B}\varpi_1(t) \\
&\quad + 2\xi^T(t)P\mathcal{L}\varpi_2(t) + 2\xi^T(t)P\mathcal{B}_r i_r(t) \\
&\quad + 2s^{-1}e_s(t)\dot{e}_s(t) + 2a^{-1}e_a(t)\dot{e}_a(t) \\
&\quad - 2d_u\zeta(t)\zeta^T(t)\frac{a(t)}{\|\zeta(t)\|^2 d_{\min}} \\
&\le \xi^T(t)[(\mathcal{A} + d_u\mathcal{B}\mathcal{K})^T P + P(\mathcal{A} + d_u\mathcal{B}\mathcal{K})]\xi(t) \\
&\quad + 2\xi^T(t)P\mathcal{E}_s e_s(t) + 2\xi^T(t)P\mathcal{E}_a e_a(t) + 2\xi^T(t)P\mathcal{B}\varpi_1(t) \\
&\quad + 2\xi^T(t)P\mathcal{L}\varpi_2(t) + 2\xi^T(t)P\mathcal{B}_r i_r(t) \\
&\quad + 2s^{-1}e_s(t)\dot{e}_s(t) + 2a^{-1}e_a(t)\dot{e}_a(t) - 2\|\xi^T(t)P\mathcal{L}\|\hat{f}_s(t) \\
&\quad - 2\|\zeta(t)\|\hat{f}_a(t) - 2\|\zeta(t)\|\rho(t)\int_{t_0}^{t}\|\xi(\tau)\|d\tau.
\end{aligned} \tag{15}$$

By recalling the conditions in Assumption 1, (15) is reduced as

$$\begin{aligned}
\dot{V}(t) &\le \xi^T(t)[(\mathcal{A} + d_u\mathcal{B}\mathcal{K})^T P + P(\mathcal{A} + d_u\mathcal{B}\mathcal{K})]\xi(t) \\
&\quad + 2\xi^T(t)P\mathcal{E}_s e_s(t) + 2\xi^T(t)P\mathcal{E}_a e_a(t) + 2\xi^T(t)P\mathcal{B}_r i_r(t) \\
&\quad + 2s^{-1}e_s(t)\dot{e}_s(t) + 2a^{-1}e_a(t)\dot{e}_a(t) - 2\|\xi^T(t)P\mathcal{L}\|\hat{f}_s(t) \\
&\quad - 2\|\zeta(t)\|\hat{f}_a(t) - 2\|\zeta(t)\|\rho(t)\int_{t_0}^{t}\|\xi(\tau)\|d\tau \\
&\quad + 2\|\zeta(t)\|\|\xi(t)\|^\alpha + 2\|\zeta(t)\|\bar{\varpi}_1 + 2\|\xi^T(t)P\mathcal{L}\|\bar{\varpi}_2.
\end{aligned} \tag{16}$$

Similar to [13], the following inequality will hold

$$\begin{aligned}
\|\zeta^T(t)\|\bar{\varpi}_1 &\le \|\zeta^T(t)\|f_a(t) \\
\|\xi^T(t)P\mathcal{L}\|\bar{\varpi}_2 &\le \|\xi^T(t)P\mathcal{L}\|f_s(t).
\end{aligned} \tag{17}$$

The nonlinear function $\rho(t)\int_{t_0}^{t}\|\xi(\tau)\|d\tau$ is obviously a monotonically increasing function of the augmented vector $\xi(t)$. Therefore, when $\xi(t) > 0$ holds, if the parameter ρ is large enough, and if the parameter $\alpha \le 2$ exists, one obtains

$$\|\xi(t)\|^\alpha \le \rho(t)\int_{t_0}^{t}\|\xi(\tau)\|d\tau. \tag{18}$$

Then, combining (6), (17), and (18), the inequality (16) is reduced as

$$\begin{aligned}
\dot{V}(t) &\le \xi^T(t)[(\mathcal{A} + d_u\mathcal{B}\mathcal{K})^T P + P(\mathcal{A} + d_u\mathcal{B}\mathcal{K})]\xi(t) \\
&\quad + 2\xi^T(t)P\mathcal{E}_s e_s(t) + 2\xi^T(t)P\mathcal{E}_a e_a(t) + 2\xi^T(t)P\mathcal{B}_r i_r(t).
\end{aligned} \tag{19}$$

Similar to [9], by introducing $\bar{\xi}(t) = \begin{bmatrix}\xi^T(t) & \bar{w}^T(t)\end{bmatrix}^T$ with $\bar{w}(t) = \begin{bmatrix}e_s^T(t) & e_a^T(t) & i_r^T(t)\end{bmatrix}^T$ and the slack matrix $\Psi = \Psi^T$, based on the membership function information and its characters, there exists $\sum_{i=1}^{m}\sum_{l=1}^{m}\sum_{j=1}^{o} g_i s_l \times (s_j - h_j)\Psi = \sum_{i=1}^{m}\sum_{l=1}^{m}(\sum_{j=1}^{o} s_j - \sum_{j=1}^{o} h_j)\Psi = \sum_{i=1}^{m}\sum_{l=1}^{m}(1-1)\Psi = 0$. One has

$$\begin{aligned}
&\sum_{i=1}^{m}\sum_{l=1}^{m}\sum_{j=1}^{o} g_i s_l h_j \bar{\xi}^T(t)\Lambda_{ilj}\bar{\xi}(t) \\
&+ \sum_{i=1}^{m}\sum_{l=1}^{m}\sum_{j=1}^{o} g_i s_l \times (s_j - h_j)\Psi \\
\le &\sum_{i=1}^{m}\sum_{l=1}^{m} g_i g_i(\hat{x}(t)) s_l \bar{\xi}^T(t)(\eta_i\Lambda_{ili} - \eta_i\Psi + \Psi)\bar{\xi}(t) \\
&+ \sum_{i=1}^{m}\sum_{l=1}^{m}\sum_{j=1}^{o} g_i s_l (h_j - \eta_i g_j)\bar{\xi}(t)(\Lambda_{ilj} - \Psi)\bar{\xi}^T(t) \\
&+ \sum_{i=1}^{m}\sum_{l=1}^{m}\sum_{i<j} g_i s_l h_j \times \bar{\xi}^T(t)(\eta_j\Lambda_{ilj} + \eta_i\Lambda_{jli} - \eta_j\Psi \\
&- \eta_i\Psi + 2\Psi)\bar{\xi}(t).
\end{aligned} \tag{20}$$

Furthermore, using congruence properties in (10)–(12) yields

$$\dot{V}(t) - J(t) < 0. \tag{21}$$

If the given matrices $\Xi_1 = -I, \Xi_2 = \gamma^2 I$, the above inequality is reduced to

$$\dot{V}(t) + e_y^T(t)e_y(t) - \gamma^2\bar{w}^T(t)\bar{w}(t) < 0. \tag{22}$$

When external input variable $\bar{w}(t) = 0$, with the situation of $e_y^T(t)e_y(t) > 0$, that means $\dot{V}(t) < 0$, so the adaptive FTC system (8) is asymptotically stable.

When external input variable $\bar{w}(t) \neq 0$, under zero initial conditions, integral from 0 to t_a at both ends of the inequality (22), one obtains

$$\int_0^{t_a} J(\tau)d\tau > V(t_a) - V(0) = V(t_a) \tag{23}$$

with the condition $V(t_a) \geq 0$ and $\Xi_3 = 0$, the $\mathcal{H}_\infty$ performance condition $\int_0^{t_a} e_y^T(t)e_y(t)d\tau < \gamma^2\int_0^{t_a}\bar{w}^T(t)\bar{w}(t)d\tau$ is obtained.

In addition, using congruence properties with $\Xi_1 = 0$, $\Xi_2 = \gamma^2 I$, $\Xi_4 = I$, and $\hat{\xi}(t) = \begin{bmatrix}\xi^T(t) & e_s^T(t) & e_a^T(t)\end{bmatrix}^T$ to inequality (13) yields

$$\begin{aligned}
&e_y^T(t)e_y(t) - [\xi^T(t)P\xi(t) + s^{-1}e_s^T(t)e_s(t) \\
&\quad + a^{-1}e_a^T(t)e_a(t)] \\
&= e_y^T(t)e_y(t) - V(t) \leq 0.
\end{aligned} \tag{24}$$

Furthermore, with the situation $0 \leq t \leq t_a$, one has

$$e_y^T(t_a)e_y(t_a) - V(t_a) \leq 0. \tag{25}$$

By combining inequality (23), we can obtain the result

$$\sup_{0\leq t\leq t_a}\{e_y^T(t)e_y(t)\} \leq \gamma^2\int_0^{t_a}\bar{w}^T(t)\bar{w}(t)d\tau$$

which implies that the system (8) satisfies $L_2 - L_\infty$ performance. The proof is completed. □

4. Fuzzy Observer and Controller Design

The nonlinear coupling terms in Theorem 1 mean that the unknown observer and controller gain matrices cannot be solved directly, so they need to be designed and obtained through the following theorem obtained by some lemmas.

Theorem 2. *Consider the adaptive FTC system (8). For given performance index γ, positive parameters β_1, β_2, $\wp$, η_i, partial degradation failure coefficients d_y, d_u, if there exist matrices $P_1 > 0$, $P_2 > 0$, $\bar{L}_l$, $\bar{K}_j$, $\bar{K}_{rj}$, S, $\mathbb{T}_2^1$, $\mathbb{T}_2^2$, and $\bar{\Psi} = \bar{\Psi}^T$ such that the inequalities hold with $i = 1, 2, \cdots, m; l = 1, 2, \cdots, m; j = 1, 2, \cdots, o$*

$$\hat{\Lambda}_{ilj} - \bar{\Psi} < 0 \tag{26}$$

$$\eta_i \hat{\Lambda}_{ili} - \eta_i \bar{\Psi} + \bar{\Psi} < 0 \tag{27}$$

$$\eta_j \hat{\Lambda}_{ilj} + \eta_i \hat{\Lambda}_{jli} - \eta_j \bar{\Psi} - \eta_i \bar{\Psi} + 2\bar{\Psi} < 0 \tag{28}$$

$$\sum_{i=1}^{m} g_i \bar{\Gamma} \leq 0 \tag{29}$$

where

$$\hat{\Lambda}_{ilj} = \begin{bmatrix} \bar{\mathbb{X}}_0 & * \\ \wp \bar{\mathbb{X}}_1^T + \mathbb{S}\bar{\mathbb{X}}_2 & -He\{\wp \mathbb{S}\} \end{bmatrix}, \bar{\mathbb{X}}_0 = \begin{bmatrix} \bar{\mathbb{X}}_{01} & * \\ \bar{\mathbb{X}}_{02} & \Lambda_3 \end{bmatrix}$$

$$\bar{\mathbb{X}}_0 = \begin{bmatrix} \hat{\mathbb{X}}_0 & * \\ \mathbb{T}_2^1 \mathbb{T}_3^1 & -He\{\beta_1 \mathbb{T}_2^1\} + \beta_1^2 I \end{bmatrix}$$

$$\bar{\mathbb{X}}_{01} = \begin{bmatrix} \bar{X}_1 & * & * \\ \bar{X}_2 & \bar{X}_3 & * \\ C_r^T \bar{K}_{rj}^T B_i^T & 0 & He\{P_2 A_r\} \end{bmatrix}$$

$$\bar{X}_1 = He\{P_1 A_i - \bar{d}_y \bar{L}_l C_i + B_i \bar{K}_j C_i\}$$

$$\bar{X}_2 = -\bar{d}_y \bar{L}_l C_i - d_y C_i^T \bar{L}_l^T, \bar{X}_3 = He\{P_1 A_i - d_y \bar{L}_l C_i\}$$

$$\bar{\mathbb{X}}_2 = S^{-T} \begin{bmatrix} d_u B_i^T P_1^T - S^T B_i^T & \boldsymbol{0}_6 \end{bmatrix}, \mathbb{S} = S^T$$

$$\bar{\mathbb{X}}_1 = \begin{bmatrix} \bar{K}_j C_i & 0 & \bar{K}_{rj} C_r & \bar{K}_j G_i & \boldsymbol{0}_3 \end{bmatrix}^T, \mathbb{T}_3^1 = \begin{bmatrix} \mathcal{C} & \mathcal{G}_1 \end{bmatrix}$$

$$\bar{\mathbb{X}}_{02} = \begin{bmatrix} G_i^T \bar{K}_j^T B_i^T - G_i^T \bar{L}_l^T & -G_i^T \bar{L}_l^T & 0 \\ 0 & F_i^T P_1 & 0 \\ 0 & 0 & B_r^T P_2 \end{bmatrix}$$

$$\bar{\Gamma} = \begin{bmatrix} \mathbb{T}_0^2 & * \\ \mathbb{T}_2^2 \mathbb{T}_3^2 & -He\{\beta_2 \mathbb{T}_2^2\} + \beta_2^2 I \end{bmatrix}$$

$$\mathbb{T}_0^2 = -diag\{P_1, P_1, P_2, s^{-1} I, a^{-1} I\}, \mathbb{T}_3^2 = \begin{bmatrix} \mathcal{C} & \mathcal{G}_2 \end{bmatrix}.$$

Then, the fuzzy observer (5) and controller (7) can ensure the adaptive FTC system (8) is asymptotically stable and has the mixed $\mathcal{H}_\infty$ and $L_2 - L_\infty$ performances. Accordingly, the gains of a fuzzy tracking controller and observer are obtained as follows

$$L_l = P_1^{-1} \bar{L}_l, K_j = S^{-1} \bar{K}_j, K_{rj} = S^{-1} \bar{K}_{rj}. \tag{30}$$

Proof. By choosing the matrix $P = diag\{P_1, P_1, P_2\}$ to the (10)–(13) and defining the following matrices

$$\mathbb{T}_0^1 = \begin{bmatrix} \bar{\Lambda}_1 & * \\ \bar{\Lambda}_2 & \Lambda_3 \end{bmatrix}, \mathbb{T}_1^1 = \mathbb{T}_1^2 = I$$
$$\bar{\Lambda}_1 = \begin{bmatrix} X_1 & * & * \\ X_2 & X_3 & * \\ d_u C_r^T K_{rj}^T B_i^T P_1^T & 0 & He\{P_2 A_r\} \end{bmatrix}$$
$$X_1 = He\{P_1 A_i - \bar{d}_y P_1 L_l C_i + d_u P_1 B_i K_j C_i\}$$
$$X_2 = -\bar{d}_y P_1 L_l C_i - d_y C_i^T L_l^T P_1^T, X_3 = He\{P_1 A_i - d_y P_1 L_l C_i\}$$
$$\bar{\Lambda}_2 = \begin{bmatrix} d_u G_i^T K_j^T B_i^T P_1^T - G_i^T L_l^T P_1^T & -G_i^T L_l^T P_1^T & 0 \\ 0 & F_i^T P_1^T & 0 \\ 0 & 0 & B_r^T P_2^T \end{bmatrix}.$$

Recalling the matrices $\mathbb{T}_2^1$, $\mathbb{T}_3^1$, $\mathbb{T}_0^2$, $\mathbb{T}_2^2$, $\mathbb{T}_3^2$ and introducing the scalars β_1, β_2. By using Lemma 1 to (10)–(13), the condition (29) is obtained and there is

$$\begin{bmatrix} \mathbb{T}_0^1 & * \\ \mathbb{T}_2^1 \mathbb{T}_3^1 & -He\{\beta_1 \mathbb{T}_2^1\} + \beta_1^2 I \end{bmatrix} < 0. \tag{31}$$

Furthermore, recalling the matrices $\mathbb{X}_2$, $\mathbb{S}$ and defining the matrices

$$\mathbb{X}_0 = \begin{bmatrix} \begin{bmatrix} \hat{\Lambda}_1 & * \\ \hat{\Lambda}_2 & \Lambda_3 \end{bmatrix} & * \\ \mathbb{T}_2^1 \mathbb{T}_3^1 & -He\{\beta_1 \mathbb{T}_2^1\} + \beta_1^2 I \end{bmatrix}$$
$$\hat{\Lambda}_1 = \begin{bmatrix} \hat{X}_1 & * & * \\ X_2 & X_3 & * \\ C_r^T K_{rj}^T S^T B_i^T & 0 & He\{P_2 A_r\} \end{bmatrix}$$
$$\hat{X}_1 = He\{P_1 A_i - \bar{d}_y P_1 L_l C_i + B_i S K_j C_i\}$$
$$\hat{\Lambda}_2 = \begin{bmatrix} G_i^T K_j^T S^T B_i^T - G_i^T L_l^T P_1^T & -G_i^T L_l^T P_1^T & 0 \\ 0 & F_i^T P_1^T & 0 \\ 0 & 0 & B_r^T P_2^T \end{bmatrix}$$
$$\mathbb{X}_1 = (S\begin{bmatrix} K_j C_i & 0 & K_{rj} C_r & K_j G_i & \mathbf{0}_3 \end{bmatrix})^T.$$

Then, by using the Lemma 2 to (31), by defining the matrices $\bar{L}_l = P_1 L_l, \bar{K}_j = S K_j$, $\bar{K}_{rj} = S K_{rj}$, so that the feasibility conditions (26)–(29) are obtained. The proof is completed. □

Remark 2. *In actual engineering, due to different models, environmental changes, human factors, aging and other reasons, if the same membership function is used to model the system modules (observer and controller) and the nonlinear system, an accurate fuzzy model cannot be established. However, IT2 fuzzy modeling is designed to model each module separately with the upper and lower membership degree and membership function, and the method in [9] is adopted. The slack matrix and membership function properties are introduced to obtain (20), which further describes the mismatching and uncertainty of membership functions between system modules.*

5. Simulations

A mass-spring-damping system [35,39] is selected to demonstrate the effectiveness of the designed method. According to Newton's law,

$$m\ddot{x} + F_f + F_s = u \tag{32}$$

where $F_f = \bar{c}\dot{x}$, $F_s = \bar{k}(1 + \bar{a}^2x^2)x$, m, and u are the friction force, hardening spring force, mass, and control input, respectively, and $\bar{c} > 0$ and $\bar{k}$ and $\bar{a}$ are constants. Then, (32) is rewritten as

$$m\ddot{x} + \bar{c}\dot{x} + \bar{k}x + \bar{k}\bar{a}^2x^3 = u \tag{33}$$

where x is the displacement of mass from the reference point. Defending $x(t) = \begin{bmatrix} x_1^T(t) & x_2^T(t) \end{bmatrix}^T = \begin{bmatrix} x^T & \dot{x}^T \end{bmatrix}^T$ and $\bar{b}(t) = (-\bar{k} - \bar{k}\bar{a}^2x_1^2(t))/m$, assume $x_1(t) \in [-1, 1]$, $m = 2$ kg, $\bar{c} = 6$ N $\cdot$ m/s, $\bar{a} = 0.5$ m^{-1}, and $\bar{k} \in [5, 8]$, so that $\bar{b}(t) \in [\bar{b}_{min}, \bar{b}_{max}] = [-2, -1]$.

Then, the IT2 T–S fuzzy system matrices are

$$A_{1,2} = \begin{bmatrix} 0 & 1 \\ \bar{b}(t) & -\frac{\bar{c}}{m} \end{bmatrix},\ B_1 = B_2 = \begin{bmatrix} 0 \\ \frac{1}{m} \end{bmatrix}.$$

Based on the property of membership function $\alpha_1 + \alpha_2 = 1$, there has $\bar{b}(t) = \alpha_1\bar{b}_{min} + \alpha_2\bar{b}_{max}$ with $\alpha_1 = \frac{\bar{b}_{max} - \bar{b}(t)}{\bar{b}_{max} - \bar{b}_{min}}$ and $\alpha_2 = \frac{\bar{b}(t) - \bar{b}_{min}}{\bar{b}_{max} - \bar{b}_{min}}$. Then, with the parameter $\bar{k}$, the homologous upper and lower membership functions are

$$\begin{aligned} &\underline{\alpha}_1 = \alpha_1, \underline{\alpha}_2 = \alpha_2,\ \bar{k} = 5 \\ &\overline{\alpha}_1 = \alpha_1, \overline{\alpha}_2 = \alpha_2,\ \bar{k} = 8. \end{aligned}$$

Define the nonlinear weighting functions $\underline{p}_1 = \underline{r}_1 = \underline{q}_1 = \sin^2(x_1(t))$, $\overline{p}_1 = \overline{r}_1 = \overline{q}_1 = 1 - \sin^2(x_1(t))$, $\underline{p}_2 = \underline{r}_2 = \underline{q}_2 = \cos^2(x_1(t))$, $\overline{p}_2 = \overline{r}_2 = \overline{q}_2 = 1 - \cos^2(x_1(t))$. The membership functions of the observer and controller are selected as $\underline{\vartheta}_1 = \underline{\beta}_1 = e^{-\hat{x}_1^2(t)/0.5}$, $\overline{\vartheta}_1 = \overline{\beta}_1 = e^{-\hat{x}_1^2(t)}$, $\underline{\vartheta}_2 = \underline{\beta}_2 = 1 - e^{-\hat{x}_1^2(t)}$, $\overline{\vartheta}_2 = \overline{\beta}_2 = 1 - e^{-\hat{x}_1^2(t)/0.5}$.

The corresponding matrices are

$$\begin{aligned} &A_1 = \begin{bmatrix} 0 & 1 \\ -2 & -3 \end{bmatrix},\ A_2 = \begin{bmatrix} 0 & 1 \\ -1 & -3 \end{bmatrix} \\ &B_1 = B_2 = \begin{bmatrix} 0 \\ 0.5 \end{bmatrix},\ E_1 = E_2 = \begin{bmatrix} -0.2 \\ -0.1 \end{bmatrix},\ F_1 = F_2 = \begin{bmatrix} -0.5 \\ -0.3 \end{bmatrix} \\ &C_1 = C_2 = \begin{bmatrix} 0.1 & 0.2 \end{bmatrix},\ G_1 = G_2 = 0.3. \end{aligned}$$

Assume that the disturbance $w(t) = 0.5e^{-0.3t}\sin(0.2t)$; then, the corresponding mathematical expression of sensor fault and actuator fault are

$$f_s(t) = \begin{cases} 0.5, & 100 \le t \le 150, \\ 0.2, & 200 \le t \le 250, \\ 0, & else. \end{cases}$$

$$f_a(t) = \begin{cases} 0.5, & 130 \le t \le 170, \\ 0.3, & 230 \le t \le 250, \\ 0, & else. \end{cases}$$

Moreover, the matrices in the reference system are

$$\begin{aligned} &A_r = \begin{bmatrix} 0.1 & 1.6 \\ -0.3 & -1 \end{bmatrix},\ B_r = \begin{bmatrix} 0.2 \\ -0.2 \end{bmatrix} \\ &C_r = \begin{bmatrix} -0.5 & 0.8 \end{bmatrix}. \end{aligned}$$

with the reference input

$$i_r(t) = \begin{cases} -0.2, & t \le 150, \\ 0.2\cos(0.2t), & 150 \le t \le 350, \\ 0, & else. \end{cases}$$

Set the parameters $\eta_1 = 0.4$, $\eta_2 = 0.7$; then, the observer and controller gain matrices are obtained as

$$L_1 = \begin{bmatrix} 0.2597 & -1.0683 \end{bmatrix}^T$$
$$L_2 = \begin{bmatrix} -0.1621 & 0.6746 \end{bmatrix}^T$$
$$K_1 = -0.4141,\ K_2 = 0.5073$$
$$K_{r1} = 0.0104,\ K_{r2} = -0.0383.$$

The system and observer initial values are selected as $x(0) = \hat{x}(0) = \begin{bmatrix} 0 & 0 \end{bmatrix}^T$. Figure 2 shows the observer's estimation of the system states, indicating that the observer has good estimation performance. In Figure 3, a comparison is added with the method proposed in reference [13]. Initially, the system output with faults $y_f(t)$ can be quickly achieved under the action of disturbance compensation. Next, when the fault occurs, the tracking effect is better than the method in [13], and the reference output $y_r(t)$ can be tracked as soon as the fault ends. Figures 3 and 4 illustrate the tracking effect of the system output on the reference output. It can be seen that the system can still achieve the tracking effect even under the influence of external disturbances and faults. Figure 5 represents the control signals that vary with the faults and external inputs. The ratio history curves of $\sqrt{\sup_{0 \le t \le t_a} \{e_y^T(t) e_y(t)\} / \int_0^{t_a} \bar{w}^T(\tau)\bar{w}(\tau)d\tau}$ and $\sqrt{\int_0^{t_a} e_y^T(\tau) e_y(\tau) d\tau / \int_0^{t_a} \bar{w}^T(\tau)\bar{w}(\tau)d\tau}$ (i.e., the trajectories of $L_2 - L_\infty$ and $\mathcal{H}_\infty$ performance) are shown in Figures 6 and 7, which means, under the influence of disturbance $w(t)$ and faults ($f_s(t)$ and $f_a(t)$), the ratio curve can quickly tends to stabilize, and the maximum value 0.0166 of $L_2 - L_\infty$ performance and 0.0480 of $\mathcal{H}_\infty$ performance are lower than the performance index $\gamma = 1$. To sum up, these simulation results demonstrate that the FTC method is effective and can ensure asymptotic stability and desired mixed $\mathcal{H}_\infty$ and $L_2 - L_\infty$ performances for the system (8).

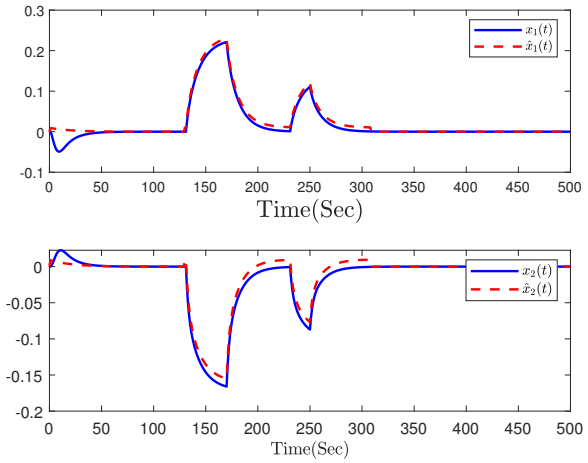

Figure 2. System states $x(t)$ and observer states $\hat{x}(t)$.

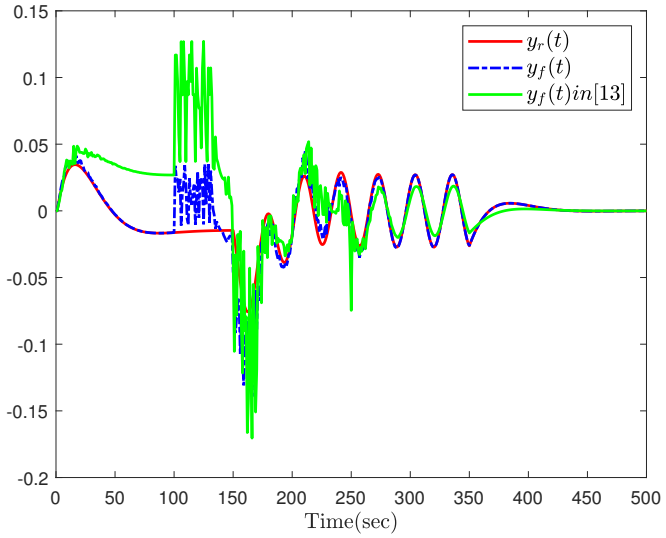

Figure 3. System output with faults $y_f(t)$ and reference output $y_r(t)$.

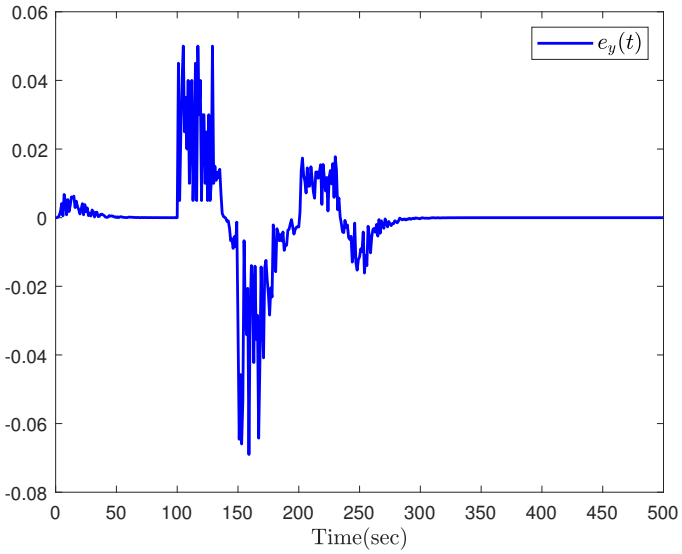

Figure 4. System tracking error $e_y(t)$.

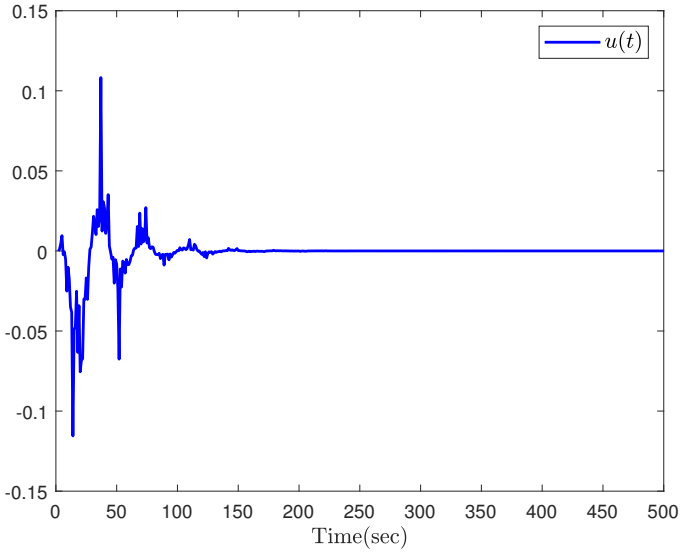

Figure 5. Adaptive control signal $u(t)$.

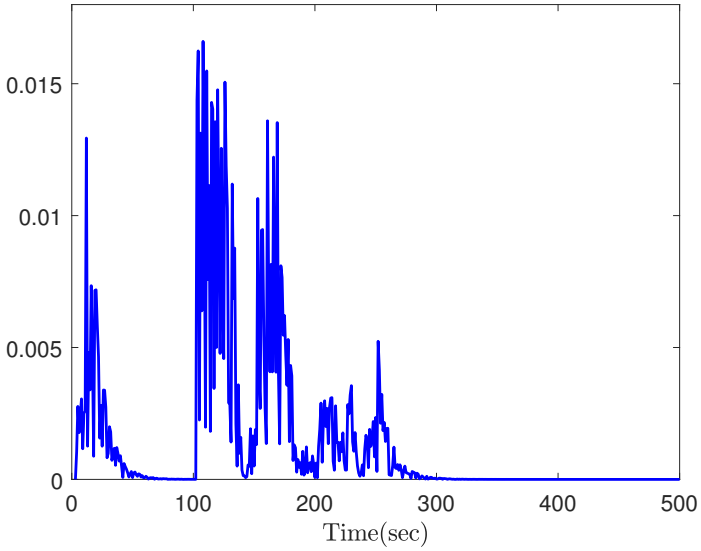

Figure 6. The trajectory of $L_2 - L_\infty$ performance.

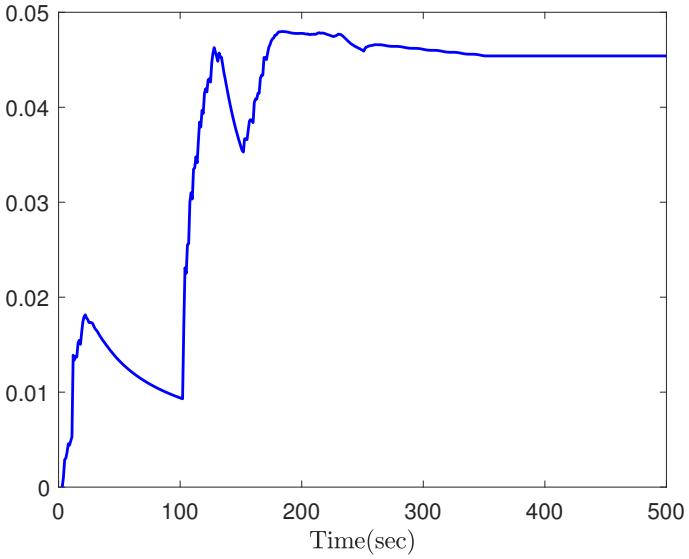

Figure 7. The trajectory of $\mathcal{H}_\infty$ performance.

In order to further verify the tracking effect of the system, the reference input is changed to $i_r(t) = 0.2\sin(0.3t)$. Compared with the results without the adaptive sensor fault compensation term in [13], we can see from Figure 8 that the system output containing faults has a good tracking effect following the reference output, which shows the effectiveness of the consequence.

Comparative Explanations: Compared with the design schemes of adaptive FTC for actuator faults in [11,13] and overcompensation for external disturbances, that is, compensation item $\int_{t_0}^{t} \|\xi(\tau)\| d\tau$ will always exist after the disturbance and fault disappear. Therefore, this paper designs an adaptive compensation scalar $\rho(t)$ based on this, which avoids channel congestion caused by too much data and saves communication resources under the condition of limited bandwidth. Moreover, a more practical application scenario of FTC is considered. The fault cases under consideration include not only partial degenerate faults of multiplicative type but also stuck fault of additive type. Both the observer and controller of the joint design meet the mixed $\mathcal{H}_\infty$ and $L_2 - L_\infty$ performances, and the conservative design is reduced by introducing appropriate Lemmas 1 and 2.

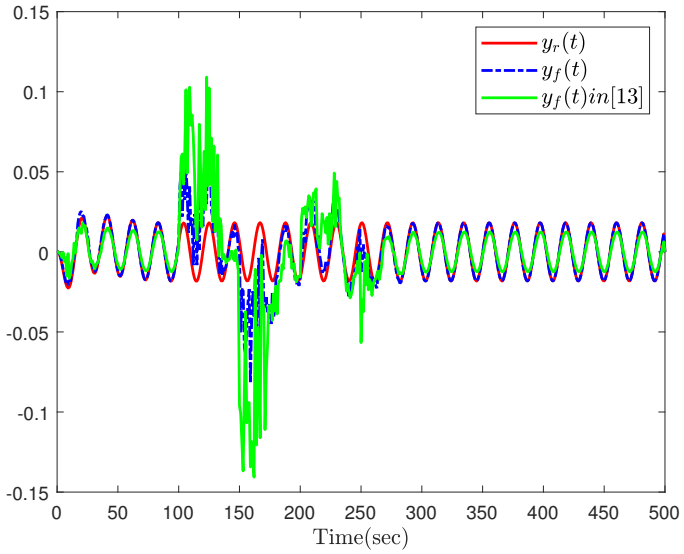

Figure 8. System output with faults $y_f(t)$ and reference output $y_r(t)$.

6. Conclusions

In this paper, the tracking problem of mixed $\mathcal{H}_\infty$ and $L_2 - L_\infty$ adaptive FTC for continuous-time IT2FSs is studied. The IT2 fuzzy model was used to figure out the problem of mismatch and uncertainty of membership functions between system modules, while the fuzzy observer and adaptive fault estimation functions were used to estimate the system state and fault signals, in order for the adaptive tracking controller to realize the tracking control of the reference output under disturbance and fault conditions. Both the jointly designed observer and controller can satisfy the mixed $\mathcal{H}_\infty$ and $L_2 - L_\infty$ performances while ensuring the asymptotic stability of the system. In addition, the designed adaptive control law can achieve the purpose of dynamic compensation for disturbances and faults, and the conservatism of the observer and controller was further reduced by the slack parameters in the lemmas. Finally, a mass-spring-damping system effectively validated the design method. Our future work will improve the adaptive control algorithm on this basis or adopt an active fault tolerance scheme to further improve the FTC capability of the system.

Author Contributions: Conceptualization, M.-Y.Q. and X.-H.C.; methodology, M.-Y.Q. and X.-H.C.; software, M.-Y.Q. and X.-H.C.; formal analysis, M.-Y.Q. and X.-H.C.; investigation, writing—original draft preparation, and writing—review and editing, M.-Y.Q. and X.-H.C. All authors have read and agreed to the published version of the manuscript.

Funding: This work was supported in part by the National Natural Science Foundation of China under Grant 62173261.

Data Availability Statement: The original contributions presented in the study are included in the article, further inquiries can be directed to the corresponding author.

Conflicts of Interest: The authors declare no conflicts of interest.

References

1. Witczak, M. *Fault Diagnosis and Fault-Tolerant Control Strategies for Non-Linear Systems*; Springer: Heidelberg, Germany, 2014.
2. Long, Y.; Park, J.H.; Ye, D. Asynchronous fault detection and isolation for Markov jump systems with actuator failures under networked environment. *IEEE Trans. Syst. Man, Cybern. Syst.* **2021**, *51*, 3477–3487. [CrossRef]
3. Zhu, Z.; Zhu, Q. Adaptive event-triggered fuzzy control for stochastic highly nonlinear systems with time delay and non-triangular structure interconnections. *IEEE Trans. Fuzzy Syst.* **2024**, *32*, 27–37. [CrossRef]
4. Wang, X. Active fault tolerant control for unmanned underwater vehicle with sensor faults. *IEEE Trans. Instrum. Meas.* **2020**, *69*, 9485–9495. [CrossRef]
5. Han, S.Y.; Zhou, J.; Chen, Y.H.; Zhang, Y.F.; Tang, G.y.; Wang, L. Active fault-tolerant control for discrete vehicle active suspension via reduced-order observer. *IEEE Trans. Syst. Man, Cybern. Syst.* **2021**, *51*, 6701–6711. [CrossRef]

6. Rudin, K.; Ducard, G.J.J.; Siegwart, R.Y. Active fault-tolerant control with imperfect fault detection information: Applications to UAVs. *IEEE Trans. Aerosp. Electron. Syst.* **2020**, *56*, 2792–2805. [CrossRef]
7. Zhang, K.; Jiang, B.; Yan, X.; Mao, Z.; Polycarpou, M.M. Fault-tolerant control for systems with unmatched actuator faults and disturbances. *IEEE Trans. Autom. Control* **2021**, *66*, 1725–1732. [CrossRef]
8. Mu, Y.; Zhang, H.; Xi, R.; Wang, Z.; Sun, J. Fault-tolerant control of nonlinear systems with actuator and sensor faults based on T–S fuzzy model and fuzzy observer. *IEEE Trans. Syst. Man Cybern. Syst.* **2022**, *52*, 5795–5804. [CrossRef]
9. Li, X.; Song, W.; Li, Y.; Tong, S. Finite-time dynamic event-triggered fuzzy output fault-tolerant control for interval type-2 fuzzy systems. *IEEE Trans. Fuzzy Syst.* **2022**, *30*, 4926–4938. [CrossRef]
10. Zhu, X.; Li, W.; Xia, Y. Finite-time fault estimate and fault-tolerant control for discrete-time Markov jump systems with actuator and sensor faults. *Int. J. Robust Nonlinear Control* **2023**, *33*, 6233–6249. [CrossRef]
11. Jin, X.Z.; Yang, G.H. Robust adaptive fault-tolerant compensation control with actuator failures and bounded disturbances. *Acta Autom. Sin.* **2009**, *35*, 305–309. [CrossRef]
12. Bounemeur, A.; Chemachema, M. Adaptive fuzzy fault-tolerant control using Nussbaum-type function with state-dependent actuator failures. *Neural Comput. Appl.* **2021**, *33*, 191–208. [CrossRef]
13. Jin, X.Z.; Che, W.W.; Wu, Z.G.; Wang, H. Analog control circuit designs for a class of continuous-time adaptive fault-tolerant control systems. *IEEE Trans. Cybern.* **2022**, *52*, 4209–4220. [CrossRef] [PubMed]
14. Zhao, Z.; Tan, Z.; Liu, Z.; Efe, M.O.; Ahn, C.K. Adaptive inverse compensation fault-tolerant control for a flexible manipulator with unknown dead-zone and actuator faults. *IEEE Trans. Ind. Electron.* **2023**, *70*, 12698–12707. [CrossRef]
15. Chen, C.; Lewis, F.L.; Xie, S.; Modares, H.; Liu, Z.; Zuo, S.; Davoudi, A. Resilient adaptive and $\mathcal{H}_\infty$ controls of multi-agent systems under sensor and actuator faults. *Automatica* **2019**, *102*, 19–26. [CrossRef]
16. Tahoun, A.H.; Arafa, M. A new unmatched-disturbances compensation and fault-tolerant control for partially known nonlinear singular systems. *ISA Trans.* **2020**, *104*, 310–320. [CrossRef]
17. Wang, B.; Zhang, Y. An adaptive fault-tolerant sliding mode control allocation scheme for multirotor helicopter subject to simultaneous actuator faults. *IEEE Trans. Ind. Electron.* **2018**, *65*, 4227–4236. [CrossRef]
18. Bey, O.; Chemachema, M. Finite-time event-triggered output-feedback adaptive decentralized echo-state network fault-tolerant control for interconnected pure-feedback nonlinear systems with input saturation and external disturbances: A fuzzy control-error approach. *Inf. Sci.* **2024**, *669*, 120557. [CrossRef]
19. Li, H.; Wu, Y.; Chen, M. Adaptive fault-tolerant tracking control for discrete-time multiagent systems via reinforcement learning algorithm. *IEEE Trans. Cybern.* **2021**, *51*, 1163–1174. [CrossRef]
20. Zare, I.; Setoodeh, P.; Asemani, M.H. Fault-tolerant tracking control of discrete-time T–S fuzzy systems with input constraint. *IEEE Trans. Fuzzy Syst.* **2022**, *30*, 1914–1928. [CrossRef]
21. Liu, X.M.; Chang, X.H. Adaptive event-triggered tracking control for nonlinear networked systems with dynamic quantization and deception attacks. *Int. J. Robust Nonlinear Control* **2024**, *34*, 8311–8333. [CrossRef]
22. Zou, A.M.; Kumar, K.D.; Ruiter, A.H.J.d. Fixed-time attitude tracking control for rigid spacecraft. *Automatica* **2020**, *113*, 108792. [CrossRef]
23. Lee, H.; Kim, H.J. Trajectory tracking control of multirotors from modelling to experiments: A survey. *Int. J. Control. Autom. Syst.* **2017**, *15*, 281–292. [CrossRef]
24. Amer, N.H.; Zamzuri, H.; Hudha, K.; Kadir, Z.A. Modelling and control strategies in path tracking control for autonomous ground vehicles: A review of state of the art and challenges. *J. Intell. Robot. Syst.* **2017**, *85*, 225–254. [CrossRef]
25. Li, W.; Xie, Z.; Wong, P.K.; Zhang, X.; Zhao, J.; Zhao, J. Interval type-2 fuzzy path tracking control for autonomous ground vehicles under switched triggered and sensor attacks. *IEEE Trans. Intell. Transp. Syst.* **2024**, *25*, 16024–16035. [CrossRef]
26. Chang, X.H.; Han, X. Observer-based fuzzy $l_2 - l_\infty$ control for discrete-time nonlinear systems. *IEEE Trans. Fuzzy Syst.* **2024**, *32*, 2523–2528. [CrossRef]
27. Chang, X.H.; Liu, X.M.; Hou, L.W.; Qi, J.H. Quantized fuzzy feedback control for electric vehicle lateral dynamics. *IEEE Trans. Syst. Man Cybern. Syst.* **2024**, *54*, 2331–2341. [CrossRef]
28. Liu, H.; Wang, Z.; Fei, W.; Li, J. $\mathcal{H}_\infty$ and $l_2 - l_\infty$ state estimation for delayed memristive neural networks on finite horizon: The Round-Robin protocol. *Neural Netw.* **2020**, *132*, 121–130. [CrossRef]
29. Zhang, Z.; Dong, J. Observer-based interval type-2 $L_2 - L_\infty/\mathcal{H}_\infty$ mixed fuzzy control for uncertain nonlinear systems under measurement outliers. *IEEE Trans. Syst. Man Cybern. Syst.* **2021**, *51*, 7652–7662. [CrossRef]
30. Zhu, Q. Event-triggered sampling problem for exponential stability of stochastic nonlinear delay systems driven by Levy processes. *IEEE Trans. Autom. Control* **2024**, 1–8. [CrossRef]
31. Zhu, Q. Stabilization of stochastic nonlinear delay systems with exogenous disturbances and the event-triggered feedback control. *IEEE Trans. Autom. Control* **2019**, *64*, 3764–3771. [CrossRef]
32. Takagi, T.; Sugeno, M. Fuzzy identification of systems and its application to modeling and control. *IEEE Trans. Syst. Man Cybern.* **1985**, *SMC-15*, 116–132. [CrossRef]
33. Zhao, X.Y.; Chang, X.H. $\mathcal{H}_\infty$ filtering for nonlinear discrete-time singular systems in encrypted state. *Neural Process. Lett.* **2022**, *55*, 2843–2866. [CrossRef]
34. Mendel, J.M.; John, R.I.; Liu, F. Interval type-2 fuzzy logic systems made simple. *IEEE Trans. Fuzzy Syst.* **2006**, *14*, 808–821. [CrossRef]

35. Li, X.; Ye, D. Asynchronous event-triggered control for networked interval type-2 fuzzy systems against DoS attacks. *IEEE Trans. Fuzzy Syst.* **2021**, *29*, 262–274. [CrossRef]
36. Ge, C.; Sun, R.; Liu, Y.; Feng, W. Interval type-2 fuzzy sampled-date control for nonlinear systems with packet dropouts via a switched system approach. *Int. J. Fuzzy Syst.* **2024**. [CrossRef]
37. Pan, Y.; Yang, G.H. Event-driven fault detection for discrete-time interval type-2 fuzzy systems. *IEEE Trans. Syst. Man Cybern. Syst.* **2021**, *51*, 4959–4968. [CrossRef]
38. Zhang, Z.; Su, S.F.; Niu, Y. Dynamic event-triggered control for interval type-2 fuzzy systems under fading channel. *IEEE Trans. Cybern.* **2021**, *51*, 5342–5351. [CrossRef]
39. Tang, X.; Wu, M.; Li, M.; Ding, B. On designing the event-triggered multistep model predictive control for nonlinear system over networks with packet dropouts and cyber attacks. *IEEE Trans. Cybern.* **2022**, *52*, 11200–11212. [CrossRef]
40. Zhang, X.; Huang, W. Adaptive sliding mode fault tolerant control for interval type-2 fuzzy singular fractional-order systems. *J. Vib. Control* **2022**, *28*, 465–475. [CrossRef]
41. Feng, Z.; Yang, Y.; Lam, H.K. Extended-dissipativity-based adaptive event-triggered control for stochastic polynomial fuzzy singular systems. *IEEE Trans. Fuzzy Syst.* **2022**, *30*, 3224–3236. [CrossRef]

MDPI AG
Grosspeteranlage 5
4052 Basel
Switzerland
Tel.: +41 61 683 77 34

Mathematics Editorial Office
E-mail: mathematics@mdpi.com
www.mdpi.com/journal/mathematics

Academic Open
Access Publishing

mdpi.com

ISBN 978-3-7258-4312-1